Development of rifampicin loaded in surface-modified 4.0 G PAMAM dendrimer as a novel antituberculosis pulmonary drug delivery system

Rami M. Y. Ahmed

A thesis submitted in fulfillment of the requirement for the degree of

Doctor of Philosophy

Department of Pharmaceutics, School of Pharmacy

Faculty of Natural Science

University of the Western Cape

Supervisor: Prof. Halima Samsodien

Co-supervisors: Prof. Marique Aucamp/Dr. Naushaad Ebrahim

December 2020

Keywords

Tuberculosis

Rifampicin

Pulmonary delivery

Macrophage targeting

Nanoparticles

PAMAM dendrimer

PEGylated dendrimer

Mannosylated dendrimer

Surface-modified dendrimer

Abstract

Introduction: Tuberculosis (TB) is a serious bacterial infections caused by the *Mycobacterium Tuberculosis* (MTB) organism affecting mainly the lungs. Occasionally, MTB bacilli may be transported out of the pulmonary region and infect peripheral organs causing extra-pulmonary tuberculosis. Many therapeutic agents were developed over the years to combat TB, however the rapid emergence of resistant strains hampered their use. Furthermore, most of the current anti-TB drugs experience many challenges, which can be summarized in treatment regimen factors, drug-drug interactions, and physicochemical characteristics factors (such as hydrophobicity and low permeability into alveolar macrophages). These challenges have a significant role in treatment failure and the emergence of resistant TB. Due to the lack of newly discovered anti-TB drugs, and the absence of effective vaccines, many scientists have suggested the use of novel modalities for the current anti-TB drugs to enhance their efficacy and overcome some of the drawbacks. One of these modalities is nanotechnology-based drug delivery systems.

Most of the anti-TB drugs experience low drug distribution to the lung and particularly alveolar macrophages within which the MTB resides, leading to treatment failure. Employing nanoparticles as drug delivery systems can have a significant impact on improving the pharmacokinetic profile of anti-TB drugs, the feasibility of different routes of administration, enhancing drug permeability, controlled/sustained drug release, and targeting specific disease sites. Collectively, these impacts will aid in enhancing drug concentration at the site of infection and reduce dosing and regimen duration.

Dendrimers, such as polyamidoamine (PAMAM) dendrimers, are synthetic polymeric nanoparticles that have unique features that afford a dendrimer-conjugate complex the possibility to overcome the most common hurdles associated with drug delivery and treatment of diseases. Obstacles associated with solubility, permeability, inadequate biodistribution associated side effects may be enhanced. Manipulating the outermost surface functional groups with various ligands and polymers, will enhance the dendrimer properties and targeting potential.

Aim: This study aims to develop a novel pulmonary delivery system for the anti-TB drug rifampicin using surface-modified G4 PAMAM dendrimer nanoparticles (polyethylene glycol (PEG) or mannose moieties), to improve drug solubility, prolong-release, enhance permeability into the macrophages, and decrease the toxicity of the drug-dendrimer conjugates.

Methods: PAMAM dendrimers having increasing concentrations of poly(ethylene glycol) (PEG) 2 kDa or mannose residues were synthesized. The 4-nitrophenyl chloroformate was used as an activator in the case of PEG functionalization, while for the mannose conjugation the 4-isothiocyanatophenyl alpha-D-mannopyranoside (4-ICPMP) directly interacted with the primary amines of the dendrimer. The conjugated PEG polymers and mannose moieties on the dendrimer periphery were confirmed using FTIR and ^{1}H NMR analytical techniques. Thereafter, rifampicin was loaded into the native and surface-modified dendrimers *via* a simple dissolution solvent evaporation method. Rifampicin-loaded dendrimers were then characterized using several analytical techniques namely; FTIR, DSC, NMR, SEM, and DLS. The polymer encapsulation efficiency (EE%) and percentage of drug loading (DL%) were determined directly using a validated HPLC method. *In vitro* drug release was studied at pH 7.4 and pH 4.5. The MTT technique was used to assess the cytotoxicity of the dendrimer formulations against raw 264.7 cell lines. Finally, the uptake of dendrimer nanoparticles by raw macrophages was studied using a flow cytometer and fluorescence microscopy techniques.

Results: The percentage coverage of 4.0 G PAMAM dendrimer peripheral with PEG was achieved in a range of 38% - 100%, while for mannose moieties was from 44% - 100%. The EE% of unmodified dendrimer was 7.5% (w/w). The EE% of PEGylated dendrimers ranged from 65.0% - 78.75% (w/w), whereas for mannosylated dendrimers was from 43.43% - 57.91% (w/w). The size of the unloaded dendrimer nanoparticles was less than 25 nm, a gradual increase in the size after drug conjugation followed. The zeta potential of dendrimers was positive with values greater than 12 mV, the nanoparticle's zeta potential decreased upon increasing the density of PEG/mannose and after drug loading. FTIR and NMR data showed that rifampicin molecules were conjugated to the dendrimer at three sites; at the surface amines *via* electrostatic linkages, within the PEG/mannose, and into

the dendrimer interior. SEM images of dendrimer nanoparticles confirmed the spherical shape of particles, and DSC data verified drug entrapment. Drug release was found to be affected by the pH of the medium and the extent of dendrimer functionalization. At the physiologic pH, surface-modified dendrimers showed a slower release rate compared to the unmodified dendrimer and free drug. Among surface-modified dendrimers, the release rate was inversely associated with the density of PEG/mannose molecules. At pH 4.5, a relatively higher drug release from all formulations was observed which suggests a burst release inside the alveolar macrophages. Toxicity studies showed that the unmodified dendrimer experienced time-dependent and concentration-dependent cytotoxicity against raw 264.7 cells. The toxicity gradually decreased upon increasing the density of PEG/mannose, and negligible toxicity was detected for formulations with 100% functionalization. Dendrimer nanoparticles were successfully internalized into raw cells after 24 hrs of incubation. The order of nanoparticles permeability was PEG 100% < PEG 85% < PEG 70% < PEG 49% < PEG 38% < unmodified dendrimer < mannose 44% < mannose 69% < mannose 93% < mannose 100%. The significant increase in the uptake of mannosylated dendrimers was due to the interaction with lectin receptors at the surface of raw macrophages, whereas the lower internalization of PEGylated dendrimers was due to the shielding of the surface positive charges.

Conclusion: The *in-vitro* and *ex-vivo* data studies suggested that the developed novel surface-modified G4 PAMAM dendrimers are suitable drug carriers in terms of biocompatibility, release behaviour, and site-specific delivery of the anti-TB drug rifampicin.

Publications and presentations

Articles relevant to the thesis under process for publishing in scientific journals:

- Ahmed, R.M.Y, Samsodien, H., Aucamp, M., Ebrahim, N. Functionalization of dendrimers using mannose residues: Characteristic features and applications (Review article). (Ready for submission).

- Ahmed, R.M.Y, Samsodien, H., Aucamp, M., Ebrahim, N. Supramolecular assembly of rifampicin and PEGylated G4 PAMAM dendrimer as a novel conjugate for tuberculosis. (Ready for submission).

- Ahmed, R.M.Y, Samsodien, H., Aucamp, M., Ebrahim, N. Mannosylated dendrimer nanoconjugates for pulmonary delivery of rifampicin: Development and *in vitro* studies. (Ready for submission).

Presentations and conference attendance

- Pulmonary delivery of anti-tuberculosis drug rifampicin loaded in surface-modified fourth-generation PAMAM dendrimer as a novel drug delivery system (2019). Ahmed, R.M.Y, Samsodien, H., Aucamp, M., Ibrahim, N. At the *5th UWC School of Pharmacy Research Symposium*. Cape Town, South Africa.

- Attended the First Conference of Biomedical and Natural Sciences and Therapeutics (CoBNeST) (October 2018), Spier Estate, Stellenbosch, Cape Town, South Africa.

Declaration

I declare that: "***Development of rifampicin loaded in surface-modified 4.0 G PAMAM dendrimer as a novel antituberculosis pulmonary drug delivery system****"* is my own work, that has not been submitted for any degree or examination in any other university, and that all the sources I have used or quoted have been indicated and acknowledged by complete references.

Signed: 

Full name: Rami M.Y. Ahmed Date:…11/12/2020…….

Acknowledgment

First and foremost, I would like to thank Allah for His endless mercy, blessings and gifts. I thank Allah for His grace that enabled me to successfully complete this thesis.

There are no proper words to convey my deep gratitude and respect for my supervisor **Prof. Halima Samsodien** for her invaluable guidance, advice, support, criticism and encouragement throughout this project. It is an honor to know her as a supervisor and researcher and as a supervisor for my thesis. I will always be indebted to her.

My sincerest gratitude is extended to my thesis co-supervisors **Prof. Marique Aucamp** and **Dr. Naushaad Ebrahim** for the continuous support, guidance, cooperation, encouragement and for facilitating all the requirements. No words can convey my sincere gratitude.

My special words of thanks should also go to **Prof**. **Admire Dube**, for providing me with invaluable assistance and support. He always helped and supported me in various ways. Words cannot express my gratitude.

I owe my deepest gratitude to my better half and beloved wife **Lina Algasim** for her support and understanding of my goals and aspirations. Her love and support have always been my strength. Her patience and sacrifice will remain my inspiration throughout my life. Without her help, this thesis could not be completed. I love you.

I would like to express my gratitude to **Mr. Yunus Kippie** for the analytical expertise he shared, to **Mr. Sandile Dyantyi** and **Mrs. Eloise Braaf** for the procurement of essentials

for the project, to **Dr. Franscious Cummings** for assistance with SEM analysis, and to **Prof Edith Antunes** for making the analysis of NMR easy and interesting.

I greatly appreciate all the hard work and the tremendous support of **Dr. Nicole Sibuyi, Dr. Adewale Fadaka**, and **Dr. Nadine Pringle** for the extensive help with the *Tissue culture studies* and for always providing me with positive energy through my PhD journey.

I also thank **Prof Samsodien's research group**: Jean, Bjorn, and Zene for their insight, constructive criticism and support.

I gratefully acknowledge the **School of Pharmacy** staff, University of the Western Cape, for providing me with all the facilities, support and to allow me to carry out my research in this esteemed institute.

I greatly appreciate and acknowledge the support received from the **DST/Mintek Nanotechnology Innovation Center**, Department of Biotechnology, Faculty of Natural Science, University of the Western Cape. Most of the results described in this thesis would not have been obtained without their support.

Last but not least I greatly appreciate the fund that I received from **Medical Research Council-MRC** that enabled me to complete this project.

Dedication

I dedicate this thesis to my lovely wife Lina, My compassionate mother and my father

****

To my pretty daughters, Rina and Jana

***

To my siblings Dalia, Dina, Yousra, & Maiada for constantly putting me in their prayers during my studies.

****

To my friends Amir, Hassan, Ashraf, and Gassan for their invaluable advice and support, and for making it a positive competition.

***

Finally, to postgraduate colleagues at the School of Pharmacy, University of the Western Cape, I say thank you for good working relationships.

Content

Keywords i
Abstract ii
Publications and presentations v
Declaration vi
Acknowledgment vii
Dedication ix
Content x
List of Figures xvi
List of Tables xxvi
List of abbreviations xxix
Chapter 1 Tuberculosis: Background and treatment challenges 1
1.1 Tuberculosis 1
1.1.1 Overview and epidemiology 1
1.1.2 Causative organism 2
1.1.3 Transmission 3
1.1.4 Pathophysiology 3
1.1.5 Treatment 7
1.2 Challenges for the current anti-TB drugs 12
1.2.1 Treatment regimen 12
1.2.2 Co-infection and drug-drug interaction 12
1.2.3 Route of administration and drug properties 14
1.3 Towards a better treatment 15
1.3.1 Nanotechnology-based drug delivery system for treatment of tuberculosis 16
1.3.2 The pulmonary administration route 17
1.4 Rationale of the study 19
1.5 Aims and objectives of the study 20
1.6 Null hypothesis 21
1.7 Thesis outline 21
1.8 References 23

Chapter 2 Dendrimers: Characteristics and features 30
2.1 Background 30
2.2 Overview and general consideration 33
2.3 Characteristics of dendrimers 35
2.4 Dendrimers and hyperbranched polymers 37
2.5 Methods of dendrimer synthesis 40
2.6 Types of dendrimers 42
2.6.1 PPI dendrimer 43
2.6.2 Tecto (core-shell) dendrimer 43
2.6.3 Chiral dendrimers 43
2.6.4 Hybrid dendrimers 43
2.6.5 Amphiphilic and micellar dendrimers 43
2.6.6 Multiple antigen peptide dendrimers 44
2.6.7 Frèchet dendrimers 44
2.6.8 Glycodendrimers 44
2.6.9 PAMAM dendrimer 44
2.7 Dendrimers and tuberculosis 55
2.8 References 57
Chapter 3 Synthesis and characterization of rifampicin loaded PEGylated and non-PEGylated 4.0 G PAMAM dendrimers 64
3.1 Introduction 64
3.2 Review of the literature 64
3.2.1 PEGylation 64
3.2.2 Approaches of dendrimer-PEG conjugate 66
3.2.3 PEG-PAMAM dendrimer conjugate and drug delivery 68
3.2.4 Factors to be considered in PEGylated nanoparticulate drug delivery 71
3.2.5 Methods to quantify PEG density 73
3.3 Aim and the Objectives of the chapter 74
3.3.1 Aim 74
3.3.2 Objectives 74
3.4 Materials 75
3.4.1 Consumables 75

3.4.2 Equipment 76
3.5 Methods 76
3.5.1 Activation of mPEG 2000 by synthesizing mPEG-4-nitrophenyl carbonate 76
3.5.2 Conjugation of activated mPEG on the surface of G4 PAMAM dendrimer 77
3.5.3 Confirmation and quantification of the degree of PEGylation using ^{1}H NMR technique 78
3.5.4 Encapsulation of rifampicin by PEGylated and non-PEGylated G4 PAMAM dendrimers 79
3.5.5 Characterization of rifampicin loaded PAMAM dendrimer nanoparticles 79
3.5.6 Development and validation of reversed-phase high-performance liquid chromatography (RP-HPLC) method 82
3.5.7 Encapsulation efficiency (EE %) and drug loading (DL %) 86
3.6 Data analysis 86
3.7 Results and discussion 86
3.7.1 Activation of mPEG 2000 by synthesizing mPEG-4-nitrophenyl carbonate 86
3.7.2 Conjugation of activated mPEG-4NPC on the surface of G4 PAMAM dendrimer 89
3.7.3 Confirming and quantifying the degree of PEGylation using ^{1}H NMR technique 94
3.7.4 Characterization of rifampicin loaded PAMAM dendrimers 96
3.7.5 Development and validation of Reverse-phase high performance/pressure liquid chromatography (RP-HPLC) method 127
3.7.6 Encapsulation efficiency (EE%) and drug loading (DL%) 130
3.8 Conclusion 134
3.9 References 136
Chapter 4 Synthesis and characterization of rifampicin loaded mannosylated 4.0 G PAMAM dendrimer 142
4.1 Introduction 142
4.2 Review of the literature 142
4.2.1 Protein-carbohydrate interactions in cell recognition background 142
4.2.2 Design of multivalent biomimetic ligands 143
4.2.3 Macrophages role in drug delivery 146
4.2.4 The interaction of functionalized PAMAM dendrimers and the alveolar macrophages 147
4.2.5 Methods of PAMAM functionalization with mannose residues 149

4.2.6 Mannosylated dendrimer and tuberculosis 151
4.2.7 Methods to quantify the mannose content on dendrimers 151
4.3 Aim and the Objectives of the Chapter 153
4.3.1 Aim 153
4.3.2 Objectives 153
4.4 Materials 153
4.4.1 Consumables 153
4.4.2 Equipment 154
4.5 Methods 155
4.5.1 Functionalization of the surface of G4 PAMAM dendrimer with various mannose residues 155
4.5.2 Confirming and quantifying the degree of mannosylation using ^{1}H NMR technique 156
4.5.3 Encapsulation of rifampicin by mannosylated G4 PAMAM dendrimers 157
4.5.4 Characterization of rifampicin loaded mannosylated PAMAM dendrimer nanoparticles 157
4.5.5 Development and validation of Reverse-phase high performance/pressure liquid chromatography (RP-HPLC) method 159
4.5.6 Encapsulation efficiency (EE%) and drug loading (DL%) 159
4.6 Data analysis 160
4.7 Results and discussion 161
4.7.1 Functionalization of the surface of G4 PAMAM dendrimer with various mannose residues 161
4.7.2 Confirming and quantifying the degree of mannosylation using ^{1}H NMR technique 167
4.7.3 Characterization of rifampicin loaded mannosylated PAMAM dendrimers 169
4.7.4 Development and validation RP-HPLC method 190
4.7.5 Encapsulation efficiency (EE%) and drug loading (DL%) 191
4.8 Conclusion 195
4.9 References 196
Chapter 5 *In-vitro* drug release studies 201
5.1 Introduction 201
5.2 Review of the literature 201
5.2.1 Mechanisms of drug release from polymeric nanoparticles 201
5.2.2 Evaluation of *in vitro* drug release from polymeric nanoparticles 204

5.2.3 Analysis and modelling of drug release 207
5.2.4 The effect of dendrimer surface modification on drug release 211
5.3 Aim and the Objectives of the Chapter 213
5.3.1 Aim 213
5.3.2 Objectives 213
5.4 Materials 214
5.4.1 Consumables 214
5.4.2 Equipments 214
5.5 Methodology 215
5.5.1 Development and validation of RP-HPLC method for assessing rifampicin in phosphate buffer saline (PBS) pH 7.4 and acetate buffer pH 4.5 215
5.5.2 Stability studies of rifampicin in the release medium solutions within the study time-frame 218
5.5.3 *In-Vitro* drug release 219
5.5.4 Mathematical modelling of drug release data 220
5.6 Data analysis 221
5.7 Results and Discussion 221
5.7.1 Validation of RP-HPLC method for rifampicin determination in PBS pH 7.4 and acetate buffer solution pH 4.5 221
5.7.2 Stability of rifampicin in the release medium within the release studies time-frame 226
5.7.3 *In vitro* release of rifampicin from 4.0 G PAMAM dendrimer having different PEG content 230
5.7.4 *In vitro* release of rifampicin from 4.0 G PAMAM dendrimer having different mannose content 240
5.7.5 Fitting of drug release data into mathematical models 246
5.8 Conclusion 256
5.9 References 257
Chapter 6 *In vitro* cytotoxicity and permeability studies 262
6.1 Introduction 262
6.2 Review of the literature 262
6.2.1 Toxicity and biocompatibility 262
6.2.2 Toxicity of drug delivery systems: Dendrimer toxicity 263
6.2.3 Functionalization strategies 265

6.2.4 Dendrimer cellular uptake 272
6.2.5 Dendrimer uptake by alveolar macrophages 273
6.3 Aim and the Objectives of the Chapter 277
6.3.1 Aim 277
6.3.2 Objectives 277
6.4 Materials 278
6.4.1 Consumables 278
6.4.2 Equipment 278
6.5 Methods 279
6.5.1 Cell culture 279
6.5.2 Cytotoxicity assay 279
6.5.3 Labeling of the dendrimer nanoparticles 279
6.5.4 Cellular uptake studies 280
6.5.5 Fluorescence microscope analysis 280
6.6 Data analysis 281
6.7 Results and discussion 281
6.7.1 Cytotoxicity studies 281
6.7.2 Microscopic analysis 296
6.7.3 Labeling of the dendrimer nanoparticles 298
6.7.4 Cellular uptake studies 299
6.7.5 Fluorescence microscope analysis 305
6.8 Conclusion 308
6.9 References 310
Chapter 7 Summary, conclusion, and recommendations 316
7.1 Summary and conclusion of the thesis 316
7.2 Recommendations for this study 319

List of Figures

Figure 1.1 Illustration of TB pathophysiology and the consequences of the interaction between the MTB and the immune system [adapted from (Kaufmann and McMichael, 2005)]. 4

Figure 1.2 The maturation of TB granuloma [adapted from (Dube, Agrawal and Vyas, 2012)]. 6

Figure 1.3 Time-line for the discovered anti-TB drugs (1940 – 2000) [adapted from (Al-Humadi, Al-Saigh and Al-Humadi, 2017)]. 7

Figure 1.4 Clinical problems associated with the current TB therapeutic drugs [adapted from (Pinheiro *et al.*, 2011)]. 13

Figure 1.5 Illustration for the required properties of the novel anti-TB drugs/modalities [adapted from (Shehzad *et al.*, 2013)]. 15

Figure 2.1 The development track of dendrimers [Adapted from (Singh *et al.*, 2017)].....31

Figure 2.2 Main components of 3.0 G dendrimer, (A) 2-dimensional (2-D), and (B) 3- dimensional (3-D) representations [adapted from (Svenson, 2009)]. 33

Figure 2.3 Illustration of dendrimer generation number [adapted from (Hu, Hu and Cheng, 2016)]. 34

Figure 2.4 Summary of dendrimer characteristics [Adapted from (Singh *et al.*, 2017)]. 36

Figure 2.5 The structure of (a) hyperbranched polymers and (b) dendrimer [Adapted from (Grayson and Fréchet, 2001)]. 38

Figure 2.6 Development of the dendrimer over a time frame of 50 years [adapted from (Tomalia and Fréchet, 2002)]. 39

Figure 2.7 Illustration of the divergent method for dendrimer synthesis [Adapted from (Grayson and Fréchet, 2001)]. 41

Figure 2.8 Illustration of the convergent method for dendrimer synthesis [Adapted from (Grayson and Fréchet, 2001)]. 42

Figure 2.9 Comparison of several PAMAM dendrimers having ammonia core with different proteins, lipid bilayers, and DNA [Adapted from (Esfand and Tomalia, 2001)]. 47

Figure 2.10 Types of PAMAM dendrimer – drug encapsulation mechanisms [Adapted from (Singh *et al.*, 2017)]. 51

Figure 2.11 Illustration for the approaches of drug release by dendrimers (a) structure conformational changes approach (Boas and Heegaard, 2004), and b) stimulus cleavage approach (Zhu and Shi, 2013)..... 52

Figure 2.12 Hypothetical scheme for the interaction of dendrimer with (A) lipid bilayers membrane (Martinho *et al.*, 2014), and (B) red blood cells [Adapted from (Labieniec-Watala *et al.*, 2013)]..... 53

Figure 2.13 Different techniques to minimize the toxicity of PAMAM dendrimers [Adapted from (Luong *et al.*, 2016)]. 54

Figure 3.1 Outline of PEGylation techniques [adapted from (Veronese and Pasut, 2005; Damodaran and Fee, 2010)]……..65

Figure 3.2 Synthesis of PEGylated 4.0 G PAMAM dendrimer [adapted from (Kojima *et al.*, 2000)]. 66

Figure 3.3 The main types of PEG-dendrimer conjugate [adapted from (Thakur *et al.*, 2015)]. (a) Surface-conjugation PEGylated dendrimer, (b) Dendrimer having PEG core, (c) Dendrimer with PEG as a branching monomer unit, (d) PEGylated-diagnostic agent conjugated dendrimer, (e) PEGylated-ligand conjugated dendrimer, (f) PEGylated-bioactive agent (drug) conjugated dendrimer..... 68

Figure 3.4 Synthesis of PEGylated G4 PAMAM dendrimer [adapted from (Diaz *et al.*, 2018b)]. . 77

Figure 3.5 ^{1}H NMR spectra of mPEG-4NPC after (a) 24 hrs, and (b) 48 hrs of reaction..... 87

Figure 3.6 ^{1}H NMR spectra of (a) mPEG 2 kDa, (b) 4-nitrophenyl chloroformate (4-NPC), and (c) mPEG-4-nitrophenyl carbonate (mPEG-4NPC). 88

Figure 3.7 FTIR spectra of: (a) mPEG 2 kDa, (b) 4-NPC, and (c) mPEG-4NPC. 89

Figure 3.8 ^{1}H NMR spectra of, (i) mPEG-4NPC in $CDCl_3$, (ii) G4 PAMAM dendrimer (iii) G4-PEG 1:25, (iv) G4-PEG 1:38, (v) G4-PEG 1:51, (vi) G4-PEG 1:62, and (vii) G4-PEG 1:200, in deuterated water. 91

Figure 3.9 FTIR spectra of: (a) G4 PAMAM dendrimer, (b) mPEG-4NPC, (c) G4-mPEG 1:25, (d) G4-mPEG 1:38, (e) G4-mPEG 1:51, (f) G4-mPEG 1:62, and (g) G4-mPEG 1:200. 92

Figure 3.10 The ^{1}H NMR spectra of (a) G4-mPEG 1:25, (b) G4-mPEG 1:38, (c) G4-mPEG 1:51, (d) G4-mPEG 1:62, and (e) G4-mPEG 1:200, in deuterated water, with integration values of methylene protons next to the carbonyl groups of PAMAM dendrimer at δ of 2.30 ppm**,** methylene of (-***CH2***-O-CO-**)** group at δ of 4.11 ppm, and the terminal methyl group protons peak of the mPEG at δ of 3.3 ppm..... 95

Figure 3.11 FTIR spectra of: (a) G4 PAMAM dendrimer, (b) G4-mPEG 38%, (c) rifampicin, and (d) RIF loaded G4- mPEG 38%. 97
Figure 3.12 FTIR spectra of: (a) G4 PAMAM dendrimer, (b) G4-mPEG 49% (1:38), (c) rifampicin, and (d) RIF loaded G4-mPEG 49% (1:38). 99
Figure 3.13 FTIR spectra of: (a) G4 PAMAM dendrimer, (b) G4-mPEG 70% (1:51), (c) rifampicin, and (d) RIF loaded G4-mPEG 70% (1:51). 100
Figure 3.14 FTIR spectra of: (a) G4 PAMAM dendrimer, (b) G4-mPEG 85% (1:62), (c) rifampicin, and (d) RIF loaded G4-mPEG 85% (1:62). 100
Figure 3.15 FTIR spectra of: (a) G4 PAMAM dendrimer, (b) G4-mPEG 100% (1:200), (c) rifampicin, and (d) RIF loaded G4-mPEG 100% (1:200). 101
Figure 3.16 FTIR spectra of (a) G4 PAMAM dendrimer, (b) rifampicin, and (c) RIF loaded G4 dendrimer (0% mPEG). 102
Figure 3.17 The structure of rifampicin. 103
Figure 3.18 ^{1}H NMR spectra of (a) PEGylated G4 PAMAM dendrimer (38%), (b) rifampicin, and (c) rifampicin loaded PEGylated G4 PAMAM dendrimer (38%), in DMSO-d_6. 107
Figure 3.19 ^{1}H NMR spectra of (a) PEGylated G4 PAMAM dendrimer (49%), (b) rifampicin, and (c) rifampicin loaded PEGylated G4 PAMAM dendrimer (49%), in DMSO-d_6. 109
Figure 3.20 ^{1}H NMR spectra of (a) PEGylated G4 PAMAM dendrimer (70%), (b) rifampicin, and (c) rifampicin loaded PEGylated G4 PAMAM dendrimer (70%), in DMSO-d_6. 109
Figure 3.21 ^{1}H NMR spectra of (a) PEGylated G4 PAMAM dendrimer (85%), (b) rifampicin, and (c) rifampicin loaded PEGylated G4 PAMAM dendrimer (85%), in DMSO-d_6. 110
Figure 3.22 ^{1}H NMR spectra of (a) PEGylated G4 PAMAM dendrimer (100%), (b) rifampicin, and (c) rifampicin loaded PEGylated G4 PAMAM dendrimer (100%), in DMSO-d_6. 110
Figure 3.23 2D NOESY NMR spectra of rifampicin loaded PEGylated G4 PAMAM dendrimer (38%), in DMSO-d_6. 111
Figure 3.24 ^{1}H NMR spectra of (a) G4 PAMAM dendrimer in D_2O, (b) rifampicin in DMSO-d_6, and (c) rifampicin loaded G4- dendrimer (mPEG 0%) in DMSO-d_6. 112
Figure 3.25 2D NOESY NMR spectra of rifampicin loaded non-PEGylated G4 PAMAM dendrimer (0% mPEG), in DMSO-d_6. 113
Figure 3.26 SEM micrographs of (a) pure G4 PAMAM dendrimer, (b) PEGylated dendrimer (85% PEG), and (c) rifampicin-loaded PEGylated dendrimer (85% PEG). 115

Figure 3.27 SEM images of (A) RIF-G4 dendrimer (0% mPEG), (B) RIF-G4 dendrimer (38% mPEG), (C) RIF-G4 dendrimer (49% mPEG), (D) RIF-G4 dendrimer (70% mPEG), (E) RIF-G4 dendrimer (85% mPEG), and (F) RIF-G4 dendrimer (100% mPEG). 116
Figure 3.28 DSC thermograms of (1) rifampicin, (2) RIF-dendrimer physical mixture (100% mPEG), (3) PEGylated dendrimer (100% mPEG), and (4) RIF-dendrimer (100% mPEG). 117
Figure 3.29 DSC thermograms of (1) rifampicin, (2) rifampicin-dendrimer physical mixture (100% mPEG), (3) RIF-dendrimer (38% mPEG), (4) RIF-dendrimer (49% mPEG), (5) RIF-dendrimer (70% mPEG), (6) RIF-dendrimer (85% mPEG), and (7) RIF-dendrimer (100% mPEG). 118
Figure 3.30 The hydrodynamic (D_H) diameters of unloaded (blue) and rifampicin-loaded (red) dendrimer nanoparticle formulations with different mPEG content. Results show a mean ± SD (n = 3). Error bars represent the calculated SD from the mean. 121
Figure 3.31 Molecular dynamic snapshot illustrating the effect of mPEG size and density on the G4 PAMAM dendrimer. Black dots symbolize G4 PAMAM dendrimer beads, and transparent pink dots symbolize mPEG chains [adapted from (Lee and Larson, 2011)]. 122
Figure 3.32 Polydispersity index (PDI) of unloaded (blue) and rifampicin-loaded (red) dendrimer nanoparticle formulations with different mPEG content. Results show as mean ± SD (n=3). Error bars represent the calculated SD from the mean. 124
Figure 3.33 Zeta potential of empty (blue) and rifampicin-loaded (red) dendrimer nanoparticle formulations with different mPEG content. Results showed as mean ± SD (n=3). Error bars represent the calculated SD from the mean. 125
Figure 3.34 Rifampicin standard calibration curve at a wavelength of 475 nm in the mobile phase. 128
Figure 3.35 HPLC chromatograms of (a) non-degraded rifampicin standard, (b) unloaded PEGylated dendrimer, and (c) the mobile phase. 130
Figure 3.36 Nanoparticle encapsulation efficiency (EE%) of different dendrimer-mPEG formulations. 132
Figure 3.37 Nanoparticle percentage drug loading (DL%) of different dendrimer-mPEG formulations. 133
Figure 4.1 Examples of biological conjugations that are mainly mediated *via* protein-carbohydrate interactions; [adapted from (Sharon and Lis, 1993; Woller, 2003)]..... 142

Figure 4.2 Summary for different modes of interactions, (A) monovalent, (B) multivalent, (C) glycoside cluster effect, (D) combination of multivalent and glycoside cluster, and (E) cross-linking interaction; [adapted from (Woller, 2003)]. 144

Figure 4.3 Representation of the two glycodendrimer classes: a) when the saccharides are conjugated to the outer layer of the dendrimer, and b) when the saccharides are the building units of the dendrimer; [adapted from (Jayaraman, Nepogodiev and Stoddart, 1997)]..... 148

Figure 4.4 Various techniques of synthesis glycoPAMAM dendrimers; [adapted from (Woller, 2003)]. 150

Figure 4.5 Synthesis of mannosylated G4 PAMAM dendrimers. 155

Figure 4.6 Chemical structure of mannosylated G4 PAMAM dendrimer. 161

Figure 4.7 ^{1}H NMR spectra (1.8 ppm – 9.0 ppm) of, (i) G4 PAMAM dendrimer in D_2O, (ii) Mannose (4-ICPMP), (iii) G4-mannose 1:30, (iv) G4-mannose 1:45, (v) G4-mannose 1:60, and (vi) G4-mannose 1:100, in DMSO-d_6. 163

Figure 4.8 ^{1}H NMR spectra (8.80 ppm – 14.80 ppm) of, (i) G4 PAMAM dendrimer in D_2O, (ii) Mannose (4-ICPMP), (iii) G4-mannose 1:30, (iv) G4-mannose 1:45, (v) G4-mannose 1:60, and (vi) G4-mannose 1:100, in DMSO-d_6. 163

Figure 4.9 FTIR spectra of (a) G4 PAMAM dendrimer, (b) mannose (4-ICPMP), (c) G4-mannose 1:30, (d) G4-mannose 1:45, (e) G4-mannose 1:60, and (f) G4-mannose 1:100. 164

Figure 4.10 The ^{1}H NMR spectra of (a) G4-mannose 1:30, (b) G4-mannose 1:45, (c) G4-mannose 1:60, and (d) G4-mannose 1:100, in DMSO-d_6, with integration values of methylene protons next to the carbonyl groups of G4 PAMAM dendrimer at δ of 2.30 ppm, anomeric protons (peak L) at δ of 5.31 ppm, and aromatic protons (peaks M & N) at δ of 7.02 ppm and 7.25 ppm from mannose residues. 167

Figure 4.11 FTIR spectra of (a) G4 PAMAM dendrimer, (b) G4-mannose 1:30 (44%), (c) rifampicin, and (d) RIF loaded G4- mannose 1:30 (44%). 169

Figure 4.12 FTIR spectra of (a) G4 PAMAM dendrimer, (b) G4-mannose 69%, (c) rifampicin, and (d) RIF loaded G4- mannose 69%. 171

Figure 4.13 FTIR spectra of (a) G4 PAMAM dendrimer, (b) G4-mannose 93%, (c) rifampicin, and (d) RIF loaded G4- mannose 93%. 171

Figure 4.14 FTIR spectra of (a) G4 PAMAM dendrimer, (b) G4-mannose 100%, (c) rifampicin, and (d) RIF loaded G4- mannose 100%. 172

Figure 4.15 The structures of (a) rifampicin, and (b) mannosylated dendrimer, with highlighting on atoms that show changes in their ^{1}H NMR chemical shift. 173
Figure 4.16 ^{1}H NMR spectra of (a) mannosylated G4 PAMAM dendrimer (44%), (b) rifampicin, and (c) rifampicin loaded mannosylated G4 PAMAM dendrimer (44%), in DMSO-d_6 solvent. 174
Figure 4.17 ^{1}H NMR spectra of (a) mannosylated G4 PAMAM dendrimer (69%), (b) rifampicin, and (c) rifampicin loaded mannosylated G4 PAMAM dendrimer (69%), in DMSO-d_6 solvent. 175
Figure 4.18 ^{1}H NMR spectra of (a) mannosylated G4 PAMAM dendrimer (93%), (b) rifampicin, and (c) rifampicin loaded mannosylated G4 PAMAM dendrimer (93%), in DMSO-d_6 solvent. 175
Figure 4.19 ^{1}H NMR spectra of (a) mannosylated G4 PAMAM dendrimer (100%), (b) rifampicin, and (c) rifampicin loaded mannosylated G4 PAMAM dendrimer (100%), in DMSO-d_6 solvent. 176
Figure 4.20 2D NOESY NMR spectra of rifampicin loaded mannosylated G4 PAMAM dendrimer (44%), in DMSO-d_6 solvent. 177
Figure 4.21 SEM images of (a) G4-mannose 1:30 (44%), (b) G4-mannose 1:45 (69%), (c) G4-mannose 1:60 (93%), and (d) G4-mannose 1:100 (100%). 179
Figure 4.22 SEM images of (a) RIF loaded G4-mannose 1:30 (44%), (b) RIF loaded G4-mannose 1:45 (69%), (c) RIF loaded G4-mannose 1:60 (93%), and (d) RIF loaded G4-mannose 1:100 (100%). 180
Figure 4.23 DSC thermograms of (a) rifampicin, (b) rifampicin-dendrimer (44% mannose) physical mixture, (c) unloaded mannosylated dendrimer (44%), and (d) rifampicin loaded mannosylated dendrimer (44%). 181
Figure 4.24 DSC thermograms of (a) rifampicin, (b) rifampicin loaded mannosylated dendrimer (44%), (c) rifampicin loaded mannosylated dendrimer (69%), (d) rifampicin loaded mannosylated dendrimer (93%), and (e) rifampicin loaded mannosylated dendrimer (100%). 183
Figure 4.25 The hydrodynamic (D_H) diameters of unloaded (blue) and rifampicin-loaded (red) dendrimer nanoparticle formulations with different mannose residues. Results showed a mean ± SD (n = 3). Error bars represent the calculated SD from the mean. 185
Figure 4.26 Polydispersity index (PDI) of unloaded (blue) and rifampicin-loaded (red) dendrimer nanoparticle formulations with different mannose residues. Results showed as mean ± SD (n=3). Error bars represent the calculated SD from the mean. 187

Figure 4.27 Zeta potential values of unloaded (blue) and rifampicin-loaded (red) dendrimer nanoparticle formulations with different mannose residues. Results showed as mean ± SD (n=3). Error bars represent the calculated SD from the mean. 188

Figure 4.28 HPLC chromatograms of (a) rifampicin standard, (b) the mobile phase, and (c) unloaded mannosylated dendrimer. 191

Figure 4.29 Rifampicin standard calibration curve in the mobile phase at a wavelength of 475 nm. 192

Figure 4.30 Nanoparticle encapsulation efficiency (EE%) of different dendrimer-mannose formulations. 192

Figure 4.31 Nanoparticle percentage drug loading (DL%) of different dendrimer-mannose formulations. 194

Figure 5.1 Schematic of drug release mechanisms from polymeric nanocarriers (Son, Lee and Cho, 2017), (a) diffusion release; (b) solvent-controlled release; (c) polymer degradation release; and (d) stimuli-controlled release 202

Figure 5.2 Possible mechanisms of drug release from PAMAM dendrimers. 204

Figure 5.3 Schematic of dialysis bag technique (D'Souza and DeLuca, 2006). 205

Figure 5.4 Rifampicin calibration curves at a wavelength of 475 nm. (A) in PBS spiked with ascorbic acid 200 µg/ml, and (B) in acetate buffer pH 4.5 spiked with ascorbic acid 50 µg/ml. 221

Figure 5.5 Chromatograms of **(a)** standard rifampicin, **(b)** unloaded PEGylated dendrimer, **(c)** unloaded mannosylated dendrimer, **(d)** the mobile phase, **(e)** PBS (spiked with ascorbic acid), and **(f)** acetate buffer pH 4.5 (spiked with ascorbic acid). 224

Figure 5.6 HPLC chromatograms of **(a)** non-degraded rifampicin standard, alkaline force degraded (0.1 M NaOH) of rifampicin in **(b)** the mobile phase, **(c)** PBS, and **(d)** acetate buffer pH 4.5. ... 225

Figure 5.7 HPLC chromatograms of **(a)** non-degraded rifampicin standard, acidic force degraded (0.1 M HCL) of rifampicin in **(b)** the mobile phase, **(c)** PBS, and **(d)** acetate buffer pH 4.5. 226

Figure 5.8 Rifamapicin oxidative decomposition pathway (Sorokoumova *et al.*, 2008). 227

Figure 5.9 Pathway of rifampicin degradation in acidic medium adapted from (Singh *et al.*, 2000). 228

Figure 5.10 Rifampicin (20.0 µg/ml) degradation in acetate buffer pH 4.5, and comparison between using the derived correlation factor and sum of RIF and 3FRSV AUCs. 230

Figure 5.11 *In vitro* release profiles of rifampicin from 4.0 G PAMAM dendrimer having different PEG content, incubated in PBS pH 7.4 spiked with ascorbic acid 200 µg/ml at 37 °C under continuous stirring at 100 rpm (n = 3)..... 231
Figure 5.12 *In vitro* release profiles of rifampicin from 4.0 G PAMAM dendrimer having different PEG content, incubated in acetate medium pH 4.5 spiked with ascorbic acid 50 µg/ml at 37 °C under continuous stirring at 100 rpm (n = 3). 236
Figure 5.13 3-D and 2-D depictions for the effect of pH on the conformational change of amino-terminated dendrimers [adapted from (Boas and Heegaard, 2004)]. 238
Figure 5.14 *In vitro* release profiles of rifampicin from 4.0 G PAMAM dendrimer having different mannose content, incubated in PBS pH 7.4 spiked with ascorbic acid 200 µg/ml at 37 °C under continuous stirring at 100 rpm (n = 3)..... 240
Figure 5.15 *In vitro* release profiles of rifampicin from 4.0 G PAMAM dendrimer having different mannose content, incubated in acetate medium pH 4.5 spiked with ascorbic acid at 37 °C under continuous stirring at 100 rpm (n = 3)..... 244
Figure 5.16 Kinetic models of best fit for *in vitro* release of rifampicin from PEGylated and non-PEGylated dendrimer nano-formulations at pH 7.4..... 248
Figure 5.17 Kinetic models of best fit for *in vitro* release of rifampicin from PEGylated and non-PEGylated dendrimer nano-formulations at pH 4.5..... 250
Figure 5.18 Kinetic models of best fit for *in vitro* release of rifampicin from mannosylated dendrimer nano-formulations at pH 7.4. 254
Figure 5.19 Kinetic models of best fit for *in vitro* release of rifampicin from mannosylated dendrimer nano-formulations at pH 4.5. 255
Figure 6.1 Difference between biocompatibility and toxicity [adapted from (Duncan and Izzo, 2005)]..... 262
Figure 6.2 Commonly reported techniques to overcome dendrimer toxicity (Thakur *et al.*, 2015). 266
Figure 6.3 The structure of PEGylated dendrimer [adapted from (Mishra, Gupta and Jain, 2009)]. 266
Figure 6.4 Illustration for the expected interaction between dendrimer and cell membrane [adapted from (Jain *et al.*, 2010; Thakur *et al.*, 2015)]..... 268
Figure 6.5 Glycodendrimers structure of (a) surface-modified with mannose (Pagé and Roy, 1997), and (b) surface-modified with galactose (Mishra, Gupta and Jain, 2009). 270

Figure 6.6 The structure of a dendritic box [adapted from (Mishra, Gupta and Jain, 2009)]..... 272
Figure 6.7 Illustration of the phagocytosis process by the alveolar macrophages [adapted from pathogens (Patel, Gupta and Ahsan, 2015)]. 275
Figure 6.8 Cell survival (%) on raw cells for increasing PEGylated dendrimer concentrations (1.25 µM – 10 µM), after (a) 24 hrs, (b) 48 hrs, and (c) 72 hrs of incubation. The untreated cells were employed as a negative control and doxorubicin drug was used as a positive control. (n = 3). (*) denotes statistical significance difference compared to the unmodified dendrimer at each concentration, while letter (a,b, and c) symbols denote statistical significance difference compared to the control. 283
Figure 6.9 Cell survival (%) on raw cells for increasing unmodified G4 PAMAM dendrimer concentrations (1.25 µM – 10 µM), after 24 hrs, 48 hrs, and 72 hrs of incubation (n = 3)..... 285
Figure 6.10 Cell survival (%) on raw cells for increasing rifampicin-loaded PEGylated dendrimer concentrations (0.125 µM – 2 µM), after (a) 24 hrs, (b) 48 hrs, and (c) 72 hrs of incubation. The untreated cells were employed as a negative control (n = 3). (*) denotes statistical significance difference compared to the unmodified dendrimer at each concentration, while letter (a,b, and c) symbols denote statistical significance difference compared to the control. 289
Figure 6.11 Cell survival (%) on raw cells for increasing mannosylated dendrimer concentrations (1.25 µM – 10 µM), after (a) 24 hrs, (b) 48 hrs, and (c) 72 hrs of incubation. The untreated cells were employed as a negative control and doxorubicin drug was used as a positive control (n = 3). (*) denotes statistical significance difference compared to the unmodified dendrimer at each concentration, while letter (a,b, and c) symbols denote statistical significance difference compared to the control. 291
Figure 6.12 Cell survival (%) on raw cells for increasing rifampicin-loaded mannosylated dendrimer concentrations (0.125 µM – 2 µM), after (a) 24 hrs, (b) 48 hrs, and (c) 72 hrs of incubation. The untreated cells were employed as a negative control (n = 3). (*) denotes statistical significance difference compared to the unmodified dendrimer (0% mannose) at each concentration, while letter (a,b, and c) symbols denote statistical significance difference compared to the control. 295
Figure 6.13 Microscopic images of raw cells treated with 5 µM of DOX and dendrimers for 24 hrs. The images were obtained by the Invitrogen EVOS cell imaging system. (a) include the –ve control, +ve control and the native G4, (b) PEGylated dendrimers, (c) mannosylated dendrimers. 297
Figure 6.14 ^{1}H NMR spectra of (a) 38% PEGylated dendrimer, (b) FITC, and (c) FITC-labeled PEGylated dendrimer (38%). 298

Figure 6.15 Endocytic uptake of FITC-labeled PEGylated dendrimers (5 μM) in raw cells after 24 hrs of incubation. (a) Flow cytometric analysis, (b) percentage of +ve-FITC-staining cells, and (c) mean fluorescence intensity of dendrimer nanoformulations (n = 3). (*) denotes statistical significance difference compared to the unmodified dendrimer. 300
Figure 6.16 Endocytic uptake of FITC-labeled mannosylated dendrimers (5 μM) in raw cells after 24 hrs of incubation. (a) Flow cytometric analysis, (b) percentage of +ve-FITC-staining cells, and (c) mean fluorescence intensity of dendrimer nanoformulations (n = 3). (*) denotes statistical significance difference compared to the unmodified dendrimer. 302
Figure 6.17 Fluorescence images of raw264.7 cells incubated with 5 μM of FITC-labeled dendrimers (green dye) (a) unmodified dendrimer, (b) 38% PEG-dendrimer, (c) 100% PEG-dendrimer, (d) 44% mannose-dendrimer, and (e) 69% mannose-dendrimer, showing uptake after 24 hrs. The nuclei were stained with DAPI (blue dye). 307

List of Tables

Table 1.1 Current anti-TB drugs and their mechanism of action [adapted from (Dube, Agrawal and Vyas, 2012)]. 10

Table 2.1 Timeline of dendrimer development until 2010 (Singh et al., 2017).....32

Table 2.2 Summary of approximate molecular mass and the number of surface groups of G0 - G10 PAMAM dendrimers (Tomalia et al., 1985; Maiti et al., 2004; Müller et al., 2007). 46

Table 2.3 Summary of factors affecting the characteristics of PAMAM dendrimers. 49

Table 3.1 Comparison between PEGylated and non-PEGylated dendrimers [adapted from (Thakur *et al.*, 2015)].....71

Table 3.2 Characteristics of PEG-PAMAM dendrimer conjugates. 78

Table 3.3 Selected IR functional groups with their frequencies for G4 PAMAM dendrimer, activated mPEG-4NPC, and PEGylated dendrimers. 93

Table 3.4 Characterization of mPEG-G4 PAMAM dendrimer conjugates (n = 3). 96

Table 3.5 The IR functional group assignments of G4 PAMAM dendrimer, G4-mPEG 38%, rifampicin, and RIF loaded G4- mPEG 38%. 98

Table 3.6 The ^{1}H NMR, ^{13}C NMR resonance assignments, multiplicity, integration, and coupling constants of rifampicin atoms in DMSO-d6. 104

Table 3.7 Comparison of the dendrimer's endothermic peaks before and after drug conjugation. 117

Table 3.8 The physicochemical characteristics of the unloaded and rifampicin-loaded dendrimers having different mPEG content. Results illustrated as mean ± SD (n = 3). 120

Table 3.9 Summary of the linearity data of rifampicin standard (λ_{max} = 475 nm) in the mobile phase. 128

Table 3.10 Intra-day and inter-day precision and accuracy of rifampicin (λ_{max} = 475) in the mobile phase (Potassium phosphate buffer pH 7.4: ACN). 129

Table 3.11 DL%, EE% of rifampicin in different dendrimer formulations, results shown as mean ± SD (n = 3). 131

Table 4.1 Characteristics of mannose-dendrimer conjugates.....156

Table 4.2 Selected IR functional groups with their frequencies (cm^{-1}) for G4 PAMAM dendrimer, mannose, and mannosylated dendrimers..... 166
Table 4.3 Characterization of mannosylated G4 PAMAM dendrimer conjugates. 168
Table 4.4 The IR functional group assignments of G4 PAMAM dendrimer, G4-mannose 44%, rifampicin, and RIF loaded G4- mannose 44%. 170
Table 4.5 Comparison of the dendrimer's endothermic peaks before and after drug conjugation. 182
Table 4.6 The physicochemical characteristics of the unloaded and rifampicin-loaded dendrimers having different mannose residues. Results illustrated as mean ± SD (n = 3). 185
Table 4.7 DL%, EE% of rifampicin in different dendrimer formulations, results displayed as mean ± SD (n = 3)..... 193
Table 5.1 Examples of drug release assessing methods with dendrimer nanoparticles.....207
Table 5.2 Summary of the linearity data of rifampicin (λ_{max} = 475 nm) at pH 7.5 and pH 4.5. ... 222
Table 5.3 Intra-day and inter-day precision and accuracy of rifampicin (λ_{max} = 475 nm) at pH 7.4 and 4.5. 223
Table 5.4 Developing a correlation between rifampicin (20.0 µg/ml) and 3FRSV using AUCs value as a function of time, in acetate buffer pH 4.5 at 37 °C under continuous stirring at 100 rpm (n = 3)..... 229
Table 5.5 Comparison of the effect of dendrimer PEG content on rifampicin release after 11 hrs, 24 hrs, 48 hrs, and 72 hrs of incubation in PBS 7.4 fortified with ascorbic acid at 37 °C under continuous stirring of 100 rpm. 232
Table 5.6 Comparison of the effect of dendrimer PEG content on rifampicin release after 6 hrs, 11 hrs, 24 hrs, and 48 hrs of incubation in acetate buffer medium pH 4.5 fortified with ascorbic acid at 37 °C under continuous stirring of 100 rpm. 237
Table 5.7 Comparison of the effect of dendrimer mannose content on rifampicin release after 12 hrs, 24 hrs, 48 hrs, and 72 hrs of incubation in acetate buffer medium pH 7.4 fortified with ascorbic acid at 37 °C under continuous stirring of 100 rpm. 241
Table 5.8 Comparison of the effect of dendrimer mannose content on rifampicin release after 6 hrs, 11 hrs, 24 hrs, and 48 hrs of incubation in acetate buffer medium pH 4.5 fortified with ascorbic acid at 37 °C under continuous stirring of 100 rpm. 245
Table 5.9 Parameter values and R^2_{adj} values acquired from fitting the rifampicin release data from PEGylated and non-PEGylated dendrimers in PBS into 6 mathematical models. The highlighted

values in red colour correspond to the highest values of R^2_{adj} obtained when the six models were compared, for each formulation. 249
Table 5.10 Parameter values and R^2_{adj} values acquired from fitting the rifampicin release data from PEGylated and non-PEGylated dendrimers in acetate medium into 6 mathematical models. The highlighted values in red colour correspond to the highest values of R^2_{adj} obtained when the six models were compared, for each formulation. 251
Table 5.11 Parameter values and R^2_{adj} values acquired from fitting the rifampicin release data from unmodified and mannosylated dendrimer in [a] PBS and [b] acetate into 6 mathematical models. The highlighted values in red colour correspond to the highest values of R^2_{adj} obtained when the six models were compared, for each formulation. 253
Table 6.1 Approaches to increase or decrease the phagocytic potential of drug carriers by alveolar macrophages (Patel, Gupta and Ahsan, 2015)……..276

List of abbreviations

AUC	Area Under the Curve
BSC	Biopharmaceutical Classification System
^{13}C NMR	Carbon Nuclear Magnetic Resonance spectroscopy
DAPI	Diamidino-2-phenylindole
DMEM	Dulbecco's Modified Eagle's Medium
DL%	Drug Loading Percentage
DLS	Dynamic Light Scattering
DOTs	Directly Observed Treatment short-course
DSC	Differential Scanning Calorimetry
EE%	Encapsulation Efficiency Percentage
EPR	Enhanced Permeability and Retention effect
FBS	Fetal Bovine Serum
FDC	Fixed-Dose Combination
FITC	Fluorescein-5-isothiocyanate
FTIR	Fourier Transform Infrared spectroscopy
^{1}H NMR	Proton Nuclear Magnetic Resonance spectroscopy
HPLC	High Performance Liquid Chromatography
HR-SEM	High Resolution-Scanning Electron Microscope
ICH	International Conference on Harmonization
LOD	Limit of Detection

LOQ	Limit of Quantification
MDR-TB	Multidrug-resistant tuberculosis
MFI	Mean Fluorescence Intensity
mPEG	Methoxy Poly(ethylene Glycol)
MTB	Mycobacterium Tuberculosis
MTT	(3-(4,5-dimethylthiazol-2-yl)-2,5-diphenyl tetrazolium bromide)
MWCO	Molecular Weight Cut-off
NMR	Nuclear Magnetic Resonance spectroscopy
NOESY NMR	Nuclear Overhauser Effect spectroscopy
NP	Nanoparticle
PAMAM dendrimer	Poly(amidoamine) dendrimer
PBS	Phosphate Buffer Saline
PDI	Polydispersity Index
PENSTREP	Penicillin-Streptomycin mixture
PFA	Paraformaldehyde
PPI dendrimer	Poly(propyleneimine) dendrimer
RIF	Rifampicin
TB	Tuberculosis
TEA	Triethylamine
WHO	World Health Organization
XDR-TB	Extensively Drug-Resistant Tuberculosis

ZP	Zeta potential
3-FRSV	3-Formylrifamycin SV
4.0 G/G4 dendrimer	Fourth Generation dendrimer
4-ICPMP	4-Isothiocyanatophenyl α-D-mannopyranoside
4-NPC	4-Nitrophenyl Chloroformate

Chapter 1

Tuberculosis: Background and treatment challenges

1.1 Tuberculosis

1.1.1 Overview and epidemiology

Tuberculosis (TB) is an old enemy of the human race; it is a ubiquitous and highly transferable bacterial disease caused by *Mycobacterium tuberculosis* (MTB) (WHO, 2019). TB is considered a global public health concern, according to the World Health Organization (WHO) report in 2019, TB ranks as one of the highest 10 causes of death and the foremost reason of death from a single infectious pathogen superior to the human immunodeficiency virus (HIV/AIDS) (WHO, 2019). In 2018, there were approximately 1.2 million deaths from TB amongst HIV-negative patients and further 251,000 deaths amongst HIV-positive patients (WHO, 2019). The global incidence rate in 2018 was around 10 million cases of TB, Africa and the South-East Asia regions have recorded 24% and 44%, respectively. According to the WHO's list of top burden areas, 30 countries accounted for about 87% of the global TB cases, South Africa has 3% of the total cases (WHO, 2019). A WHO self-study estimated that for every second past there is a new case of TB infection occurring (WHO, 2004). Annually, billions of dollars have been expended by governments all over the world to eradicate TB, nevertheless, the disease stays out of control, infecting millions and killing millions of people.

A significant percentage of HIV patients are co-infected with TB, about 1/3 of the 36 million HIV patients are co-infected with TB (Colebunders and Lambert, 2002). The co-infection between HIV and TB is considered one of the socio-economic calamities since 30 % of the annual income of the infected people will be expended in direct and indirect costs (Sharma *et al*., 2005). Moreover, the highest rate of co-infection occurs between the ages of 25 - 44 (WHO, 2006), which signifies the main sector of the labor force for any country, therefore the impact on the economy is huge.

Several reasons contribute to the continual increasing of TB prevalence, such as traveling between countries especially those that acquire a high prevalence of the disease, deficiencies of basic hygienic facilities, migration of citizens from rural to urban slum sites, increasing the number of HIV patients, emergence of bacterial resistance towards TB antibiotics, and the increase in homelessness and drug addiction (Goldrick, 2004).

Based on the site of infection, TB as a disease is classified into two types: pulmonary TB and extra-pulmonary TB. In pulmonary TB the lung represents the main organ being affected by the MTB bacilli, while extra-pulmonary TB expression is usually used to describe TB infection in other organs except for the lung such as in the kidney, liver, spine, brain, etc. (WHO, 2019). Sometimes the extra-pulmonary TB may co-exist with pulmonary TB. Tuberculosis is also classified into progressive primary TB and progressive secondary TB based on the development manner of the disease. Progressive primary TB develops from first-time exposure to the MTB bacilli (primary infection) that replicates to invade lung tissues, typically only 5% – 10% of the primary infection will develop active TB disease (Geng *et al.,* 2005; Knechel, 2009). While progressive secondary TB develops either by reinfection with other pathogens (secondary infection) or by reactivation of old lesions after a period of dormancy (Geng *et al.*, 2005).

1.1.2 Causative organism

TB is an infectious disease caused by *Mycobacterium tuberculosis* (MTB), it was discovered in 1882 by the German scientist, Robert Koch (Porth, 2002). TB bacterium is obligate aerobic which grows well in oxygen-rich organs like the lung. It is an acid-fast bacillus, rod-shaped, non-encapsulated or spore-forming, and non-motile with a size range of 0.5 – 3.0 µm (Porth, 2002; Knechel, 2009). MTB bacilli are characterized by a distinctive cell wall, built of mycolic acid and fatty acids that are covalently conjugated to the underlying peptidoglycan-bound polysaccharide arabinogalactan (Knechel, 2009). The unique mycobacterium's cell wall is attributed to various properties including, its survival in hostile environments and many anti TB drug resistance behaviors (Lee *et al.,* 2005). The rigidity of the cell wall is mainly offered by the peptidoglycan components. While the lipoarabinomannan component that is located at the external part of the cell wall represents the bacterial antigen, is attributed to various immunogenic reactions, it also has an

important role in the survival of the bacilli inside the alveolar macrophages (Lee *et al.*, 2005; Joe *et al.*, 2007).

Cell multiplication of the MTB bacilli takes about 15 - 20 hrs, which is relatively slower than other bacteria. Another characteristic of MTB is its capability to survive within the macrophages in its dormant/latent state (without multiplication) for a long period, therefore multi-drug treatment and extended regimen durations are usually recommended (Pieters, 2008; Astaire-Dequeker *et al.*, 2010).

1.1.3 Transmission

TB bacilli can transfer from the infected patient during coughing, sneezing, talking, or even singing, through airborne droplets that can suspend in the air carrying the bacilli for many hours (Lee *et al.*, 2005). Many factors influence the transmission process including, the number of bacilli in the airborne droplets, the level of ventilation, and general conditions for aerosolization (American Thoracic Society, 2000). Once the TB bacilli inhaled by the person and diffused to the respiratory system, it can either infect lung tissues to develop pulmonary tuberculosis, or may relocate to other organs such as bone/joints, meninges, and the lymphatic system causing extra-pulmonary tuberculosis (Knechel, 2009).

1.1.4 Pathophysiology

After MTB is inhaled into the respiratory system, the majority of the bacilli will be confined by the first body defensive system, the mucociliary escalator, which is located in the upper part of the airways and comprises of ciliated and goblet cells (Knechel, 2009). The mucous is consistently released by the goblet cells to trap foreign particles and microorganisms, and the cilia are located on the surface of the ciliated cells with mucous containing foreign particles/microorganisms pointing outward for complete elimination (Frieden *et al.*, 2003).

The MTB bacilli that escape the mucociliary escalator and diffuse to the alveolar region will be confronted by the most copious immune cells, alveolar macrophage that represents the second body defense system (American Thoracic Society, 2000; Frieden *et al.*, 2003; Korf *et al.*, 2006). Alveolar macrophages are in a continuous fighting mode of various infectious pathogens even if they are invading the body for the first time (Ottenhoff, 2002).

The main ligand that mediates recognition and engulfment of MTB by the alveolar macrophage is the lipoarabinomannan on their cell wall (Ottenhoff, 2002). The process of recognition and engulfment of MTB is enhanced by another part of the immune system known as the complement system. This system mediates rapid opsonization of the MTB cell wall by protein C3 even for the first-time exposure (Ferguson, Weis, Martin, & Schlesinger, 2004; Li, Petrofsky, & Bermudez, 2002). Opsonization is the process by which bacteria are altered by opsonins so as to become more readily and more efficiently engulfed by phagocytes. The interaction between alveolar macrophages and MTB is expected to be mediated *via* pattern recognition receptors (PRR), through the cholesterol components of the bacteria (Kaufmann, 2001). The degree of PRR interactions has a significant impact on the destiny of MTB and their locking within the alveolar macrophages (Pieters, 2008).

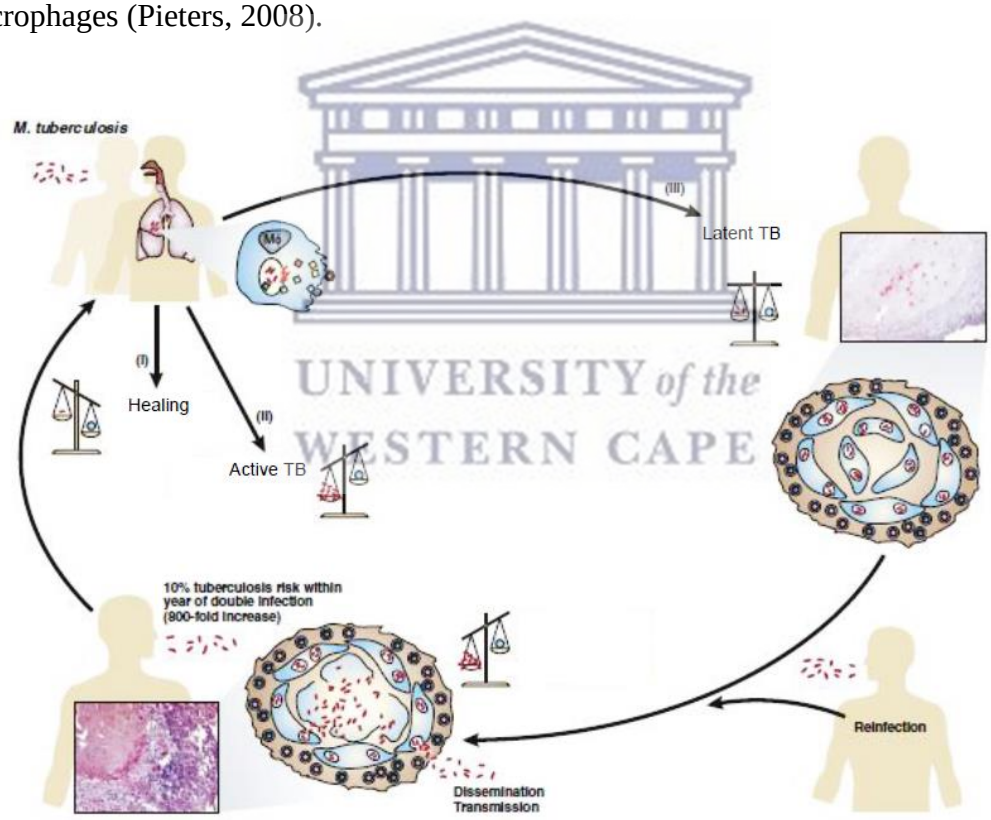

Figure 1.1 Illustration of TB pathophysiology and the consequences of the interaction between the MTB and the immune system [adapted from (Kaufmann and McMichael, 2005)].

Three scenarios (Figure 1.1) will pursue the interaction between the MTB and the macrophages, (i) total eradication of the invading pathogens (healing), or (ii) MTB may overcome the immune system to develop active infection (i.e., progressive primary tuberculosis), or (iii) the immune system may control the progression of the infection by engulfing the MTB within macrophages to develop dormant/latent tuberculosis (Frieden *et al.*, 2003). In latent TB, the bacilli can survive and replicate within the macrophages by generating a dynamic balance with the immune defense system for a long period (Ottenhoff, 2002; Guyot-Revol *et al.*, 2006).

The mechanism(s) by which MTB are capable to survive inside the macrophages are expected to be *via* (1) interference with the phagolysosomal fusion process, which is an important step for acidification of infected phagosomes, (2) inhibition of various interferon (IFN)-ϒ mediated signaling, which are usually induced by macrophages to kill intracellular pathogens (Flynn and Chan, 2003; Vandal, Nathan and Ehrt, 2009), and (3) a few types of MTB may undergo some phenotypic expression mutations (e.g. protein regulation) to adapt them to survive in the phagolysosomal environment (pH 4.5 - pH 5.0) (Li, Petrofsky and Bermudez, 2002; Vandal, Nathan and Ehrt, 2009).

The engulfed MTB bacilli can replicate at a slow rate inside the macrophages (Frieden *et al.*, 2003) with cell multiplication taking place every 25 - 32 hrs (American Thoracic Society, 2000; Porth *et al.*, 2002). Irrespective of the state of the disease whether it is active or dormant, macrophages mediate primary responses which include the release of cytokines and other enzymes trying to destroy the invading bacilli (Ottenhoff, 2002). These mediators invite cell-mediated immunity, T lymphocytes, to the site of infection. Then, the MTB antigens will appear on the surface of macrophages to attract T lymphocyte cells (Ottenhoff, 2002). The interaction between T lymphocytes and the MTB antigens activate them. After that, T lymphocytes release different cytokines and chemokines to stimulate macrophages, in addition, to entice other immune cells to the site of infection. These primary immune interactions take from 2 to 12 weeks; MTB bacilli continue to replicate till they achieve maximum stimulation of the cell-mediated immune reactions, which can be detected by a skin test (Ottenhoff, 2002; Frieden *et al.*, 2003).

People with intact immune functions are likely to convert the macrophage loaded with MTB (infected macrophages) into nodular-type lesions, known as granuloma, in an attempt to limit bacterial growth and progress (Figure 1.2) (Frieden *et al.*, 2003). Granuloma is a cluster structure comprised of infected macrophages in the middle and enclosed with various immune cells mainly T-lymphocytes and macrophages (Figure 1.2) (Rosenkrands *et al.*, 2002). Granulomas produce an extraordinary microenvironment to control the multiplication and progress of MTB bacilli. This unusual condition mediates the rupture of macrophages to generate solid necrosis at the center of the cluster. However, some MTB bacilli can survive by undergoing manipulation in their phenotypic expression (Li, Petrofsky and Bermudez, 2002). After 2 – 3 weeks, the necrotic lesions turn into low oxygen, low pH, and limited nutrients for further managing the bacilli growth which creates a soft cheese-like shape known as caseous necrosis (Dheda *et al.*, 2005; Knechel, 2009). Granulomas may undergo calcification and fibrosis of the cluster for further enclosing of the bacilli within the lesions (Figure 1.2) (Dheda *et al.*, 2005; Knechel, 2009).

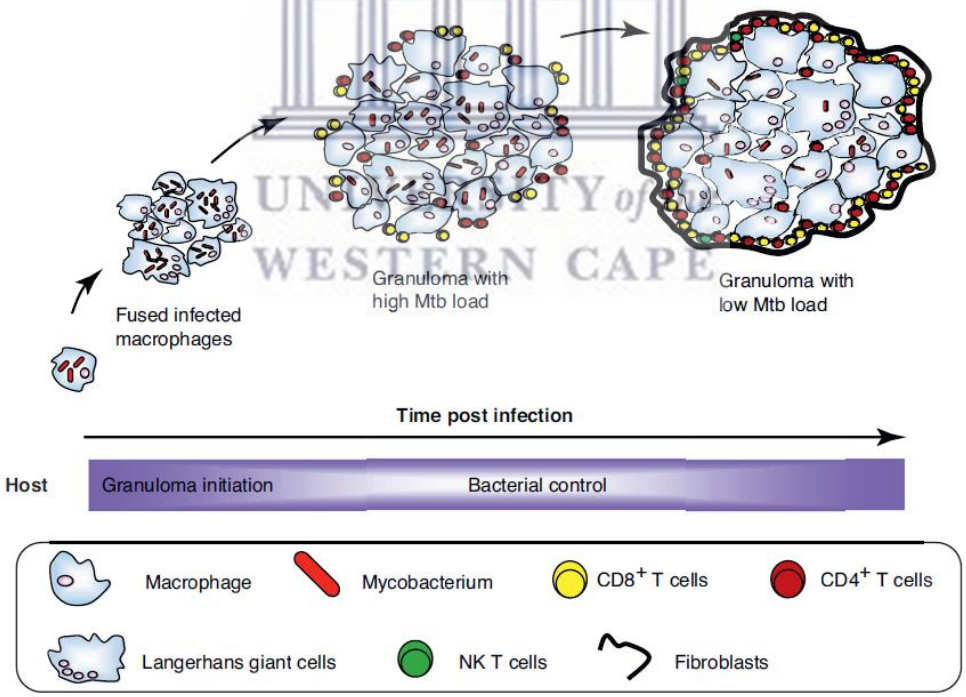

Figure 1.2 The maturation of TB granuloma [adapted from (Dube, Agrawal and Vyas, 2012)].

For the weakened immune system, the wall of the lesion loses its integrity and the bacilli can escape out of granulomas to infect other pulmonary tissues to develop active tuberculosis (Li, Petrofsky and Bermudez, 2002; Frieden *et al.*, 2003; Dheda *et al.*, 2005; Porth *et al*., 2002). The liberated bacilli can either drain to the lymphatic system to develop new granulomas or diffuse to adjacent blood vessels and distribute peripherally to progress extra-pulmonary tuberculosis (Dheda *et al.*, 2005) which at this stage MTB may reach the bronchus and be liable to transmit and infect another person (Dheda *et al.*, 2005).

1.1.5 Treatment

Despite the early discovery of the most anti-TB drugs (Figure 1.3), MTB resistance strains quickly emerged, for example, MTB has acquired resistance to streptomycin after three years of discovery (1943 – 1946) (Shehzad *et al.*, 2013). It was observed that the rate of resistance by MTB is almost similar for active and latent TB, therefore it is suggested that bacterial genetic mutation is taking place in a time-dependant mode rather than by a replication-dependent mode (Rittershaus, Baek and Sassetti, 2013).

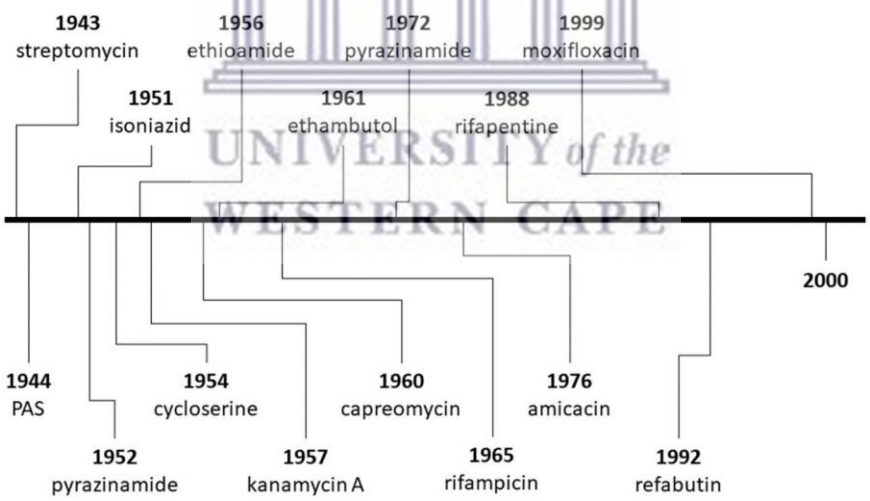

Figure 1.3 Time-line for the discovered anti-TB drugs (1940 – 2000) [adapted from (Al-Humadi, Al-Saigh and Al-Humadi, 2017)].

Unlike other bacteria types, resistance to anti-TB drugs is not occurring *via* horizontal gene transfer but it is expected to be mediated through independent chromosomal mutations and non-chromosomal mechanisms such as synthesis of drug inhibitor enzymes (Smith, Wolff and Nguyen, 2012; Louw and Sampson, 2017). Since the genes attributed to various drug

resistance are unlinked genes (Shehzad *et al.*, 2013), thus employing three drugs to treat TB is estimated to decrease the mutation frequency from $10^{-6} – 10^{-8}$ to a negligible chance, i.e. $10^{-18} – 10^{-20}$ (Slayden and Barry, 2000). Therefore, multi-drugs are always recommended throughout the treatment protocol of TB to try to negate the possibility of drug resistance.

The aim of TB treatment guidelines suggested by the WHO is to assist all national TB directors in settling policies to achieve cure without relapse or recurrence, diminish transmission, decrease drug resistance, and minimize global prevalence (WHO, 2010; Dube, Agrawal and Vyas, 2012). To attain that, long term regimens with multi-drugs are required. Various classes of drugs that are currently used in the management of TB are summarized in Table 1.1. In 1994, WHO launched a program called directly observed treatment, short-course (DOTs) to improve the adherence of TB patients to treatment under direct monitoring of trained healthcare workers (Raviglione and Pio, 2002).

The WHO recommendations for the treatment of TB are categorized into two panels, panel 1 includes recommendations for drug-sensitive tuberculosis (DOTs) (Dube, Agrawal and Vyas, 2012). Here the first-line anti-TB drugs (Table 1.1) are highly recommended to be used for 6 months in two phases. The intensive phase of two months comprise of isoniazid (H), rifampicin (R), pyrazinamide (Z), and ethambutol (E) (H + R + Z + E), followed by a continuous phase of 4 months of isoniazid and rifampicin (H + R) (WHO, 2010; Dube, Agrawal and Vyas, 2012). For patients with known or susceptible isoniazid resistance, a combination of H + R + E is usually suggested as a substitute for H + R for the continuous phase (WHO, 2010). In cases where relapse occurs after the first treatment regimen, patients are recommended to repeat the regimen using H + R + Z + E + streptomycin (S) for the first 2 months followed by H + R + Z + E for one month and lastly H + R + E for 5 months, if there is no previous multidrug resistance recorded (WHO, 2010).

There are two types of resistance to anti-TB drugs, multidrug resistance TB (MDR-TB) and extensive drug resistance TB (XDR-TB). MDR-TB is resistant to the most effective first-line anti-TB drugs isoniazid and rifampicin, while XDR-TB status when MTB strains are resistant to isoniazid or rifampicin, any fluoroquinolone drugs and at least one of the injectable second-line anti-TB drugs (Chan *et al.*, 2004; Caminero, 2006; Mitnick *et al.*,

2008).

Panel 2 encompasses recommendations for the treatment of multidrug-resistant TB adapted from WHO guidelines (WHO, 2010). This regimen comprises of at least 4 drugs in the intensive phase for not less than 6 months or for at least 4 months after the culture had become negative, and a total treatment duration period of 18 months (Caminero *et al.*, 2010). In panel 2, WHO recommends the use of DOTs-plus, which indicates using DOTs in addition to the second-line anti-TB drugs (Table 1.1) (Dube, Agrawal and Vyas, 2012). Generally, treatment of multidrug resistance is costly, it takes a long time, and is associated with numerous side-effects (Orenstein *et al.*, 2009; Caminero *et al.*, 2010). The success of the treatment is approximately 2/3 of patients (Orenstein *et al.*, 2009). Further treatment recommendation is available *via* the Treatment of tuberculosis guidelines (*4Th Edition)* issued by WHO (WHO, 2010).

Rifampicin and isoniazid are the most essential drugs in the treatment regimen of TB, they have good clinical outcomes when used within recommended concentrations (Peloquin, 2002). Isoniazid causes the highest decrease in the number of colony-forming units of MTB bacilli within 2 days of treatment (Mitchison, 2000). Rifampicin molecules show a rapid onset when interacting with MTB bacilli and are capable of destroying the bacilli under different conditions (Mitchison, 2000).

Table 1.1 Current anti-TB drugs and their mechanism of action [adapted from (Dube, Agrawal and Vyas, 2012)].

Drug	Mechanism of action
	First-line therapeutic drugs
Rifampicin	Inhibits bacterial RNA synthesis by inhibiting bacterial DNA-dependent RNA-polymerase.
Isoniazid	A pro-drug that inhibits the synthesis of MTB cell wall by inhibiting the formation of mycolic acids.
Pyrazinamide	A pro-drug that inhibit MTB growth. After activation it is estimated to prevent fatty acids formation by inhibiting fatty acid synthase enzyme, also it is believed to inhibit trans-translation which is an important cellular process for treating damaged proteins and non-functioning ribosomes in MTB.
Ethambutol	Inhibits MTB cell wall synthesis by inhibiting arabinosyl transferases, an essential enzyme that mediates polymerization of D-arabinofuranose to arabinoglycan, which represents one of the main constituents of the cell wall.
Aminoglycosides	Inhibits protein synthesis of the bacteria through binding to the 30S ribosomal subunit that leads to misinterpretation of the genetic code.
	Second-line therapeutic drugs
P-aminosalicylic acid	Inhibits folic acid synthesis, also interferes with the cell wall synthesis by inhibiting the synthesis of their components, mycobactin.

Cycloserine	Interfere with the bacterial cell wall synthesis, since cycloserine is considered an analogue of D-alanine, it disrupts their incorporation of D-alanine into peptidoglycan during the cell wall synthesis process.
Other therapeutic drugs	
Clofazimine	Not clearly understood, the proposed mechanism involves binding to some DNA bases of the MTB, which lead to inhibit their growth.
Amoxicillin and/or clavulanic acid	Amoxicillin inhibits bacterial cell wall synthesis, and Clavulanic acid is a b-lactamase enzyme inhibitor.
Clarithromycin	Inhibits protein synthesis through binding to the 50S subunit of the bacterial ribosomal RNA, which blocks the translation of peptides.
Rifabutin	Similar to rifampicin, it inhibits bacterial RNA synthesis by inhibiting bacterial DNA-dependent RNA-polymerase
Thiacetazone	Not clearly understood.

1.2 Challenges for the current anti-TB drugs

Most of the anti-TB therapeutic drugs have been discovered in the last century (Figure 1.3), where drug development and regulation policies were considerably different from today (Laurenzi, Ginsberg and Spigelman, 2007; WHO, 2007). With new drug discoveries taking a very long time to reach the market with the extensive cost involved, not to mention the increase of resistance to anti-TB drugs, a significant decrease of interest to develop new chemical entities by pharmaceutical industries is observed (Laurenzi, Ginsberg and Spigelman, 2007; WHO, 2007). The main factors that are considered as challenges for the current anti-TB drugs are treatment regimen, co-infection and drug-drug interaction, route of administration, and drug properties (Figure 1.4).

1.2.1 Treatment regimen

As discussed earlier, the necessity for the use of multi-drugs for a long duration will ensure the success of the treatment and minimize the possibility of resistance. The complex regimen is the first obstacle associated with current anti-TB drugs since it has a negative impact on the patient's adherence to the treatment protocol (Laurenzi, Ginsberg and Spigelman, 2007). Although, the intervention of the DOTs program by the WHO has been considered as one of the best tools that have enhanced the success of TB treatment (Raviglione and Pio, 2002), however the degree of application varies as it is somewhat challenging for patients and health care providers (Laurenzi, Ginsberg and Spigelman, 2007). TB regimen elements such as the period of the treatment, the number of drugs and doses, besides drug dosage forms and their quality determine the suitability of treatment (Laurenzi, Ginsberg and Spigelman, 2007). The inappropriate treatment may play an important role in treatment failure and the appearance of resistant TB, i.e., MDR and XDR.

1.2.2 Co-infection and drug-drug interaction

Another obstacle associated with TB treatment is the high rate of co-infection with TB and HIV/AIDS. TB and AIDS are considered comorbid diseases (Laurenzi, Ginsberg and Spigelman, 2007). Around 12 million patients are co-infected with TB and AIDS (WHO, 2003), and about 50% of HIV-positive patients are estimated to develop TB (Corbett *et al.*, 2003). Annually, TB causes the death of 15% of AIDS patients (WHO, 2003). In addition,

the possibility of latent TB to turn into active TB is estimated to be fifty times greater for HIV-positive patients compared to HIV-negative patients (De Cock *et al.*, 1992; Markowitz *et al.*, 1997). One of the main difficulties to manage patients co-infected with TB and AIDS is the interactions of the anti-TB drug (e.g rifampicin) and antiretroviral drugs (i.e., protease inhibitors (PIs), non-nucleoside reverse transcriptase inhibitors (NNRTIs)) with cytochrome P450 3A4 (Laurenzi, Ginsberg and Spigelman, 2007). Accordingly, concomitant treatment with rifampicin and PIs or NNRTIs is not recommended, especially when a lower level of the monitoring program is used, since drug-drug interactions could fortify the total therapeutic toxicity (Michalets, 1998; Burman and Jones, 2001; Dean *et al.*, 2002). Also, it is observed that co-treatment using anti-TB drug isoniazid and the antiretroviral drugs could enhance the toxicity since both of them have reported causing peripheral neuropathy.

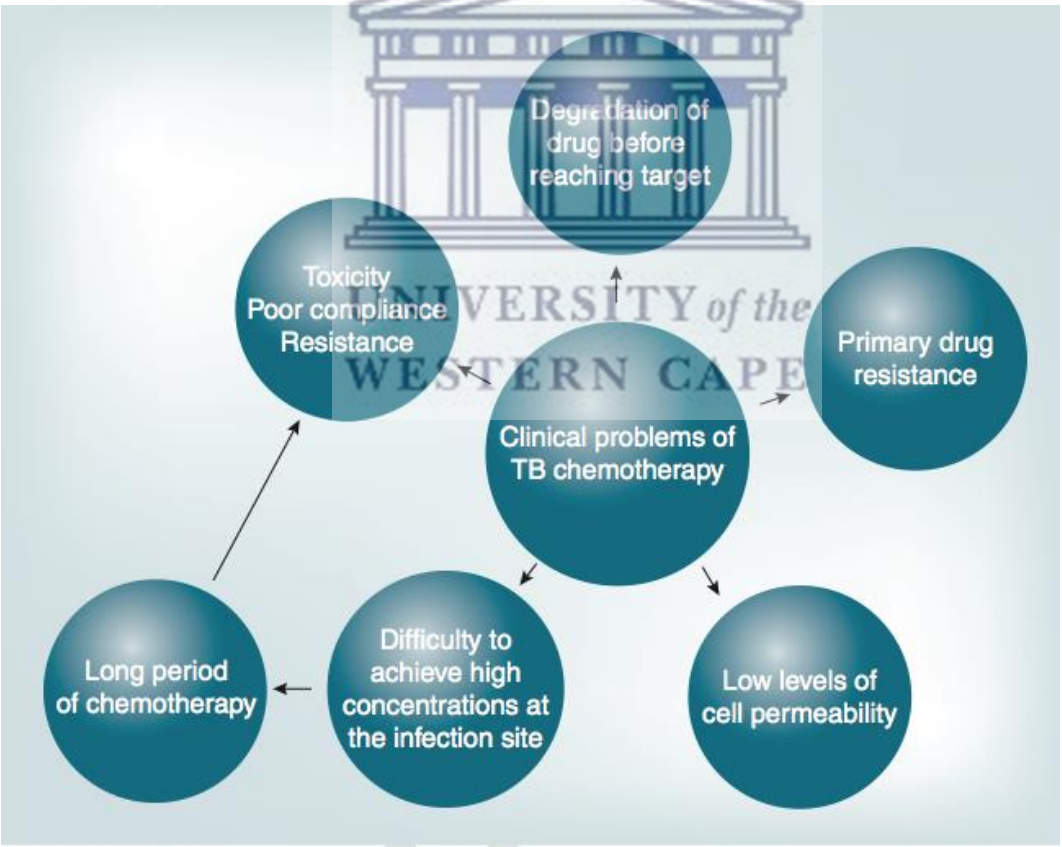

Figure 1.4 Clinical problems associated with the current TB therapeutic drugs [adapted from (Pinheiro *et al.*, 2011)].

1.2.3 Route of administration and drug properties

The current anti-TB drugs are usually administered *via* the oral or parenteral routes. The oral route is a simple, convenient, safe, and low-cost route of drug administration. It experiences some drawbacks such as the slow onset of action, reduced drug concentration due to the first-pass effect, lower bioavailability due to physiological and physicochemical factors, and drug interaction problems (Turner *et al.*, 2011). Although the parenteral route is characterized by better bioavailability profiles, bypasses the hepatic first-pass metabolism, and the possibility to precisely control drug concentration delivered to different body sites can be achieved (Clark *et al.*, 2012), it is also a painful route and requisite trained health care personnel. Both routes may perhaps deliver sub-therapeutic doses to the lung, as in the case of TB, due to poor pulmonary distribution for the majority of systemically administered TB drugs (Conte *et al.*, 2002). Therefore, treatment failure and resistance will possibly emerge rapidly (Conte *et al.*, 2002). The anti-TB drugs that succeed to reach the lung tissues with an effective therapeutic level may face difficulties to diffuse into the macrophages and granulomas that contained the MTB bacilli.

Since the TB treatment is used for a prolonged duration, monitoring of anti-TB drugs that have a narrow therapeutic window should be implemented, as it may affect patient's compliance and adherence to treatment protocol (Conte *et al.*, 2002).

Another important complication associated with treatment failure is the degradation of therapeutic drugs before reaching the site of action. Many literature reports revealed that concomitant administration of the first-line anti-TB drugs, i.e. rifampicin, isoniazid, ethambutol, and pyrazinamide, in fixed-dose combination (FDC) was attributed with various chemical and physical instability events (Bhutani, Singh and Jindal, 2005). This obstacle mediates drug degradations and decreases the therapeutic level, hence treatment failure may be expected. The degradation process is highly observed between rifampicin and isoniazid especially in the acid environment (such as in the stomach) (Singh *et al.*, 2000).

1.3 Towards a better treatment

The challenges for the current anti-TB drugs suggest the necessity to develop novel therapeutics/modalities that is potent, have lower dosing frequency, minimal drug-drug interactions, and can be used to shorten time regimens to treat TB (Figure 1.5) (Laurenzi, Ginsberg and Spigelman, 2007; Shehzad *et al.*, 2013).

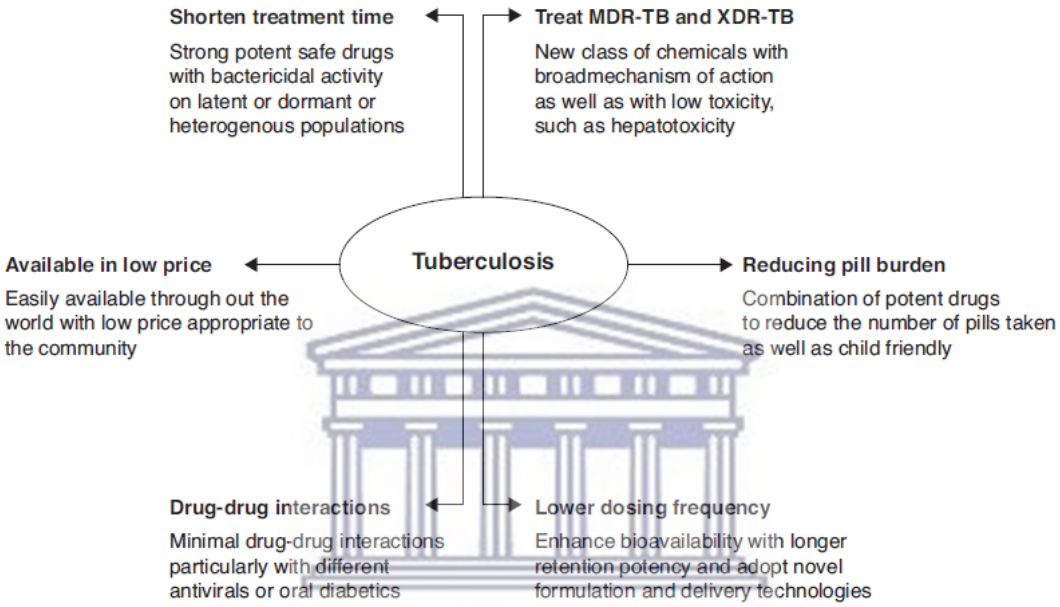

Figure 1.5 Illustration for the required properties of the novel anti-TB drugs/modalities [adapted from (Shehzad *et al.*, 2013)].

Different academic institutes, governmental research sectors, numerous organizations, private and public corporations, are in continuous work to develop novel anti-TB drugs/modalities to attain unique characteristics, including (Laurenzi, Ginsberg and Spigelman, 2007; Shehzad *et al.*, 2013):

a) Shorten time TB regimens to enhance patient compliance and adherence to the protocols, this will facilitate the success of TB treatment, minimize the burden on the health care providers, and decrease the probability of resistant TB.

b) Developing potent therapeutic drugs that are capable to treat MDR-TB and XDR-TB *via* unique mechanisms; the suggested drugs should be safe and tolerable.

c) The absence of drug-drug interactions particularly with antiretroviral drugs when co-infection between TB and AIDS exists, this can be attained by developing drug molecules that are not inducers or inhibitors to cytochrome P450.

d) Novel drugs/modalities that are safe and effective against latent TB, also capable to diffuse into granulomas and alveolar macrophages within which the MTB bacilli resides.

e) Minimal dosing frequency as well as low drug concentration by using a variety of drug delivery technologies.

f) Safe effective drugs that are child-friendly and elderly-friendly.

One of the effective approaches for disease prevention is by using vaccines. Unfortunately, the only existing TB vaccine, i.e. Bacillus Calmette-Guerin (BCG), against MTB bacilli suffers from very limited efficacy towards inhibiting pulmonary TB (Khademi *et al.*, 2018). Moreover, there has been a lack of newly discovered drugs to treat TB for decades (Shehzad *et al.*, 2013). Consequently, developing safe and effective vaccines together with novel treatment modalities is a promising tactic for the efficient control of the TB disease. One of the suggested treatment modalities is the use of nanotechnology-based drug delivery systems and the pulmonary route of administration to overcome some of the difficulties associated with current therapeutics.

1.3.1 Nanotechnology-based drug delivery system for treatment of tuberculosis

Nanotechnology represents the future platform for the pharmaceutical and biotechnology industries, as the pipelines for most of them are diminishing besides many patent drugs are near the end of patency (Farokhzad and Langer, 2009; da Silva *et al.*, 2016). So, the implementation of nanotechnology in drug delivery will create an additional field of competition (Farokhzad and Langer, 2009; da Silva *et al.*, 2016). Nanotechnology is paving the road for pharmaceutical industries from two perspectives, either through participation in the synthesis of new molecule entities (NMEs) that did not exist before or by improving the pharmacokinetic profiles of the available molecules (Farokhzad and Langer, 2009). Many advantages can be acquired from the application of nanotechnology in drug delivery,

including enhancing the delivery of poorly water-soluble drugs, precise site targeting of the drugs by using different routes of administration or targeting ligands, enhance drug permeability across various biological membranes, decrease the therapeutic toxicity, improve drug stability, and controlled or prolonged drug release (Farokhzad and Langer, 2009; da Silva *et al.*, 2016). For example, some of the first-line anti-TB drugs suffer from lower water solubility, poor permeability, and rapid disappearance from the plasma (half-life only 1 - 4 hrs) due to high liver metabolism (da Silva *et al.*, 2016). Using nanotechnology-based drug delivery systems to anti-TB drugs have enhanced their stability, release behavior, pharmacokinetic parameters, reduced the frequency, reduced drug concentrations, and offered the possibility to use various route of administrations (Kumar *et al.*, 2011; da Silva *et al.*, 2016).

The lipid vesicle was the first nanotechnology-based drug delivery system that appeared, it was developed in 1960, later known as liposomes (Bangham, Standish and Watkins, 1965; Farokhzad and Langer, 2009). Then, different types of organic and inorganic systems were developed (Farokhzad and Langer, 2009). A variety of nanotechnology-based drug delivery systems have been utilized to improve the properties of the anti-TB drugs, such as polymeric nanoparticles (Anisimova *et al.*, 2000; Pandey *et al.*, 2003), solid lipid nanoparticles (Pandey and G.K. Khuller, 2005; Chuan *et al.*, 2013; Singh, Bhandari and Kaur, 2013), dendrimers (Kumar *et al.*, 2006; Rajabnezhad *et al.*, 2016; Dineshkumar *et al.*, 2017), liposomes (Agarwal *et al.*, 1994; Deol and Khuller, 1997; Adams *et al.*, 1999), nano-micelles (Silva *et al.*, 2006; Jiang *et al.*, 2007; Jeetah, Bhaw-Luximon and Jhurry, 2013), nano-emulsions (Ahmed *et al.*, 2008), cyclodextrins (Rao, Suresh and Narendra, 2006), and gold and silver nanoparticles (Lu and Zu, 2013; Praba *et al.*, 2013).

1.3.2 The pulmonary administration route

1.3.2.1 The rationale for pulmonary delivery in tuberculosis

The lung is the main organ that is exposed to the TB infection, where the MTB bacilli utilize the lung tissues to proliferate and progress into active pulmonary TB, or it may relocate to invade other organs to develop extra-pulmonary TB (Misra *et al.*, 2011; Sethi and Agrawal, 2011). Using the pulmonary route for drug delivery of anti-TB drugs is

considered an interesting assumption to treat TB (Muttil, Wang and Hickey, 2009; Amani *et al.*, 2011; Hokey and Misra, 2011). Various characteristics of the pulmonary route to deliver anti-TB drugs have been reported in literature which include: (1) direct delivery to the lung could improve the drug absorption as a result of a large surface area and thin alveolar epithelium membrane of the lung (Patton and Platz, 1992; Misra *et al.*, 2011), (2) lower drug concentration and dosing frequency are required to achieve the therapeutic effects compared to the oral route (Willis, Hayes and Mansour, 2012), this will help to decrease therapeutic side effects, (3) it is a non-invasive route and can be self-administered in comparison to the parenteral route (Mehanna, Mohyeldin and Elgindy, 2014), (4) availability of high drug concentration at the pulmonary tissues may assist to reduce the regimen duration (Misra *et al.*, 2011), (5) one of the suggested routes to treat extra-pulmonary TB due to high vascularization and the large surface area of the lung, which will enhance drug bioavailability (Pandey and Khuller, 2005; Das, Tucker and Stewart, 2015), (6) the possibility of drug targeting to the alveolar macrophage *via* different techniques, which will result in enhancing therapeutic outcomes and minimal systemic toxicity (Misra *et al.*, 2011) and finally, (7) overcoming drug instability issues in the GIT, beside waiving hepatic first-pass metabolism and other metabolizing enzymes in the GIT resulting in improved drug bioavailability (Misra *et al.*, 2011; Lee *et al.*, 2015).

1.3.2.2 Lung deposition and targeting

The biological barriers are not the only challenge for the disposition of inhaled therapeutic particles, but also the physicochemical properties of particles, such as size, shape, charge, density and aerodynamic size distribution (Ferron, 1994; Ferron *et al.*, 2013; Mehanna, Mohyeldin and Elgindy, 2014).

Particle size is the most vital parameter that determines where the inhaled particles will be deposited (Sung, Pulliam and Edwards, 2007). Particles with size > 5 µm, inertial impaction mechanism will mediate their disposition in the mouth and the upper airways. Particles with a size of 1 - 5 µm are expected to achieve deep lung disposition through inertial impaction and sedimentation mechanisms (Mitchison and Fourie, 2010; Shegokar, Shaal and Mitri, 2011). Particles with size < 1 µm, diffusion and sedimentation mechanisms are expected to mediate the disposition at the pulmonary alveoli region.

Besides pulmonary disposition, particle size plays an important role for passive targeting of the alveolar macrophages that accommodate the MTB bacilli, particles having a diameter size of 100 - 200 nm or 1-5 µm have superior macrophages uptake (Patel, Gupta and Ahsan, 2015). The inhaled particles can be optimized to induce active targeting of the macrophages through surface modification using sugar residues such as mannose (Nimje *et al.*, 2009) and lactose (Jain *et al.*, 2010). Targeting the mannose receptors is the most frequently used technique to enhance macrophage internalization since these receptors are highly expressed in alveolar macrophages (Nimje *et al.*, 2009; Jain *et al.*, 2010; Patel, Gupta and Ahsan, 2015). Other targeting ligands include maleylated bovine serum albumin (MBSA), O-steroyl amylopectin (O-SAP), tuftsin and anionic lipid such as dicetylphosphate (DCP) (Pinheiro *et al.*, 2011; Patel, Gupta and Ahsan, 2015).

1.4 Rationale of the study

The current drugs that are used to treat TB disease experience various challenges, which can be summarized in treatment regimen factors, drug-drug interaction, route of administration, and drug properties. These hurdles have a major role in treatment failure and the emergence of resistant TB. Moreover, due to the lack of newly discovered drugs for TB treatment over the past decades (Shehzad *et al.*, 2013), and the absence of more effective TB vaccines (Khademi *et al.*, 2018), many researchers have suggested the use of novel modalities for the current anti-TB drugs to enhance their efficiency and overcome some drawbacks, one of these modalities is the nanotechnology-based drug delivery systems (Kumar *et al.*, 2011; da Silva *et al.*, 2016).

The most commonly reported nanocarriers for anti-TB drugs are liposomes and polymeric systems. Even though these systems have improved the properties of anti-TB drugs, they have limited applications due to some drawbacks. The liposome system suffers from physical and chemical instability, while the polymeric system, especially the linear polymers are characterized by polydisperse molecules that may exert different pharmacokinetic profiles (Langer, 1998). Dendrimers are synthetic, globular shaped, three-dimensional, hyperbranched, monodispersed, and well-ordered polymeric compounds. PAMAM dendrimers have precise constitutional and compositional properties such as size (less than 100 nm), shape, and molecular weight. They can encapsulate drug molecules at

high loading capacity due to high internal voids besides the dense peripheral functional groups. The surface groups can further be manipulated to improve the dendrimer properties (such as improving the targeting potential) and enhance the drug/guest molecule's attachment. Due to structural conformational changes at different pH environments, PAMAM dendrimers are proposed as a promising carrier to deliver anti-TB drugs inside the alveolar macrophages. Studying the effect of surface functionalization of G4 PAMAM dendrimer on improving the physicochemical properties, cytotoxicity, and cellular internalization of anti-TB drug rifampicin has not been fully understood.

In this study, a novel nanotechnology-based drug delivery system for the anti-TB drug rifampicin was developed using fourth-generation (G4) PAMAM dendrimer nanoparticles having an increased concentration of poly(ethylene glycol) densities or mannose residues, in order to overcome some of the shortcomings of rifampicin and improve its efficacy.

1.5 Aims and objectives of the study

This study aims to develop a novel pulmonary delivery system for the anti-TB drug rifampicin using surface-modified G4 PAMAM dendrimer nanoparticles (PEG and mannose molecules) to improve drug solubility, prolong drug release, enhance drug permeability into the macrophages, and decrease the toxicity of the drug-dendrimer conjugates.

The objectives of the study were:

i. To manipulate the surface of G4 PAMAM dendrimer with various PEG densities.

ii. To manipulate the surface of G4 PAMAM dendrimer with various mannose residues.

iii. To encapsulate rifampicin on PEGylated and non-PEGylated dendrimer formulations.

iv. To encapsulate rifampicin on mannosylated dendrimer formulations.

v. To characterize rifampicin conjugated on surface-modified dendrimer nanoparticles.

vi. To assess the release manner of rifampicin from different dendrimer formulations at pH 7.4 and pH 4.5.

vii. To evaluate the cytotoxicity of rifampicin, G4 PAMAM dendrimer, unloaded and loaded surface-modified G4 PAMAM dendrimer nanoparticles.

viii. To compare the permeability of dendrimer formulations into the alveolar macrophages.

1.6 Null hypothesis

i. PEG chains and mannose residues do not have any impact on the encapsulation efficiency or the loading capacity of the dendrimer nanoparticles.

ii. The release manner of rifampicin from the native dendrimer is not significantly different from surface-modified dendrimers.

iii. There is no significant difference in the cytotoxicity effect or macrophage uptake between the native and surface-modified dendrimers.

1.7 Thesis outline

This thesis is divided into seven chapters and is designed as follows:

Chapter 1: This chapter is an introduction presenting a brief overview of the literature regarding TB epidemiology and pathophysiology. Furthermore, it provides a brief review of the challenges for the current anti-TB drugs and the suggested modalities towards better treatment. The rationale and objective for conducting this thesis are outlined and finally, the framework of the thesis design is provided.

Chapter 2: This chapter provides an overview of the characteristics and features of dendrimers. It reviews the benefits of employing dendrimers, and particularly PAMAM dendrimers, in the drug delivery field.

Chapter 3: This chapter aims to synthesize and characterize rifampicin loaded in the native and PEGylated dendrimers. Various analytical techniques were used to characterize the nanoparticles such as FTIR, NMR, SEM, DSC, HPLC, and Zetasizer. It also provides a

review of the literature on the use of PEG polymers and their advantages when conjugating dendrimer nanoparticles.

Chapter 4: This chapter aims to synthesize and characterize rifampicin loaded in mannosylated dendrimers. Various analytical techniques were used to characterize the nanoparticles such as FTIR, NMR, SEM, DSC, HPLC, and Zetasizer. It also provides an outline on the importance of functionalizing dendrimer nanocarriers with carbohydrate moieties for site-specific targeting.

Chapter 5: This chapter evaluates the release behaviour of rifampicin from the native and surface-modified dendrimer at pH 7.4 and pH 4.5. In addition, it describes the mechanism of drug release from the nanoparticles by determining the best mathematical model using DDSolver software.

Chapter 6: This chapter aims to study the cytotoxicity of the native and surface-modified dendrimers by evaluating its effect on the growth rate of raw 264.7 cells. Furthermore, this chapter assesses the internalization of the dendrimer nanoparticles into the raw cells.

Chapter 7: This chapter summarizes the findings of this thesis, shows the recommendations and provides the prospective studies that can be generated from this thesis.

1.8 References

Adams, L.B., Sinha, I., Franzblau, S.G., Krahenbuhl, J.L. and Mehta, R.T., (1999). Effective treatment of acute and chronic murine tuberculosis with liposome-encapsulated clofazimine. *Antimicrobial agents and chemotherapy*, 43(7), pp.1638-1643.

Agarwal, A.N.S.H.U., Kandpal, H.E.M.A., Gupta, H.P., Singh, N.B. and Gupta, C.M., (1994). Tuftsin-bearing liposomes as rifampin vehicles in treatment of tuberculosis in mice. *Antimicrobial agents and chemotherapy*, *38*(3), pp.588-593.

Ahmed, M., Ramadan, W., Rambhu, D. and Shakeel, F., (2008). Potential of nanoemulsions for intravenous delivery of rifampicin. *Die Pharmazie-An International Journal of Pharmaceutical Sciences*, *63*(11), pp.806-811.

Al-Humadi, H.W., Al-Saigh, R.J. and Al-Humadi, A.W., (2017). Addressing the Challenges of Tuberculosis: A brief historical account. *Frontiers in pharmacology*, *8*, p.689.

Amani, A., Amini, M.A., Ali, H.S. and York, P., (2011). Alternatives to conventional suspensions for pulmonary drug delivery by nebulisers: a review. *Journal of pharmaceutical sciences*, *100*(11), pp.4563-4570.

American Thoracic Society (2000). Diagnostic standards and classification of tuberculosis in adults and children. *Am J Respir Crit Care Med*, 161, pp. 1376–1395.

Anisimova, Y.V., Gelperina, S.I., Peloquin, C.A. and Heifets, L.B., (2000). Nanoparticles as antituberculosis drugs carriers: effect on activity against Mycobacterium tuberculosis in human monocyte-derived macrophages. *Journal of Nanoparticle Research*, 2(2), pp.165-171.

Astarie-Dequeker, C., Nigou, J., Passemar, C. and Guilhot, C., (2010). The role of mycobacterial lipids in host pathogenesis. *Drug Discovery Today: Disease Mechanisms*, *7*(1), pp.e33-e41.

Bangham, A. D., Standish, M. M. and Watkins, J. C. (1965) 'Diffusion of univalent ions across the lamellae of swollen phospholipids', *Journal of Molecular Biology*. Academic Press, 13(1), pp. IN26–IN27. doi: 10.1016/S0022-2836(65)80093-6.

Bhutani, H., Singh, S. and Jindal, K.C., (2005). Drug-drug interaction studies on first-line anti-tuberculosis drugs. *Pharmaceutical development and technology*, *10*(4), pp.517-524.

Burman, W.J. and Jones, B.E., (2001). Treatment of HIV-related tuberculosis in the era of effective antiretroviral therapy. *American journal of respiratory and critical care medicine*, *164*(1), pp.7-12.

Caminero, J.A., (2006). Treatment of multidrug-resistant tuberculosis: evidence and controversies. *The International Journal of Tuberculosis and Lung Disease*, *10*(8), pp.829-837.

Caminero, J.A., Sotgiu, G., Zumla, A. and Migliori, G.B., (2010). Best drug treatment for multidrug-resistant and extensively drug-resistant tuberculosis. *The Lancet infectious diseases*, *10*(9), pp.621-629.

Chan, E.D., Laurel, V., Strand, M.J., Chan, J.F., Huynh, M.L.N., Goble, M. and Iseman, M.D., (2004). Treatment and outcome analysis of 205 patients with multidrug-resistant tuberculosis. *American journal of respiratory and critical care medicine*, *169*(10), pp.1103-1109.

Chuan, J., Li, Y., Yang, L., Sun, X., Zhang, Q., Gong, T. and Zhang, Z., (2013). Enhanced

rifampicin delivery to alveolar macrophages by solid lipid nanoparticles. *Journal of nanoparticle research*, *15*(5), p.1634.

Clark, M.A., Finkel, R.S., Rey, J.A. and Whalen, K. eds., (2012). *Lippincott's illustrated reviews: pharmacology* (Vol. 526, pp. 530-541). Wolters Kluwer Health/Lippincott Williams & Wilkins.

Colebunders, R. and Lambert, M.L., (2002). Management of co-infection with HIV and TB: improving tuberculosis control programmes and access to highly active antiretroviral treatment is crucial, *British Medical Journal*, 324(7341), pp. 802–803.

Conte, J.E., Golden, J.A., McQuitty, M., Kipps, J., Duncan, S., McKenna, E. and Zurlinden, E., (2002). Effects of gender, AIDS, and acetylator status on intrapulmonary concentrations of isoniazid. *Antimicrobial agents and chemotherapy*, *46*(8), pp.2358-2364.

Corbett, E.L., Watt, C.J., Walker, N., Maher, D., Williams, B.G., Raviglione, M.C. and Dye, C., (2003). The growing burden of tuberculosis: global trends and interactions with the HIV epidemic. *Archives of internal medicine*, *163*(9), pp.1009-1021.

da Silva, P.B., de Freitas, E.S., Bernegossi, J., Gonçalez, M.L., Sato, M.R., Leite, C.Q.F., Pavan, F.R. and Chorilli, M., (2016). Nanotechnology-based drug delivery systems for treatment of tuberculosis—A review. *Journal of biomedical nanotechnology*, *12*(2), pp.241-260.

De Cock, K.M., Soro, B., Coulibaly, I.M. and Lucas, S.B., (1992). Tuberculosis and HIV infection in sub-Saharan Africa. *Jama*, *268*(12), pp.1581-1587.

Das, S., Tucker, I. and Stewart, P., (2015). Inhaled dry powder formulations for treating tuberculosis. *Current drug delivery*, *12*(1), pp.26-39.

Dean, G.L., Edwards, S.G., Ives, N.J., Matthews, G., Fox, E.F., Navaratne, L., Fisher, M., Taylor, G.P., Miller, R., Taylor, C.B. and de Ruiter, A., (2002). Treatment of tuberculosis in HIV-infected persons in the era of highly active antiretroviral therapy. *Aids*, *16*(1), pp.75-83.

Deol, P. and Khuller, G.K., (1997). Lung specific stealth liposomes: stability, biodistribution and toxicity of liposomal antitubercular drugs in mice. *Biochimica et Biophysica Acta (BBA)-General Subjects*, *1334*(2-3), pp.161-172.

Dheda, K., Booth, H., Huggett, J.F., Johnson, M.A., Zumla, A. and Rook, G.A., (2005). Lung remodeling in pulmonary tuberculosis. *The Journal of infectious diseases*, *192*(7), pp.1201-1210.

Dineshkumar, P., Panneerselvam, T., Deepti Brundavani, K., Selvaraj, K. and Vijayaraj Kumar, P., (2017). Formulation of Rifampicin Loaded PEGylated 5.0 G EDA-PAMAM Dendrimers as Effective Long-Duration Release Drug Carriers. *Current Drug Therapy*, *12*(2), pp.115-126.

Dube, D., Agrawal, G.P. and Vyas, S.P., (2012). Tuberculosis: from molecular pathogenesis to effective drug carrier design. *Drug discovery today*, *17*(13-14), pp.760-773.

Farokhzad, O.C. and Langer, R., (2009). Impact of nanotechnology on drug delivery. *ACS nano*, *3*(1), pp.16-20.

Ferguson, J.S., Weis, J.J., Martin, J.L. and Schlesinger, L.S., (2004). Complement protein C3 binding to Mycobacterium tuberculosis is initiated by the classical pathway in human bronchoalveolar lavage fluid. *Infection and immunity*, *72*(5), pp.2564-2573.

Ferron, G.A., (1994). Aerosol properties and lung deposition. *European Respiratory Journal*, *7*(8),

pp.1392-1394.

Ferron, G.A., Upadhyay, S., Zimmermann, R. and Karg, E., (2013). Model of the deposition of aerosol particles in the respiratory tract of the rat. II. Hygroscopic particle deposition. *Journal of aerosol medicine and pulmonary drug delivery*, *26*(2), pp.101-119.

Flynn, J.L. and Chan, J., (2003). Immune evasion by Mycobacterium tuberculosis: living with the enemy. *Current opinion in immunology*, *15*(4), pp.450-455.

Frieden, T. R., Sterling, T. R., Munsiff, S. S., Watt, C. J., Dye, C., (2003) 'Tuberculosis', in *Lancet*, 362(9387) pp. 887–899. doi: 10.1016/S0140-6736(03)14333-4.

Geng, E., Kreiswirth, B., Burzynski, J. and Schluger, N.W., (2005). Clinical and radiographic correlates of primary and reactivation tuberculosis: a molecular epidemiology study. *Jama*, *293*(22), pp.2740-2745.

Goldrick, B.A., (2004). Once Dismissed, Still Rampant: Tuberculosis, the second deadliest infectious disease worldwide. *AJN The American Journal of Nursing*, *104*(9), pp.68-70.

Guyot-Revol, V., Innes, J.A., Hackforth, S., Hinks, T. and Lalvani, A., (2006). Regulatory T cells are expanded in blood and disease sites in patients with tuberculosis. *American journal of respiratory and critical care medicine*, *173*(7), pp.803-810.

Hokey, D.A. and Misra, A., (2011). Aerosol vaccines for tuberculosis: a fine line between protection and pathology. *Tuberculosis*, *91*(1), pp.82-85.

Jain, S.K., Gupta, Y., Ramalingam, L., Jain, A., Jain, A., Khare, P. and Bhargava, D., (2010). Lactose-conjugated PLGA nanoparticles for enhanced delivery of rifampicin to the lung for effective treatment of pulmonary tuberculosis. *PDA journal of pharmaceutical science and technology*, *64*(3), pp.278-287.

Jeetah, R., Bhaw-Luximon, A. and Jhurry, D., (2013). Dual encapsulation and controlled delivery of anti-TB drugs from PEG-block-poly (ester-ether) nanomicelles. *Journal of Nanopharmaceutics and Drug Delivery*, *1*(3), pp.240-257.

Jiang, Z., You, Y., Deng, X. and Hao, J., (2007). Injectable hydrogels of poly (ε-caprolactone-co-glycolide)–poly (ethylene glycol)–poly (ε-caprolactone-co-glycolide) triblock copolymer aqueous solutions. *Polymer*, *48*(16), pp.4786-4792.

Joe, M., Bai, Y., Nacario, R.C. and Lowary, T.L.,(2007). Synthesis of the docosanasaccharide arabinan domain of mycobacterial arabinogalactan and a proposed octadecasaccharide biosynthetic precursor. *Journal of the American Chemical Society*, *129*(32), pp.9885-9901.

Kaufmann, S.H., (2001). How can immunology contribute to the control of tuberculosis?. *Nature Reviews Immunology*, *1*(1), pp.20-30.

Kaufmann, S.H. and McMichael, A.J., (2005). Annulling a dangerous liaison: vaccination strategies against AIDS and tuberculosis. *Nature medicine*, *11*(4), pp.S33-S44.

Khademi, F., Derakhshan, M., Yousefi-Avarvand, A. and Tafaghodi, M., (2018). Potential of polymeric particles as future vaccine delivery systems/adjuvants for parenteral and non-parenteral immunization against tuberculosis: A systematic review. *Iranian journal of basic medical sciences*, *21*(2), p.116-123.

Knechel, N.A., (2009). Tuberculosis: pathophysiology, clinical features, and diagnosis. *Critical care nurse*, *29*(2), pp.34-43.

Korf, J.E., Pynaert, G., Tournoy, K., Boonefaes, T., Van Oosterhout, A., Ginneberge, D., Haegeman, A., Verschoor, J.A., De Baetselier, P. and Grooten, J., (2006). Macrophage reprogramming by mycolic acid promotes a tolerogenic response in experimental asthma. *American journal of respiratory and critical care medicine*, *174*(2), pp.152-160.

Kumar, N., Kumar, P., Kumar, P., Kumar, M. and Kumar, R., (2011). Nanotechnology: A focus on treatment of tuberculosis. *International Journal of Drug Delivery*, *3*(1), pp. 25-42.

Kumar, P.V., Asthana, A., Dutta, T. and Jain, N.K., (2006). Intracellular macrophage uptake of rifampicin loaded mannosylated dendrimers. *Journal of drug targeting*, *14*(8), pp.546-556.

Langer, R., (1998). Drug delivery and targeting. *Nature*, *392*(6679 Suppl), pp.5-10.

Laurenzi, M., Ginsberg, A. and Spigelman, M., (2007). Challenges associated with current and future TB treatment. *Infectious Disorders-Drug Targets (Formerly Current Drug Targets-Infectious Disorders)*, *7*(2), pp.105-119.

Lee, R.E., Li, W., Chatterjee, D. and Lee, R.E., (2005). Rapid structural characterization of the arabinogalactan and lipoarabinomannan in live mycobacterial cells using 2D and 3D HR-MAS NMR: structural changes in the arabinan due to ethambutol treatment and gene mutation are observed. *Glycobiology*, *15*(2), pp.139-151.

Lee, W.H., Loo, C.Y., Traini, D. and Young, P.M., (2015). Nano-and micro-based inhaled drug delivery systems for targeting alveolar macrophages. *Expert opinion on drug delivery*, *12*(6), pp.1009-1026.

Li, Y.J., Petrofsky, M. and Bermudez, L.E., (2002). Mycobacterium tuberculosis uptake by recipient host macrophages is influenced by environmental conditions in the granuloma of the infectious individual and is associated with impaired production of interleukin-12 and tumor necrosis factor alpha. *Infection and immunity*, *70*(11), pp.6223-6230.

Louw, G.E. and Sampson, S.L., (2017). Implications of chromosomal mutations for mycobacterial drug resistance. In *Drug Resistance in Bacteria, Fungi, Malaria, and Cancer* (pp. 233-262). Springer, Cham.

Lu, W. and Zu, Y., (2013). Metal-based nanoparticles: Their potential clinical applications and limitations. *Rev. Nanosci. Nanotechnol*, *2(3)*, pp..208-224.

Markowitz, N., Hansen, N.I., Hopewell, P.C., Glassroth, J., Kvale, P.A., Mangura, B.T., Wilcosky, T.C., Wallace, J.M., Rosen, M.J. and Reichman, L.B., (1997). Incidence of tuberculosis in the United States among HIV-infected persons. *Annals of Internal Medicine*, *126*(2), pp.123-132.

Mehanna, M.M., Mohyeldin, S.M. and Elgindy, N.A., (2014). Respirable nanocarriers as a promising strategy for antitubercular drug delivery. *Journal of Controlled Release*, *187*, pp.183-197.

Michalets, E.L., (1998). Update: clinically significant cytochrome P-450 drug interactions. *Pharmacotherapy: The Journal of Human Pharmacology and Drug Therapy*, *18*(1), pp.84-112.

Misra, A., Hickey, A.J., Rossi, C., Borchard, G., Terada, H., Makino, K., Fourie, P.B. and

Colombo, P., (2011). Inhaled drug therapy for treatment of tuberculosis. *Tuberculosis*, *91*(1), pp.71-81.

Mitchison, D.A., (2000). Role of individual drugs in the chemotherapy of tuberculosis. *The international journal of tuberculosis and lung disease*, *4*(9), pp.796-806.

Mitchison, D.A. and Fourie, P.B., (2010). The near future: improving the activity of rifamycins and pyrazinamide. *Tuberculosis*, *90*(3), pp.177-181.

Mitnick, C.D., Shin, S.S., Seung, K.J., Rich, M.L., Atwood, S.S., Furin, J.J., Fitzmaurice, G.M., Alcantara Viru, F.A., Appleton, S.C., Bayona, J.N. and Bonilla, C.A., (2008). Comprehensive treatment of extensively drug-resistant tuberculosis. *New England Journal of Medicine*, *359*(6), pp.563-574.

Muttil, P., Wang, C. and Hickey, A.J., (2009). Inhaled drug delivery for tuberculosis therapy. *Pharmaceutical research*, *26*(11), pp.2401-2416.

Nimje, N., Agarwal, A., Saraogi, G.K., Lariya, N., Rai, G., Agrawal, H. and Agrawal, G.P., (2009). Mannosylated nanoparticulate carriers of rifabutin for alveolar targeting. *Journal of drug targeting*, *17*(10), pp.777-787.

Ottenhoff, T.H., (2002). Innate immunity to Mycobacterium tuberculosis. *Clinical microbiology reviews*, *15*(2), pp.294-309.

Orenstein, E.W., Basu, S., Shah, N.S., Andrews, J.R., Friedland, G.H., Moll, A.P., Gandhi, N.R. and Galvani, A.P., (2009). Treatment outcomes among patients with multidrug-resistant tuberculosis: systematic review and meta-analysis. *The Lancet infectious diseases*, *9*(3), pp.153-161.

Pandey, R., Sharma, A., Zahoor, A., Sharma, S., Khuller, G.K. and Prasad, B., (2003). Poly (DL-lactide-co-glycolide) nanoparticle-based inhalable sustained drug delivery system for experimental tuberculosis. *Journal of Antimicrobial Chemotherapy*, *52*(6), pp.981-986.

Pandey, R. and Khuller, G.K., (2005). Antitubercular inhaled therapy: opportunities, progress and challenges. *Journal of Antimicrobial Chemotherapy*, *55*(4), pp.430-435.

Pandey, R. and Khuller, G.K., (2005). Solid lipid particle-based inhalable sustained drug delivery system against experimental tuberculosis. *Tuberculosis*, *85*(4), pp.227-234.

Patel, B., Gupta, N. and Ahsan, F., (2015). Particle engineering to enhance or lessen particle uptake by alveolar macrophages and to influence the therapeutic outcome. *European Journal of Pharmaceutics and Biopharmaceutics*, *89*, pp.163-174.

Patton, J. S. and Platz, R. M. (1992). Pulmonary delivery of peptides and proteins for systemic action, *Advanced Drug Delivery Reviews*, 8, pp. 179–196.

Peloquin, C.A., (2002). Therapeutic drug monitoring in the treatment of tuberculosis. *Drugs*, *62*(15), pp.2169-2183.

Pieters, J., (2008). Mycobacterium tuberculosis and the macrophage: maintaining a balance. *Cell host & microbe*, *3*(6), pp.399-407.

Pinheiro, M., Lúcio, M., Lima, J.L. and Reis, S., (2011). Liposomes as drug delivery systems for the treatment of TB. *Nanomedicine*, *6*(8), pp.1413-1428.

Porth, C.M., (2002). Alterations in respiratory function: respiratory tract infections, neoplasms, and childhood disorders. *Porth CM, Kunert MP. Pathophysiology: Concepts of Altered Health States. Philadelphia, PA: Lippincott Williams & Wilkins*, pp.615-619.

Praba, V.L., Kathirvel, M., Vallayyachari, K., Surendar, K., Muthuraj, M., Jesuraj, P.J., Govindarajan, S. and Raman, K.V., (2013). Bactericidal effect of silver nanoparticles against Mycobacterium tuberculosis. *Journal of Bionanoscience*, *7*(3), pp.282-287.

Rajabnezhad, S., Casettari, L., Lam, J.K., Nomani, A., Torkamani, M.R., Palmieri, G.F., Rajabnejad, M.R. and Darbandi, M.A., (2016). Pulmonary delivery of rifampicin microspheres using lower generation polyamidoamine dendrimers as a carrier. *Powder Technology*, *291*, pp.366-374.

Rao, B.P., Suresh, S. and Narendra, C., (2006). Physicochemical characterization of β-cyclodextrin and hydroxy ethyl β-cyclodextrin complexes of rifampicin. *Ars Pharmaceutica*, *47*(1), pp.37-59.

Raviglione, M. C. and Pio, A. (2002). Evolution of WHO policies for tuberculosis control, 1948-2001, *Lancet*, 359, pp. 775–780. doi: 10.1016/S0140-6736(02)07880-7.

Rittershaus, E.S., Baek, S.H. and Sassetti, C.M., (2013). The normalcy of dormancy: common themes in microbial quiescence. *Cell host & microbe*, *13*(6), pp.643-651.

Rosenkrands, I., Slayden, R.A., Crawford, J., Aagaard, C., Clifton III, E. and Andersen, P., (2002). Hypoxic response of Mycobacterium tuberculosis studied by metabolic labeling and proteome analysis of cellular and extracellular proteins. *Journal of bacteriology*, *184*(13), pp.3485-3491.

Sethi, T. and Agrawal, A., (2011). Structure and function of the tuberculous lung: Considerations for inhaled therapies. *Tuberculosis*, *91*(1), pp.67-70.

Sharma, S.K., Mohan, A. and Kadhiravan, T., (2005). HIV-TB co-infection: epidemiology, diagnosis & management. *Indian J Med Res*, *121*(4), pp.550-567.

Shegokar, R., Al Shaal, L. and Mitri, K., (2011). Present status of nanoparticle research for treatment of tuberculosis. *Journal of Pharmacy & Pharmaceutical Sciences*, *14*(1), pp.100-116.

Shehzad, A., Rehman, G., Ul-Islam, M., Khattak, W.A. and Lee, Y.S., (2013). Challenges in the development of drugs for the treatment of tuberculosis. *The Brazilian journal of infectious diseases*, *17*(1), pp.74-81.

Silva, M., Ricelli, N.L., El Seoud, O., Valentim, C.S., Ferreira, A.G., Sato, D.N., Leite, C.Q. and Ferreira, E.I., (2006). Potential Tuberculostatic Agent: Micelle-forming Pyrazinamide Prodrug. *Archiv der Pharmazie: An International Journal Pharmaceutical and Medicinal Chemistry*, *339*(6), pp.283-290.

Singh, H., Bhandari, R. and Kaur, I.P., (2013). Encapsulation of Rifampicin in a solid lipid nanoparticulate system to limit its degradation and interaction with Isoniazid at acidic pH. *International journal of pharmaceutics*, *446*(1-2), pp.106-111.

Singh, S., Mariappan, T.T., SHARDA, N. and SINGH, B., (2000). Degradation of rifampicin, isoniazid and pyrazinamide from prepared mixtures and marketed single and combination products under acid conditions. *Pharmacy and Pharmacology Communications*, *6*(11), pp.491-494.

Slayden, R.A. and Barry III, C.E., (2000). The genetics and biochemistry of isoniazid resistance in Mycobacterium tuberculosis. *Microbes and Infection*, *2*(6), pp.659-669.

Smith, T., Wolff, K.A. and Nguyen, L., (2012). Molecular biology of drug resistance in Mycobacterium tuberculosis. In *Pathogenesis of Mycobacterium tuberculosis and its Interaction with the Host Organism*, pp. 53-80. Springer, Berlin, Heidelberg.

Sung, J.C., Pulliam, B.L. and Edwards, D.A., (2007). Nanoparticles for drug delivery to the lungs. *Trends in biotechnology*, *25*(12), pp.563-570.

Turner, P.V., Brabb, T., Pekow, C. and Vasbinder, M.A., (2011). Administration of substances to laboratory animals: routes of administration and factors to consider. *Journal of the American Association for Laboratory Animal Science*, *50*(5), pp.600-613.

Vandal, O.H., Nathan, C.F. and Ehrt, S., (2009). Acid resistance in Mycobacterium tuberculosis. *Journal of bacteriology*, *191*(15), pp.4714-4721.

World Health Organization (WHO), (2003). State of the art of new vaccines: research and development. *Initiative for Vaccine Research. Geneva, Switzerland: World Health Organization*.

WHO (2004) *Avoiding tuberculosis Selfstudy Program on Tuberculosis*. Available at: http://www.who.int/healthacademy/WHO_TB.pdf.

WHO (2007) Tuberculosis Fact sheet N 104-Global and regional incidence.

WHO (2010) 'Treatment of tuberculosis: guidelines', in *4Th Edition*, p. 160.

WHO (2019) *WHO | Global tuberculosis report 2019, World Health Organization*. World Health Organization.

Willis, L., Hayes, D. and Mansour, H.M., (2012). Therapeutic liposomal dry powder inhalation aerosols for targeted lung delivery. *Lung*, *190*(3), pp.251-262.

Chapter 2

Dendrimers: Characteristics and features

2.1 Background

The term dendrimer is commonly used to describe a tree-like architectural pattern and does not indicate a particular molecule or group of compounds. The earliest suggestion of this pattern was conceptualized by the scientist Flory in 1941 (Flory, 1941), while the first experimental synthesis of dendrimers was developed by Donald Tomalia in 1984 - 1985 (Tomalia *et al.*, 1985; Tomalia, 1995). By the end of the 1970s, Tomalia and his group in the Dow Corporate laboratory, successfully synthesized a dendritic molecule using new synthesis concepts (Tomalia and Fréchet, 2002). These concepts have been directed to produce monodispersed artificial macromolecules (Tomalia and Fréchet, 2002). Between 1978 to 1980, it was reported that Fritz Vogtle and co-workers also succeeded in synthesizing the first cascade molecules (Figure 2.1, Table 2.1) (Buhleier, Wehner and Vögtle, 1978). These achievements, at that time, were the first instances in the field of synthetic polymers to produce biotic macromolecules without utilizing the biological system.

The first illustration of a synthesized dendrimer was poly(amidoamine) (PAMAM) dendrimer in 1984 (Figure 2.1, Table 2.1) by Tomalia *et al.*, 1984. It was presented at the 1st International Polymer Conference, Society of Polymer Science, Japan (SPSJ), and was published in Polymer Journal in 1985 (Tomalia *et al.*, 1985). According to many literature reports, the announcement of dendrimer synthesis in 1985 happened simultaneously with the synthesis of tree-like macromolecules called arborols by the scientist Newkome at the Louisiana State University (Figure 2.1, Table 2.1) (Newkome *et al.*, 1985).

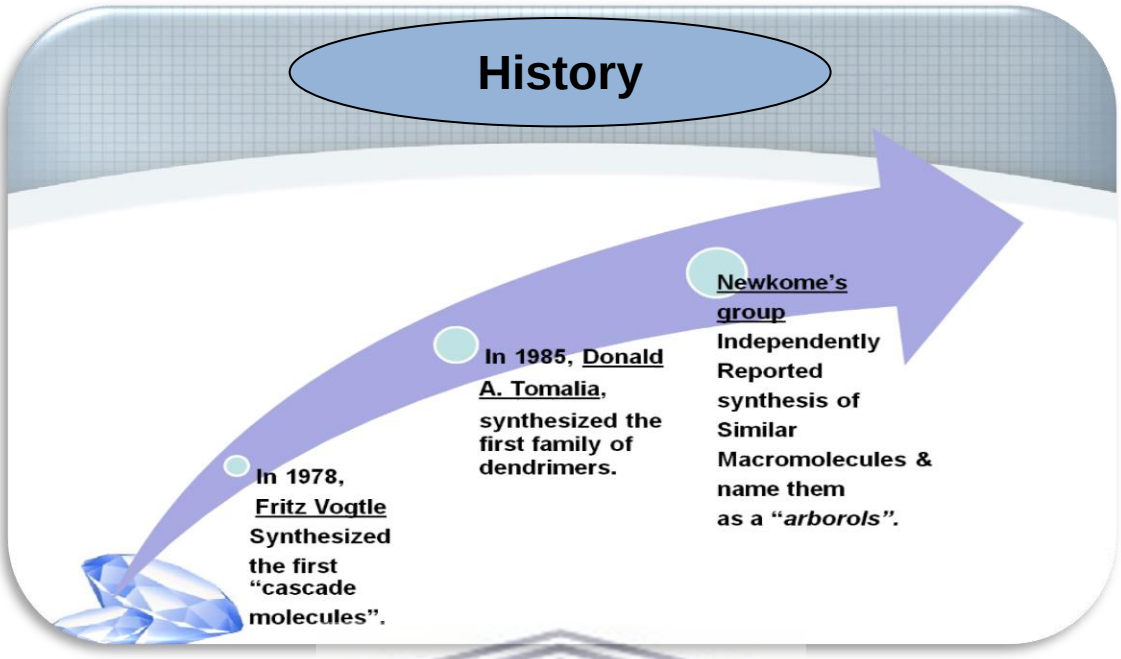

Figure 2.1 The development track of dendrimers [Adapted from (Singh *et al.*, 2017)].

Table 2.1 reviews the timeline of dendrimer development from the earliest theory suggested by Flory in 1941, going through different types of dendrimers and also list examples for dendrimer-based products under clinical trials.

Table 2.1 Timeline of dendrimer development until 2010 (Singh et al., 2017).

Year	Features of development
1941–1942	Evidence for branched-chain macromolecules
1973	Stepwise strategies for the synthesis of macro-cyclic rings
1978	Cascade synthesis
1981	Lysine-dendrimer patent
1983	First theoretical study on dendrimers
1985	First modular dendrimer synthesis, the first reference to unimolecular micelles
1985	First high-generation dendrimers-based on linear monomers
1989	Metallo-dendrimers
1990	First convergent synthesis
1990	Silicone-based dendrimers
1991	Phenylacetylene dendrimers
1993	Improved Vogtle technique and later developed the dendritic box
1993	Chiral dendrimers
1993	DNA-based dendrimers
1994	Phosphorous-based dendrimers
1995	Self-Assembly of dendrimers
1995	Dendronized-Polymers
1999	PAMAM dendrimers non-viral vectors for gene transfer
1999	Starpharma is in phase II trials of dendrimers
2001	Treatment of several viral diseases
2003	US FDA for human trials of their dendrimer-based anti-HIV product
2004	Vaginal gel, SPL7013 human trials of their dendrimer-based anti-HIV product
2010	PEGylated dendrimers

2.2 Overview and general consideration

Dendrimers are synthetic, globular-shaped, three-dimensional, hyperbranched, well-ordered polymeric compounds (Singh *et al.*, 2017). Dendrimers have precise constitutional and compositional properties such as size (less than 100 nm), shape, and molecular weight (Singh *et al.*, 2017). They are produced by repetitive growth reactions that start from the center atom or group of atoms known as the "initiator multi-functional core" such as ammonia or ethylenediamine. From the core, step-wise sequential addition of branching units will form the shell of the dendrimer which contains the radiated repeated monomers (such as polyamidoamines and polyethers). The generated internal spaces/voids within the dendrimer shell (Figure 2.2) are essential to accommodate various metals, organic and inorganic molecules (Tomalia *et al.*, 1986). Figure 2.2 illustrates the main components of the dendrimer architecture: the multi-functional core, the shell which comprises of a layer or multi-layers known as a generation made up of repeating monomers attached to the core. This radiates out with outer multivalent surface functional groups (Singh *et al.*, 2017).

The dendrimer generation (G) stands for the hyperbranching when moving from the dendrimer's core towards the outer surface to form homostructural layers between branching points (focal points).

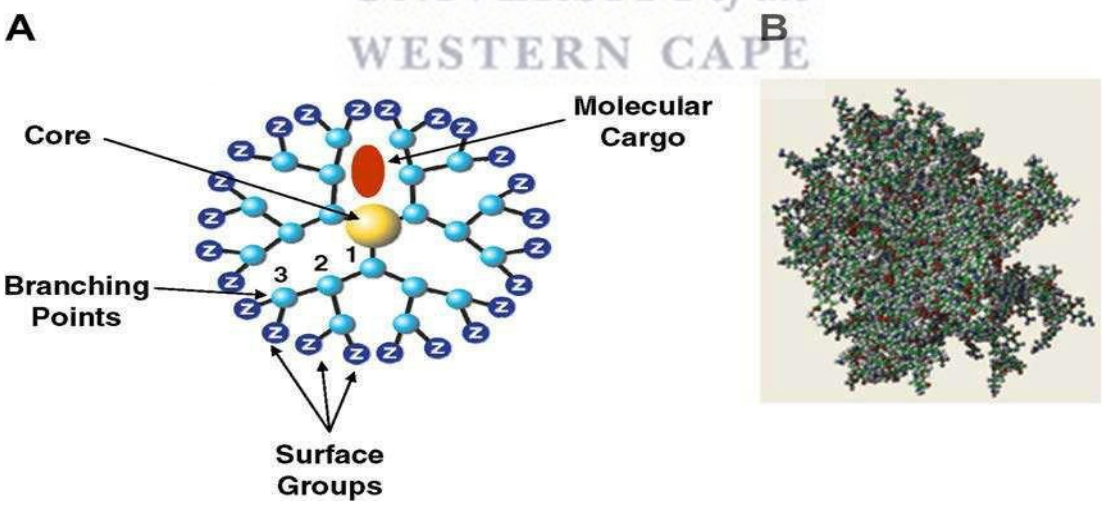

Figure 2.2 Main components of 3.0 G dendrimer, (A) 2-dimensional (2-D), and (B) 3-dimensional (3-D) representations [adapted from (Svenson, 2009)].

The number of focal points from the core to the outer dendrimer surface accounts for the generation number (Figure 2.3). For example, if a dendrimer molecule has 4 focal points starting from the core towards the outer surface, it is referred to as a 4^{th} generation dendrimer, which can be further shortened to a 4.0 G PAMAM dendrimer or G4 PAMAM dendrimer. Sometimes dendrimers could hold half-generation numbers such as 0.5 G and 1.5 G, and this happens for the intermediate synthesis products of the dendrimers. One of the common half-generation dendrimers is a carboxylic acid-terminated dendrimer.

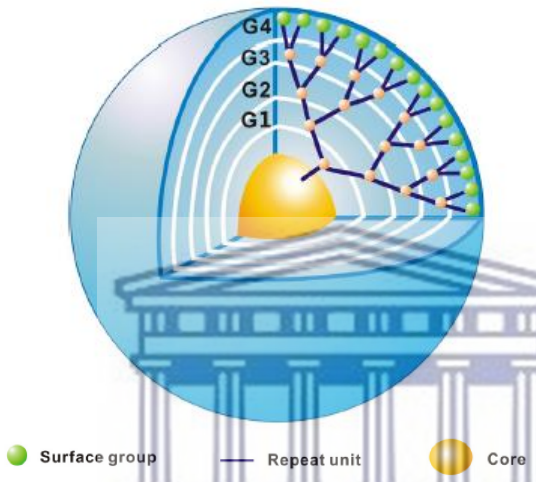

Figure 2.3 Illustration of dendrimer generation number [adapted from (Hu, Hu and Cheng, 2016)].

The properties of dendrimer such as size, shape, surface chemistry, and molecular weight can be controlled at different stages of the synthesis (Tomalia, Naylor and Goddard, 1990). This can be achieved by managing the nature of the core, the level of radiated monomers (generations) and the nature and number of functional groups at the periphery (Bosman, Janssen and Meijer, 1999; Svenson and Tomalia, 2005).

The possibility of peripheral surface modification suggests dendrimers as multifunctional platform molecules. Manipulating the outermost surface functional groups with various ligands and polymers (Esfand and Tomalia, 2001), will enhance the dendrimer properties and targeting potential which is extremely beneficial in the field of drug delivery (Tomalia, Naylor and Goddard, 1990). The highly dense surface groups and the appropriate internal voids recommend dendrimers as one of the promising drug and gene delivery systems

(Kojima *et al.*, 2000; Malik *et al.*, 2000; Konda *et al.*, 2001; Jevprasesphant *et al.*, 2003; Chauhan *et al.*, 2004; Yang, Morris and Lopina, 2004; Ertürk, Gürbüz and Tülü, 2017).

2.3 Characteristics of dendrimers

Dendrimers have unique features that afford a dendrimer-conjugate complex the possibility to overcome the most common hurdles associated with drug delivery and treatment of diseases. Obstacles associated with solubility, permeability, inadequate biodistribution, and associated side effects may be enhanced. The dendrimer-conjugate complex may acquire the following properties (Figure 2.4):

a) Enhance permeability and retention effect (EPR)

The nano-size (e.g., 4.0 G is approximately 4.4 nm) property of dendrimers suggests the possibility of drug carriers for cancer treatment due to enhanced permeability and retention effect (EPR) (Singh *et al.*, 2017). Drug-loaded dendrimers distribute preferentially into tumor tissue due to the small particle size (nanosize) and higher tissue vascularization compared to the normal tissues. The diffusion of these nanoparticles occurs through the leaky endothelium membrane of the tumour tissues. Due to lack of adequate lymphatic drainage, nanoparticles could be retained inside the tumor tissues for days and sometimes weeks (Purohit, Sakthivel and Florence, 2001; Bae *et al.*, 2005; Patri, Kukowska-Latallo and Baker, 2005).

b) Enhance permeability

Dendrimers and dendrimer-loaded molecules are competent to diffuse across the biological barriers such as the blood-brain barrier and cell membrane (Singh *et al.*, 2017). The monodispersity and nano-size of dendrimers have a high impact on enhancing their cell membrane permeability as well as reducing the rapid hepatic and spleen clearance (Jansen, De Brabander-van den Berg and Meijer, 1994; Newkome *et al.*, 1996; Zhuo, Du and Lu, 1999).

c) Prolong duration effect

Dendrimers are capable of releasing the loaded molecules in sustained/controlled behaviour (Tawfik, Tadros and Mohamed, 2019). Manipulating the surface of dendrimers with polyethylene glycol will not only improve the distribution behaviour but also obviate nonspecific interactions with biomolecules. This results in extending the circulating time, which is necessary to achieve the intended therapeutic effect (Newkome *et al.*, 1991).

d) Enhanced solubility

According to previous literature reports, dendrimers are able to improve the solubility of the hydrophobic molecules *via* three mechanisms, i.e. hydrogen bonding, ionic interaction and hydrophobic interaction (Galia *et al.*, 1998; Twyman *et al.*, 1999; Milhem *et al.*, 2000; Chauhan *et al.*, 2004; Kolhe *et al.*, 2006; Rupal *et al.*, 2009).

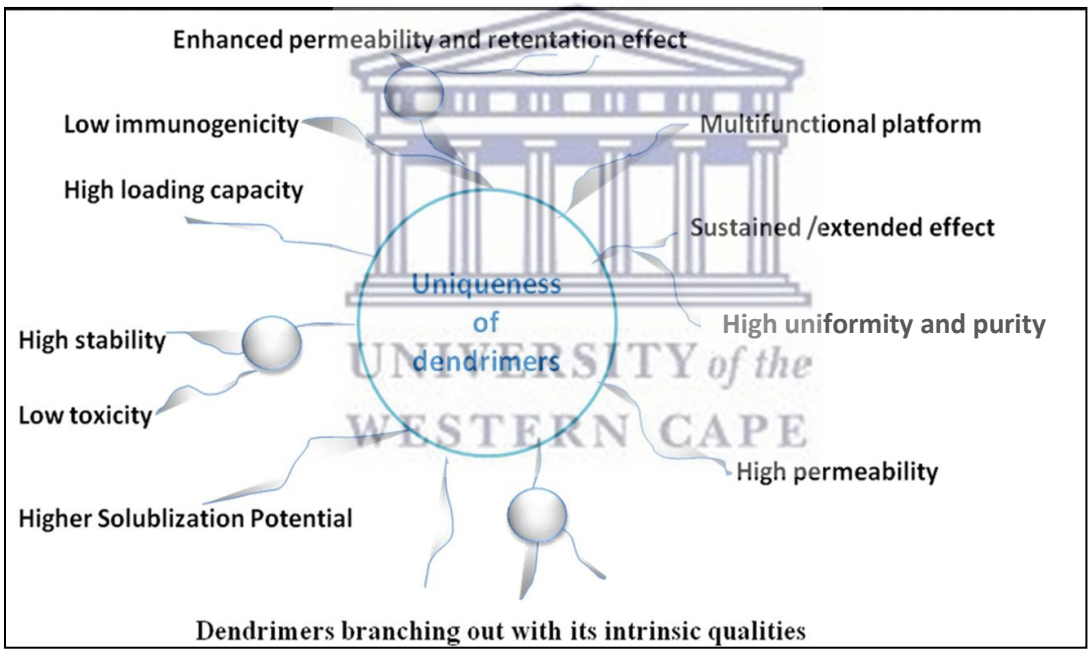

Figure 2.4 Summary of dendrimer characteristics [Adapted from (Singh *et al.*, 2017)].

e) High purity and monodispersity

The synthesis of dendrimers follows highly controlled sequential addition reactions to produce particles with a uniform size range, exact molecular weight, multifunction surface,

and minimal impurities (Singh *et al.*, 2017). The consistent monodispersed particles will help to achieve precise drug delivery (El-Sayed *et al.*, 2001, 2002).

f) Multivalent platform

The peripheral surface groups of dendrimers can form conjugates with drug molecules, polymers, and targeting ligands. Attaching site-specific ligands, solubility enhancers, and stealth polymers on the surface of the dendrimer are considered essential to improve the biodistribution and decrease body clearance (Devarakonda, Li and de Villiers, 2005).

g) High loading potential

Dendrimers are capable of encapsulating different metals and drug molecules in a high loading percentage. Drug conjugation could take place at the dendrimer interior *via* physical entrapment within the internal voids (Newkome *et al.*, 1991; Jansen, De Brabander-van den Berg and Meijer, 1994) or through non-covalent interactions with the core and the branching monomers (Kojima *et al.*, 2000). Sometimes the conjugation may arise at the exterior surface through electrostatic interactions with the dense peripheral groups (Milhem *et al.*, 2000; Tripathy and Das, 2013).

h) Better stability

Many drug molecules exhibited improvement in their stability following encapsulation in the dendrimer scaffold (Singh *et al.*, 2017).

i) Low toxicity and immunogenicity

The majority of dendrimers show low cytotoxicity behaviour, as well as an insignificant immunogenic reaction when used topically or parenterally (Duncan and Izzo, 2005).

2.4 Dendrimers and hyperbranched polymers

The two types of polymers that consist of repeating branched components are the dendrimers and the hyperbranched polymers (Figure 2.5) (Grayson and Fréchet, 2001; Singh *et al.*, 2009). The hyperbranched polymers are synthesized by the non-iterative polymerization process (Kim and Webster, 1990; Hawker, Lee and Frécnet, 1991; Wang,

Gan and Wooley, 2001). Therefore, they exhibit an asymmetrical structure with sometimes incomplete reacted branch points in their structure (Fréchet *et al.*, 1996; Hawker, 1999).

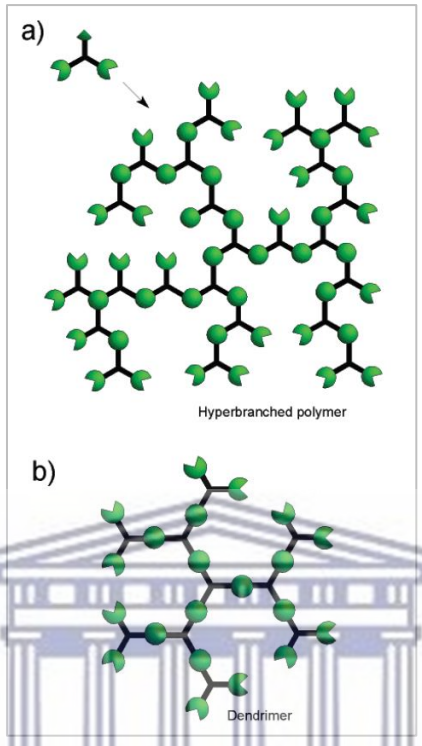

Figure 2.5 The structure of (a) hyperbranched polymers and (b) dendrimer [Adapted from (Grayson and Fréchet, 2001)].

On the other hand, dendrimers are synthesized by sequential additional reactions that generate a well-ordered structure with regular branching and precise surface functional groups (Klajnert and Bryszewska, 2001).

In addition, dendrimers differ from the traditional linear polymers on the following characteristics (Grayson and Fréchet, 2001):

a) The synthesis techniques of dendrimers produce monodisperse compounds, while linear polymer synthesis techniques generate polydisperse compounds.

b) Increasing the dendrimer generation will exponentially increase the number of surface groups. Dendrimer properties such as solubility and chemical interaction depend significantly on the nature and the number of surface groups (Grayson and Fréchet, 2001). Therefore, increasing the density of surface groups will help to improve the

dendrimer properties whereas linear polymers possess only two functional groups in their structure that mainly control the molecule properties.

c) The growth of linear polymers can continue infinitely, unless solubility matters arise, while the dendrimers' growth is mathematically limited. In dendrimers, when the number of branch units increases doubly with the generation addition, the space presented to the molecule only rises by the cube of its radius. Adding more generations will result in a globular structure due to physical restrictions generated by the terminal groups. At a particular stage, the steric hindrance will hamper the normal growth of the dendrimer, which is known as the de Gennes dense packing (de Gennes and Hervet, 1983; Grayson and Fréchet, 2001). Sometimes the growth may exceed the de Gennes dense packing, which could enhance the possibility of irregular dendrimer structures, including defects and backfolding within the dendrimer shell (Grayson and Fréchet, 2001).

Figure 2.6 illustrates the development of the dendrimer compared to other polymers as time evolved.

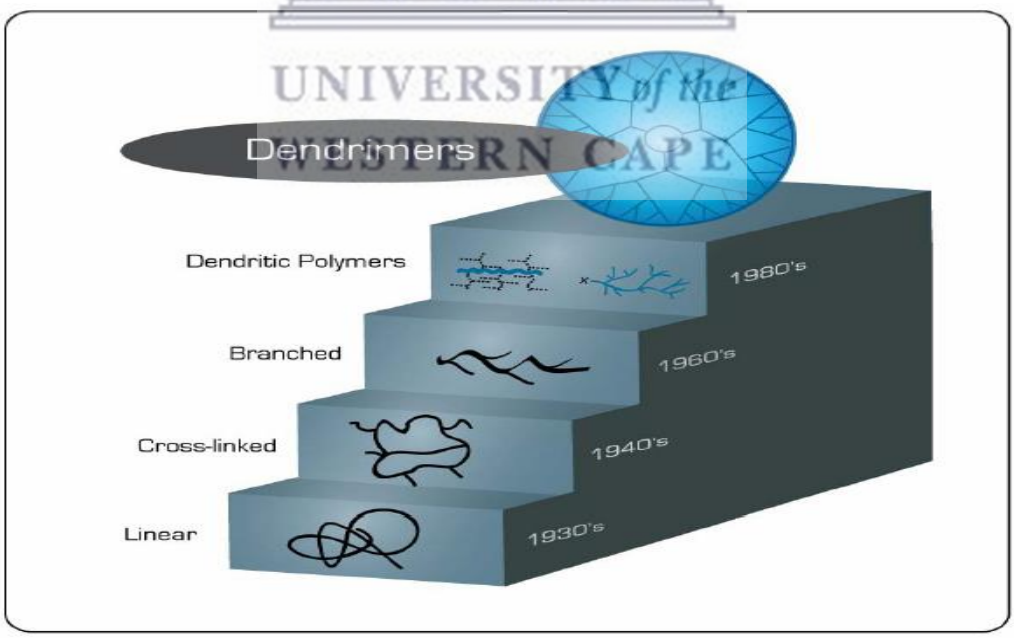

Figure 2.6 Development of the dendrimer over a time frame of 50 years [adapted from (Tomalia and Fréchet, 2002)].

2.5 Methods of dendrimer synthesis

Dendrimers are frequently synthesized by two approaches, (a) the divergent method, and (b) the convergent method (Hodge, 1993; Kesharwani, Jain and Jain, 2014). The concept of the divergent method was firstly reported in 1978 by the scientist Vögtle (Buhleier, Wehner and Vögtle, 1978), who created an iterative cascade technique to synthesize low molecular weight branched amines. After that, Tomalia and his group (1980 -1985) used the divergent method to synthesize the first member of dendrimers, i.e. the PAMAM dendrimer (Tomalia *et al.*, 1985). Later, between 1989 to 1990 the two scientists Hawker and Jean Fréchet developed a new synthesis technique of dendrimers known as the convergent method (Hawker and Fréchet, 1990).

a) Divergent method (Grayson and Fréchet, 2001)

It was reported that the earliest model developed to synthesize the first cascade molecule using an iterative technique was done by Vögtle and co-workers (1978) (Buhleier, Wehner and Vögtle, 1978). Applying the divergent method to synthesize dendrimers and the arborols macromolecules were reported by Tomalia and co-workers (1984) (Tomalia *et al.*, 1984) and Newkome and co-workers (1985) (Newkome *et al.*, 1985), respectively. The divergent process consists of two stages, firstly there is the activation of the peripheral functional groups, and then the addition of the dendrimer branching units (Figure 2.7). The synthesis starts from the multifunctional core towards the outer surface through a series of sequential addition of monomer units. This is followed by the deshielding step of the monomer's end groups, which is known as the activation step. This then generates a new reactive platform for further monomer addition and hence raises the number of surface groups by two-fold. The monomer units are usually characterized by inert functional groups to manage uncontrolled hyperbranched polymerization. The monomers addition step and activation step are repeated many times until the dendrimer of the desired generation and properties is achieved.

The divergent method has some advantages such as the simple purification step of dendrimer from other reactant monomers due to molecular weight variation. Also, the

physicochemical properties of the dendrimer can be easily controlled to the exact requirements (Ong *et al.*, 2001; Islam, Majoros and Baker, 2005).

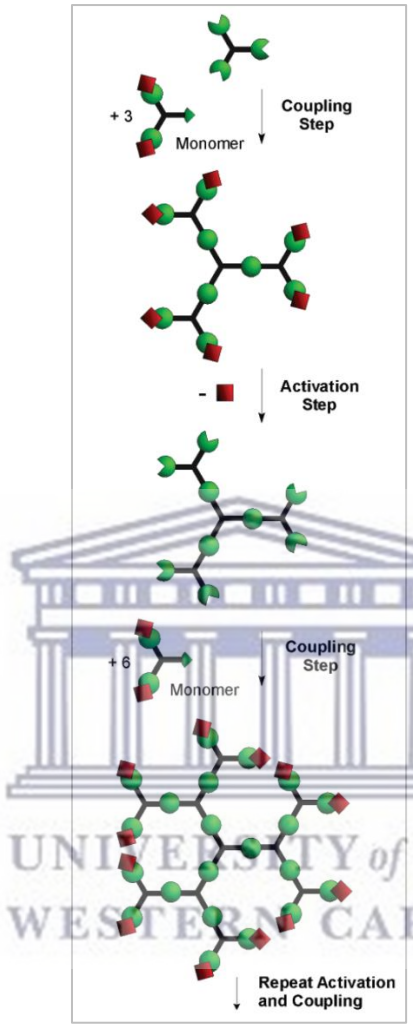

Figure 2.7 Illustration of the divergent method for dendrimer synthesis [Adapted from (Grayson and Fréchet, 2001)].

b) Convergent method (Grayson and Fréchet, 2001)

The convergent method was developed by the two scientists, Hawker and Fréchet, between 1989 - 1990 (Hawker and Fréchet, 1990). In this approach, the growth begins at the periphery and progresses inwards by coupling the intended surface groups with the branching monomers, followed by an activation step to form a dendron (Figure 2.8). A series of monomer coupling and activation steps continue to achieve the desired dendron

generation. After that, dendrons are joined to the multifunctional core to generate the globular shaped dendrimer.

In the convergent method, lesser reaction steps and a lower amount of reactants were observed compared to the divergent method. On the other hand, producing a higher generation (above the sixth generation), by the convergent method, is difficult, due to the steric hindrance of the dendrons at the coupling step with the core.

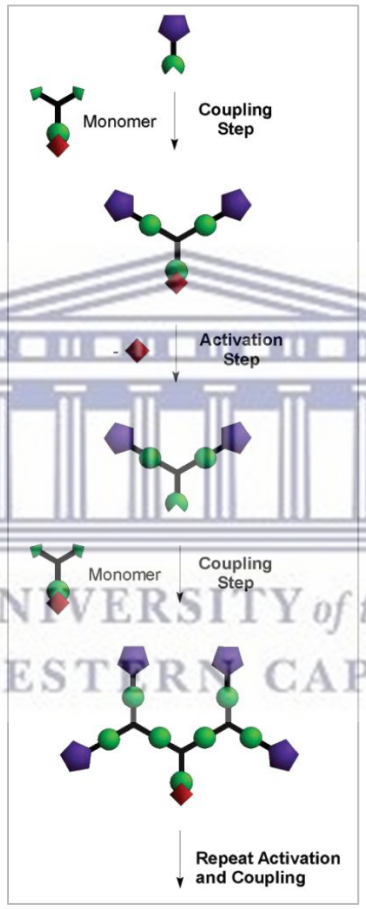

Figure 2.8 Illustration of the convergent method for dendrimer synthesis [Adapted from (Grayson and Fréchet, 2001)].

2.6 Types of dendrimers

Different types of dendrimers have been developed in a few years as a result of the advances in synthetic chemistry and analytical tools; some of these dendrimers are described below:

2.6.1 PPI dendrimer

The poly(Propyleneimine) (PPI) dendrimer is an amine-terminated macromolecule, developed by Vögtle and mostly synthesized by the divergent method (Koper *et al.*, 1997). The PPI dendrimer holds two types of nitrogen atoms in its structure, the nitrogen of the tertiary tris-propylene amines and the nitrogen of surface primary amines. Usually, 1,4 diaminobutane (DAB) is used as a PPI dendrimer core; accordingly, sometimes it is symbolized as DAB dendrimer. PPI is available up to the fifth-generation (G5) and is widely used in material science and biology (Kesharwani, Jain and Jain, 2014).

2.6.2 Tecto (core-shell) dendrimer

Tecto dendrimer consists of a core dendrimer that is covalently surrounded by other dendrimer molecules where drug molecules are commonly loaded in the core dendrimer (Kesharwani, Jain and Jain, 2014). Tecto dendrimer is regularly synthesized by the divergent method. Tecto dendrimer has promising applications in biological sciences and multidrug delivery.

2.6.3 Chiral dendrimers

Chiral dendrimers are macromolecules that are synthesized by the convergent method. The chirality in these dendrimers is based on the building up of branches that have different constituents but are chemically comparable to the chiral core (Kesharwani, Jain and Jain, 2014).

2.6.4 Hybrid dendrimers

The hybrid dendrimers are a combination of linear polymers and dendrimers in a hybrid block, that possess the features of both (Kesharwani, Jain and Jain, 2014).

2.6.5 Amphiphilic and micellar dendrimers

The amphiphilic dendrimers are synthesized with two separate sites of chain ends; the first part is electron-donating, and the second part is electron-withdrawing (Tripathy and Das, 2013). The micellar dendrimers are unimolecular hydrophilic hyper-branched polyphenylene micelles. Micellar dendrimers are synthesized by the divergent method and

are usually used in drug delivery and various biological applications (Tripathy and Das, 2013).

2.6.6 Multiple antigen peptide dendrimers

Multiple antigen peptide dendrimers are a dendron-like architecture that comprises of polylysine units. Lysine contains an alkyl amino side-chain which is considered a superior building monomer that gives better flexibility. Multiple antigen peptide dendrimers have been used in various biological applications such as vaccines in addition to uses in magnetic resonance imaging (Tripathy and Das, 2013).

2.6.7 Frèchet dendrimers

Frèchet dendrimers were developed by Frèchet and Hawker, which consists of a poly-benzyl ether hyper-branched scaffold. These dendrimers are hydrophobic molecules. Usually, Frèchet dendrimers encompass carboxyl groups at their surface that increases the hydrophilicity of the dendrimer and provides a platform for further surface manipulation (Hawker and Fréchet, 1990; Cheng *et al.*, 2008).

2.6.8 Glycodendrimers

Glycodendrimers are dendrimers that contain sugar moieties, such as mannose, galactose, and glucose in their structure (Kesharwani, Jain and Jain, 2014). The sugar moieties are either attached to the outer dendrimer surface or represent the dendrimer core from which the branched monomers manifest. The most-reported application of these dendrimers is targeting drug delivery, particularly lectin-rich sites (Kesharwani, Jain and Jain, 2014).

2.6.9 PAMAM dendrimer

The term PAMAM refers to poly(amidoamine) dendrimer, which was firstly synthesized by Tomalia in 1985 using the divergent method (Tomalia *et al.*, 1985). Tomalia used ammonia or ethylenediamine (EDA) as an initiator core for synthesizing PAMAM dendrimer (Tomalia *et al.*, 1985). The branching out of monomers from the center core took place through a series of sequential additions of methyl acrylate and ethylenediamine that ends with amine groups (in the case of full generation), and carboxyl/carboxylic acid

groups (in the case of half generation) (Kesharwani *et al.*, 2015). The surface groups can further be manipulated to improve the dendrimer properties and enhance the drug/guest molecule's attachment. PAMAM dendrimers are the first dendrimer to be synthesized, characterized, and commercialized (Esfand and Tomalia, 2001). Generally, PAMAM dendrimers are available as a methanol solution in amber glass containers since they degrade in light (Chauhan *et al.*, 2004), therefore all their reactions are recommended to be in the dark. Starburst® is the trademark of PAMAM dendrimer, which corresponds to the star-like pattern, especially for a higher generation (Hawker and Fréchet, 1990).

PAMAM dendrimers have a size ranging from a few nanometers about 2 nm for the first generation (G1) up to about 13 nm for the tenth generation (G10) (Tomalia *et al.*, 1985; Maiti *et al.*, 2004; Müller *et al.*, 2007). They exhibit several conformational shapes based on the number of generations. Adding a new generation will exponentially increase the number of surface groups while the volume increases by the cube of its radius. For example, G1 and G2 PAMAM dendrimers are characterized by open flat architecture with 8 and 16 surface groups, respectively. While G4 PAMAM dendrimer will only reside in the 64 surface amine groups in a 4.4 nm volume if the shape turns into a spheroid (Grayson and Fréchet, 2001). The highly compact package called De Gennes dense packing will be attained for dendrimers above G6 due to the congested surface (Grayson and Fréchet, 2001; Tomalia, 2001; Yang and Kao, 2006).

PAMAM dendrimers can be synthesized either in full generations (e.g. G0 - G10) with amine surface groups, or in half generations (e.g. G0.5, G1.5, and G2.5, etc,) with carboxyl surface groups. Table 2.2 below summarizes the molecular weight and number of surface groups for PAMAM dendrimers from G0 to G10 of ammonia and ethylenediamine core.

Table 2.2 Summary of approximate molecular mass and the number of surface groups of G0 - G10 PAMAM dendrimers (Tomalia et al., 1985; Maiti et al., 2004; Müller et al., 2007).

Generation (G)	Ammonia core (NH_3)		Ethylenediamine core ($C_2H_8N_2$)	
	Molecular mass	No of surface groups	Molecular mass	No of surface groups
G0	359	3	516	4
G1	1043	6	1428	8
G2	2411	12	3252	16
G3	5147	24	6900	32
G4	10619	48	14196	64
G5	21563	96	28788	128
G6	43451	192	57972	256
G7	87227	384	116340	512
G8	174779	768	233076	1024
G9	349883	1536	466548	2048
G10	700091	3072	933492	4096

2.6.9.1 Common properties and uniqueness of PAMAM dendrimers

PAMAM dendrimers own the general characteristics of dendrimers such as monodispersity and well-ordered architecture as a result of its highly controlled synthesis and purification methods. The precise iterative synthesis reaction of PAMAM dendrimer offers an accurate expectation of molecular mass, biodegradability, and biocompatibility, and accordingly, they are considered promising drug delivery and site targeting systems (Tomalia *et al.*, 1986; Duncan and Izzo, 2005; Kumar *et al.*, 2006; Dineshkumar *et al.*, 2017). PAMAM dendrimers have appropriate internal voids and dense surface groups for superior drug/guest molecular attachment. Loading drug/guest molecules on PAMAM dendrimers have been reported to improve their solubility, diffusion across biological membranes, and site targeting delivery (Kojima *et al.*, 2000; Pan *et al.*, 2005; Kumar *et al.*, 2006). The exterior surface of PAMAM dendrimer has an additional important role in controlling the movement of encapsulated molecules in and out of the polymer, which will help to improve

drug biodistribution and prediction of drug pharmacokinetics (Pan *et al.*, 2005; Bellini *et al.*, 2015; Dineshkumar *et al.*, 2017).

Based on some unique characteristics such as highly organized structure, electrophoretic properties (Brothers, Piehler and Tomalia, 1998), dimensional size and other bio-similar properties (Jiang and Aida, 1996; Dandliker *et al.*, 1997; Weyermann *et al.*, 1999; Hecht and Fréchet, 2001), PAMAM dendrimers are sometimes considered as artificial proteins. For example, G3, G4, and G5 PAMAM dendrimers have a comparable size to insulin (≈30 Å), cytochrome C (≈40 Å), and hemoglobin (≈55 Å), respectively (Figure 2.9) (Esfand and Tomalia, 2001). As well as, G5 and G6 approximately have similar diameters to that of the lipid bilayers of biological cells (Figure 2.9) (Esfand and Tomalia, 2001).

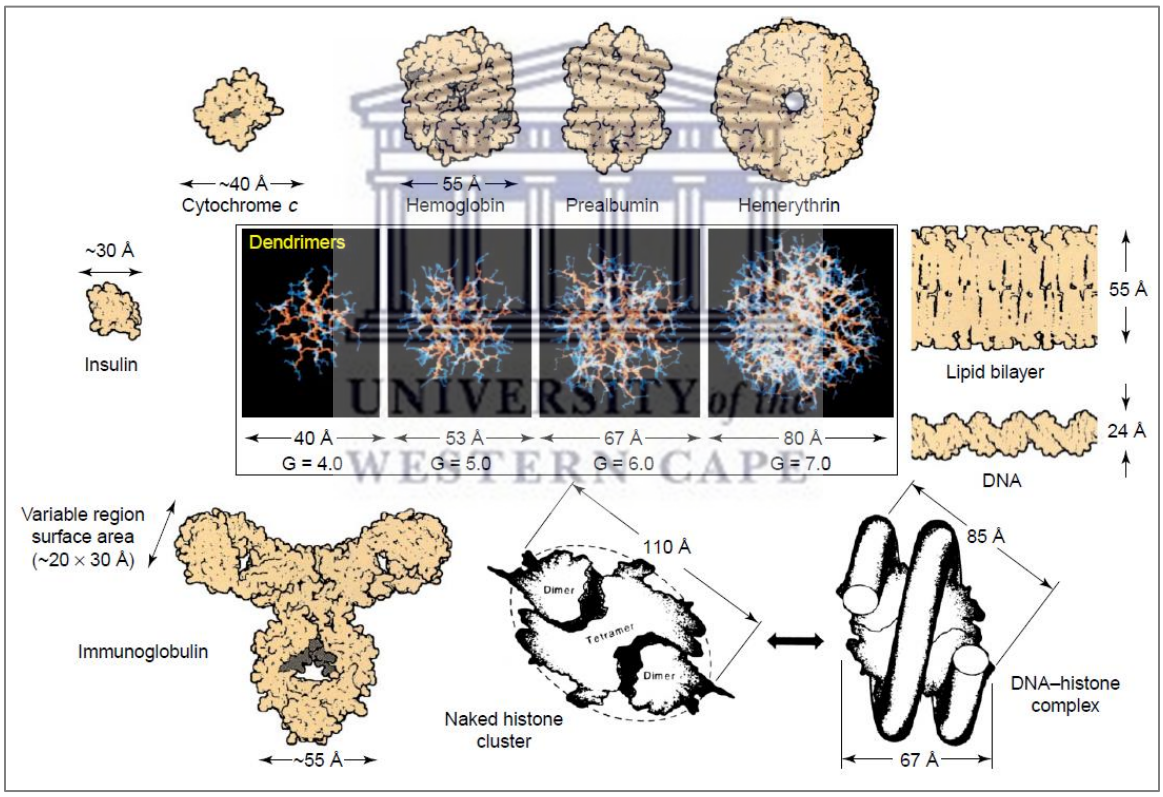

Figure 2.9 Comparison of several PAMAM dendrimers having ammonia core with different proteins, lipid bilayers, and DNA [Adapted from (Esfand and Tomalia, 2001)].

The DNA duplexes (≈ 24 Å width) are commonly accumulated inside the nucleosome of the cells after forming stable hybrid complexes with the histone protein clusters (≈ 110 Å × 80 Å) (Figure 2.9). Due to the shape and size similarities between PAMAM dendrimers

(G7-G10) and the histone proteins, they are considered synthetic histone macromolecules (Esfand and Tomalia, 2001). Their similarities account for the exceptional stability of DNA-PAMAM dendrimer complexes. For example, better gene expression was noticed for G7-G10 PAMAM dendrimers compared to that with the lower generation (G1-G5) (Hudde *et al.*, 1999; Eichman *et al.*, 2000). Due to these similarities, PAMAM dendrimers are suggested to be a suitable and feasible substitute for globular protein in immunodiagnostic applications (Singh *et al.*, 1994, 1996; Singh, 1998).

PAMAM dendrimers have been observed to be non-immunogenic with minimal toxicity behavior, mainly when the surface groups include anionic or neutral charges, such as carboxyl and hydroxyl groups (Roberts, Bhalgat and Zera, 1996).

2.6.9.2 Factors affecting the characteristics of PAMAM dendrimers

Numerous factors such as the pH of the solution, type of solvent, salt concentration, and the dendrimer concentration may affect the nature of the amino group's charge, as well as the structural conformation of the dendrimer molecules. Table 2.3 discuss the effect of these factors on PAMAM dendrimer at different levels:

Table 2.3 Summary of factors affecting the characteristics of PAMAM dendrimers.

Factor	Level	Outcome
Effect of pH (Wang and Imae, 2004; Gupta, Agashe and Jain, 2007)	Low	- At low pH, particularly < 4 both primary surface amines and interior tertiary amines are protonated. - Repulsion will arise between the protonated atoms to generate a hollow-shell molecule (dense-shell).
	Neutral	- At neutral pH, only peripheral amines will be protonated. - Backfolding might happen *via* hydrogen bonding between the protonated primary amines and interior tertiary amines.
	High	- At high pH, particularly > 10 dendrimer molecules are regularly not carrying charges (neutral). The molecule shape is getting contracted (globular, dense core) as a result of minimal repulsion forces. - A high degree of backfolding is usually observed due to low repulsive forces.
Effect of solvent (Chai *et al.*, 2001)		- Non-solvent encourages the backfolding as a result of intra-dendron interaction (dense core). - Non-solvent may decrease the polarity of hydrophobic dendrimer that holds hydrophilic surface groups.

		- Solvent interacts with dendrimer arms which decrease the backfolding and therefore allow for extended conformation (dense shell).
Effect of salt (Gupta, Agashe and Jain, 2007)	High	- High salt concentration will diminish the dendrimer's total charges, which will directly decrease the repulsive forces and enhance the possibility of contracted conformation due to a higher degree of backfolding.
	Low	- Low salt concentration has a slighter influence on the dendrimer's total charges, and hence the repulsive forces between the charged atoms will be maintained. The molecule appears in an extended conformation shape (dense shell).
Effect of other dendrimer concentration (Gupta, Agashe and Jain, 2007)		- The conformation of dendrimers is also affected by the concentration of other dendrimer molecules in the solution. - Increasing dendrimers concentration will decrease the intra-dendron repulsive forces due to the interactions with other dendrimer entities in the solution. As a result of that, a decrease in the repulsive forces and dendrimer molecules will possibly be existing in packed conformation (dense core).

2.6.9.3 PAMAM dendrimer - guest interaction

Many articles evaluated the nature of dendrimer-drug/bioactive molecule interactions and their potential in drug delivery (Newkome *et al.*, 1996; Kojima *et al.*, 2000; Milhem *et al.*, 2000; Choi *et al.*, 2004; Kim, Klutz and Jacobson, 2008; Pisal *et al.*, 2008).

Based on the site of conjugation, drug-dendrimer interactions can be categorized into two approaches (Figure 2.10):

a) The first approach commonly occurs for low molecular weight drugs, where the guest molecules are probably encapsulated inside the dendrimer either in the hydrophobic core or within the dendrimer shell. The interactions can either take place *via* hydrogen bonding (Newkome *et al.*, 1996) or hydrophobic interaction (Kojima *et al.*, 2000), or physical entrapment (Newkome *et al.*, 1991; Jansen, De Brabander-van den Berg and Meijer, 1994).

b) In the second approach, the guest molecules are either electrostatically or covalently connected to the dendrimer surface. The high density of surface groups such as amine and carboxyl on the dendrimer's surface will facilitate electrostatic attachment with guest molecules (Milhem *et al.*, 2000; Tripathy and Das, 2013). Covalent interaction corresponds to the connection of one or more drug molecules to the surface of the dendrimer *via* strong covalent bonds. The covalent linkage is hard to be ruptured as it needs chemical or enzymatic cleavage and therefore enables highly controlled drug release (Wolinsky and Grinstaff, 2008).

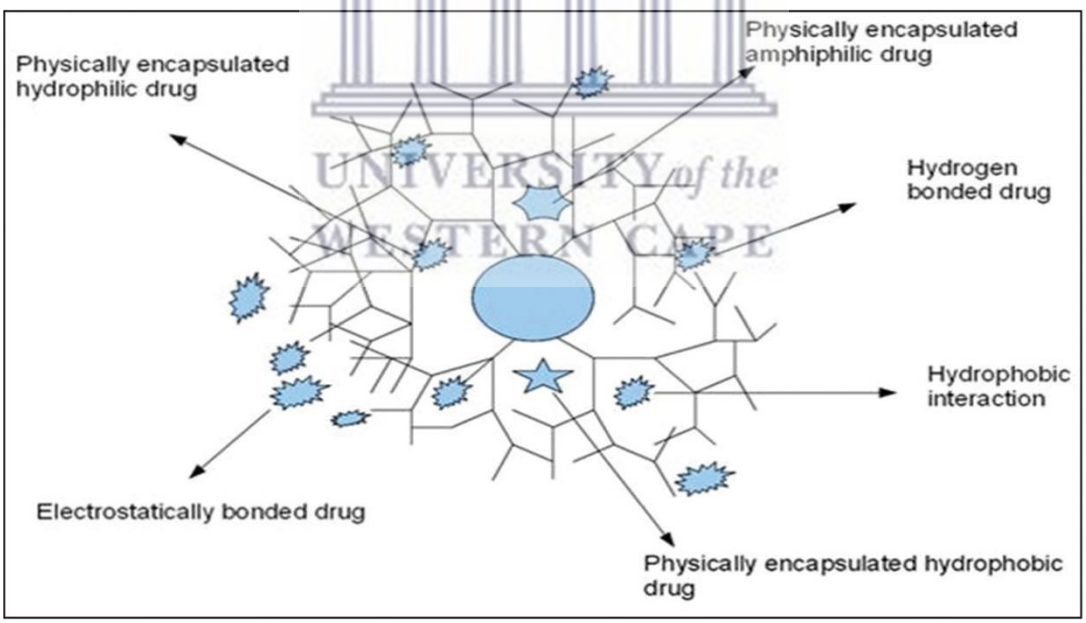

Figure 2.10 Types of PAMAM dendrimer – drug encapsulation mechanisms [Adapted from (Singh *et al.*, 2017)].

2.6.9.4 Mechanisms of drug delivery by PAMAM dendrimers

PAMAM dendrimers have been considered a promising drug delivery system that accommodates drug molecules either within the shell voids or at the outer surface. Two main approaches can attain drug delivery by PAMAM dendrimers:

a) The first approach takes place due to changes in physical circumstances such as pH and temperature. These variations could trigger a conformational change of PAMAM dendrimers (Figure 2.11), which will facilitate the release of conjugated drug molecules outside the polymer (Wang and Imae, 2004; Gupta, Agashe and Jain, 2007).

b) The second approach happens for the covalently linked molecules; the release can only occur through appropriate *in-vivo* enzymatic cleavage of the covalent bonds.

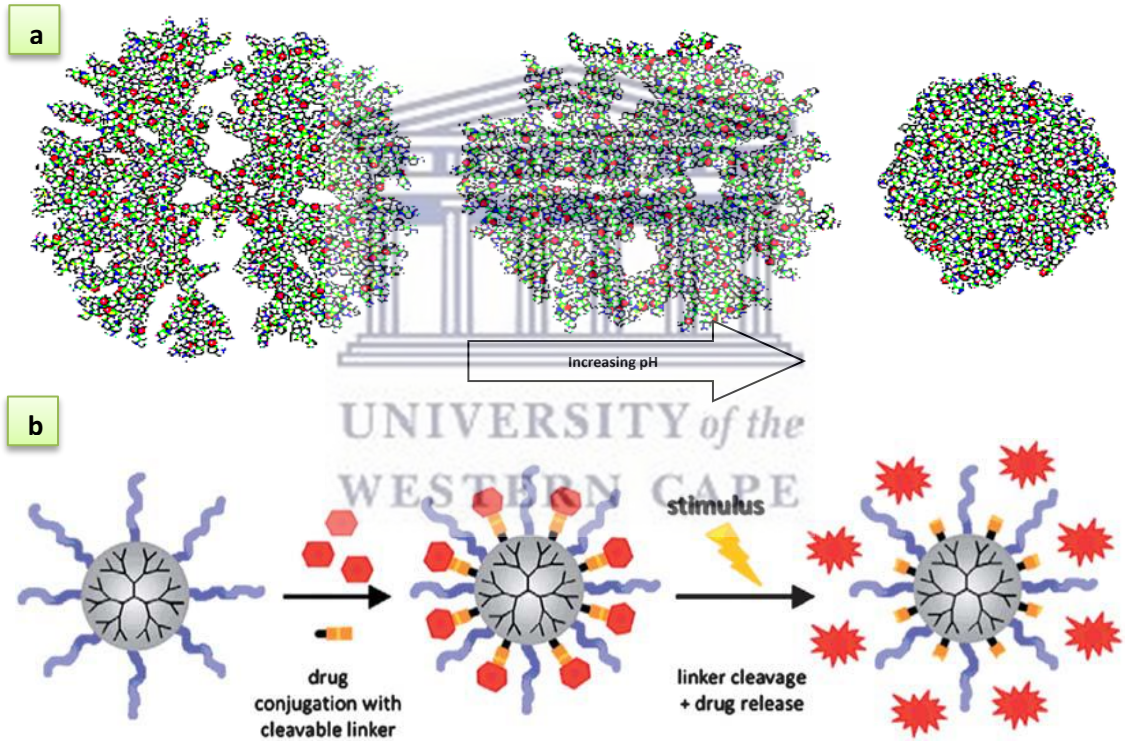

Figure 2.11 Illustration for the approaches of drug release by dendrimers (a) structure conformational changes approach (Boas and Heegaard, 2004), and (b) stimulus cleavage approach (Zhu and Shi, 2013)

2.6.9.5 PAMAM dendrimers toxicity

Regardless of the numerous advantages of PAMAM dendrimers and the promising application as a drug delivery system, toxicity issues represent the main obstacle for their

use (Duncan and Izzo, 2005). PAMAM dendrimers and particularly the cationic amino-terminated PAMAM dendrimers exhibit significant toxicity towards the biological system (cytotoxicity and hemolytic toxicity) (Duncan and Izzo, 2005). The most-reported mechanism through which the toxicity arises is through the interaction of the positively charged amino groups with the negatively charged components of the biological lipid bilayers (Malik *et al.*, 2000; Chen *et al.*, 2004; Mecke *et al.*, 2005; Kolhatkar *et al.*, 2007), that will produce permeable holes of 15 - 40 nm diameter (Figure 2.12, A). Accordingly, the decrease of membrane integrity will boost the escape of electrolytes and intracellular contents outside the cells, that leads to cell lysis as well as hemolysis (Figure 2.12) (Malik *et al.*, 2000; Chen *et al.*, 2004; Mecke *et al.*, 2005; Kolhatkar *et al.*, 2007).

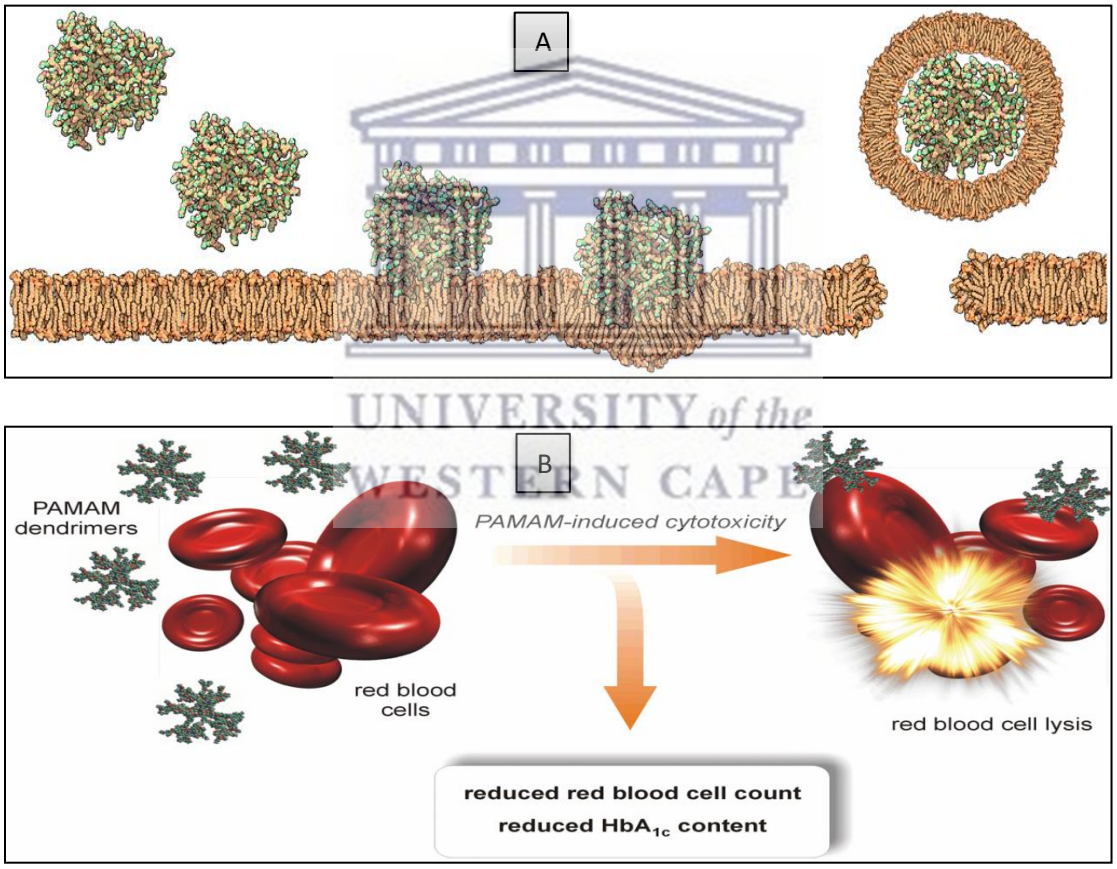

Figure 2.12 Hypothetical scheme for the interaction of dendrimer with (A) lipid bilayers membrane (Martinho *et al.*, 2014), and (B) red blood cells [Adapted from (Labieniec-Watala *et al.*, 2013)].

An alternative explanation of dendrimer toxicity was discussed by Thomas and co-workers (2009), they observed that cationic PAMAM dendrimers at therapeutically relevant concentrations induced cellular death following the lysosomal-induced apoptosis pathway (Thomas *et al.*, 2009). Thomas and co-workers detected a significant increase in the lysosomal pH after cationic PAMAM dendrimers being endocytosed (lysosomal alkalinization), and it induced mitochondria-mediated cellular death (Thomas *et al.*, 2009).

The dendrimer's toxicity is influenced by the nature of surface charges and the number of generations, a high degree of toxicity is usually observed with higher dendrimer generations (Duncan and Izzo, 2005), which is attributed to the higher charge density that accounts for lipid membrane interactions and nano-hole formations. PAMAM dendrimer with higher generations having positive or neutral surface groups shows more significant cytotoxicity and hemolysis effects compared to the lower generations which have negatively charged groups (Chen *et al.*, 2004). Therefore, dendrimer toxicity is a function of the principal surface charges as well as their densities.

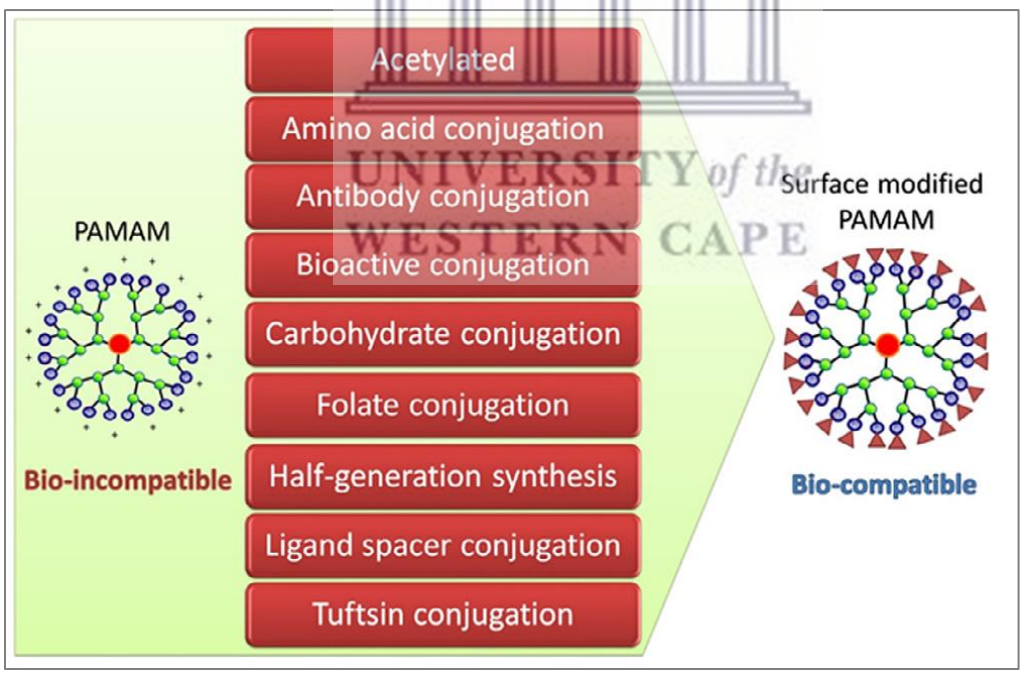

Figure 2.13 Different techniques to minimize the toxicity of PAMAM dendrimers [Adapted from (Luong *et al.*, 2016)].

The toxicity of amino-terminated PAMAM dendrimers on different cell lines and tissues was extensively reported in the literature (Jevprasesphant *et al.*, 2003; Rachaneekorn Jevprasesphant *et al.*, 2003; Jones *et al.*, 2012; Bodewein *et al.*, 2016). All findings indicated that PAMAM dendrimers, particularly cationic molecules, showed significant toxicity to various biological tissues. There are a variety of techniques that have been applied to enhance the biocompatibility of PAMAM dendrimers without losing its potential by reducing the polymer toxicity. Figure 2.13 summarizes the most common techniques to minimize the toxicity of PAMAM dendrimers in the literature.

2.7 Dendrimers and tuberculosis

The application of dendrimers as drug delivery and targeting systems for anti-tuberculosis drugs was reported in the literature (Kumar *et al.*, 2006; Bellini *et al.*, 2015; Rajabnezhad *et al.*, 2016; Dineshkumar *et al.*, 2017).

Bellini and co-workers (2015) studied the association of rifampicin on 4.0 G PAMAM dendrimer using molecular dynamics simulation techniques (Bellini *et al.*, 2015). Results indicated that about 20 rifampicin molecules could be loaded on the 4.0 G PAMAM dendrimer at neutral pH. The loaded drug molecules exhibited better stability with the dendrimer at neutral pH, while at the acidic pH, a burst release from the dendrimer was noticed. This characteristic was recommended as a useful drug delivery tool to the acidic domain of the alveolar macrophage (i.e. lysosome) within which *Mycobacterium tuberculosis* resides (Bellini *et al.*, 2015).

According to several reports indicating the toxicity of dendrimers, especially the cationic PAMAM dendrimers, researchers have manipulated the surface functional groups to decrease the positive charge density of the polymer. Surface grafting of dendrimers with poly(ethylene glycol) (PEG) chains and sugar-based molecules were the commonly reported techniques in literature (Kojima *et al.*, 2000; Pan *et al.*, 2005; Kumar *et al.*, 2006; Ly *et al.*, 2013; Dineshkumar *et al.*, 2017; Diaz *et al.*, 2018). Surface graft with sugar molecules is usually applied to reduce the charge density of dendrimer, besides targeting lectin receptors present on the membrane of alveolar macrophages (Lee *et al.*, 2016).

Kumar and co-workers (2006) developed rifampicin loaded in mannosylated 5.0 G PPI dendrimers (Kumar *et al.*, 2006). Carbohydrate molecules (mannose) were covalently connected to the surface groups to minimize the positive charges and to target the lectin receptors on macrophages. Drug-loaded dendrimers were studied to assess drug release, cytotoxicity, and macrophage uptake. *In vitro* MTT cytotoxicity assay on Vero cells showed a significant decrease in the toxicity of the drug-loaded mannosylated dendrimers, and hence enhanced the biocompatibility of the drug carrier. Release studies revealed a lower drug release at the physiological pH (7.4) compared to a burst release manner at pH (4.5). Targeting the lectin receptors on the alveolar macrophages by mannosylated dendrimers was confirmed to increase the macrophage uptake of rifampicin loaded dendrimer compared to pure rifampicin.

Another study was performed by Dineshkumar (2017) to evaluate PEGylated 5.0 G PAMAM dendrimer as a sustain-release drug delivery system for anti-tuberculosis drug, rifampicin, with minimal toxicity (Dineshkumar *et al.*, 2017). *In vitro* release studies showed prolonged drug release from PEGylated dendrimer compared to a non-PEGylated dendrimer at physiological pH (7.4). The drug was also observed in plasma for an extended period with rifampicin loaded onto PEGylated dendrimer, while the standard drug was rapidly excreted. A significant decrease in hemolytic toxicity to about 2.5% for rifampicin loaded PEGylated dendrimer was observed, while non-PEGylated dendrimer showed 11.6% to 25.3% of toxicity.

To conclude, surface-modified cationic PAMAM dendrimers are suggested as biocompatible drug delivery targeting systems.

The proposed work is different than the research work done before on PAMAM dendrimer-rifampicin by other researchers. Firstly this study highlights the G4 PAMAM dendrimer having various concentrations of PEG content as a drug carrier. Previous studies did not explore the different concentrations. Furthermore, a full physicochemical an *in-vitro* analysis of each concentration is explained. Secondly, for the mannosylated dendrimer, it is the first study to explore and develop mannosylated PAMAM dendrimer for the delivery of rifampicin to alveolar macrophages.

2.8 References

Bae, Y., Nishiyama, N., Fukushima, S., Koyama, H., Yasuhiro, M. and Kataoka, K., (2005). Preparation and biological characterization of polymeric micelle drug carriers with intracellular pH-triggered drug release property: tumor permeability, controlled subcellular drug distribution, and enhanced in vivo antitumor efficacy. *Bioconjugate chemistry*, *16*(1), pp.122-130.

Bellini, R.G., Guimarães, A.P., Pacheco, M.A., Dias, D.M., Furtado, V.R., de Alencastro, R.B. and Horta, B.A., (2015). Association of the anti-tuberculosis drug rifampicin with a PAMAM dendrimer. *Journal of Molecular Graphics and Modelling*, *60*, pp.34-42.

Boas, U. and Heegaard, P.M., (2004). Dendrimers in drug research. *Chemical Society Reviews*, *33*(1), pp.43-63.

Bodewein, L., Schmelter, F., Di Fiore, S., Hollert, H., Fischer, R. and Fenske, M., (2016). Differences in toxicity of anionic and cationic PAMAM and PPI dendrimers in zebrafish embryos and cancer cell lines. *Toxicology and applied pharmacology*, *305*, pp.83-92.

Bosman, D.A., Janssen, H.M. and Meijer, E.W., (1999). About dendrimers: structure, physical properties, and applications. *Chemical reviews*, *99*(7), pp.1665-1688.

Brothers II, H.M., Piehler, L.T. and Tomalia, D.A., (1998). Slab-gel and capillary electrophoretic characterization of polyamidoamine dendrimers. *Journal of Chromatography A*, *814*(1-2), pp.233-246.

Buhleier, E., Wehner, W. and Vögtle, F. (1978). "Cascade"- And "nonskid-chain-like" syntheses of molecular cavity topologies', *Synthesis (Germany)*, 1978(2), pp. 155–158.

Chai, M., Niu, Y., Youngs, W.J. and Rinaldi, P.L., (2001). Structure and conformation of DAB dendrimers in solution via multidimensional NMR techniques. *Journal of the American Chemical Society*, *123*(20), pp.4670-4678.

Chauhan, A.S., Jain, N.K., Diwan, P.V. and Khopade, A.J., (2004). Solubility enhancement of indomethacin with poly (amidoamine) dendrimers and targeting to inflammatory regions of arthritic rats. *Journal of drug targeting*, *12*(9-10), pp.575-583.

Chen, H.T., Neerman, M.F., Parrish, A.R. and Simanek, E.E., (2004). Cytotoxicity, hemolysis, and acute in vivo toxicity of dendrimers based on melamine, candidate vehicles for drug delivery. *Journal of the American Chemical Society*, *126*(32), pp.10044-10048.

Cheng, Y., Xu, Z., Ma, M. and Xu, T., (2008). Dendrimers as drug carriers: applications in different routes of drug administration. *Journal of pharmaceutical sciences*, *97*(1), pp.123-143.

Choi, J.S., Nam, K., Park, J.Y., Kim, J.B., Lee, J.K. and Park, J.S., (2004). Enhanced transfection efficiency of PAMAM dendrimer by surface modification with L-arginine. *Journal of controlled release*, *99*(3), pp.445-456.

Dandliker, P.J., Diederich, F., Zingg, A., Gisselbrecht, J.P., Gross, M., Louati, A. and Sanford, E., (1997). Dendrimers with porphyrin cores: synthetic models for globular heme proteins. *Helvetica chimica acta*, *80*(6), pp.1773-1801.

Devarakonda, B., Li, N. and de Villiers, M.M., (2005). Effect of polyamidoamine (PAMAM) dendrimers on the in vitro release of water-insoluble nifedipine from aqueous gels. *AAPS*

PharmSciTech, *6*(3), pp.E504-E512.

Diaz, C., Guzmán, J., Jiménez, V.A. and Alderete, J.B., (2018). Partially PEGylated PAMAM dendrimers as solubility enhancers of Silybin. *Pharmaceutical development and technology*, *23*(7), pp.689-696.

Dineshkumar, P., Panneerselvam, T., Deepti Brundavani, K., Selvaraj, K. and Vijayaraj Kumar, P., (2017). Formulation of Rifampicin Loaded PEGylated 5.0 G EDA-PAMAM Dendrimers as Effective Long-Duration Release Drug Carriers. *Current Drug Therapy*, *12*(2), pp.115-126.

Duncan, R. and Izzo, L., (2005). Dendrimer biocompatibility and toxicity. *Advanced drug delivery reviews*, *57*(15), pp.2215-2237.

Eichman, J.D., Bielinska, A.U., Kukowska-Latallo, J.F. and Baker Jr, J.R., (2000). The use of PAMAM dendrimers in the efficient transfer of genetic material into cells. *Pharmaceutical science & technology today*, *3*(7), pp.232-245.

El-Sayed, M., Kiani, M.F., Naimark, M.D., Hikal, A.H. and Ghandehari, H., (2001). Extravasation of poly (amidoamine) (PAMAM) dendrimers across microvascular network endothelium. *Pharmaceutical research*, *18*(1), pp.23-28.

El-Sayed, M., Ginski, M., Rhodes, C. and Ghandehari, H., (2002). Transepithelial transport of poly (amidoamine) dendrimers across Caco-2 cell monolayers. *Journal of Controlled Release*, *81*(3), pp.355-365.

Ertürk, A.S., Gürbüz, M.U. and Tülü, M., (2017). The effect of PAMAM dendrimer concentration, generation size and surface functional group on the aqueous solubility of candesartan cilexetil. *Pharmaceutical development and technology*, *22*(1), pp.111-121.

Esfand, R. and Tomalia, D.A., (2001). Poly (amidoamine)(PAMAM) dendrimers: from biomimicry to drug delivery and biomedical applications. *Drug discovery today*, *6*(8), pp.427-436.

Flory, P. J. (1941). Molecular Size Distribution in Three Dimensional Polymers. I. Gelation. *Journal of the American Chemical Society*, 63(11), pp. 3083–3090.

Fréchet, J.M., Hawker, C.J., Gitsov, I. and Leon, J.W., (1996). Dendrimers and hyperbranched polymers: two families of three-dimensional macromolecules with similar but clearly distinct properties. *Journal of Macromolecular Science, Part A: Pure and Applied Chemistry*, *33*(10), pp.1399-1425.

Galia, E., Nicolaides, E., Hörter, D., Löbenberg, R., Reppas, C. and Dressman, J.B., (1998). Evaluation of various dissolution media for predicting in vivo performance of class I and II drugs. *Pharmaceutical research*, *15*(5), pp.698-705.

de Gennes, P.G. and Hervet, H., (1983). Statistics of «starburst» polymers. *Journal de Physique Lettres*, *44*(9), pp.351-360.

Grayson, S.M. and Frechet, J.M., (2001). Convergent dendrons and dendrimers: from synthesis to applications. *Chemical Reviews*, *101*(12), pp.3819-3868.

Gupta, U., Agashe, H.B. and Jain, N.K., (2007). Polypropylene imine dendrimer mediated solubility enhancement: effect of pH and functional groups of hydrophobes. *J Pharm Pharm Sci*, *10*(3), pp.358-367.

Hawker, C. and Fréchet, J.M., (1990). A new convergent approach to monodisperse dendritic macromolecules. *Journal of the Chemical Society, Chemical Communications*, (15), pp.1010-1013.

Hawker, C.J., (1999). Dendritic and hyperbranched macromolecules—precisely controlled macromolecular architectures. In *Macromolecular Architectures*, 147, pp. 113–160. Springer, Berlin, Heidelberg.

Hawker, C.J. and Frechet, J.M., (1990). Preparation of polymers with controlled molecular architecture. A new convergent approach to dendritic macromolecules. *Journal of the American Chemical Society*, *112*(21), pp.7638-7647.

Hawker, C.J., Lee, R. and Fréchet, J.M.J., (1991). One-step synthesis of hyperbranched dendritic polyesters. *Journal of the American Chemical Society*, *113*(12), pp.4583-4588.

Hecht, S. and Fréchet, J.M., (2001). Dendritic encapsulation of function: applying nature's site isolation principle from biomimetics to materials science. *Angewandte Chemie International Edition*, *40*(1), pp.74-91.

Hodge, P., (1993). Polymer science branches out. *Nature*, *362*(6415), pp.18-19.

Hu, J., Hu, K. and Cheng, Y., (2016). Tailoring the dendrimer core for efficient gene delivery. *Acta biomaterialia*, *35*, pp.1-11.

Hudde, T., Rayner, S.A., Comer, R.M., Weber, M., Isaacs, J.D., Waldmann, H., Larkin, D.F.P. and George, A.J.T., (1999). Activated polyamidoamine dendrimers, a non-viral vector for gene transfer to the corneal endothelium. *Gene therapy*, *6*(5), pp.939-943.

Islam, M.T., Majoros, I.J. and Baker Jr, J.R., (2005). HPLC analysis of PAMAM dendrimer based multifunctional devices. *Journal of Chromatography B*, *822*(1-2), pp.21-26.

Jansen, J.F., De Brabander-van den Berg, E. M. M and Meijer, E.W., (1994). Encapsulation of guest molecules into a dendritic box. *Science*, *266*(5188), pp.1226-1229.

Jevprasesphant, R., Penny, J., Attwood, D., McKeown, N.B. and D'emanuele, A., (2003). Engineering of dendrimer surfaces to enhance transepithelial transport and reduce cytotoxicity. *Pharmaceutical Research*, *20*(10), pp.1543-1550.

Jevprasesphant, R., Penny, J., Jalal, R., Attwood, D., McKeown, N.B. and D'emanuele, A., (2003). The influence of surface modification on the cytotoxicity of PAMAM dendrimers. *International journal of pharmaceutics*, *252*(1-2), pp.263-266.

Jiang, D.L. and Aida, T., (1996). A dendritic iron porphyrin as a novel haemoprotein mimic: effects of the dendrimer cage on dioxygen-binding activity. *Chemical Communications*, (13), pp.1523-1524.

Jones, C.F., Campbell, R.A., Franks, Z., Gibson, C.C., Thiagarajan, G., Vieira-de-Abreu, A., Sukavaneshvar, S., Mohammad, S.F., Li, D.Y., Ghandehari, H. and Weyrich, A.S., (2012). Cationic PAMAM dendrimers disrupt key platelet functions. *Molecular pharmaceutics*, *9*(6), pp.1599-1611.

Kesharwani, P., Banerjee, S., Gupta, U., Amin, M.C.I.M., Padhye, S., Sarkar, F.H. and Iyer, A.K., (2015). PAMAM dendrimers as promising nanocarriers for RNAi therapeutics. *Materials Today*, *18*(10), pp.565-572.

Kesharwani, P., Jain, K. and Jain, N.K., (2014). Dendrimer as nanocarrier for drug delivery. *Progress in Polymer Science*, *39*(2), pp.268-307.

Kim, Y.H. and Webster, O.W., (1990). Water soluble hyperbranched polyphenylene:" a unimolecular micelle?". *Journal of the American Chemical Society*, *112*(11), pp.4592-4593.

Kim, Y., Klutz, A.M. and Jacobson, K.A., (2008). Systematic investigation of polyamidoamine dendrimers surface-modified with poly (ethylene glycol) for drug delivery applications: synthesis, characterization, and evaluation of cytotoxicity. *Bioconjugate chemistry*, *19*(8), pp.1660-1672.

Klajnert, B. and Bryszewska, M., (2001). Dendrimers: properties and applications. *Acta biochimica polonica*, *48*(1), pp.199-208.

Kojima, C., Kono, K., Maruyama, K. and Takagishi, T., (2000). Synthesis of polyamidoamine dendrimers having poly (ethylene glycol) grafts and their ability to encapsulate anticancer drugs. *Bioconjugate chemistry*, *11*(6), pp.910-917.

Kolhatkar, R.B., Kitchens, K.M., Swaan, P.W. and Ghandehari, H., (2007). Surface acetylation of polyamidoamine (PAMAM) dendrimers decreases cytotoxicity while maintaining membrane permeability. *Bioconjugate chemistry*, *18*(6), pp.2054-2060.

Kolhe, P., Khandare, J., Pillai, O., Kannan, S., Lieh-Lai, M. and Kannan, R.M., (2006). Preparation, cellular transport, and activity of polyamidoamine-based dendritic nanodevices with a high drug payload. *Biomaterials*, *27*(4), pp.660-669.

Konda, S.D., Aref, M., Wang, S., Brechbiel, M. and Wiener, E.C., (2001). Specific targeting of folate–dendrimer MRI contrast agents to the high affinity folate receptor expressed in ovarian tumor xenografts. *Magnetic resonance materials in physics, Biology and Medicine*, *12*(2-3),

Koper, G.J.M., Van Genderen, M.H.P., Elissen-Roman, C., Baars, M.W.P.L., Meijer, E.W. and Borkovec, M., (1997). Protonation mechanism of poly (propylene imine) dendrimers and some associated oligo amines. *Journal of the American Chemical Society*, *119*(28), pp.6512-6521.

Kumar, P.V., Asthana, A., Dutta, T. and Jain, N.K., (2006). Intracellular macrophage uptake of rifampicin loaded mannosylated dendrimers. *Journal of drug targeting*, *14*(8), pp.546-556.

Labieniec-Watala, M., Karolczak, K., Siewiera, K. and Watala, C., (2013). The Janus face of PAMAM dendrimers used to potentially cure nonenzymatic modifications of biomacromolecules in metabolic disorders—A critical review of the pros and cons. *Molecules*, *18*(11), pp.13769-13811.

Lee, W.H., Loo, C.Y., Young, P.M. and Traini, D., (2016). The Potential of Nanotechnology for Tuberculosis Treatment.

Luong, D., Kesharwani, P., Deshmukh, R., Amin, M.C.I.M., Gupta, U., Greish, K. and Iyer, A.K., (2016). PEGylated PAMAM dendrimers: Enhancing efficacy and mitigating toxicity for effective anticancer drug and gene delivery. *Acta biomaterialia*, *43*, pp.14-29.

Ly, T.U., Tran, N.Q., Hoang, T.K.D., Phan, K.N., Truong, H.N. and Nguyen, C.K., (2013). Pegylated dendrimer and its effect in fluorouracil loading and release for enhancing antitumor activity. *Journal of biomedical nanotechnology*, *9*(2), pp.213-220.

Maiti, P.K., Çağın, T., Wang, G. and Goddard, W.A., (2004). Structure of PAMAM dendrimers: Generations 1 through 11. *Macromolecules*, *37*(16), pp.6236-6254.

Malik, N., Wiwattanapatapee, R., Klopsch, R., Lorenz, K., Frey, H., Weener, J. W., Meijer, E. W., Paulus, W., and Duncan, R. (2000). Dendrimers: relationship between structure and biocompatibility in vitro, and preliminary studies on the biodistribution of 125I-labelled polyamidoamine dendrimers in vivo. *Journal of controlled release*, *65*(1-2), 133–148.

Martinho, N., Florindo, H., Silva, L., Brocchini, S., Zloh, M. and Barata, T., (2014). Molecular modeling to study dendrimers for biomedical applications. *Molecules*, *19*(12), pp.20424-20467.

Mecke, A., Lee, D.K., Ramamoorthy, A., Orr, B.G. and Banaszak Holl, M.M., (2005). Synthetic and natural polycationic polymer nanoparticles interact selectively with fluid-phase domains of DMPC lipid bilayers. *Langmuir*, *21*(19), pp.8588-8590.

Milhem, O.M., Myles, C., McKeown, N.B., Attwood, D. and D'Emanuele, A., (2000). Polyamidoamine Starburst® dendrimers as solubility enhancers. *International journal of pharmaceutics*, *197*(1-2), pp.239-241.

Müller, R., Laschober, C., Szymanski, W.W. and Allmaier, G., (2007). Determination of molecular weight, particle size, and density of high number generation PAMAM dendrimers using MALDI− TOF− MS and nES− GEMMA. *Macromolecules*, *40*(15), pp. 5599-5605.

Newkome, G.R., Yao, Z., Baker, G.R. and Gupta, V.K., (1985). Micelles. Part 1. Cascade molecules: a new approach to micelles. A [27]-arborol. *The Journal of Organic Chemistry*, *50*(11), pp.2003-2004.

Newkome, G.R., Moorefield, C.N., Baker, G.R., Saunders, M.J. and Grossman, S.H., (1991). Unimolecular micelles. *Angewandte Chemie International Edition in English*, *30*(9), pp.1178-1180.

Newkome, G.R., Woosley, B.D., He, E., Moorefield, C.N., Güther, R., Baker, G.R., Escamilla, G.H., Merrill, J. and Luftmann, H., (1996). Supramolecular chemistry of flexible, dendritic-based structures employing molecular recognition. *Chemical Communications*, (24), pp.2737-2738.

Ong, K.K., Jenkins, A.L., Cheng, R., Tomalia, D.A., Durst, H.D., Jensen, J.L., Emanuel, P.A., Swim, C.R. and Yin, R., (2001). Dendrimer enhanced immunosensors for biological detection. *Analytica chimica acta*, *444*(1), pp.143-148.

Pan, G., Lemmouchi, Y., Akala, E.O. and Bakare, O., (2005). Studies on PEGylated and drug-loaded PAMAM dendrimers. *Journal of bioactive and compatible polymers*, *20*(1), pp.113-128.

Patri, A.K., Kukowska-Latallo, J.F. and Baker Jr, J.R., (2005). Targeted drug delivery with dendrimers: comparison of the release kinetics of covalently conjugated drug and non-covalent drug inclusion complex. *Advanced drug delivery reviews*, *57*(15), pp.2203-2214.

Pisal, D.S., Yellepeddi, V.K., Kumar, A., Kaushik, R.S., Hildreth, M.B., Guan, X. and Palakurthi, S., (2008). Permeability of surface-modified polyamidoamine (PAMAM) dendrimers across Caco-2 cell monolayers. *International journal of pharmaceutics*, *350*(1-2), pp.113-121.

Purohit, G., Sakthivel, T. and Florence, A.T., (2001). Interaction of cationic partial dendrimers with charged and neutral liposomes. *International journal of pharmaceutics*, *214*(1-2), pp.71-76.

Rajabnezhad, S., Casettari, L., Lam, J.K., Nomani, A., Torkamani, M.R., Palmieri, G.F., Rajabnejad, M.R. and Darbandi, M.A., (2016). Pulmonary delivery of rifampicin microspheres using lower generation polyamidoamine dendrimers as a carrier. *Powder Technology*, *291*, pp.366-

374.

Roberts, J.C., Bhalgat, M.K. and Zera, R.T., (1996). Preliminary biological evaluation of polyamidoamine (PAMAM) Starburst™ dendrimers. *Journal of Biomedical Materials Research: An Official Journal of The Society for Biomaterials and The Japanese Society for Biomaterials*, *30*(1), pp.53-65.

Rupal, J., Kaushal, J., Mallikarjuna, S.C. and Dipti, P., (2009). Preparation and evaluation of solid dispersions of aceclofenac. *Int J Pharm Sci Drug Res*, *1(1)*, pp.32-35.

Singh, M.P., Gautam, S.P., Gupta, A.K., Gupta, R., and Gautam, T., (2017). Dendrimers: A Glimpse of History, Current Progress, and Applications. In *Drug Delivery Approaches and Nanosystems, Volume 1* (pp. 213-236). Apple Academic Press.

Singh, P., Moll 3rd, F., Lin, S.H., Ferzli, C., Yu, K.S., Koski, R.K., Saul, R.G. and Cronin, P., (1994). Starburst dendrimers: enhanced performance and flexibility for immunoassays. *Clinical chemistry*, *40*(9), pp.1845-1849.

Singh, P., MOLL III, F., Lin, S.H. and Ferzli, C., (1996). Starburst dendrimers: a novel matrix for multifunctional reagents in immunoassays. *Clinical chemistry (Baltimore, Md.)*, *42*(9), pp.1567-1569.

Singh, P., (1998). Terminal groups in starburst dendrimers: activation and reactions with proteins. *Bioconjugate chemistry*, *9*(1), pp.54-63.

Singh, S. *et al.* (2009) 'Dendrimer a versatile polymer in drug delivery', *Asian Journal of Pharmaceutics*, pp. 178–187. doi: 10.4103/0973-8398.56295.

Singh, S.K., Lohiya, G.K., Limburkar, P.P., Dharbale, N.B. and Mourya, V.K., (2009). Dendrimer a versatile polymer in drug delivery. *Asian Journal of Pharmaceutics*, *3*(3), pp. 178–187.

Svenson, S., (2009). Dendrimers as versatile platform in drug delivery applications. *European Journal of Pharmaceutics and Biopharmaceutics*, *71*(3), pp.445-462.

Svenson, S. and Tomalia, D.A., (2005). Dendrimers in biomedical applications—reflections on the field. *Advanced drug delivery reviews*, *57(15)*, pp.2106-2129.

Tawfik, M.A., Tadros, M.I. and Mohamed, M.I., (2019). Polyamidoamine (PAMAM) dendrimers as potential release modulators and oral bioavailability enhancers of vardenafil hydrochloride. *Pharmaceutical development and technology*, *24*(3), pp.293-302.

Thomas, T.P., Majoros, I., Kotlyar, A., Mullen, D., Banaszak Holl, M.M. and Baker Jr, J.R., (2009). Cationic poly (amidoamine) dendrimer induces lysosomal apoptotic pathway at therapeutically relevant concentrations. *Biomacromolecules*, *10*(12), pp.3207-3214.

Tomalia, D.A., Dewald, J., Hall, M., Martin, S. and Smith, P., (1984). Reprints of the 1st SPSJ International Polymer Conference. *Soc Polym Sci*, *65*.

Tomalia, D.A., Baker, H., Dewald, J., Hall, M., Kallos, G., Martin, S., Roeck, J., Ryder, J. and Smith, P., (1985). A new class of polymers: starburst-dendritic macromolecules. *Polymer journal*, *17*(1), pp.117-132.

Tomalia, D.A., Baker, H., Dewald, J., Hall, M., Kallos, G., Martin, S., Roeck, J., Ryder, J. and Smith, P., (1986). Dendritic macromolecules: synthesis of starburst

dendrimers. *Macromolecules*, *19*(9), pp.2466-2468.

Tomalia, D.A., (1995). Dendrimer molecules. *Scientific American*, *272*(5), pp.62-66.

Tomalia, D.A., 2001. Architecturally driven properties based on the dendritic state. *High Performance Polymers*, *13*(2), pp.S1-S10.

Tomalia, D.A. and Fréchet, J.M., (2002). Discovery of dendrimers and dendritic polymers: a brief historical perspective. *Journal of Polymer Science Part A: Polymer Chemistry*, *40*(16), pp.2719-2728.

Tomalia, D.A., Naylor, A.M. and Goddard III, W.A., (1990). Starburst dendrimers: molecular-level control of size, shape, surface chemistry, topology, and flexibility from atoms to macroscopic matter. *Angewandte Chemie International Edition in English*, *29*(2), pp.138-175.

Tripathy, S. and Das, M.K., (2013). Dendrimers and their applications as novel drug delivery carriers. *J Appl Pharm Sci*, *3*(9), pp.142-149.

Twyman, L.J., Beezer, A.E., Esfand, R., Hardy, M.J. and Mitchell, J.C., (1999). The synthesis of water soluble dendrimers, and their application as possible drug delivery systems. *Tetrahedron Letters*, *40*(9), pp.1743-1746.

Wang, D. and Imae, T., (2004). Fluorescence emission from dendrimers and its pH dependence. *Journal of the American Chemical Society*, *126*(41), pp.13204-13205.

Wang, M., Gan, D. and Wooley, K.L., (2001). Linear and hyperbranched poly (silyl ester) s: Synthesis via cross-dehydrocoupling-based polymerization, hydrolytic degradation properties, and morphological analysis by atomic force microscopy. *Macromolecules*, *34*(10), pp.3215-3223.

Weyermann, P., Gisselbrecht, J.P., Boudon, C., Diederich, F. and Gross, M., (1999). Dendritic iron porphyrins with tethered axial ligands: new model compounds for cytochromes. *Angewandte Chemie International Edition*, *38*(21), pp.3215-3219.

Wolinsky, J.B. and Grinstaff, M.W., (2008). Therapeutic and diagnostic applications of dendrimers for cancer treatment. *Advanced drug delivery reviews*, *60*(9), pp.1037-1055.

Yang, H. and Kao, W.J., (2006). Dendrimers for pharmaceutical and biomedical applications. *Journal of biomaterials science, polymer edition*, *17*(1-2), pp.3-19.

Yang, H., Morris, J.J. and Lopina, S.T., (2004). Polyethylene glycol–polyamidoamine dendritic micelle as solubility enhancer and the effect of the length of polyethylene glycol arms on the solubility of pyrene in water. *Journal of colloid and interface science*, *273*(1), pp.148-154.

Zhuo, R.X., Du, B. and Lu, Z.R., (1999). In vitro release of 5-fluorouracil with cyclic core dendritic polymer. *Journal of controlled release*, *57*(3), pp.249-257.

Zhu, J. and Shi, X., 2013. Dendrimer-based nanodevices for targeted drug delivery applications. *Journal of Materials Chemistry B*, *1*(34), pp.4199-4211.

Chapter 3

Synthesis and characterization of rifampicin loaded PEGylated and non-PEGylated 4.0 G PAMAM dendrimers

3.1 Introduction

This chapter gives a detailed account of the materials, methods, and a clear description of the analytical techniques applied to synthesize and characterize rifampicin loaded in PEGylated and non-PEGylated 4.0 G PAMAM dendrimers. Also, this chapter displays the results achieved from various surface-modified dendrimer formulations, with discussion and conclusion.

3.2 Review of the literature

3.2.1 PEGylation

Poly(ethylene glycol) (PEG) is a safe, non-antigenic, non-immunogenic, extremely water-soluble and FDA approved polymer (Veronese and Pasut, 2005). PEGylation is the covalent conjugation of PEG chains to nano-drug delivery systems, proteins, peptides, non-peptide molecules, and bioactives (Thakur *et al.*, 2015). The word PEGylation was firstly used by Davies and Abucvhowsky in 1970 in the case of catalase and albumin (Abuchowski *et al.*, 1977), this technique allowed them to adapt the enzyme while maintaining its activity.

Generally, polymeric nano-carriers are employed to allow proper drug delivery to the site of action with desired release properties. The carrier must be biodegradable, biocompatible, and non-toxic (Thakur *et al.*, 2015). Dendrimers and in particular cationic groups such as PAMAM dendrimers are hampered by considerable *in vitro* cytotoxicity and hemolytic effects (Malik *et al*., 2000; Chen *et al*., 2004; Mecke *et al*., 2005; Kolhatkar *et al*., 2007). The toxicity can be significantly minimized by surface modification of peripheral

positively charged groups; one of these techniques is surface amine PEGylation (Jevprasesphant *et al.*, 2003). Beside toxicity, PEGylation is also applied to improve the biodistribution and pharmacokinetic properties such as the circulating time and solubility of the dendrimer system (Quintana *et al.*, 2002), as well as, to enhance drug loading capacity (Liu, Kono and Fréchet, 1999), and to control drug release (Männistö *et al.*, 2002).

Alongside dendrimers, a variety of nanocarriers have also been PEGylated for similar reasons of enhancing safety and efficacy, such as liposomes, carbon nanotubes, quantum dot, and polymeric nanoparticles (Jevprasesphant *et al.*, 2003; Puskas, Seo and Sen, 2011; Shim and Kwon, 2012).

Conjugation of PEG can be achieved by a variety of strategies that can be summarized in Figure 3.1, in which PEG-amino functionality conjugation represents the most common approach (Thakur *et al.*, 2015).

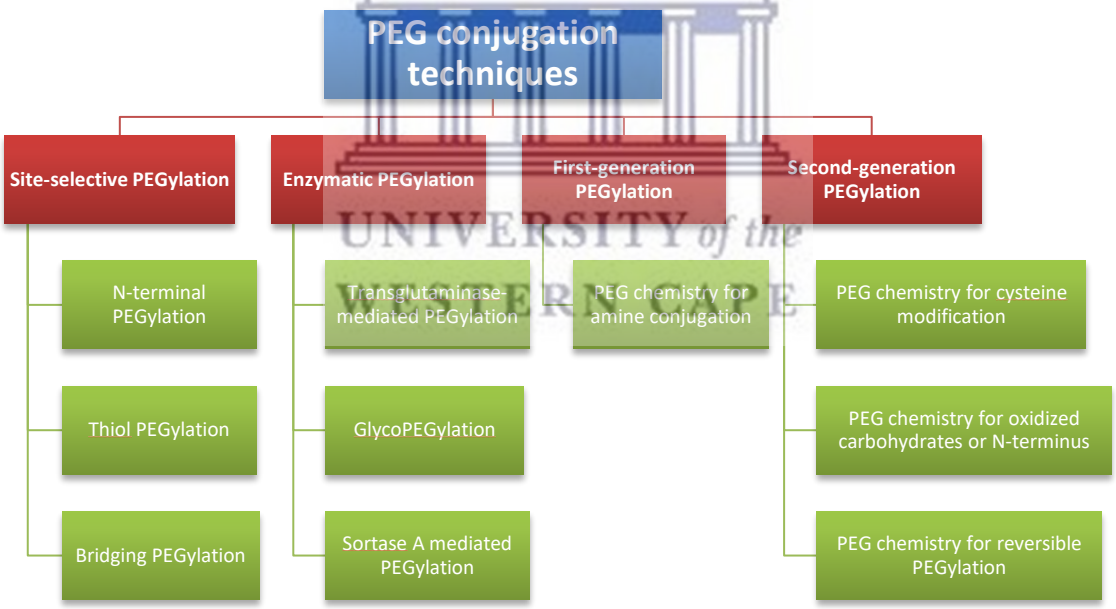

Figure 3.1 Outline of PEGylation techniques [adapted from (Veronese and Pasut, 2005; Damodaran and Fee, 2010)].

Since the PEG chain has a two side hydroxyl group, which might facilitate cross-linking with various molecules in the solution *via* a covalent bond, methoxy poly(ethylene glycol) (mPEG) is usually advised to be used in PEGylation (Luong *et al.*, 2016). One of the

suggested methods to synthesize PEGylated PAMAM dendrimer is *via* Michael's addition which motivates PEG chain conjugation (Figure 3.2). This is mostly done by adding 4-nitrophenyl chloroformate (4-NPC) and triethylamine to activate mPEG polymer (Kojima *et al.*, 2000; Lim and Tam, 2011).

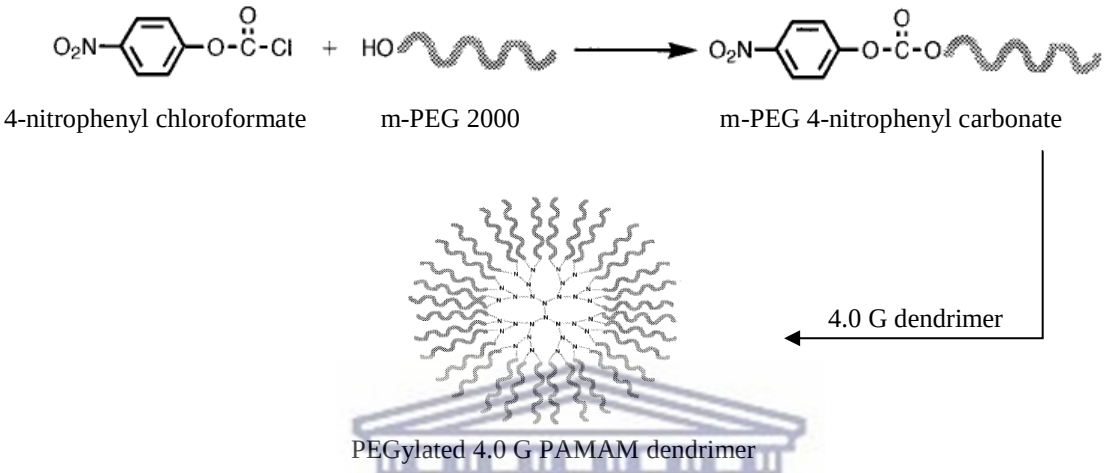

Figure 3.2 Synthesis of PEGylated 4.0 G PAMAM dendrimer [adapted from (Kojima *et al.*, 2000)].

3.2.2 Approaches of dendrimer-PEG conjugate

Based on the location of PEG chains at the dendrimer structure, the PEGylated dendrimer can be categorized into five groups: surface conjugation, dendrimer with PEG core, dendrimer with PEG as a branching monomer unit, drug/diagnostic agents conjugated PEGylated dendrimer, and ligand PEGylated dendrimer (Thakur *et al.*, 2015) (Figure 3.3).

a) Surface conjugation

Surface conjugation also known as conventional PEGylation is the exterior attachment of one or more PEG chains to the positively charged amino groups. Surface conjugation represents the most common style of dendrimer PEGylation (Thakur *et al.*, 2015). It has been widely reported in the literature to improve the carrier safety and enhance drug efficacy (Kojima *et al.*, 2000; Jevprasesphant *et al.*, 2003; Pan *et al.*, 2005; Vijayaraj Kumar *et al.*, 2007; Dineshkumar *et al.*, 2017; Diaz *et al.*, 2018b).

b) Dendrimer with PEG core

In this approach, PEG represents the core from which the dendrimer growth process takes place (Thakur *et al.*, 2015). Bhadra *et al.* (2005) synthesized a dendrimer with PEG core to improve the solubility and release characteristic of an anti-malarial drug, artemether (Bhadra, Bhadra and Jain, 2005).

c) Dendrimer with PEG as a branching monomer unit

In this approach, the branching monomer units of dendrimer are replaced by PEG chains. Ooya, Lee, and Park (2003) synthesized star-shaped graft polymers consisting of PEG-400 chains to enhance the solubility and the release characteristics of anticancer drug, paclitaxel (Ooya, Lee and Park, 2003).

d) Drug (bioactive)/diagnostic agents conjugated PEGylated dendrimer

In this category, the drug/diagnostic agents and PEG chains are attached to the dendrimer peripheral. It is a modified form of conventional PEGylated dendrimer in which PEG chains act as connectors between dendrimer and drug molecules. Reports showed that the PEGylation of dendrimer could affect drug loading and the release properties of the conjugated drug/diagnostic agents, due to the generated steric hindrance over the dendrimer structure (Liu, Kono and Fréchet, 1999; Yang and Lopina, 2003; Thakur *et al.*, 2015).

e) Ligand PEGylated dendrimer

This approach is an advanced delivery system in which ligand and PEG chains are attached to the dendrimer functionality surface to improve the targeting potential and biopharmaceutical characteristics of the loaded drugs. Sideratou *et al.* (Sideratou *et al.*, 2010) and Singh *et al.* (Singh *et al.*, 2008) synthesized folate conjugated dendrimers to target anticancer drugs, etoposide and 5-fluorouracil, respectively. Results indicated better targeting of folate receptors compared to the drug-loaded pure dendrimer. Thus, improving the bioavailability, therapeutic efficacy, solubility, loading capacity, and decreasing the toxicity.

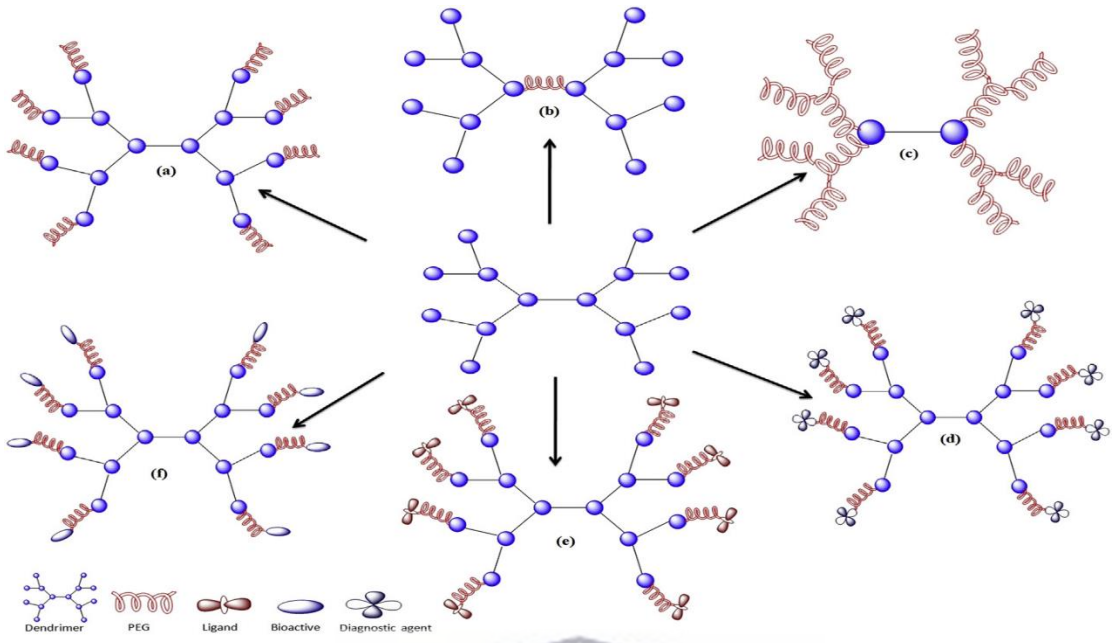

Figure 3.3 The main types of PEG-dendrimer conjugate [adapted from (Thakur *et al.*, 2015)]. (a) Surface-conjugation PEGylated dendrimer, (b) Dendrimer having PEG core, (c) Dendrimer with PEG as a branching monomer unit, (d) PEGylated-diagnostic agent conjugated dendrimer, (e) PEGylated-ligand conjugated dendrimer, and (f) PEGylated-bioactive agent (drug) conjugated dendrimer.

3.2.3 PEG-PAMAM dendrimer conjugate and drug delivery

The incorporation of PEG chains to the dendrimer scaffold will provide additional features to the conjugate, such as the following:

i. Solubility improvement

One of the beneficial features of using PEGylated PAMAM dendrimer is to enhance the solubility of poorly water-soluble drugs, to improve their bioavailability. For example, one of the effective anticancer drugs, methotrexate is characterized by low water solubility. Various techniques were implemented to enhance its solubility, such as particle size reduction, cyclodextrin inclusion, and micellar system. However, drawbacks such as high cost, instability, and toxicity hampered its use (Thakur *et al.*, 2015). Recently, using PEGylated PAMAM dendrimer not only improved the solubility of methotrexate but also enabled controlled/sustained release from the dendrimer scaffold due to dense PEG chains over the dendrimer system (Tekade *et al.*, 2009).

PEGylation could enhance the solubility of hydrophobic drugs by solubilizing drug molecules within PEG chains in addition to the encapsulation inside the dendrimer core. The use of PEGylated PAMAM dendrimer as a solubility enhancer for therapeutic drugs has been widely reported (Kojima *et al.*, 2000; Pan *et al.*, 2005; Zhu *et al.*, 2010b; Ly *et al.*, 2013; Dineshkumar *et al.*, 2017; Diaz *et al.*, 2018b).

ii. Drug loading enhancement

Different therapeutic and diagnostic agents have been conjugated with dendrimers either *via* covalent (Wolinsky and Grinstaff, 2008) or non-covalent interactions such as hydrophobic interaction (Kojima *et al.*, 2000) and electrostatic interaction (Milhem *et al.*, 2000; Thakur *et al.*, 2015). Numerous studies have reported that PEGylation enhances drug loading by offering a further platform for interaction at the dendrimer surface (Kojima *et al.*, 2000; Sideratou, Tsiourvas and Paleos, 2001; Thakur *et al.*, 2015).

iii. Physicochemical properties

PEGylation alters some of the dendrimer's physicochemical properties such as size, polydispersity index (PDI), and zeta potential (ZP) (Motoyama *et al.*, 2012; Peng *et al.*, 2012). Since the physicochemical properties such as size and ZP are essential factors for managing the particle biodistribution (Okuda *et al.*, 2006), PEGylation can, therefore, influence the biodistribution properties of dendrimer nanoparticles.

iv. Drug bioavailability

Surface modification of dendrimers has a high impact on enhancing the therapeutic efficiency of drugs through site targeting, control release, and reduce toxicity. Site-specific delivery *via* linking targeting ligands on the dendrimer surface will offer high chances of accumulation at the site of action, and bioavailability improvement will be expected (Satija, Gupta and Jain, 2007). Moreover, PEGylation and other surface engineering techniques are considered to enhance the fate of circulating the drug delivery system and improve its bioavailability (Patri *et al.*, 2004; Nam *et al.*, 2009).

v. PEGylation and immunogenicity

PEG is one of the most common material that has been used in the field of drug delivery due to its chemical and biological inertness. As indicated that PEGylation was used to

reduce the immunogenicity of some biopharmaceuticals and proteins (Gefen *et al.*, 2013; Turecek *et al.*, 2016), therefore conjugation of PEG to drug carriers (such as dendrimers) are recommended to reduce the possibility of any immunological reaction and enhance its biocompatibility (Hoffman, 2016).

vi. PEGylation and dendrimer toxicity

Regardless of the various potential advantages of dendrimers and their promising application in drug delivery, toxicity issues represent the main difficulty for their use (Luong *et al.*, 2016).

Cytotoxicity is believed to be a function of the surface charges as well as their densities (Wang *et al.*, 2009). This probably arises as a consequence of the interaction of the positively charged surface amines with the negatively charged components of the biological lipid bilayer membrane (Leroueil *et al.*, 2007, 2008). The dendrimer-biological membrane interaction is capable of forming permeable holes of 15 - 40 nm in diameter (Prajapati *et al.*, 2009; Kesharwani *et al.*, 2011). This opening will decrease the membrane integrity and therefore enhance the escape of electrolytes and intracellular contents out the cells, that leads to cell lysis as well as hemolysis (Malik *et al.*, 2000; Chen *et al.*, 2004; Mecke *et al.*, 2005; Kolhatkar *et al.*, 2007).

Surface modification of dendrimer peripheral amines by PEG is likely to decrease/shield the surface positive charges and hence reduce their toxicity (Jevprasesphant *et al.*, 2003), in addition to improving the efficacy of encapsulated drugs (Kojima *et al.*, 2000; Wang *et al.*, 2009; Zhu *et al.*, 2010b; Ly *et al.*, 2013; Diaz *et al.*, 2018a; Diaz *et al.*, 2018b; Ho *et al.*, 2019).

Table 3.1 summarizes some of the improved characteristics of dendrimers after being PEGylated, compared to non-PEGylated dendrimers.

Table 3.1 Comparison between PEGylated and non-PEGylated dendrimers [adapted from (Thakur *et al.*, 2015)].

Features	Non-PEGylated dendrimer	PEGylated dendrimer
Cytotoxicity	Higher	Lower
Hemolysis	Higher	Lower
Targeting potential	Lower	Higher
Drug loading capacity	Lower	Higher
Immunogenicity	Higher	Lower
Solubilization potential	Higher	Highest
Drug release behavior	Burst to sustained	More sustained
Transepithelial transport	Higher	Lower
Stability	Lower	Higher
Macrophage uptake	Higher	Lower

3.2.4 Factors to be considered in PEGylated nanoparticulate drug delivery

a) PEG molecular weight

PEG chains exist in a wide range of molecular weight, which has a significant impact on the solubility and loading capacity of hydrophobic drugs. Increasing the molecular weight of PEG will offer a superior solubilizer platform for the drug to interact with. A study was done by Yang, Morris, and Lopina (2004) to improve the solubility of pyrene using three molecular weights of mPEG, mPEG 750, mPEG 2000, and mPEG 5000 to graft 3.0 G PAMAM dendrimer surface (Yang, Morris and Lopina, 2004). The results indicated that for the shorter mPEG chains (750) limited solubility improvement was observed. PEGylated dendrimer (mPEG 2000) exhibited the highest drug loading/solubility compared to the other mPEG chains (750 and 5000), whereas mPEG (5000) showed

comparatively lower solubility than mPEG 2000. The authors suggested that PEGylation with shorter chains does not offer a great platform of interaction between pyrene and mPEG and so limited solubility potential. While PEGylation with mPEG (2000) generates a large cluster around the dendrimer surface and much interaction with pyrene took place. For mPEG (5000), Yang and co-authors have speculated that increasing chain length even at low concentrations may allow the PEG arms to penetrate the cavity of near dendrimer molecules. This will allow agglomeration between dendrimers and reduce the inner space capacity for the guest drugs.

Kojima *et al.* (2000) reported another study to evaluate the effect of PEGylated 3.0 G and 4.0 G PAMAM dendrimers on improving the water-solubility of anti-cancer drugs, methotrexate and adriamycin (Kojima *et al.*, 2000). Two molecular weights mPEG 550 and mPEG 2000 were used to graft the dendrimer's surface. Results for both anticancer drugs indicated a significant increase in encapsulation potential when using mPEG (2000) in PEGylation compared to mPEG (550).

From these two studies done by Kojima *et al.* (2000) and Yang, Morris and Lopina, (2004), using mPEG 2000 was recommended for dendrimer PEGylation, compared to mPEG 550, 750, and 5000, to improve solubility, drug-loading capability, reduce toxicity, and control release of therapeutic drugs.

b) PEG content and density

The degree of dendrimer PEGylation not only improves the solubility potential of conjugated molecules but also includes the dendrimer as a locked box from which the drug is released in a controlled and sustained behaviour (Thakur *et al.*, 2015).

Sideratou and co-workers (2001) investigated the extent of PEGylation of diaminobutyric poly(propyleneimine) (DAB-PPI) dendrimer on the solubility improvement potential of pyrene (Sideratou, Tsiourvas and Paleos, 2001). The results showed that a higher quantity of pyrene was loaded in dendrimer grafted with 8 PEG chains compared to that with 4 PEG chains. This finding confirmed that, besides entrapment inside the dendrimer core, pyrene was also dissolved within PEG chains.

PEG chains of PEGylated dendrimer are widely reported to have a significant role in facilitating the encapsulation of drugs (Kojima *et al.*, 2000; Sideratou, Tsiourvas and Paleos, 2001). A contrary opinion was reported by Pan *et al.* (2005), they synthesized methotrexate-loaded G3 PEGylated PAMAM dendrimers. The data analysis revealed that there was no significant relationship between the degree of PEGylation (i.e., 23, 43, and 99% surface coverage) and the encapsulation potential of methotrexate (Pan *et al.*, 2005). Whereas the drug release was significantly affected by the extent of PEGylation and different release patterns were observed for each formulation.

3.2.5 Methods to quantify PEG density

Many techniques have been used to estimate the extent of PEGylation on the surface of the dendrimer nanoparticles. The most-reported methods are NMR and molecular weight determination techniques (Kojima *et al.*, 2000; Bharti and Roy, 2012; Ly *et al.*, 2013).

a) NMR technique

Proton nuclear magnetic resonance (^{1}H NMR) was used to prove the conjugation of PEG chains on the dendrimer surface as well as the percentage of coverage (Bharti and Roy, 2012). Quantitatively, Pan *et al*., (2005) and Kojima *et al*., (2000) estimated the number of mPEG chains attached from the integral ratio of the signal which corresponds to the protons of methylene next to the carbonyl groups of the PAMAM dendrimer, to the signal which corresponds to the protons of the terminal methyl group (OCH_3) of mPEG chains (Kojima *et al.*, 2000; Pan *et al.*, 2005).

b) Molecular weight determination technique

This technique was applied to determine the approximate number of PEG chains conjugated by calculating the difference in the molecular weight (M.wt) of the dendrimer before and following PEG conjugation. One of the practices to determine dendrimer molecular weight (M.wt) is by using gel permeation chromatography (GPC) (Kojima *et al.*, 2000). As done previously by Ly *et al*., (2013) where GPC was used to calculate the M.wt of PAMAM dendrimer before and after PEG conjugation. The difference in the M.wt

was then used to determine the approximate number of PEG attached and the percentage of PEGylation (Ly *et al.*, 2013).

Another approach to estimate dendrimer molecular weight is by using mass spectroscopy, particularly mass-assisted laser desorption/ionization-time of flight (MALDI-TOF) technique (Uppuluri *et al.*, 1998).

3.3 Aim and the Objectives of the chapter

3.3.1 Aim

The study aimed to synthesize and characterize rifampicin loaded in surface-modified 4.0 G PAMAM dendrimer having a range of mPEG content.

3.3.2 Objectives

i. To activate mPEG 2kD polymer by synthesizing mPEG-4-nitrophenyl carbonate using Michael's addition technique.

ii. To graft the surface of the dendrimer with increasing concentrations of mPEG.

iii. To encapsulate rifampicin into PEGylated and non-PEGylated dendrimers.

iv. To characterize rifampicin-loaded nanoparticles particularly size, PDI, ZP, shape, and the nature of drug-dendrimer interaction.

v. To estimate the encapsulation efficiency (EE %) and percentage drug loading (DL %) by the direct technique using a validated HPLC method.

3.4 Materials

3.4.1 Consumables

Reagents and solvents: Methoxy poly(ethylene glycol) m-PEG 2kD (Creative PEGWorks, China), fourth-generation (G4) ethylenediamine polyamidoamine (PAMAM) dendrimer 10 wt % in methanol (Aldrich, USA), 4-nitrophenyl chloroformate (NPC) (Aldrich, China), triethylamine (TEA) (Sigma, Belgium), rifampicin (DB Fine Chemicals, South Africa), potassium phosphate monobasic (Sigma, USA), potassium phosphate dibasic (Sigma-Aldrich, Spain), sodium hydroxide NaOH pellets (Merck, South Africa), ultrapure water (18.2 MΩ cm, O-purity filtration system, Lasec, South Africa), hydrochloric acid (HCl) (Fluka, Austria), tetrahydrofuran (THF) (Sigma-Aldrich, Germany), diethyl ether (Aldrich, USA), HPLC grade acetonitrile (Merck, Germany), dimethyl sulfoxide (DMSO) (Sigma Aldrich, Poland), HPLC grade methanol (Sigma Aldrich, France), deuterated chloroform ($CDCl_3$) (Merck, Switzerland), deuterium oxide (D_2O) 99.9% (Aldrich, Canada), and deuterated methanol 99.8% (Merck, Germany).

Other consumables: 125 mm filter paper (Advantec TOYO, Japan), Nylon 0.22µm syringe filter (Micron Separation Inc., USA), Nylon 0.45µm syringe filters (KimLab, India), poly top glass vials NO. 1, 2 and 4 (Kimix, South Africa), Pur-A-Lyzer® Maxi MWCO 25 kDa dialysis tubes (Sigma, Israel), Pur-A-Lyzer® Midi MWCO 3.5 kDa dialysis tubes (Sigma, Israel), folded capillary zeta cell (DTS 1070) (Malvern, UK), disposable 12 mm square polystyrene cuvettes (Malvern, UK), 5 mm thin wall 7″ NMR tubes (Wilmad Labglass, USA), DSC aluminum pan and lid (Kimix, South Africa), 2 ml HPLC vials with PTFE screw (Cronus, UK), HVLP 0.45 µm membrane filter (Millipore, Ireland), Parafilm® (Bemis, USA), micropipette 20, 200, 1000 and 5000 µl (DLAB, China), pipette tips 20, 200, 1000 and 5000 µl (Lasec, South Africa), and 10 ml centrifuge tube (Plastpro Scientific, South Africa).

3.4.2 Equipment

NMR spectrometer (Bruker Advance IIID Nanobay, Bruker BioSpin GmbH, Rheinstetten, Germany), Upright ultralow -86°C freezer (NU-9668E, NuAire, USA), Freeze-dryer (Virtis, Freeze mobile model 125L, Malvern instrument Ltd, UK), Fourier transform infrared spectrometer (Perkin-Elmer Spectrum-400 controlled with spectrum® software version 6.3.5, USA), Rotary evaporator (Büchi, Labotec, South Africa), HPLC system (Agilent 1200® series controlled with Agilent ChemStation software® version G2173-60101L, Germany), HPLC column (Phenomenex LC Luna® 250 x 4.6 mm, 5µm C18, USA), differential scanning calorimeter (Perkin Elmer DSC 8000, USA), scanning electron microscope (Auriga HR-SEM F50, Zeiss, Germany), Malvern Zetasizer NanoZS90 (Malvern Instruments, Ltd., UK), Ultrasonic bath (ScienTech®, South Africa), pH meter (XS®, Italy), filter apparatus (Millipore®, USA), vacuum pump (Dry Vac 400, USA), Vortex-Genie2, model-560E (scientific industries, USA), magnetic stirrer (IKA®-WERKE, Germany), and semi micron electronic balance (Shimadzu, Japan).

3.5 Methods

3.5.1 Activation of mPEG 2000 by synthesizing mPEG-4-nitrophenyl carbonate

mPEG was activated following the protocol described by Kojima *et al.* (2000) (Figure 3.4, Step 1). 0.4 g (0.2 mmol) of mPEG 2.0 kDa was dissolved in 20 ml of THF, afterward, 80.6 mg (0.4 mmol) of 4-nitrophenyl chloroformate (4-NPC) and 56 µl (0.4 mmol) of triethylamine (TEA) were added. The mixture was kept at room temperature with continuous stirring for two days (Kojima *et al.*, 2000). The precipitated triethylamine hydrochloride salt was removed, and the filtrate concentrated *via* solvent evaporation. The synthesized mPEG-4-nitrophenyl carbonate was precipitated from the THF solution into cold ether, collected, and left to air dry at room temperature (25 ˚C). The product was confirmed using Fourier-transform infrared (FTIR) and proton nuclear magnetic resonance (^{1}H NMR) ($CDCl_3$) techniques.

3.5.2 Conjugation of activated mPEG on the surface of G4 PAMAM dendrimer

Five PEGylated G4 PAMAM dendrimer formulations were synthesized to achieve surface coverage ranging between 39% and 100%, following the method reported earlier by Kojima *et al*. (2000) (Kojima *et al.*, 2000) (Figure 3.4, Step 2) with some modification. To five solutions of G4 PAMAM dendrimer (11.0 mg, 0.8 μmol) in 10 ml of dimethyl sulfoxide DMSO, various quantities of activated mPEG-4NPC were added (Table 3.2). The molar ratio between the 4.0 G PAMAM dendrimer and the activated mPEG-4NPC was as follows 1:25, 1:38.4, 1:51.2, 1:62, and 1:200. The solutions were slowly stirred for five days at room temperature. After this, the solutions were diluted with deionized water and dialyzed for seven days against deionized water to purify the crude products using Pur-A-lyzer Maxi 25 kDa cut-off dialysis tubes. The products were recovered from aqueous solutions by lyophilization, then characterized using ^{1}H NMR (D_2O) and FTIR techniques.

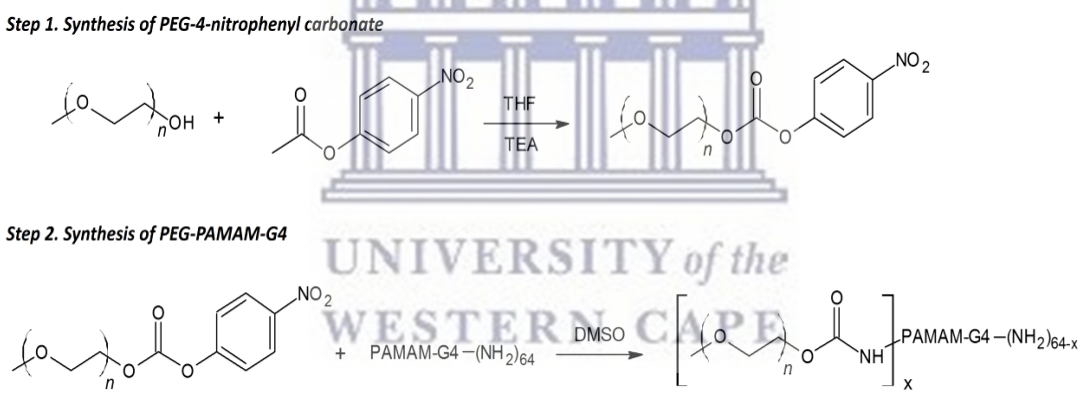

Figure 3.4 Synthesis of PEGylated G4 PAMAM dendrimer [adapted from (Diaz *et al.*, 2018b)].

Table 3.2 Characteristics of PEG-PAMAM dendrimer conjugates.

Target surface PEGylation %	Ratio G4: mPEG-4NPC (mol: mol)	Amount of dendrimer (Feeding)	Amount of mPEG-4NPC (Feeding)
39	1:25	0.8 µmol = 11.0 mg	20 µmol = 43.0 mg
60	1:38.4	0.8 µmol = 11.0 mg	31 µmol = 67.0 mg
80	1:51.2	0.8 µmol = 11.0 mg	41 µmol = 89.0 mg
96	1:62	0.8 µmol = 11.0 mg	50 µmol = 110.0 mg
100	1:200	0.8 µmol = 11.0 mg	160 µmol = 350.0 mg

3.5.3 Confirmation and quantification of the degree of PEGylation using ^{1}H NMR technique

Proton ^{1}H NMR was used to authenticate the conjugation of mPEG with PAMAM dendrimer *via* an amide-linkage, as well as estimating the degree of PEGylation as previously reported by Kojima *et al*. (2000) and Pan *et al.* (2005) (Kojima *et al.*, 2000; Pan *et al.*, 2005). In preparation for analysis, 5 mg of the freeze-dried sample was dissolved in 1 ml of deuterium oxide (D_2O), filtered and analyzed by a Buker 400 REM instrument running at 400 MHz. Each sample was scanned 64 times, and the data was interpreted using TopSpin® software version 4.0.6. The data is expressed as chemical shift (δ, ppm), and D_2O with δ 4.7 ppm is used as an internal solvent reference. The integral ratio of the peak area which corresponds to the methylene protons next to the carbonyl groups of PAMAM dendrimer, to the peak area corresponds to the protons of the terminal methyl group of the mPEG 2000 was employed to determine the approximate number of mPEG attached. The

analysis was done in triplicate, and the average ± standard deviation for each formulation was reported.

3.5.4 Encapsulation of rifampicin by PEGylated and non-PEGylated G4 PAMAM dendrimers

Drug loading was carried out using simple dissolution solvent evaporation method with slight modification following the protocol described by Kumar *et al.* (2007) (Vijayaraj Kumar *et al.*, 2007). To a methanolic solution of rifampicin (8.20 mg, 10 µmol), 0.1 µmol of PEGylated dendrimers or non-PEGylated dendrimer was added. All mixtures were kept at a slow stirring rate of 50 rpm for 24 hrs at room temperature (25 ˚C) (Bellini *et al*., 2015). Then, methanol was removed from the solutions using a rotary evaporator operating at a temperature of 40˚C and speed 3. Rifampicin loaded dendrimer was extracted from all mixtures by dissolving the precipitates in deionized water. After this, the aqueous solutions were filtered through a 0.22 µm syringe filter and twice dialyzed for 10 min against deionized water using Pur-A-Lyzer Midi 3.5 kDa dialysis tubes. Rifampicin-dendrimer conjugates were retrieved by lyophilization from the aqueous solutions and characterized using ^{1}H NMR, FTIR, Zetasizer, SEM, and DSC. The encapsulated efficiency (EE %) and the percentage drug loading (DL %) were determined directly using a validated HPLC method at wavelength 475 nm.

3.5.5 Characterization of rifampicin loaded PAMAM dendrimer nanoparticles

3.5.5.1 Fourier transform infrared spectroscopy (FTIR) analysis

FTIR analysis was done to study the conjugation of mPEG on the dendrimer, as well as drug-dendrimer interaction based on the vibration of atoms within a molecule. An IR spectrum is generated by transmitting IR radiation through a sample to determine which part of the incident radiation is absorbed at a specific energy. The energy used to generate the IR spectrum corresponds to the frequency of vibration of functional groups of a sample.

IR spectrums of 4.0 G PAMAM dendrimer, rifampicin, PEGylated PAMAM dendrimers, and rifampicin loaded PEGylated and non-PEGylated dendrimers were generated by scanning samples between 650 - 4000 cm^{-1} using a Fourier transform infrared spectrometer

(Perkin-Elmer Spectrum-400, USA) having diamond attenuated total reflectance (ATR) accessories with a diamond crystal.

A small granule of a fresh freeze-dried sample was placed on the top of the FTIR crystal, the force was applied using a pressure gauge (up to 60%). IR-spectra were captured using Spectrum® software version 6.3.5. The data were interpreted for functional groups at their relevant wave-number (cm^{-1}). The FTIR spectra of the rifampicin conjugated dendrimer formulations were compared to that of the rifampicin and their corresponding empty dendrimers. Differences in the absorbance band features such as appearance and disappearance of peaks, change in peak intensity, and shift in wave-number were employed to authenticate complex formation.

3.5.5.2 Nuclear magnetic resonance (NMR) studies

NMR is one of the essential techniques used to study the structure of compounds. Proton ^{1}H NMR, carbon ^{13}C NMR, carbon dept-135, correlation spectroscopy (COSY), total correlation spectroscopy (TOCSY), heteronuclear single-quantum correlation spectroscopy (HSQC), heteronuclear multiple-bond correlation spectroscopy (HMBC), and nuclear overhauser effect spectroscopy (NOESY) were used to confirm entrapment of rifampicin within the PAMAM dendrimer and PEGylated PAMAM dendrimers. Resonance data were also used to expect the site(s) of interaction between the rifampicin and the polymer. 5 mg from each sample was dissolved in 1 ml of deuterated DMSO and filtered before analysis using a Bruker 400 REM instrument running at 400 MHz. Tetramethylsilane was used as an internal standard. The data were interpreted using TopSpin 4.0.6® software; expressed as chemical shift (δ, ppm), and DMSO-d_6 with δ 2.5 ppm, 3.33 ppm used as an internal solvent reference.

3.5.5.3 Morphology of the nanoparticles

The shape of G4 PAMAM dendrimer, PEGylated PAMAM dendrimers, and rifampicin loaded PEGylated and non-PEGylated PAMAM dendrimers were studied using scanning electron microscopy (SEM). SEM generates images as a result of scanning the surface of the sample by an electron beam passed through a very fine probe. The generated beam contains accelerated electrons that hit the sample and sequentially liberate secondary and

backscattered electrons which are collected by the SEM detector and transformed as a signal. Samples must be conducive to ensure there is no build-up of static electric charge as the probe passes through the sample (Kailasam, 2008; Johansson, 2010), so the non-conductive samples are coated by one of the conductive materials such as carbon or gold before analysis.

Dendrimer samples were mounted on double-sided carbon conductive adhesive tape fixed on aluminium stubs and left to dry at room temperature, then coated by a thin film of gold using a sputtering method. The shape of the samples was observed and captured under an Auriga HR-SEM F50 scanning electron microscope (Zeiss®, Germany).

3.5.5.4 Differential scanning calorimetry (DSC) studies

Differential scanning calorimetry (DSC) technique was used to study the thermal performance as well as the crystallinity transformation over a range of temperatures. Approximately, 2 mg of rifampicin, PEGylated PAMAM dendrimers, rifampicin-dendrimer physical mixture, and rifampicin loaded PEGylated or non-PEGylated dendrimer formulations were weighed in individual aluminum pans which were then crimped at the edges. The sample was placed in the cell holder of a Perkin Elmer DSC 8000, and analyzed at an increasing heating rate of 10 ˚C/min from 35 ˚C to 220 ˚C under N_2 gas flow; a blank pan of the same dimension was crimped and used as a reference.

The DSC thermogram of each drug-loaded dendrimer was compared to their corresponding empty dendrimer, pure rifampicin, and rifampicin-dendrimer physical mixture to confirm drug conjugation.

3.5.5.5 Dynamic light scattering analysis (Size, PDI, and ZP)

Dynamic light scattering (DLS) was used to estimate the hydrodynamic diameter of the nanoparticles. The analysis was done on a Malvern Zetasizer Nano ZS90 that measures light scattering at a 90˚ angle using dynamic light scattering (DLS) theory. The system determines the intensity of scattered light that results from particles being in stable Brownian motion. Studying the particle size of nano-formulations is useful to predict some

behaviour of the nanoparticles, particularly the physicochemical features, biological half-life, and biodistribution (Blanco, Shen and Ferrari, 2015).

The extent of the distribution of molecular mass in a definite sample is called the polydispersity index (PDI). Values of PDI closer to one signify a heterogeneous distribution of nanoparticles in a sample whereas values closer to zero signify a homogenous distribution of nanoparticles in a sample.

The size and the PDI of the dendrimer nanoparticles were measured directly after synthesis. Two milligrams of freeze-dried dendrimer formulations were dissolved in 2 ml of PBS pH 7.4. After that, one milliliter from each dendrimer suspension was placed in cuvettes and analyzed. Three independent measurements for ten cycles were performed for each sample. The z-average particle diameters were automatically calculated by the system using cumulant analysis with the zetasizer software version 7.12 installed. The average diameter ± standard deviation for each sample was calculated and tabulated.

Zeta potential is the role of particle surface charge in suspension or colloidal dispersion (Demir *et al.*, 2014). The analysis was also done on a Malvern Zetasizer Nano ZS90 system. Measurement was carried out in triplicate after preparing a 1 mg/ml dispersion from each sample, which was transferred to a zeta-potential capillary cell (DTS 1070) and filled up until both electrodes were covered with the nanoparticle dispersion. The average zeta potential ± standard deviation for each sample was calculated and tabulated.

3.5.6 Development and validation of reversed-phase high-performance liquid chromatography (RP-HPLC) method

An isocratic RP-HPLC method to quantify rifampicin concentration was developed and validated following the International Conference on Harmonization (ICH) guidelines (ICH, 2005).

3.5.6.1 Instrumentation

Agilent 1200 HPLC system was used to analyze samples. The system was equipped with a quaternary pump (G1311A, Germany), autosampler (G1329A, Germany), diode array detector (G1315B, Germany), and a dual lamp design (i.e., ultraviolet and visible lamps),

and an analyte fraction collector (G164C, Germany). The system is also capable of controlling the column temperature throughout the analysis by the thermostat column compartment (G1322A, Japan). The data was recorded and interpreted by ChemStation software (G2173-60101L, Germany).

3.5.6.2 Chromatographic conditions

The HPLC analysis was performed *via* passing the mobile phase through a Phenomenex Luna® 250 x 4.6 mm, 5µm C18 column using a quaternary pump at a flow rate of 1 ml/min and a total run time of 6 minutes. The sample injection volume was set to be 10 µl. The column temperature was controlled throughout the analysis at 25 °C. Before sample injection, the column equilibrated for 30 minutes *via* passing the mobile phase throughout the system until a stable baseline was achieved. Drug elution was detected by a diode array detector at a wavelength of 475 nm.

3.5.6.3 Mobile phase preparation

The mobile phase consisted of solvent A: 0.01 M potassium phosphate buffer of pH 7.4, prepared by dissolving 1.21 g of potassium phosphate dibasic (K_2HPO_4) and 0.41 g of potassium phosphate monobasic (KH_2PO_4) in 800 ml of deionized (dH_2O). The volume was adjusted to 1 L using dH_2O, and solvent B comprised of HPLC grade acetonitrile (ACN). The ratio of A:B was 40:60 (v/v). The mixture was continuously stirred for 5 minutes, then filtered using a filter apparatus (Millipore®, USA) using HVLP 0.45 µm membrane filter (Millipore, Ireland). Finally, the mixture was degassed using an ultrasonic bath for 10 minutes (intensity 5) before use.

3.5.6.4 Preparation of calibration standards

Rifampicin stock solution having a concentration of 100 µg/ml was prepared on the day of analysis by weighing accurately 1 mg of rifampicin powder. Then transferred rifampicin to a 10 ml volumetric flask, and diluted with the mobile phase up to 10 ml. The rifampicin stock solution was vortexed for two minutes to ensure complete dissolution. Standard solutions with a range concentration were prepared on the day of injection by diluting the

stock solution using the mobile phase to make concentrations of 4, 10, 20, 50, and 100 µg/ml.

3.5.6.5 Key parameters of the analytical method validation

The method was validated according to the International Conference on Harmonization (ICH) guidelines (ICH, 2005). The following parameters were tested: the range, linearity, precision, accuracy, specificity, and sensitivity.

A. Determination of linearity and range

The linearity of an analytical method is the capability (within a given range) to get test results that are directly related to the concentration of an analyte in the sample (ICH, 2005).

The linearity and range were assessed for the standard solutions (4.0 – 100.0 µg/ml). One milliliter from each standard solution was transferred to HPLC vials after filtration through a 0.45 µm nylon syringe filter. Samples were analyzed using the Agilent 1200 HPLC system with the setup as described in the preceding paragraphs. A calibration curve was generated by plotting each sample concentration with their corresponding mean peak areas (AUC). Linear regression analysis was used to study the linearity by calculating the correlation coefficient, slope, and y-intercept of the curve over concentrations.

B. Determination of accuracy and precision

Accuracy is one of the validation parameters that is commonly used to determine the closeness between the expected values and calculated results (ICH, 2005), by calculating the percentage recovery of a known injected sample concentration. Recovery studies were carried out on three standard concentrations 10 µg/ml, 20 µg/ml, and 50 µg/ml. The analysis was done in triplicate, and the percentage recovery for the selected standard concentrations was determined using equation 3.1.

$$\% \text{ Recovery } = \frac{\text{Calculated concentration}}{\text{Injected concentration}} \times 100 \qquad \textbf{Equation 3.1}$$

The precision of an analytical method determines the extent of scattering between several measurements collected from the same sample under the prescribed situations (ICH, 2005). Intra-day (repeatability) and inter-day (intermediate precision) were assessed by measuring triplicates of rifampicin standards 10 µg/ml, 20 µg/ml, and 50 µg/ml, at three periods per day and at three-periods on three consecutive days, respectively. Results at each occasion were interpreted statistically by calculating the average ± standard deviation (SD), and relative standard deviation (RSD) to evaluate inter-day and intra-day precision.

C. Sensitivity

Limit of quantification (LOQ) and limit of detection (LOD) were determined to estimate the sensitivity of the analytical method. LOD is the minimal amount of analyte in a sample that can be identified but not essentially quantitated precisely, whereas the LOQ is the minimum amount of analyte in a sample that can be accurately and precisely quantified (ICH, 2005).

LOQ and LOD for the HPLC method were calculated using the calibration curve technique. From the calibration curve linearity data, the standard deviation of the y-intercepts and the slope of the regression line were used and equations 3.2 & 3.3 were applied to determine LOQ and LOD.

$$LOQ = 10 \text{ X } \frac{\sigma}{S} \qquad \textbf{Equation 3.2}$$

$$LOD = 3.3 \text{ X } \frac{\sigma}{S} \qquad \textbf{Equation 3.3}$$

Where σ represents the standard deviation of the y-intercepts, and S represents the slope of the calibration curve.

D. Specificity

Specificity is the capability to distinguish between the intended analyte (s) and other components within a sample (ICH, 2005). The specificity of the HPLC method was evaluated by injecting the mobile phase (phosphate buffer: acetonitrile) and unloaded dendrimer dispersions at similar analysis conditions to ensure no overlapping or interference with the rifampicin peak. In addition, 20 µg/ml rifampicin standard solution

was force degraded for 24 hr in pH 1.0 and pH 10, using HCl and NaOH solutions, respectively. After 24 hr, both solutions were analyzed to observe the degradant product peaks relative to the intended analyte peak.

3.5.7 Encapsulation efficiency (EE %) and drug loading (DL %)

The direct calculation technique was used to estimate the encapsulation efficiency percentage (EE %) and the percentage drug loading (DL %) using a validated HPLC method. One milligram of freeze-dried rifampicin loaded PEGylated, and non-PEGylated dendrimers were transferred to 10 ml volumetric flasks, the volume was adjusted to 10 ml by the mobile phase. Samples were sonicated for 2 minutes in a ScienTech ultrasonic bath to ensure complete dissolution, then filtered using a nylon 0.45 μm syringe filter, and finally analyzed using HPLC as described earlier. The resulting peak area was interpreted as rifampicin concentration using a generated calibration curve prepared on the day of study. The analysis was done in triplicate, and the average ± standard deviation for each sample was reported. DL% and EE% for dendrimer formulations were determined using equations 3.4 and 3.5, respectively.

$$\mathrm{DL\%} = \frac{\text{Amount of encapsulated rifampicin per (g) of dendrimer}}{\text{weight of dry nanoparticles (g)}} \quad \textbf{Equation 3.4}$$

$$\mathrm{EE\ \%} = \frac{\text{Total amount of encapsulated rifampicin}}{\text{The total theoretical amount of rifampicin added}} \quad \textbf{Equation 3.5}$$

3.6 Data analysis

The data, expressed as mean ± standard deviation, were interpreted using GraphPad® Prism 7.04. A one-way ANOVA test was applied to set up the significance of any differences between the means. Values were considered significant if the *p*-value was ≤ 0.05.

3.7 Results and discussion

3.7.1 Activation of mPEG 2000 by synthesizing mPEG-4-nitrophenyl carbonate

The mPEG was activated *via* Michael's addition technique using 4NPC and TEA reagents to form mPEG-4-nitrophenyl carbonate (mPEG-4NPC), following the protocol described by Kojima *et al.* (Kojima *et al.*, 2000). ^{1}H NMR technique was used to monitor the

conversion of mPEG into the activated form (i.e., mPEG-4NPC). ^{1}H NMR was applied to calculate the integral value of the aromatic protons after 24 hrs and 48 hrs (Figure 3.5 a & b). Results showed that the aromatic proton's integral values after 24 hrs and 48 hrs were 1.14, 1.17 and 1.86, 1.89, respectively. This indicated that the majority of the mPEG was successfully converted into activated mPEG-4NPC after 48 hrs of reaction (≈ 2 ortho Hs and 2 meta Hs/molecule) (Figure 3.5) with a yield of about 75%.

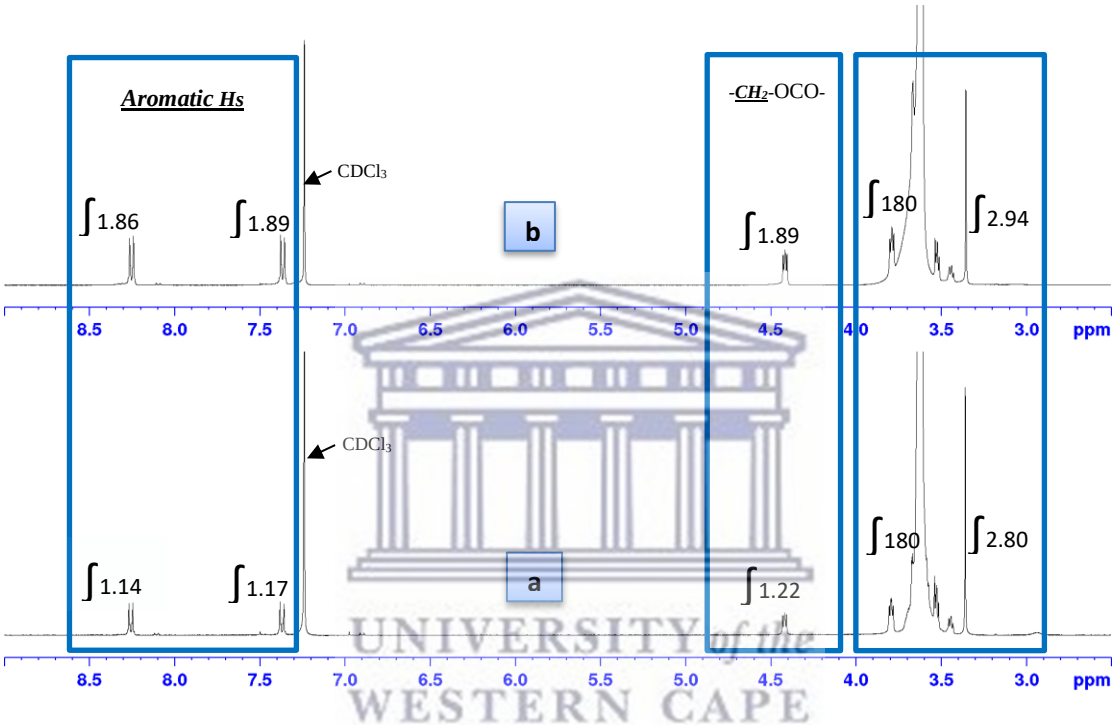

Figure 3.5 ^{1}H NMR spectra of mPEG-4NPC after (a) 24 hrs, and (b) 48 hrs of reaction.

^{1}H NMR was used to confirm the successful conversion of mPEG to mPEG-4-NPC. In Figure 3.6 (b), ^{1}H NMR spectra showed two doublets at δ of 7.45 - 7.47 ppm and 8.34 - 8.36 ppm which correspond to the protons at the meta- and ortho- positions of the aromatic rings of 4-nitrophenyl chloroformate, respectively. These two doublets were shifted to δ of 7.38 - 7.40 ppm and 8.27 - 8.29 ppm in the case of activated mPEG (Figure 3.6 (c)). Additionally, the appearance of a triplet signal at δ of 4.36 - 4.38 ppm which corresponds to (-***CH***$_2$-OCO-) confirms the synthesis of conjugated mPEG-4NPC (Figure 3.6 (c)). The presence of signals which correspond to ethylene protons and (-O***CH3***) protons of the mPEG chain in the spectra of mPEG-4NPC at δ of 3.62 ppm and 3.30 ppm, respectively, also suggest the formation of the conjugated product.

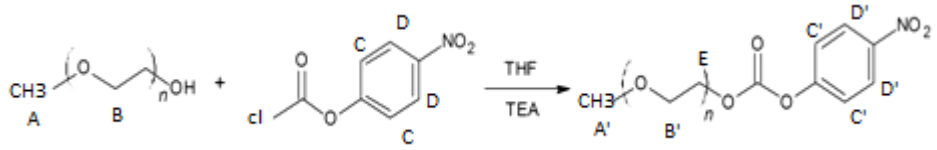

(a) mPEG (b) 4-NPC (c) mPEG-4NPC

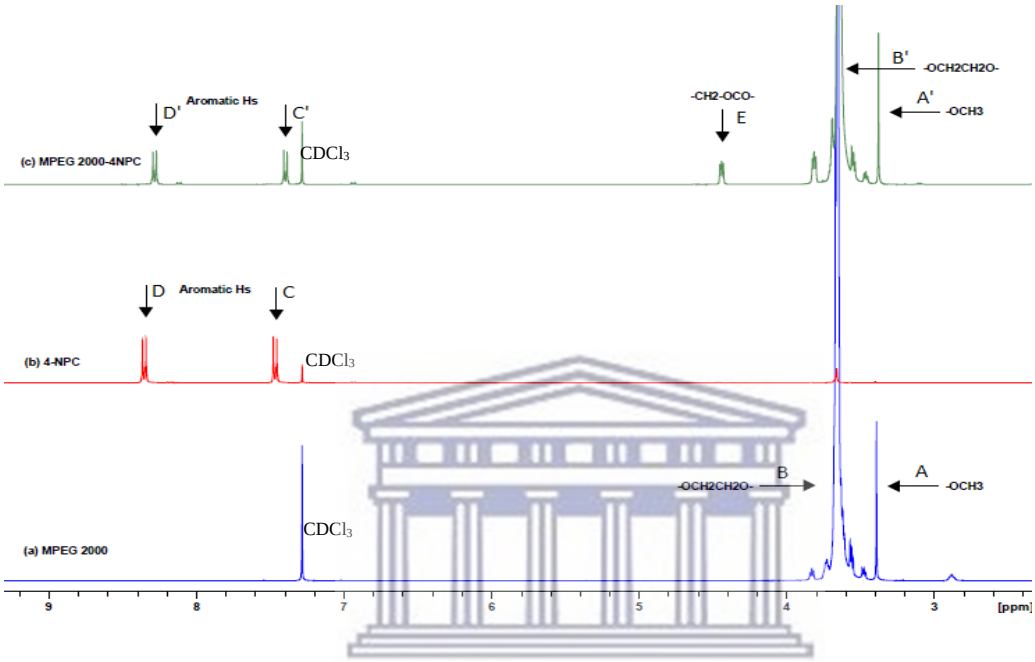

Figure 3.6 ^{1}H NMR spectra of (a) mPEG 2 kDa, (b) 4-nitrophenyl chloroformate (4-NPC), and (c) mPEG-4-nitrophenyl carbonate (mPEG-4NPC).

FTIR analysis was achieved for the mPEG, 4-NPC, and the activated mPEG-4NPC product (Figure 3.7). The FTIR spectrum of mPEG-4NPC (Figure 3.7 (c)) was characterized by the appearance of new peaks at 1767 cm^{-1}, 1594 cm^{-1}, and 1525 cm^{-1} attributed to C=O stretching, $–NO_2$ group, and an aromatic C-C stretching obtained from 4-nitrophenyl chloroformate, respectively. The appearance of the aforementioned IR peaks suggests that mPEG-4NPC was successfully synthesized.

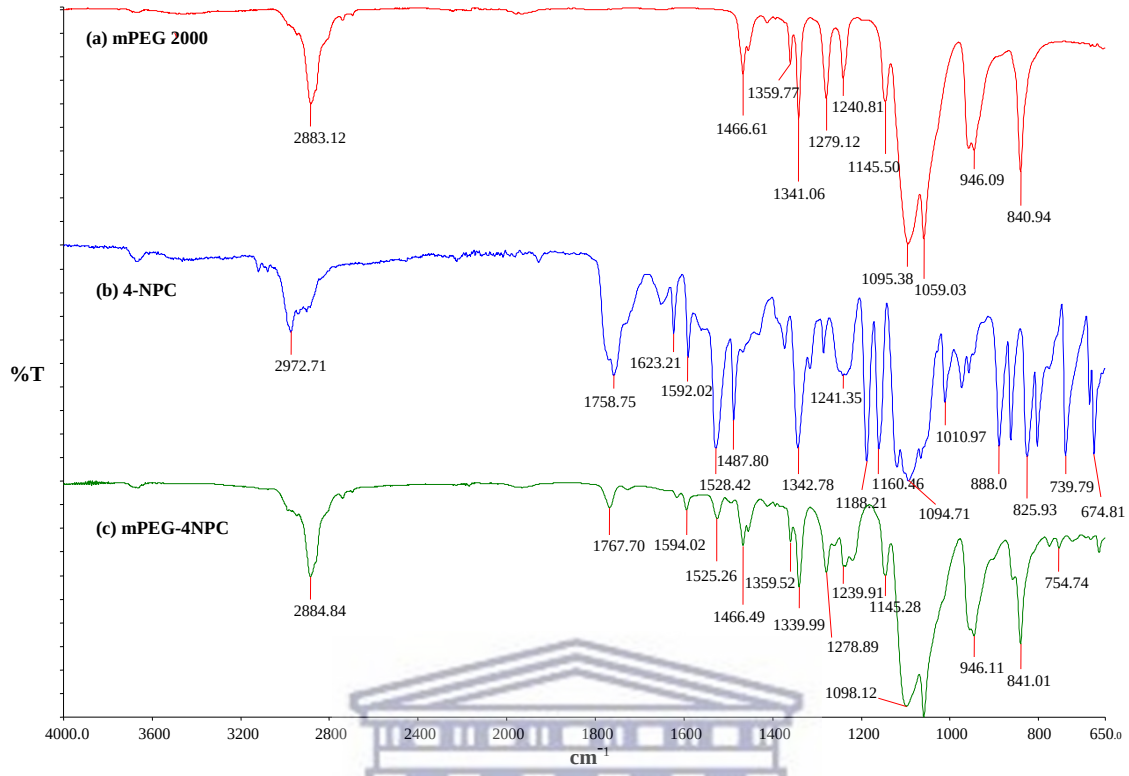

Figure 3.7 FTIR spectra of: (a) mPEG 2 kDa, (b) 4-NPC, and (c) mPEG-4NPC.

3.7.2 Conjugation of activated mPEG-4NPC on the surface of G4 PAMAM dendrimer

Partially and fully surface-modified 4.0 G PAMAM dendrimers were synthesized by adding increasing concentrations of activated mPEG-4NPC to the dendrimer to achieve surface coverage ranging from 39% to 100%. The molar ratio between the 4.0 G PAMAM dendrimer and the activated mPEG-4NPC was as follows 1:25, 1:38.4, 1:51.2, 1:62, and 1:200. The mixtures were kept under slow stirring for five days to ensure maximum conjugation of PEG chains on the surface of the dendrimer. The recovered products were characterized using ^{1}H NMR as well as FTIR techniques.

^{1}H NMR analysis was done for G4 PAMAM dendrimer alone, mPEG-4NPC, and PEGylated dendrimer formulations (Figure 3.8). Spectra of PEGylated dendrimers suggested the attachment of PEG chains possibly *via* carbamate bonds. In all PEGylated dendrimers spectra, the dendrimer's methylene protons appeared at a similar chemical shift to that of the pure G4 dendrimer. The signal which corresponds to the methylene protons

close to the carbonyl group in the PEG chain shifted from 4.36 - 4.38 ppm to 4.11 ppm (Figure 3.8 (G & G' symbols)). It was also noticed that the upfield shift of methylene protons of the PEG end chain from 3.38 ppm to 3.30 ppm arose when conjugated to the dendrimer (Figure 3.8 (E & E' symbols)). The upfield shift of (G') and (E') peaks of the activated mPEG-4NPC after conjugation could be a result of a lower deshielding effect relative to unconjugated mPEG-4NPC. These groups of the unconjugated mPEG-4NPC were attached to the nitrobenzene group that could exhibit a greater deshielding effect compared to the chemical part of the PEGylated dendrimer.

The spectra of PEGylated dendrimers corroborated the existence of peaks for PEG ethylene protons at δ of 3.62 ppm. Furthermore, the aromatic proton peaks of the activated mPEG-4NPC disappeared in the case of PEGylated dendrimers which confirms the formation of carbamate bonds between activated mPEG-4NPC molecules and the dendrimer surface amines.

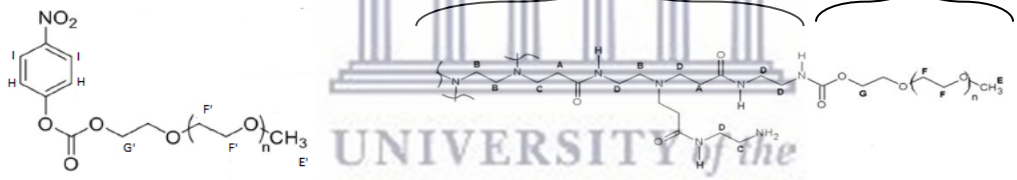

mPEG-4NPC | PEGylated G4 dendrimer

mPEG-4NPC	
Peak label	Peak chemical shift δ (ppm)
E'	3.38
F'	3.64
G'	4.36, 4.38
H	7.41
I	8.29

PEGylated dendrimer	
Peak label	Peak chemical shift δ (ppm)
A	2.33
B	2.54
C	2.74
D	3.21
E	3.30
F	3.62
G	4.11

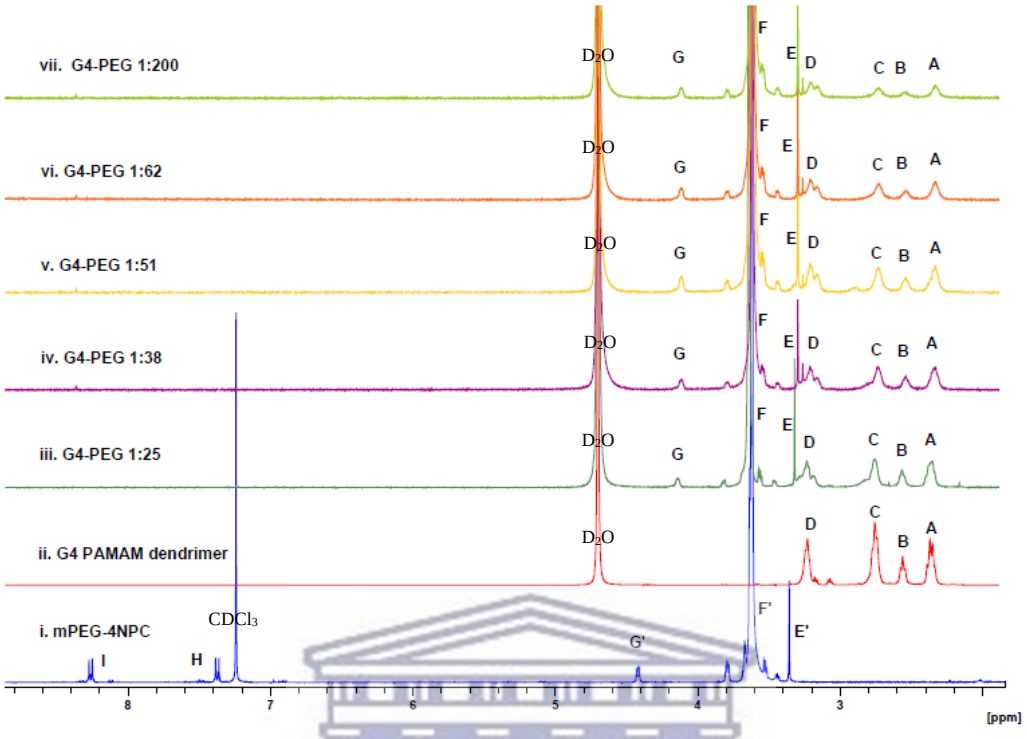

Figure 3.8 ^{1}H NMR spectra of, (i) mPEG-4NPC in $CDCl_3$, (ii) G4 PAMAM dendrimer (iii) G4-PEG 1:25, (iv) G4-PEG 1:38, (v) G4-PEG 1:51, (vi) G4-PEG 1:62, and (vii) G4-PEG 1:200, in deuterated water.

FTIR analysis was done for G4 PAMAM dendrimer alone, mPEG-4NPC, and PEGylated dendrimer formulations, illustrated in Figure 3.9 and Table 3.3. IR data of PEGylated dendrimers showed peaks at 2883 - 2884 cm^{-1} and 1098 - 1102 cm^{-1} which correspond to C-H stretching vibration of methylene and C-O ether stretching vibration of the mPEG backbone, respectively. Figure 3.9 observes the C-H stretching of the G4 dendrimer shifting from 2836 cm^{-1} to 2883 - 2884 cm^{-1} in the case of PEGylated dendrimer. Also, the C-H peak intensity was significantly higher in the surface-modified dendrimer due to a large number of methylene groups of the mPEG chains attached to the dendrimer. The appearance of the C-O ether peak in all PEGylated dendrimers suggested the conjugation of mPEG chains to the dendrimer structure.

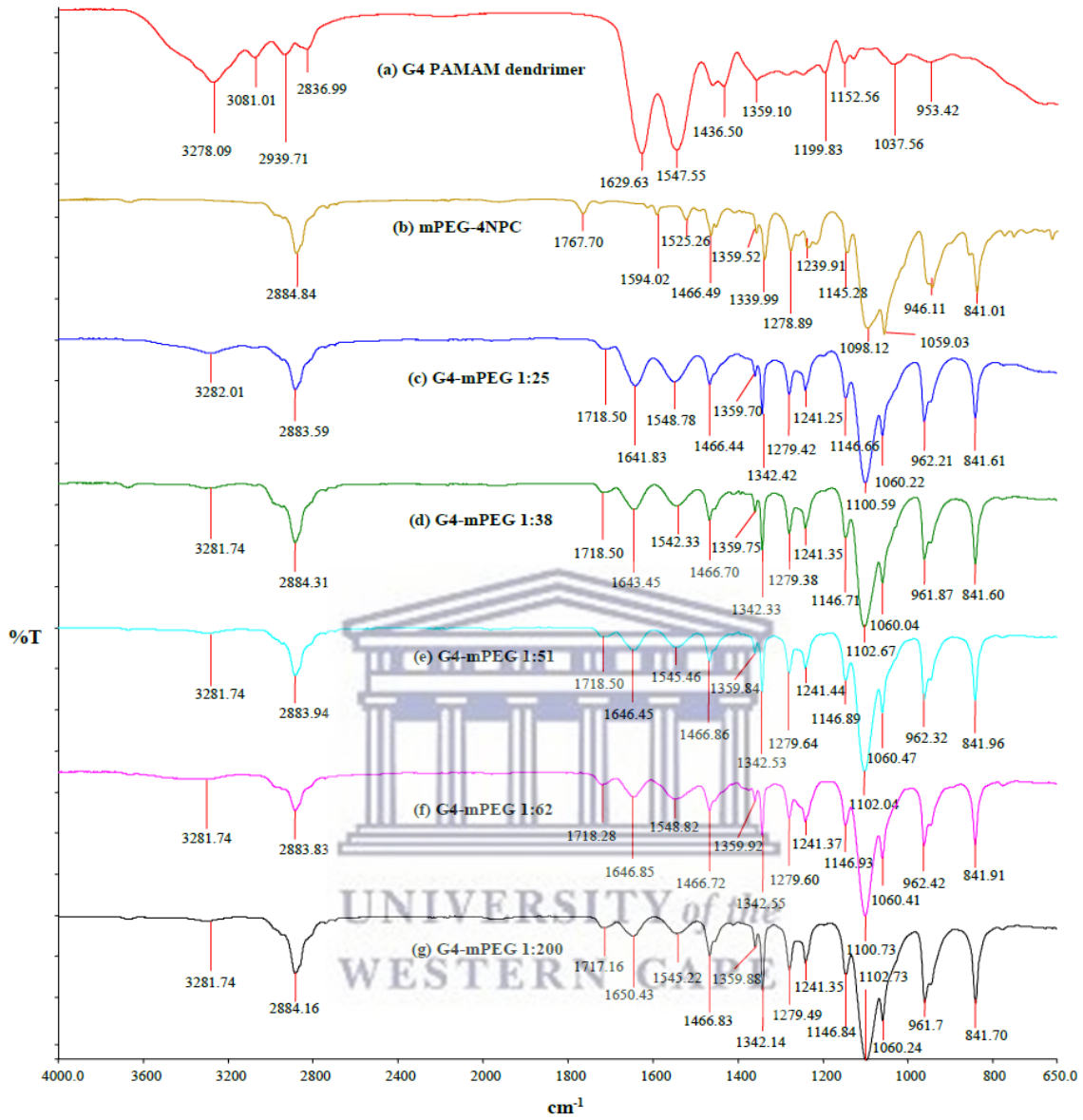

Figure 3.9 FTIR spectra of: (a) G4 PAMAM dendrimer, (b) mPEG-4NPC, (c) G4-mPEG 1:25, (d) G4-mPEG 1:38, (e) G4-mPEG 1:51, (f) G4-mPEG 1:62, and (g) G4-mPEG 1:200.

FTIR data of PEGylated dendrimers showed peaks at 1717 - 1718 cm^{-1}, and at 3281 - 3282 cm^{-1} which were assigned to the C=O group of the mPEG chains and N-H stretching vibration of the G4 dendrimer, respectively. Moreover, the amide groups of the G4 dendrimer which appeared as two peaks at 1629 cm^{-1} and 1547 cm^{-1} were also observed in all PEGylated dendrimers at 1641 - 1650 cm^{-1} and 1542 - 1548 cm^{-1} (Table 3.3). In Figure 3.9, the intensity of the N-H peak of the G4 dendrimer decreased significantly in PEGylated

dendrimers. Among the PEGylated dendrimers, the decrease in the intensity of the N-H peak was directly related to the extent of PEGylation with relatively higher peak intensity seen for G4-mPEG 1:25 and a small peak observed for G4-mPEG 1:200. The decrease in N-H peak intensity was possibly due to the conjugation of mPEG chains to the peripheral amines of the G4 dendrimer and therefore shielding their IR absorption potential. The shielding effect was directly related to the amount of mPEG available on the dendrimer periphery. The FTIR analysis suggests that mPEG chains were successfully conjugated to the dendrimer surface amines *via* amide linkages to form a PEGylated dendrimer.

Table 3.3 Selected IR functional groups with their frequencies for G4 PAMAM dendrimer, activated mPEG-4NPC, and PEGylated dendrimers.

Sample	Functional group frequency (cm^{-1})				
	N-H group	$-CH_2-$ group	C=O of the carbonyl group	-NH-CO- group	C-O ether of PEG
G4 dendrimer	3278, 3081 (s)	2939 (s), 2836 (s), & 1436 (b)	-	1629 (s), 1547 (b)	-
mPEG-4NPC	-	2884 (s), 1466 (b)	1767 (s)	-	1098 (s)
G4-mPEG 1:25	3282 (s)	2883 (s), 1466 (b)	1718 (s)	1641 (s), 1548 (b)	1100 (s)
G4-mPEG 1:38	3281 (s)	2884 (s), 1466 (b)	1718 (s)	1643 (s), 1542 (b)	1102 (s)
G4-mPEG 1:51	3281 (s)	2883 (s), 1466 (b)	1718 (s)	1646 (s), 1545 (b)	1102 (s)
G4-mPEG 1:62	3281 (s)	2883 (s), 1466 (b)	1718 (s)	1646 (s), 1548 (b)	1100 (s)
G4-mPEG 1:200	3281 (s)	2884 (s), 1466 (b)	1717 (s)	1650 (s), 1545 (b)	1102 (s)

*s = stretching vibration; b = bending vibration

The IR spectra of PEGylated dendrimers were also used to confirm the extent of PEGylation. The ratio of peak area at 1718 cm^{-1} (C=O stretch of carbonyl group) to that at

1643 cm^{-1} (C=O of amide group) and the ratio of peak area at 1643 cm^{-1} to the area at 1100 cm^{-1} were determined for all PEGylated dendrimers. Results indicated a direct increase in the carbamate groups and ethylene oxide moieties of the PEGylated dendrimers by increasing the proportion of mPEG added (from 1:25 to 1:200 molar ratio).

3.7.3 Confirming and quantifying the degree of PEGylation using ^{1}H NMR technique

^{1}H NMR was used to verify the conjugation of the mPEG chains to the dendrimer surface *via* an amide-linkage, as well as to determine the number of substituted peripheral amines of the G4 dendrimer by mPEG chains as previously reported by Kojima *et al.* (2000) and Pan *et al.* (2005) (Kojima *et al.*, 2000; Pan *et al.*, 2005). The integral ratio of the peak area which corresponds to the methylene protons next to the carbonyl groups of PAMAM dendrimer, to the peak area corresponds to the protons of the terminal methyl group of the mPEG was used to determine the approximate number of mPEG attached. The analysis was done in triplicate, and the average ± standard deviation for each formulation was reported.

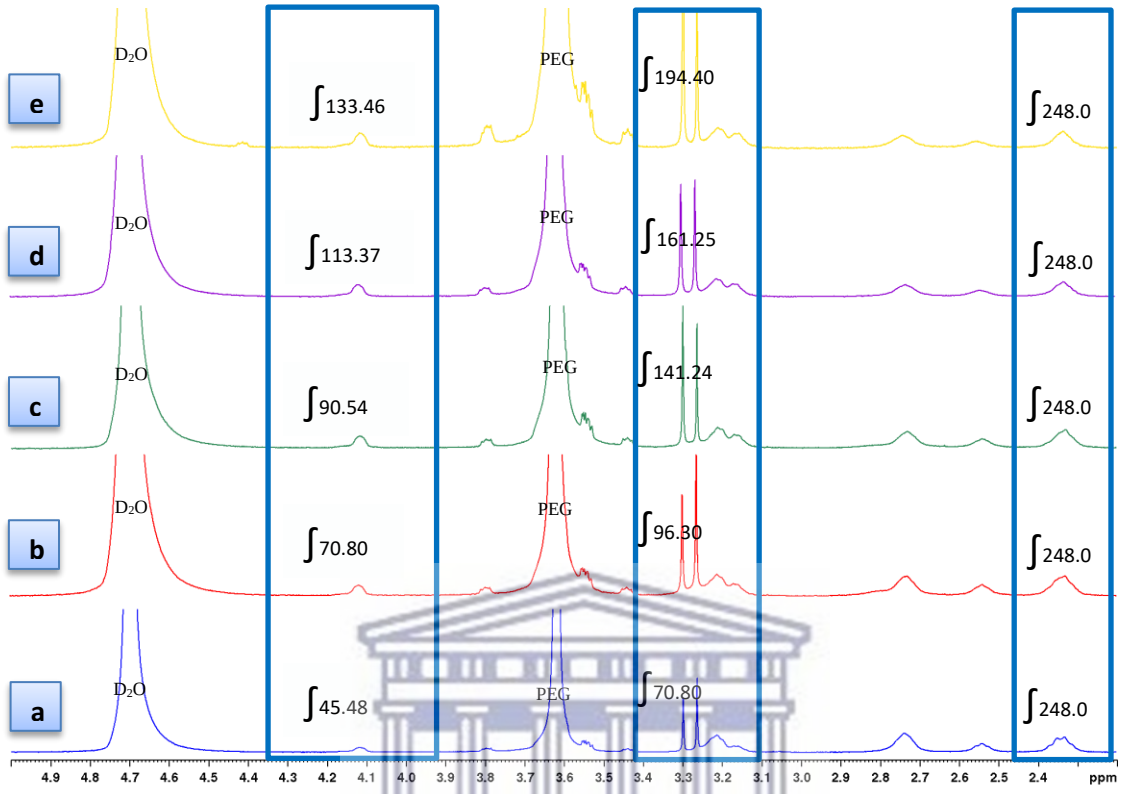

Figure 3.10 The ^{1}H NMR spectra of (a) G4-mPEG 1:25, (b) G4-mPEG 1:38, (c) G4-mPEG 1:51, (d) G4-mPEG 1:62, and (e) G4-mPEG 1:200, in deuterated water, with integration values of methylene protons next to the carbonyl groups of PAMAM dendrimer at δ of 2.30 ppm**,** methylene of (-***CH2***-O-CO-**)** group at δ of 4.11 ppm, and the terminal methyl group protons peak of the mPEG at δ of 3.3 ppm.

In Figure 3.10a, the AUC of methylene protons of PAMAM dendrimer at δ of 2.3 ppm was 248 (which approximately represent the number of methylene protons next to carbonyl groups for one G4 dendrimer molecule), and the AUC of the terminal methyl group protons (–OCH_3) of the mPEG was 70.80. It is known that there are approximately three methyl protons for each mPEG chain, accordingly, the number of conjugated mPEG chains was determined by dividing the calculated AUC of (–OCH_3) by the three methyl protons. Thus for Figure 3.10a, it was 23.60 which represents the number of mPEG chains substituted on the surface amines of the dendrimer. Formulations b, c, d, and e in Figure 3.10, have 32.10, 47.08, 53.75, and 64.80 conjugated mPEG chains, respectively.

Table 3.4 Characterization of mPEG-G4 PAMAM dendrimer conjugates (n = 3).

Formulation	Ratio G4: mPEG-4NPC	Amount of dendrimer (Feeding)	Amount of mPEG-4NPC (Feeding)	Yield wt (mg)	No of NH_2 substituted Mean ± SD	% Coverage
1	(1:25) mol:mol	0.80 µmol = 11.0 mg	20 µmol = 43.0 mg	12.70	24.70 ± 1.28	38.59%
2	(1:38.4) mol:mol	0.80 µmol = 11.0 mg	31 µmol = 67.0 mg	12.11	31.90 ± 2.11	49.84%
3	(1:51.2) mol:mol	0.80 µmol = 11.0 mg	41 µmol = 89.0 mg	28.01	45.10 ± 3.03	70.47%
4	(1:62) mol:mol	0.80 µmol = 11.0 mg	50 µmol = 110.0 mg	38.22	54.70 ± 2.32	85.47%
5	(1:200) mol:mol	0.80 µmol = 11.0 mg	160 µmol = 350.0 mg	28.33	64.60 ± 2.72	100.94%

Listed in Table 3.4 are the substitutions by activated mPEG 2kDa (i.e., five batches at different ratios of activated mPEG) on the surface of G4 dendrimer and their % coverage. The number of substituted primary amines for each formulation was reported as mean ± SD determined from the ^{1}H NMR integration results for 3 samples. The percentage of coverage was calculated from the ratio of substituted amines to the total peripheral amines, which are approximately 64 amine groups in the case of G4 PAMAM dendrimer.

3.7.4 Characterization of rifampicin loaded PAMAM dendrimers

3.7.4.1 Fourier transform infrared (FTIR) studies

FTIR analysis was performed to study rifampicin-dendrimer interaction based on the vibration of atoms within the molecules. The FTIR spectra of the rifampicin conjugated dendrimer formulations were compared to that of the rifampicin and their corresponding empty dendrimer. Differences in the band's features such as appearance, disappearance, peak intensity, and shift in wave-number (cm^{-1}) were used to verify complex formation.

Figure 3.11 illustrates the IR spectra of G4 PAMAM dendrimer, G4-mPEG 1:25, rifampicin, and rifampicin loaded G4-mPEG 1:25 with their functional groups wave-number (cm^{-1}). Whereas Table 3.5 highlights particular functional groups for comparison.

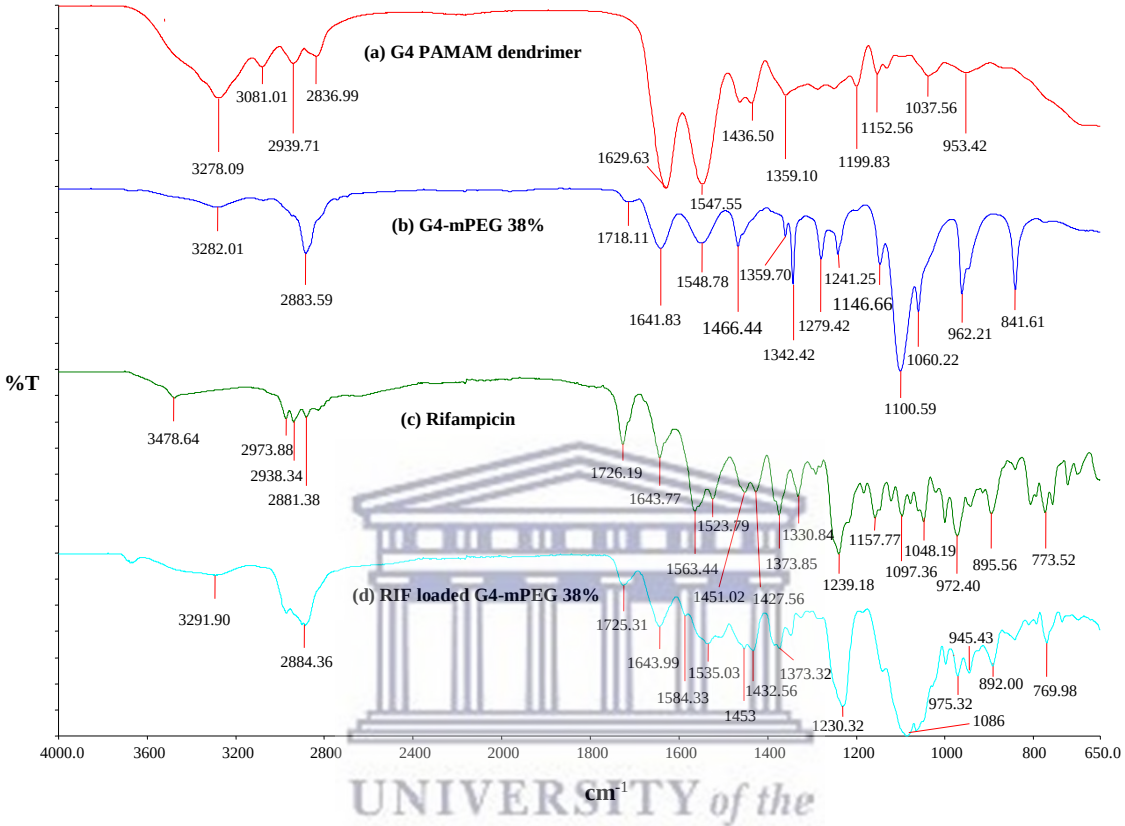

Figure 3.11 FTIR spectra of: (a) G4 PAMAM dendrimer, (b) G4-mPEG 38%, (c) rifampicin, and (d) RIF loaded G4- mPEG 38%.

From Figure 3.11, the IR spectra of G4 dendrimer (a) and PEGylated dendrimer (1:25) (b) is characterized by the appearance of N-H vibration of the peripheral amines at 3278 cm^{-1} / 3081 cm^{-1} and 3282 cm^{-1}, respectively (Uppuluri *et al.*, 1998). Rifampicin (c) showed a broad peak at 3478 cm^{-1} which corresponds to O-H and N-H stretching vibration (Date, Samad and Devarajan, 2010; Dineshkumar *et al.*, 2017). For rifampicin conjugated dendrimer (d), the N-H peaks of dendrimer were expected to be hidden under the broad O-H peak of the rifampicin, however, the O-H peak was shifted to 3291 cm^{-1}. Comparing the IR spectra of empty PEGylated dendrimer (b) to the loaded PEGylated dendrimer (d) indicated the appearance of new bands at 1453 cm^{-1}, 1230 cm^{-1}, 975 cm^{-1}, and 770 cm^{-1}, which were attributed to aromatic C-C (stretch), aromatic-O-R (C-O stretch), C=C

(bending), and di-substituted C-H bending obtained from rifampicin, respectively (Date, Samad and Devarajan, 2010). Once the PEGylated dendrimer was loaded, the peaks at 1718 cm^{-1} (C=O stretch of the carbonyl groups), 1641 cm^{-1} / 1548 cm^{-1} (amide groups vibration), and 1100 cm^{-1} (C-O ether) were shifted to 1725 cm^{-1}, 1643 cm^{-1}/1535 cm^{-1}, and 1086 cm^{-1} (Table 3.5), respectively.

Table 3.5 The IR functional group assignments of G4 PAMAM dendrimer, G4-mPEG 38%, rifampicin, and RIF loaded G4- mPEG 38%.

Functional groups	Frequency (cm^{-1})			
	G4-PAMAM (a)	G4-mPEG (38%) (b)	Rifampicin (c)	RIF-PEGylated dendrimer (38%) (d)
O-H (stretch)	-	-	3478	3291
N-H (stretch)	3278, 3081	3282	3478	3291
$-CH_2-$ (stretch)	2939, 2836	2883	2973, 2938, 2881	2884
C=O (stretch)	-	1718	1726	1725
-NH-CO-	1629, 1547	1641, 1548	1643, 1563	1643, 1535
C=C, C=N (stretch)	-	-	1643	1643
Ar C-C (stretch)	-	-	1451	1453
Ar-O-R (C-O stretch)	-	-	1239	1230
C-O ether (stretch)	-	1100	1097	1086
C=C (bending)	-	-	972	975
C-H (bending) di-substituted	-	-	773	770

A new peak emerged at about 1584 cm^{-1} for the rifampicin loaded PEGylated dendrimer spectra. This new peak could result in hydrogen bonding between the amide carbonyl of some of the amide groups within the dendrimer and the amino group and/or –OH groups of rifampicin. The formation of a new peak at 1584 cm^{-1} could account for the appearance of the amide amino groups at lower wave-number (i.e., 1535 cm^{-1}) relative to the unloaded molecule (1548 cm^{-1}). These findings suggested possible inter-molecular interaction

between rifampicin and dendrimer interior. The appearance of the new peak at 1584 cm^{-1} was also confirmed by the IR spectra of drug-loaded PEGylated (1:38, 1:51, 1:62, and 1:200) and non-PEGylated dendrimers (see Figure 3.12 to Figure 3.16, respectively). Comparing the drug conjugated dendrimers with the corresponding unloaded dendrimers, suggested the formation of H-bonding between the rifampicin and some amide carbonyl of the dendrimer is corroborated in Figure 3.12 to Figure 3.16. The IR spectra of drug-loaded PEGylated dendrimers (Figures 3.12 to Figure 3.15) showed approximately similar absorption peaks as that displayed for drug-loaded PEGylated dendrimer (1:25) (Figure 3.11 and Table 3.5).

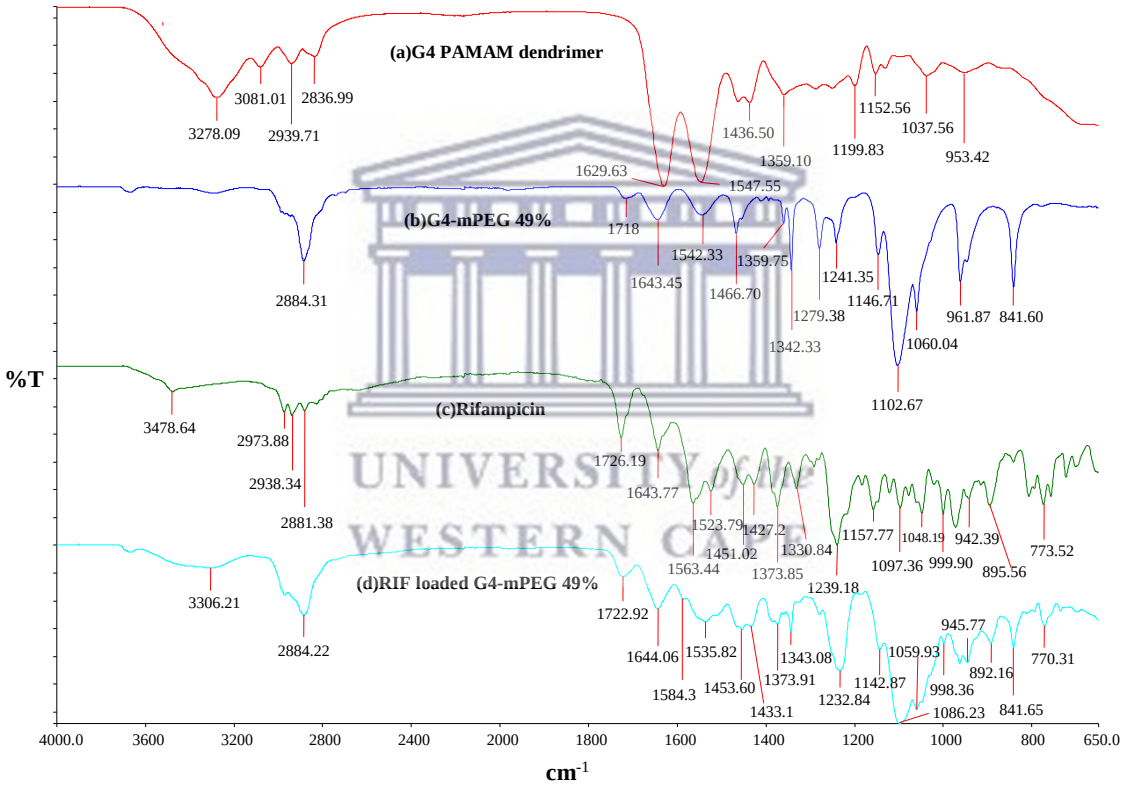

Figure 3.12 FTIR spectra of: (a) G4 PAMAM dendrimer, (b) G4-mPEG 49% (1:38), (c) rifampicin, and (d) RIF loaded G4-mPEG 49% (1:38).

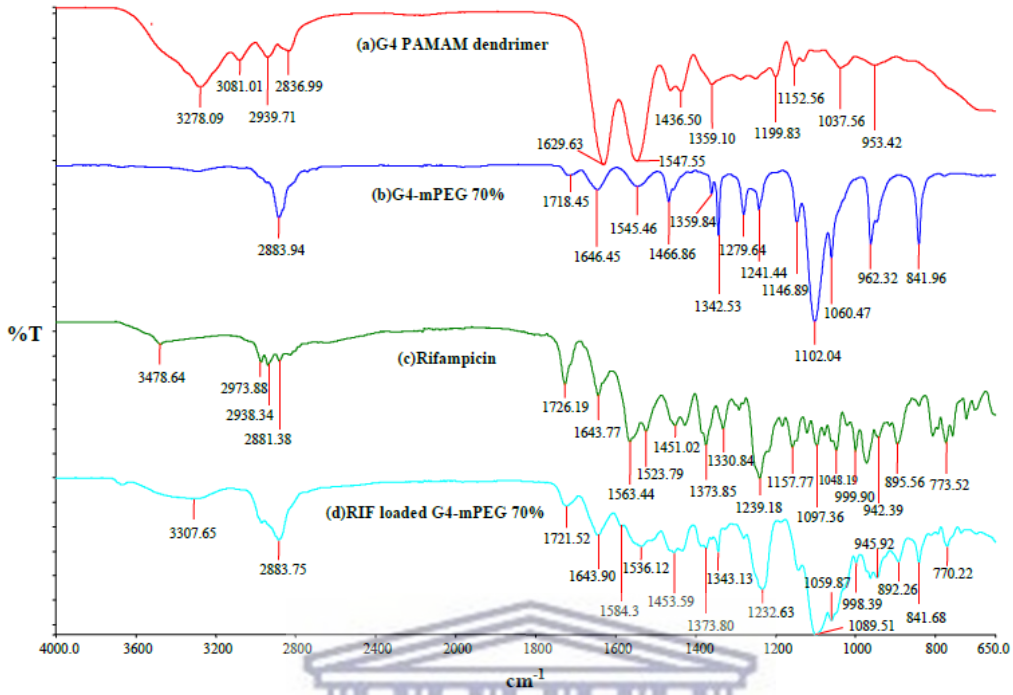

Figure 3.13 FTIR spectra of: (a) G4 PAMAM dendrimer, (b) G4-mPEG 70% (1:51), (c) rifampicin, and (d) RIF loaded G4-mPEG 70% (1:51).

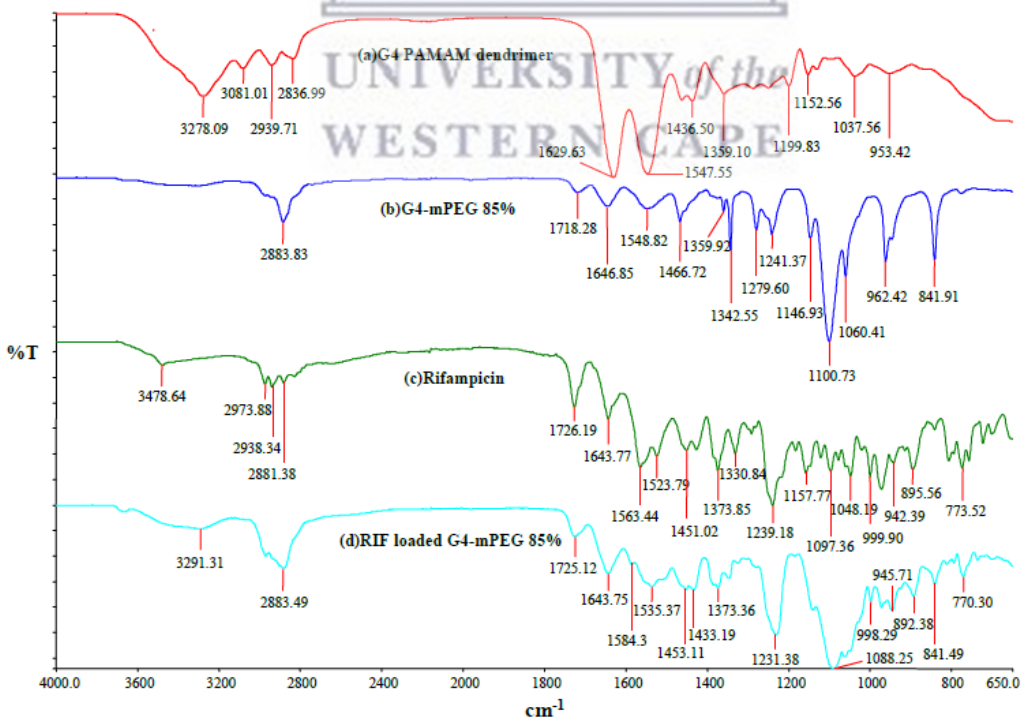

Figure 3.14 FTIR spectra of: (a) G4 PAMAM dendrimer, (b) G4-mPEG 85% (1:62), (c) rifampicin, and (d) RIF loaded G4-mPEG 85% (1:62).

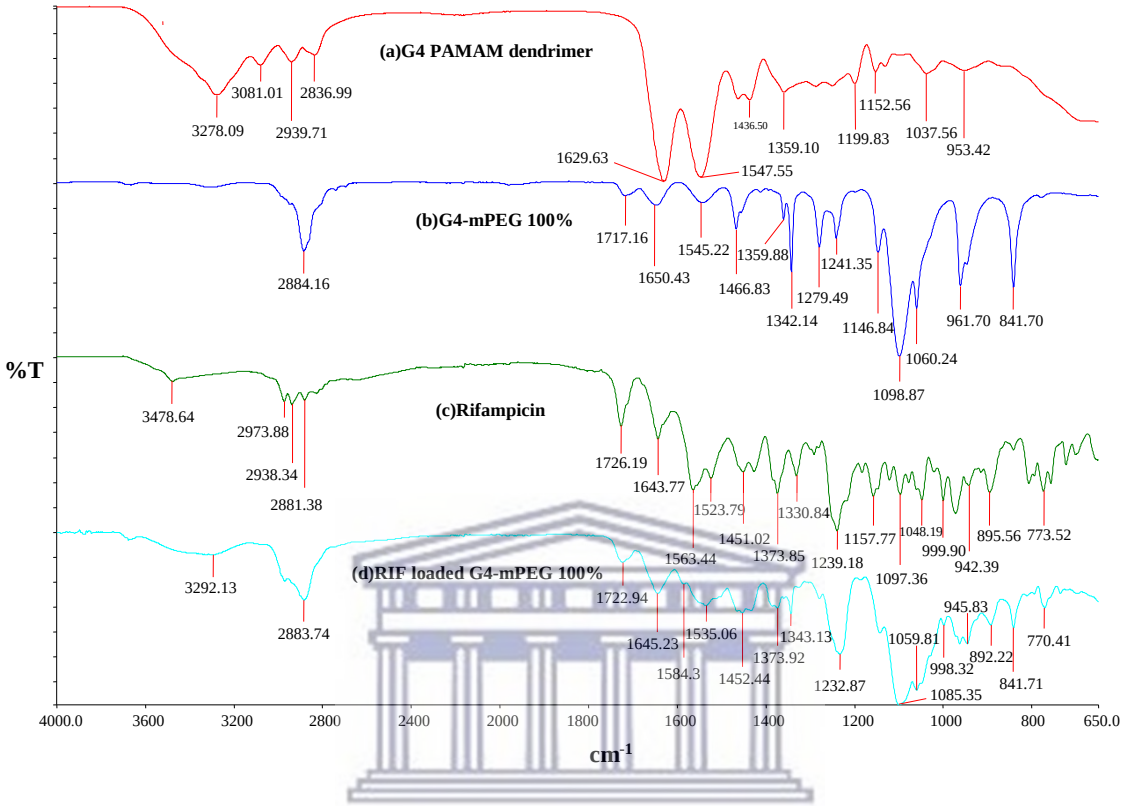

Figure 3.15 FTIR spectra of: (a) G4 PAMAM dendrimer, (b) G4-mPEG 100% (1:200), (c) rifampicin, and (d) RIF loaded G4-mPEG 100% (1:200).

For rifampicin loaded dendrimer (0% mPEG) (Figure 3.16 c), the IR spectra showed a broad O-H stretching at 3455 cm^{-1}, and a peak at 3675 cm^{-1} expected to be for free -OH groups. Methylene C-H stretching was noticed at 2901 cm^{-1} and 2988 cm^{-1}. The appearance of absorption peaks at 1723 cm^{-1}, 1647 cm^{-1}, and 1535 cm^{-1} were attributed to C=O of the carbonyl groups, C=O of the amide groups, and N-H of the amide groups (Figure 3.16 c), respectively. As aforementioned for all drug-loaded dendrimers, the new peak at 1584 cm^{-1}, as a result of H-bonding between the rifampicin and the dendrimer was also observed for rifampicin conjugated dendrimer (0% mPEG) at 1581 cm^{-1} (c). Once rifampicin was loaded to the dendrimer (0% mPEG), peaks at 1453 cm^{-1}, 1230 cm^{-1}, 1066 cm^{-1}, 892 cm^{-1}, and 771 cm^{-1} were observed and assigned to Ar (C-C) stretching, Ar (C-O) stretching, ester (C-O) stretching, C=C bending, and di-substituted C-H bending (c), respectively.

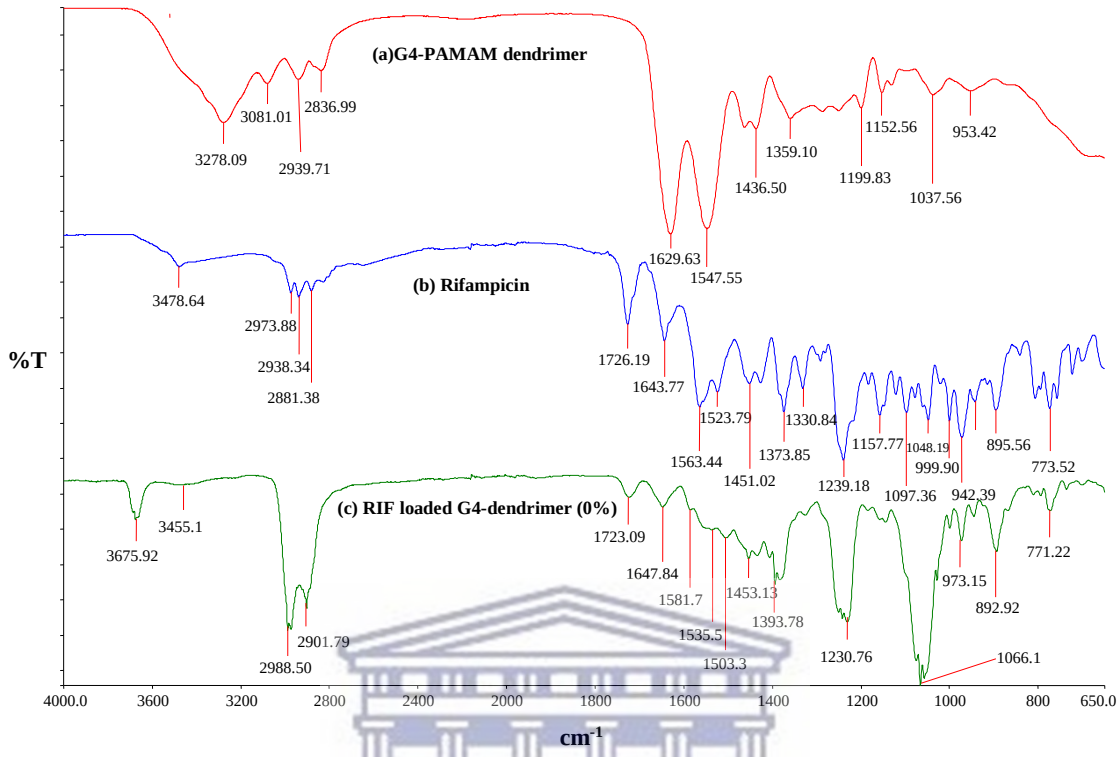

Figure 3.16 FTIR spectra of (a) G4 PAMAM dendrimer, (b) rifampicin, and (c) RIF loaded G4 dendrimer (0% mPEG).

3.7.4.2 Nuclear magnetic resonance (NMR) studies

The NMR analysis technique was employed to study rifampicin, and the rifampicin loaded dendrimer conjugates. ^{1}H NMR, ^{13}C NMR, COSY, TOCSY, HSQC, and HMBC were utilized to assign the chemical shifts of rifampicin atoms (Table 3.6). Furthermore, the change in the proton chemical shift and the 2D NOESY NMR data were employed to predict the preferred site(s) of interaction between the rifampicin molecules and the dendrimer scaffold.

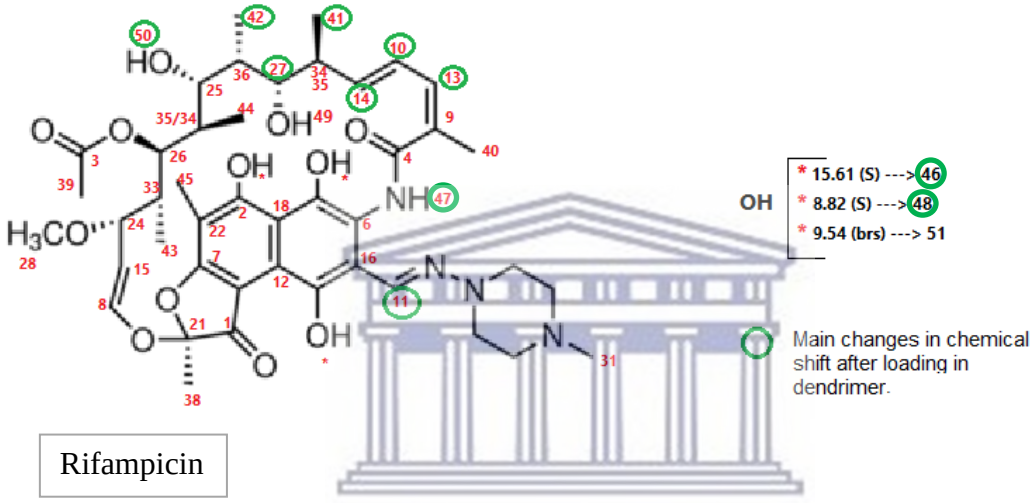

Figure 3.17 The structure of rifampicin.

Table 3.6 The ^{1}H NMR, ^{13}C NMR resonance assignments, multiplicity, integration, and coupling constants of rifampicin atoms in DMSO-d6.

Atom #	δ_C (mult.)	δ_H (RIF)	δ_H (PEGylated Conjugate)	δ_H (non-PEGylated Conjugate)	*J* = Hz	Integration	multiplicity	COSY	HMBC	TOCSY
1	184.5	-			-	-	-	-	-	
2	171.8	-			-	-	-	-	-	
3	169.5	-			-	-	-	-	-	
4	166.2	-			-	-	-	-	-	
5	148.6								-	
6	145.4	-			-	-	-	-	-	
7	143.59	-			-	-	-	-	-	
8	142.8	6.19			13.0	1H	d	H15	C21; C15/C16; C24	H15; H43; H24
9	138.2	-			-	-	-	-	-	
10	138.1	5.91	5.89	5.84	6.9; 16.2	1H	dd	H-14; H-34	C13	H13; H34; H41; H14; H27; H40
11	137.4	8.08	8.05	7.96	-	1H	s	-	C18; C16; C6	
12	132.3	-			-	-	-	-	-	
13	132.0	6.24	6.23	6.23	10.8	1H	d	H14; H40/H45	C4; C9; C39	H10; H34; H41; H14
14	127.7	7.11	7.08	6.99	11.1; 15.7			H10; H13	C34/C35	H10; H34; H41; H13
15	117.6	4.93			8.2; 12.7	1H	dd	H8; H24	C7	H8; H24; H43
16	117.2	-			-	-	-	-	-	
17	117.2	-			-	-	-	-	-	
18	115.6	-			-	-	-	-	-	
19	115.6	-			-	-	-	-	-	

20	114.2	-			-	-	-	-	-	
21	108.6	-			-	-	-	-	-	
22	101.0	-			-	-	-	-	-	
23	98.5								-	
24	76.5	3.23			8.4	1H	d	H15	C28; C43; C32	H26; H8; H15
25	76.2	2.82			8.8	1H	t	H50; H35	-	
26	73.6	5.07			10.8	1H	d	H33	C3; C24; C43	H34/35; H50; H33; H24
27	72.1	3.76	3.75	3.71	8.4	1H	d	H36; H34	C7	H41; H42; H34/35; H49
28	55.7	2.89			-	3H	s	H50; H35	C24	-
29	51.5								-	
30	47.9								-	
31	42.4	2.77			-	3H	s	-	-	
32	40.3	-			-	-	-	-	-	
33	40.1	1.03			-	1H	m	H43; H26	-	H26; H43
34	38.4	2.21			-	1H	m	H41/H42; H27; H10	-	
35	38.1	1.33			-	1H	m	H43; H25/H28/H31	-	
36	32.9	1.60			-	1H	m	-	-	
37	29.0	1.24			-	0.5H	s	-	-	
38	22.2	1.64			-	3H	s	H42; H40/H45	C1; C21	-
39	20.7	1.98			-	3H	s	-	C40; C3	
40	20.6	1.91			-	3H	s	H13; H36/H38	C4; C12	H13; H14; H10
41	17.8	0.83	0.84	0.84	6.7	3H	d	H34	C34; C27; C10; C9	H34/35; H10; H14; H49; H27
42	11.4	0.89	0.88	0.87	6.8	3H	d	H36/H38	C36; C27; C25	H27
43	8.98	-0.25			6.6	3H	d	H33	C33; C26; C24	H33; H26; H15; H8

44	8.7	0.44			6.6	3H	d	H35	C34; C26; C25	H35; H50; H25
45	7.5	1.91			-	3H	s	-	C2; C1; C22	
46		15.61	15.50	15.46	-	1H	br s	-	-	-
47		12.52	12.49	12.45	-	1H	br s	-	C16; C6	-
48		8.80	8.91	9.13	-	1H	br s	-	-	
49		5.05			-	1H	br s	H27	-	H34; H27; H41
50		4.18	4.21	4.31	8.4	1H	d	H25/H28/H31	-	H25; H35; H44
51		9.54			-	1H	br s			

*s= singlet; d= doublet; m= multiplet, br s= broad singlet; t= triplet; dd= doublet of doublets; J = coupling constant, COSY= correlation spectroscopy; HMBC= heteronuclear multiple-bond correlation spectroscopy; TOCSY= total correlation spectroscopy.

Table 3.6 lists the resonance data of the rifampicin atoms and rifampicin in conjugated dendrimers. Comparing the ^{1}H NMR spectra of the rifampicin loaded PEGylated dendrimer (38%) to that of the pure rifampicin (Figure 3.18), revealed the existence of most rifampicin proton peaks at relatively similar chemical shifts in both spectra. The only exception is that of the atoms that are circled in Table 3.6 i.e., proton numbers 10, 11, 13, 14, 27, 41, 42, 46, 47, 48, and 50. Atom numbers 41, 48, and 50 of the rifampicin conjugated dendrimer emerged at relatively higher chemical shifts (δ_H) (downfield) compared to that of the pure rifampicin. While atom numbers 10, 11, 13, 14, 27, 42, 46, and 47 emerged at lower chemical shifts (δ_H) (upfield) comparative to the pure rifampicin. Hydrogen bonding between the rifampicin and the dendrimer could account for the changes in the chemical shifts of these 11 atoms. The lower intensities of the proton peaks of rifampicin in the conjugate complex were due to the lower rifampicin concentration present in the dendrimer nanoparticles compared to the crude drug sample.

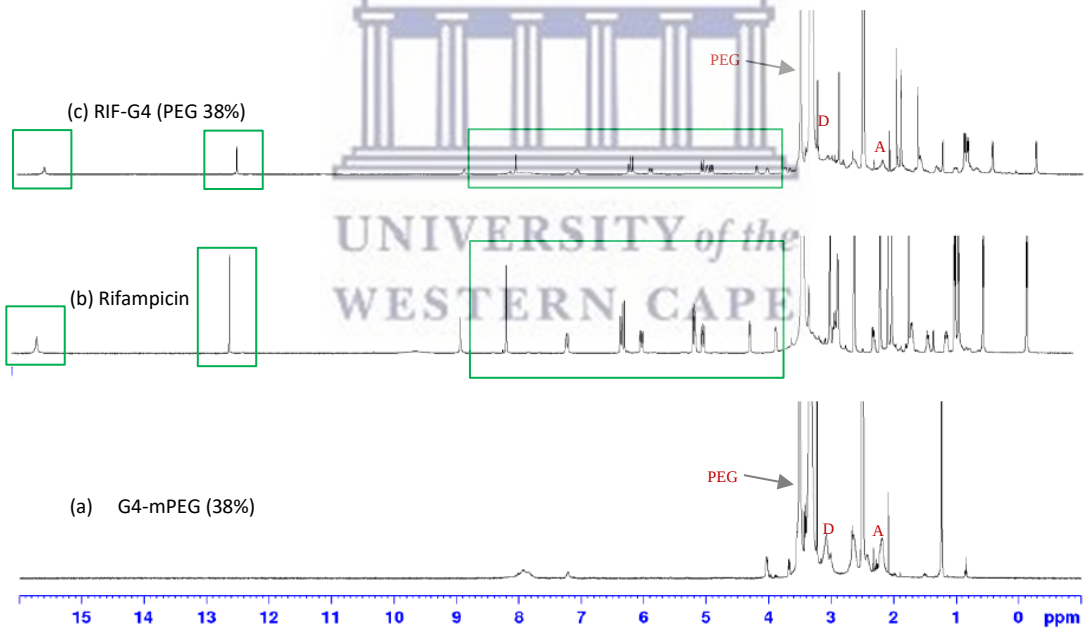

Figure 3.18 ^{1}H NMR spectra of (a) PEGylated G4 PAMAM dendrimer (38%), (b) rifampicin, and (c) rifampicin loaded PEGylated G4 PAMAM dendrimer (38%), in DMSO-d_6.

For the PEGylated dendrimer, the proton peaks that correspond to the mPEG part and the methylenes of the dendrimer were also observed in the ^{1}H NMR spectrum of the rifampicin

loaded PEGylated dendrimer (38%) (Figure 3.18). The proton peak which corresponds to the methylene of (-***CH*$_2$**-OCO-) on the mPEG chain appeared at a relatively higher chemical shift when the rifampicin was loaded. While the other proton peaks of the mPEG chain were detected at approximately similar chemical shifts to the unloaded PEGylated dendrimer. The methylene proton peaks of the dendrimer part were observed at comparable chemical shifts to the unloaded dendrimer. Only methylene protons adjacent to the carbonyl groups (Figure 3.18, peak A), and adjacent to the secondary amino groups (Figure 3.18, peak D) were observed at higher chemical shifts compared to the unloaded dendrimer. Again, H-bonding between rifampicin and the dendrimer could be the reason behind the changes in the chemical shifts of the proton peaks of the PEGylated dendrimer as a result of deshielding.

The proton NMR spectra of the other PEGylated dendrimer formulations have further corroborated the formation of non-covalent interactions between rifampicin molecules and dendrimers. The ^{1}H NMR spectra of rifampicin loaded 49% (Figure 3.19), 70% (Figure 3.20), 85% (Figure 3.21), and 100% (Figure 3.22) PEGylated dendrimers showed similar findings, i.e., δ_H of unloaded and rifampicin loaded PEGylated dendrimers, change in the chemical shifts of 11 rifampicin atoms circled in Table 3.6, to that of the rifampicin-loaded 38% PEGylated dendrimer (Figure 3.18, Table 3.6).

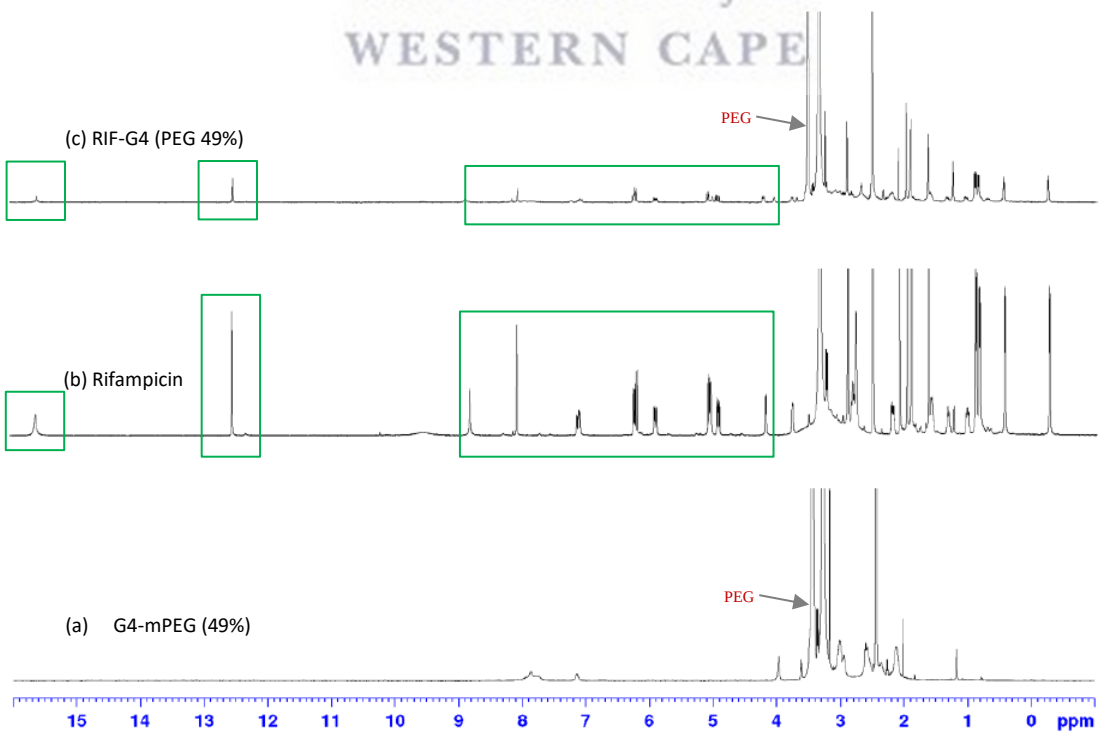

Figure 3.19 ^{1}H NMR spectra of (a) PEGylated G4 PAMAM dendrimer (49%), (b) rifampicin, and (c) rifampicin loaded PEGylated G4 PAMAM dendrimer (49%), in DMSO-d_6.

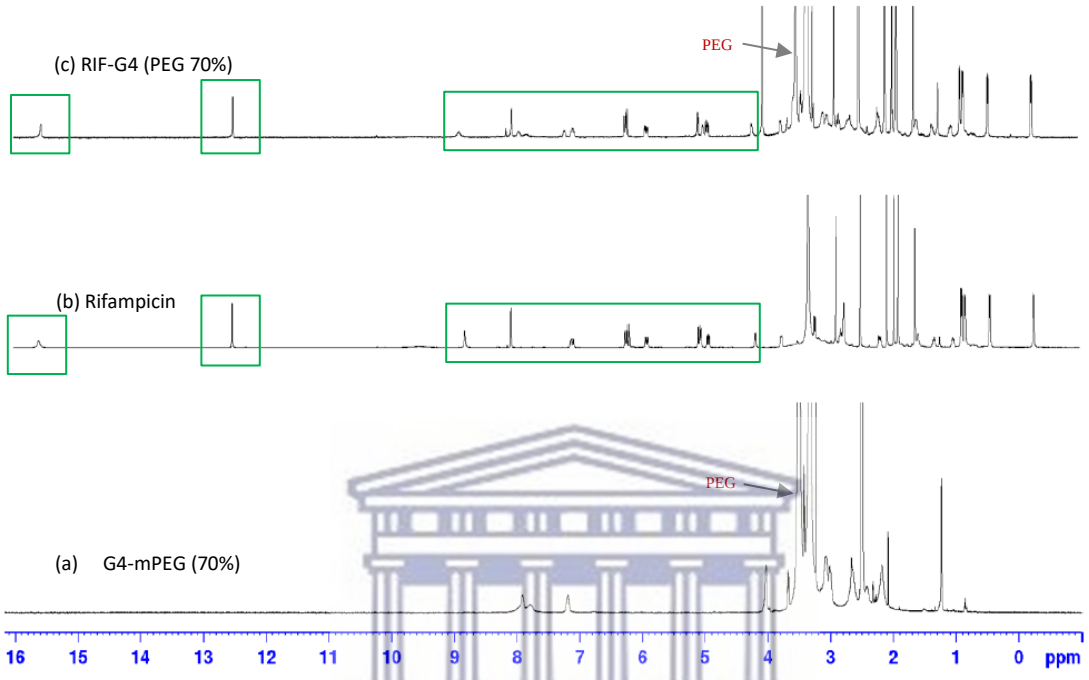

Figure 3.20 ^{1}H NMR spectra of (a) PEGylated G4 PAMAM dendrimer (70%), (b) rifampicin, and (c) rifampicin loaded PEGylated G4 PAMAM dendrimer (70%), in DMSO-d_6.

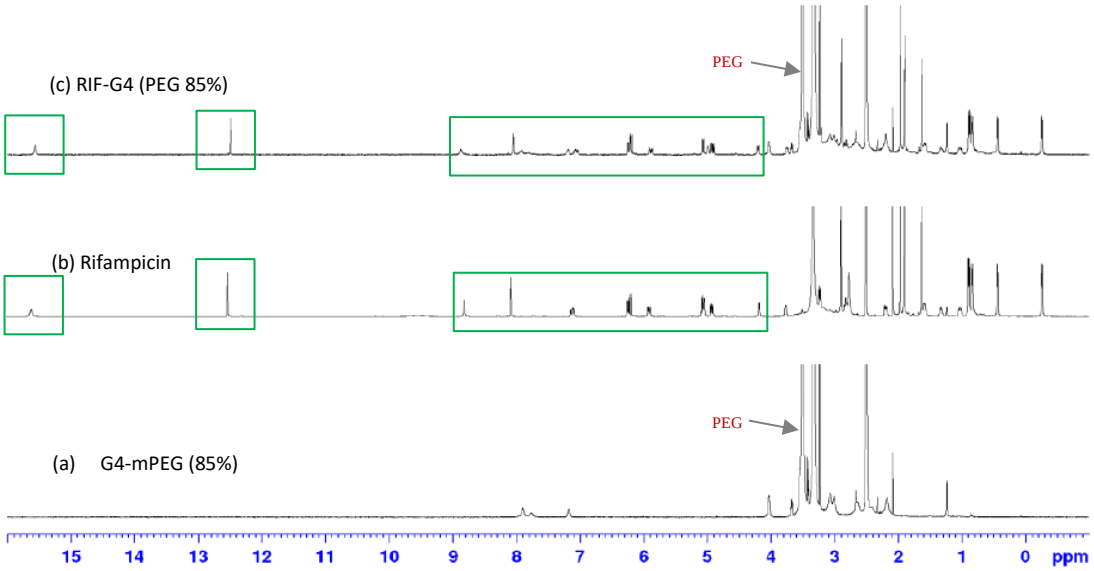

Figure 3.21 ^{1}H NMR spectra of (a) PEGylated G4 PAMAM dendrimer (85%), (b) rifampicin, and (c) rifampicin loaded PEGylated G4 PAMAM dendrimer (85%), in DMSO-d_6.

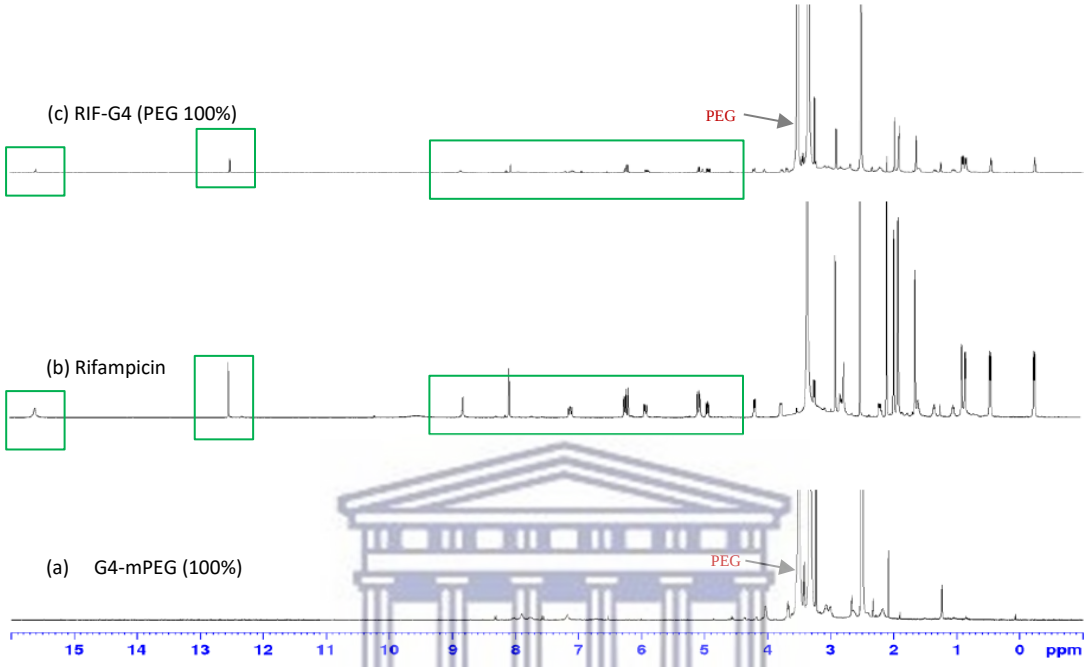

Figure 3.22 ^{1}H NMR spectra of (a) PEGylated G4 PAMAM dendrimer (100%), (b) rifampicin, and (c) rifampicin loaded PEGylated G4 PAMAM dendrimer (100%), in DMSO-d_6.

In Figure 3.23, the 2D NOESY NMR of rifampicin loaded PEGylated G4 PAMAM dendrimer was studied. The 2D NOESY NMR analysis was performed to validate the supramolecular conjugation of rifampicin molecules within the PEGylated dendrimer. Also, 2D NOESY data was employed to identify the site(s) of interaction between the drug molecules and the dendrimer. The cross-peaks in the NOESY spectra indicating nearby proton atoms interacting at a distance of < 5 Å (Diaz *et al.*, 2018b). From Figure 3.23, the observed cross-peaks predict the interaction of rifampicin molecules with the mPEG portion besides the dendrimer's methylene portion. Particularly, rifampicin atom numbers 10 (δ_H = 5.89 ppm), 14 (δ_H = 7.08 ppm), 27 (δ_H = 3.75 ppm), and 42 (δ_H = 0.88 ppm) interacted with the dendrimer's methylene protons adjacent to the carbonyl groups (δ_H = 2.19 ppm). While rifampicin atom numbers 11 (δ_H = 8.05 ppm), and 39 (δ_H = 1.98 ppm) preferentially interacted with the ethylene protons of the mPEG moieties (δ_H = 3.51 ppm).

These findings suggesting the dual conjugation of rifampicin molecules in the internal shell of the dendrimer and at the peripheral mPEG chains.

The NOESY NMR spectra of the other rifampicin-loaded PEGylated dendrimers (49%, 70%, 85%, and 100%) also confirmed the interaction of rifampicin molecules with the inner dendrimer methylene protons, as well as, with the outer PEG chains. Our results propose that surface modification of G4 PAMAM dendrimer with 38% - 100% of 2.0 kDa mPEG chains does not completely hinder the diffusion of rifampicin molecules towards the dendrimer's interior.

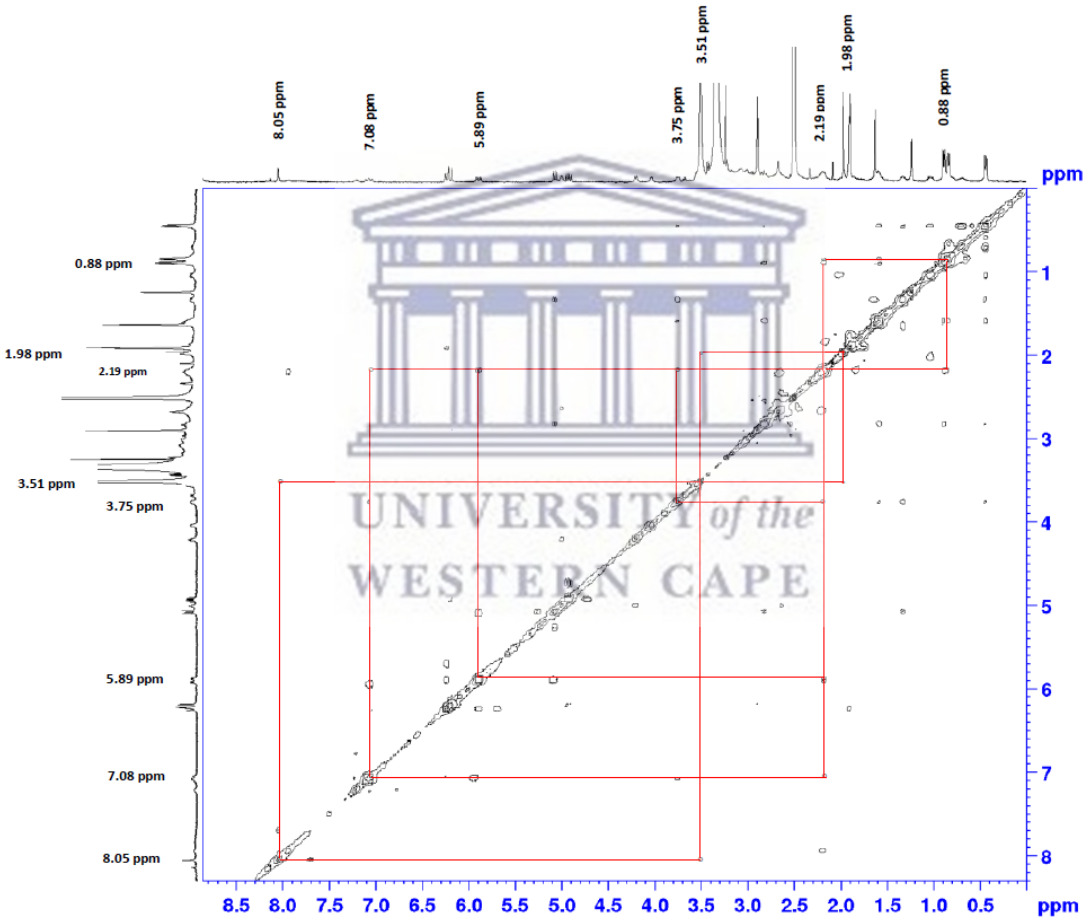

Figure 3.23 2D NOESY NMR spectra of rifampicin loaded PEGylated G4 PAMAM dendrimer (38%), in DMSO-d_6.

A similar finding was previously observed by Diaz and co-workers (2017), their results indicated that surface modification of G4 PAMAM dendrimer with 50% of 2.0 kDa mPEG

chains does not prevent the encapsulation of silybin molecules inside the dendrimer cavities (Diaz *et al.*, 2018b). Barraza and co-authors (2015, 2016), observed that when increasing the degree of PEGylation of G4 PAMAM dendrimer by more than 50%, a significant decrease in the amount of 5-fluorouracil or methotrexate molecules that diffuse into the dendrimer interior and the majority of drug molecules interacted with the outer mPEG chains (Barraza, Jiménez and Alderete, 2015, 2016).

The ^{1}H NMR spectrum of the rifampicin loaded non-PEGylated dendrimer (0% mPEG) was illustrated in Figure 3.24. Rifampicin protons, as well as, the dendrimer methylene proton peaks, were detected in the spectrum of the rifampicin conjugate complex. Proton numbers 10, 11, 13, 14, 27, 41, 42, 46, 47, 48, and 50 of the rifampicin in the non-PEGylated dendrimer showed slightly different chemical shifts compared to that of the pure rifampicin (Table 3.6, Figure 3.24). Atom numbers 41, 48, and 50 appeared at higher

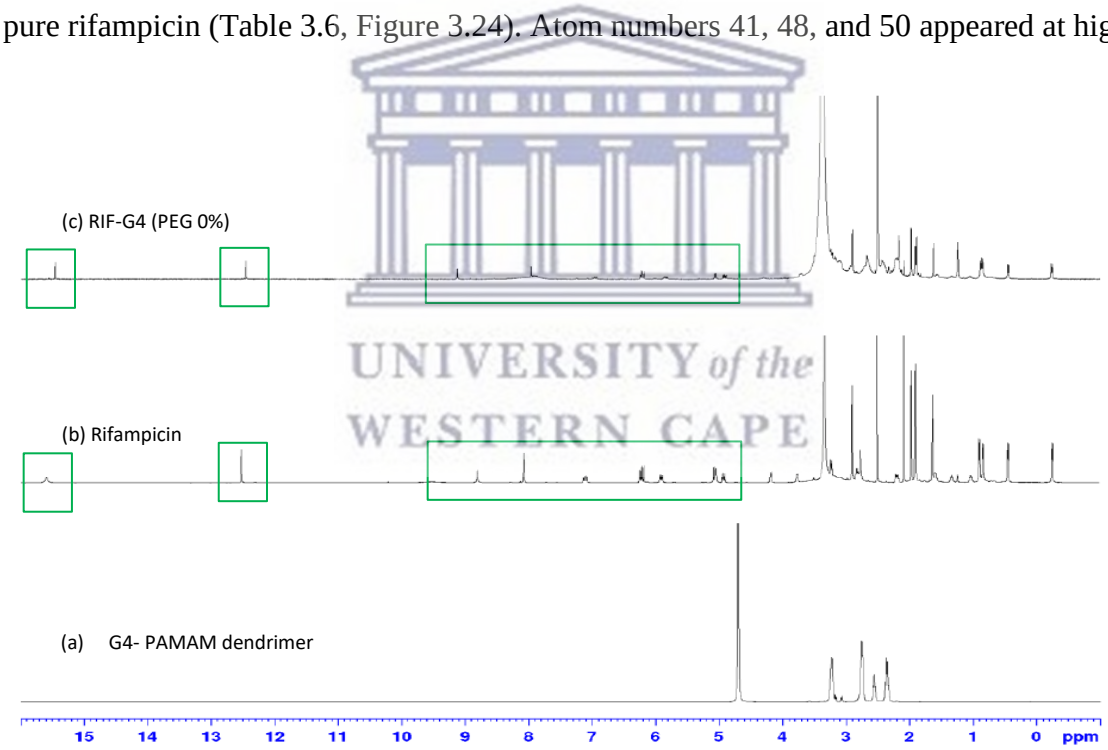

Figure 3.24 ^{1}H NMR spectra of (a) G4 PAMAM dendrimer in D_2O, (b) rifampicin in DMSO-d_6, and (c) rifampicin loaded G4- dendrimer (mPEG 0%) in DMSO-d_6.

chemical shifts (δ_H) compared to that of the pure rifampicin. Whereas atom numbers 10, 11, 13, 14, 27, 42, 46, and 47 appeared at lower chemical shifts comparative to the pure rifampicin. Furthermore, the methylene protons of the dendrimer appeared at higher

chemical shifts when rifampicin was loaded. Principally, the methylene protons that are close to the carbonyl groups and the secondary amino groups exhibit higher chemical shifts relative to that in the G4 PAMAM dendrimer. H-bonding between the drug molecules and the dendrimer interior could be the reason for the observed chemical shifting.

Figure 3.25 illustrates the 2D NOESY data of rifampicin loaded non-PEGylated dendrimer. The observed cross-peaks in Figure 3.25 account for the interaction between rifampicin proton number 11 (δ_H = 7.96 ppm) and the inner methylene protons of the G4 PAMAM

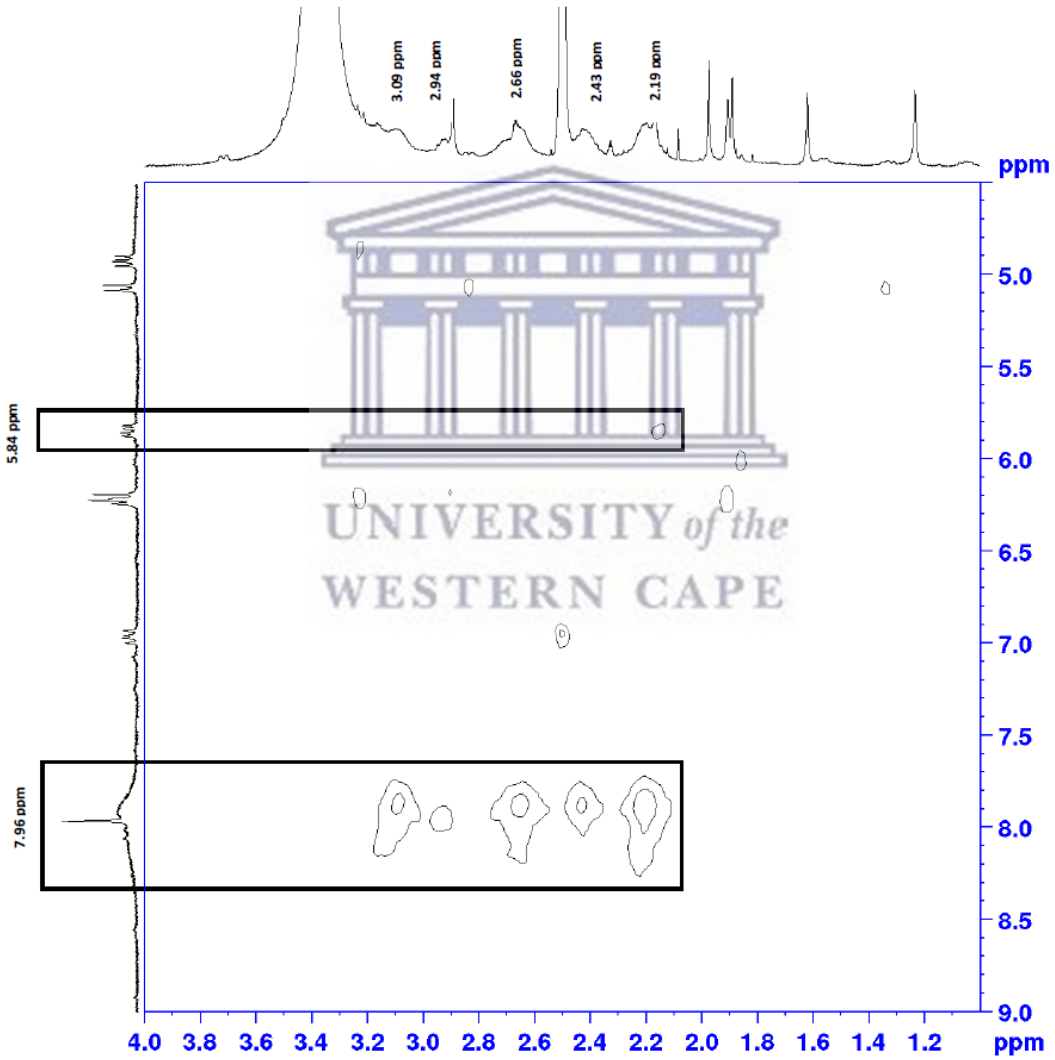

Figure 3.25 2D NOESY NMR spectra of rifampicin loaded non-PEGylated G4 PAMAM dendrimer (0% mPEG), in DMSO-d_6.

dendrimer (δ_H = 2.19 ppm; δ_H = 2.43 ppm; δ_H = 2.66 ppm; δ_H = 2.94 ppm; δ_H = 3.09 ppm). The interaction of the dendrimer's methylene protons (δ_H = 2.19 ppm) with the rifampicin proton number 10 (δ_H = 5.84 ppm) was detected as a cross-peak in Figure 3.25. The 2D NOESY data of rifampicin loaded non-PEGylated dendrimer corroborates that rifampicin molecules have mainly interacted with the internal methylene protons of the G4 PAMAM dendrimer.

3.7.4.3 Morphology of the nanoparticles

The shape of G4 PAMAM dendrimer, PEGylated PAMAM dendrimers, rifampicin-loaded PEGylated and non-PEGylated G4 PAMAM dendrimers were characterized using scanning electron microscopy (SEM).

SEM images of G4 PAMAM dendrimer (Figure 3.26 a) indicate the spherical shape of the nanoparticles. It was observed that the mPEG conjugation and rifampicin loading decrease the smoothness of the spherical nanoparticles (Figure 3.26 (b & c)), due to their presence on the dendrimer surface.

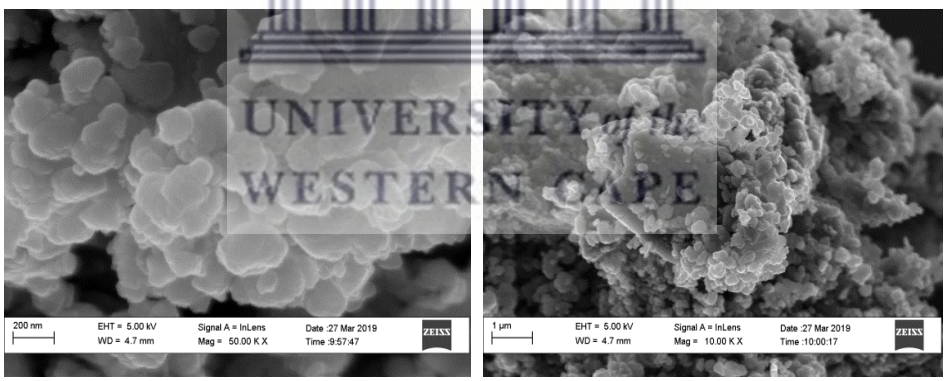

(a) G4 PAMAM dendrimer alone

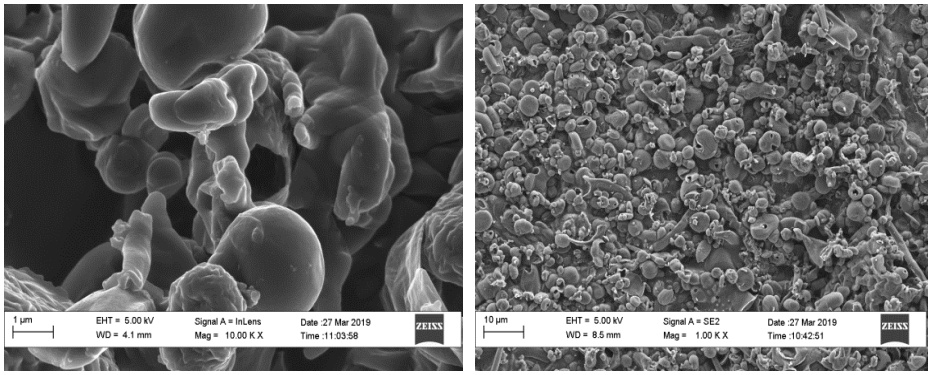

(b) PEGylated dendrimer (85%)

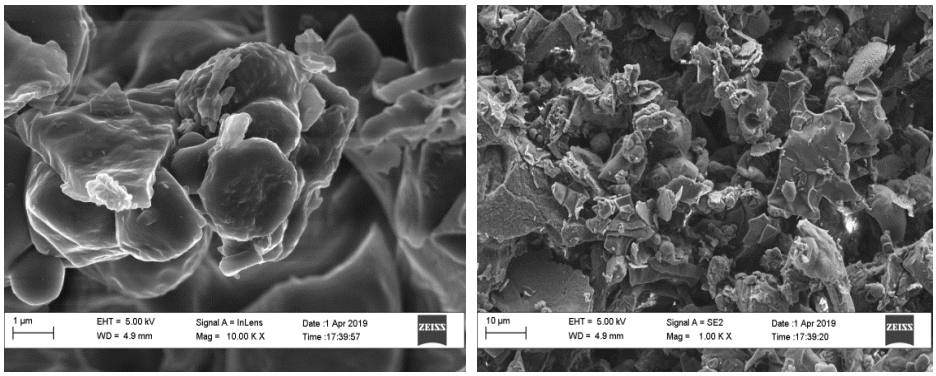

(c) Rifampicin loaded PEGylated dendrimer (85%)

Figure 3.26 SEM micrographs of (a) pure G4 PAMAM dendrimer, (b) PEGylated dendrimer (85% PEG), and (c) rifampicin-loaded PEGylated dendrimer (85% PEG).

Increasing the degree of dendrimer PEGylation resulted in the transition of the dendrimer surface from smooth spherical to coarse spherical shape, as illustrated in Figure 3.27 (A-F). This observable fact can be elucidated by the characteristic of the conjugated polymer (mPEG). Synthesis of the PEGylated dendrimer was done using long-chain 2kD mPEG polymer (Kojima et al., 2000), which may collapse on the dendrimer surface forming an irregular coat under SEM (Samkange et al., 2019).

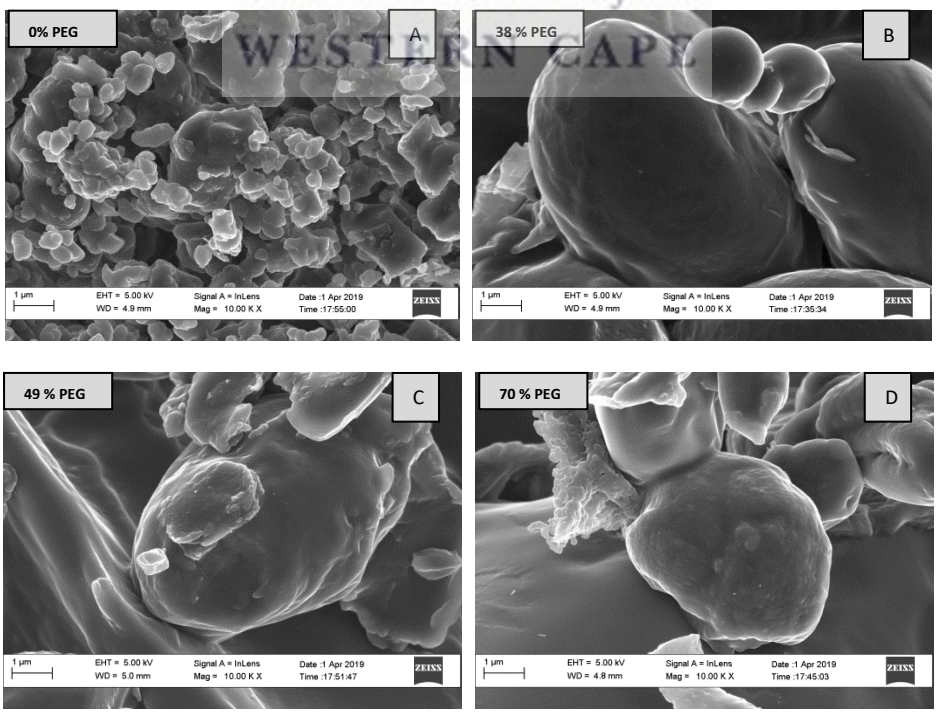

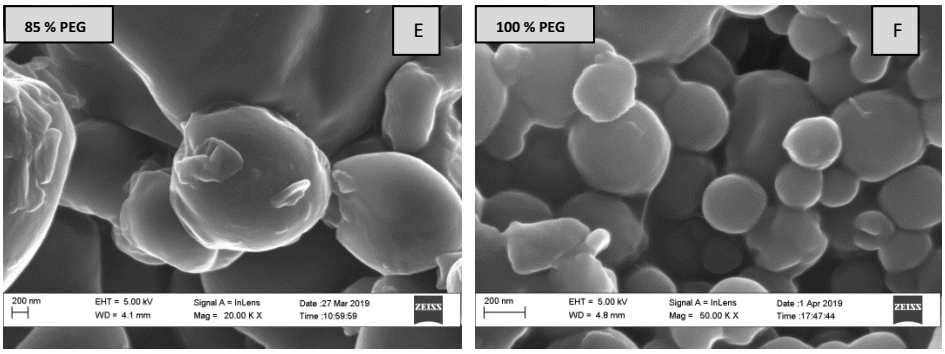

Figure 3.27 SEM images of (A) RIF-G4 dendrimer (0% mPEG), (B) RIF-G4 dendrimer (38% mPEG), (C) RIF-G4 dendrimer (49% mPEG), (D) RIF-G4 dendrimer (70% mPEG), (E) RIF-G4 dendrimer (85% mPEG), and (F) RIF-G4 dendrimer (100% mPEG).

3.7.4.4 Differential scanning calorimetry DSC studies

Differential scanning calorimetry (DSC) analysis was performed to study the physical state of rifampicin and the dendrimer in the formulation, as well as to predict any potential interactions between the drug and the dendrimer (Vijayaraj Kumar *et al.*, 2007). The analysis was done for pure rifampicin, rifampicin loaded dendrimers, their corresponding unloaded dendrimers, and drug-dendrimer physical mixtures, at an increasing heating rate of 10 °C/ min from 35 °C to 220 °C under N_2 gas flow.

For the temperature range studied, pure rifampicin experienced a broad endothermic transition which started at about 183.98 °C and ended at 202.10 °C with a peak at 196.27 °C (Figure 3.28 (1)). This temperature was previously reported as the melting point of rifampicin (Pelizza *et al.*, 1977). A sharp endothermic peak for the unloaded PEGylated (100% PEG) was observed at about 54.33 °C (Figure 3.28 (3)). The characteristic peaks of the rifampicin and the unloaded PEGylated dendrimer (100%) disappeared in the DSC curve of rifampicin loaded PEGylated dendrimer (100%) and a new peak exhibited at about 53.0 °C (Figure 3.28 (4)). While the peaks of rifampicin and unloaded PEGylated dendrimer were detected in the drug-dendrimer physical mixture curve (Figure 3.28 (2)). The overall finding suggested that the rifampicin loaded PEGylated dendrimer (100%) was not a physical mixture.

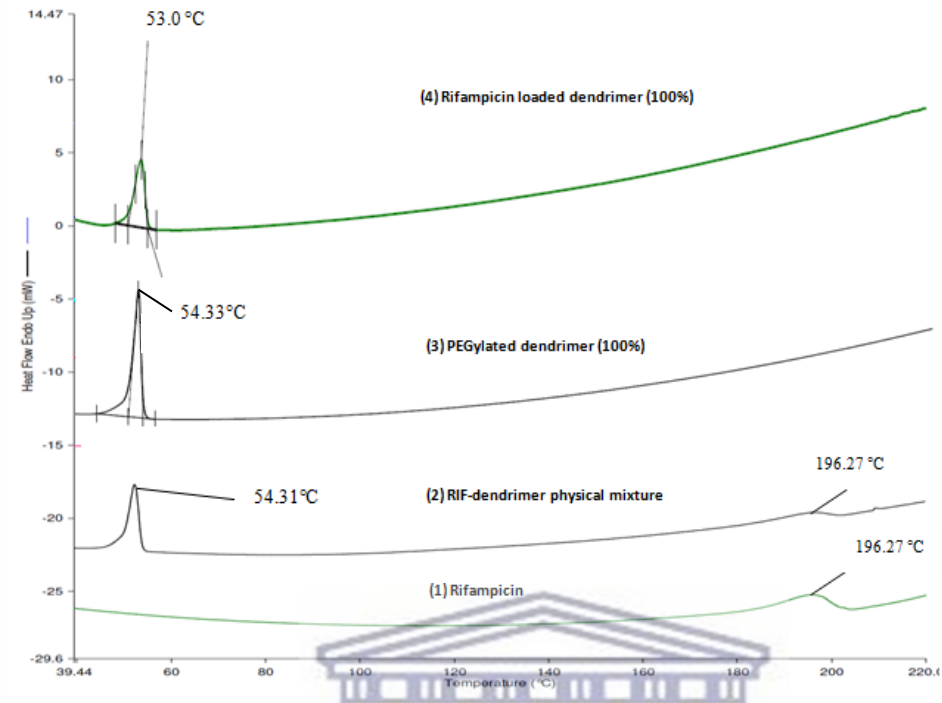

Figure 3.28 DSC thermograms of (1) rifampicin, (2) RIF-dendrimer physical mixture (100% mPEG), (3) PEGylated dendrimer (100% mPEG), and (4) RIF-dendrimer (100% mPEG).

In Figure 3.29 and Table 3.7, drug-loaded dendrimer formulations show new endothermic peaks with a lower transitional temperature comparative to their corresponding unloaded

Table 3.7 Comparison of the dendrimer's endothermic peaks before and after drug conjugation.

Type of the dendrimer	Endothermic peak (°C)	
	Unloaded dendrimer	Drug-loaded dendrimer
Dendrimer (38% mPEG)	53.10	51.49
Dendrimer (49% mPEG)	54.63	53.31
Dendrimer (70% mPEG)	53.40	52.31
Dendrimer (85% mPEG)	52.26	49.03
Dendrimer (100% mPEG)	54.33	53.00

dendrimers. In addition, we observe the disappearance of the rifampicin peak in all drug conjugated dendrimer nanoparticles. Physical mixtures of rifampicin and other PEGylated formulations (38%, 49%, 70%, and 85%) confirmed the presence of both endothermic peaks correspond to unloaded PEGylated dendrimers (Table 3.7), as well as, rifampicin peaks at about 196.27 °C. These results suggest that drug-dendrimer complexes were not physical mixtures and the expected drug-dendrimer interactions induced a lowering of the transitional temperature, as observed previously (Vijayaraj Kumar *et al.*, 2007).

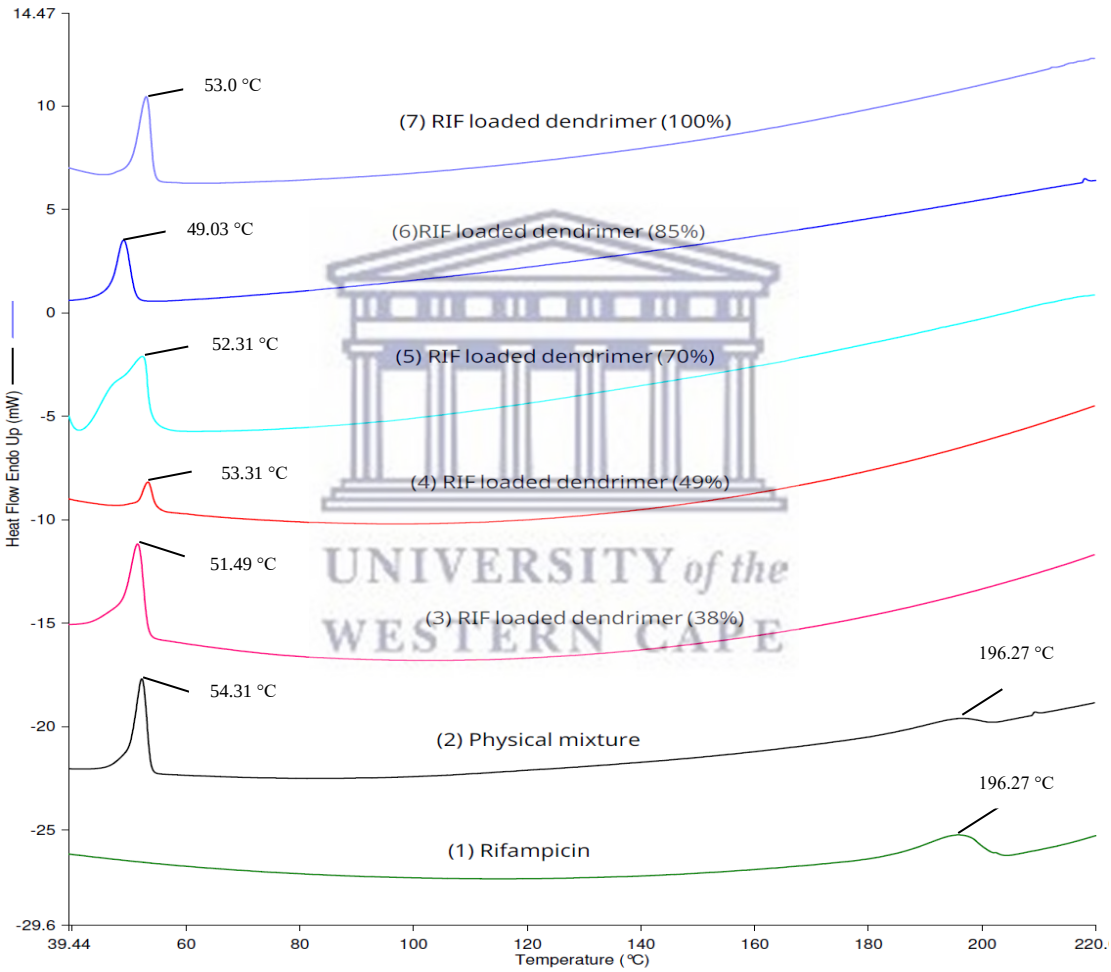

Figure 3.29 DSC thermograms of (1) rifampicin, (2) rifampicin-dendrimer physical mixture (100% mPEG), (3) RIF-dendrimer (38% mPEG), (4) RIF-dendrimer (49% mPEG), (5) RIF-dendrimer (70% mPEG), (6) RIF-dendrimer (85% mPEG), and (7) RIF-dendrimer (100% mPEG).

3.7.4.5 Nanoparticles size, PDI, and ZP studies

DLS technique was used to determine the hydrodynamic diameter (D_H), PDI, and the zeta potential of dendrimer nanoparticles (Table 3.8). The analysis was done on a Malvern Zetasizer Nano ZS90 using dynamic light scattering (DLS) theory.

i) Nanoparticle size and polydispersity index (PDI)

The hydrodynamic size of the unloaded dendrimer formulations ranged from 4.22 nm ± 1.30 nm for native dendrimer (0% mPEG) to 21.27 nm ± 2.60 nm for 100% PEGylated dendrimer. While for rifampicin loaded dendrimer formulations, the hydrodynamic size was ranged from 5.14 nm ± 1.20 nm for drug-loaded dendrimer (0% mPEG) to 21.19 nm ± 2.50 nm for drug-loaded 100% PEGylated dendrimer (Table 3.8).

There was a statistically significant difference in the hydrodynamic diameter (D_H) among unloaded dendrimer nanoparticles verified by a one-way ANOVA test ($p < 0.05$). Applying Tukey post hoc test, which is commonly used to compare the mean of one sample to the mean of each of the other samples, the result indicated that 49% mPEG, 70% mPEG, and 100% mPEG dendrimers had diameters which were significantly greater than that of pure dendrimer (0% mPEG) ($p < 0.05$) (Table 3.8, Figure 3.30). In addition, data analysis revealed that 38% mPEG, 49% mPEG, and 85% mPEG dendrimers exhibited D_H significantly smaller than the 100% mPEG dendrimer ($p < 0.05$). The coefficient of determination (R^2) obtained from one-way ANOVA analysis signified a strong relationship between the degree of dendrimer PEGylation and the hydrodynamic diameter of nanoparticles ($R^2 = 0.8918$) (Table 3.8 and Figure 3.30).

Following drug conjugation, ANOVA analysis (Tukey post hoc test) indicated that all rifampicin-loaded PEGylated dendrimers (38% mPEG - 100% mPEG) had diameters that are significantly greater than rifampicin-loaded non-PEGylated dendrimer (0% mPEG) ($p < 0.05$). Among the drug-loaded PEGylated dendrimers, 70% mPEG and 85% mPEG formulations exhibited a D_H which was significantly smaller compared to 38% mPEG and 100% mPEG formulations ($p < 0.05$). No significant difference was observed between 38%, 49%, and 100% drug-loaded formulations ($p > 0.05$).

Comparing each dendrimer formulations before and after drug loading revealed that no statistically significant difference in their D_H was observed ($p > 0.05$). The only exception was noticed with the 38% formulation that exhibited a significant increase in the size following the drug conjugation, from 9.32 nm ± 1.78 nm to 22.15 nm ± 1.82 nm ($p < 0.05$) (Table 3.8 and Figure 3.30).

Table 3.8 The physicochemical characteristics of the unloaded and rifampicin-loaded dendrimers having different mPEG content. Results illustrated as mean ± SD (n = 3).

Dendrimer-PEG content	Hydrodynamic diameter (nm)		PDI		Zeta potential (mV)	
	unloaded	Loaded	unloaded	Loaded	unloaded	Loaded
0% mPEG	4.22 ± 1.30	5.14 ± 1.20	0.29 ± 0.02	0.31 ± 0.09	36.97 ± 3.46	31.87 ± 1.01
38% mPEG	9.32 ± 1.78	22.15 ± 1.82	0.32 ± 0.01	0.34 ± 0.04	28.37 ± 2.46	15.17 ± 0.76
49% mPEG	13.64 ± 1.57	15.80 ± 2.18	0.25 ± 0.13	0.35 ± 0.02	31.00 ± 1.85	20.33 ± 3.61
70% mPEG	14.47 ± 3.33	12.50 ± 2.63	0.37 ± 0.11	0.39 ± 0.09	18.47 ± 3.59	17.10 ± 2.09
85% mPEG	8.81 ± 1.32	13.11 ± 1.88	0.27 ± 0.03	0.28 ± 0.07	17.07 ± 1.12	13.37 ± 1.43
100% mPEG	21.27 ± 2.60	21.19 ± 2.50	0.31 ± 0.07	0.37 ± 0.05	13.83 ± 0.99	17.03 ± 0.78

mPEG chains, which were confirmed previously in this chapter, conjugated to the surface of the dendrimer *via* an amide bond. The long-chain mPEG (i.e., 2 kDa M.wt) could increase the nanoparticle size due to peripheral mPEG-mPEG crowding that stretches dendrimer arms towards the exterior and therefore enlarges their size (Lee and Larson, 2011), which was observed for the unloaded PEGylated dendrimers compared to the pure

dendrimer. From the coefficient of determination (R^2 = 0.8918), the degree of PEGylation has a significant impact on increasing the nanoparticle size, particularly for the 49% mPEG, 70% mPEG, and 100% mPEG dendrimers ($p < 0.05$). No significant increase in the size of the 38% PEGylated dendrimer was noticed, this could be due to lower mPEG chains conjugated compared to the other PEGylated dendrimers.

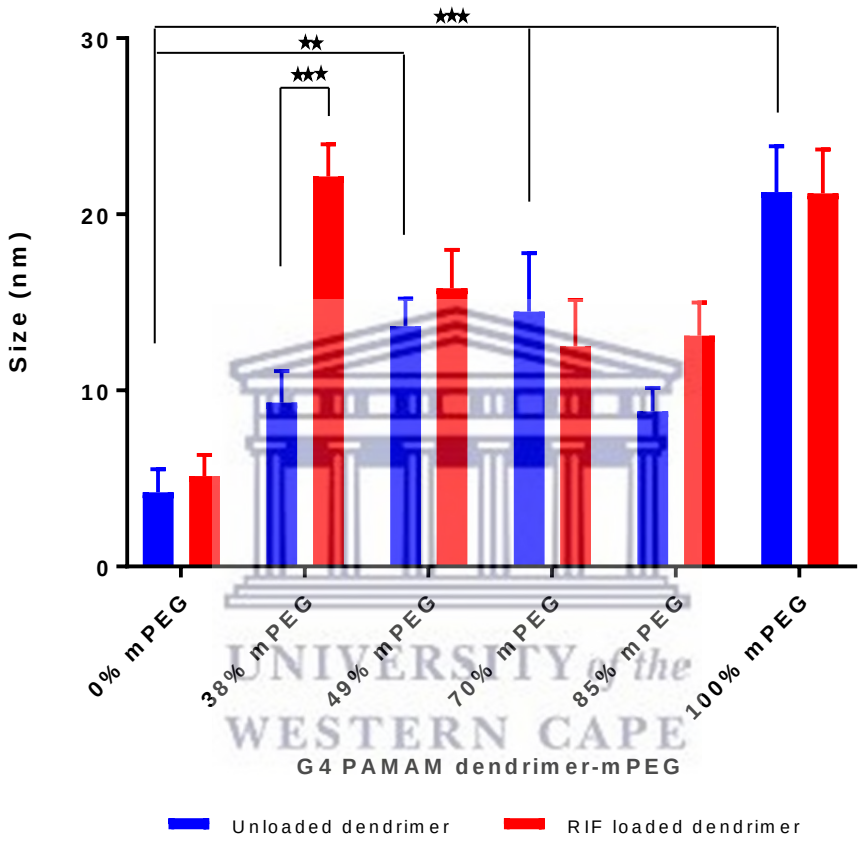

(* = p ≤ 0.05; ** = p ≤ 0.01; *** = p ≤ 0.001)

Figure 3.30 The hydrodynamic (D_H) diameters of unloaded (blue) and rifampicin-loaded (red) dendrimer nanoparticle formulations with different mPEG content. Results show a mean ± SD (n = 3). Error bars represent the calculated SD from the mean.

Increasing in the dendrimer size after PEGylation was also previously reported by (Zhu *et al.*, 2010a; Li *et al.*, 2017; Ho *et al.*, 2019)

A molecular dynamics study performed by Lee and Larson (2011) assessed the effect of PEGylation on the size of G4, G5, and G7 PAMAM dendrimers (Lee and Larson, 2011).

The results illustrated that pure dendrimers are characterized by dense-core conformational structures at a neutral pH, where the dendrimer has higher monomer density at the interior core with a decrease toward its periphery as shown in Figure 3.31 (left image). After PEGylation with mPEG 550 and 5000, the dendrimer structures shifted to dense-shell conformations for the long-length mPEG, where a lower monomer density at the dendrimer core developed increasing toward the periphery (Figure 3.31- right image). No significant conformational change was observed for the lower mPEG chain. The change in the conformational structure showed an increase in the size of the nanoparticle due to the stretch effect of the mPEG chains. The study also noticed that the stretching effect and conformational transition is not only a function of the mPEG chain length but also their densities on the dendrimer surface (Lee and Larson, 2011).

Our results confirmed that the increase in the dendrimer size was directly proportional to the degree of PEGylation (i.e., PEG density). From Table 3.8, ANOVA analysis verified that 0% mPEG, 38% mPEG, 49% mPEG, and 85% mPEG formulations have sizes that are significantly lower than the 100% mPEG formulation. The findings in our study agree with molecular dynamic results done by Lee and Larson (Lee and Larson, 2011).

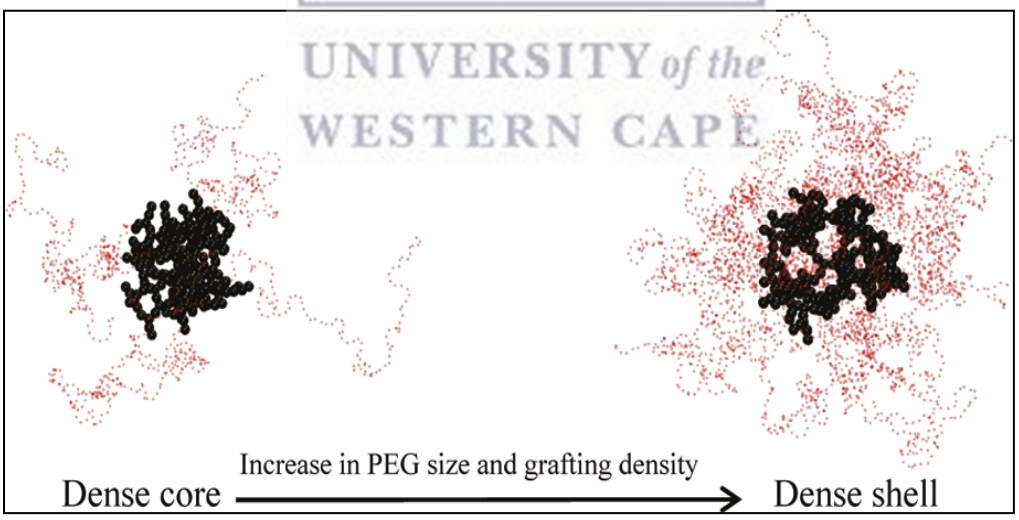

Figure 3.31 Molecular dynamic snapshot illustrating the effect of mPEG size and density on the G4 PAMAM dendrimer. Black dots symbolize G4 PAMAM dendrimer beads, and transparent pink dots symbolize mPEG chains [adapted from (Lee and Larson, 2011)].

Another molecular dynamic study was carried out by Yang and Da Rocha (2014) to investigate the change in the microstructure of G2-G5 PAMAM dendrimers once PEGylated with 500 mPEG and 1000 mPEG (Yang and Da Rocha, 2014). Their findings determined that the increase in the dendrimer size is principally affected by the mPEG length more than the mPEG density. Using the same total molecular weight of the two PEG chains 500 and 1000 (16 mPEG 500 and 8 mPEG 1000), revealed that higher size enlargement was detected with 8 mPEG 1000. Although the stretching effect of both mPEGs was similar for dendrimer monomers, the difference in the dendrimer size could be due to the higher unmodified surface amines in the case of 8 mPEG 1000 compared to 16 mPEG 500. The high percentage of unmodified surface amines ensures a more positive charge and stronger repulsion that increases the dendrimer size.

For drug-loaded dendrimers, no significant increase in the size of the nanoparticles after drug conjugation occurred, the only exception was observed with the 38% formulation. Rifampicin is a hydrophobic chemical entity (Williams and Piddock, 1998) with an isoelectric point of about 7.11 (Khan *et al.*, 2017) and pKa of 1.7 and 7.9 (Kumar *et al.*, 2006). During drug loading, rifampicin molecules are expected to carry negative charges as a result of deprotonation. Consequently, the significant size increase of 38% dendrimer after drug adding could be due to electrostatic attachment between positively charged surface amines and some of the deprotonated rifampicin. The 38% PEGylated dendrimer has the highest unmodified surface amine compared to the other PEGylated dendrimers. This enhances the possibilities for maximum electrostatic attachment with rifampicin and could be the principal rationale for size increasing.

The polydispersity index (PDI) of the unloaded PEGylated and non-PEGylated dendrimers ranged from 0.25 to 0.37 (Table 3.8). After drug loading, the PDI was observed between 0.28 and 0.39 (Table 3.8). No statistically significant difference was observed among empty dendrimers, as well as among drug-loaded dendrimers ($p > 0.05$) using ANOVA analysis (Tukey post hoc test). Comparing each formulation before and after drug conjugation also illustrated that no significant difference was detected ($p > 0.05$). The coefficient of determination (R^2) obtained from ANOVA analysis of the empty dendrimers and for drug-loaded dendrimers was 0.2693 and 0.3019, respectively. The ANOVA

analysis data confirmed that both the degree of PEGylation and rifampicin addition has no significant influence on the PDI of the dendrimers (Figure 3.32, Table 3.8).

Both unloaded and drug-loaded dendrimers have PDI values < 0.4. These values are considered to indicate a moderate homogenized distribution of nanoparticles. PDI values of 0.1 - 0.4 are regarded as a moderately distributed sample, while PDI value ≥ 0.5 indicates a broad polydisperse sample (Sabeti *et al.*, 2014; Bhattacharjee, 2016). Therefore, the synthesized unloaded and drug-loaded dendrimers are considered as moderately distributed samples.

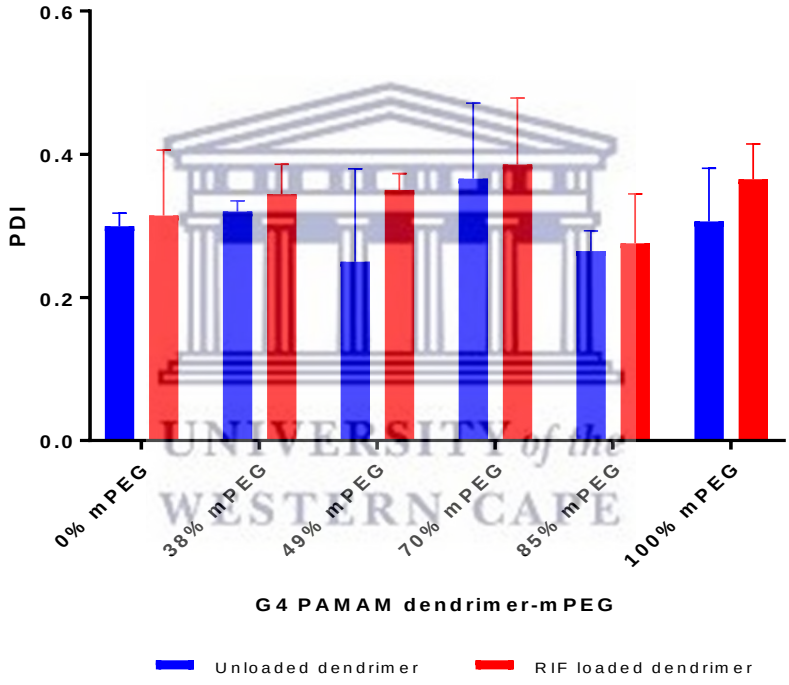

Figure 3.32 Polydispersity index (PDI) of unloaded (blue) and rifampicin-loaded (red) dendrimer nanoparticle formulations with different mPEG content. Results show as mean ± SD (n=3). Error bars represent the calculated SD from the mean.

ii) Nanoparticle zeta potential

Zeta potential analysis was carried out to assess the stability of the nanoparticle. For the empty dendrimers, values ranged from 36.97 ± 3.46 (Mv) for 0% mPEG dendrimer to

13.83 ± 0.99 (Mv) for 100% mPEG dendrimer. The non-PEGylated dendrimer was observed to have a higher zeta potential compared to the PEGylated dendrimers ($p < 0.05$) (except the 49% formulation) (Figure 3.33). Among the PEGylated dendrimers, the decrease in the zeta potential was proportional to the extent of dendrimer PEGylation. The 38% mPEG and 49% mPEG dendrimers showed values that are significantly higher than 70% mPEG, 85% mPEG, and 100% mPEG formulations ($p < 0.05$) (Table 3.8). No statistical significance was detected between 38% mPEG and 49% mPEG ($p > 0.05$), as well as between 70% mPEG, 85% mPEG, and 100% mPEG ($p > 0.05$).

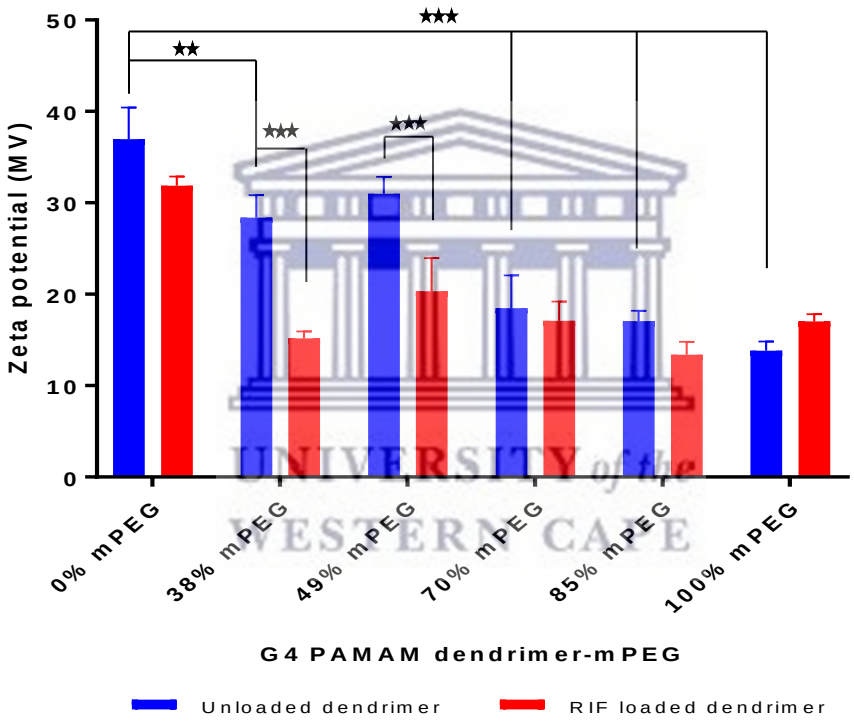

(* = p ≤ 0.05; ** = p ≤ 0.01; *** = p ≤ 0.001)

Figure 3.33 Zeta potential of empty (blue) and rifampicin-loaded (red) dendrimer nanoparticle formulations with different mPEG content. Results showed as mean ± SD (n=3). Error bars represent the calculated SD from the mean.

The coefficient of determination (R^2) obtained from the ANOVA analysis of the empty dendrimers was 0.9498, which indicated a strong association between the degree of dendrimer PEGylation and the decrease in the zeta potential.

Following drug conjugation, the zeta potential of nanoparticles was shifted to lower values compared to unloaded nanoparticles, ranging from 31.87 ± 1.01 (Mv) for 0% mPEG dendrimer to 13.37 ± 1.43 (Mv) for 85% mPEG dendrimer (Table 3.8). The zeta potential of drug-loaded dendrimer (0% mPEG) exhibited a value that was significantly higher than drug-loaded PEGylated dendrimers *($p < 0.05$*). Among the drug-loaded PEGylated dendrimers, no significant difference was noticed (*$p > 0.05$*), the only exception observed was between drug-loaded 49% mPEG and 85% mPEG (*$p < 0.05$*). The coefficient of determination (R^2) obtained from the ANOVA analysis of drug-loaded dendrimers was 0.8297, which indicates a moderate association between the extent of dendrimer PEGylation besides the rifampicin loading and the decrease in the zeta potential.

Evaluating each dendrimer nanoparticle before and after drug conjugation revealed that no significant change was observed in their zeta potential, the only exception was noticed in 38% mPEG and 49% mPEG formulations (Figure 3.33) (*$p < 0.05$*).

G4 PAMAM dendrimer has approximately 64 surface amino groups, at neutral pH, these amines will be protonated (Wang and Imae, 2004; Gupta, Agashe and Jain, 2007), and be accountable for its zeta potential value and the stability of a colloidal formulation. As previously discussed in this chapter mPEG chains are covalently conjugated to the surface amines *via* amide bonds, surface PEGylation will reduce the number of unmodified amines, and therefore decreasing the molecule's positive charges and its zeta potential. The results in this chapter agree with this observation from Table 3.8 with the zeta potential values of the unloaded dendrimers that were inversely related to the amount of mPEG added. A higher value was noticed with 0% mPEG (36.97 ± 3.46 mV), while the lowest value was achieved by 100% mPEG (13.83 ± 0.99 mV).

For drug-loaded dendrimers, two aspects are involved in managing the zeta potential of the nanoparticles. Firstly, the number of mPEG chains attached to the surface amines, and secondly the electrostatic conjugation between the protonated dendrimer amines and the negatively charged rifampicin, at neutral pH. This could be the reason behind the lower zeta potential values of drug-loaded dendrimers compared to the unloaded dendrimers. Among PEGylated dendrimers, the shift in the zeta potential was insignificant for 70% mPEG, 85% mPEG, and 100% mPEG loaded dendrimers. While a significant shift in the

zeta potential was observed for 38% mPEG and 49% mPEG loaded dendrimers. This observation could be because these two formulations are the lowest dendrimers being PEGylated, so a higher number of unmodified amines exist. Consequently, they provide a superior opportunity for some of the deprotonated rifampicin molecules to conjugate. This observation was not noticed in higher PEGylated dendrimers because most of the dendrimer surface amines were modified.

The zeta potential results agree with the dendrimer size results in this chapter. A significant increase in the nanoparticle size after the drug conjugation was observed with 38% mPEG formulation, The 38% mPEG has the highest unmodified amines among PEGylated dendrimers that offer a superior opportunity for electrostatic conjugation. Accordingly, the size and zeta potential analysis results confirm drug conjugation in the dendrimer interior, as well as on the peripheral surface.

3.7.5 Development and validation of Reverse-phase high performance/pressure liquid chromatography (RP-HPLC) method

The linearity of the HPLC method was determined by analyzing a range of rifampicin standards 4.0 – 100.0 µg/ml at an absorbance wavelength of 475 nm. Linear regression analysis was applied to assess the correlation between rifampicin absorbance and concentration. A plot of average rifampicin absorbance versus its concentration was generated as illustrated in Figure 3.34. This relationship model creates a basis for the prediction of rifampicin concentration by measuring sample absorbance.

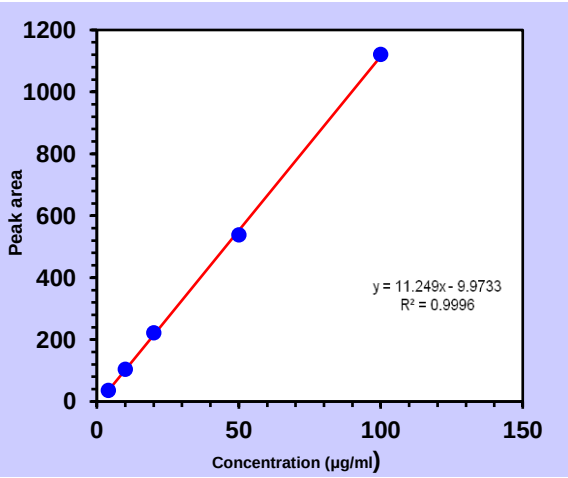

Figure 3.34 Rifampicin standard calibration curve at a wavelength of 475 nm in the mobile phase.

The linear regression equation was, y = 11.249x – 9.9733, with correlation coefficient r^2 = 0.9996. The generated linear equation displays a strong relationship between rifampicin concentration and its absorbance. Where x is rifampicin concentration in µg/ml and y is the absorbance peak area in mAU.

Table 3.9 Summary of the linearity data of rifampicin standard (λ_{max} = 475 nm) in the mobile phase.

Validation parameters	**Value**
r^2	0.9996
Slope ± SD	11.25 ± 0.13
Intercept ± SD	-9.9733 ± 6.43
Concentration range (µg/ml)	4.0 – 100.0
LOD ± SD (µg/ml)	1.89 ± 0.13
LOQ ± SD (µg/ml)	5.72 ± 1.01

The sensitivity of the method was assessed by calculating the limit of detection (LOD) and limit of quantification (LOQ) values. Results indicated that the method was sensitive, where the LOD and the LOQ values were 1.89 µg/ml and 5.72 µg/ml, respectively (Table 3.9).

Inter-day (intermediate precision) and intra-day (repeatability) precision of the HPLC method were evaluated by analyzing triplicates of three rifampicin standards (i.e., 10.0 µg/ml, 20.0 µg/ml, and 50.0 µg/ml). As shown in Table 3.10, intermediate precision and repeatability of the method were expressed as % RSD. The degree of scattering was less than 2.10% for repeatability and intermediate precision, this finding suggested that the method is reproducible (ICH, 2005; Shabir, 2006).

For accuracy, the method was assessed using recovery study techniques. Three selected rifampicin standards (i.e., 10.0 µg/ml, 20.0 µg/ml, and 50.0 µg/ml) were triplicated and

analyzed at λ_{max} 475 nm. Results were expressed as a percentage of the mean calculated concentration to the theoretical injected concentration. In Table 3.10, the determined percentage recoveries were within the range of 98.0 - 110.0 %, which proves the accuracy of the method as the acceptance criteria for non-regulated products should be within 90 - 110% (Shabir, 2006).

Table 3.10 Intra-day and inter-day precision and accuracy of rifampicin (λ_{max} = 475) in the mobile phase (Potassium phosphate buffer pH 7.4: ACN).

Parameter	**Value**		
Rifampicin standard (µg/ml)	10.0	20.0	50.0
	Intra-day (n = 3)		
Mean absorbance	109.33	222.07	561.70
SD	2.22	3.16	7.55
RSD	2.03	1.43	1.35
Mean determined Conc. (µg/ml)	10.61	20.63	50.82
% Recovery	106.10	103.10	101.60
	Inter-day (n = 3)		
Mean absorbance	112.69	225.13	545.87
SD	1.67	1.89	8.10
RSD	1.48	0.84	1.48
Mean determined Conc. (µg/ml)	10.90	20.90	49.41
% Recovery	109.0	104.50	98.80

Analysis of unloaded PEGylated dendrimer and the mobile phase did not show any interference with the rifampicin elution peak (~ 2.9 mins) (Figure 3.35), which suggested the suitability of the method for rifampicin.

Furthermore, rifampicin was forced degraded by the addition of 0.1 M NaOH and 0.1 M HCl to ensure specificity with regards to its degradants. The degraded sample showed lower peak height and an area relative to the non-degraded sample due to a decrease in rifampicin concentration as a result of degradation in acidic and basic mediums. Results confirmed the specificity of the method to detect rifampicin even when degraded by HCl and NaOH.

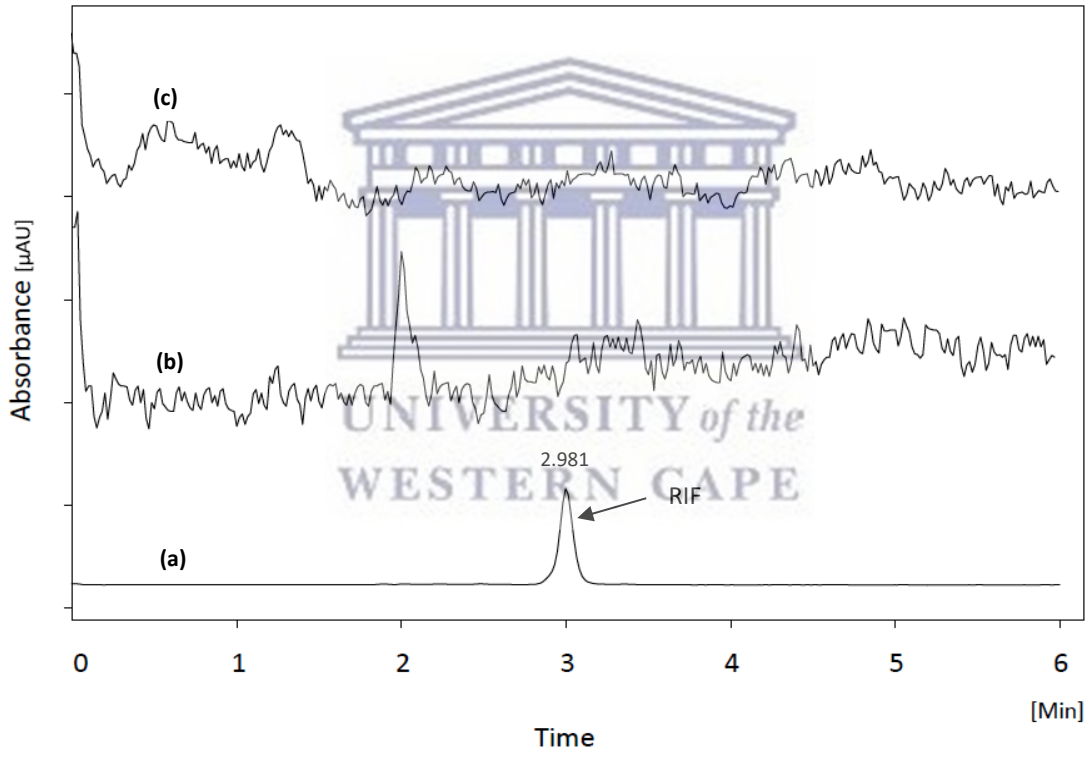

Figure 3.35 HPLC chromatograms of (a) non-degraded rifampicin standard, (b) unloaded PEGylated dendrimer, and (c) the mobile phase.

3.7.6 Encapsulation efficiency (EE%) and drug loading (DL%)

The encapsulation efficiency percentage (EE%) and the percentage drug loading (DL%) were determined directly using a validated HPLC method. EE% and DL% were calculated using equation 3.3 and equation 3.4, which were previously discussed.

Figure 3.36 and Table 3.11 illustrated the dendrimers mean EE%, which ranged from 7.50 ± 1.15% (w/w) for 0% mPEG dendrimer to 78.75 ± 0.75% (w/w) for 100% mPEG dendrimer. ANOVA analysis (Tukey post hoc test) revealed that EE% significantly increased after dendrimer PEGylation ($p < 0.05$) (Figure 3.36). This finding confirmed that mPEG chains have a high impact on the incorporation of rifampicin molecules.

Table 3.11 DL% and EE% of rifampicin in different dendrimer formulations, results shown as mean ± SD (n = 3).

Dendrimer -mPEG content	Amount of G4-mPEG	Amount of RIF	Yield wt (mg)	Total RF in NP (mg)	DL% (w/w)	EE% (w/w)
0% mPEG	0.1 µmol = 1.50 mg	10 µmol = 8.0 mg	2.30 (24.21%)	0.60	26.09 ± 1.35	7.50 ± 1.15
38% mPEG	0.1 µmol = 6.0 mg	10 µmol = 8.0 mg	12.60 (90.0%)	5.80	46.03 ± 1.01	72.50 ± 1.64
49% mPEG	0.1 µmol = 8.0 mg	10 µmol = 8.0 mg	13.0 (81.25%)	5.70	43.85 ± 1.69	71.25 ± 2.80
70% mPEG	0.1 µmol = 11.0 mg	10 µmol = 8.0 mg	17.10 (90.0%)	5.60	32.75 ± 1.50	70.0 ± 3.20
85% mPEG	0.1 µmol = 13.0 mg	10 µmol = 8.0 mg	18.30 (87.14%)	5.20	28.42 ± 0.76	65.0 ± 1.77
100% mPEG	0.1 µmol = 14.0 mg	10 µmol = 8.0 mg	20.80 (94.55%)	6.30	30.29 ± 0.66	78.75 ± 0.75

Among the PEGylated dendrimers, 100% mPEG formulation exhibited a higher EE% value compared to the other formulations ($p < 0.05$) (except 38% mPEG) (Figure 3.36). In addition, the lower PEGylated dendrimers, i.e., 38% mPEG and 49% mPEG, showed higher EE% values relative to 85% mPEG ($p < 0.05$). No statistically significant difference was observed between 38% mPEG, 49% mPEG, and 70% mPEG ($p > 0.05$).

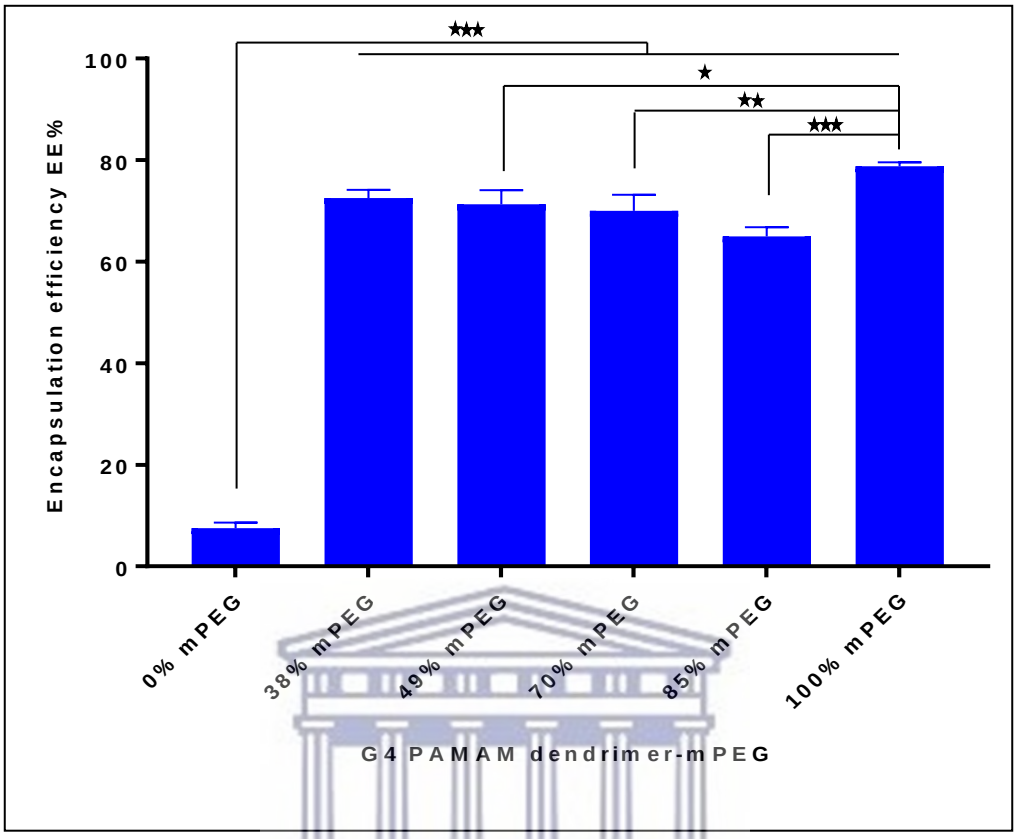

(* = p ≤ 0.05; ** = p ≤ 0.01; *** = p ≤ 0.001)

Figure 3.36 Nanoparticle encapsulation efficiency (EE%) of different dendrimer-mPEG formulations.

The percentage drug loading (DL%) was determined for dendrimer formulations as illustrated in Table 3.11 and Figure 3.37. The DL % ranged from 26.09 % (w/w) for 0% mPEG dendrimer to 46.03 % (w/w) for 38% mPEG dendrimer. Analysis of DL% results indicated that a significant increase was noticed with PEGylated dendrimers compared to non-PEGylated dendrimer ($p < 0.05$) (Figure 3.37). Among the PEGylated dendrimers, the DL% was inversely proportional to the degree of dendrimer PEGylation. Higher values were observed with 38% mPEG and 49% mPEG dendrimers and lower values were linked with 85% mPEG and 100% mPEG dendrimers (Figure 3.37). No statistically significant difference was detected between 38% mPEG and 49% mPEG dendrimers, as well as between 85% mPEG and 100% mPEG dendrimers ($p > 0.05$).

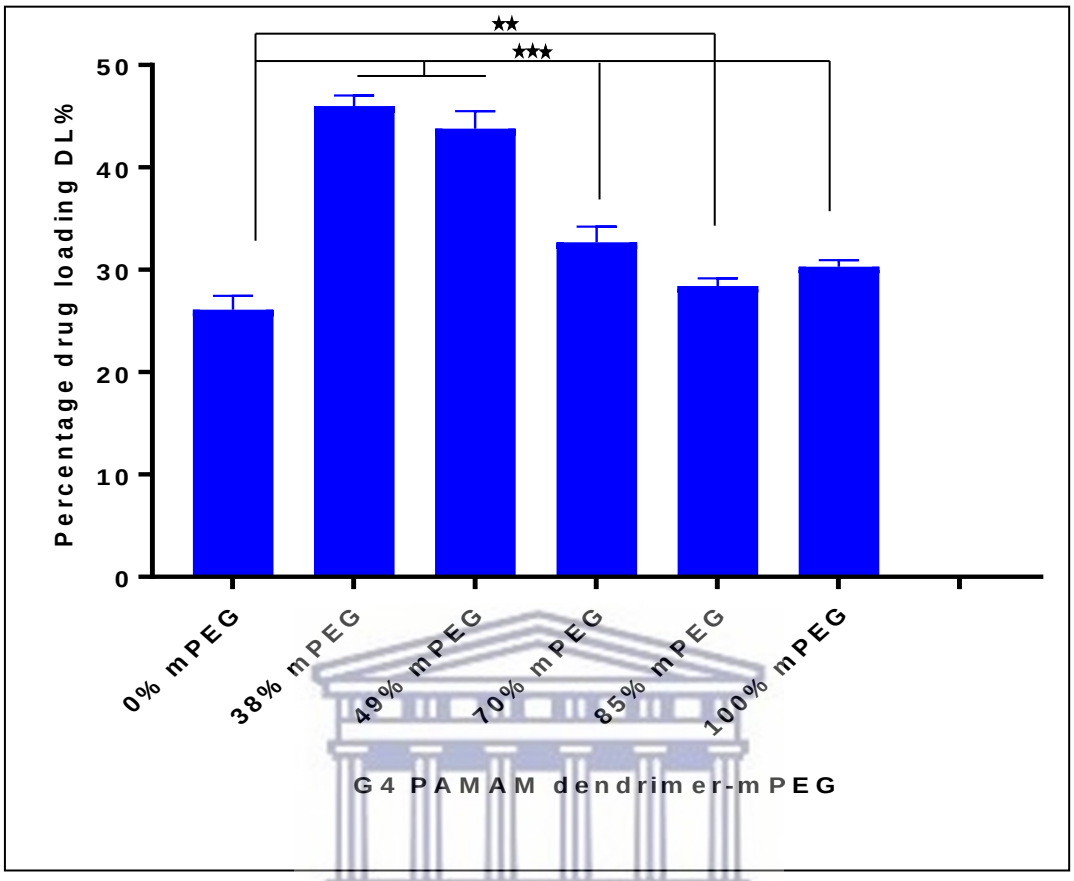

Figure 3.37 Nanoparticle percentage drug loading (DL%) of different dendrimer-mPEG formulations.

As discussed before, the PEGylation of a dendrimer could enhance the solubility of hydrophobic drugs by incorporating drug molecules within the PEG chains beside the dendrimer core. Several studies have reported that PEGylation enhances drug loading by offering a further platform for interaction at the dendrimer surface (Kojima *et al.*, 2000; Sideratou, Tsiourvas and Paleos, 2001; Pan *et al.*, 2005; Zhu *et al.*, 2010b; Thakur *et al.*, 2015; Dineshkumar *et al.*, 2017; Diaz *et al.*, 2018b). The results in this study are in line with the aforementioned reports, the EE% and DL% were significantly increased following dendrimer PEGylation (Table 3.11).

The reduction in the DL% upon increasing the mPEG content could be explained by two scenarios: the steric hindrance effect and the decrease in the number of unmodified surface amines (positive charge). Even though increasing the density of PEG chains will enhance drug solubilization potential, it will also form a dense cloud that surrounds the dendrimer,

which acts as a physical barrier that minimizes the movement of the drug molecules toward the dendrimer interior. A similar observation was reported by Pan *et al.*, (2005), where authors noticed a decrease in the number of methotrexate molecules encapsulated with the G3 PAMAM dendrimer having a higher PEG content (i.e., 99%), compared to lower PEGylated dendrimer (i.e., 43%). The second explanation for the reduction in DL% is the decrease in the number of unmodified surface amine by PEGylation. Increasing the extent of PEGylation will minimize the number of unmodified surface amines, these functional groups offer an additional platform for electrostatic interaction with rifampicin molecules. For higher PEGylated dendrimers, the possibility for electrostatic interactions will be low and therefore influence the number of drug molecules conjugated. Moreover, the repulsion between surface positive charges could stretch the dendrimer arms which change the dendrimer from the dense-core into dense-shell conformational structure (Lee and Larson, 2011). This transition will generate cavities within the dendrimer shell and enhance the loading capacity (Lee and Larson, 2011). Consequently, increasing the degree of dendrimer PEGylation will decrease the amount of the positive charges and hence a lower level of repulsion and drug-loading potential. In conclusion, the suggested explanations create a basis for the interpretation of the decrease in DL% as a function of mPEG content.

3.8 Conclusion

As a conclusion, G4 PAMAM dendrimers having concentration range from 38% to 100% mPEG were successfully synthesized. NMR and FTIR techniques were applied to confirm the conjugation of mPEG chains on the dendrimer surface *via* amide linkages, as well as to quantify the degree of PEGylation. Rifampicin molecules were encapsulated into the native and PEGylated dendrimers in varying proportions. The EE% of nanoparticles was 7.50 ± 1.15% (w/w) for native G4 dendrimer, whilst for PEGylated dendrimers ranged from 65.0 ± 1.77% (w/w) to 78.75 ± 0.75% (w/w). The DL% of nanoparticles was 26.09 ± 1.35% (w/w) for the native dendrimer, and for PEGylated dendrimers the range was between 28.42 ± 0.76% (w/w) – 46.03 ± 1.01% (w/w). FTIR and NMR techniques indicated that rifampicin molecules were conjugated to the dendrimer scaffold at three sites, at the surface amines *via* electrostatic bonds, within the PEG chain, and into the dendrimer core. The shape of the nanoparticles was observed as spherical under the SEM

instrument. DSC analysis confirmed that rifampicin was loaded in the dendrimer and PEGylated dendrimers were not physical mixtures. The size of the unloaded nanoparticles was less than 25 nm and no significant difference was noticed after rifampicin conjugation except for 38% mPEG formulation. PDI values of all formulations were below 0.4 which indicates moderately distributed samples. The zeta potential of nanoparticles was positive with values greater than 13 mV and zeta potential values were decreased by increasing the degree of PEGylation since PEG chains are attaching to the surface amines. Finally, the native dendrimer has the highest value of zeta potential i.e., 36.97 ± 3.46 mV and 31.87 ± 1.01 mV for unloaded and loaded G4 PAMAM dendrimer, respectively.

3.9 References

Abuchowski, A., Van Es, T., Palczuk, N.C. and Davis, F.F., (1977). Alteration of immunological properties of bovine serum albumin by covalent attachment of polyethylene glycol. *Journal of Biological Chemistry*, *252*(11), pp.3578-3581.

Barraza, L.F., Jiménez, V.A. and Alderete, J.B., (2015). Effect of PEGylation on the structure and drug loading capacity of PAMAM-G4 dendrimers: a molecular modeling approach on the complexation of 5-fluorouracil with native and PEGylated PAMAM-G4. *Macromolecular Chemistry and Physics*, *216*(16), pp.1689-1701.

Barraza, L.F., Jiménez, V.A. and Alderete, J.B., (2016). Methotrexate Complexation with Native and PEGylated PAMAM-G4: Effect of the PEGylation Degree on the Drug Loading Capacity and Release Kinetics. *Macromolecular Chemistry and Physics*, *217*(4), pp.605-613.

Bellini, R.G., Guimarães, A.P., Pacheco, M.A., Dias, D.M., Furtado, V.R., de Alencastro, R.B. and Horta, B.A., (2015). Association of the anti-tuberculosis drug rifampicin with a PAMAM dendrimer. *Journal of Molecular Graphics and Modelling*, *60*, pp.34-42.

Bhadra, D., Bhadra, S. and Jain, N.K., (2005). PEGylated peptide-based dendritic nanoparticulate systems for delivery of artemether. *Journal of Drug Delivery Science and Technology*, *15*(1), pp.65-73.

Bharti, S.K. and Roy, R., (2012). Quantitative 1H NMR spectroscopy. *TrAC Trends in Analytical Chemistry*, *35*, pp.5-26.

Bhattacharjee, S., (2016). DLS and zeta potential–what they are and what they are not?. *Journal of controlled release*, *235*, pp.337-351.

Blanco, E., Shen, H. and Ferrari, M., (2015). Principles of nanoparticle design for overcoming biological barriers to drug delivery. *Nature biotechnology*, *33*(9), pp.941-951.

Chen, H.T., Neerman, M.F., Parrish, A.R. and Simanek, E.E., (2004). Cytotoxicity, hemolysis, and acute in vivo toxicity of dendrimers based on melamine, candidate vehicles for drug delivery. *Journal of the American Chemical Society*, *126*(32), pp.10044-10048.

Damodaran, V.B. and Fee, C., (2010). Protein PEGylation: An overview of chemistry and process considerations. *European Pharmaceutical Review*, *15*(1), pp.18-26.

Demir, B.Ü.Ş.R.A., Barlas, F.B., Guler, E., Gumus, P.Z., Can, M., Yavuz, M., Coskunol, H. and Timur, S.U.N.A., (2014). Gold nanoparticle loaded phytosomal systems: synthesis, characterization and in vitro investigations. *RSC advances*, *4*(65), pp.34687-34695.

Diaz, C., Benitez, C., Vidal, F., Barraza, L.F., Jiménez, V.A., Guzman, L., Fuentealba, J., Yevenes, G.E. and Alderete, J.B., (2018a). Cytotoxicity and in vivo plasma kinetic behavior of surface-functionalized PAMAM dendrimers. *Nanomedicine: Nanotechnology, Biology and Medicine*, *14*(7), pp.2227-2234.

Diaz, C., Guzmán, J., Jiménez, V.A. and Alderete, J.B., (2018b). Partially PEGylated PAMAM dendrimers as solubility enhancers of Silybin. *Pharmaceutical development and technology*, *23*(7), pp.689-696.

Dineshkumar, P., Panneerselvam, T., Deepti Brundavani, K., Selvaraj, K. and Vijayaraj Kumar, P.,

(2017). Formulation of Rifampicin Loaded PEGylated 5.0 G EDA-PAMAM Dendrimers as Effective Long-Duration Release Drug Carriers. *Current Drug Therapy*, *12*(2), pp.115-126.

Gefen, T., Vaya, J., Khatib, S., Harkevich, N., Artoul, F., Heller, E.D., Pitcovski, J. and Aizenshtein, E., (2013). The impact of PEGylation on protein immunogenicity. *International immunopharmacology*, *15*(2), pp.254-259.

Ho, M.N., Bach, L.G., Nguyen, T.H., Ho, M.H., Nguyen, D.H., Nguyen, C.K., Nguyen, C.H., Nguyen, N.V. and Thi, T.T.H., (2019). PEGylated poly (amidoamine) dendrimers-based drug loading vehicles for delivering carboplatin in treatment of various cancerous cells. *Journal of Nanoparticle Research*, *21*(2), p.43.

Hoffman, A.S., (2016). The early days of PEG and PEGylation (1970s–1990s). *Acta biomaterialia*, *40*, pp.1-5.

ICH (2005) 'ICH harmonised tripartite guideline validation of analytical procedures: text and methodology Q2(R1)'. In *International conference on harmonization, Geneva, Switzerland* (Vol. 11).

Jevprasesphant, R., Penny, J., Jalal, R., Attwood, D., McKeown, N.B. and D'emanuele, A., (2003). The influence of surface modification on the cytotoxicity of PAMAM dendrimers. *International journal of pharmaceutics*, *252*(1-2), pp.263-266.

Johansson, E.M., (2010). *Controlling the pore size and morphology of mesoporous silica* (Doctoral dissertation, Linköping University Electronic Press).

Kailasam, K., (2008). Synthesis and characterization of mesoporous silica and metal oxide based stationary phase materials (Doctoral dissertation, University of Stuttgart).

Kesharwani, P., Gajbhiye, V., K Tekade, R. and K Jain, N., (2011). Evaluation of dendrimer safety and efficacy through cell line studies. *Current drug targets*, *12*(10), pp.1478-1497.

Khan, M.F., Rita, S.A., Kayser, M., Islam, M., Asad, S., Bin Rashid, R., Bari, M., Rahman, M.M., Aman, A., Anwar, D.A. and Setu, N.I., (2017). Theoretically guided analytical method development and validation for the estimation of rifampicin in a mixture of isoniazid and pyrazinamide by UV spectrophotometer. *Frontiers in Chemistry*, *5*, p.27.

Kojima, C., Kono, K., Maruyama, K. and Takagishi, T., (2000). Synthesis of polyamidoamine dendrimers having poly (ethylene glycol) grafts and their ability to encapsulate anticancer drugs. *Bioconjugate chemistry*, *11*(6), pp.910-917.

Kolhatkar, R.B., Kitchens, K.M., Swaan, P.W. and Ghandehari, H., (2007). Surface acetylation of polyamidoamine (PAMAM) dendrimers decreases cytotoxicity while maintaining membrane permeability. *Bioconjugate chemistry*, *18*(6), pp.2054-2060.

Kumar, P.V., Asthana, A., Dutta, T. and Jain, N.K., (2006). Intracellular macrophage uptake of rifampicin loaded mannosylated dendrimers. *Journal of drug targeting*, *14*(8), pp.546-556.

Lee, H. and Larson, R.G., (2011). Effects of PEGylation on the size and internal structure of dendrimers: self-penetration of long PEG chains into the dendrimer core. *Macromolecules*, *44*(7), pp.2291-2298.

Leroueil, P.R., Hong, S., Mecke, A., Baker Jr, J.R., Orr, B.G. and Banaszak Holl, M.M., (2007). Nanoparticle interaction with biological membranes: does nanotechnology present a Janus

face?. *Accounts of chemical research*, *40*(5), pp.335-342.

Leroueil, P.R., Berry, S.A., Duthie, K., Han, G., Rotello, V.M., McNerny, D.Q., Baker Jr, J.R., Orr, B.G. and Banaszak Holl, M.M., (2008). Wide varieties of cationic nanoparticles induce defects in supported lipid bilayers. *Nano letters*, *8*(2), pp.420-424.

Li, Y., He, H., Lu, W. and Jia, X., (2017). A poly (amidoamine) dendrimer-based drug carrier for delivering DOX to gliomas cells. *RSC advances*, *7*(25), pp.15475-15481.

Lim, A.H. and Tam, K.C., (2011). Stabilization of polyamidoamine (PAMAM) dendrimers/sodium dodecyl sulfate complexes via PEGylation. *Colloids and Surfaces A: Physicochemical and Engineering Aspects*, *380*(1-3), pp.47-52.

Liu, M., Kono, K. and Fréchet, J.M., (1999). Water-soluble dendrimer–poly (ethylene glycol) starlike conjugates as potential drug carriers. *Journal of Polymer Science Part A: Polymer Chemistry*, *37*(17), pp.3492-3503.

Luong, D., Kesharwani, P., Deshmukh, R., Amin, M.C.I.M., Gupta, U., Greish, K. and Iyer, A.K., (2016). PEGylated PAMAM dendrimers: enhancing efficacy and mitigating toxicity for effective anticancer drug and gene delivery. *Acta biomaterialia*, *43*, pp.14-29.

Ly, T.U., Tran, N.Q., Hoang, T.K.D., Phan, K.N., Truong, H.N. and Nguyen, C.K., (2013). Pegylated dendrimer and its effect in fluorouracil loading and release for enhancing antitumor activity. *Journal of biomedical nanotechnology*, *9*(2), pp.213-220.

Malik, N., Wiwattanapatapee, R., Klopsch, R., Lorenz, K., Frey, H., Weener, J.W., Meijer, E.W., Paulus, W. and Duncan, R., (2000). Dendrimers:: Relationship between structure and biocompatibility in vitro, and preliminary studies on the biodistribution of 125I-labelled polyamidoamine dendrimers in vivo. *Journal of Controlled Release*, *65*(1-2), pp.133-148.

Männistö, M., Vanderkerken, S., Toncheva, V., Elomaa, M., Ruponen, M., Schacht, E. and Urtti, A., (2002). Structure–activity relationships of poly (L-lysines): effects of pegylation and molecular shape on physicochemical and biological properties in gene delivery. *Journal of controlled release*, *83*(1), pp.169-182.

Mecke, A., Lee, D.K., Ramamoorthy, A., Orr, B.G. and Banaszak Holl, M.M., (2005). Synthetic and natural polycationic polymer nanoparticles interact selectively with fluid-phase domains of DMPC lipid bilayers. *Langmuir*, *21*(19), pp.8588-8590.

Milhem, O.M., Myles, C., McKeown, N.B., Attwood, D. and D'Emanuele, A., (2000). Polyamidoamine Starburst® dendrimers as solubility enhancers. *International journal of pharmaceutics*, *197*(1-2), pp.239-241.

Motoyama, K., Hayashida, K., Higashi, T. and Arima, H., (2012). Polypseudorotaxanes of pegylated α-cyclodextrin/polyamidoamine dendrimer conjugate with cyclodextrins as a sustained release system for DNA. *Bioorganic & medicinal chemistry*, *20*(4), pp.1425-1433.

Nam, H.Y., Nam, K., Hahn, H.J., Kim, B.H., Lim, H.J., Kim, H.J., Choi, J.S. and Park, J.S., (2009). Biodegradable PAMAM ester for enhanced transfection efficiency with low cytotoxicity. *Biomaterials*, *30*(4), pp.665-673.

Okuda, T., Kawakami, S., Maeie, T., Niidome, T., Yamashita, F. and Hashida, M., (2006). Biodistribution characteristics of amino acid dendrimers and their PEGylated derivatives after

intravenous administration. *Journal of controlled release*, *114*(1), pp.69-77.

Ooya, T., Lee, J. and Park, K., (2003). Effects of ethylene glycol-based graft, star-shaped, and dendritic polymers on solubilization and controlled release of paclitaxel. *Journal of controlled release*, *93*(2), pp.121-127.

Pan, G., Lemmouchi, Y., Akala, E.O. and Bakare, O., (2005). Studies on PEGylated and drug-loaded PAMAM dendrimers. *Journal of bioactive and compatible polymers*, *20*(1), pp.113-128.

Patri, A.K., Myc, A., Beals, J., Thomas, T.P., Bander, N.H. and Baker, J.R., (2004). Synthesis and in vitro testing of J591 antibody− dendrimer conjugates for targeted prostate cancer therapy. *Bioconjugate chemistry*, *15*(6), pp.1174-1181.

Pelizza, G., Nebuloni, M., Ferrari, P. and Gallo, G.G., (1977). Polymorphism of rifampicin. *Il Farmaco; edizione scientifica*, *32*(7), pp.471-481.

Peng, C., Zheng, L., Chen, Q., Shen, M., Guo, R., Wang, H., Cao, X., Zhang, G. and Shi, X., (2012). PEGylated dendrimer-entrapped gold nanoparticles for in vivo blood pool and tumor imaging by computed tomography. *Biomaterials*, *33*(4), pp.1107-1119.

Prajapati, R.N., Tekade, R.K., Gupta, U., Gajbhiye, V. and Jain, N.K., (2009). Dendimer-mediated solubilization, formulation development and in vitro− in vivo assessment of piroxicam. *Molecular pharmaceutics*, *6*(3), pp.940-950.

Prosa, T.J., Bauer, B.J. and Amis, E.J., (2001). From stars to spheres: A SAXS analysis of dilute dendrimer solutions. *Macromolecules*, *34*(14), pp.4897-4906.

Puskas, J.E., Seo, K.S. and Sen, M.Y., (2011). Green polymer chemistry: Precision synthesis of novel multifunctional poly (ethylene glycol) s using enzymatic catalysis. *European polymer journal*, *47*(4), pp.524-534.

Quintana, A., Raczka, E., Piehler, L., Lee, I., Myc, A., Majoros, I., Patri, A.K., Thomas, T., Mulé, J. and Baker, J.R., (2002). Design and function of a dendrimer-based therapeutic nanodevice targeted to tumor cells through the folate receptor. *Pharmaceutical research*, *19*(9), pp.1310-1316.

Sabeti, B., Noordin, M.I., Mohd, S., Hashim, R., Dahlan, A. and Akbari Javar, H., (2014). Development and characterization of liposomal doxorubicin hydrochloride with palm oil. *BioMed research international*, *2014*.

Samkange, T., D'Souza, S., Obikeze, K. and Dube, A., (2019). Influence of PEGylation on PLGA nanoparticle properties, hydrophobic drug release and interactions with human serum albumin. *Journal of Pharmacy and Pharmacology*, *71*(10), pp.1497-1507.

Satija, J., Gupta, U. and Jain, N.K., (2007). Pharmaceutical and biomedical potential of surface engineered dendrimers. *Critical Reviews™ in Therapeutic Drug Carrier Systems*, *24*(3), pp. 257–306.

Shabir, G. A. (2006). 'Step-by-Step Analytical Protocol in the Quality System Methods Validation and Compliance Industry', *Analytical Methods Validation*, 40(6), pp. 951–961.

Shim, M.S. and Kwon, Y.J., (2012). Stimuli-responsive polymers and nanomaterials for gene delivery and imaging applications. *Advanced drug delivery reviews*, *64*(11), pp.1046-1059.

Sideratou, Z., Kontoyianni, C., Drossopoulou, G.I. and Paleos, C.M., (2010). Synthesis of a folate

functionalized PEGylated poly (propylene imine) dendrimer as prospective targeted drug delivery system. *Bioorganic & medicinal chemistry letters*, *20*(22), pp.6513-6517.

Sideratou, Z., Tsiourvas, D. and Paleos, C.M., (2001). Solubilization and release properties of PEGylated diaminobutane poly (propylene imine) dendrimers. *Journal of colloid and interface science*, *242*(1), pp.272-276.

Singh, P., Gupta, U., Asthana, A. and Jain, N.K., (2008). Folate and folate− PEG− PAMAM Dendrimers: synthesis, characterization, and targeted anticancer drug delivery potential in tumor bearing mice. *Bioconjugate chemistry*, *19*(11), pp.2239-2252.

Tekade, R.K., Dutta, T., Gajbhiye, V. and Jain, N.K., (2009). Exploring dendrimer towards dual drug delivery: pH responsive simultaneous drug-release kinetics. *Journal of microencapsulation*, *26*(4), pp.287-296.

Thakur, S., Kesharwani, P., Tekade, R.K. and Jain, N.K., (2015). Impact of pegylation on biopharmaceutical properties of dendrimers. *Polymer*, *59*, pp.67-92.

Turecek, P.L., Bossard, M.J., Schoetens, F. and Ivens, I.A., (2016). PEGylation of biopharmaceuticals: a review of chemistry and nonclinical safety information of approved drugs. *Journal of pharmaceutical sciences*, *105*(2), pp.460-475.

Uppuluri, S., Dvornic, P.R., Klimash, J.W., Carver, P.I. and Tan, N.C., (1998). *The properties of dendritic polymers I: generation 5 poly (amidoamine) dendrimers* (No. ARL-TR-1606). ARMY RESEARCH LAB ABERDEEN PROVING GROUND MD.

Veronese, F.M. and Pasut, G., (2005). PEGylation, successful approach to drug delivery. *Drug discovery today*, *10*(21), pp.1451-1458.

Vijayaraj Kumar, P., Agashe, H., Dutta, T. and Jain, N.K., (2007). PEGylated dendritic architecture for development of a prolonged drug delivery system for an antitubercular drug. *Current drug delivery*, *4*(1), pp.11-19.

Wang, W., Xiong, W., Wan, J., Sun, X., Xu, H. and Yang, X., (2009). The decrease of PAMAM dendrimer-induced cytotoxicity by PEGylation via attenuation of oxidative stress. *Nanotechnology*, *20*(10), p.105103.

Williams, K.J. and Piddock, L.J., (1998). Accumulation of rifampicin by Escherichia coli and Staphylococcus aureus. *The Journal of antimicrobial chemotherapy*, *42*(5), pp.597-603.

Wolinsky, J.B. and Grinstaff, M.W., (2008). Therapeutic and diagnostic applications of dendrimers for cancer treatment. *Advanced drug delivery reviews*, *60*(9), pp.1037-1055.

Yang, H. and Lopina, S.T., (2003). Penicillin V-conjugated PEG-PAMAM star polymers. *Journal of Biomaterials Science, Polymer Edition*, *14*(10), pp.1043-1056.

Yang, H., Morris, J.J. and Lopina, S.T., (2004). Polyethylene glycol–polyamidoamine dendritic micelle as solubility enhancer and the effect of the length of polyethylene glycol arms on the solubility of pyrene in water. *Journal of colloid and interface science*, *273*(1), pp.148-154.

Yang, L. and da Rocha, S.R., (2014). PEGylated, NH2-terminated PAMAM dendrimers: a microscopic view from atomistic computer simulations. *Molecular pharmaceutics*, *11*(5), pp.1459-1470.

Zhu, S., Hong, M., Tang, G., Qian, L., Lin, J., Jiang, Y. and Pei, Y., (2010a). Partly PEGylated polyamidoamine dendrimer for tumor-selective targeting of doxorubicin: the effects of PEGylation degree and drug conjugation style. *Biomaterials*, *31*(6), pp.1360-1371.

Zhu, S., Hong, M., Zhang, L., Tang, G., Jiang, Y. and Pei, Y., (2010b). PEGylated PAMAM dendrimer-doxorubicin conjugates: in vitro evaluation and in vivo tumor accumulation. *Pharmaceutical research*, *27*(1), pp.161-174.

Chapter 4

Synthesis and characterization of rifampicin loaded mannosylated 4.0 G PAMAM dendrimer

4.1 Introduction

This chapter gives a detailed account of the materials, methods, and a clear description of the analytical techniques employed to synthesize and characterize rifampicin loaded in 4.0 G PAMAM dendrimer grafted with various mannose concentrations. This chapter also displays the results of the surface-modified dendrimer formulations, with discussion and conclusion.

4.2 Review of the literature

4.2.1 Protein-carbohydrate interactions in cell recognition background

The protein-carbohydrate interactions represent the necessary initial step for the majority of biological processes. Figure 4.1 illustrates that bacterial/viral interactions, antibody-antigen interactions, various hormone interactions, and several cell-cell interactions mainly depend on protein-carbohydrate interactions as an initial step in the recognition process (Sharon and Lis, 1993; Dwek, 1996; Kiessling, 1998; Lis and Sharon, 1998; Mammen, Choi, S and Whitesides, 1998; Williams and Davies, 2001).

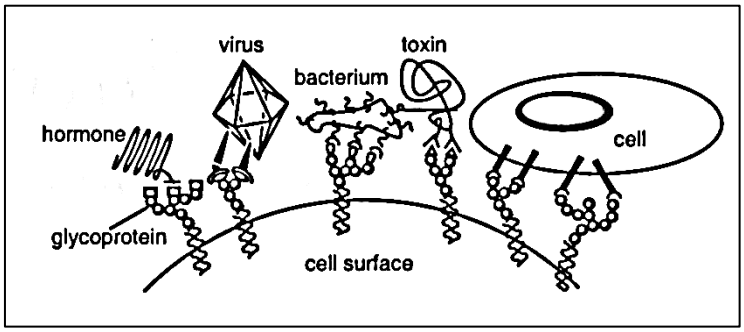

Figure 4.1 Examples of biological conjugations that are mainly mediated *via* protein-carbohydrate interactions; [adapted from (Sharon and Lis, 1993; Woller, 2003)].

The protein-carbohydrate interactions may take place *via* various modes, the two major modes are the monovalent and the multivalent interactions. For the monovalent, the interaction occurs between one binding site and a single ligand (Toone, 1994; Lundquist and Toone, 2002). This type of biological interaction is characterized by a relatively weak binding affinity of a glycoprotein receptor for the interacting ligand (Toone, 1994; Lundquist and Toone, 2002). On the other hand, multivalent interaction refers to the interaction of a ligand (such as carbohydrate residues) that conjugate to two or more distant binding spots on the glycoprotein receptor (Lee *et al.*, 1983). Multivalent interaction is a highly specific interaction and is characterized by a strong binding affinity of the glycoprotein receptor for the interacting ligands (Quesenberry, Lee and Lee, 1997).

An example of the multivalent interaction is the engulfment of the bacteria by the macrophages that are mediated by antibodies. Without antibodies, macrophages will not be able to recognize the bacteria and destroy them. According to the nature of the antibody, their tail may hold 2, 4, 6, or 10 binding spots. Antibodies are capable of identifying and conjugating to the pathogen based on their surface antigen. Multivalent interaction between the pathogens and the antibodies is important to guarantee a strong association between them. Once interactions arise, the carbohydrate residues at the tail of the antibodies will direct the targeting of mannose receptors on the surface of the macrophages. Consequently, when adequate antibodies are conjugated to macrophages, the immune cells will then digest and destroy the invading pathogens. Multivalent interaction between the antibodies and the macrophages is highly required since the interaction of a single antibody to the mannose receptor will result in slightly or sometimes no induction of the macrophages (Mammen, Choi, S and Whitesides, 1998).

4.2.2 Design of multivalent biomimetic ligands

With the advances in scientific research, many scientists have synthesized molecules that mimic the innate ligands that are capable to achieve comparable biological effects (activators or inhibitors). An example of the inhibitory biomimetic ligand is the influenza virus ligand. Usually, for the infection to occur the antigen on the influenza virus is (hemagglutinin) requisite to interact with the sialic acid of the epithelial cell *via* multivalent interaction (Kamitakahara *et al.*, 1998; Mammen, Choi, S and Whitesides, 1998). The

synthesized ligand holds sialic acid on its surface which is designed to favorably bind the virus more than the sialic acid of the epithelial cells. The interaction between the synthetic ligand and the invading virus will result in preventing the progress of the virus. Activating biomimetic ligands are usually employed to induce a biological response by interacting with receptor binding sites on the cell surface.

Many factors should be considered before designing the biomimetic ligands to achieve the proposed biological effect, some of these factors are the mode of interaction and the type of the ligand.

4.2.2.1 Mode of the biological interactions

Before designing biomimetic ligands, it is important to consider the mode of interaction with the biological receptors. Various modes of interaction may lead to different biological outcomes. Several modes of interaction were reported earlier, the most common and essential are: monovalent, multivalent, glycoside cluster effect, and cross-linking interactions (Kiessling, Gestwicki and Strong, 2000).

I. Monovalent interactions

Monovalent interactions represent the simplest style of interaction between the ligand and the biological receptor. It takes place between one ligand and a single binding site (Figure 4.2 (A)).

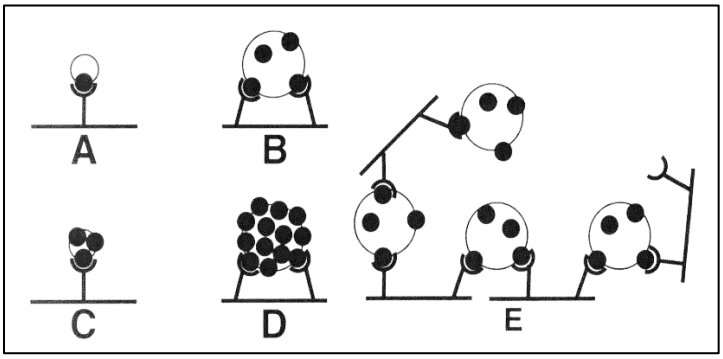

Figure 4.2 Summary for different modes of interactions, (A) monovalent, (B) multivalent, (C) glycoside cluster effect, (D) combination of multivalent and glycoside cluster, and (E) cross-linking interaction; [adapted from (Woller, 2003)].

This type of interaction exhibits a weak affinity of the receptor to the ligand; usually, no biological outcomes are generated of monovalent interactions (Woller, 2003).

II. Multivalent interactions

The multivalent interaction occurs when a ligand is capable of conjugating to numerous binding sites on a receptor (Figure 4.2 (B)). The multivalent interaction exhibits a relatively higher affinity of the binding sites to the ligand compared to the monovalent interaction.

III. Glycoside cluster effect

According to earlier reports, the two terms 'glycoside cluster effect' and 'multivalent interaction' are sometimes interchangeable (Lee and Lee, 1995, 2000; Olsen *et al.*, 1997; Dimick *et al.*, 1999; Lundquist and Toone, 2002). As illustrated in Figure 4.2 (C), the glycoside cluster effect is a result of local concentration around one receptor. The only difference between the glycoside cluster effect and the monovalent interaction is that when the interacting epitope of the ligand dissociates from the binding spot of the receptor, the ligand with a high epitope concentration has a greater possibility to re-conjugate to the receptor. Sometimes a combination of multivalent and glycoside clusters may take place with the biological receptor (Figure 4.2 (D)).

IV. Cross-linking

The cross-linking interaction occurs when a ligand conjugates to several biological receptors (Figure 4.2 (E)).

4.2.2.2 Type of the ligand

Based on the molecular size, ligands are classified into three main groups: small molecules, medium molecules, and large molecule ligands (Lindhorst, 2002; Lundquist and Toone, 2002). An example of a medium molecule and a large molecule ligand are dendritic glycosides, and polymeric ligands, respectively (Lindhorst, 2002; Lundquist and Toone, 2002).

Burke and co-workers (2000) studied the mode of interaction of mannose (small molecule) attached to a rigid macrocyclic scaffold and the concanavalin A (ConA) receptor (Burke *et*

al., 2000). They expected that the mode of interaction had occurred *via* the clustering effect or cross-linking interactions. Furthermore, a higher response was observed with the trivalent ligand compared to the monovalent ligand. The authors did not expect the multivalent interaction as the mannose is too small a molecule to span numerous binding spots (Burke *et al.*, 2000). The multivalent interaction is usually observed with large molecular ligands (such as glycopolymers) (Spaltenstein and Whitesides, 1991).

4.2.3 Macrophages role in drug delivery

Macrophages are one of the key components of innate immunity, besides their function in biological homeostasis, development, and tissue repair (Wynn, Chawla and Pollard, 2013). In chronic infectious diseases, macrophages represent the main hosts of intracellular pathogens, such as alveolar macrophages in tuberculosis disease. Unlike the previous concept that regarded the macrophages as an unwanted interceptor of the drug delivery system, targeting macrophages with several therapeutic drugs has gained an increasing interest in the field of drug delivery (Pei and Yeo, 2016). Targeting the macrophages may help to destroy the intracellular pathogens as in the case of chronic infectious diseases. Also, some cancer immunotherapy has employed macrophages to target the cancerous tissues due to their complex role in the tumor microenvironment (Pei and Yeo, 2016).

4.2.3.1 Targeting the macrophages with therapeutic agents

Targeting the macrophages have got increasing attention in the field of drug delivery, mostly to treat intracellular infections such as salmonellosis, brucellosis, and tuberculosis (Pei and Yeo, 2016). For these infections, macrophages act as an immune-privileged reservoir for the invading bacteria, within which may proliferate or remain dormant (Monack, Mueller and Falkow, 2004; Casadevall, 2008). Although the control of these infections is normally managed using antibiotics, the therapeutic outcomes are usually unsuccessful due to the difficulty to obtain an effective drug concentration in the macrophages (Imbuluzqueta *et al.*, 2010). Targeting the macrophages with the different delivery system are suggested to improve the therapeutic effectiveness of the antibiotics to enhance the contact between drug molecules and the intracellular bacteria (Pei and Yeo, 2016).

4.2.3.2 Macrophages as a drug delivery system

It has been reported that macrophages are sometimes employed as a carrier for drugs and imaging agents in cancer treatment due to their ability to diffuse into tumors besides their tropism to hypoxia (Choi *et al.*, 2007; Huang *et al.*, 2015). Macrophages are also capable of crossing the blood-brain barrier which may help to deliver therapeutic drugs to treat Alzheimer's and Parkinson's diseases (Anselmo and Mitragotri, 2014). The development of macrophages as drug carriers are performed in two steps, firstly drug molecules are loaded into nanoparticles, and then the nanoconjugates interact with macrophages *via* ligand-receptor conjugation, non-covalent adsorption, or covalent coupling (Batrakova, Gendelman and Kabanov, 2011; Anselmo and Mitragotri, 2014; Anselmo *et al.*, 2015).

4.2.4 The interaction of functionalized PAMAM dendrimers and the alveolar macrophages

Dendrimers are a synthetic polymer that differs from other polymers in which the mixture shows uniform particle distribution (monodisperse), while other polymers are characterized by heterogeneous particle distribution (polydisperse) (Grayson and Fréchet, 2001). For that reason, dendrimers are a well-suggested scaffold for the formation of medium-sized ligands of mannose to interact with lectin receptors on the alveolar macrophages. By controlling the number of dendrimer's generation and the degree of mannosylation, it could be possible to evaluate the influence of the multivalent interaction and the clustering effect independently.

4.2.4.1 Functionalization of PAMAM dendrimer with carbohydrates

The term glycoconjugate is commonly used when carbohydrates are attached to biological compounds such as polymers, peptides, and proteins to produce glycopolymers (Roy, 1996), glycopeptides (Kunz, 1987), and glycoproteins (Kimura *et al.*, 1999), respectively. These glycoconjugates have various biological functions. In the case of synthetic polymers such as dendrimers, conjugation of sugar residues onto a scaffold will generate macromolecules known as glycodendrimers. The glycodendrimer is formed when the sugar molecules are covalently conjugated to the peripheral groups of the dendrimer. It has gained a worthy research impact and is widely stated in mutual interaction reports of

proteins and sugars at the molecular level. According to the location of sugar molecules, glycodendrimers are classified into two types:

a) The first class is when the sugar molecules (generally monosaccharides or disaccharides) are covalently attached to the outer surface of the dendrimer. Such as in the case of PAMAM and PPI dendrimers (Figure 4.3 a).

b) The second class is when the sugar molecules are the building units (monomers) of the dendrimer (Figure 4.3 b).

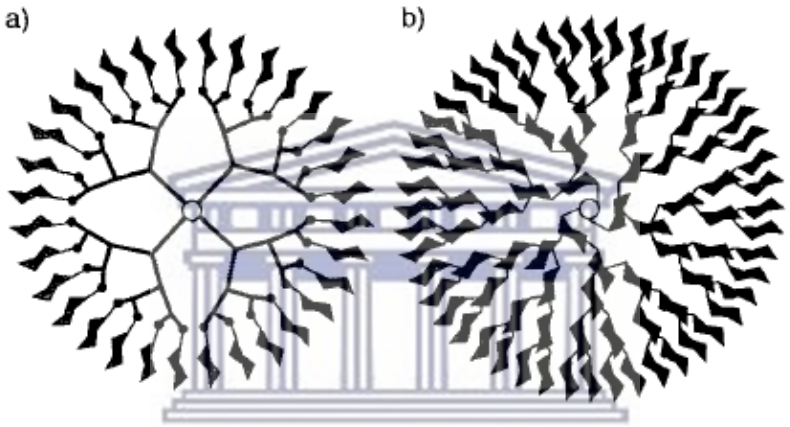

Figure 4.3 Representation of the two glycodendrimer classes: a) when the saccharides are conjugated to the outer layer of the dendrimer, and b) when the saccharides are the building units of the dendrimer; [adapted from (Jayaraman, Nepogodiev and Stoddart, 1997)].

4.2.4.2 Mannose receptors

Mannose receptors belong to the C-type lectin receptors that are presented on the surface of the alveolar macrophages (Ishii and Akira, 2008). Mannose receptors are one of the innate immune receptors that interact with carbohydrate-containing pathogens, particularly those that have fructose or mannose residues (Ishii and Akira, 2008). The mannose receptors have another important role in the clearing of the internal injurious molecules, such as glycosylated ligands (Ishii and Akira, 2008). Targeting the mannose receptors using carbohydrate ligands is one of the strategies that is commonly used to enhance drug delivery to the alveolar macrophages (Kumar *et al.*, 2006; Nimje *et al.*, 2009; Song *et al.*, 2015).

4.2.5 Methods of PAMAM functionalization with mannose residues

Several methods to modify the peripheral functional groups of PAMAM dendrimer with carbohydrate residues (i.e., mannose) have been reported in literature (Turnbull and Stoddart, 2002). Meijer and co-workers (1998) have modified the peripheral amines of 5.0 G PPI dendrimer using *N*-succinimidyl activated ester (Figure 4.4 (**1a**)) (I. Peerlings *et al.*, 1998). The resultant yield of the glycodendrimer was approximately 95% (Figure 4.4 (**1b**)) (I. Peerlings *et al.*, 1998).

Another method of glycodendrimer synthesis was reported by Roy and Baek (2002) (Baek and Roy, 2002). They successfully synthesized T-antigen (Figure 4.4 (**2a**)) coupled to 3.0 G glycoPAMAM dendrimer, with a yield of 73% (Figure 4.4 (**2b**)), by using 2-(1H-benzotriazole-1-yl)-1,1,3,3-tetramethyluronium tetra-fluoroborate (TBTU) and *N*,*N*-diisopropylethylamine (DIPEA) (Baek and Roy, 2002).

A further technique to functionalize the peripheral amines of the G0 - G3 PAMAM dendrimers were reported by Pagé and co-workers (1997) using isothiocyanates (Figure 4.4 (**3a**)) (Pagé and Roy, 1997). Synthesis of G0 - G2 glycoPAMAM dendrimers were achieved in refluxing dichloromethane for 3 hrs while refluxing for 48 hrs in DMF to synthesize G3 glycoPAMAM dendrimer (Pagé and Roy, 1997). One advantage of employing isothiocyanates is its selectivity to interact with peripheral amines of the PAMAM dendrimer, therefore shielding the hydroxyl groups of the sugar is not necessary.

Sashiwa and co-authors in 2000 and 2002 developed a new method to synthesize glycodendrimers (Figure 4.4 (**4b**)) *via* a reductive amination reaction to conjugate sialic acid (i.e., *p*-formyl phenyl-α-sialoside) (Figure 4.4 (**4a**)), to the dendrimer using $NaCNBH_3$ (Figure 4.3) (Sashiwa, Shigemasa and Roy, 2000, 2002).

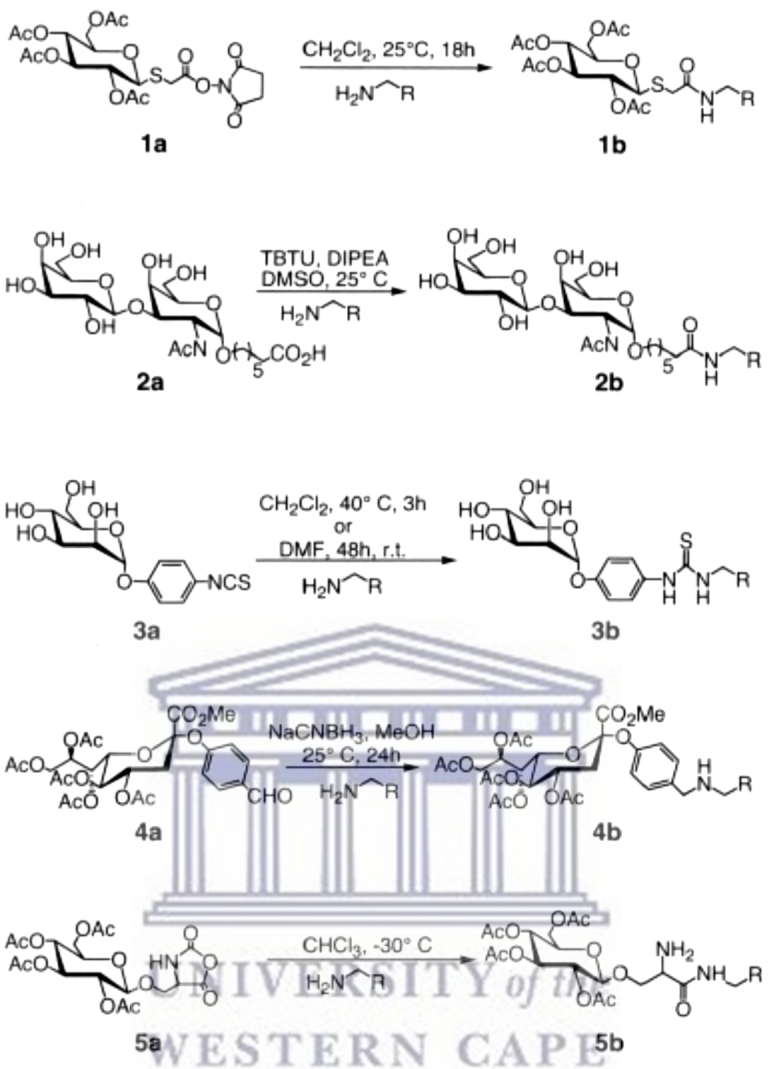

Figure 4.4 Various techniques of synthesis glycoPAMAM dendrimers; [adapted from (Woller, 2003)].

Lastly, a unique method was reported by Okada and co-workers (1998) to graft the surface of PAMAM dendrimers using sugar-substituted α-amino acid *N*-carboxyanhydrides, particularly O-(tetra-O-acetyl)-β-D-glucopyranosyl)-L-serine *N*-carboxyanhydride (Figure 4.4 (**5a**)), to generate glycodendrimers (Figure 4.4 (**5b**)) (Aoi *et al.*, 1998). An extra benefit of employing this reaction is the formation of additional primary amines on the glycodendrimer product which can further be modified.

4.2.6 Mannosylated dendrimer and tuberculosis

Dendrimers are one of the drug carriers that have been modified for targeted delivery of anti-TB drugs to alveolar macrophages (Filatova, Klyachko and Kudryashova, 2018). Targeting the alveolar macrophages using mannosylated dendrimers is the commonly reported strategy in the literature (Woller and Cloninger, 2001; Kumar *et al.*, 2006; Dutta *et al.*, 2007; Jain *et al.*, 2015; Filatova, Klyachko and Kudryashova, 2018). Mannosylated dendrimers were observed to increase the concentration of anti-TB drugs in the alveolar macrophages which are expected to improve the drug efficiency as a result of enhancing the co-localization of drugs and the pathogens (Filatova, Klyachko and Kudryashova, 2018).

Kumar and co-workers (2006) developed a mannosylated 5.0 G PPI dendrimer for targeted delivery of rifampicin to alveolar macrophages (Kumar *et al.*, 2006). Rifampicin was conjugated to the dendrimer *via* H-bonding, hydrophobic interactions, and electrostatic interactions. Surface modification of dendrimers with mannose (~30 mannose molecules) was observed to decrease the hemolytic toxicity as well as the cytotoxicity of the polymer, due to the shielding of the peripheral cationic amines. Drug release from mannosylated dendrimer showed sustained/prolonged release behavior at pH 7.4 compared to free rifampicin (Kumar *et al.*, 2006). While a higher drug release rate was observed at pH 5.0 (simulated phagolysosomal pH) compared to the release at pH 7.4. Comparing to free rifampicin, mannosylated dendrimer was observed to enhance rifampicin internalization into the alveolar macrophages (Kumar *et al.*, 2006).

4.2.7 Methods to quantify the mannose content on dendrimers

Several techniques have been used to estimate the number of mannose residues on the surface of the dendrimer nanoparticles. The most-reported methods are NMR, molecular weight determination techniques (Woller and Cloninger, 2001; Kumar *et al.*, 2006), and resorcinol assay.

a) NMR technique

^{1}H NMR has been employed to corroborate the conjugation of mannose residues on the dendrimer surface (Pagé and Roy, 1997; Woller and Cloninger, 2001; Kumar *et al.*, 2006), as well as the percentage of coverage (Woller and Cloninger, 2001; Kumar *et al.*, 2006). Quantitatively, Woller and Cloninger (2001) estimated the number of mannose residues attached on G4 PAMAM dendrimer from the integral ratio of the signal which corresponds to the protons of methylene next to the carbonyl groups of the PAMAM dendrimer (~ 248 Hs/molecule of G4 PAMAM dendrimer), to the signal which corresponds to the aromatic protons of the mannose residue (~ 4 Hs/molecule) (Woller and Cloninger, 2001).

b) Molecular weight determination technique

This technique was applied to determine the approximate number of mannose residues conjugated by calculating the difference in the molecular weight (M.wt) of the dendrimer before and following mannosylation (Woller and Cloninger, 2001). The mass-assisted laser desorption/ionization-time of flight (MALDI-TOF) technique was used by Woller and Cloninger (2001) to determine the difference in the molecular weight (M.wt) of G4, G5, and G6 PAMAM dendrimers before and after mannosylation (Woller and Cloninger, 2001). The different values were then divided by 313.33 (which represents the M.wt of the mannose residue) to estimate the number of mannose residues attached to each dendrimer (Pagé and Roy, 1997; Woller and Cloninger, 2001).

c) Resorcinol assay

The resorcinol assay is one of the commonly used techniques to calculate the density of monosaccharides in the polymeric scaffold (Diebold *et al.*, 1999).

4.3 Aim and the Objectives of the Chapter

4.3.1 Aim

The study aimed to synthesize and characterize rifampicin loaded in surface-modified 4.0 G PAMAM dendrimer having a range of mannose residues.

4.3.2 Objectives

i. To graft the surface of 4.0 G PAMAM dendrimer with increasing concentrations of mannose residues.

ii. To encapsulate rifampicin into 4.0 G PAMAM dendrimers having different mannose content.

iii. To characterize rifampicin loaded in mannosylated 4.0 G PAMAM dendrimer nanoparticles by size, PDI, ZP, shape, and the nature of drug-dendrimer interaction.

iv. To estimate the encapsulation efficiency (EE%) and percentage drug loading (DL%) by the direct technique using a validated HPLC method ***(Chapter 3)***.

4.4 Materials

4.4.1 Consumables

Reagents and solvents: 4-isothiocyanatophenyl alpha-D-mannopyranoside (4-ICPMP) (Toronto Research Chemicals, Canada), fourth-generation (G4) ethylenediamine polyamidoamine (PAMAM) dendrimer 10 wt % in methanol (Aldrich, USA), rifampicin (DB Fine Chemicals, South Africa), potassium phosphate monobasic (Sigma, USA), potassium phosphate dibasic (Sigma-Aldrich, Spain), Ultrapure water (18.2 MΩ cm, O-purity filtration system, Lasec, South Africa), HPLC grade acetonitrile (Merck, Germany), dimethyl sulfoxide (DMSO) (Sigma Aldrich, Poland), and HPLC grade methanol (Sigma Aldrich, France).

Other consumables: Nylon 0.22µm syringe filter (Micron separation Inc., USA), Nylon 0.45µm syringe filters (KimLab, India), poly top glass vials NO. 1, 2 and 4 (Kimix, South Africa), Pur-A-Lyzer MWCO 6 - 8 kDa dialysis tubes (Sigma, Israel), folded capillary zeta

cell (DTS 1070) (Malvern, UK), disposable 12 mm square polystyrene cuvettes (Malvern, UK), 5 mm thin wall 7″ NMR tubes (Wilmad Labglass, USA), DSC aluminum pan and lid (Kimix, South Africa), 2 ml HPLC vials with PTFE screw (Cronus, UK), HVLP 0.45 µm membrane filter (Millipore, Ireland), parafilm (Bemis, USA), micropipette 20, 200, 1000 and 5000 µl (DLAB, China), pipette tips 20, 200, 1000 and 5000 µl (Lasec, South Africa), and 10 ml centrifuge tube (Plastpro Scientific, South Africa).

4.4.2 Equipment

NMR spectrometer (Bruker Avance IIID Nanobay, Bruker BioSpin GmbH, Rheinstetten, Germany), Upright ultralow -86°C freezer (NU-9668E, NuAire, USA), Freeze-dryer (Virtis, Freeze mobile model 125L, Malvern instrument Ltd, UK), Fourier transform infrared spectrometer (Perkin-Elmer Spectrum-400 controlled with spectrum® software version 6.3.5, USA), Rotary evaporator (Büchi, Labotec, South Africa), HPLC system (Agilent 1200 series controlled with Agilent Chem-station software version G2173-60101L, Germany), HPLC column (phenomenex LC Luna® 250 x 4.6 mm, 5µm C-18, USA), differential scanning calorimeter (Perkin Elmer DSC 8000, USA), scanning electron microscope (Auriga HR-SEM F50, Zeiss, Germany), Malvern Zetasizer NanoZS90 (Malvern instruments, Ltd., UK), Ultrasonic bath (ScienTech®, South Africa), pH meter (XS®, Italy), filter apparatus (Millipore®, USA), vacuum pump (Dry Vac 400, USA), Vortex-Genie2, model-560E (scientific industries, USA), magnetic stirrer (IKA®-WERKE, Germany), and semi micron electronic balance (Shimadzu, Japan).

4.5 Methods

4.5.1 Functionalization of the surface of G4 PAMAM dendrimer with various mannose residues

The 4-isothiocyanatophenyl alpha-D- mannopyranoside (4-ICPMP) compound was used to functionalize the surface of the G4 PAMAM dendrimer with a range of mannose residues, following the protocol describes by Woller and Cloninger (2001) with few modifications. The 4-ICPMP has an advantage over the other mannose compounds as previously verified where the isothiocyanates interact selectively with peripheral amines of the PAMAM dendrimer, thereby shielding the hydroxyl groups of the mannose is not required (Pagé and Roy, 1997; Woller and Cloninger, 2001).

As illustrated in Table 4.1, four mannosylated G4 PAMAM dendrimer formulations were synthesized to achieve surface coverage ranging between 40% and 100%. To four solutions of G4 PAMAM dendrimer (14.20 mg, 1.0 µmol) in 10 ml of DMSO, various quantities of 4-ICPMP were added (Table 4.1). The molar ratio between the G4 PAMAM dendrimer and the 4-ICPMP was as follows 1:30, 1:45, 1:60, and 1:100. The mixtures were kept under slow stirring (50 rpm), at room temperature (25˚C), for 48 hrs (Figure 4.5). Then, the solutions were diluted with dH_2O and dialyzed for 48 hrs against a water/DMSO mixture using Pur-A-Lyzer 6 - 8 kDa MWCO dialysis tubes. The mannosylated dendrimer products were recovered by lyophilization and characterized using ^1H NMR (DMSO-d_6) and FTIR techniques.

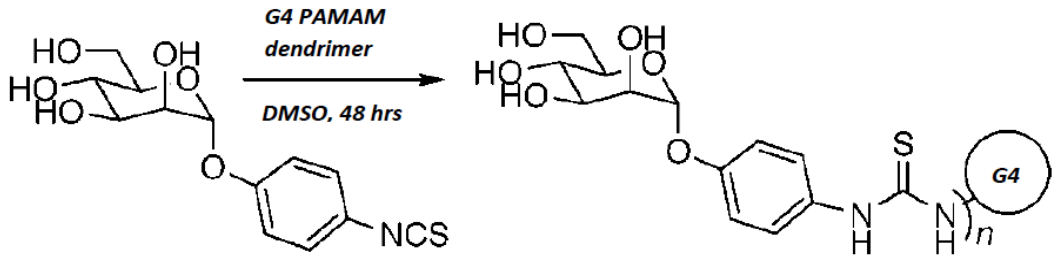

4-isothiocyanatophenyl alpha-D- mannopyranoside *Mannosylated G4 PAMAM dendrimer*

Figure 4.5 Synthesis of mannosylated G4 PAMAM dendrimers.

Table 4.1 Characteristics of mannose-dendrimer conjugates.

Target surface mannosylation (%)	Ratio G4: Mannose (mol: mol)	Amount of dendrimer (Feeding)	Amount of mannose (Feeding)
40 - 50	1:30	1 µmol = 14.22 mg	30 µmol = 9.39 mg
60 - 70	1:45	1 µmol = 14.22 mg	45 µmol = 14.09 mg
80 - 95	1:60	1 µmol = 14.22 mg	60 µmol = 18.78 mg
100	1:100	1 µmol = 14.22 mg	100 µmol = 31.30 mg

4.5.2 Confirming and quantifying the degree of mannosylation using ^{1}H NMR technique

^{1}H NMR technique was used to confirm the conjugation of mannose residues to the peripheral amino groups of the PAMAM dendrimer *via* expected thiourea linkage. Also, this technique was employed to estimate the number of conjugated sugar molecules on the surface of the PAMAM dendrimer as previously reported by Woller and Cloninger (2001). The analysis was performed by dissolving 5 mg of freeze-dried sample in 1 ml of deuterated DMSO solvent, filtered and examined using a Bruker 400 REM instrument running at 400 MHz. The data were collected and interpreted using TopSpin® software version 4.0.6. The integral ratio of the peak area which corresponds to the methylene protons next to the carbonyl groups of G4 PAMAM dendrimer, to the peak areas which correspond to the aromatic protons of the mannose part, was used to estimate the approximate number of conjugated mannose residues. The analysis was done for three batches, and the average ± standard deviation for each formulation was reported.

4.5.3 Encapsulation of rifampicin by mannosylated G4 PAMAM dendrimers

Rifampicin was loaded into mannosylated dendrimers following the reported protocol (Kumar *et al.*, 2006), with slight modifications. Briefly, 10 µmol of rifampicin was dissolved in DMSO, then 0.1 µmol of mannosylated dendrimers was added. All mixtures were incubated with slow stirring of 50 rpm for 24 hrs at room temperature (25˚C). After that, the mixtures were diluted with dH_2O and dialyzed twice against dH_2O/DMSO mixture using Pur-A-Lyzer dialysis tubes (MWCO of 6 - 8 kDa), under strict sink conditions for 10 min to remove unconjugated drug molecules. Rifampicin-dendrimer conjugates were retrieved by lyophilization from their solutions and then characterized using NMR, FTIR, Zetasizer, SEM, and DSC techniques. The encapsulated efficiency (EE%) and the percentage drug loading (DL%) were determined directly at a wavelength of 475 nm using a validated HPLC method.

4.5.4 Characterization of rifampicin loaded mannosylated PAMAM dendrimer nanoparticles

4.5.4.1 Fourier transform infrared spectroscopy (FTIR) analysis

FTIR analysis was carried out to study the interaction between rifampicin molecules and the mannosylated dendrimers. The analysis was performed by scanning samples between 650 - 4000 cm^{-1} using a Fourier transform infrared spectrometer (Perkin-Elmer Spectrum-400, USA) having diamond attenuated total reflectance (ATR) accessories with a diamond crystal.

A small granule of a fresh freeze-dried sample was placed on top of the FTIR crystal, a force was applied using a pressure gauge (up to 60%). IR-spectra were captured using spectrum® software version 6.3.5. The data were interpreted for functional groups at their relevant wave-number (cm^{-1}). The FTIR spectra of the rifampicin conjugated mannosylated dendrimer formulations were compared to that of the rifampicin and their corresponding unloaded mannosylated dendrimers. Differences in the band's features such as appearance and disappearance of peaks, change in peak intensity, and shift in wave-number were employed to verify conjugate formation.

4.5.4.2 Nuclear magnetic resonance (NMR) studies

NMR technique was used to study the chemical structure of the nanoparticles. ^{1}H NMR and NOESY techniques were used to confirm the conjugation of rifampicin in mannosylated G4 PAMAM dendrimers. Resonance data were also employed to predict the site(s) of interaction between the rifampicin molecules and the mannosylated PAMAM dendrimer. 5 mg from each sample was dissolved in 1 ml of deuterated DMSO and filtered before analysis by a Bruker NMR instrument running at 400 MHz. The data were interpreted using TopSpin 4.0.6® software.

4.5.4.3 Morphology of the nanoparticles

The morphology of the G4 PAMAM dendrimer, the unloaded mannosylated G4 PAMAM dendrimers, and the rifampicin-loaded mannosylated PAMAM dendrimers were examined using scanning electron microscopy (SEM).

Dendrimer samples were mounted on double-sided carbon conductive adhesive tape fixed on aluminium stubs and left to dry at room temperature, then coated by a thin film of gold using a sputtering method. The morphology of the samples was observed and captured under an Auriga HR-SEM F50 scanning electron microscope (Zeiss®, Germany).

4.5.4.4 Differential scanning calorimetry (DSC) studies

The DSC technique was used to study the thermal performance as well as the crystallinity transformation over a range of temperatures. Approximately 2 mg of rifampicin, unloaded mannosylated G4 PAMAM dendrimers, rifampicin-dendrimer physical mixtures, and rifampicin loaded mannosylated dendrimer formulations were packed in individual aluminum pans which were then crimped at the edges. The sample was placed in the cell holder of a Perkin Elmer DSC 8000, and analyzed at an increasing heating rate of 10 ˚C/min from 30 ˚C to 220 ˚C under N_2 gas flow; a blank pan of the same dimension was crimped and used as a reference. The DSC thermogram of each drug-loaded dendrimer was compared to their corresponding unloaded dendrimer formulation, pure rifampicin, and rifampicin-dendrimer physical mixture to approve drug conjugation.

4.5.4.5 Nanoparticle size, polydispersity (PDI) and zeta potential (ZP) studies

Dynamic light scattering (DLS) was used to examine the hydrodynamic diameter, PDI, and Zeta potential of the dendrimer samples. The analysis was done on a Malvern Zetasizer Nano ZS90 that measures light scattering at a 90˚ angle using the dynamic light scattering (DLS) theory.

The size and the PDI of the unloaded and loaded mannosylated G4 PAMAM dendrimer nanoparticles were measured directly after synthesis. Two milligrams of each sample was added to 2 ml of PBS pH 7.4. Afterward, one milliliter from each dendrimer dispersion was placed in a zeta cell and analyzed. Three independent measurements for ten cycles were performed for each sample. The z-average particle diameters were automatically calculated by the system using cumulant analysis with the zetasizer software version 7.12 installed. The average diameter ± standard deviation for each sample was calculated and tabulated.

Zeta potential analysis was carried out in triplicate after preparing 1 mg/ml dispersion from each sample, which was transferred to a zeta-potential capillary cell (DTS 1070) and filled up until both electrodes were covered with the nanoparticle dispersion. The average zeta potential ± standard deviation for each sample was calculated and tabulated.

4.5.5 Development and validation of Reverse-phase high performance/pressure liquid chromatography (RP-HPLC) method

The RP-HPLC method that was validated in Chapter 3, was also employed in this Chapter to calculate rifampicin concentration. The HPLC method was additionally assessed for the specificity parameter for the unloaded mannosylated dendrimer to ensure no overlapping with the rifampicin peak.

4.5.6 Encapsulation efficiency (EE%) and drug loading (DL%)

The direct technique was applied to determine the encapsulation efficiency percentage (EE%) and the percentage drug loading (DL%) using a validated HPLC method. One milligram of freeze-dried rifampicin-loaded mannosylated dendrimer was transferred to 10 ml volumetric flasks, the volume was adjusted to 10 ml by the mobile phase. Samples were

sonicated for 2 minutes in an ultrasonic bath to ensure complete dissolution, then filtered using a Nylon 0.45 μm syringe filter, and finally analyzed on an Agilent 1200 HPLC at 475 nm wavelength. The resulting peak area was interpreted as rifampicin concentration using a generated calibration curve prepared on the day of study. The analysis was done in triplicate, and the average ± standard deviation for each sample was reported. EE% and DL% for dendrimer formulations were determined using equations 3.4 and 3.5 (Chapter), respectively.

4.6 Data analysis

The data, expressed as mean ± standard deviation, were interpreted using GraphPad® Prism 7.04. A one-way ANOVA test was applied to set up the significance of any differences between the means. Values were considered significant if the *p*-value was ≤ 0.05.

4.7 Results and discussion

4.7.1 Functionalization of the surface of G4 PAMAM dendrimer with various mannose residues

Functionalization of the surface of G4 PAMAM dendrimer with various concentrations of mannose residues was performed to achieve surface coverage ranging from 40% to 100% (Figure 4.6). This was attained by adding incremental amounts of 4-ICPMP to four G4 PAMAM dendrimer solutions, the molar ratio between the dendrimer and 4-ICPMP was as follows: 1:30, 1:45, 1:60, and 1:100.

^{1}H NMR technique was used to examine G4 PAMAM dendrimer, mannose (4-ICPMP), and the synthesized mannosylated dendrimer formulations (Figure 4.7). ^{1}H NMR spectra of mannosylated G4 PAMAM dendrimers characterized by the appearance of peaks that correspond to the dendrimer part (A, B, C, & D peaks), besides other peaks of the mannose part (E, F, G, H, I, J, K, L, M, & N peaks) (Figure 4.7) were identified. It was observed that some of the mannose proton peaks i.e., K, L, M, and N, were upfield shifted after conjugation with the dendrimer, the shifts were from 5.05, 5.40, 7.13, and 7.39 ppm to 5.03, 5.31, 7.02, and 7.25, respectively. Moreover, comparing the ^{1}H NMR spectra (Figures 4.7 & 4.8) of dendrimer (i) and mannose (ii) to that of mannosylated dendrimers (iii-vi) confirmed the emergence of new proton peaks at 8.01 – 8.08 ppm (P) and 9.42 – 9.61 ppm (Q) for surface-functionalized dendrimers only.

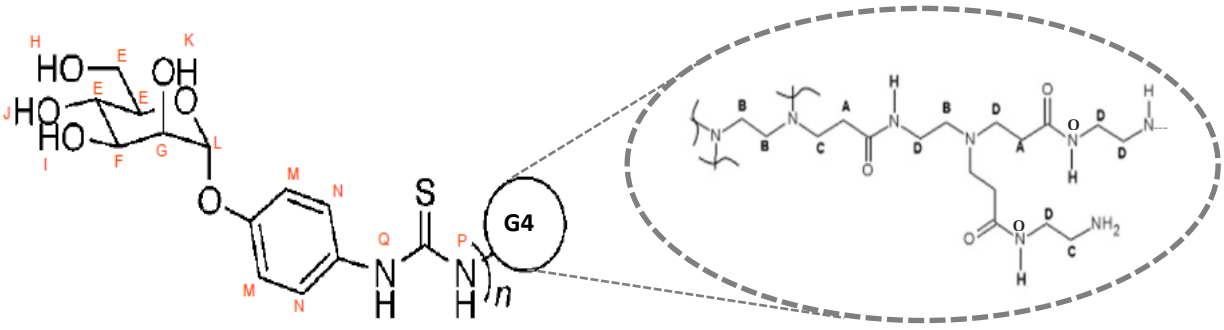

Figure 4.6 Chemical structure of mannosylated G4 PAMAM dendrimer.

These new peaks (P & Q) are expected to be formed as a result of the interaction of mannose molecules with the surface amines of the dendrimer *via* thiourea linkages to generate thiourea NH groups. Altogether, the change in the chemical shift of some proton

peaks of mannose molecules besides the appearance of new peaks that correspond to thiourea NH groups corroborated the successful conjugation of mannose residues to the surface amines of the G4 PAMAM dendrimer through thiourea linkages.

Mannosylated G4 PAMAM dendrimer	
Peak label	Peak chemical shift δ (ppm)
A	2.21
B	2.43
C	2.62
D	3.23
E	3.40 - 3.60
F	3.67
G	3.82
H	4.47
I	4.77

Mannosylated G4 PAMAM dendrimer	
Peak label	Peak chemical shift δ (ppm)
J	4.85
K	5.03
L	5.31
M	7.02
N	7.25
O	7.61 - 7.86
P	8.01 – 8.08
Q	9.42 - 9.61

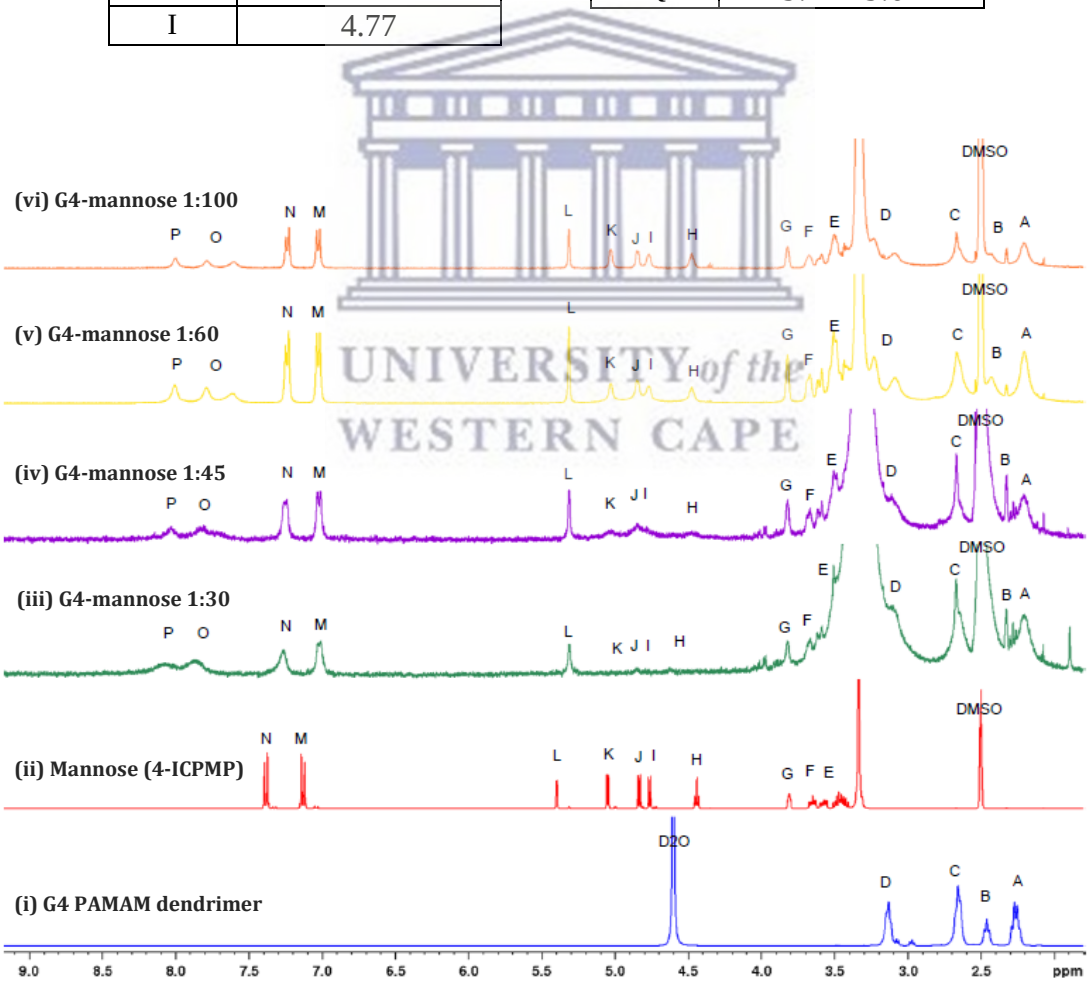

Figure 4.7 ^{1}H NMR spectra (1.8 ppm – 9.0 ppm) of, (i) G4 PAMAM dendrimer in D_2O, (ii) Mannose (4-ICPMP), (iii) G4-mannose 1:30, (iv) G4-mannose 1:45, (v) G4-mannose 1:60, and (vi) G4-mannose 1:100, in DMSO-d_6.

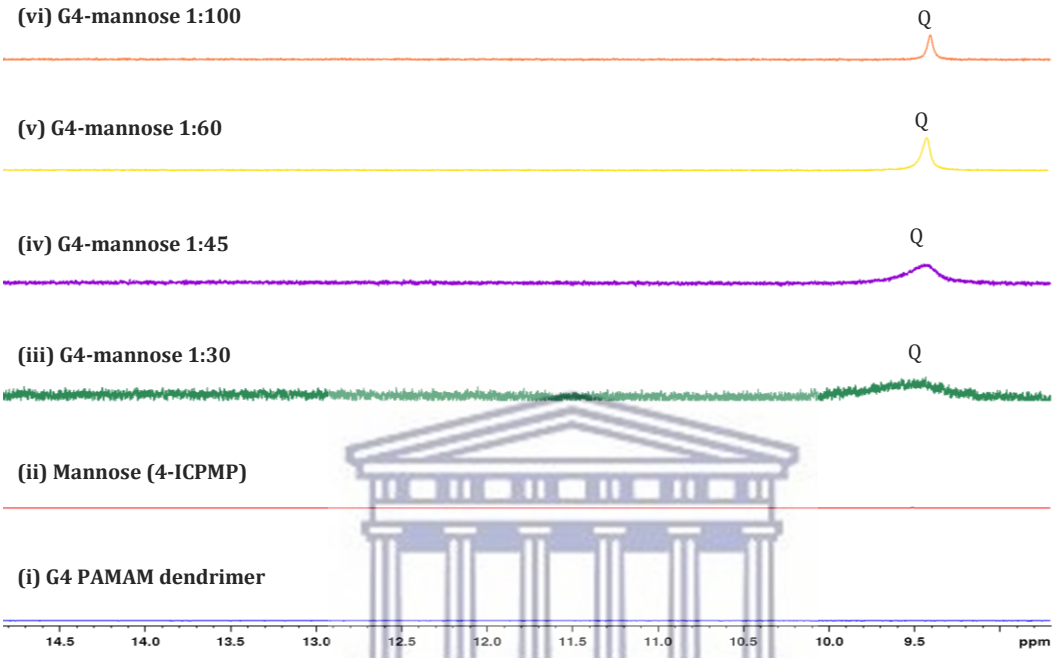

Figure 4.8 ^{1}H NMR spectra (8.80 ppm – 14.80 ppm) of, (i) G4 PAMAM dendrimer in D_2O, (ii) Mannose (4-ICPMP), (iii) G4-mannose 1:30, (iv) G4-mannose 1:45, (v) G4-mannose 1:60, and (vi) G4-mannose 1:100, in DMSO-d_6.

FTIR technique was also applied to confirm the conjugation of mannose molecules on the surface of the G4 PAMAM dendrimer. Scanning G4 PAMAM dendrimer, mannose (4-ICPMP), and mannosylated dendrimers between 650 - 4000 cm^{-1} using a Fourier transform infrared spectrometer (Perkin-Elmer Spectrum-400, USA), generated IR spectra as shown in Figure 4.8. The IR data of mannosylated dendrimers (Figure 4.9 and Table 4.2) confirmed the existence of dendrimer peaks as well as mannose peaks. The IR peaks of mannosylated dendrimers (c – f) at 3071 - 3079 cm^{-1}, 1632 - 1634 cm^{-1}, and 1534 - 1541 cm^{-1} are attributed to NH stretching, carbonyl stretching of (-NH-***CO***-) group, and NH bending of (-***NH***-CO) group of the dendrimer part, respectively (Uppuluri *et al.*, 1998). While the IR peaks at 1504 - 1507 cm^{-1}, 1335 - 1339 cm^{-1}, 1218 - 1222 cm^{-1}, 1121 - 1125 cm^{-1}, and 1066 – 1068 cm^{-1} are associated with the aromatic (C=C) stretching, aromatic

(C-N) stretching, aromatic (C-O-R) stretching, (C=S) group, and (C-O) stretching of the mannose part, respectively (Liu, Li and Li, 2018). It was also observed that the absorption peak at 2125 cm^{-1} which corresponds to (–N=C=S) group of the mannose (b), had disappeared in the spectra of all mannosylated dendrimers (c – f). This could suggest the formation of thiourea bonds between the mannose molecules and surface-amines of the dendrimer to generate thiourea amines.

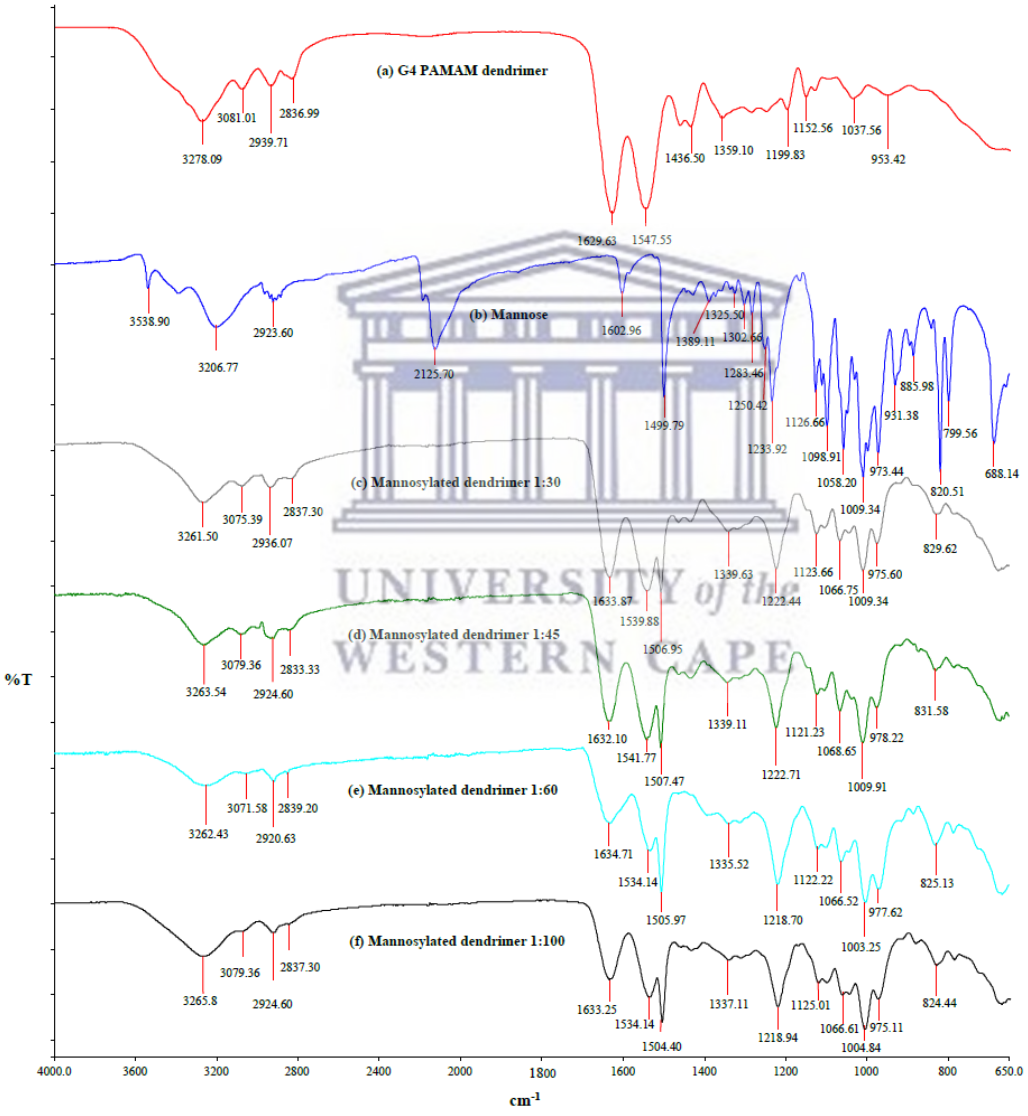

Figure 4.9 FTIR spectra of (a) G4 PAMAM dendrimer, (b) mannose (4-ICPMP), (c) G4-mannose 1:30, (d) G4-mannose 1:45, (e) G4-mannose 1:60, and (f) G4-mannose 1:100.

The O-H peaks of the mannose (b) were observed at 3538 cm^{-1} and 3206 cm^{-1}, it is expected that the broad peaks at 3261 – 3265 cm^{-1} in the spectra of mannosylated dendrimers (c – f) be attributed to O-H stretching vibration shielding the NH stretching of the dendrimer. FTIR analysis suggests that mannose molecules were successfully conjugated to the peripheral amines of the dendrimer *via* thiourea linkages to form mannosylated dendrimer.

Table 4.2 Selected IR functional groups with their frequencies (cm^{-1}) for G4 PAMAM dendrimer, mannose, and mannosylated dendrimers.

Functional groups	Frequency (cm^{-1})					
	G4-PAMAM	Mannose	G4-mannose (1:30)	G4-mannose (1:45)	G4-mannose (1:60)	G4-mannose (1:100)
O-H (S)	-	3538, 3206	3261	3263	3262	3265
N-H (S)	3278, 3081	-	3261, 3075	3263, 3079	3262, 3071	3265, 3079
-CH_2- (S)	2939, 2836	2923	2936, 2837	2924, 2833	2920, 2839	2924, 2837
-N=C=S (S)	-	2125	-	-	-	-
-NH-***CO***- (S)	1629	-	1633	1632	1634	1633
-***NH***-CO- (B)	1547	-	1539	1541	1534	1534
Ar C=C (S)	-	1602, 1499	1506	1507	1505	1504
Ar C-N (S)	-	1325	1339	1339	1335	1337
Ar-O-R (S)	-	1233	1222	1222	1218	1218
Thiocarbonyl C=S	-	1126	1123	1121	1122	1125
C-O (S)	-	1058	1066	1068	1066	1066
AR - disubstituted	-	820	829	831	825	824

*S = stretching vibration, B = bending vibration, Ar = aromatic.

4.7.2 Confirming and quantifying the degree of mannosylation using ^{1}H NMR technique

^{1}H NMR technique was used to estimate the approximate number of mannose molecules that have been conjugated to peripheral amines of G4 PAMAM dendrimer. The integral ratio of peak area which corresponds to methylene protons (A-peak) next to the carbonyl groups of the PAMAM dendrimer, to the peak areas corresponding to aromatic (M-peak & N-peak) and/or anomeric protons (L-peak) from the mannose residues were employed to determine the degree of mannosylation (Woller and Cloninger, 2001). The analysis was done for three batches, the average ± standard deviation for each formulation was reported (Table 4.3).

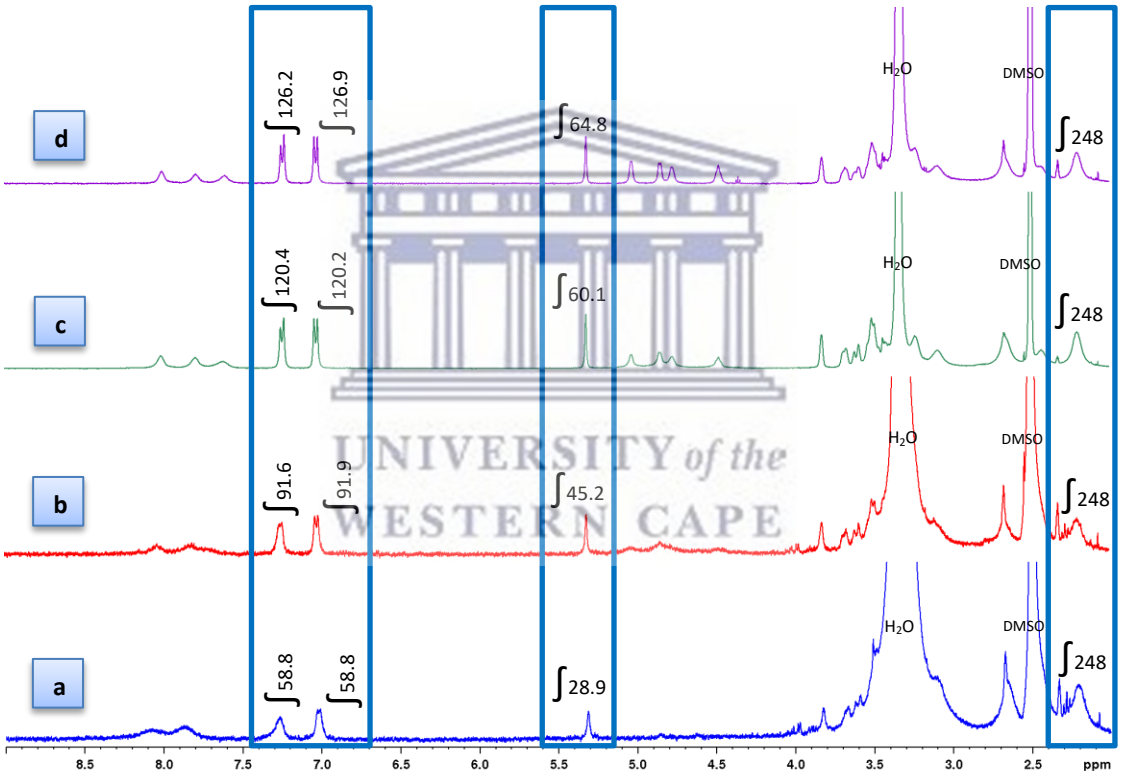

Figure 4.10 The ^{1}H NMR spectra of (a) G4-mannose 1:30, (b) G4-mannose 1:45, (c) G4-mannose 1:60, and (d) G4-mannose 1:100, in DMSO-d_6, with integration values of methylene protons next to the carbonyl groups of G4 PAMAM dendrimer at δ of 2.30 ppm, anomeric protons (peak L) at δ of 5.31 ppm, and aromatic protons (peaks M & N) at δ of 7.02 ppm and 7.25 ppm from mannose residues.

G4 PAMAM dendrimer theoretically has 248 protons from methylene adjacent to the carbonyl groups, and the mannose molecule (4-ICPMP) holds 4 aromatic protons (i.e., 2 protons at ortho position and 2 protons at the meta position). In Figure 4.10, the ratio of methylene protons (A-peak) to aromatic protons (M-peak & N-peak) indicated that approximately 29.40, 45.90, 60.15, and 63.28 mannose residues were successfully conjugated to G4 PAMAM dendrimer formulations a, b, c, and d, respectively.

Table 4.3 Characterization of mannosylated G4 PAMAM dendrimer conjugates (n = 3).

Formulation	Ratio G4: Mannose	Amount of dendrimer (Feeding)	Amount of mannose (Feeding)	Yield wt (mg)	No of NH2 substituted Mean ± SD	% Coverage achieved
1	(1:30) mol:mol	1 µmol = 14.22 mg	30 µmol = 9.39 mg	14.73 ± 2.29	27.90 ± 2.21	43.59%
2	(1:45) mol:mol	1 µmol = 14.22 mg	45 µmol = 14.09 mg	13.83 ± 1.76	44.02 ± 0.63	68.78%
3	(1:60) mol:mol	1 µmol = 14.22 mg	60 µmol = 18.78 mg	17.15 ± 2.90	59.70 ± 0.08	93.28%
4	(1:100) mol:mol	1 µmol = 14.22 mg	100 µmol = 31.30 mg	15.35 ± 1.48	64.20 ± 0.79	100.31%

Table 4.3 summarizes the developed mannosylated dendrimer formulations with the average number of conjugated mannose residues to the surface of the dendrimer *via* thiourea linkages. The number of substituted primary amines of each formulation was reported as mean ± SD determined from the ^{1}H NMR integration results for 3 samples. The percentage of coverage that is listed in the last column of Table 4.3, was calculated based on the ratio of substituted amines to the theoretical total amines of G4 PAMAM dendrimer i.e., 64 amine groups.

4.7.3 Characterization of rifampicin loaded mannosylated PAMAM dendrimers

4.7.3.1 Fourier transform infrared (FTIR) studies

Figure 4.11 shows the IR spectra of G4 PAMAM dendrimer, G4-mannose 1:30 (44%), rifampicin, and rifampicin loaded G4-mannose 1:30 (44%), and Table 4.4 highlights particular functional groups for comparison.

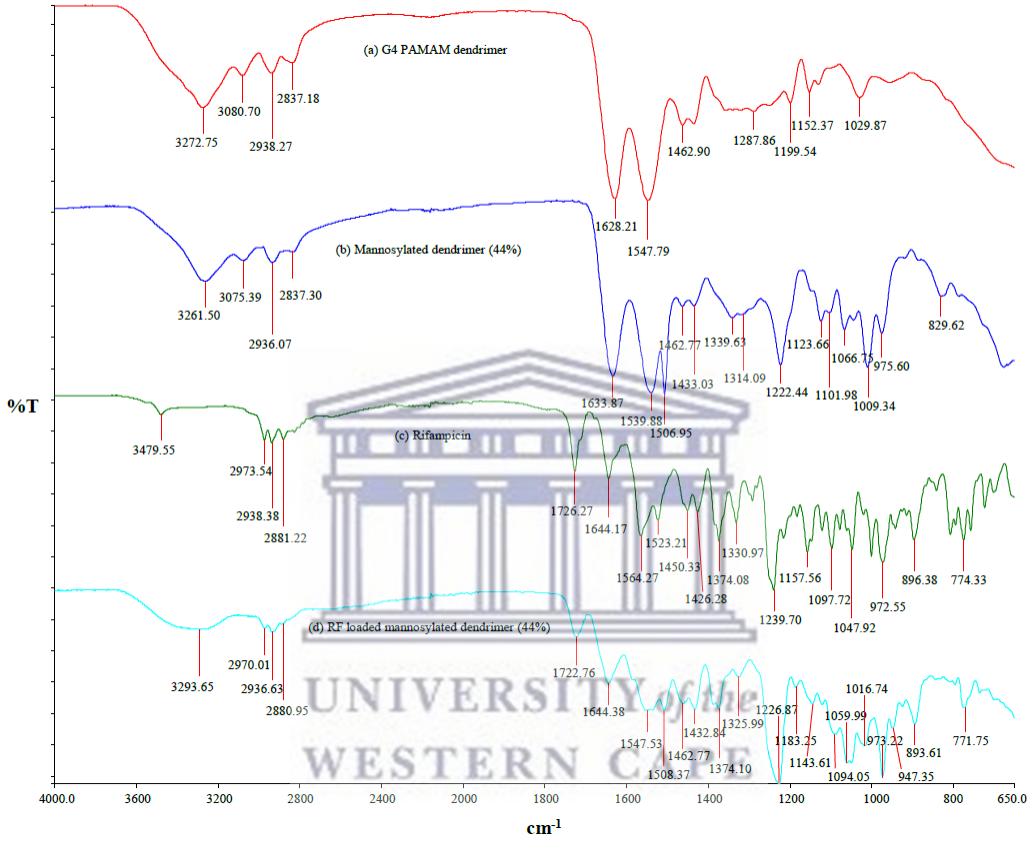

Figure 4.11 FTIR spectra of (a) G4 PAMAM dendrimer, (b) G4-mannose 1:30 (44%), (c) rifampicin, and (d) RIF loaded G4- mannose 1:30 (44%).

From Figure 4.11, the IR spectrum of rifampicin (c) showed numerous peaks, absorption bands of O-H and N-H at 3479 cm^{-1}, C=O stretching at 1726 cm^{-1}, -C=N stretching at 1644 cm^{-1}, aromatic C=C stretching at 1523 cm^{-1}, aromatic C-N stretching at 1374 cm^{-1}, -C-O- ether stretching at 1097 cm^{-1}, and C=C bending at 972 cm^{-1} (Date, Samad and Devarajan, 2010). Comparing the spectrum of rifampicin-loaded mannosylated dendrimer (d) to their corresponding empty dendrimer (b) indicated the appearance of a broad absorption peak at 3293 cm^{-1} which is expected to be for the O-H groups from the mannosylated dendrimer and rifampicin. This broad peak probably covers the N-H peaks of the mannosylated dendrimer. In the spectrum of rifampicin

conjugated dendrimer (d), a new peak at 1722 cm^{-1} had emerged which corresponds to the carbonyl functional groups obtained from rifampicin.

Table 4.4 The IR functional group assignments of G4 PAMAM dendrimer, G4-mannose 44%, rifampicin, and RIF loaded G4- mannose 44%.

Functional groups	Frequency (cm^{-1})			
	G4-PAMAM **(a)**	G4-mannose (44%) **(b)**	Rifampicin **(c)**	RIF-mannosylated dendrimer (44%) **(d)**
O-H (S)	-	3261	3479	3293
N-H (S)	3272, 3080	3261, 3075	3479	Underneath 3293
-CH_2- (S)	2938, 2837	2936, 2837	2973, 2938, 2881	2970, 2936, 2880
C=O (S)	-	-	1726	1722
-C=N- (S)	-	-	1644	1644
-NH-***CO***- (S)	1628	1633	1644	1644
-***NH***-CO- (B)	1547	1539	1564	1547
Ar C=C (S)	-	1506	1523	1508
Ar C-N (S)	-	1339	1374	1374
Ar-O-R (C-O (S))	-	1222	1239	1226
C-O ether (S)	-	1066	1097	1059
C=C (B)	-	975	972	973
C-H di-substituted (B)	-	-	774	771

*S = stretching vibration, B = bending vibration, Ar = aromatic.

The spectrum of rifampicin loaded nanoparticles maintained most of the mannosylated dendrimer peaks with slight shifting, as demonstrated in Table 4.4. Also, the absorption peak from rifampicin at 774 cm^{-1} appeared in the spectrum of rifampicin loaded nanoparticles with a slight shift. The main peaks corresponding to rifampicin (c) could also be detected in the spectrum of rifampicin loaded nanoparticles (d) (Table 4.4). These findings could suggest the successful encapsulation of rifampicin molecules into mannosylated dendrimer nanoparticles. Similar findings were observed in the spectra of other rifampicin-loaded mannosylated dendrimers (Figures 4.12, 4.13, and 4.14).

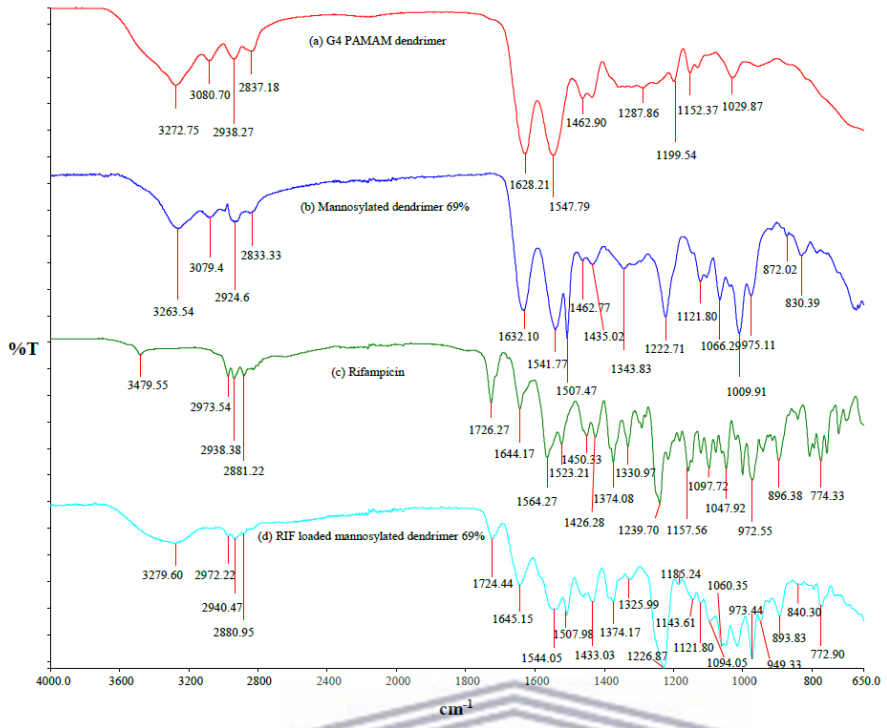

Figure 4.12 FTIR spectra of (a) G4 PAMAM dendrimer, (b) G4-mannose 69%, (c) rifampicin, and (d) RIF loaded G4- mannose 69%.

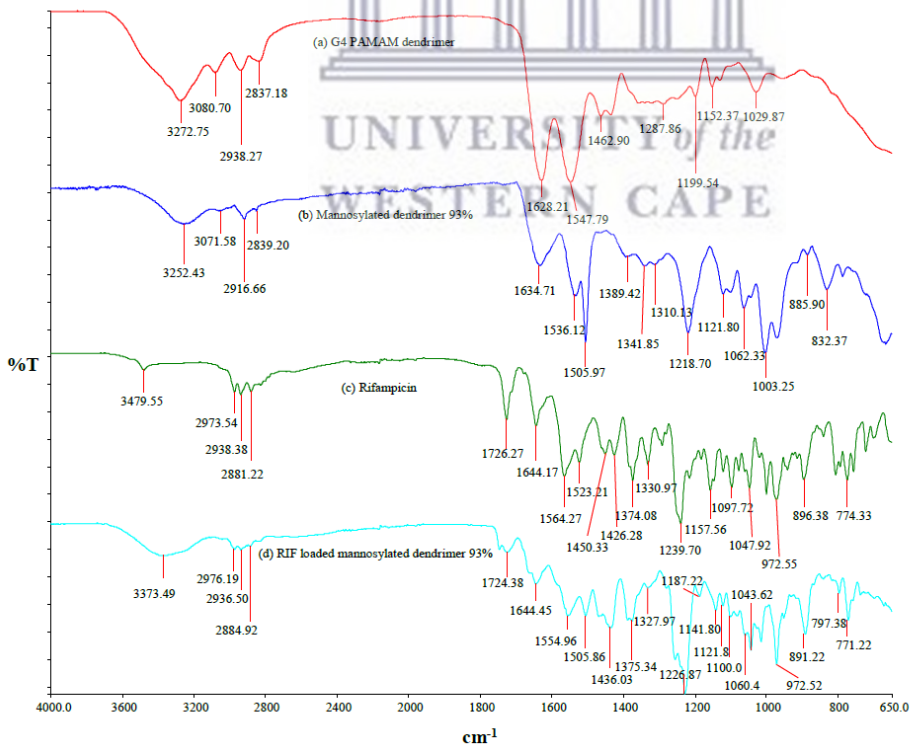

Figure 4.13 FTIR spectra of (a) G4 PAMAM dendrimer, (b) G4-mannose 93%, (c) rifampicin, and (d) RIF loaded G4- mannose 93%.

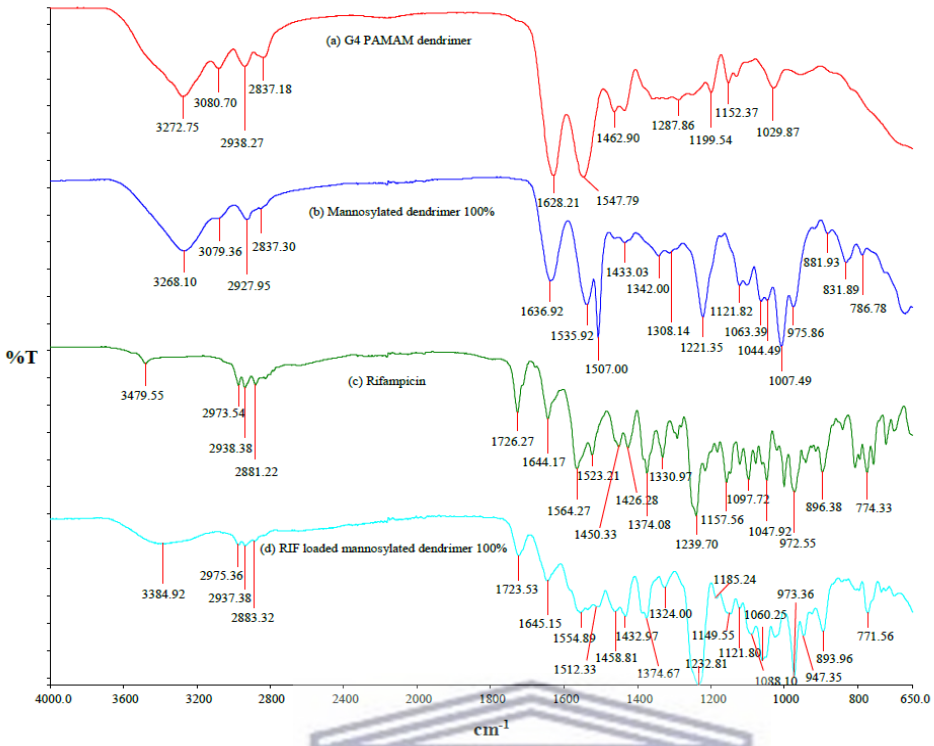

Figure 4.14 FTIR spectra of (a) G4 PAMAM dendrimer, (b) G4-mannose 100%, (c) rifampicin, and (d) RIF loaded G4- mannose 100%.

4.7.3.2 Nuclear magnetic resonance (NMR) studies

^{1}H NMR technique was used to study the rifampicin nanoconjugates. The protons of the unloaded mannosylated dendrimers were already assigned in this chapter, while rifampicin protons have been previously assigned in Chapter 3 (section 3.7.4.2). The change in the proton chemical shift besides 2D NOESY NMR data were used to predict the preferred site(s) of interaction between rifampicin molecules and the mannosylated dendrimer.

Figure 4.16, comparing the ^{1}H NMR of rifampicin (b) to that of rifampicin loaded mannosylated dendrimer (c), revealed the appearance of most rifampicin proton peaks at relatively comparable chemical shifts in the spectrum of rifampicin nanoconjugates (c). Only a few atoms were observed at somewhat higher or lower chemical shifts after being conjugated to the dendrimer scaffold. Particularly, atom numbers 48 and 50 were detected at higher chemical shifts (downfield) after conjugation, while atom numbers 10, 11, 13, 14, 26, 27, 42, and 47 were observed at lower chemical shifts (upfield) after drug conjugation. These rifampicin atoms are highlighted with green circles as

illustrated in Figure 4.15a. H-bonding between the rifampicin protons and the dendrimer scaffold could account for the changes in their chemical shifts.

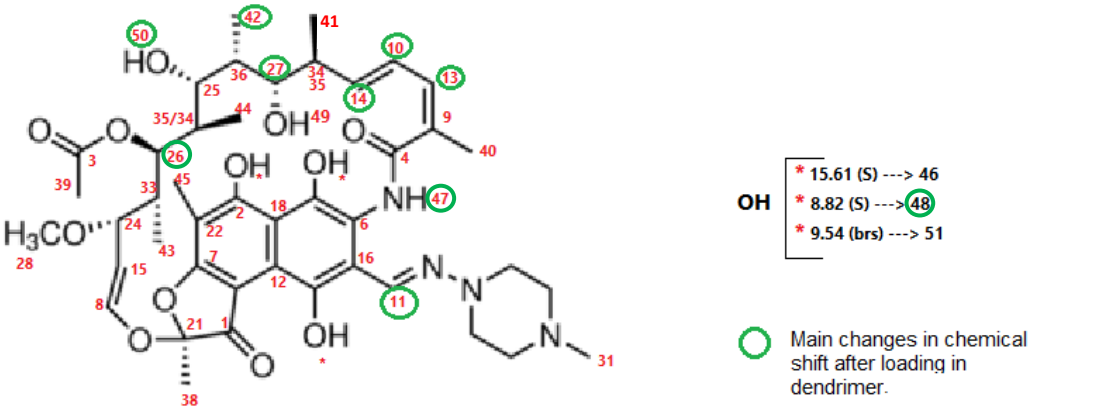

(a) Rifampicin

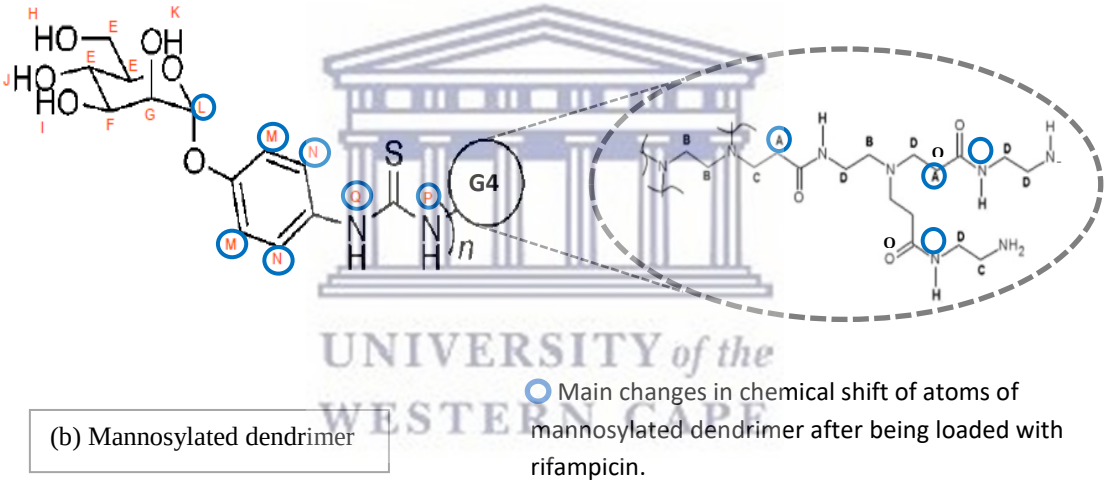

(b) Mannosylated dendrimer

Figure 4.15 The structures of (a) rifampicin, and (b) mannosylated dendrimer, with highlighting on atoms that show changes in their ^{1}H NMR chemical shift.

In addition, comparing the ^{1}H NMR spectrum of the unloaded mannosylated G4 PAMAM dendrimer (Figure 4.16 a) to the loaded one (4.16 c) has verified the existence of the dendrimer methylene protons as well as the peaks correspond to the mannose part. The lower proton peak intensities of the mannosylated dendrimer in the conjugate complex were due to the lower concentration present compared to the pure unloaded sample. The atoms that are encircled with blue circles (Figure 4.15 b) were noticed at slightly higher or lower chemical shifts. Atoms L and M were downfield shifted after conjugation, whereas atoms A, N, O, P, and Q were upfield shifted after rifampicin

conjugation. Again, H-bonding between rifampicin and the mannosylated dendrimer could be the reason for the variation in the proton chemical shifts.

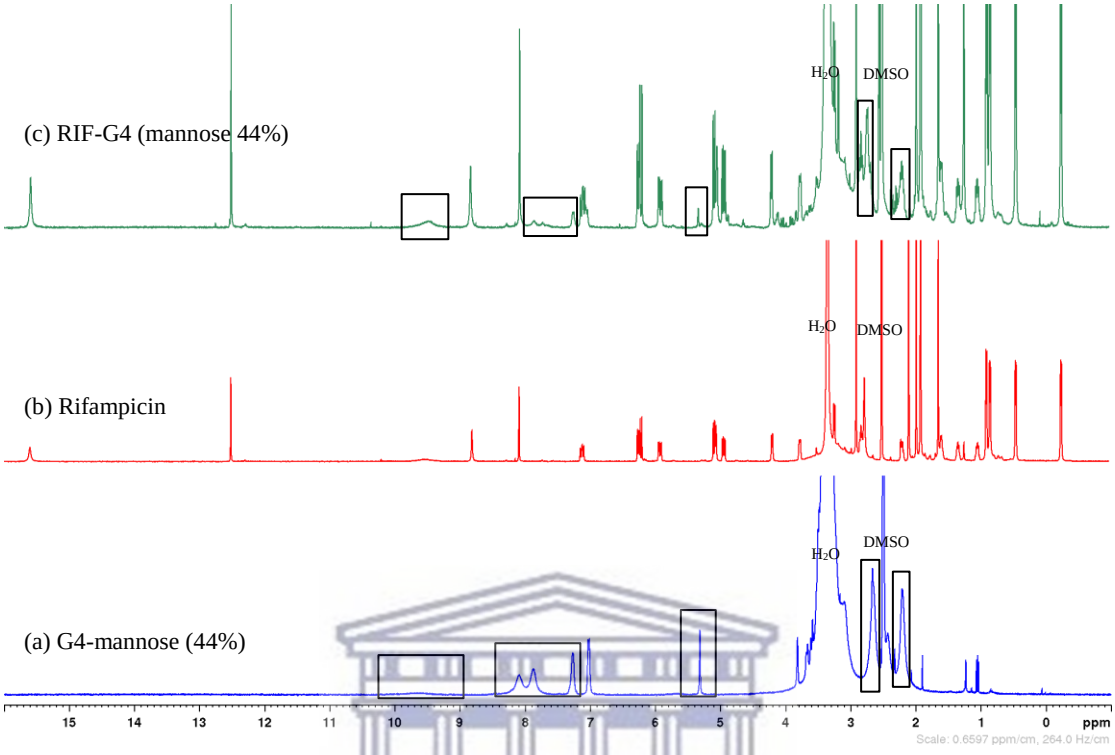

Figure 4.16 ^{1}H NMR spectra of (a) mannosylated G4 PAMAM dendrimer (44%), (b) rifampicin, and (c) rifampicin loaded mannosylated G4 PAMAM dendrimer (44%), in DMSO-d_6 solvent.

The ^{1}H NMR spectra of the other rifampicin-loaded mannosylated dendrimers (Figures 4.17 – 4.19) have also supported the formation of non-covalent interactions between rifampicin molecules and the dendrimer nanoparticles, as a result of changes in the proton chemical shifts in the conjugate complexes. Analyzing the ^{1}H NMR of rifampicin loaded 69% (Figure 4.17), 93% (Figure 4.18), and 100% (Figure 4.19) mannosylated dendrimers have indicated comparable findings to that of the rifampicin loaded 44% mannosylated dendrimer, i.e., δ_H of rifampicin loaded mannosylated dendrimers and a change in the chemical shifts of the 10 rifampicin atoms and 7 mannosylated dendrimer atoms.

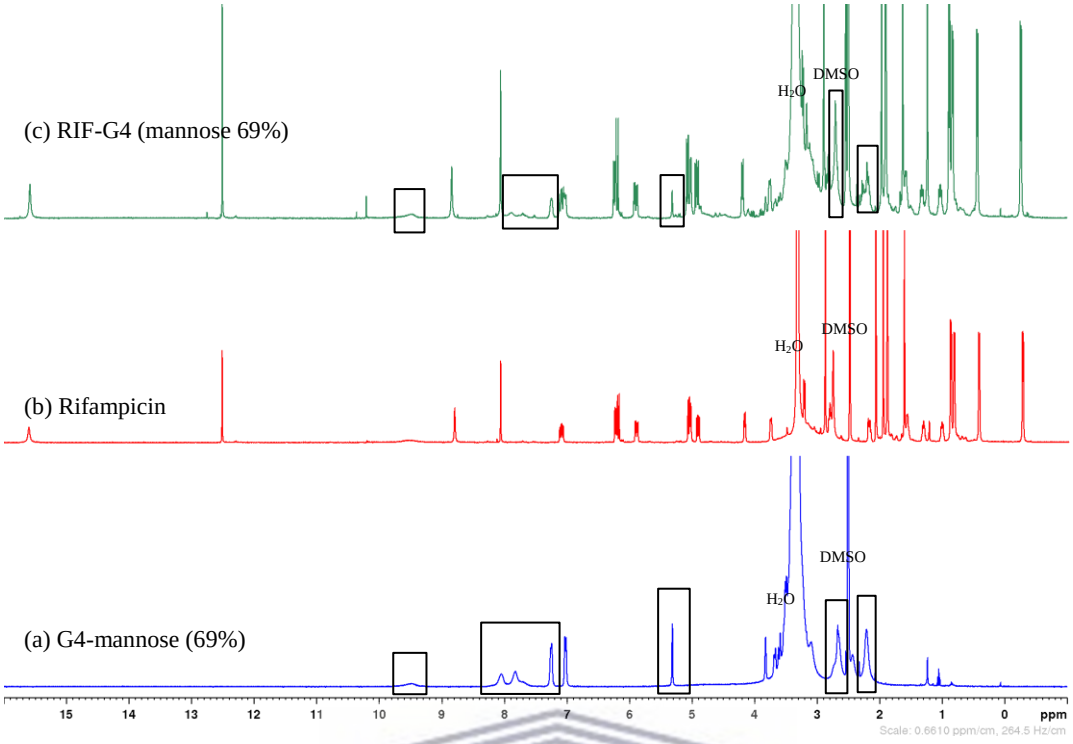

Figure 4.17 ^{1}H NMR spectra of (a) mannosylated G4 PAMAM dendrimer (69%), (b) rifampicin, and (c) rifampicin loaded mannosylated G4 PAMAM dendrimer (69%), in DMSO-d_6 solvent.

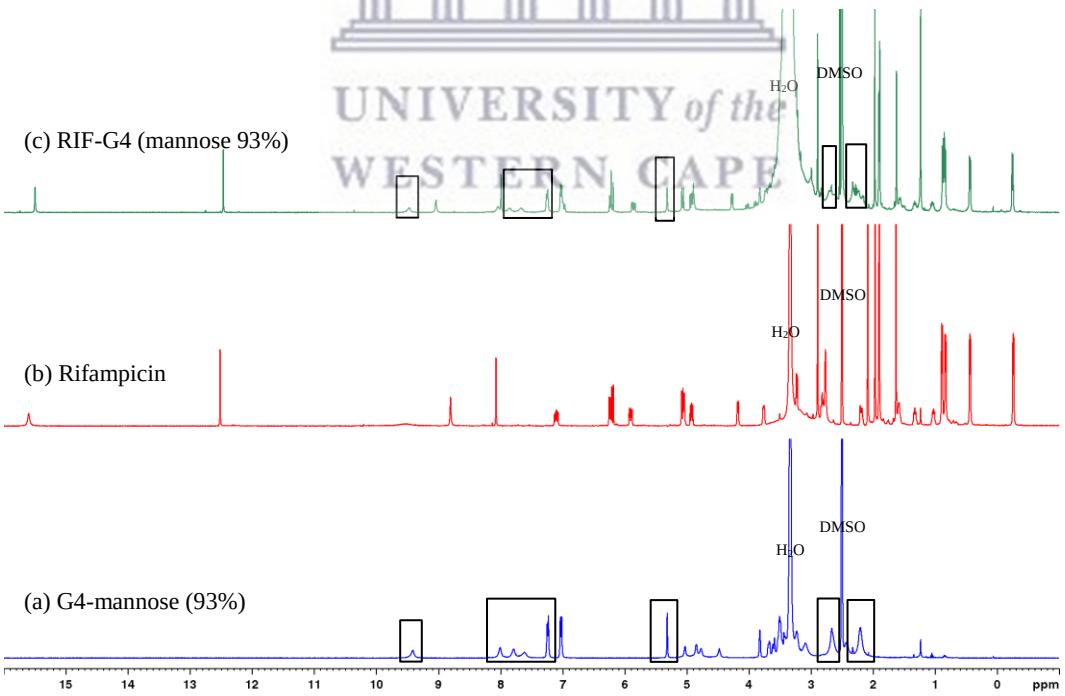

Figure 4.18 ^{1}H NMR spectra of (a) mannosylated G4 PAMAM dendrimer (93%), (b) rifampicin, and (c) rifampicin loaded mannosylated G4 PAMAM dendrimer (93%), in DMSO-d_6 solvent.

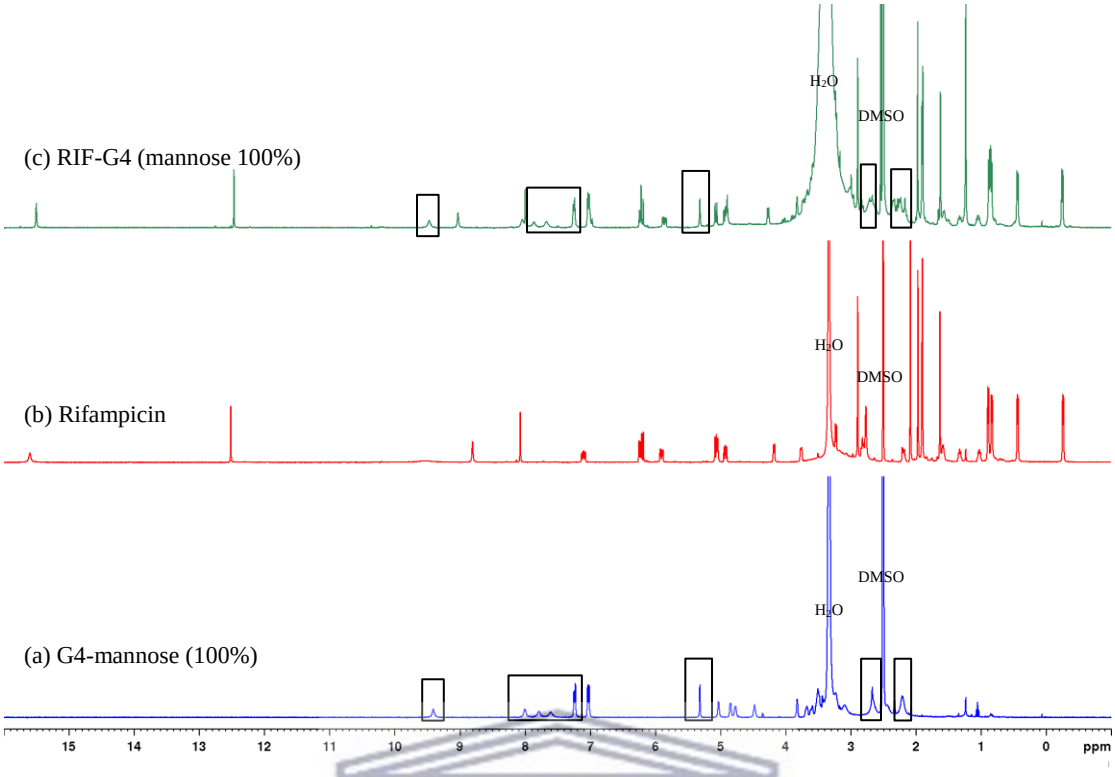

Figure 4.19 ^{1}H NMR spectra of (a) mannosylated G4 PAMAM dendrimer (100%), (b) rifampicin, and (c) rifampicin loaded mannosylated G4 PAMAM dendrimer (100%), in DMSO-d_6 solvent.

The 2D NOESY NMR was applied to confirm the supramolecular conjugation of rifampicin molecules into the mannosylated dendrimer, besides identifying the preferred site(s) of interaction. The cross-peaks in NOESY spectra signifying adjacent proton atoms interacting at a distance of < 5 Å (Diaz *et al.*, 2018). The 2D NOESY NMR of rifampicin loaded mannosylated dendrimer (44%) was studied as illustrated in Figure 4.20. The observed cross-peaks in Figure 4.20 suggesting that interactions between rifampicin molecules and the mannosylated dendrimer were taking place at the outer mannose part as well as in the interior shell of the dendrimer. In Figure 4.20, rifampicin atom numbers 10 (δ_H = 5.88 ppm), 11(δ_H = 8.06 ppm), 14 (δ_H = 7.09 ppm), 27 (δ_H = 3.74 ppm), 40 (δ_H = 1.90 ppm), and 42 (δ_H = 0.87 ppm) interacted with the dendrimer methylene protons adjacent to the carbonyl groups (atom A, δ_H = 2.19 ppm). Furthermore, rifampicin atom numbers 11 (δ_H = 8.06 ppm) and 14 (δ_H = 7.09 ppm) were observed interacting with amide amine protons of the dendrimer monomers (atom O) (δ_H = 7.71 ppm). In addition, rifampicin protons of atom 14 (δ_H = 7.09 ppm) were interacted with the mannose residue at two sites, with atom G (δ_H = 3.81 ppm) and atom Q (δ_H = 9.47 ppm) (cross-peak between atom 14 and atom Q is not included in Figure

4.20). These outcomes suggesting that rifampicin molecules were dual conjugated to the dendrimer scaffold, in the interior dendrimer shell and at the peripheral mannose residues.

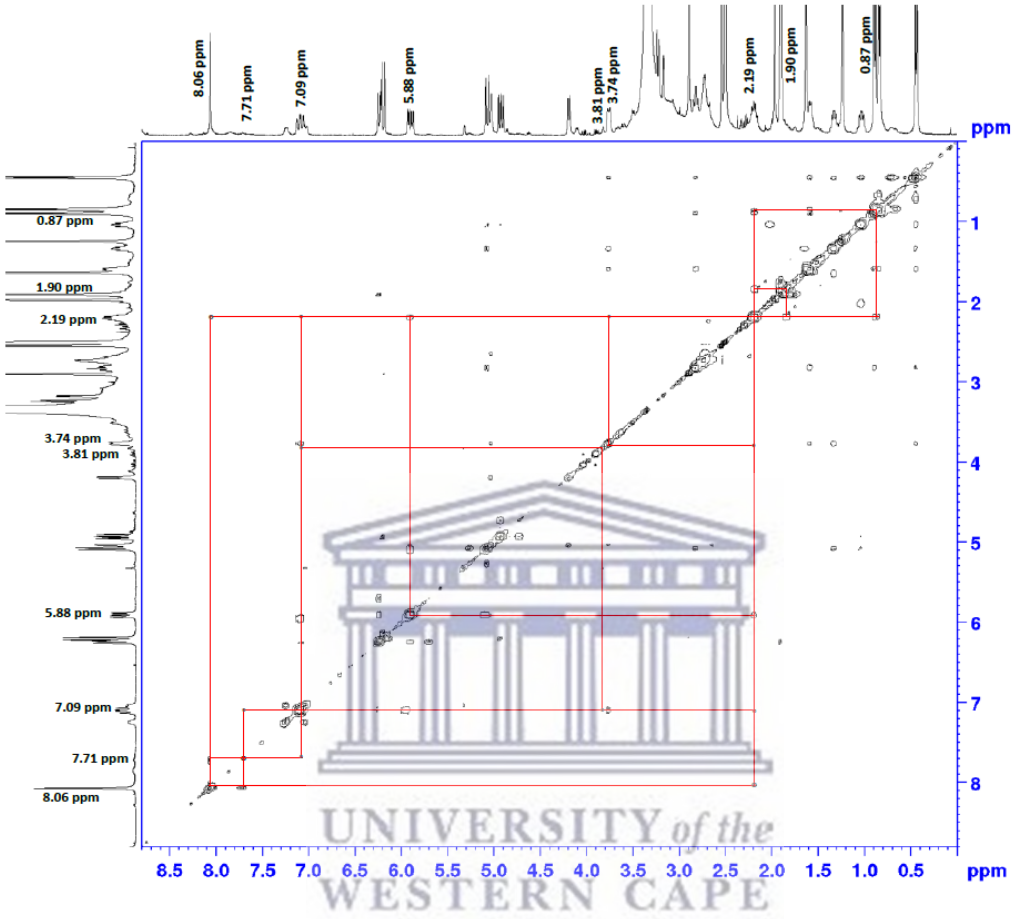

Figure 4.20 2D NOESY NMR spectra of rifampicin loaded mannosylated G4 PAMAM dendrimer (44%), in DMSO-d_6 solvent.

The 2D NOESY NMR data of the other rifampicin-loaded mannosylated dendrimers (69%, 93%, and 100%) were further corroborated for the interaction of rifampicin molecules with both internal dendrimer shell and peripheral mannose part.

Rifampicin is a hydrophobic molecule (Williams and Piddock, 1998). Based on previous reports, rifampicin molecules are expected to be encapsulated into the hydrophobic interior of the PAMAM dendrimer more than the peripheral amines (Bellini *et al.*, 2015; Dineshkumar *et al.*, 2017), *via* hydrophobic interaction (Kojima *et al.*, 2000) or H-bonding (Newkome *et al.*, 1996) or physical entrapment (Newkome *et al.*, 1991; Jansen, De Brabander-van den Berg and Meijer, 1994). Our results are

aligned with the previous reports since 2D NOESY NMR findings proved that rifampicin molecules interacted with the dendrimer interior at two sites (Figure 4.15b atoms A & O). Moreover, the 4-isothiocyanatophenyl alpha-D- mannopyranoside (4-ICPMP) compound has an XLogP3 of 1 (PubChem, 2019) which suggests that the molecule is hydrophobic. The hydrophobic properties of the mannose residues could provide an additional platform for rifampicin molecules to interact with. This was clearly observed in the ^{1}H NMR and 2D NOESY NMR results that confirmed the interaction of rifampicin molecules with the mannose residues of the outer mannosylated dendrimer.

4.7.3.3 Morphology of the nanoparticles

The shape of dendrimer formulations was studied under SEM. Figure 4.21 shows the SEM images of mannosylated dendrimer formulations, which indicate the spherical or semi-spherical shape of the nanoparticles. It was observed that the surface smoothness of the nanoparticles was slightly decreased by increasing the density of mannose residues, which could be due to their peripheral presence as a result of conjugation to surface amines of the dendrimer.

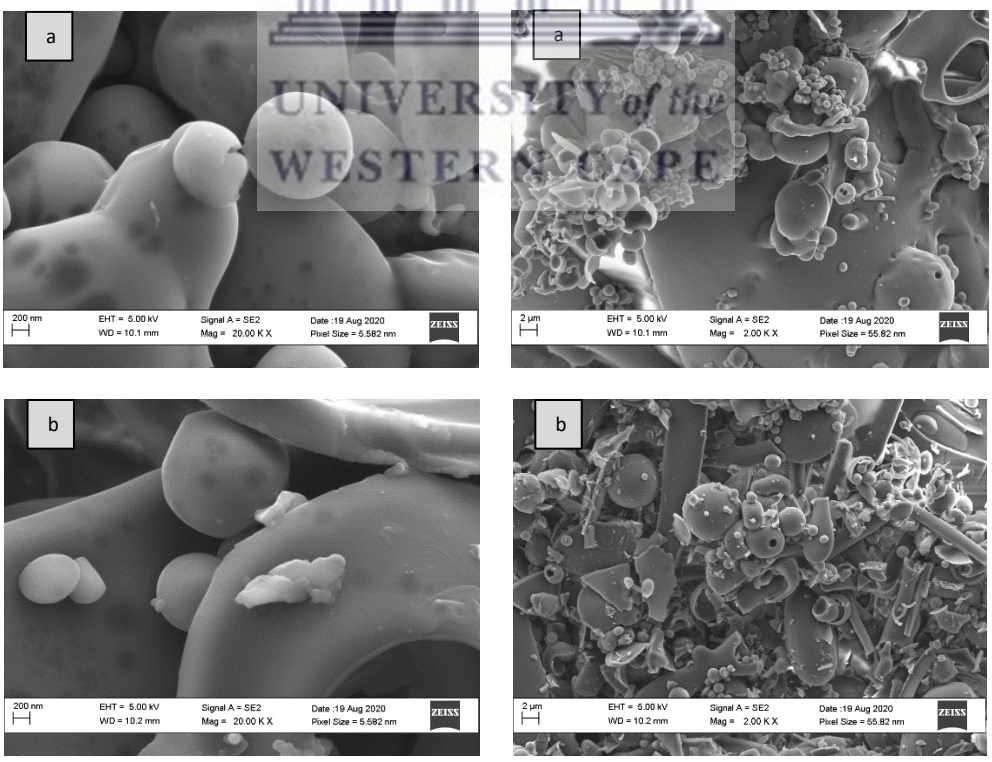

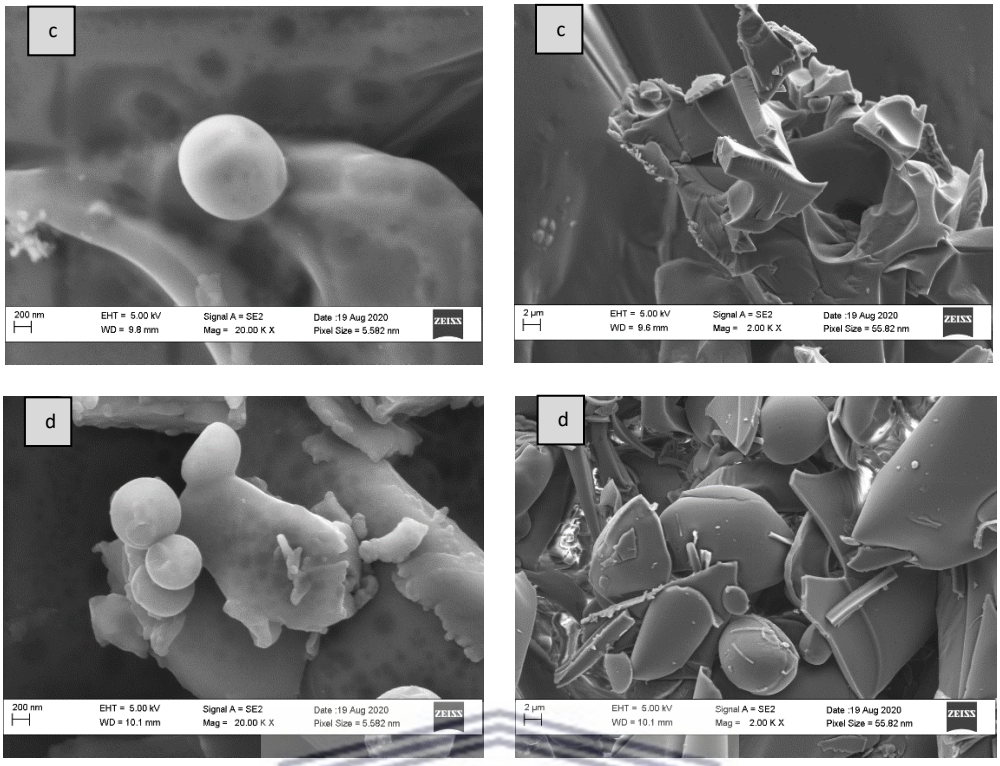

Figure 4.21 SEM images of (a) G4-mannose 1:30 (44%), (b) G4-mannose 1:45 (69%), (c) G4-mannose 1:60 (93%), and (d) G4-mannose 1:100 (100%).

Following rifampicin loading (Figure 4.22), the shape of nanoconjugates is also seen under SEM as spherical or semi-spherical. Surface smoothness was considerably decreased by increasing the degree of surface mannosylation. Conjugation of mannose residues to the peripheral amines besides the attachment of rifampicin molecules on the surface of the dendrimer could account for the decrease in the smoothness of the nanoparticle's surface.

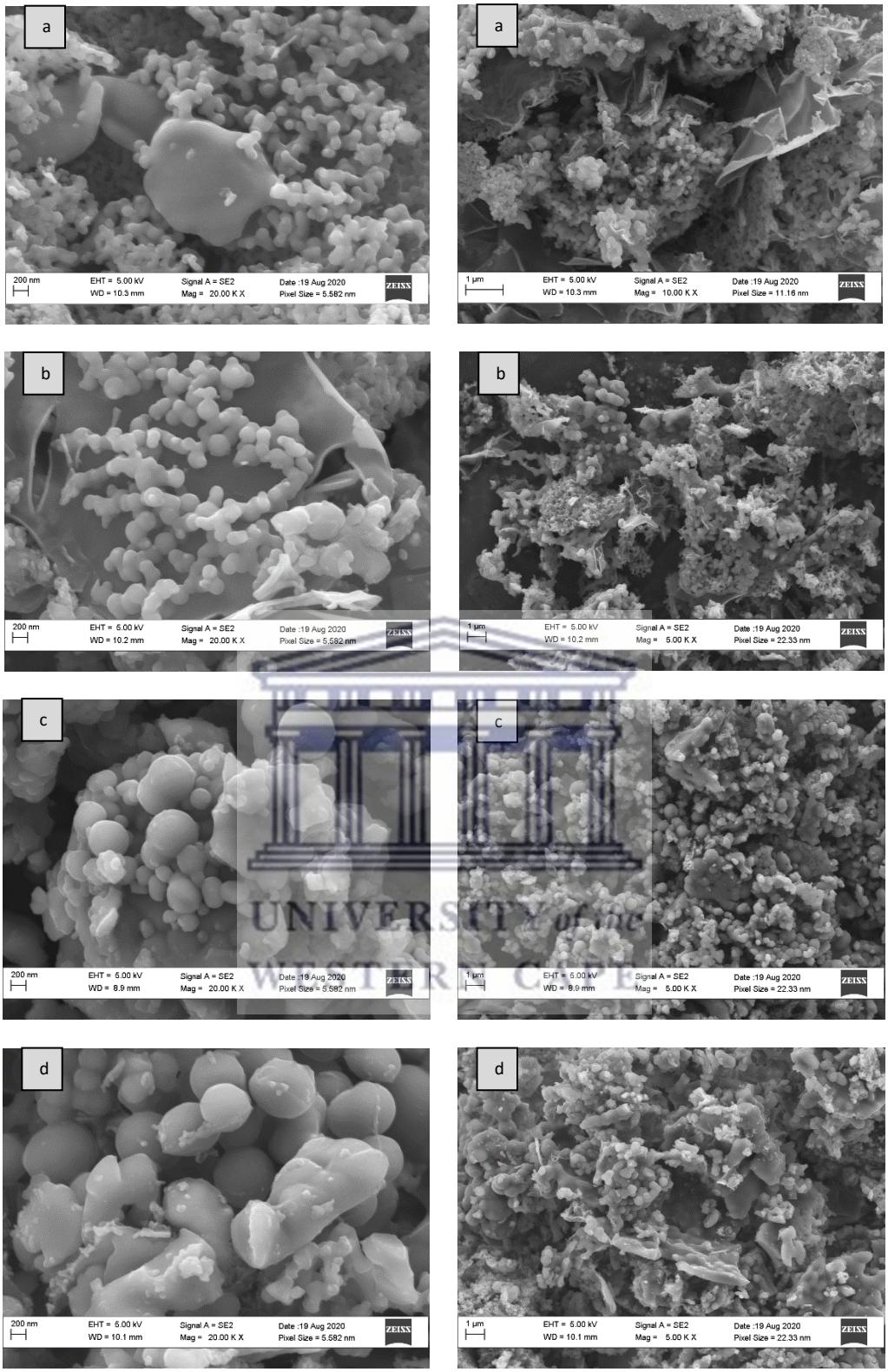

Figure 4.22 SEM images of (a) RIF loaded G4-mannose 1:30 (44%), (b) RIF loaded G4-mannose 1:45 (69%), (c) RIF loaded G4-mannose 1:60 (93%), and (d) RIF loaded G4-mannose 1:100 (100%).

4.7.3.4 Differential scanning calorimetry (DSC) studies

DSC analysis was performed to study the thermal behavior and changes in the crystallinity of the dendrimer nanoparticles over a range of temperatures (i.e., 30˚C to 220˚C). DSC thermograms of loaded and unloaded mannosylated dendrimer (44%) were compared to pure rifampicin and their corresponding physical mixture (Figure 4.23). Pure rifampicin (Figure 4.23 a) showed a broad endothermic peak just below 200˚C (i.e., 195.83˚C), which was previously reported as its melting point (Pelizza *et al.*, 1977). The unloaded mannosylated dendrimer (44%) was characterized by two endothermic peaks at 56.56˚C and 97.45˚C (Figure 4.23 c).

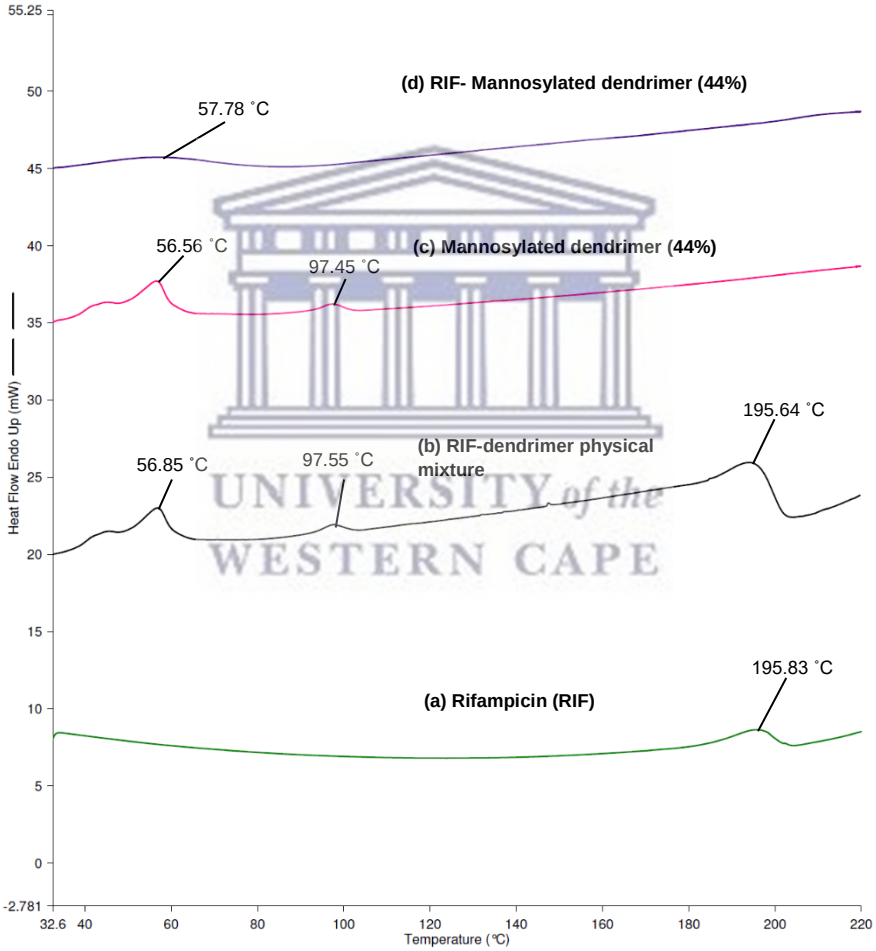

Figure 4.23 DSC thermograms of (a) rifampicin, (b) rifampicin-dendrimer (44% mannose) physical mixture, (c) unloaded mannosylated dendrimer (44%), and (d) rifampicin loaded mannosylated dendrimer (44%).

The characteristic peaks of rifampicin and the unloaded mannosylated dendrimer almost disappeared in the DSC thermogram of rifampicin loaded mannosylated

dendrimer (Figure 4.23 d). However, rifampicin loaded mannosylated dendrimer (44%) experienced a new broad endothermic peak which started at 38.46˚C and ended at 76.51˚C with a peak at 57.78˚C, besides a very broad peak between 100˚C - 200˚C (very small endothermic peak). The rifampicin-dendrimer physical mixture curve maintained rifampicin peak as well as peaks corresponding to mannosylated dendrimer (Figure 4.23 b). Overall, the results suggest that the rifampicin loaded mannosylated dendrimer (44%) was not a physical mixture.

Table 4.5 Comparison of the dendrimer's endothermic peaks before and after drug conjugation.

Type of the dendrimer	Endothermic peak (°C)	
	Unloaded dendrimer	**RIF-loaded dendrimer**
Dendrimer (44% mannose)	56.56 & 97.45	57.78
Dendrimer (69% mannose)	64.45 & 198.73	67.67 & 180.84
Dendrimer (93% mannose)	61.16 & 203.10	64.53 & 179.75
Dendrimer (100% mannose)	62.72 & 198.72	70.79 & 175.24

Table 4.5 and Figure 4.24 illustrate the DSC data of other mannosylated dendrimer formulations (69%, 93%, and 100%). It was observed that after drug conjugation each formulation experienced new endothermic peaks compared to their corresponding unloaded nanoparticles (Table 4.5 and Figure 4.24). Furthermore, the rifampicin peak at 195.83˚C disappeared in all rifampicin loaded mannosylated formulations. Comparing the loaded dendrimers (69%, 93%, and 100%) with their corresponding physical mixtures corroborates the existence of both rifampicin peak and mannosylated dendrimer peaks. Therefore, the DSC data of rifampicin nanoconjugates confirmed the successful conjugation of rifampicin molecules into the dendrimer scaffold and they are not physical mixtures. Comparable findings were previously reported by Kumar and co-workers using G5 PPI dendrimer (Kumar *et al.*, 2006).

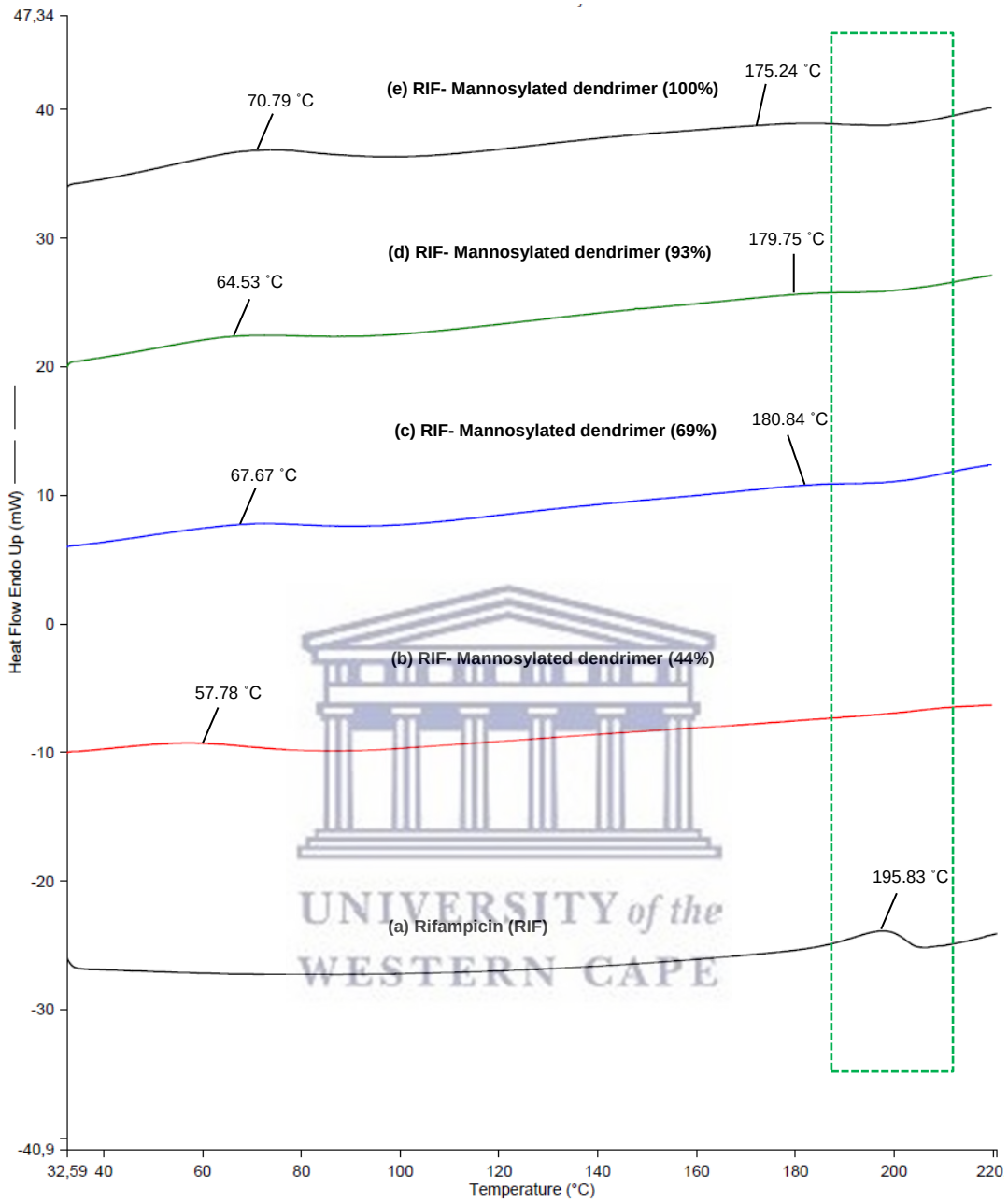

Figure 4.24 DSC thermograms of (a) rifampicin, (b) rifampicin loaded mannosylated dendrimer (44%), (c) rifampicin loaded mannosylated dendrimer (69%), (d) rifampicin loaded mannosylated dendrimer (93%), and (e) rifampicin loaded mannosylated dendrimer (100%).

4.7.3.5 DLS studies

The DLS technique was used to determine the hydrodynamic diameter (D_H), PDI, and the zeta potential of dendrimer nanoparticles (Table 4.6). The analysis was done on a Malvern Zetasizer Nano ZS90 using dynamic light scattering (DLS) theory.

a) Nanoparticle size and polydispersity index (PDI)

The hydrodynamic size of the unloaded dendrimer formulations ranged from 4.21 nm ± 0.50 nm for the native dendrimer (0% mannose) to 10.92 nm ± 1.35 nm for 44% mannosylated dendrimer. While for rifampicin loaded dendrimer formulations, the hydrodynamic size ranged from 5.14 nm ± 0.57 nm for drug-loaded dendrimer (0% mannose) to 82.87 nm ± 14.16 nm for drug-loaded 69% mannosylated dendrimer (Table 4.6).

Among the unloaded mannosylated dendrimers, there was no statistically significant difference in the D_H detected by a one-way ANOVA test (Tukey post hoc test) ($p > 0.05$). Comparing the D_H of the unloaded native dendrimer (0% mannose) to that of mannosylated dendrimers indicated a significant difference between the 44% and 100% formulations and the native dendrimer ($p < 0.05$) (Figure 4.25).

The coefficient of determination (R^2) obtained from a one-way ANOVA analysis showed a weak relationship between the degree of dendrimer mannosylation and the D_H of the nanoparticles ($R^2 = 0.5938$). After drug loading, one-way ANOVA analysis (Tukey post hoc test) signified that all rifampicin-loaded mannosylated dendrimers (44% to 100% mannose resides) had D_Hs that are significantly greater than rifampicin loaded dendrimer (0% mannose) ($p < 0.05$). No statistically significant difference in the D_Hs had been noticed between drug-loaded mannosylated dendrimer formulations ($p > 0.05$).

Studying each formulation before and after drug conjugation revealed that rifampicin molecules have significantly increased the D_H of the nanoparticles ($p < 0.05$), the only exception of the dendrimer formulations was with 0% mannose (Figure 4.25).

Table 4.6 The physicochemical characteristics of the unloaded and rifampicin-loaded dendrimers having different mannose residues. Results illustrated as mean ± SD (n = 3).

Dendrimer -mannose content	Hydrodynamic diameter (nm)		PDI		Zeta potential (mV)	
	unloaded	Loaded	unloaded	unloaded	unloaded	Loaded
0% mannose	4.21 ± 0.50	5.14 ± 0.57	0.29 ± 0.02	0.31 ± 0.07	36.54 ± 2.96	31.71 ± 0.88
44% mannose	10.92 ± 1.35	79.56 ± 13.28	0.35 ± 0.03	0.30 ± 0.08	23.88 ± 1.56	19.55 ± 2.67
69% mannose	8.54 ± 2.20	82.87 ± 14.16	0.22 ± 0.09	0.19 ± 0.02	21.13 ± 1.65	12.85 ± 0.90
93% mannose	8.16 ± 2.19	77.48 ± 10.34	0.20 ± 0.05	0.35 ± 0.02	18.45 ± 0.85	14.83 ± 2.56
100% mannose	10.34 ± 3.68	69.16 ± 13.83	0.14 ± 0.04	0.31 ± 0.07	19.93 ± 2.09	20.23 ± 1.50

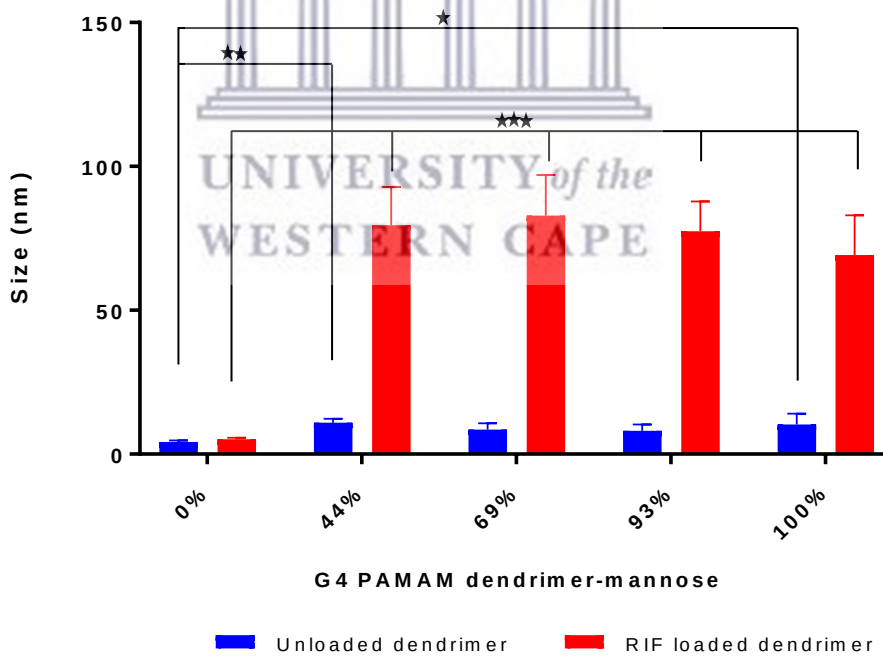

(* = p ≤ 0.05; ** = p ≤ 0.01; *** = p ≤ 0.001)

Figure 4.25 The hydrodynamic (D_H) diameters of unloaded (blue) and rifampicin-loaded (red) dendrimer nanoparticle formulations with different mannose residues. Results showed a mean ± SD (n = 3). Error bars represent the calculated SD from the mean.

As confirmed earlier in this chapter, mannose residues are attached to the dendrimer periphery *via* thiourea linkages. Since G4 PAMAM dendrimer is characterized by a dense-core conformational structure at a neutral pH (Lee and Larson, 2011), conjugation of mannose molecules to the dendrimer amines could stretch the dendrimer monomers and convert the structure into dense-shell conformations. Molecular dynamic studies on G4 PAMAM dendrimer confirmed that the stretching effect and conformational changes of the dendrimer structure depend on the chain length and the density of the conjugated molecules (Lee and Larson, 2011). Mannose compound (4-ICPMP) that was used to graft the dendrimer surface is a short molecule with a molecular weight of 313.33 (Burke *et al.*, 2000; Woller and Cloninger, 2001). The short-length molecule is probably exerting a low stretching effect to the dendrimer scaffold and therefore no significant changes in the D_H of the nanoparticles will be expected especially those with a lower mannose concentration, as previously noticed with short-chain mPEG 550 (Lee and Larson, 2011). This explanation is further corroborated by the coefficient of determination value (R^2 = 0.5938), which illustrates a weak relationship between the density of the mannose residues and the change in the D_H of the dendrimer nanoparticles. The only exception to that trend was 44% and 100% mannosylated formulations. A considerable increase in the D_H of 100% mannosylated formulation is anticipated due to the highest concentration of mannose residues.

A significant increase in the D_H of all dendrimer nanoparticles is seen after rifampicin conjugation, the only exception is 0% mannose formulation. As mentioned in Chapter 3, rifampicin has an isoelectric point of about 7.11 (Khan *et al.*, 2017) and pKa of 1.7 and 7.9 (Kumar *et al.*, 2006). During the loading process, rifampicin molecules were deprotonated and therefore they had carried negative charges. This encouraged the formation of electrostatic linkages with the free positively charged surface amines. Accordingly, rifampicin molecules are expected to conjugate into a dendrimer structure either *via* electrostatic interactions or hydrophobic interactions (in the interior and within mannose residues). As observed here, many reports have noticed a significant increase in the size of the mannosylated PPI dendrimer after being conjugated with genetic materials (siRNA and DNA) at the periphery through electrostatic linkages (Kim *et al.*, 2012; Hu *et al.*, 2014).

The polydispersity index values of unloaded dendrimer formulations ranged from 0.14 ± 0.04 to 0.35 ± 0.03, while rifampicin loaded dendrimer formulations ranged from

0.19 ± 0.02 to 0.35 ± 0.02 (Table 4.6). Among the unloaded dendrimers, it was observed that the 44% mannosylated dendrimer showed a greater PDI value compared to 69%, 93%, and 100 mannosylated dendrimers ($p < 0.05$). Also, the 100% mannosylated dendrimer exhibited a lower PDI value comparative to the unmodified dendrimer (0% mannose) ($p < 0.05$) (Figure 4.26). The coefficient of determination value was about 0.7551 which suggested an intermediate relationship between the degree of the dendrimer mannosylation and the change in the PDI value. From the PDI results of the unloaded dendrimer formulations, a negative relationship between the density of mannose residues and the PDI value of nanoparticles was observed (Figure 4.26).

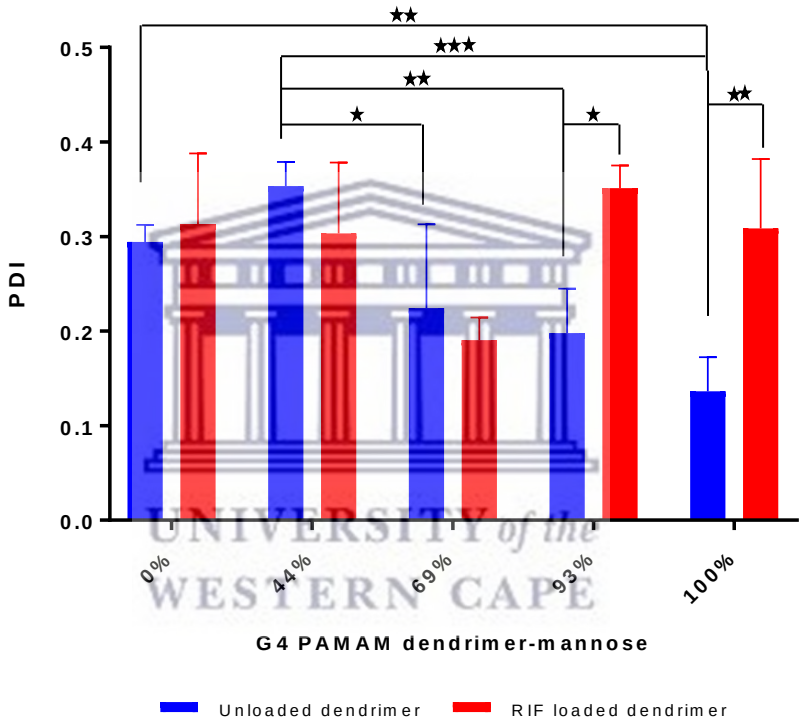

(* = p ≤ 0.05; ** = p ≤ 0.01; *** = p ≤ 0.001)

Figure 4.26 Polydispersity index (PDI) of unloaded (blue) and rifampicin-loaded (red) dendrimer nanoparticle formulations with different mannose residues. Results showed as mean ± SD (n=3). Error bars represent the calculated SD from the mean.

No significant difference in the PDI of the nanoparticles was noticed among loaded dendrimer formulations ($p > 0.05$), the only exception was observed between 69% and 93% mannosylated formulations ($p < 0.05$). Statistical analysis of the PDI values of the loaded and unloaded dendrimer formulations indicated a significant increase in the PDI of 93% and 100% formulations following rifampicin conjugation ($p < 0.05$).

The loaded and unloaded dendrimer formulations are characterized by PDI values < 0.4. These values indicate a moderate homogenized distribution of the nanoparticles. As mentioned in Chapter 3, PDI values of 0.1 - 0.4 are regarded as a moderately distributed sample, while PDI value ≥ 0.5 indicates a broad polydisperse sample (Sabeti *et al.*, 2014; Bhattacharjee, 2016). Therefore, the developed unloaded and drug-loaded dendrimer nanoparticles are considered as moderately distributed samples.

b) Nanoparticle zeta potential

The zeta potential of dendrimer formulations was studied to evaluate the stability of nanoparticles. For the unloaded dendrimers, values ranged from 36.54 ± 2.96 (Mv) to 18.45 ± 0.85 (Mv) (Table 4.6). Analysis of zeta potential data of the unloaded dendrimer formulations showed a negative relationship between the concentration of mannose residues and the zeta potential values of dendrimers. A one-way ANOVA method

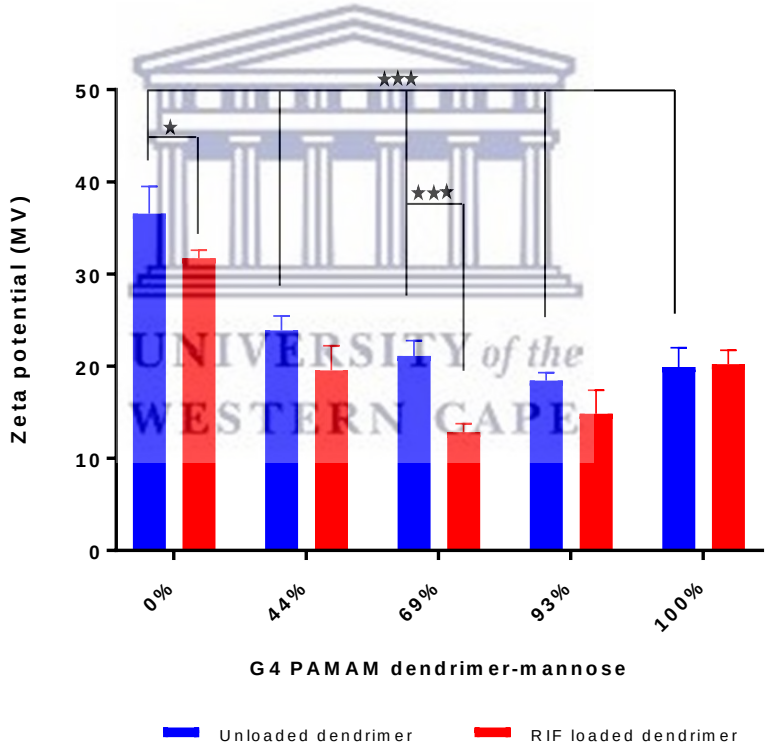

(* = p ≤ 0.05; ** = p ≤ 0.01; *** = p ≤ 0.001)

Figure 4.27 Zeta potential values of unloaded (blue) and rifampicin-loaded (red) dendrimer nanoparticle formulations with different mannose residues. Results showed as mean ± SD (n=3). Error bars represent the calculated SD from the mean.

indicated a significant decrease in the zeta potential values of mannosylated dendrimers compared to the unmodified dendrimer (0% mannose) ($p < 0.05$) (Figure 4.27). Among

mannosylated dendrimers, no significant variance has been noticed between nanoparticles ($p > 0.05$), except for 44% formulation that displayed a greater zeta potential value relative to 93% formulation ($p < 0.05$). The coefficient of determination (R^2) obtained by a one-way ANOVA was about 0.9373, which suggests a somewhat strong association between the change in the zeta potential of nanoparticles and the density of mannose residues.

After drug loading, the zeta potential values of dendrimer nanoparticles are further decreased and ranged from 31.71 ± 0.88 to 12.85 ± 0.90. All rifampicin mannosylated dendrimer nanoparticles exhibited zeta potential values that were lower than that of rifampicin loaded unmodified dendrimer nanoparticles (0% mannose) ($p < 0.05$) (Figure 4.27). Among rifampicin mannosylated dendrimers, 44% and 100% formulations showed greater zeta potential values comparative to 69% and 93% loaded dendrimers ($p < 0.05$). The R^2 of rifampicin-loaded dendrimers was about 0.9427 which confirms a strong link between the change in the zeta potential of nanoparticles and the degree of surface mannosylation beside rifampicin conjugation.

Assessing each formulation before and after drug loading indicates a change in the zeta potential of the nanoparticles after rifampicin conjugation. Particularly, unmodified (0% mannose) and 69% mannosylated dendrimers displayed significant decrease in their zeta potential values after drug loading ($p < 0.05$) (Figure 4.27).

When the zeta potential of dendrimer nanoparticles are positive values, this suggests a function of the dendrimer surface amines (Wang and Imae, 2004; Gupta, Agashe and Jain, 2007). Since mannose residues are conjugated to these surface amines *via* thiourea linkages, a shift in the zeta potential of the mannosylated dendrimer nanoparticles is expected due to the shield of the positive charges. The change in the zeta potential values of the nanoparticles is directly correlated to the density of the mannose residues, a lower decrease in zeta potential will probably occur with a dendrimer being grafted with a small concentration of mannose residues. The zeta potential data of the unloaded mannosylated dendrimers are aligned with what we are expecting, a negative relationship was observed between the density of mannose on the dendrimer and the zeta potential values of nanoparticles.

For drug-loaded dendrimers, a further decrease in the zeta potential of the nanoparticles was noticed. It is expected that the electrostatic interactions between the unmodified

positively charged amines and the deprotonated rifampicin molecules could account for the additional decrease in the zeta potential of the nanoparticles. In Figure 4.27, the significant shift of the zeta potential to lower values after drug conjugation was noticed with the unmodified dendrimer (0% mannose) and dendrimer with low mannose concentration (69%) ($p < 0.05$). Whereas, for formulations that have the highest mannose concentration, no significant change in the zeta potential values after drug conjugation ($p > 0.05$) was identified. It can be speculated that for a lower mannose concentration the number of unmodified surface amines is high which could offer an additional platform for the deprotonated rifampicin molecules to interact with them *via* electrostatic bonds and hence provide extra shielding of positive charges. On the other hand, dendrimers with the highest mannose concentration on their surface amines have been modified by 93% and 100%, so most of the positive charges were shielded and became unavailable to interact with rifampicin molecules. Many previous reports have mentioned that electrostatic interaction at the surface of cationic dendrimers significantly decreased their zeta potential values (Kim *et al.*, 2012; Hu *et al.*, 2014).

4.7.4 Development and validation RP-HPLC method

As mentioned earlier in the method section of this chapter that the validated HPLC method for quantifying rifampicin in Chapter 3 was also employed in this chapter to determine the EE% and DL% of the nanoparticles. The HPLC method was also assessed for the specificity parameter for the unloaded mannosylated dendrimer to ensure no overlapping with the rifampicin peak.

As illustrated in Figure 4.28, the mannosylated dendrimer did not exhibit any interference with the rifampicin absorption peak (~ 2.9 mins), which suggests the suitability of the method to quantify rifampicin in the dendrimer formulations.

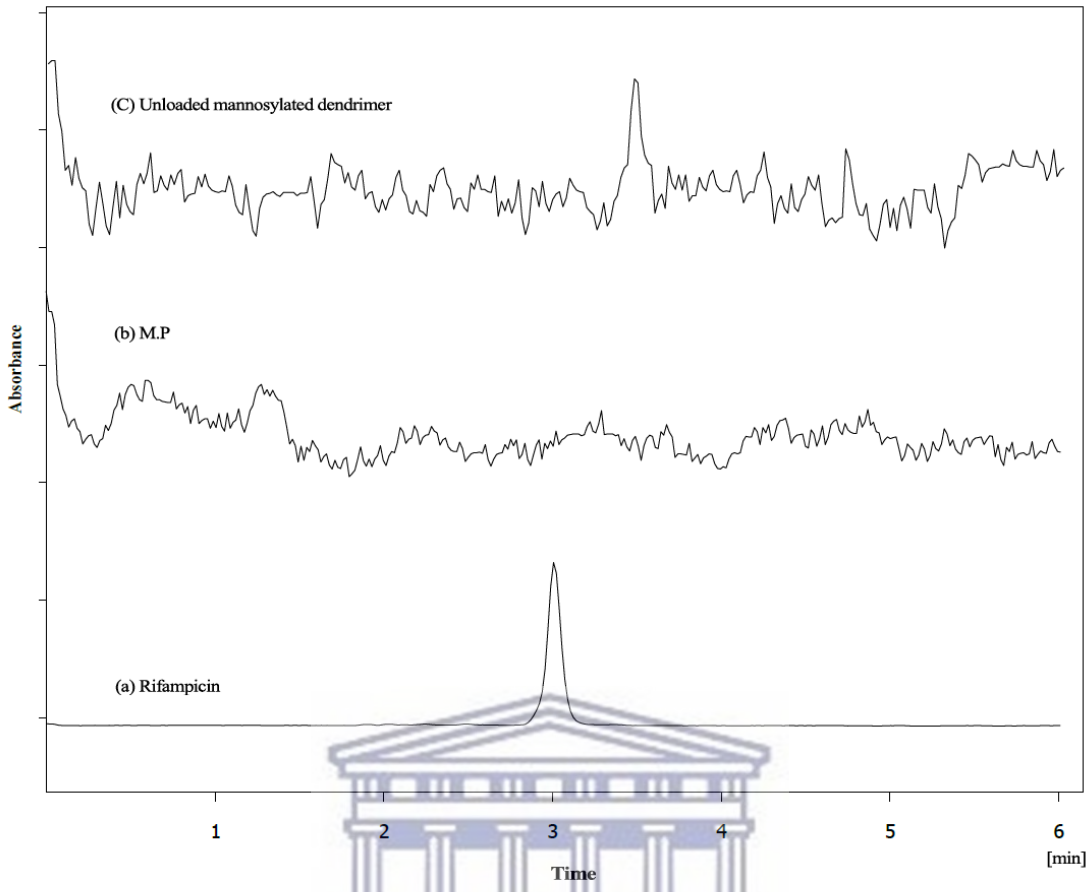

Figure 4.28 HPLC chromatograms of (a) rifampicin standard, (b) the mobile phase, and (c) unloaded mannosylated dendrimer.

4.7.5 Encapsulation efficiency (EE%) and drug loading (DL%)

The rifampicin standard calibration curve was generated by analyzing a range of rifampicin standards 5.0 – 100.0 µg/ml at an absorbance wavelength of 475 nm. Linear regression analysis was applied to assess the correlation between rifampicin absorbance and concentration. A plot of average rifampicin absorbance versus its concentration was generated as illustrated in Figure 4.29. This relationship model creates a basis for the prediction of rifampicin concentration by measuring sample absorbance.

The linear regression equation was, y = 12.875x – 2.8713, with correlation coefficient r^2 = 0.9999. The generated linear equation displays a strong relationship between rifampicin concentration and its absorbance. Where x is rifampicin concentration in µg/ml and y is the absorbance peak area in mAU.

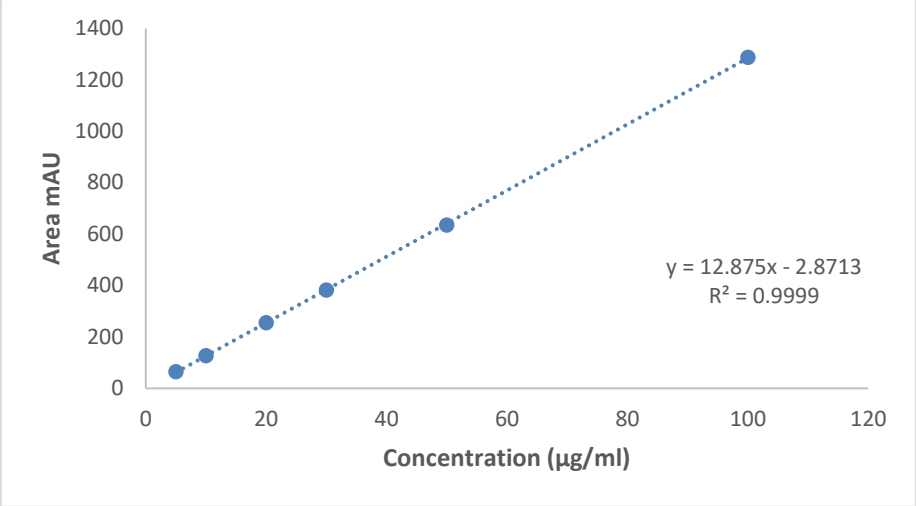

Figure 4.29 Rifampicin standard calibration curve in the mobile phase at a wavelength of 475 nm.

The encapsulation efficiency percentage (EE%) and the percentage drug loading (DL%) were determined directly using a validated HPLC method. EE% and DL% were calculated using equation 3.3 and equation 3.4, which were previously discussed in Chapter 3.

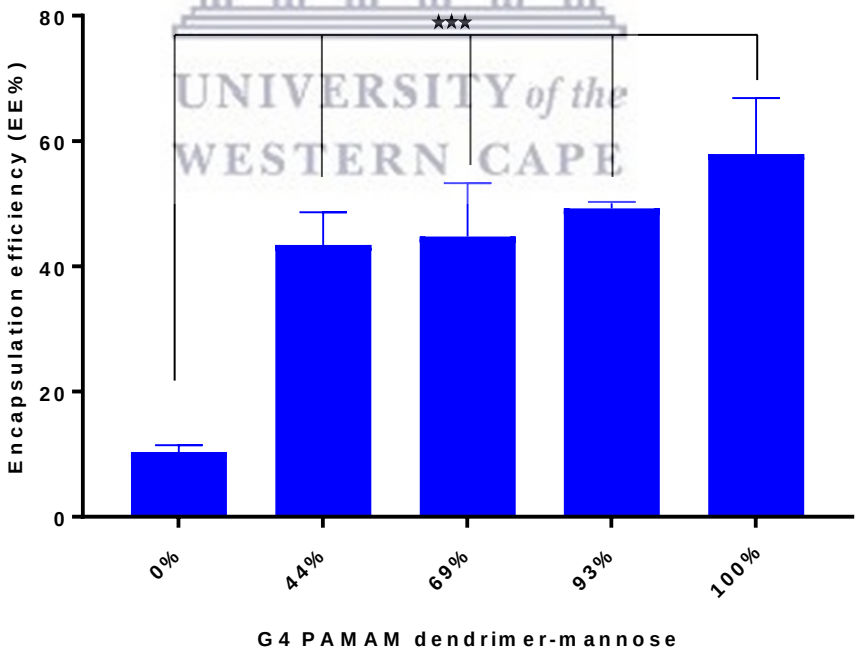

(* = $p \leq 0.05$; ** = $p \leq 0.01$; *** = $p \leq 0.001$)

Figure 4.30 Nanoparticle encapsulation efficiency (EE%) of different dendrimer-mannose formulations.

The EE% of the dendrimer nanoparticles ranged from 10.34 ± 1.11 % (w/w) for the unmodified dendrimer to 57.91 ± 5.18 % (w/w) for 100% mannosylated dendrimer (Table 4.7). Data analysis using one-way ANOVA (Tukey post hoc test) revealed that EE% of the dendrimer nanoparticles significantly increased after dendrimer mannosylation ($p < 0.05$) (Figure 4.30). This finding suggested that mannose residues have offered an additional platform of interaction with rifampicin molecules. Earlier in this chapter, it was confirmed that rifampicin molecules interacted with the dendrimer scaffold in the interior as well as with mannose residues. EE% data are therefore aligned with NMR and physicochemical results since higher values are achieved by the dendrimer that has the highest mannose content.

Table 4.7 DL%, EE% of rifampicin in different dendrimer formulations, results displayed as mean ± SD (n = 3).

Mannose content	G4-mannose (mol)	Rifampicin (mol)	Yield (mg)	Yield %	Total RF in NP (mg)	DL% w/w	EE% w/w
0% mannose	0.1 µmol = 1.50 mg	10 µmol = 8.22 mg	2.20 ± 0.25	22.63%	0.85 ± 0.09	34.20 ± 0.95	10.34 ± 1.11
44% mannose	0.1 µmol = 2.30 mg	10 µmol = 8.22 mg	5.90 ± 0.72	56.08%	3.57 ± 0.30	60.51 ± 1.84	43.43 ± 3.00
69% mannose	0.1 µmol = 2.80 mg	10 µmol = 8.22 mg	6.43 ± 1.01	58.35%	3.68 ± 0.50	57.11 ± 3.21	44.77 ± 4.92
93% mannose	0.1 µmol = 3.30 mg	10 µmol = 8.22 mg	6.50 ± 0.40	56.42%	4.05 ± 0.05	62.34 ± 1.93	49.27 ± 0.58
100% mannose	0.1 µmol = 3.40 mg	10 µmol = 8.22 mg	6.77 ± 0.99	58.26%	4.76 ± 0.52	70.57 ± 5.80	57.91 ± 5.18

Figure 4.30 and Table 4.7 data showed a direct relationship between the increases in EE% values and the density of mannose residues. Lower EE% values are linked to dendrimers having low mannose concentration, while the highest values are obtained by dendrimers that have been modified by the most mannose residues. Statistical analysis did not show any significant difference in the EE% values among the mannosylated dendrimers ($p > 0.05$)

For the percentage drug loading (DL%) of the nanoparticles, values ranged from 34.20 ± 0.95 % (w/w) for unmodified dendrimer (0% mannose) to 70.57 ± 5.80 % (w/w) for 100% mannosylated dendrimer (Table 4.7). Figure 4.31 showed a significant increase in the DL% value of the dendrimer nanoparticles observed after dendrimer mannosylation ($p < 0.05$). In the case of EE%, a positive relationship exists between the DL% value and the degree of dendrimer mannosylation (Table 4.7, Figure 4.31). The uppermost values were recorded by dendrimers that have been functionalized with the highest mannose residues. A one-way ANOVA analysis revealed no significant difference in the DL% values among mannosylated dendrimers ($p > 0.05$), the only exception was noticed between 69% and 100% mannosylated dendrimers ($p < 0.05$) (Figure 4.31).

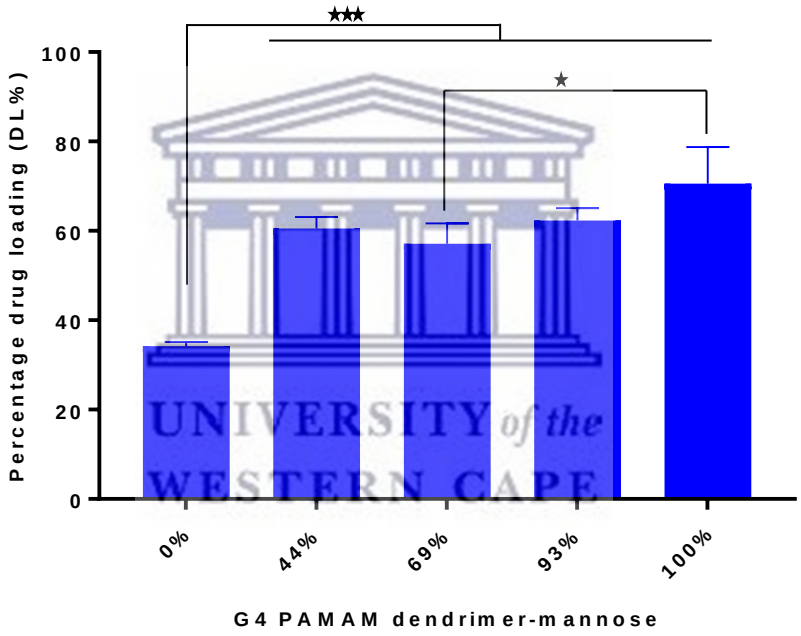

(* = p ≤ 0.05; ** = p ≤ 0.01; *** = p ≤ 0.001)

Figure 4.31 Nanoparticle percentage drug loading (DL%) of different dendrimer-mannose formulations.

The positive relationship that has been observed between the DL% values and the extent of mannosylation is further corroborated by the fact that mannose residues have conjugated rifampicin molecules *via* hydrophobic interactions. In addition, the DL% data could suggest that mannose residues on the dendrimer surface did not exhibit steric hindrance (dense shell) around the dendrimer, as previously noticed on PEG 2000, and so rifampicin incorporation into the nanoparticles was not significantly influenced.

The increase in the EE% and DL% of dendrimers after manipulating the surface with mannose residues was also previously reported in literature since peripheral mannosylation could increase the density of the functional groups for complexation (Kumar *et al.*, 2006; Dutta and Jain, 2007; Jain *et al.*, 2015).

4.8 Conclusion

As a conclusion, G4 PAMAM dendrimers having a concentration range from 44% to 100% mannose residues were successfully synthesized using 4-isothiocyanatophenyl alpha-D-mannopyranoside (4-ICPMP) compound. The conjugated product was confirmed using NMR and FTIR techniques, which suggested the formation of thiourea linkages between the surface amines of the dendrimer and the 4-ICPMP molecules. In addition, ^{1}H NMR was employed to calculate the number of attached mannose residues. Rifampicin molecules were encapsulated into dendrimer formulations in varying proportions. The EE% of nanoparticles was 10.34 ± 1.11 % (w/w) for the unmodified dendrimer, whilst for mannosylated dendrimers this ranged from 43.43 ± 3.00 % (w/w) to 57.91 ± 5.18% (w/w). The DL% of the unmodified dendrimer was 34.20 ± 0.95 % (w/w), while for mannosylated dendrimers the range was from 57.11 ± 3.21 % (w/w) to 70.57 ± 5.80 % (w/w). FTIR and NMR techniques indicated that rifampicin molecules were conjugated to the dendrimer scaffold at three places, at the surface amines *via* electrostatic bonds, within the mannose residues, and into the dendrimer core. The shape of the nanoparticles was observed as spherical under the SEM instrument. DSC analysis confirmed that rifampicin was loaded in dendrimer formulations and were not physical mixtures. The size of the unloaded nanoparticles was less than 15 nm and significant differences were noticed after rifampicin conjugation except for unmodified dendrimer formulation. PDI values were ≤ 0.35 which suggests a moderately distributed sample. The zeta potential of nanoparticles was positive with values greater than 12 mV, a significant decrease in the zeta potential values were noticed after dendrimer mannosylation as well as after rifampicin conjugation.

4.9 References

Anselmo, A.C., Gilbert, J.B., Kumar, S., Gupta, V., Cohen, R.E., Rubner, M.F. and Mitragotri, S., (2015). Monocyte-mediated delivery of polymeric backpacks to inflamed tissues: a generalized strategy to deliver drugs to treat inflammation. *Journal of Controlled Release*, *199*, pp.29-36.

Anselmo, A.C. and Mitragotri, S., (2014). Cell-mediated delivery of nanoparticles: taking advantage of circulatory cells to target nanoparticles. *Journal of controlled release*, *190*, pp.531-541.

Aoi, K., Tsutsumiuchi, K., Yamamoto, A. and Okada, M., (1998). Globular carbohydrate macromolecule "sugar balls", 2. Synthesis of mono (glycopeptide)-persubstituted dendrimers by polymer reaction with sugar-substituted α-amino acid N-carboxyanhydrides (glycoNCAs). *Macromolecular rapid communications*, *19*(1), pp.5-9.

Baek, M.G. and Roy, R., (2002). Synthesis and protein binding properties of T-antigen containing GlycoPAMAM dendrimers. *Bioorganic & medicinal chemistry*, *10*(1), pp.11-17.

Batrakova, E.V., Gendelman, H.E. and Kabanov, A.V., (2011). Cell-mediated drug delivery. *Expert opinion on drug delivery*, *8*(4), pp.415-433.

Bellini, R.G., Guimarães, A.P., Pacheco, M.A., Dias, D.M., Furtado, V.R., de Alencastro, R.B. and Horta, B.A., (2015). Association of the anti-tuberculosis drug rifampicin with a PAMAM dendrimer. *Journal of Molecular Graphics and Modelling*, *60*, pp.34-42.

Bhattacharjee, S., (2016). DLS and zeta potential–what they are and what they are not?. *Journal of controlled release*, *235*, pp.337-351.

Burke, S.D., Zhao, Q., Schuster, M.C. and Kiessling, L.L., (2000). Synergistic formation of soluble lectin clusters by a templated multivalent saccharide ligand. *Journal of the American Chemical Society*, *122*(18), pp.4518-4519.

Casadevall, A., (2008). Evolution of intracellular pathogens. *Annu. Rev. Microbiol.*, *62*, pp.19-33.

Choi, M.R., Stanton-Maxey, K.J., Stanley, J.K., Levin, C.S., Bardhan, R., Akin, D., Badve, S., Sturgis, J., Robinson, J.P., Bashir, R. and Halas, N.J., (2007). A cellular Trojan Horse for delivery of therapeutic nanoparticles into tumors. *Nano letters*, *7*(12), pp.3759-3765.

Date, P.V., Samad, A. and Devarajan, P.V., (2010). Freeze thaw: a simple approach for prediction of optimal cryoprotectant for freeze drying. *Aaps Pharmscitech*, *11*(1), pp.304-313.

Diaz, C., Guzmán, J., Jiménez, V.A. and Alderete, J.B., (2018). Partially PEGylated PAMAM dendrimers as solubility enhancers of Silybin. *Pharmaceutical development and technology*, *23*(7), pp.689-696.

Diebold, S.S., Kursa, M., Wagner, E., Cotten, M. and Zenke, M., (1999). Mannose polyethylenimine conjugates for targeted DNA delivery into dendritic cells. *Journal of biological chemistry*, *274*(27), pp.19087-19094.

Dimick, S.M., Powell, S.C., McMahon, S.A., Moothoo, D.N., Naismith, J.H. and Toone, E.J., (1999). On the meaning of affinity: cluster glycoside effects and concanavalin A. *Journal of the American Chemical Society*, *121*(44), pp.10286-10296.

Dineshkumar, P., Panneerselvam, T., Deepti Brundavani, K., Selvaraj, K. and Vijayaraj Kumar, P., (2017). Formulation of Rifampicin Loaded PEGylated 5.0 G EDA-PAMAM Dendrimers as

Effective Long-Duration Release Drug Carriers. *Current Drug Therapy*, *12*(2), pp.115-126.

Dutta, T., Agashe, H.B., Garg, M., Balasubramanium, P., Kabra, M. and Jain, N.K., (2007). Poly (propyleneimine) dendrimer based nanocontainers for targeting of efavirenz to human monocytes/macrophages in vitro. *Journal of drug targeting*, *15*(1), pp.89-98.

Dutta, T. and Jain, N.K., (2007). Targeting potential and anti-HIV activity of lamivudine loaded mannosylated poly (propyleneimine) dendrimer. *Biochimica et Biophysica Acta (BBA)-General Subjects*, *1770*(4), pp.681-686.

Dwek, R.A., (1996). Glycobiology: toward understanding the function of sugars. *Chemical reviews*, *96*(2), pp.683-720.

Filatova, L.Y., Klyachko, N.L. and Kudryashova, E.V., (2018). Targeted delivery of anti-tuberculosis drugs to macrophages: targeting mannose receptors. *Russian Chemical Reviews*, *87*(4), p.374-391.

Grayson, S.M. and Frechet, J.M., (2001). Convergent dendrons and dendrimers: from synthesis to applications. *Chemical reviews*, *101*(12), pp.3819-3868.

Gupta, U., Agashe, H.B. and Jain, N.K., (2007). Polypropylene imine dendrimer mediated solubility enhancement: effect of pH and functional groups of hydrophobes. *J Pharm Pharm Sci*, *10*(3), pp.358-67.

Hu, Y., Xu, B.H., Xu, J.J., Shou, D. and Gao, J.Q., (2014). Synthesis of mannosylated polyethylenimine and its potential application as cell-targeting non-viral vector for gene therapy. *Polymers*, *6*(10), pp.2573-2587.

Huang, W.C., Chiang, W.H., Cheng, Y.H., Lin, W.C., Yu, C.F., Yen, C.Y., Yeh, C.K., Chern, C.S., Chiang, C.S. and Chiu, H.C., (2015). Tumortropic monocyte-mediated delivery of echogenic polymer bubbles and therapeutic vesicles for chemotherapy of tumor hypoxia. *Biomaterials*, *71*, pp.71-83.

I. Peerlings, H.W., Nepogodiev, S.A., Stoddart, J.F. and Meijer, E.W., (1998). Synthesis of Spacer-Armed Glucodendrimers Based on the Modification of Poly (propylene Imine) Dendrimers. *European journal of organic chemistry*, *1998*(9), pp.1879-1886.

Imbuluzqueta, E., Gamazo, C., Ariza, J. and Blanco-Prieto, M.J., (2010). Drug delivery systems for potential treatment of intracellular bacterial infections. *Frontiers in Bioscience*, 15(2), pp. 397–417.

Ishii, K. J. and Akira, S. (2008). Innate immunity, in *Clinical Immunology*. Elsevier Ltd, pp. 39–51.

Jain, K., Verma, A.K., Mishra, P.R. and Jain, N.K., (2015). Surface-engineered dendrimeric nanoconjugates for macrophage-targeted delivery of amphotericin B: formulation development and in vitro and in vivo evaluation. *Antimicrobial agents and chemotherapy*, *59*(5), pp.2479-2487.

Jansen, J.F., De Brabander-van den Berg, E. M. M., and Meijer, E.W., (1994). Encapsulation of guest molecules into a dendritic box. *Science*, *266*(5188), pp.1226-1229.

Jayaraman, N., Nepogodiev, S.A. and Stoddart, J.F., (1997). Synthetic Carbohydrate-Containing Dendrimers. *Chemistry–A European Journal*, *3*(8), pp.1193-1199.

Kamitakahara, H., Suzuki, T., Nishigori, N., Suzuki, Y., Kanie, O. and Wong, C.H., (1998). A Lysoganglioside/Poly-L-glutamic Acid Conjugate as a Picomolar Inhibitor of Influenza Hemagglutinin. *Angewandte Chemie International Edition*, *37*(11), pp.1524-1528.

Khan, M.F., Rita, S.A., Kayser, M., Islam, M., Asad, S., Bin Rashid, R., Bari, M., Rahman, M.M., Aman, A., Anwar, D.A. and Setu, N.I., (2017). Theoretically guided analytical method development and validation for the estimation of rifampicin in a mixture of isoniazid and pyrazinamide by UV spectrophotometer. *Frontiers in Chemistry*, *5*, p.27.

Kiessling, L.L., (1998). The Molecular Recognition of Saccharides and Glycoprotein-Inspired Materials. In *Recent Trends in Molecular Recognition*, pp. 183-212. Springer, Berlin, Heidelberg.

Kiessling, L.L., Gestwicki, J.E. and Strong, L.E., (2000). Synthetic multivalent ligands in the exploration of cell-surface interactions. *Current opinion in chemical biology*, *4*(6), pp.696-703.

Kim, N., Jiang, D., Jacobi, A.M., Lennox, K.A., Rose, S.D., Behlke, M.A. and Salem, A.K., (2012). Synthesis and characterization of mannosylated pegylated polyethylenimine as a carrier for siRNA. *International journal of pharmaceutics*, *427*(1), pp.123-133.

Kimura, M., Mizuno, K., Muto, T., Hanabusa, K. and Shirai, H., (1999). Synthesis and characterization of a ligand-substituted poly (amidoamine) dendrimer with external terpyridine units and its iron (II) complexes. *Macromolecular rapid communications*, *20*(2), pp.98-102.

Kojima, C., Kono, K., Maruyama, K. and Takagishi, T., (2000). Synthesis of polyamidoamine dendrimers having poly (ethylene glycol) grafts and their ability to encapsulate anticancer drugs. *Bioconjugate chemistry*, *11*(6), pp.910-917.

Kumar, P.V., Asthana, A., Dutta, T. and Jain, N.K., (2006). Intracellular macrophage uptake of rifampicin loaded mannosylated dendrimers. *Journal of drug targeting*, *14*(8), pp.546-556.

Kunz, H., (1987). Synthesis of glycopeptides, partial structures of biological recognition components [New synthetic methods (67)]. *Angewandte Chemie International Edition in English*, *26*(4), pp.294-308.

Lee, H. and Larson, R.G., (2011). Effects of PEGylation on the size and internal structure of dendrimers: self-penetration of long PEG chains into the dendrimer core. *Macromolecules*, *44*(7), pp.2291-2298.

Lee, R.T. and Lee, Y.C., (2000). Affinity enhancement by multivalent lectin–carbohydrate interaction. *Glycoconjugate journal*, *17*(7-9), pp.543-551.

Lee, Y.C., Townsend, R.R., Hardy, M.R., Lönngren, J., Arnarp, J., Haraldsson, M. and Lönn, H., (1983). Binding of synthetic oligosaccharides to the hepatic Gal/GalNAc lectin. Dependence on fine structural features. *Journal of Biological Chemistry*, *258*(1), pp.199-202.

Lee, Y.C. and Lee, R.T., (1995). Carbohydrate-protein interactions: basis of glycobiology. *Accounts of chemical research*, *28*(8), pp.321-327.

Lindhorst, T.K.,(2002). Artificial multivalent sugar ligands to understand and manipulate carbohydrate-protein interactions. In *Host-Guest Chemistry*, pp. 201-235. Springer, Berlin, Heidelberg.

Lis, H. and Sharon, N., (1998). Lectins: carbohydrate-specific proteins that mediate cellular recognition. *Chemical reviews*, *98*(2), pp.637-674.

Liu, M., Li, J. and Li, B., (2018). Mannose-modificated polyethylenimine: a specific and effective antibacterial agent against Escherichia coli. *Langmuir*, *34*(4), pp.1574-1580.

Lundquist, J.J. and Toone, E.J., (2002). The cluster glycoside effect. *Chemical reviews*, *102*(2), pp.555-578.

Mammen, M., Choi, S.K. and Whitesides, G.M., (1998). Polyvalent interactions in biological systems: implications for design and use of multivalent ligands and inhibitors. *Angewandte Chemie International Edition*, *37*(20), pp.2754-2794.

Monack, D.M., Mueller, A. and Falkow, S., (2004). Persistent bacterial infections: the interface of the pathogen and the host immune system. *Nature Reviews Microbiology*, *2*(9), pp.747-765.

Newkome, G.R., Moorefield, C.N., Baker, G.R., Saunders, M.J. and Grossman, S.H., (1991). Unimolecular micelles. *Angewandte Chemie International Edition in English*, *30*(9), pp.1178-1180.

Newkome, G.R., Woosley, B.D., He, E., Moorefield, C.N., Güther, R., Baker, G.R., Escamilla, G.H., Merrill, J. and Luftmann, H., (1996). Supramolecular chemistry of flexible, dendritic-based structures employing molecular recognition. *Chemical Communications*, (24), pp.2737-2738.

Nimje, N., Agarwal, A., Saraogi, G.K., Lariya, N., Rai, G., Agrawal, H. and Agrawal, G.P., (2009). Mannosylated nanoparticulate carriers of rifabutin for alveolar targeting. *Journal of drug targeting*, *17*(10), pp.777-787.

Olsen, L.R., Dessen, A., Gupta, D., Sabesan, S., Sacchettini, J.C. and Brewer, C.F., (1997). X-ray crystallographic studies of unique cross-linked lattices between four isomeric biantennary oligosaccharides and soybean agglutinin. *Biochemistry*, *36*(49), pp.15073-15080.

Pagé, D. and Roy, R., (1997). Synthesis and biological properties of mannosylated starburst poly (amidoamine) dendrimers. *Bioconjugate chemistry*, *8*(5), pp.714-723.

Pei, Y. and Yeo, Y., (2016). Drug delivery to macrophages: Challenges and opportunities. *Journal of Controlled Release*, *240*, pp.202-211.

Pelizza, G., Nebuloni, M., Ferrari, P. and Gallo, G.G., (1977). Polymorphism of rifampicin. *Il Farmaco; edizione scientifica*, *32*(7), pp.471-481.

PubChem (2019) *4-Isothiocyanatophenyl alpha-D-mannopyranoside | C13H15NO6S - PubChem*. Available at: https://pubchem.ncbi.nlm.nih.gov/compound/4-Isothiocyanatophenyl-alpha-D-mannopyranoside#section=Computed-Properties&fullscreen=true (Accessed: 19 August 2020).

Quesenberry, M.S., Lee, R.T. and Lee, Y.C., (1997). Difference in the binding mode of two mannose-binding proteins: demonstration of a selective minicluster effect. *Biochemistry*, *36*(9), pp.2724-2732.

Roy, R., (1996). Blue-prints, synthesis and applications of glycopolymers. *Trends in Glycoscience and Glycotechnology*, *8*(40), pp.79-99.

Sabeti, B., Noordin, M.I., Mohd, S., Hashim, R., Dahlan, A. and Akbari Javar, H., (2014). Development and characterization of liposomal doxorubicin hydrochloride with palm oil. *BioMed research international*, *2014*.

Sashiwa, H., Shigemasa, Y. and Roy, R., (2000). Chemical modification of chitosan. 3. Hyperbranched chitosan− sialic acid dendrimer hybrid with tetraethylene glycol spacer. *Macromolecules*, *33*(19), pp.6913-6915.

Sashiwa, H., Shigemasa, Y. and Roy, R., (2002). Chemical modification of chitosan 11: chitosan–dendrimer hybrid as a tree like molecule. *Carbohydrate polymers*, *49*(2), pp.195-205.

Sharon, N. and Lis, H., (1993). Carbohydrates in cell recognition. *Scientific American*, *268*(1), pp.82-89.

Song, X., Lin, Q., Guo, L., Fu, Y., Han, J., Ke, H., Sun, X., Gong, T. and Zhang, Z., (2015). Rifampicin loaded mannosylated cationic nanostructured lipid carriers for alveolar macrophage-specific delivery. *Pharmaceutical research*, *32*(5), pp.1741-1751.

Spaltenstein, A. and Whitesides, G. M. (1991). Polyacrylamides Bearing Pendant α-Sialoside Groups Strongly Inhibit Agglutination of Erythrocytes by Influenza Virus. *Journal of the American Chemical Society*, 113(2), pp. 686–687..

Toone, E.J., (1994). Structure and energetics of protein-carbohydrate complexes. *Current Opinion in Structural Biology*, *4*(5), pp.719-728.

Turnbull, W.B. and Stoddart, J.F., (2002). Design and synthesis of glycodendrimers. *Reviews in Molecular Biotechnology*, *90*(3-4), pp. 231-255.

Uppuluri, S., Dvornic, P.R., Klimash, J.W., Carver, P.I. and Tan, N.C., (1998). *The properties of dendritic polymers I: generation 5 poly (amidoamine) dendrimers* (No. ARL-TR-1606). ARMY RESEARCH LAB ABERDEEN PROVING GROUND MD.

Wang, D. and Imae, T., (2004). Fluorescence emission from dendrimers and its pH dependence. *Journal of the American Chemical Society*, *126*(41), pp.13204-13205.

Williams, K.J. and Piddock, L.J., (1998). Accumulation of rifampicin by Escherichia coli and Staphylococcus aureus. *The Journal of antimicrobial chemotherapy*, *42*(5), pp.597-603.

Williams, S.J. and Davies, G.J., (2001). Protein–carbohydrate interactions: learning lessons from nature. *Trends in biotechnology*, *19*(9), pp.356-362.

Woller, E.K., (2003). *Mannose-functionalized PAMAM dendrimers: their synthesis, characterization and use in refining the model of protein-carbohydrate interactions* (Doctoral dissertation, Montana State University-Bozeman, College of Letters & Science).

Woller, E.K. and Cloninger, M.J., (2001). Mannose functionalization of a sixth generation dendrimer. *Biomacromolecules*, *2*(3), pp.1052-1054.

Wynn, T.A., Chawla, A. and Pollard, J.W., (2013). Macrophage biology in development, homeostasis and disease. *Nature*, *496*(7446), pp.445-455.

Chapter 5

In-vitro drug release studies

5.1 Introduction

This chapter provides a detailed description of the materials, methods, and analytical techniques used to study the release behaviour of rifampicin at pH 7.4 and pH 4.5 with various dendrimer formulations synthesized in **Chapter 3** and **Chapter 4**. Drug release kinetics were also studied to predict the mechanism(s) of release from each formulation at both pH levels. Finally, this chapter also displays the results obtained with discussion and conclusion.

5.2 Review of the literature

5.2.1 Mechanisms of drug release from polymeric nanoparticles

Drug release from polymeric nanoparticles, such as PAMAM dendrimer, is influenced by many factors including the nature and the proportion of its conjugate components (polymer, drug, and additives), the method of nanoparticle synthesis, drug loading, and the nature of the drug-polymer interaction (Langer and Peppas, 1983; Siegel and Rathbone, 2012). The mechanisms of drug release from polymeric carriers can be classified into four categories: diffusion release, solvent-controlled release, polymer-degraded release, and stimuli-controlled release (Figure 5.1 and Figure 5.2) (Son, Lee and Cho, 2017).

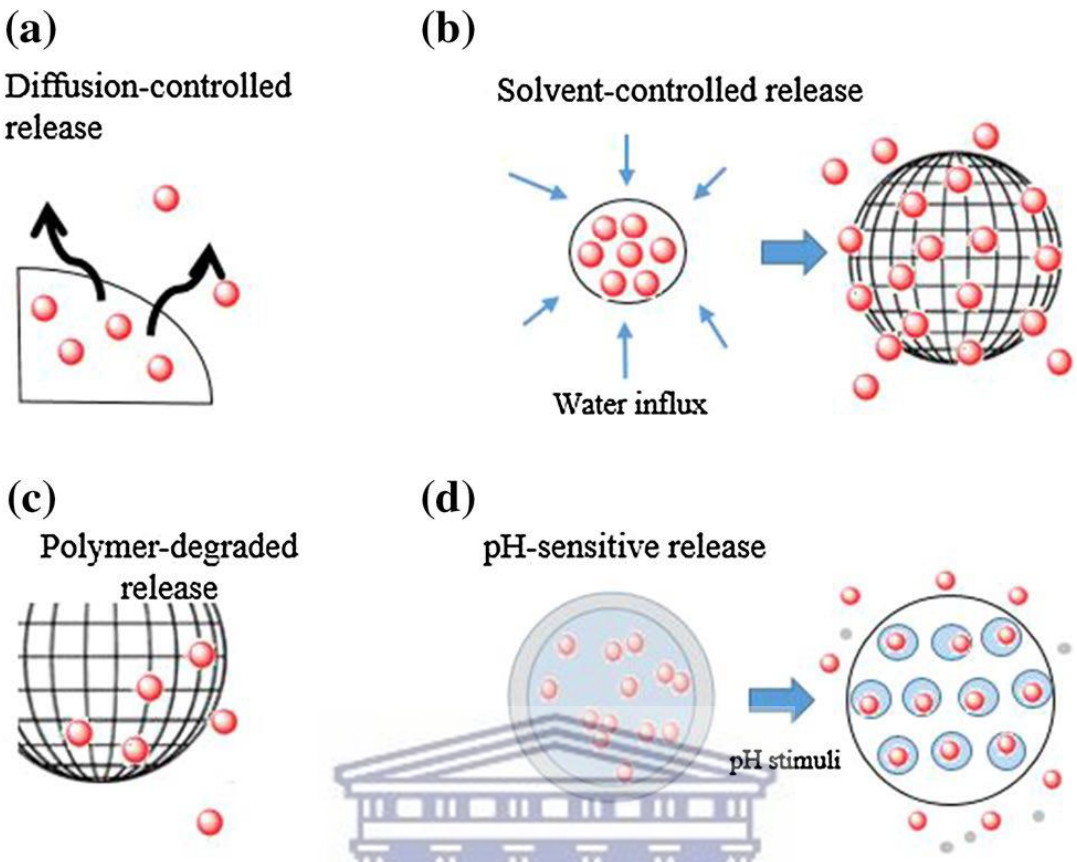

Figure 5.1 Schematic of drug release mechanisms from polymeric nanocarriers (Son, Lee and Cho, 2017), (a) diffusion release; (b) solvent-controlled release; (c) polymer degradation release; and (d) stimuli-controlled release.

a) Diffusion-controlled release

The diffusion-controlled release mechanism (Figure 5.1 (a)) takes place in shell-like systems where the drug is either dissolved in the inner core (nanocapsules) or dispersed (nanosphere) into the polymer matrix (Cauchetier *et al.*, 2003). The difference in concentration gradient across the semi-permeable membrane is the vital driving force for the movement of dissolved drug molecules from the nanoparticle core. While in the nanosphere systems, the nature of the matrix component is the main controlling factor of the diffusion rate of the dispersed drugs. The release profile of the nanosphere system is usually characterized by an initial burst phase, after a while the release rate decreases due to increasing the diffusion distance or due to a weakly bound/adsorbed drug to the surface of nanoparticles (Lee and Yeo, 2015).

b) Solvent-controlled release

The access of solvent molecules inside the drug-delivery systems may affect the release behaviour of the drug to the exterior. The solvent-controlled release is classified into the osmotic-controlled release and swelling-controlled release based on the behaviour of release (Langer and Peppas, 1983) (Figure 5.2). The osmotic release occurs in a carrier composed of a semi-permeable membrane. The transport of water molecules from the low drug concentration region to a high drug concentration core generates osmotic pressure across the membrane, which controls drug release. As a result, the zero-order kinetic release will take place across the membrane. Where in the swelling release system, the carrier composed of a three-dimensional cross-linked network polymer material such as a hydrogel, and the mesh size is the chief control of drug release (Peppas *et al.*, 2000; Chilin and Metters, 2006).

c) Degradation-controlled release

Degradation-controlled release (Figure 5.1 (c)) arises when the carrier consists of biodegradable polymers such as polysaccharides and polyesters. Drug release is a consequence of the enzymatic breakdown of the ester or amide bonds or *via* polymer hydrolysis (Figure 5.2) (Yoo and Park, 2001; Prabaharan *et al.*, 2009; Lee *et al.*, 2011). The degradation process is commonly happening in two ways: In the first type, degradation occurs simultaneously on the whole bulk matrix, for example, a matrix composed of polylactic-co-glycolic acid (PLGA) polymer. In the second type, erosion starts from the surface towards the centre and causes the degradation of the polymer and drug release, for example, a matrix composed of polymeric anhydrides (Burkersroda, Schedl and Gopferich, 2002).

d) Stimuli-controlled release

Drug release from polymeric nanocarriers can be controlled along with targeting properties by responding to localize stimulation such as pH (Figure 5.1 (d)), ultrasound, temperature, electricity, and magnetic field (Abouelmagd, Hyun and Yeo, 2014) (Figure 5.2).

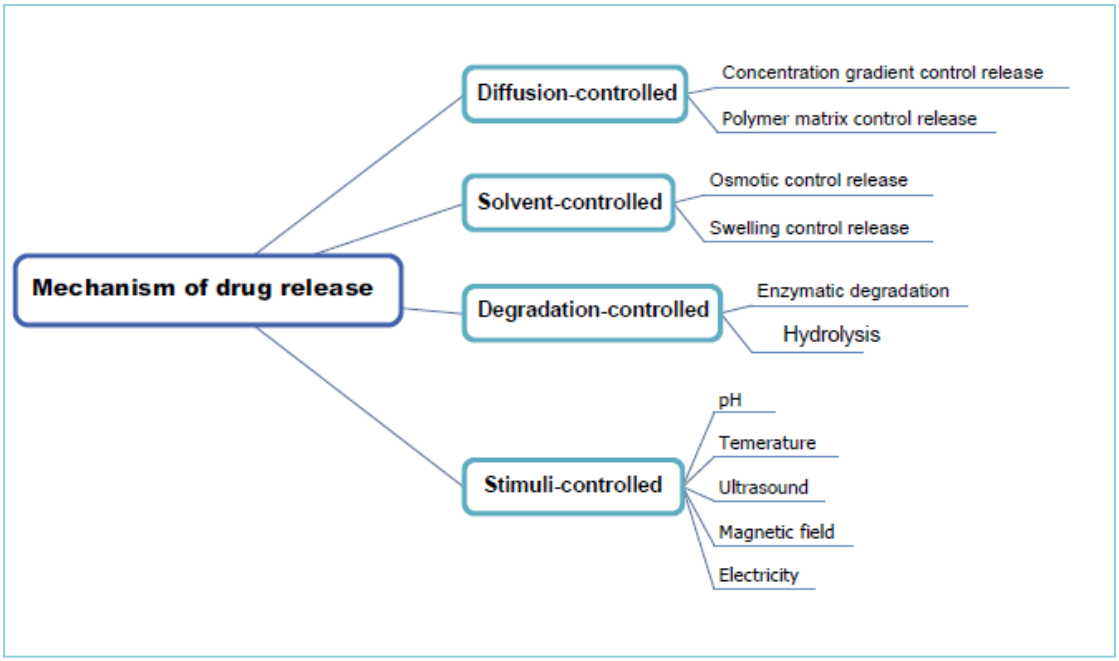

Figure 5.2 Possible mechanisms of drug release from PAMAM dendrimers.

5.2.2 Evaluation of *in vitro* drug release from polymeric nanoparticles

One of the main applications for using polymeric nanoparticles as a drug delivery system is to prolong and control drug release. Despite the advances and expansion in the development and synthesis of nanoformulations, no compendial or regulatory standards are available for drug release assessment (D'Souza, 2014). Different techniques have been developed to assess the drug release from nanoparticle formulations. These techniques are classified into four categories, i.e., dialysis membrane, sample and separate, continuous flow, and combination techniques (D'Souza, 2014; Xie *et al.*, 2015).

5.2.2.1 Dialysis membrane (DM) technique

Dialysis membrane is the most familiar and simple drug release test method, the physical separation of the nanocarrier from the release medium can be easily achieved by using a dialysis membrane having a definite molecular weight cut-off (MWCO). Drug-loaded nanoparticles are placed into a dialysis membrane and then immersed in the release medium (Figure 5.3). The membrane pores only allow the passing of drug molecules, whereas nanoparticles are retained inside the dialysis membrane; this attribute facilitates straightforward sampling at different time intervals.

There are three types of dialysis membrane techniques: dialysis bag, reverse dialysis, and side-by-side dialysis. Dialysis bag or sometimes known as regular dialysis is the most commonly reported dialysis membrane technique as opposed to other methods such as reverse dialysis and side-by-side dialysis (Calvo, Vila-Jato and Alonso, 1996; Chidambaram and Burgess, 1999; Yan *et al.*, 2010). Besides drug solubility in the release medium which is essential for the diffusion process across the membrane, selecting the appropriate MWCO of the dialysis membrane is also a crucial limiting factor for drug diffusion (D'Souza, 2014). Dialysis techniques are not suitable for molecules having high membrane binding affinity. Therefore, it is recommended to investigate the drug-membrane association before doing release studies (D'Souza and DeLuca, 2005).

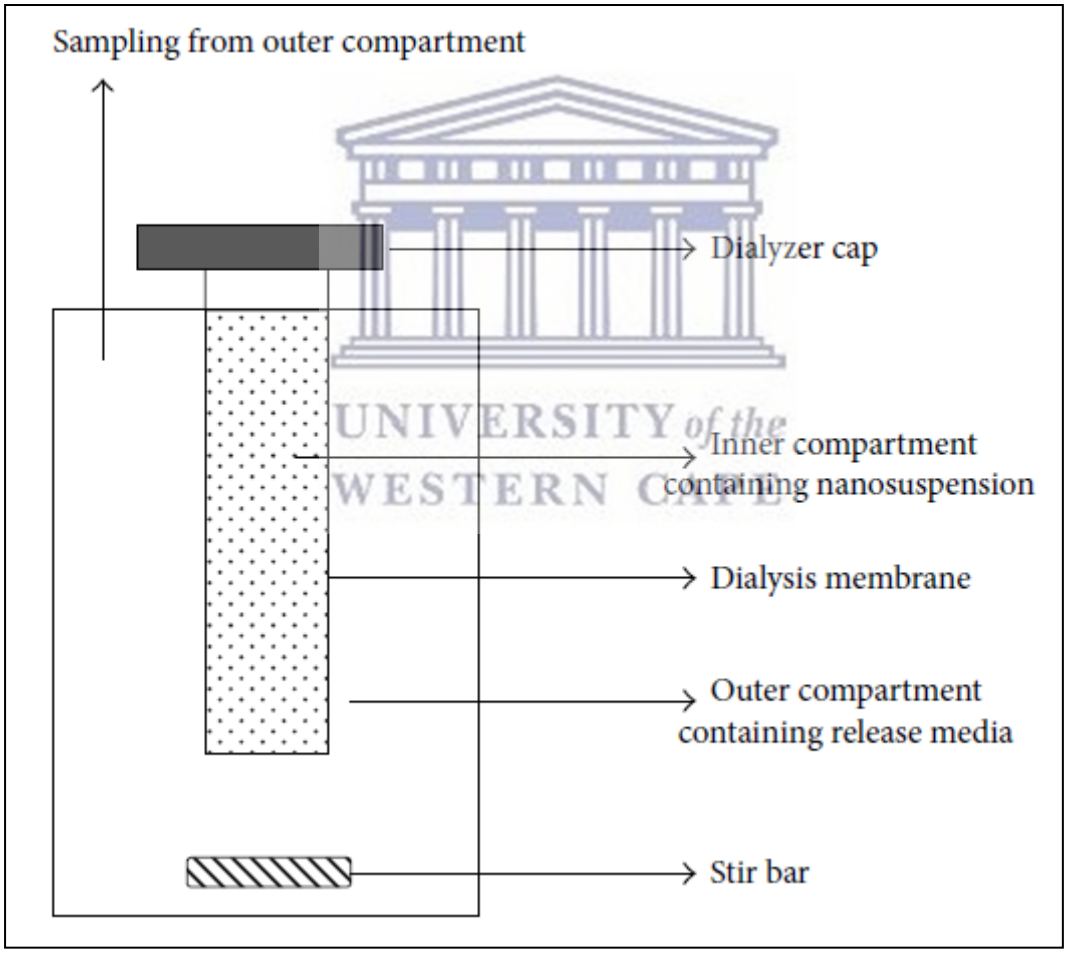

Figure 5.3 Schematic of dialysis bag technique (D'Souza and DeLuca, 2006).

5.2.2.2 Sample and separation techniques

In the sample and separation methods, the drug-loaded nanoparticles are introduced into the release medium. At various time intervals, the sample is withdrawn, and the particulates are separated from the release medium either by using filtration or centrifugation techniques after which the release medium is analyzed for drug concentration quantification. This approach allows the direct study of drug release with no membrane interfering effect. Conversely, many reports have mentioned that using centrifugation during the separation step is too vigorous and might result in forced or premature drug release (Lamprecht *et al.*, 2002; Shetab Boushehri and Lamprecht, 2015).

5.2.2.3 Continuous flow technique

In the continuous flow technique, the drug release from the nanoformulation is controlled by the USP IV apparatus or its modification. Drug release takes place by the continuous movement of the release medium throughout a column that holds an immobilized sample. The eluent is collected at different time intervals for release analysis. This technique is costly, adsorbed drug molecules may block the filter, and the release is greatly influenced by the flow rate (Shetab Boushehri and Lamprecht, 2015). Few publications of using this technique have been reported in the literature (Heng *et al.*, 2008; Sievens-Figueroa *et al.*, 2012).

5.2.2.4 Combination techniques

A limited number of reports manipulated the set-ups applied in the sample and separate, dialysis membrane, and continuous flow techniques to assess the drug release from nanoformulations. Some of them modified the sample and separate method by attaching a dialyzer to skip the separation step and hence facilitated easy sampling (Gao *et al.*, 2013). Others combined both dialysis membrane techniques and continuous flow techniques in a single apparatus (Kostanski and DeLuca, 2000).

Table 5.1 summarizes some of the previously reported *in vitro* test methods where the use of dendrimer is included as a drug delivery system.

Table 5.1 Examples of drug release assessing methods with dendrimer nanoparticles.

Type of dendrimer	Drug	Drug release test method	Reference
Mannosylated G5-PPI	rifampicin	Modified dissolution	(Kumar *et al.*, 2006)
Mannosylated G5-PPI	lamivudine	Dialysis bag	(Dutta *et al.*, 2007)
PEGylated G5 PAMAM	rifampicin	Dialysis bag	(Dineshkumar *et al.*, 2017)
PEGylated G4 PAMAM	carboplatin	Dialysis bag	(Ho *et al.*, 2019)
PEGylated G3 PAMAM	fluorouracil	Dialysis bag	(Ly *et al.*, 2013)
PEGylated G4, G5 PPI	rifampicin	Modified dissolution	(Vijayaraj Kumar *et al.*, 2007)
PEGylated G3 PAMAM	methotrexate	Dialysis bag	(Pan *et al.*, 2005)
G4.5, G5, G5.5, G6 PAMAM	vardenafil	USP dissolution type II	(Tawfik, Tadros and Mohamed, 2019)

*PPI = poly(propylene imine); PAMAM = poly(amidoamine); G = dendrimer generation.

5.2.3 Analysis and modelling of drug release

Drug release from the polymeric nanoparticles may occur by various processes to liberate drug molecules that dissolve and become available for absorption. The release is the prerequisite step before absorption and is considered as the foremost stage that determines the rate and the extent of bioavailability (Bruschi, 2015).

One of the most simple techniques to study the release behaviour of a drug delivery system is by plotting drug release profiles (Zhang *et al.*, 2010). The collected analytical data obtained from release studies using the nano-formulation at different time intervals are converted and plotted into concentration and the cumulative percentage (%) release against time. Various techniques can be used to predict the release mechanisms such as model-dependent approaches of release profile analysis through mathematical

modelling, model-independent methods, and statistical analysis. Each of these techniques has drawbacks, and some of them are regarded as a pharmaceutical inappropriate analysis tool by pharmaceutical authorization bodies like the FDA. For example, using the analysis of variance (ANOVA) to compare the release behaviour of drugs has been criticized by Zhang and co-workers (Zhang *et al.*, 2010). They mentioned that applying ANOVA for drug release comparison indicates statistical similarity and not pharmaceutical similarity. They illustrated further that in many cases where the compared profiles were different, an ANOVA statistical analysis displayed samenesses (Zhang *et al.*, 2010). For this reason, using this analysis tool will be critical, particularly for narrow therapeutic index drugs.

Drug release kinetics can be expressed by appropriate mathematical models to find out the effect of the nanocarrier on its release, besides illustrating mechanisms involved in drug release (Siepmann and Göpferich, 2001). One of the limitations of applying mathematical modelling is the fact that findings from this approach depend principally on the experimental data. Since there is no standardization for release study methods, different release kinetics might be concluded from release data of the same sample synthesized in different experimental settings.

As long as there is no universally suitable model to describe the release behaviour of all drugs, the release data are fitted into different models to evaluate the goodness of fit before choosing the best fit (Siepmann and Siepmann, 2008). Model equations are categorized into two groups: the first group offers a general description of the drug release profile, and it is known as an empirical equation. The second group is referred to as semi-empirical serves to predict the mechanism of drug release as well as the release profile description (Agata *et al.*, 2010). Examples of semi-empirical equations that have been employed in this study to elucidate the drug release from PAMAM dendrimer are Peppas-Sahlin, Korsmeyer-Peppas, and Weibull models.

A variety of mathematical models were developed to study drug release from various drug delivery systems; the most essential models are described below:

The zero-order model **(Equation 5.1)**, is designed to represent the release of therapeutic drugs from delivery systems where the release rate is slow and independent of its concentration (Bruschi, 2015; Son, Lee and Cho, 2017)

$$Q_t = K_0 t \qquad \textbf{Equation 5.1}$$

Where K_0 is the zero-order release rate constant, and t is the time.

The first-order kinetics model **(Equation 5.2)** was developed by Gibaldi and Feldman in 1967 and later on improved by Wagner in 1969. In this model, the release rate is a function of drug concentration; it has also been used to express the absorption or elimination processes of various drug molecules (Bruschi, 2015; Son, Lee and Cho, 2017).

$$Q_t = 1 - e^{-k_1 t} \qquad \textbf{Equation 5.2}$$

Where k_1 represents the first-order rate constant, and t is the time. Many drug delivery systems exhibit first-order drug release behaviour. For example, for hydrophilic drugs incorporated in a porous matrix system, the rate of release is directly proportional to the amount of remaining drug in the polymer matrix. After a while, the rate of drug released is liable to decrease as a consequence of declining drug concentration within the polymer (Bruschi, 2015).

Higuchi model **(Equation 5.3)** was developed in 1963 to illustrate the mode of release of different hydrophilic and lipophilic drugs from a range of matrix systems (Son, Lee and Cho, 2017).

$$Q_t = K_H t^{1/2} \qquad \textbf{Equation 5.3}$$

Where k_H is the Higuchi dissolution constant, and t is the time. Higuchi model describes drug release as a result of a Fickian diffusion mechanism.

Peppas-Sahlin model **(Equation 5.4)** was developed in 1989 to describe the release from delivery systems taking into consideration the involvement of both diffusion and relaxation mechanisms (Bruschi, 2015).

$$Q_t = K_1 t^m + k_2 t^{2m} \qquad \textbf{Equation 5.4}$$

Where k_1 and k_2 represent constants of diffusion and polymer relaxation respectively, and m is the diffusional exponent for a system of any geometric shape that shows controlled release. When $k_1 > k_2$ the mechanism of drug release is mainly controlled by Fickian diffusion, on the other hand, when $k_1 < k_2$ the polymer relaxation is the principal control factor of drug release (Costa and Lobo, 2001; Freire *et al.*, 2017).

Korsmeyer-Peppas model **(Equation 5.5)** was described by Korsmeyer, Gurny, Doelker, Buri, and Peppas in 1983, Ritger and Peppas in 1987. This model was developed to evaluate the drug release from a polymeric matrix such as a hydrogel. It is suitable in cases when the mechanism of release is not well understood. Also, when more than one mechanism is involved, such as Fickian diffusion and non-Fickian transport (polymer relaxation control mechanism) (Bruschi, 2015).

$$Q_t = kt^n \qquad \textbf{Equation 5.5}$$

Where k is the release constant incorporating structural and geometric characteristics of the system, and n is the diffusional exponent indicating the drug-release mechanism. According to the Korsmeyer-Peppas model, the mechanism of release can be expected from the (n) value, lower values where $n \leq 0.43$ the release is mostly governed by the Fickian diffusion mechanism. Higher values where n = 0.85, specify case II a non-Fickian model (i.e., polymer swelling and relaxation involvement), $n > 0.85$ indicates a super case II, non-Fickian model. Intermediate values, where $0.43 < n < 0.85$ indicate an anomalous release style, controlled by both diffusion and polymer swelling mechanisms (Bruschi, 2015; Son, Lee and Cho, 2017).

Weibull model **(Equation 5.6)** was developed by the two scientists Weibull in 1951 and Langenbucher in 1973 to describe and compare the release profile of matrix systems. This model can be fitted to all types of dissolution profiles to estimate the release mode (Costa and Lobo, 2001).

$$Q_t = 100\,(1 - e^{-tb/a}) \qquad \textbf{Equation 5.6}$$

Where a is the scale parameter which describes the time scale of the process, and b is the shape parameter which characterizes the dissolution curve. When b value = 1, the shape of the curve corresponds to the exponential profile. For higher value $b > 1$, the shape of the profile obtains a sigmoidal design. A lower value $b < 1$ indicates a parabolic display (Costa and Lobo, 2001; Dash *et al.*, 2010; Bruschi, 2015). Furthermore, the value of b can be used to predict the mechanism involved in the release process. If $b \leq 0.75$ the release is principally governed by the Fickian diffusion mechanism, intermediate values $0.75 < b < 1$ indicates a combined release mechanism, and with higher values, $b > 1$ identifies complex release mechanism (Papadopoulou *et al.*, 2006).

In all models, Q_t is the fraction (%) of drug released versus time t.

5.2.4 The effect of dendrimer surface modification on drug release

5.2.4.1 PEGylation and drug release

The point behind understanding the consequence of PEGylation on the drug release from nanocarriers lies in the fact that drug release analysis is one of the quality control techniques currently applied in pharmaceutical formulation development (Xie *et al.*, 2015). Furthermore, the release from nanoparticles is regarded as a significant indicator of drug efficacy (Shetab Boushehri and Lamprecht, 2015). PEGylated dendrimers usually exhibit a slower drug release in comparison to the native dendrimer, due to its superior hydrophobic interaction of drug molecules and the dendrimer core (Patri *et al.*, 2004; Singh *et al.*, 2008; Jin *et al.*, 2011; Holden *et al.*, 2012). PEGylation generates a dense surface at the dendrimer periphery, which acts as a physical barrier for drug molecule diffusion, thus slow-release behaviour will be expected (Pan *et al.*, 2005). Both the density (Sideratou, Tsiourvas and Paleos, 2001; Thakur *et al.*, 2015) and the molecular weight (Kojima *et al.*, 2000; Yang, Morris and Lopina, 2004) of the PEG chains contribute to control/sustain drug release.

A study conducted by Singh and co-workers (2008) evaluated the release of 5-fluorouracil from the folate-PEG-G4 PAMAM dendrimer (Singh *et al.*, 2008). Results indicated a lower release pattern observed for folate-PEG-PAMAM compared to folate-PAMAM dendrimer and PAMAM dendrimer formulations. The authors concluded that the reason behind slowed/sustained release behaviour might probably be due to the closed structure generated by PEG chains around dendrimer.

Pan and co-workers (2005) developed G3 PAMAM dendrimer with a range of PEG densities (i.e., 23, 43, and 99% surface coverage). Results illustrated a negative correlation between the percentage of PEG coverage and the amount of drug (i.e., methotrexate) released. The authors concluded that lower release was observed with higher PEG% due to the formation of condensed and thicker PEG layers that minimize the diffusion of drug molecules outside the dendrimer (Pan *et al.*, 2005).

5.2.4.2 Mannosylation and drug release

Manipulating the surface of a dendrimer with mannose residues could further prolong the release of encapsulated drug molecules. The conjugated mannose act as a barrier layer that slows down drug diffusion outwards.

Conjugation of mannose molecules to the surface of 5.0 G PPI dendrimer results in a prolonged release of rifampicin molecules at pH 7.4 compared to pure rifampicin (Kumar *et al.*, 2006). Since the internal tertiary nitrogens of the dendrimer interior are strongly basic with a pka of 9.5 (Asthana *et al.*, 2005), rifampicin molecules probably interact with the dendrimer core *via* hydrophobic interactions. At pH 7.4 authors suggested that surface mannosylation could minimize the hydrophobic interior cavities of the PPI dendrimer which keep drug molecules for a longer time. A higher release rate was observed at pH 5.0, due to protonation of primary as well as tertiary amines (Wang and Imae, 2004; Gupta, Agashe and Jain, 2007). The electrostatic repulsion forces could change the conformational arrangement of the dendrimer to a hollow shell structure that triggers the expelling of the loaded drug from an open structure dendrimer. Furthermore, rifampicin molecules at pH lower than 7 acquire positive charges (Khan *et al.*, 2017), which are believed to accelerate the diffusion from the inner cavities due to electrostatic repulsion with positively charged amines.

Dutta *et al*. (2007) assessed the effect of surface mannosylation of PPI dendrimer on the release properties of the antiviral drug, efavirenz (EFV). The authors determined that the release rate from mannosylated PPI dendrimer was significantly lower than that from the unmodified PPI. Up to 24 h, all the EFV was completely released from the unmodified PPI dendrimer, on the other hand, 91.0 ± 0.3% of EFV was released from mannosylated PPI dendrimer up to 144 h (Dutta *et al.*, 2007). The authors speculated that slower release from mannosylated dendrimer was due to dense crowding generated by mannose molecules at the periphery that prolongs EFV release.

Similarly, many literature reports have corroborated that conjugation of mannose molecules to the dendrimer surface has a significant influence in lowering the release rate of encapsulated drug molecules (Dutta and Jain, 2007; Jain *et al.*, 2015).

5.3 Aim and the Objectives of the Chapter

5.3.1 Aim

The study aimed to evaluate the effect of surface modification of 4.0 G PAMAM dendrimer on the release characteristics of rifampicin at pH 7.4 and pH 4.5.

5.3.2 Objectives

i. To develop and validate an RP-HPLC method for rifampicin quantification in PBS (pH 7.4) and acetate buffer solution (pH 4.5).

ii. To evaluate the stability of rifampicin throughout the study time-frame in both release mediums (i.e., phosphate buffer saline (PBS) pH 7.4 and acetate pH 4.5).

iii. To compare the release pattern of rifampicin from various formulations synthesized in **Chapter 3** and **Chapter 4** using the dialysis bag technique.

iv. To predict the kinetics of release of rifampicin from each formulation using DDSolver software.

5.4 Materials

5.4.1 Consumables

Reagents and solvents: Rifampicin (DB Fine Chemicals, South Africa), L-Ascorbic acid, 99% (Sigma-Aldrich, Germany), potassium phosphate monobasic (Sigma, USA), potassium phosphate dibasic (Sigma-Aldrich, Spain), sodium chloride (Merck, South Africa), potassium chloride (Labchem, South Africa), sodium phosphate dibasic (Merck, Germany), sodium acetate anhydrous (Merck, South Africa), sodium hydroxide NaOH pellets (Merck, South Africa), hydrochloric acid HCl (Fluka, Austria), HPLC grade acetonitrile (Merck, Germany), glacial acetic acid (SAFC, Sigma Aldrich, Ireland), and ultrapure water (18.2 MΩ cm, O-purity filtration system, South Africa).

Other consumables: Nylon 0.45 µm syringe filter (KimLab, India), Pur-A-Lyzer MWCO 12-14 kDa dialysis tubes (Sigma, Israel), Parafilm® (Bemis, USA), micropipette 20, 200, 1000 and 5000 µl (DLAB, China), pipette tips 20, 200, 1000 and 5000 µl (Lasec, South Africa), 10 ml centrifuge tube (Plastpro Scientific, South Africa), poly tops glass vials NO. 1, 2 and 4 (Kimix, South Africa), HVLP 0.45 µm membrane filter (Millipore, Ireland), and 2 ml HPLC vials with PTFE screw (Cronus, UK).

5.4.2 Equipments

Ultrasonic bath (ScienTech®, South Africa), pH meter (XS®, Italy), filter units (Millipore®, USA), vacuum pump (Dry Vac 400®, USA), Vortex-Genie2®, model-560E (Scientific Industries, USA), Computer modeling software: DDSolver (Microsoft Excel add-in program), HPLC system (Agilent 1200® series controlled with Agilent ChemStation software® version G2173-60101L, Germany), magnetic stirrer (IKA®-WERKE, Germany), semi-micron electronic balance (Shimadzu®, Japan), probe sonicator (Sonoplus HD GM 2070®, Bandelin, Germany), and orbital shaker-incubator ES-80 (Grant-bio®, England).

5.5 Methodology

5.5.1 Development and validation of RP-HPLC method for assessing rifampicin in phosphate buffer saline (PBS) pH 7.4 and acetate buffer pH 4.5

An isocratic RP-HPLC method to evaluate the drug stability, and estimating rifampicin concentration in the release medium (i.e., PBS and acetate buffer pH 4.5), was developed and validated in accordance to the International Conference on Harmonization (ICH) guidelines (ICH, 2005).

5.5.1.1 Chromatographic conditions

An Agilent 1200 HPLC system was used to run samples. The system was equipped with a quaternary pump (G1311A, Germany), autosampler (G1329A, Germany), diode array detector (G1315B, Germany), a dual lamp design (i.e., ultraviolet and visible lamps), and an analyte fraction collector (G164C, Germany). The system is capable of controlling the column temperature throughout the analysis by the thermostat column compartment (G1322A, Japan). The data was recorded and interpreted by ChemStation software (G2173-60101L, Germany).

HPLC analysis was performed *via* passing the mobile phase through a Phenomenex Luna® 250 x 4.6 mm, 5 µm C18 column using a quaternary pump at a flow rate of 1 ml/min with a total run time of 6 minutes. The sample injection volume was set to be 10 µl. The column temperature was controlled at 25 °C. Before sample injection, the column equilibrated for 30 minutes *via* passing the mobile phase through the system until a stable baseline was achieved. Drug elution was detected by a diode array detector at a wavelength of 475 nm.

5.5.1.2 Mobile phase preparations

The mobile phase consisted of solvent A: 0.01 M potassium phosphate buffer of pH 7.4, prepared by dissolving 1.21 g of potassium phosphate dibasic (K_2HPO_4) and 0.41 g of potassium phosphate monobasic (KH_2PO_4) in 800 ml of deionized water (dH_2O). The volume was adjusted to 1 L using dH_2O and solvent B comprised of HPLC grade acetonitrile (ACN). The ratio of A: B was 40:60 v/v. The mixture was continuously stirred for 5 minutes, then filtered using a filter apparatus (Millipore®, USA) using

HVLP 0.45 µm membrane filter (Millipore, Ireland). Finally, the mixture was degassed for 10 minutes (intensity 5) using an ultrasonic bath before use.

5.5.1.3 Release medium

The PBS pH 7.4 and acetate buffer pH 4.5 were used as diluents to prepare the stock solution and various concentration standard solutions as well as the release medium for the *in vitro* drug release studies. Both release media were prepared on the day of analysis.

i) Phosphate buffer (PBS) pH 7.4 preparation

PBS was prepared by dissolving 8.0 g of sodium chloride (NaCl), 0.20 g of potassium chloride (KCl), 1.44 g of sodium phosphate dibasic (Na_2HPO_4), and 0.24 g of potassium phosphate monobasic (KH_2PO_4) in a 1 L volumetric flask holding 800 ml of dH_2O. The pH was adjusted to 7.4 and the volume completed to 1 L by dH_2O.

ii) Acetate buffer (0.01 M) pH 4.5 preparation

Sodium acetate buffer (0.01 M) pH 4.5 was prepared by dissolving 0.37 g of sodium acetate (anhydrous) and 0.33 g of acetic acid in 800 ml of dH_2O, the pH was adjusted to 4.5 and the volume completed to 1 L by dH_2O.

5.5.1.4 Preparation of calibration standard solutions

Rifampicin stock solution having a concentration of 100 µg/ml was prepared on the day of analysis by weighing accurately 1 mg of rifampicin powder. This was then, transferred to a 10 ml volumetric flask, and diluted with the release medium (PBS or acetate buffer) up to 10 ml. The stock solution was probe sonicated for 5 minutes to ensure complete dissolution. Serial dilutions of the stock solution were performed using the release medium to attain standard solutions with a range concentration of 0.5, 1, 2, 4, 10, 20, and 50 µg/ml.

5.5.1.5 Key parameters of the analytical method validation

The method was validated following the ICH guidelines (ICH, 2005). The following method validation parameters were tested: the range, linearity, precision, accuracy, and sensitivity.

A. Specificity

Specificity was assessed by injecting the mobile phase (i.e., phosphate buffer: acetonitrile), release medium (i.e., PBS or acetate buffer), and the unloaded dendrimer, to ensure that no overlapping or interference with the rifampicin peak will occur. Moreover, 20.0 µg/ml rifampicin standard solution (in both release medium) was subjected to stress conditions for 24 hr under pH 1.0 and pH 10, using HCl and sodium hydroxide NaOH solutions, respectively. After 24 hrs, the solutions were analyzed to observe the degradant product peaks relative to the intended analyte peak.

B. Determination of linearity and range

The linearity and range were evaluated for the standard solutions (0.5 - 50.0 µg/ml in PBS and 0.1 - 50.0 µg/ml in acetate buffer solution). One millilitre volume from each standard solution was transferred to HPLC vials after filtration through a 0.45 µm nylon syringe filter. Samples were analyzed in triplicate using the Agilent 1200 HPLC system with the setup as described in the preceding paragraphs. Two calibration curves of rifampicin in PBS and acetate buffer were generated by plotting each sample concentration with their corresponding mean peak areas. Linear regression analysis was used to study the linearity by calculating the correlation coefficient, slope, and y-intercept of the curve over the concentrations.

C. Determination of accuracy and precision

Recovery studies were performed to evaluate the method's accuracy. Triplicate of the three concentrations, 2.0 µg/ml, 10.0 µg/ml, and 20.0 µg/ml of rifampicin standard solutions were selected to carry out the analysis. The achieved peak area for each sample was converted to concentration using the generated linear equation of the calibration curve. Results were interpreted using equation 5.7.

$$\% \text{ Recovery } = \frac{\text{Calculated concentration}}{\text{Injected concentration}} \times 100 \qquad \textbf{Equation 5.7}$$

Inter-day (intermediate precision) and intra-day (repeatability) precision were assessed to estimate the extent of scattering between several measurements of the identical sample concentration. Triplicate analysis of three levels 2.0 µg/ml, 10.0 µg/ml, and 20.0 µg/ml, at three periods in a day and three consecutive days, were calculated to

determine intra-day and inter-day precision correspondingly. Results at each occasion were interpreted statistically by calculating the average, standard deviation (SD), and relative standard deviation (RSD).

D. Sensitivity

Limit of quantification (LOQ) and limit of detection (LOD) for the HPLC method were determined to estimate the sensitivity of the analytical method, using the calibration curve technique. From the calibration curve linearity data, the standard deviation of the y-intercepts and the slope of the regression line were applied on equation 5.8 and equation 5.9 to determine LOQ and LOD.

$$\mathrm{LOQ} = 10\ \mathrm{X}\ \frac{\sigma}{\mathrm{S}} \qquad \textbf{Equation 5.8}$$

$$\mathrm{LOD} = 3.3\ \mathrm{X}\ \frac{\sigma}{\mathrm{S}} \qquad \textbf{Equation 5.9}$$

Where σ represents the standard deviation of the y-intercepts and S is the slope of the calibration curve.

5.5.2 Stability studies of rifampicin in the release medium solutions within the study time-frame

Since rifampicin undergoes rapid oxidative degradation in aqueous solutions to generate rifampicin quinone (Sorokoumova *et al.*, 2008), PBS fortified with antioxidant ascorbic acid (200 µg/ml) was used to enhance the stability of rifampicin in the aqueous solution as described previously by Kumar *et al.* (2006) and Samkange *et al.* (2019).

Furthermore, rifampicin is unstable in acidic solutions which hydrolyze quickly to 3-formylrifamycin SV (3FRSV), with studies found this to occur within 30 minutes to 1 hour which indicated that the acidic medium is inappropriate to evaluate the release behaviour of rifampicin (Gharbo, Cognion, and Williamson, 1989; Jindal *et al.*, 1994; Shishoo *et al.*, 1999). Therefore, if the rifampicin solution will only be analyzed after, for example 30 minutes, one would achieve an underestimation due to the fact that during the waiting period the rifampicin started to degrade. The degraded product will decrease the height and area of the detected rifampicin peak as a quantity of the rifampicin in the solution will be transformed into 3FRSV. Due to the difference in the molar absorptivity between rifampicin and 3FRSV at 475 nm, the total amount of

rifampicin was determined by adding both AUCs after deriving a correlation factor. The factor calculated from the AUCs data at various time intervals was reported previously by (Agrawal and Panchagnula, 2004).

Three concentrations of rifampicin standard (20.0 µg/ml, 30.0 µg/ml, and 50.0 µg/ml) were kept under the circumstances comparable to those in which dendrimer drug release studies would be conducted (i.e. PBS pH 7.4 and acetate buffer pH 4.5 spiked with ascorbic acid, maintained at 37 °C at 100 rpm). At various periods, samples were withdrawn, filtered by a 0.45 µm nylon syringe filter, and analyzed using the described RP-HPLC method. Results were interpreted to evaluate rifampicin stability in both release medium within the time frame of drug release studies.

5.5.3 *In-Vitro* drug release

Release studies of rifampicin loaded in surface-modified and unmodified G4-PAMAM dendrimers in PBS pH 7.4 and acetate buffer pH 4.5 were performed using the dialysis bag technique (Kojima *et al.*, 2000; Pan *et al.*, 2005; Kumar *et al.*, 2013).

Scheme 1 illustrates dialysis tubes (12-14 kDa MWCO) being filled with a known quantity of 0.1% w/v rifampicin-loaded dendrimer formulations. After which the loaded samples were placed in a beaker holding 100 ml of release medium spiked with ascorbic acid, and incubated at 37 °C ± 0.5 °C in an orbital shaker incubator ES-80 with slow agitation (100 rpm) over 72 hrs. At set time points (30 mins, 2.5 hrs, 4hrs, 6 hrs, 9 hrs, 11 hrs, 24 hrs, 48 hrs, and 72 hrs), aliquots of one millilitre were withdrawn from the external solutions, and subsequently, an equal volume of fresh release medium incubated at similar conditions was refilled. The concentration for each sample was determined in triplicate using a validated HPLC method on the Agilent 1200 HPLC system at 475 nm wavelength. Rifampicin release was expressed as a fraction of the amount of rifampicin encapsulated in a specified dendrimer formulation — i.e. the release profile generated by plotting the cumulative percentage release of rifampicin against time.

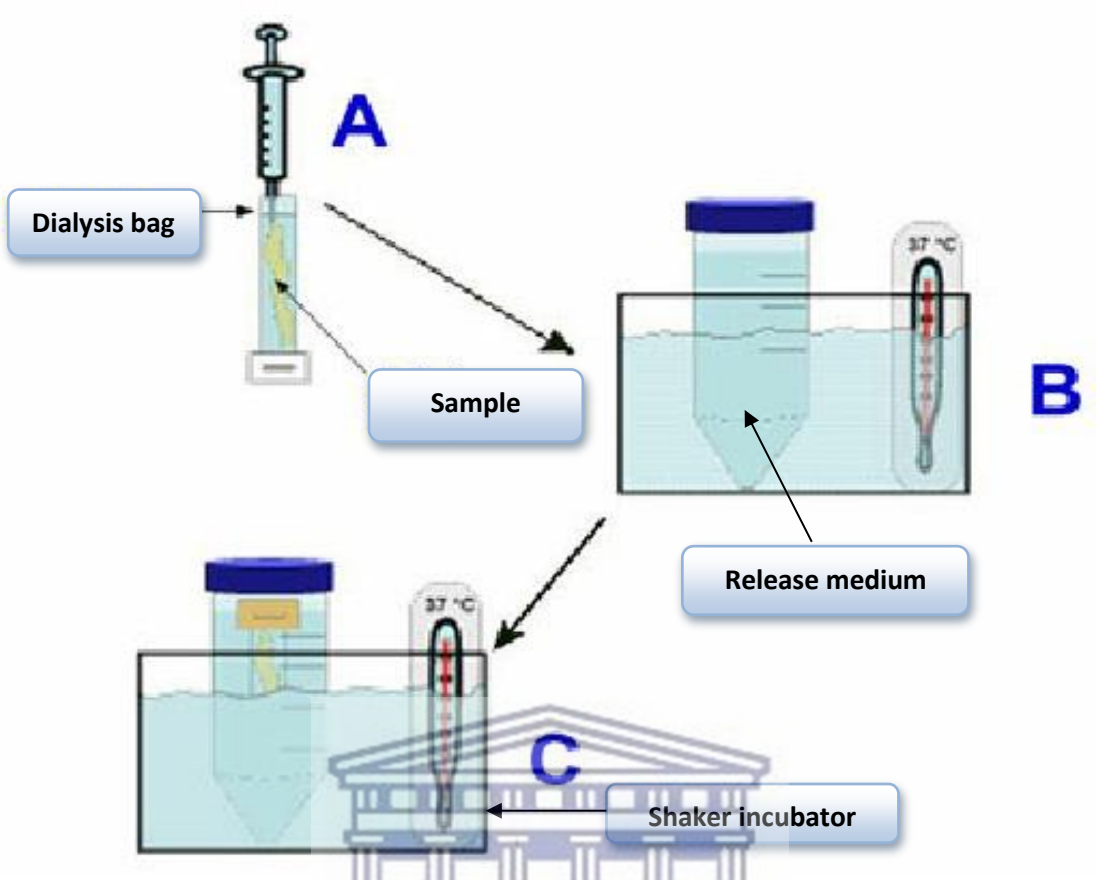

Scheme 1. *In vitro* drug release via dialysis bag technique.

5.5.4 Mathematical modelling of drug release data

Drug release kinetics from dendrimer formulations were described by determining the best mathematical model using DDSolver software (Microsoft Excel add-in program) (Zhang *et al.*, 2010) for linear regression analysis. The release data were fitted to the commonly used kinetic equations, such as zero-order (Equation 5.1), first-order (Equation 5.2), Higuchi (Equation 5.3), Peppas-Sahlin (Equation 5.4), Korsmeyer-Peppas (Equation 5.5), and Weibull (Equation 5.6) mathematical models (Costa and Lobo, 2001; Dash *et al.*, 2010; Reddy *et al.*, 2014).

From the regression analysis, the correlation coefficient of determination (R^2) and the adjusted coefficient of determination (R^2_{adj}) was used as the basis for selecting the best mathematical model. The model possessing the maximum R^2_{adj} was chosen as the best-fitting model.

5.6 Data analysis

The data were interpreted using GraphPad® Prism 7.04 and expressed as the mean ± standard deviation. One-way and two-way ANOVA tests were applied to set up the significance of any differences between means. Values were considered significant if the *p*-value was ≤ 0.05.

5.7 Results and Discussion

5.7.1 Validation of RP-HPLC method for rifampicin determination in PBS pH 7.4 and acetate buffer solution pH 4.5

The linearity of the HPLC method was determined by analyzing a range of rifampicin standards 0.5 – 50.0 µg/ml for PBS and 0.1 – 50.0 µg/ml for acetate buffer pH 4.5, at an absorbance wavelength of 475 nm. Linear regression analysis was applied to assess the correlation between rifampicin absorbance and concentration. A plot of average rifampicin absorbance versus its concentration was generated as illustrated in Figure 5.4. This relationship model creates a basis for the prediction of rifampicin concentration by measuring sample absorbance.

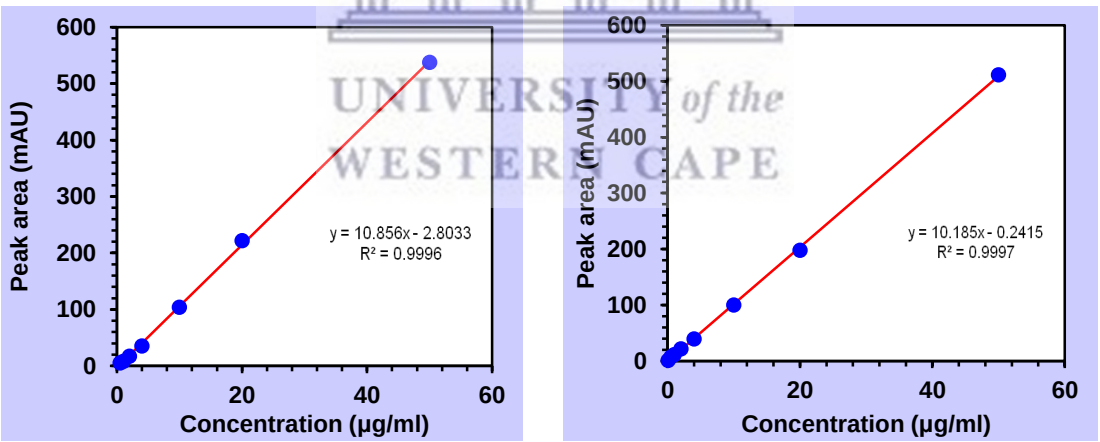

(A) **(B)**

Figure 5.4 Rifampicin calibration curves at a wavelength of 475 nm. (A) in PBS spiked with ascorbic acid 200 µg/ml, and (B) in acetate buffer pH 4.5 spiked with ascorbic acid 50 µg/ml.

The linear regression equations were, y = 10.856x – 2.8033, with correlation coefficient r^2 = 0.9996, and y = 10.185x – 0.2415, with correlation coefficient r^2 = 0.9997, at pH

7.4 and 4.5, respectively. Both generated equations exhibit a strong association between rifampicin concentration and its absorbance. Where x is rifampicin concentration in µg/ml and y is the absorbance peak area in mAU.

The sensitivity of the method was assessed at both pH values by calculating LOD and LOQ values. Results showed that the techniques were sensitive, where LOD values were 0.64 µg/ml and 0.41 µg/ml, whereas the LOQ values were 1.94 µg/ml and 1.26 µg/ml at pH 7.4 and pH 4.5, respectively (Table 5.2).

Table 5.2 Summary of the linearity data of rifampicin (λ_{max} = 475 nm) at pH 7.5 and pH 4.5.

Validation parameters	**pH 7.4**	**pH 4.5**
r^2	0.9996	0.9997
Slope ± SD	10.86 ± 0.10	10.19 ± 0.07
Intercept ± SD	-2.80 ± 2.11	-0.24 ± 1.28
Concentration range (µg/ml)	0.50 – 50.0	0.10 – 50.0
LOD ± SD (µg/ml)	0.64 ± 0.02	0.41 ± 0.01
LOQ ± SD (µg/ml)	1.94 ± 0.09	1.26 ± 0.02

Inter-day (intermediate precision) and intra-day (repeatability) precision of the HPLC method were evaluated by analysing of three rifampicin standards (i.e., 2.0 µg/ml, 10.0 µg/ml, and 20.0 µg/ml). As shown in Table 5.3, intermediate precision and repeatability of the method were expressed as % RSD. For pH 7.4 and pH 4.5, the degree of scattering was less than 2% for repeatability and intermediate precision, this finding suggested that the method is reproducible (ICH, 2005; Shabir, 2006).

For accuracy, the method was assessed using recovery study techniques. Three selected rifampicin standards (i.e., 2.0 µg/ml, 10.0 µg/ml, and 20.0 µg/ml) were triplicated and analyzed at λ_{max} 475 nm. Results are expressed as a percentage of the mean concentration calculated to the theoretical concentration injected. In Table 5.3, the determined percentage recoveries were within the range of 91% - 105%, which proves

the accuracy of the method as the acceptance criteria for non-regulated products should be within 90% - 110% (Shabir, 2006).

Table 5.3 Intra-day and inter-day precision and accuracy of rifampicin (λ_{max} = 475 nm) at pH 7.4 and 4.5.

	pH 7.4			**pH 4.5**		
Rifampicin (µg/ml)	2.0	10.0	20.0	2.0	10.0	20.0
			Intra-day (n = 3)			
Mean absorbance	17.52	102.34	220.65	17.25	110.50	224.03
SD	0.30	1.14	2.90	0.15	2.10	1.74
RSD	1.72	1.11	1.30	0.87	1.90	0.78
Mean determined Conc. (µg/ml)	1.87	9.69	20.60	1.85	10.44	20.90
% Recovery	93.60	96.91	102.94	92.42	104.41	104.54
			Inter-day (n = 3)			
Mean absorbance	17.79	101.68	219.83	17.08	103.76	221.53
SD	0.30	1.80	3.83	0.32	1.55	3.22
RSD	1.69	1.77	1.74	1.89	1.49	1.45
Mean determined Conc. (µg/ml)	1.90	9.62	20.51	1.83	9.82	20.66
% Recovery	94.84	96.22	102.50	91.63	98.22	103.31

Analysis of unloaded dendrimer, the mobile phase, PBS, and acetate buffer did not exhibit any interference with the rifampicin elution peak (~ 2.9 mins) (Figure 5.5) which proposed the suitability of the method for rifampicin.

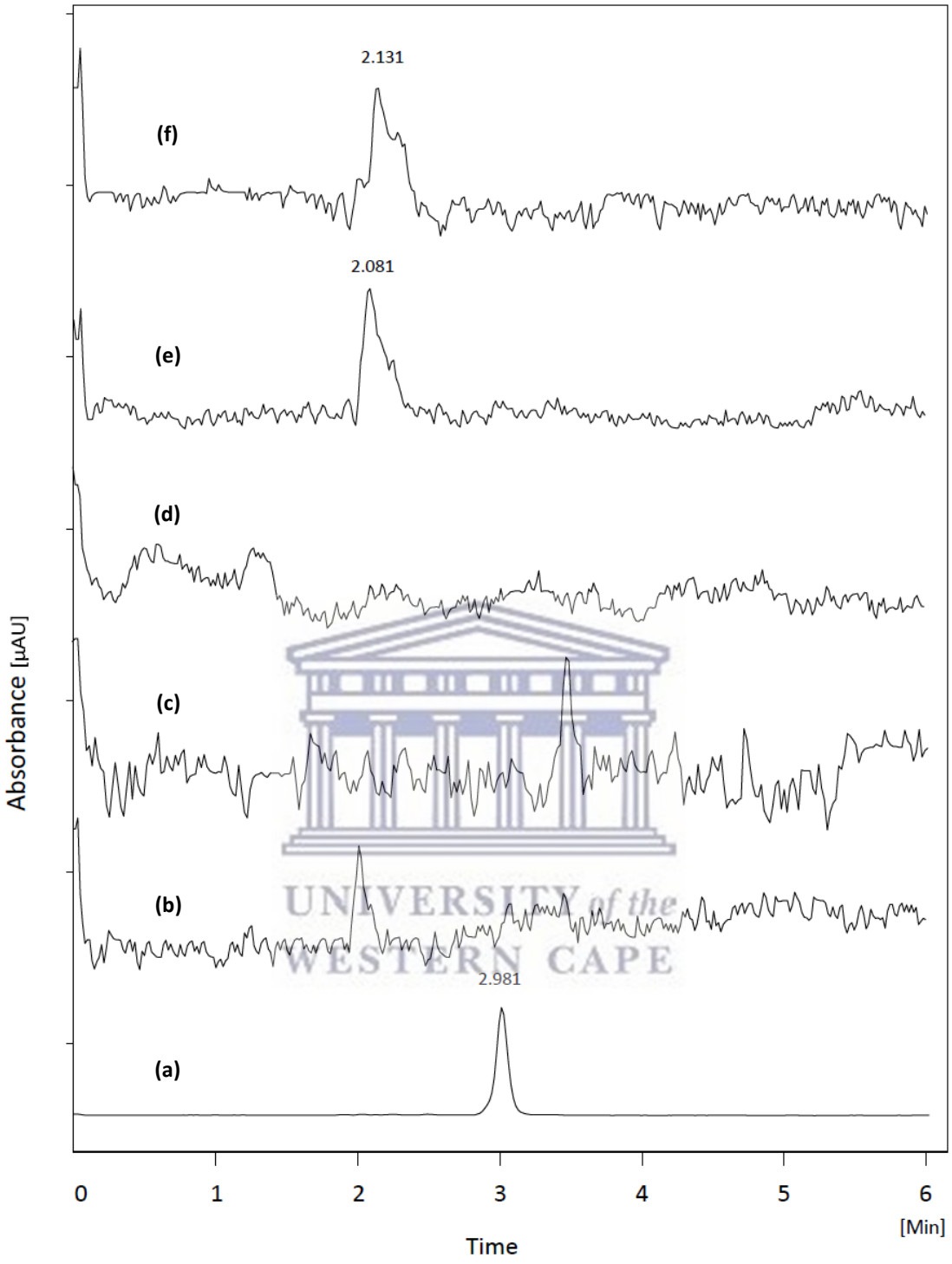

Figure 5.5 Chromatograms of **(a)** standard rifampicin, **(b)** unloaded PEGylated dendrimer, **(c)** unloaded mannosylated dendrimer, **(d)** the mobile phase, **(e)** PBS (spiked with ascorbic acid), and **(f)** acetate buffer pH 4.5 (spiked with ascorbic acid).

Furthermore, rifampicin was placed in 0.1 M NaOH and 0.1 M HCl to ensure its specificity with regards to its degradants. The degraded sample showed lower rifampicin peak height and area relative to the non-degraded sample due to a decrease

in rifampicin concentration as a result of degradation in acidic and basic mediums. Figures 5.6 and 5.7 comparing the chromatogram of the non-degraded rifampicin sample to that of alkaline and acidic force degraded rifampicin in the mobile phase, PBS, and the acetate buffer solution. Results indicated the specificity of the HPLC method to detect rifampicin even when degraded in acidic or basic media.

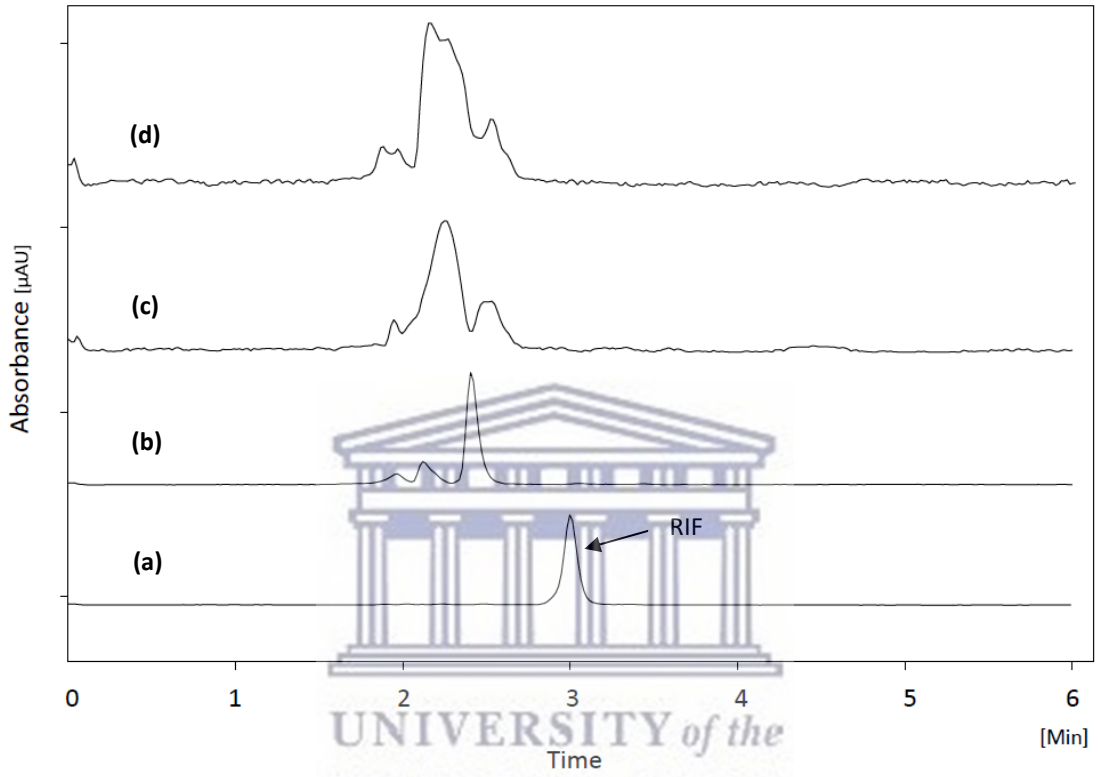

Figure 5.6 HPLC chromatograms of **(a)** non-degraded rifampicin standard, alkaline force degraded (0.1 M NaOH) of rifampicin in **(b)** the mobile phase, **(c)** PBS, and **(d)** acetate buffer pH 4.5.

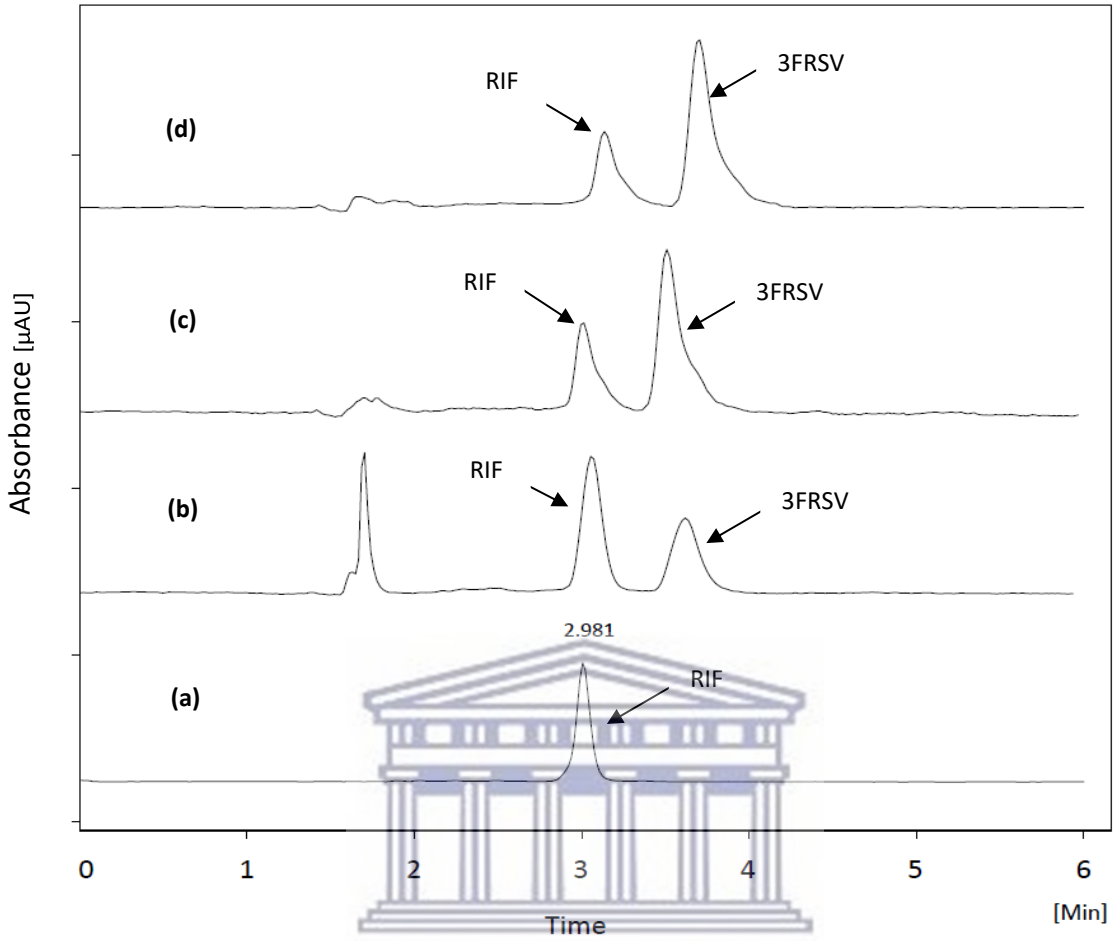

Figure 5.7 HPLC chromatograms of **(a)** non-degraded rifampicin standard, acidic force degraded (0.1 M HCL) of rifampicin in **(b)** the mobile phase, **(c)** PBS, and **(d)** acetate buffer pH 4.5.

5.7.2 Stability of rifampicin in the release medium within the release studies time-frame

5.7.2.1 Stability in PBS within the release study time-frame

As previously reported, rifampicin experienced oxidative degradation in aqueous solutions to form ineffectual rifampicin quinone (Figure 5.8) (Sorokoumova *et al.*, 2008). PBS spiked with antioxidant ascorbic acid (200 µg/ml) was used to enhance the stability of rifampicin by preventing the formation of rifampicin quinone as achieved by Kumar et al. and Samkange (Kumar *et al.*, 2006; Samkange, 2019).

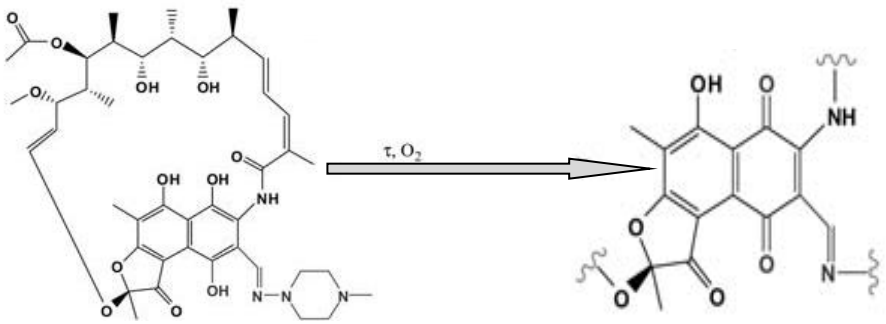

Rifampicin Rifampicin quinone

Figure 5.8 Rifamapicin oxidative decomposition pathway (Sorokoumova *et al.*, 2008).

Three rifampicin standards (20.0 µg/ml, 30.0 µg/ml, and 50.0 µg/ml) were selected based on the amount of the drug encapsulated per 1 mg of nanoparticle as calculated in Chapters 3 and 4. After incubation in conditions similar to those under which the dendrimer drug release was studied, samples were withdrawn, analyzed, and % RSD of mean absorbance readings achieved after 30 mins, 2.5 hrs, 4hr, 6 hrs, 9 hrs, 11 hrs, 24 hrs, 48 hrs, and 72 hrs were calculated. Results indicated RSD values of 1.65%, 1.87%, and 2.06% for 20 µg/ml, 30 µg/ml and 50 µg/ml rifampicin standards respectively. These findings are in line with the acceptance criteria of assay variations (Shabir, 2006).

The results verified the stability of rifampicin in PBS fortified with ascorbic acid throughout the 72 hr duration of the study as the % RSD showed no extreme variation in absorbance of samples for the selected rifampicin concentrations. Since adding ascorbic acid enhanced the stability of rifampicin in PBS solution, this will ensure the ability for consistent and reproducible release data throughout the study. Many authors identified the anti-oxidant potential of ascorbic acid towards rifampicin in *in-vitro* release studies similar to those observed in this study (Kumar *et al.*, 2006; Vijayaraj Kumar *et al.*, 2007; Rajaram, Vemuri and Natham, 2014).

5.7.2.2 Stability in acetate buffer pH 4.5 within the release study time-frame

Rifampicin suffers from rapid hydrolysis in acidic medium to form 3-formylrifamycin SV (Figure 5.9) (Gharbo, Cognion, and Williamson, 1989; Jindal *et al.*, 1994; Shishoo *et al.*, 1999), which will decrease rifampicin AUC and miscalculate the amount released. Acetate buffer spiked with ascorbic acid 50 µg/ml was used to enhance the

stability by reducing the formation of 3FRSV as recommended by Rajaram et al., (Rajaram, Vemuri and Natham, 2014).

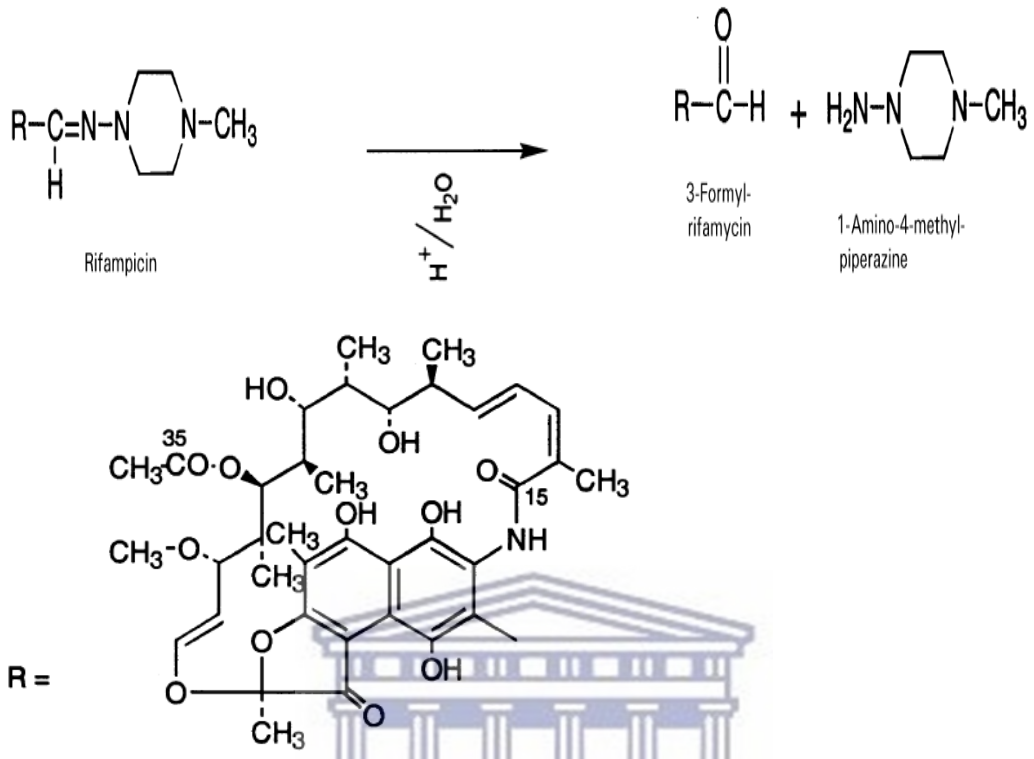

Figure 5.9 Pathway of rifampicin degradation in acidic medium adapted from (Singh *et al.*, 2000).

According to the degradation pathway of rifampicin in acidic medium (Figure 5.9), a second peak at 3.4 - 3.5 mins (Figure 5.7) is detected and attributed to 3FRSV formation. As illustrated in Table 5.4, the AUC value of 3FRSV was continually increasing as a function of time, alongside decreasing in rifampicin AUC values. It was also observed that rifampicin degraded by 51.60% in 72hrs while the emerged 3FRSV AUC represents only 27.70% of this degradation. Furthermore, the addition of rifampicin and 3FRSV AUCs shows a 23.92% decrease in 72 hrs. It was signified that for the applied HPLC method and at 475 nm wavelength, 3FRSV has less molar absorptivity than rifampicin and consequently the sum of both AUCs will not show the correct amount of rifampicin. A correlation between rifampicin and 3FRSV was derived to estimate the right total amount in acidic medium, by calculating the decrease of rifampicin AUC as a function of time relative to its initial AUC. At time zero, a small AUC of 3FRSV was detected, which may have formed during sample preparation and

injection, and hence the increase in 3FRSV AUC relative to the initial injection was adjusted by subtracting the AUC value at time zero from each period.

Outcomes determined a constant correlation between the decrease in the rifampicin AUC and the corrected 3FRSV AUC at each time stage with a mean value of 1.88. This technique was also applied for the rifampicin concentrations 10.0 μg/ml and 30.0 μg/ml (10.0 μg/ml, 20.0 μg/ml, and 30.0 μg/ml represent the range of rifampicin concentration in nanoformulations) at a similar time-frame. Equivalent values of the correlation factor for 10.0 μg/ml and 30.0 μg/ml standard solutions were also observed, i.e., 1.88. Accordingly, that value will be employed later to calculate the correct concentration of rifampicin released in the acetate buffer solution (pH 4.5), where a fraction of it is converted to 3FRSV, by using the created equation 5.9:

$$\text{Total RIF} = \text{RIF} + (1.88 \times \text{3FRSV}) \qquad \textbf{Equation 5.9}$$

Table 5.4 Developing a correlation between rifampicin (20.0 μg/ml) and 3FRSV using AUCs value as a function of time, in acetate buffer pH 4.5 at 37 °C under continuous stirring at 100 rpm (n = 3).

TIME	AUC (mAU)						
	RIF	Decrease in RIF	3FRSV	Corrected 3FRSV	DEC RIF/ corr 3FRSV	Total RIF by a factor	Sum RIF & 3FRSV
0	222.50	0	0.04	0	-	222.58	222.54
15 mins	214.30	8.20	4.44	4.40	1.86	222.65	218.74
30 mins	212.50	10.00	5.30	5.26	1.90	222.46	217.80
1 hr	202.40	20.10	11.10	11.06	1.82	223.27	213.50
3 hrs	197.20	25.30	13.33	13.29	1.90	222.26	210.53
4 hrs	186.95	35.55	18.97	18.93	1.88	222.61	205.92
6 hrs	183.81	38.69	20.39	20.35	1.90	222.14	204.20
24 hrs	131.60	90.90	49.60	49.56	1.83	224.85	181.20
48 hrs	117.51	104.99	54.40	54.36	1.93	219.78	171.91
72 hrs	107.66	114.84	61.62	61.58	1.86	223.51	169.28

At any point, the total rifampicin (20.0 µg/ml) calculated using equation 5.9 was approximately constant with an average AUC value of 222.61 and RSD of 0.57%. In parallel, total rifampicin at each instance was determined by adding rifampicin and 3FRSV AUCs as presented in the last column of Table 5.4. It was observed from Figure 5.10, the consistency of the total rifampicin AUC over the study period regardless of the degradation when using the generated equation 5.9, whereas adding rifampicin and 3FRSV AUCs showed decreasing as a function of the time. These findings suggested the suitability of the developed method to assess rifampicin in acetate buffer within the time-frame of the study.

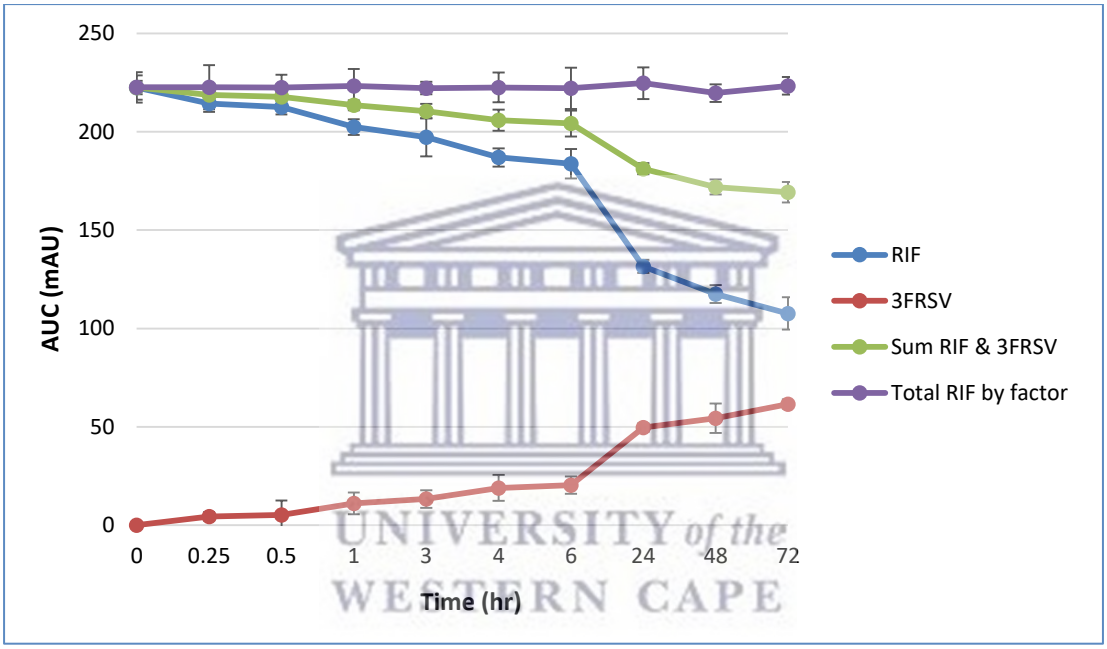

Figure 5.10 Rifampicin (20.0 µg/ml) degradation in acetate buffer pH 4.5, and comparison between using the derived correlation factor and sum of RIF and 3FRSV AUCs.

5.7.3 *In vitro* release of rifampicin from 4.0 G PAMAM dendrimer having different PEG content

A comparative evaluation of the effect of PEGylation on the release behaviour of rifampicin from 4.0 G PAMAM dendrimer was carried out at pH 7.4 and pH 4.5, i.e., simulated physiological pH of the cytoplasmic medium within the macrophage cells and acidic pH of endosomal alveolar macrophage, correspondingly. Drug release was assessed using the dialysis bag technique and to overcome the impact of the membrane on the diffusion process 12-14 kDa MWCO dialysis tubes were used in both release

media as recommended previously by Yuan Gao and co-authors (Gao *et al.*, 2013). The selected pore size of the dialysis tubes was confirmed to pass freely 50% of the dissolved rifampicin molecules across the membrane within 13 - 16 minutes at pH 7.4 and pH 4.0 (Gao *et al.*, 2013). Drug release profiles were generated by plotting the percentage of encapsulated rifampicin released for each formulation as a function of time, as shown in Figures 5.11 and 5.12.

The nano-formulations exhibited a bi-phasic release that was characterized by an initial burst release followed by a plateau phase with sustained-release in both release mediums. Among the six dendrimer formulations, PEGylated nanoparticles showed a slower release rate in comparison to the non-PEGylayed formulation.

5.7.3.1 Release in PBS medium

The overall release data in PBS indicated a negative relationship between the degree of dendrimer PEGylation and the % of rifampicin released at observed time points 11 hrs, 24hrs, 48 hrs, and 72 hrs (Table 5.5 and Figure 5.11). Moreover, the one-way ANOVA coefficient of determination (r^2) for the observed time points ranged between 0.9291 - 0.9934 which suggested a strong association between the degree of PEGylation and the amount of drug released particularly at time points 24 hrs and 48 hrs. About 54% - 88%

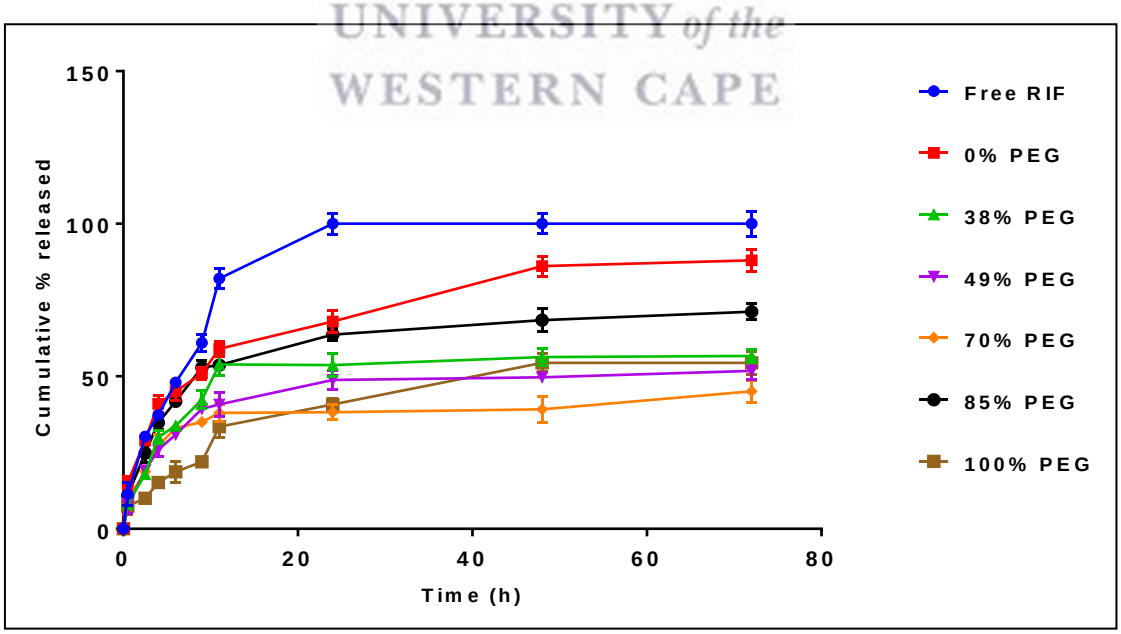

Figure 5.11 *In vitro* release profiles of rifampicin from 4.0 G PAMAM dendrimer having different PEG content, incubated in PBS pH 7.4 spiked with ascorbic acid 200 µg/ml at 37 °C under continuous stirring at 100 rpm (n = 3).

of the drug was released by 72 hrs (Table 5.5). At the time point of 11 hrs, as the degree of dendrimer PEGylation increased, there was a significant decrease in the % of rifampicin released ($p < 0.05$). The exception of that order is 38% PEG and 85% PEG formulations, which did not exhibit a significant difference to the non-PEGylated dendrimer ($p > 0.05$).

By 24 hrs, drug release was inversely proportional to the degree of dendrimer PEGylation except for 85% PEG formulation which displayed statistical insignificance to the non-PEGylated formulation. It was noticed that lower PEGylated dendrimer, i.e., 38% PEG and 49%, have comparable release pattern ($p > 0.05$), the same case was also observed for the higher PEGylated dendrimers (i.e., 70% PEG and 100% PEG). Therefore, we can conclude that until 24 hrs of release study, the lower PEGylated dendrimers behave similarly, as well as for dendrimers having a higher PEG content.

Table 5.5 Comparison of the effect of dendrimer PEG content on rifampicin release after 11 hrs, 24 hrs, 48 hrs, and 72 hrs of incubation in PBS 7.4 fortified with ascorbic acid at 37 °C under continuous stirring of 100 rpm.

Formulation	Release after 11 hr		Release after 24 hr		Release after 48 hr		Release after 72 hr	
	% RIF released	Effect of PEGylation	% RIF released	Effect of PEGylation	% RIF released	Effect of PEGylation	% RIF released	Effect of PEGylation
Free RIF	82 ± 3.35	Decrease in release % as PEG content increased $R^2 = 0.9291$	100 ± 3.45	Decrease in release % as PEG content increased $R^2 = 0.9701$	100 ± 3.25	Decrease in release % as PEG content increased $R^2 = 0.9901$	100 ± 4.1	Decrease in release % as PEG content increased $R^2 = 0.9934$
0 % PEG	59 ± 2.52		68 ± 3.6		86.1 ± 3.33		88 ± 3.55	
38% PEG	53.9 ± 3.73		53.7 ± 3.67		56.3 ± 2.92		56.7 ± 2.18	
49% PEG	40.8 ± 3.8		48.8 ± 3.1		49.7 ± 1.6		51.8 ± 2.8	
70% PEG	38.04 ± 2.94		38.2 ± 2.41		39.2 ± 4.31		45.1 ± 3.65	
85% PEG	53.7 ± 1.11		63.7 ± 2.02		68.4 ± 3.73		71.2 ± 2.67	
100% PEG	33.5 ± 3.66		40.8 ± 1.98		54.4 ± 2.99		54.4 ± 3.86	

*Release % is stated as mean ± SD (n = 3). Trend outliers are highlighted in red.

Beyond 24 hrs, all PEGylated formulations (except 85% PEG) are characterized by a significantly lower fraction of drug released compared to non-PEGylated dendrimer ($p < 0.05$). Among PEGylated formulations, the release was inversely related to the extent of dendrimer PEGylation. From the data analysis at the 72 hrs time point, no statistical

difference ($p > 0.05$) in the cumulative percentage released of rifampicin had been observed between 38% PEG, 49% PEG, and 100% PEG.

Rifampicin is a hydrophobic chemical entity (Williams and Piddock, 1998) with an isoelectric point of about 7.11 (Khan *et al.*, 2017) and pKa of 1.7 and 7.9 (Kumar *et al.*, 2006). According to the previous discussion in the literature, rifampicin molecules are likely to be encapsulated into the hydrophobic PAMAM dendrimer core more than on the surface amines (Bellini *et al.*, 2015; Dineshkumar *et al.*, 2017). In addition, the internal tertiary amines are strongly basic with pKa of 9.5 (Asthana *et al.*, 2005), which will direct deprotonation of rifampicin molecules to form quaternary nitrogens. These quaternized nitrogens are expected to trap counter ions, such as carboxylate ions, and therefore manage their dissociation and delay the release.

A significant increase in the percentage drug loading (DL%) was observed with PEGylated dendrimer as illustrated in Chapter 3 and reported earlier by Pan *et al.*, and Kojima *et al.*, (Kojima *et al.*, 2000; Pan *et al.*, 2005). These findings proposed that besides the internal incorporation of drug molecules, a fraction of the drug may perhaps be distributed within the PEG layers, which act as a solubilizer, and increases the overall amount loaded. Furthermore, the 2D NOESY results in Chapter 3 for rifampicin loaded PEGylated PAMAM dendrimers indicated that rifampicin molecules were dually interacted with the dendrimer in the interior shell and at the peripheral PEG chains. Therefore, rifampicin molecules are expected to conjugate to the dendrimer at three sections, the majority of molecules would have encapsulated within the dendrimer cavities, in addition to the electrostatic attachment to the positively charged surface amines and incorporation into PEG chains. Considering this aspect will help to understand how the drug is released from the dendrimer formulations.

The initial burst release from nano-formulations was observed up to 11 hrs for all formulations and is often due to the dissemination of drug molecules from the peripheral surface, including those incorporated within the PEG chains along with those electrostatically attached to the surface amine. Furthermore, drug diffusion from the inner cavities might contribute to the burst phase, which was noticed in the release profile of the non-PEGylated dendrimer. About 30% - 49% of the initial burst release took place after 2.5 hrs of release. Results signified a negative relationship between the percentage released and the degree of dendrimer PEGylation which is probably due to

the effect of the dense and thick outer surface produced by PEG chains around the dendrimer (Pan *et al.*, 2005) that delay drug diffusion from the interior toward the exterior. Also, back folding and self-penetration of long PEG chains, i.e., 2000 Da, inside the dendrimer cavities can be attributed to this behaviour as discussed earlier by molecular dynamic simulation reports (Yang and Da Rocha, 2014; Diaz *et al.*, 2018) that might stabilize the RIF complexes and delay the release. These two factors play an important role in delaying drug diffusion from the inner cavities. On the other hand, the physical hindrance generated by the PEG layers was not observed with the release from the 38% PEG dendrimer being 53.9% ± 3.73% compared to the non-PEGylated dendrimer being 59% ± 2.52% ($p > 0.05$). This might be due to the lower PEG content influencing the drug release or due to the possibility of the drug being conjugated peripherally via electrostatic connections with primary amines (38% PEG has the highest free primary amines) (Asthana *et al.*, 2005). The peripheral conjugations librate drug molecules at a quicker rate compared to those loaded within the internal cavities.

After 11 hrs of drug release, dendrimer formulations experienced a plateau phase and displayed a sustained drug release. The principal activity in this phase is the diffusion process of drug molecules from the dendrimer core to the release medium in a sustained manner (Shetab Boushehri and Lamprecht, 2015). The presence of dense/thick layers of PEG on the dendrimer surface decreases the diffusion rate of the drug from the interior. Increasing the degree of dendrimer surface PEGylation, i.e., increasing the thickness of the PEG layers, lead to slowing down the diffusion rate and the exit of drug molecules from dendrimer cavities. Among PEGylated dendrimers, a lower rate of drug release was linked to formulations that had higher PEG content. The exception of the trend was observed with the 85% PEG formulation at all time points. It can be surmised that the superior release rate is due to the rifampicin molecules being incorporated within the PEG chains at a high percentage comparative to interior encapsulation due to the thick or dense surface that acts as a physical barrier for rifampicin into the dendrimer cavities, as illustrated earlier (Barraza, Jiménez and Alderete, 2015). A study performed by Barraza and co-workers (2015), using molecular dynamics simulations to evaluate the effect of PEGylation of G4 PAMAM dendrimer on the DL% of 5-Fluorouracil (Barraza, Jiménez and Alderete, 2015). Barraza and co-workers noticed that increasing the degree of surface PEGylation will significantly enhance the amount of drug-loaded. 5-Fluorouracil molecules were observed at the inner cavities of the

dendrimer, as well as, at the peripheral PEG chain. Increasing the concentration of PEG chains was noticed to decrease the amount of the drug-loaded inside the dendrimer's cavities due to the generated steric hindrance, whereas the amount conjugated to the outer PEG layers was significantly increased.

During the nanoparticle-drug loading procedure of 85% PEG formulation, some of the rifampicin molecules have negative charges that facilitate electrostatic interaction with the remaining positively charged surface amine of the dendrimer. Therefore, a high percentage of the drug was expected to be peripherally conjugated, which facilitates rapid liberation and a faster release profile. While in other formulations, the majority of rifampicin molecules expected to be encapsulated in the internal core had to travel from the inner core through small channels and diffuse across PEG layers to be available in the exterior medium.

The 70% PEG formulation had the slowest release profile among the PEGylated and non-PEGylated formulations, the rationale was as a result of the extent of surface PEGylation that was not a lot to hinder drug encapsulation within the dendrimer and offered the possibility of surface electrostatic attachment for some drug molecules. During the release process, drug molecules were extensively influenced in their diffusion rate due to the high PEG layer relative to the dendrimer with lower PEG content.

It was observed that at 48 hrs and 72 hrs, the 100% PEG formulation demonstrated a release behaviour close to that of the 38% and 49% PEG formulations, the possibility of high inclusion within PEG chains and lacking electrostatic interaction due to complete PEGylation will enhance some of the drug molecules to be encapsulated inside dendrimer cavities. The low release from the interior due to the dense surface might be responsible for that release profile generated. Pan and co-worker (2005) synthesized methotrexate loaded in 3.0 G PAMAM dendrimer containing various PEG content. They also noticed that after a long period of release, PEGylated dendrimer formulations showed very similar drug release behaviour and the significant difference was only evident in the first 24 hrs of the release study (Pan *et al.*, 2005).

5.7.3.2 Release in acetate medium pH 4.5

Drug release from dendrimer formulations was assessed at pH 4.5, which mimics the phagolysosomal pH within the alveolar macrophages. Evaluating the release at this pH will provide information about how much and for how long the drug will be liberated from dendrimer and become available to kill mycobacterium bacilli.

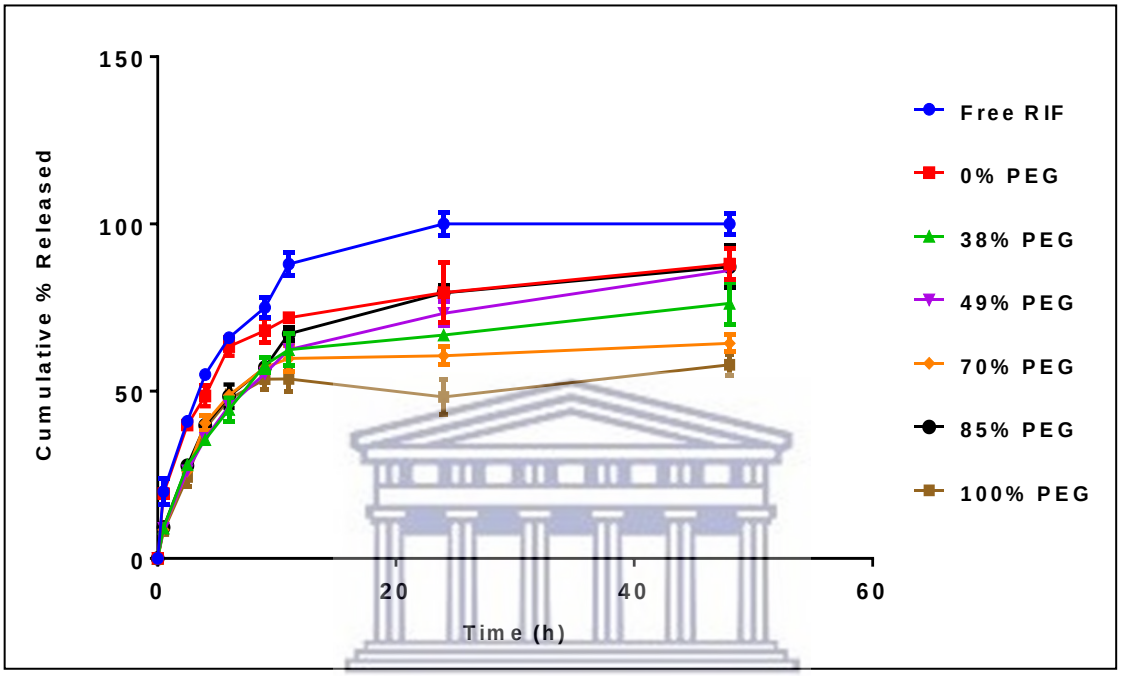

Figure 5.12 *In vitro* release profiles of rifampicin from 4.0 G PAMAM dendrimer having different PEG content, incubated in acetate medium pH 4.5 spiked with ascorbic acid 50 µg/ml at 37 °C under continuous stirring at 100 rpm (n = 3).

The release of rifampicin from dendrimer formulations showed bi-phasic release profiles (Figure 5.12), characterized by an initial burst release followed by a plateaued phase. At observed time points, i.e., 6 hrs, 11 hrs, 24 hrs, and 48 hrs, the one-way ANOVA coefficient of determination (r^2) was 0.9039, 0.9343, 0.9813, and 0.9537, respectively (Table 5.6). The calculated (r^2) for dendrimer formulations indicated a strong relationship between the degree of PEGylation and the percentage of rifampicin released, typically after 11 hrs of release. About 58% - 88% was released from the dendrimers after 48 hrs (Table 5.6).

At the time point 6 hrs, release data displayed a significant difference in the percentage of drug released between PEGylated formulations and non-PEGylated dendrimer ($p < 0.05$). PEGylated dendrimers were characterized by a slower release rate of rifampicin

compared to the non-PEGylated dendrimer. Among PEGylated dendrimers, no difference in the release behaviour was detected ($p > 0.05$).

At time point 11 hrs, the fraction of drug released from PEGylated dendrimers was significantly lower than that released from non-PEGylated dendrimer ($p < 0.05$). Among PEGylated dendrimers, the fraction released was inversely proportional to the extent of dendrimer PEGylation (except 85% PEG). A lower percentage of drug released was observed with dendrimer having high PEG content.

Beyond 11 hrs of release study, the release was vitally linked to the extent of dendrimer PEGylation; the r^2 values were 0.9813 and 0.9537 for the time points 24 hr and 48 hr respectively, suggesting a strong correlation between the extent of dendrimer PEGylation and the percentage of drug released. PEGylated dendrimers significantly released rifampicin less than the non-PEGylated dendrimer ($p < 0.05$). The only exception of this trend was noticed for 49% PEG and 85% PEG formulations ($p > 0.05$). Between PEGylated dendrimers, a lesser amount of drug released was observed with dendrimers having a high amount of PEG on the surface.

Table 5.6 Comparison of the effect of dendrimer PEG content on rifampicin release after 6 hrs, 11 hrs, 24 hrs, and 48 hrs of incubation in acetate buffer medium pH 4.5 fortified with ascorbic acid at 37 °C under continuous stirring of 100 rpm.

Formulations	Release after 6 hr		Release after 11 hr		Release after 24 hr		Release after 48 hr	
	% RIF released	Effect of PEGylation	% RIF released	Effect of PEGylation	% RIF released	Effect of PEGylation	% RIF released	Effect of PEGylation
Free RIF	66 ± 1.33	Decrease in release % as PEG content increased $R^2 = 0.9039$	88 ± 3.35	Decrease in release % as PEG content increased $R^2 = 0.9343$	99.67 ± 3.45	Decrease in release % as PEG content increased $R^2 = 0.9813$	100 ± 3.25	Decrease in release % as PEG content increased $R^2 = 0.9537$
0 % PEG	63.4 ± 2.77		72 ± 1.71		79.5 ± 8.9		88 ± 4.7	
38% PEG	44.6 ± 3.55		62.4 ± 4.84		66.8 ± 1.56		76.3 ± 6.3	
49% PEG	45.6 ± 1.62		62.4 ± 0.49		73.3 ± 3.5		86.1 ± 0.99	
70% PEG	48.8 ± 0.52		59.8 ± 3.94		60.6 ± 2.7		64.3 ± 2.58	
85% PEG	48.5 ± 3.5		67.2 ± 2.04		79.4 ± 2.2		87.2 ± 6.34	
100% PEG	47.6 ± 2.59		53.7 ± 3.8		48.3 ± 5.16		57.9 ± 3.04	

*Release % is stated as mean ± SD (n = 3). Trend outliers are highlighted in red.

PAMAM dendrimer belongs to an amino-terminated dendrimer group; these types of dendrimers exhibit extensive conformational change upon decreasing the solution pH (Boas and Heegaard, 2004). The reason behind that is due to electrostatic repulsion that arises between protonated tertiary amines in the interior as well as protonated primary amines on the surface of the dendrimer (Lee *et al.*, 2002). The repulsion forces change the conformational arrangement of a dendrimer to a hollow shell structure (Figure 5.13). This feature has been used as one of the techniques to deliver drug molecules depending on the different behaviour of dendrimers at various physiological pH values. For instance, drug release may occur as a result of conformational changes at low physiological pH (such as in alveolar macrophages) that trigger expelling of the loaded drug from an open structure dendrimer (Wang and Imae, 2004; Gupta, Agashe and Jain, 2007).

Rifampicin is a hydrophobic molecule (Williams and Piddock, 1998), the chemical structure consists of an aromatic ring system in addition to a long aliphatic bridge that contributes to its lipophilicity. At low pH, particularly less than 7, the molecule will be protonated and acquires positive charges (Khan *et al.*, 2017).

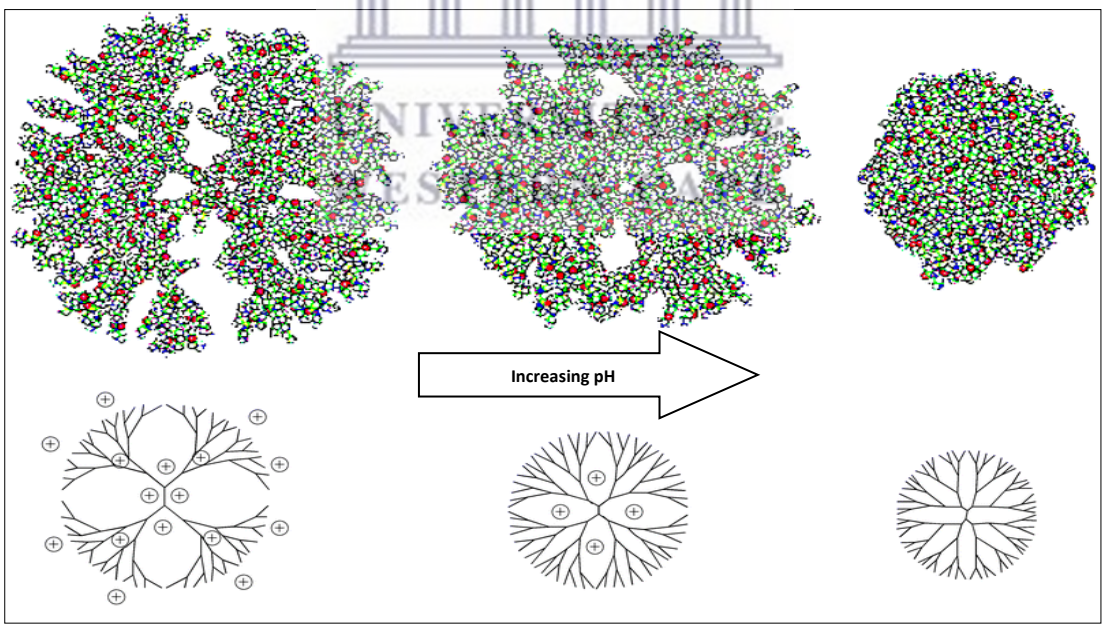

Figure 5.13 3-D and 2-D depictions for the effect of pH on the conformational change of amino-terminated dendrimers [adapted from (Boas and Heegaard, 2004)].

The initial burst phase took place after 11 hrs, and about 53% - 72% of the drug was discharged during this phase. Approximately 41.2% - 55% of the burst release occurred

at 2.5 hrs. A plateau phase was present until 48 hrs of the study and was characterized by a sustained release. Moreover, surface modification by PEG chains contributed to a slow drug release rate, hence leading to a greater extent of sustained-release behaviour.

The release in acetate medium was noticed to be higher than that in PBS, and the percentage of drug released in acetate medium up to 48 hrs was approximately equivalent to that released at 72 hrs in PBS (Tables 5.5 and 5.6). Two-way ANOVA indicated a significant difference in the amount released at all observed time points between PBS and acetate mediums ($p < 0.05$). The suggested justification for that is the possibility of conformational changes of PAMAM dendrimer at pH 4.5 as a result of amine protonation that triggers electrostatic repulsion between interior tertiary amines as well as between peripheral primary amines to form a hollow shell structure (Lee *et al.*, 2002) **(**Figure 5.13). The open-shell structure enhances drug discharge from the inner cavities to the outer media and raises the percentage released. These findings are in line with the previously reported molecular dynamic study of rifampicin loaded in 4.0 G PAMAM dendrimer done by Bellini and co-workers (Bellini *et al.*, 2015). The authors observed rapid and simultaneously force removal of rifampicin molecules from dendrimer cavities to solvent bulk at low pH.

Furthermore, rifampicin molecules at pH lower than 7 are expected to acquire positive charges (Khan *et al.*, 2017), which are believed to diffuse rapidly from the inner cavities due to electrostatic repulsion with positively charged amines. These two reasons are suggested as the driving force of enhanced release at acetate buffer. A comparable difference of *in vitro* rifampicin release data at pH 7.4 and pH 5 from mannosylated poly (propylene imine) 5.0 G dendrimer were reported earlier by Kumar and co-workers (Kumar *et al.*, 2006), authors detected a significant increase in the amount of rifampicin released at pH 5 medium relative to that at pH 7.4.

Drug release from PEGylated dendrimers was significantly less than that from the non-PEGylated dendrimer at time points 6 hrs, 11 hrs (except 85% PEG), 24 hrs (except 49% and 85% PEG), and 48 hrs (except 49% and 85% PEG). The rationale behind that is the existence of a thick layer of PEG around the dendrimer that slow down drug diffusion to the exterior. The diffusion rate was inversely proportional to the degree of dendrimer PEGylation; a lower rate was observed with dendrimer having high PEG content.

5.7.4 *In vitro* release of rifampicin from 4.0 G PAMAM dendrimer having different mannose content

A comparative analysis of the effect of surface mannosylation on the release behaviour of rifampicin from 4.0 G PAMAM dendrimer was performed at pH 7.4 and pH 4.5. Drug release was assessed using the dialysis bag technique and to overcome the impact of the membrane on the diffusion process 12-14 kDa MWCO dialysis tubes were used in both release media as recommended previously by Yuan Gao and co-authors (Gao *et al.*, 2013). Drug release profiles were generated by plotting the percentage of encapsulated rifampicin released for each formulation as a function of time, as shown in Figures 5.16 and 5.17.

5.7.4.1 Release in PBS medium pH 7.4

The nanoformulations showed a bi-phasic release manner in PBS, that characterized by an initial phase with burst release followed by a plateau phase with sustained-release (Figure 5.14).

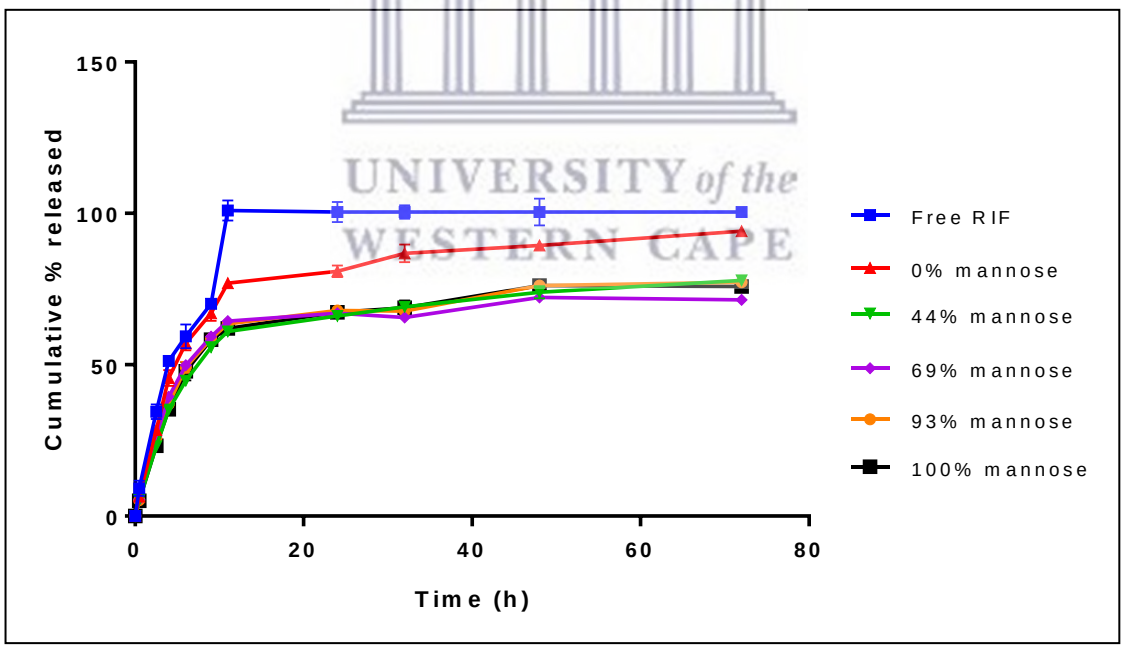

Figure 5.14 *In vitro* release profiles of rifampicin from 4.0 G PAMAM dendrimer having different mannose content, incubated in PBS pH 7.4 spiked with ascorbic acid 200 µg/ml at 37 °C under continuous stirring at 100 rpm (n = 3).

Mannosylated dendrimers exhibited lower release behaviour compared to that from the native dendrimer formulation and the free drug (Figure 5.14, Table 5.7). The one-way

ANOVA coefficient of determination (r^2) for the observed time points 11 hrs, 24 hrs, 48 hrs, and 72 hrs were 0.9943, 0.9949, 0.9738, and 0.9943, respectively. The r^2 values suggest a strong relationship between the extent of dendrimer mannosylation and the percentage of drug released especially at time points 11 hrs, 24 hrs, and 72 hrs.

At the time point 11 hrs, drug release is inversely proportional to the degree of dendrimer mannosylation, the only exception of that trend was observed for 44% mannose formulation (Table 5.7). Statistical analysis indicated that the mannosylated dendrimers exhibited a lower release rate compared to the native/unmodified (0% mannose) dendrimer ($p < 0.05$).

Similarly to that in the 11 hrs, at 24 hrs time point the mannosylated dendrimers release rifampicin at a lower rate compared to unmodified dendrimer formulation ($p < 0.05$). Among mannosylated dendrimers, drug release was approximately comparable, while statistical analysis indicated a significant difference in the release rate between them ($p < 0.05$).

Table 5.7 Comparison of the effect of dendrimer mannose content on rifampicin release after 12 hrs, 24 hrs, 48 hrs, and 72 hrs of incubation in acetate buffer medium pH 7.4 fortified with ascorbic acid at 37 °C under continuous stirring of 100 rpm.

Formulation	Release after 11 hrs		Release after 24 hrs		Release after 48 hrs		Release after 72 hrs	
	% RIF release	Effect of mannosylation	% RIF release	Effect of mannosylation	% RIF release	Effect of mannosylation	% RIF release	Effect of mannosylation
Free RIF	100.92 ± 3.38	Decrease in release % as mannose content increased $R^2 = 0.9943$	100.42 ± 3.29	Decrease in release % as mannose content increased $R^2 = 0.9949$	100.01 ± 4.47	Decrease in release % as mannose content increased $R^2 = 0.9738$	99.42 ± 0.57	Decrease in release % as mannose content increased $R^2 = 0.9943$
0 % mannose	76.95 ± 1.05		80.85 ± 1.97		89.39 ± 0.51		94.10 ± 1.16	
44% mannose	60.98 ± 0.43		66.07 ± 0.36		73.98 ± 2.07		77.87 ± 0.87	
69% mannose	64.46 ± 0.37		67.05 ± 0.17		72.26 ± 0.52		71.42 ± 0.31	
93% mannose	63.49 ± 0.28		67.88 ± 0.14		76.19 ± 1.05		77.28 ± 0.61	
100% mannose	62.00 ± 0.14		67.27 ± 0.25		76.16 ± 1.27		75.84 ± 0.18	

*****Release % is stated as mean ± SD (n = 3). Trend outliers are highlighted in red.

Beyond 24 hrs, also mannosylated dendrimers displayed a slower release rate compared to the unmodified dendrimer ($p < 0.05$). At 48 hrs time point, dendrimer formulations

with lesser mannose content (44% and 69% mannose) behave similarly ($p > 0.05$), while dendrimer formulations with the greater mannose content (93% and 100%) act in the same way ($p > 0.05$). At 72 hrs time point, the release pattern among the mannosylated dendrimers was inversely proportional to the degree of mannosylation ($p < 0.05$), except that trend was observed for 69% mannose.

As discussed earlier in this chapter that rifampicin is a hydrophobic molecule (Williams and Piddock, 1998) with an isoelectric point of 7.11 (Khan *et al.*, 2017). Accordingly, rifampicin molecules are expected to bind into the dendrimer hydrophobic core more than the peripheral amines (Bellini *et al.*, 2015; Dineshkumar *et al.*, 2017). In addition, the internal basic tertiary amines (pKa 9.5) of the dendrimer could interact with rifampicin molecules (pKa 1.7 and 7.9) after deprotonation and manage their dissociation (Asthana *et al.*, 2005; Kumar *et al.*, 2006). The 2D NOESY NMR results in chapter four have confirmed that rifampicin molecules were dually interacted with the dendrimer in the interior shell as well as at the peripheral mannose residues. Furthermore, rifampicin molecules were previously confirmed in this chapter to form electrostatic interactions with the positively charged surface amines. Therefore, rifampicin molecules are assumed to bind the mannosylated dendrimer at three sites, into the internal cavities, peripherally within the mannose residues, and with the positively charged surface amines.

The initial burst release of rifampicin molecules was noticed up to 11 hrs for the formulations under the study, which could be as a result of drug liberation from the mannose residues and those electrostatically attached to primary amines. As well, drug diffusion from the inner cavities might also contribute to the burst release, which was observed in the release profile of the unmodified dendrimer (0% mannose). About 29.5% - 37.0% of the initial burst release took place after 2.5 hrs of the study. The negative relationship between the percentage of drug release and the degree of dendrimer mannosylation is probably due to the dense mannose molecules at the periphery that form a closed structure that decreases the diffusion of encapsulated molecules.

After 11 hrs of release study, dendrimer formulations experienced a plateau phase with a sustained release manner. The expected release activity at this phase is the diffusion from the dendrimer interior to the outwards (Shetab Boushehri and Lamprecht, 2015).

At this phase, the mannosylated dendrimers are characterized by comparable release profiles, especially at 24 hrs time point. The similarity of the release pattern between 44% and 69% mannose formulations at 48 hrs could result from the fact that these nanoformulations hold the lesser mannose content which could not significantly affect the incorporation of rifampicin into the dendrimer interior. While, dendrimers that hold higher mannose content (93% and 100%) may possibly generate crowding at the periphery and therefore may interfere with the rifampicin incorporation to the inner cavities, and the loading may possibly take place at the periphery. This could account for the relatively higher release rate of 93% and 100% mannosylated dendrimer compared to 44% and 69% mannosylated dendrimers at 48 hrs time point. This observation was previously noticed in this chapter with PEGylated dendrimers.

The 69% mannose formulation had the slowest release profile among the nanoformulations at 48 hrs and 72 hrs time points. The rationale of that was due to the extent of surface mannosylation that was not a lot to hinder drug encapsulation within the dendrimer, compared to 93% and 100% mannose. During the release process, drug molecules were extensively influenced in their diffusion rate due to the thick/dense outer layer and therefore decrease their release rate.

Various literature reports have confirmed that surface mannosylation of dendrimer could slow down the release rate of encapsulation molecules compared to the unmodified dendrimer or pure drug (Kumar *et al.*, 2006; Dutta and Jain, 2007; Dutta *et al.*, 2007; Jain *et al.*, 2015).

5.7.4.2 Release in acetate medium pH 4.5

The release of rifampicin from dendrimer nanoformulations was assessed at pH 4.5, to simulate the release behaviour in the alveolar macrophages that accommodate mycobacterium tuberculosis.

The release of rifampicin from dendrimer nanoformulations showed bi-phasic profiles (Figure 5.15), an initial phase with burst release followed by a plateau phase with a sustained release. At the observed time points 6 hrs, 11 hrs, 24 hrs , and 48 hrs the one-way ANOVA (r^2) was 0.8087, 0.9298, 0.9215, and 0.9578, respectively (Table 5.8). The r^2 values suggest a strong relationship between the degree of dendrimer

mannosylation and the percentage of rifampicin released, especially after 6 hrs of the release study.

At the 6 hrs time point, lower release rates were noticed for mannosylated dendrimers compared to the unmodified dendrimer and 100% mannose formulation achieved the slowest release rate of 56.09% (Table 5.8). However, statistical analysis indicated that no significant difference in the release was observed between mannosylated dendrimer and unmodified dendrimer ($p > 0.05$).

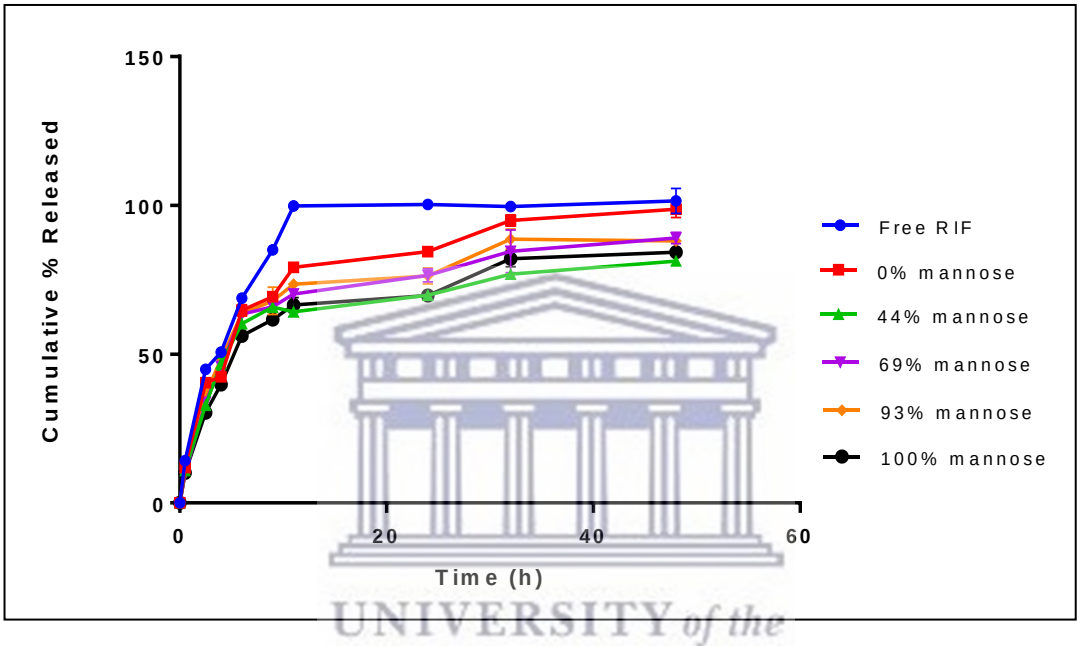

Figure 5.15 *In vitro* release profiles of rifampicin from 4.0 G PAMAM dendrimer having different mannose content, incubated in acetate medium pH 4.5 spiked with ascorbic acid at 37 °C under continuous stirring at 100 rpm (n = 3).

At 11 hrs time point, mannosylated dendrimers released rifampicin at a lower rate compared to the unmodified dendrimer but statistical analysis indicated that only 44% and 100% mannose showed a significant difference from the unmodified dendrimer ($p < 0.05$).

Beyond 11 hrs the release was inversely proportional to the degree of dendrimer mannosylation (except for 44% mannose). At 24 hrs time point, the release of rifampicin from 44% and 100% mannose formulations were significantly slower compared to unmodified dendrimer ($p < 0.05$). At 48 hrs time point, the release from all mannosylated dendrimers was significantly slower compared to the unmodified dendrimer ($p < 0.05$).

As mentioned earlier in this chapter that PAMAM dendrimer exhibit conformational change to a hollow shell structure upon decreasing the solution pH due to electrostatic repulsion that arises between protonated tertiary amines as well as between primary amine (Figure 5.13) (Lee *et al.*, 2002; Boas and Heegaard, 2004). Furthermore, below pH 7 rifampicin molecules will be protonated and carry positive charges (Khan *et al.*, 2017). These two conditions contribute to a superior drug release relative to that at PBS pH 7.4 solution.

Table 5.8 Comparison of the effect of dendrimer mannose content on rifampicin release after 6 hrs, 11 hrs, 24 hrs, and 48 hrs of incubation in acetate buffer medium pH 4.5 fortified with ascorbic acid at 37 °C under continuous stirring of 100 rpm.

Formulation	Release after 6 hrs		Release after 11 hrs		Release after 24 hrs		Release after 48 hrs	
	% RIF release	Effect of mannosylation	% RIF release	Effect of mannosylation	% RIF release	Effect of mannosylation	% RIF release	Effect of mannosylation
Free RIF	68.79 ± 1.52	Decrease in release % as mannose content increased $R^2 = 0.8087$	99.76 ± 0.96	Decrease in release % as mannose content increased $R^2 = 0.9298$	100.26 ± 1.17	Decrease in release % as mannose content increased $R^2 = 0.9215$	101.48 ± 4.25	Decrease in release % as mannose content increased $R^2 = 0.9578$
0 % mannose	64.70 ± 1.91		79.14 ± 0.76		84.44 ± 1.29		98.62 ± 2.85	
44% mannose	60.22 ± 0.30		64.20 ± 0.02		69.73 ± 0.26		81.19 ± 1.14	
69% mannose	63.43 ± 1.57		70.18 ± 1.44		76.40 ± 2.20		88.97 ± 1.96	
93% mannose	63.58 ± 1.10		73.51 ± 0.76		76.24 ± 2.65		88.05 ± 1.29	
100% mannose	56.09 ± 0.94		66.52 ± 2.49		69.66 ± 0.07		84.21 ± 065	

*****Release % is stated as mean ± SD (n = 3). Trend outliers are highlighted in red.

The initial phase took place up to 11 hrs of the release with about 64.20% – 79.14%. Almost 36.0% - 41.0% of the burst release happened up to 2.5 hrs of the study. It was observed that the percentage of drug released was inversely proportional to the extent of dendrimer mannosylation, since increasing the number of attached mannose molecules could increase the surface steric hindrance and hence decrease drug diffusion to the exterior (Dutta and Jain, 2007; Dutta *et al.*, 2007; Jain *et al.*, 2015).

The release in the acetate medium was observed higher than in the PBS medium (Tables 5.7 and 5.8). Two-way ANOVA analysis indicated significantly higher rifampicin released in acetate medium compared to that in PBS for the mannosylated dendrimer

nanoformulations at 11 hrs, 24 hrs, and 48 hrs time points ($p < 0.05$). For the unmodified dendrimer, the significant increase in the drug release was only noticed at 48 hrs time point. The electrostatic repulsion that arises between the protonated amines to generate an open-shell structure that enhances drug discharge from the interior cavities, besides the repulsion that could take place between the protonated amines and the protonated rifampicin molecules at acetate medium may enhance drug liberation. These findings are in line with what was previously observed (Kumar *et al.*, 2006; Jain *et al.*, 2015).

5.7.5 Fitting of drug release data into mathematical models

The mechanism(s) of rifampicin release from the unmodified dendrimer, as well as the effect of surface modification (PEG or mannose) on the release mechanism(s) at pH 7.4 and pH 4.5, were studied by fitting drug release data into various mathematical models. Fitting of data was done using a peer-reviewed modelling program known as DDSolver (Zhang *et al.*, 2010). Rifampicin release data were fitted into six kinetic equations which are commonly used in literature, namely: zero-order, first-order, Higuchi, Peppas- Sahlin, Korsmeyer-Peppas, and Weibull mathematical models (Costa and Lobo, 2001; Dash *et al.*, 2010; Reddy *et al.*, 2014). The adjusted coefficient of determination (R^2_{adj}), which was determined from regression analysis, was used as the basis for selecting the best mathematical model. The model possessing the highest R^2_{adj} value was chosen as the best-fitting model.

5.7.5.1 PEGylated dendrimers

Rifampicin release data in PBS medium from all dendrimers formulations were fitted into the Peppas-Sahlin model that owns the highest R^2_{adj} values, except 0% PEG formulation whose release data best fit was observed with Weibull model (Figure 5.16 and Table 5.9).

All PEGylated dendrimers had the best fit on the Peppas-Sahlin model; data analysis indicated that the constant for diffusion (K_1) was enormously bigger than the constant for polymer relaxation (K_2) for all samples (Table 5.9). Since $K_1 >> K_2$, the predominant mechanism of release from PEGylated dendrimers throughout the release study was expected to be *via* Fickian diffusion *(Section 5.2.3)*. Non-PEGylated dendrimer (0% PEG) had the best fit on the Weibull model, from Table 5.9 the **b** value was < 0.75

(0.527), this also signifies that release happened through Fickian diffusion *(Section 5.2.3)*.

Rifampicin release data in acetate medium pH 4.5 was also fitted into the six kinetic models. All formulations had the best fit on the Peppas-Sahlin model that acquired the highest R^2_{adj} values compared to the other models (Figure 5.17 and Table 5.10). The only exception is the 49% PEG formulation that possessed the uppermost R^2_{adj} value on the Weibull model. Similar to data analysis in PBS, all formulation that had the best fit on Peppas-Sahlin (i.e., 0%, 38% PEG, 70% PEG, 85% PEG, and 100% PEG), K_1 values were also higher than K_2 (Table 5.10), which suggests that Fickian diffusion was the principal mechanism for drug release from nanoparticles during the release study. Whereas for 49% PEG, the **b** value was < 0.75 (0.632), therefore signifying that release was *via* the diffusion mechanism.

Fitting of the drug release data from PBS and acetate medium on the commonly used kinetic equations indicated that the principal mechanism of drug release for all formulations (i.e., PEGylated and non-PEGylated) was *via* Fickian diffusion of rifampicin molecules from the dendrimer scaffold.

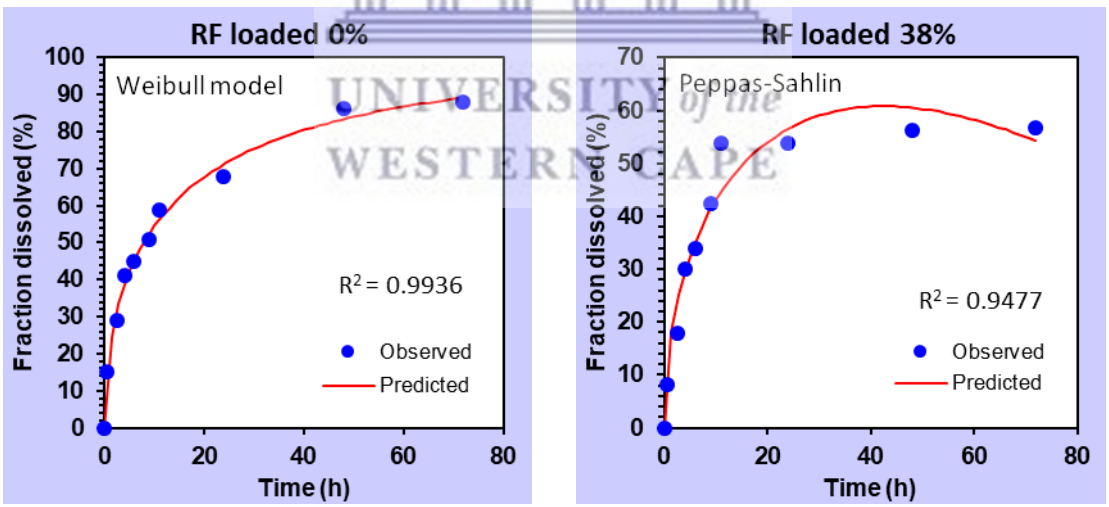

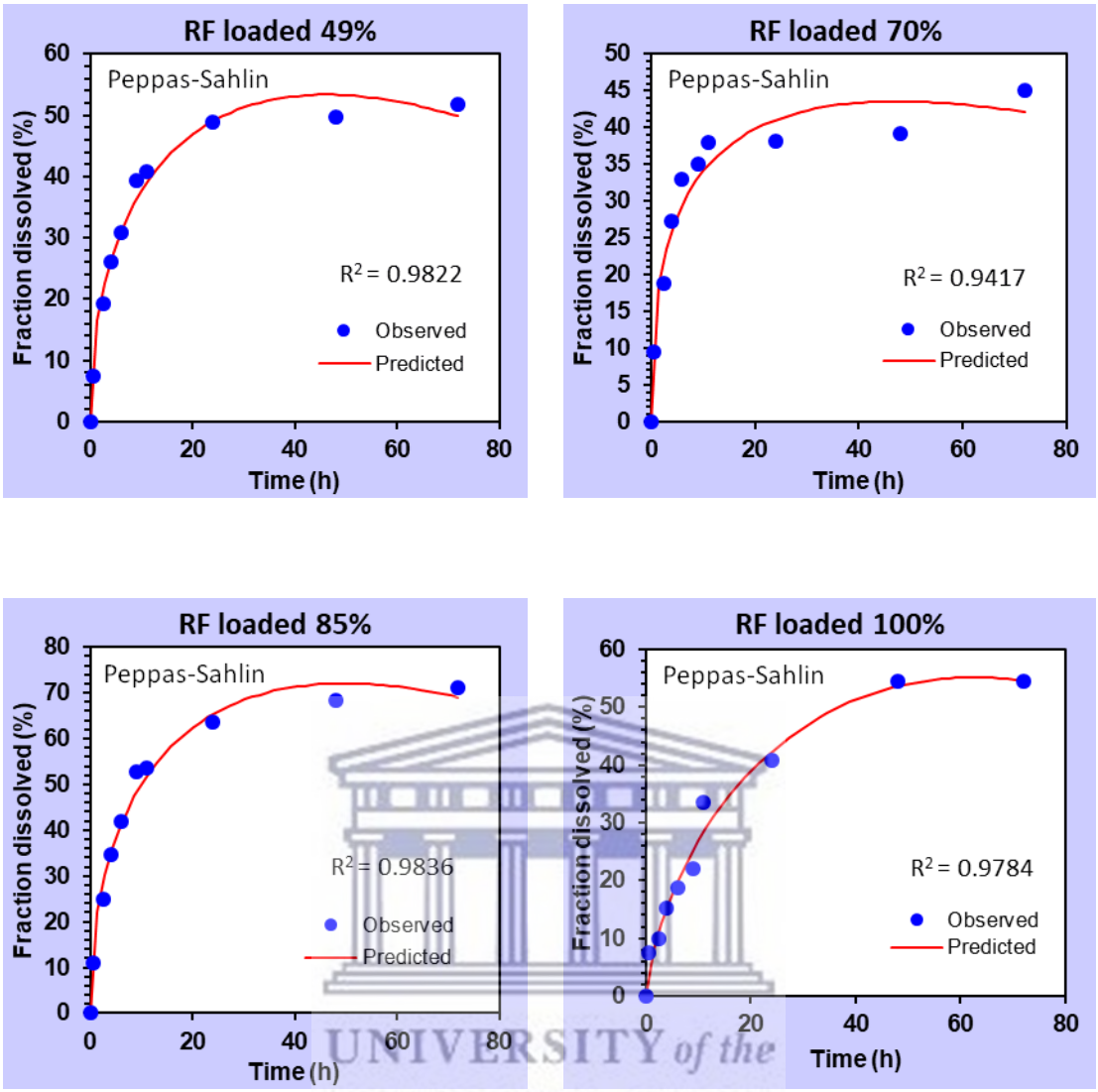

Figure 5.16 Kinetic models of best fit for *in vitro* release of rifampicin from PEGylated and non-PEGylated dendrimer nano-formulations at pH 7.4.

Table 5.9 Parameter values and R^2_{adj} values acquired from fitting the rifampicin release data from PEGylated and non-PEGylated dendrimers in PBS into 6 mathematical models. The highlighted values in red colour correspond to the highest values of R^2_{adj} obtained when the six models were compared, for each formulation.

Formulation types	Zero-order		First-order		Higuchi		Peppas-Sahlin				Korsmeyer-Peppas			Weibull		
	K_0	R^2_{adj}	k_1	R^2_{adj}	k_H	R^2_{adj}	k_1	k_2	m	R^2_{adj}	k	n	R^2_{adj}	a	b	R^2_{adj}
0% PEG	1.648	-0.0853	0.083	0.8584	12.846	0.8066	22.915	-1.478	0.462	0.9925	25.761	0.301	0.9665	4.286	0.527	**0.9936**
38% PEG	1.132	-0.4552	0.032	0.1816	9.136	0.5877	16.145	-1.072	0.538	**0.9477**	21.236	0.259	0.7810	4.635	0.366	0.8873
49% PEG	1.013	-0.4499	0.021	0.0549	8.133	0.6285	14.991	-1.053	0.512	**0.9822**	18.811	0.260	0.8602	5.175	0.346	0.9332
70% PEG	0.857	-1.0223	0.015	-0.5885	7.030	0.3556	18.266	-1.914	0.405	**0.9417**	19.572	0.205	0.7974	4.759	0.259	0.9063
85% PEG	1.377	-0.3813	0.066	0.5858	10.993	0.6659	20.193	-1.414	0.503	**0.9836**	24.799	0.268	0.8861	4.075	0.419	0.9602
100% PEG	0.994	0.4922	0.017	0.7370	7.417	0.9433	6.436	-0.188	0.687	**0.9784**	9.727	0.424	0.9406	11.514	0.544	0.9655

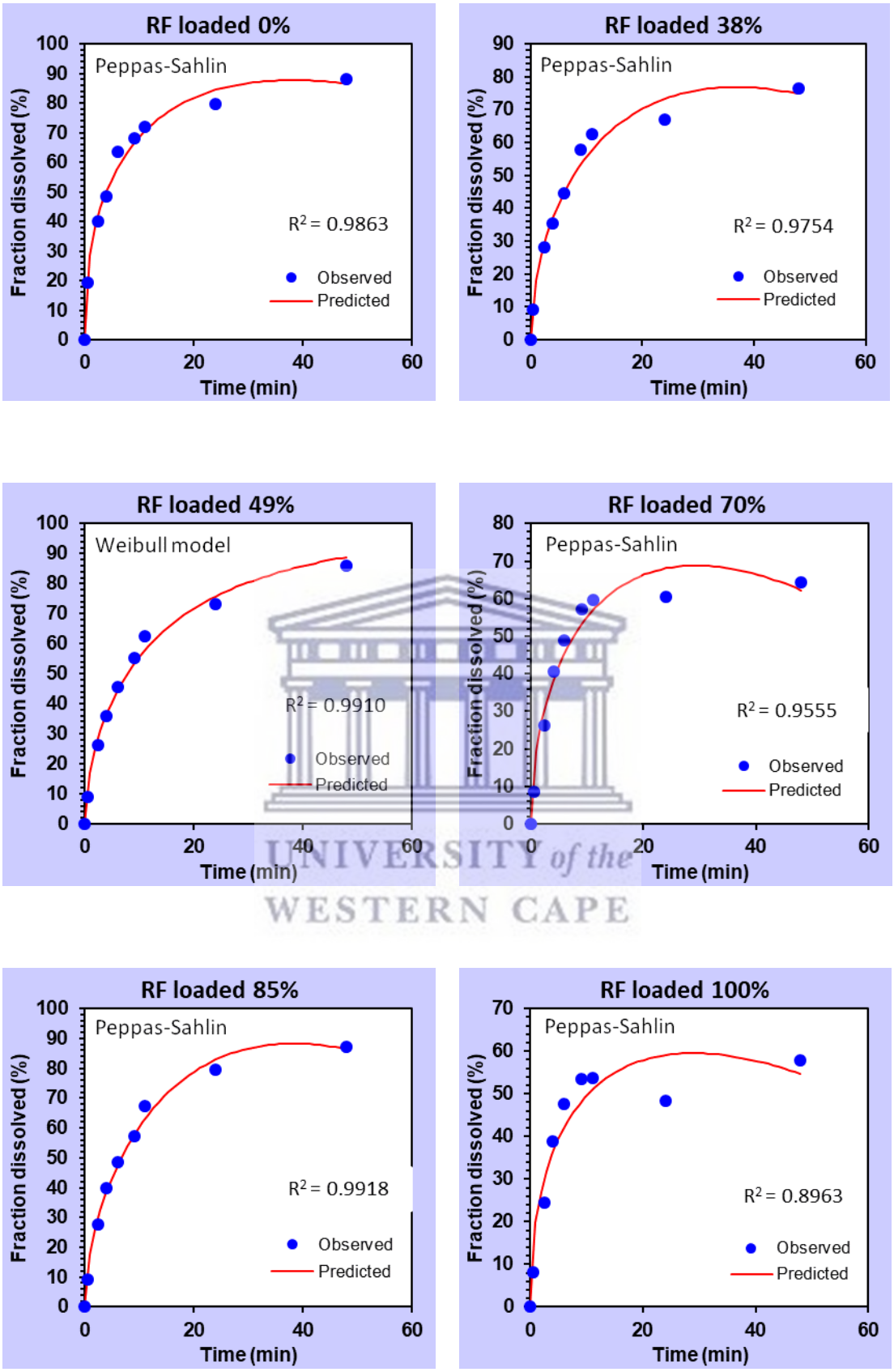

Figure 5.17 Kinetic models of best fit for *in vitro* release of rifampicin from PEGylated and non-PEGylated dendrimer nano-formulations at pH 4.5.

Table 5.10 Parameter values and R^2_{adj} values acquired from fitting the rifampicin release data from PEGylated and non-PEGylated dendrimers in acetate medium into 6 mathematical models. The highlighted values in red colour correspond to the highest values of R^2_{adj} obtained when the six models were compared, for each formulation.

Formulation types	Zero-order		First-order		Higuchi		Peppas-Sahlin				Korsmeyer-Peppas			Weibull		
	K_0	R^2_{adj}	k_1	R^2_{adj}	k_H	R^2_{adj}	k_1	k_2	m	R^2_{adj}	k	n	R^2_{adj}	a	b	R^2_{adj}
0% PEG	2.618	-0.5866	0.147	0.8786	16.872	0.6526	31.726	-2.869	0.470	**0.9863**	35.250	0.256	0.9459	2.876	0.511	0.9857
38% PEG	2.215	-0.1226	0.085	0.8047	13.973	0.7956	19.484	-1.235	0.573	**0.9754**	24.494	0.316	0.9238	4.368	0.522	0.9620
49% PEG	2.408	0.1481	0.088	0.9260	14.855	0.8941	18.081	-0.958	0.595	0.9900	22.765	0.360	0.9578	5.258	0.632	**0.9910**
70% PEG	1.986	-0.5451	0.081	0.5292	12.951	0.6028	21.491	-1.677	0.550	**0.9555**	26.786	0.260	0.8581	3.644	0.409	0.8983
85% PEG	2.505	0.0646	0.101	0.9461	15.582	0.8641	18.840	-1.004	0.614	**0.9918**	24.906	0.347	0.9442	5.004	0.658	0.9892
100% PEG	1.757	-0.7229	0.058	0.1563	11.576	0.4950	22.428	-2.111	0.496	**0.8963**	25.654	0.237	0.8161	3.651	0.343	0.8452

5.7.5.2 Mannosylated dendrimers

The mechanism of release of rifampicin from mannosylated dendrimers was also assessed by fitting the release data into mathematical models to predict the possible mechanism(s) of release.

Rifampicin release data in PBS medium from all dendrimers formulations were best fitted into the Peppas-Sahlin model that owns the highest R^2_{adj} values, except 0% mannose formulation whose release data best fit was observed with Weibull model (Figure 5.18 and Table 5.1 (a)). Since the (K_1) was extremely greater than the (K_2) for all mannosylated dendrimers (Table 5.11 (a)), the predominant mechanism of release throughout the release study was expected to occur *via* Fickian diffusion. Unmodified dendrimer (0% mannose) had the best fit on the Weibull model, from Table 5.11 (a) the **b** value was < 0.75 (0.670), this could predict that the release also happened through Fickian diffusion.

Rifampicin release data in acetate medium pH 4.5 was also fitted into the six kinetic models. All formulations had the best fit on the Weibull model that acquire the highest R^2_{adj} values compared to the other models (Figure 5.19 and Table 5.11 (b)). The only exception is the 44% mannosylated dendrimer that possesses the highest R^2_{adj} value on the Peppas-Sahlin model. As the **b** values for the nanoformulation were < 0.75 (see Table 5.11 (b)), therefore the predominant mechanism of drug release was *via* the diffusion mechanism. Furthermore, the release data of 44% mannosylated dendrimer showed that $K_1 >> K_2$ (Table 5.11 (b)), which also suggests that the Fickian diffusion was the main mechanism of release.

The release data in both PBS and acetate medium suggested that the Fickian diffusion was the main mechanism of rifampicin release from unmodified and mannosylated dendrimers.

Table 5.11 Parameter values and R^2_{adj} values acquired from fitting the rifampicin release data from unmodified and mannosylated dendrimer in [a] PBS and [b] acetate into 6 mathematical models. The highlighted values in red colour correspond to the highest values of R^2_{adj} obtained when the six models were compared, for each formulation.

[a]

Formulation types	Zero-order		First-order		Higuchi		Peppas-Sahlin				Korsmeyer-Peppas			Weibull		
	K_0	R^2_{adj}	k_1	R^2_{adj}	k_H	R^2_{adj}	k_1	k_2	m	R^2_{adj}	k	n	R^2_{adj}	a	b	R^2_{adj}
0% mannose	1.911	-0.1967	0.126	0.9519	14.540	0.7180	24.889	-1.642	0.519	0.9613	30.839	0.285	0.8546	4.368	0.670	**0.9753**
44% mannose	1.564	-0.1201	0.065	0.7362	11.840	0.7512	19.604	-1.243	0.522	**0.9636**	24.244	0.296	0.8708	4.487	0.492	0.9534
69% mannose	1.510	-0.4855	0.076	0.5754	11.687	0.5798	22.983	-1.775	0.496	**0.9438**	27.933	0.251	0.7848	3.617	0.419	0.9093
93% mannose	1.581	-0.2570	0.075	0.7094	12.066	0.6900	21.682	-1.512	0.505	**0.9532**	26.331	0.277	0.8418	4.029	0.472	0.9402
100% mannose	1.568	-0.2034	0.071	0.7227	11.943	0.7089	20.190	-1.314	0.526	**0.9569**	25.385	0.285	0.8407	4.260	0.483	0.9390

[b]

Formulation types	Zero-order		First-order		Higuchi		Peppas-Sahlin				Korsmeyer-Peppas			Weibull		
	K_0	R^2_{adj}	k_1	R^2_{adj}	k_H	R^2_{adj}	k_1	k_2	m	R^2_{adj}	k	n	R^2_{adj}	a	b	R^2_{adj}
0% mannose	2.874	0.0265	0.148	0.9645	17.616	0.8220	27.007	-1.877	0.533	0.9755	31.774	0.312	0.9092	3.984	0.705	**0.9859**
44% mannose	2.395	-0.2649	0.111	0.7496	14.924	0.6993	27.463	-2.374	0.489	**0.9549**	30.723	0.269	0.8501	3.242	0.473	0.9511
69% mannose	2.603	-0.0809	0.127	0.8908	16.068	0.7748	26.465	-2.008	0.518	0.9654	30.525	0.295	0.8809	3.582	0.571	**0.9712**
93% mannose	2.640	-0.1602	0.138	0.8997	16.379	0.7436	27.609	-2.161	0.520	0.9670	32.187	0.285	0.8671	3.400	0.574	**0.9702**
100% mannose	2.452	0.0188	0.100	0.8494	15.047	0.8142	23.254	-1.632	0.531	0.9694	27.229	0.311	0.8986	3.969	0.549	**0.9710**

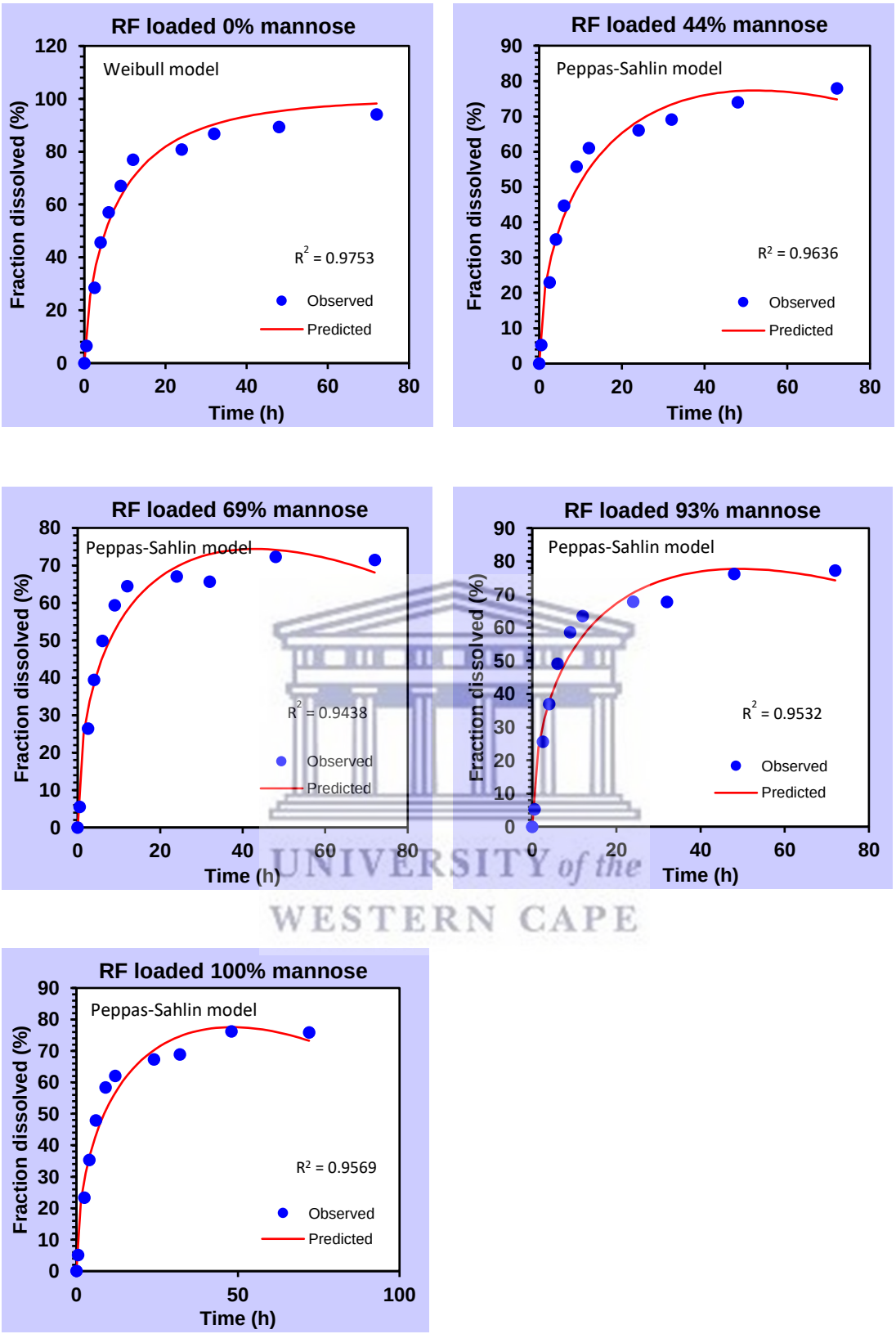

Figure 5.18 Kinetic models of best fit for *in vitro* release of rifampicin from mannosylated dendrimer nano-formulations at pH 7.4.

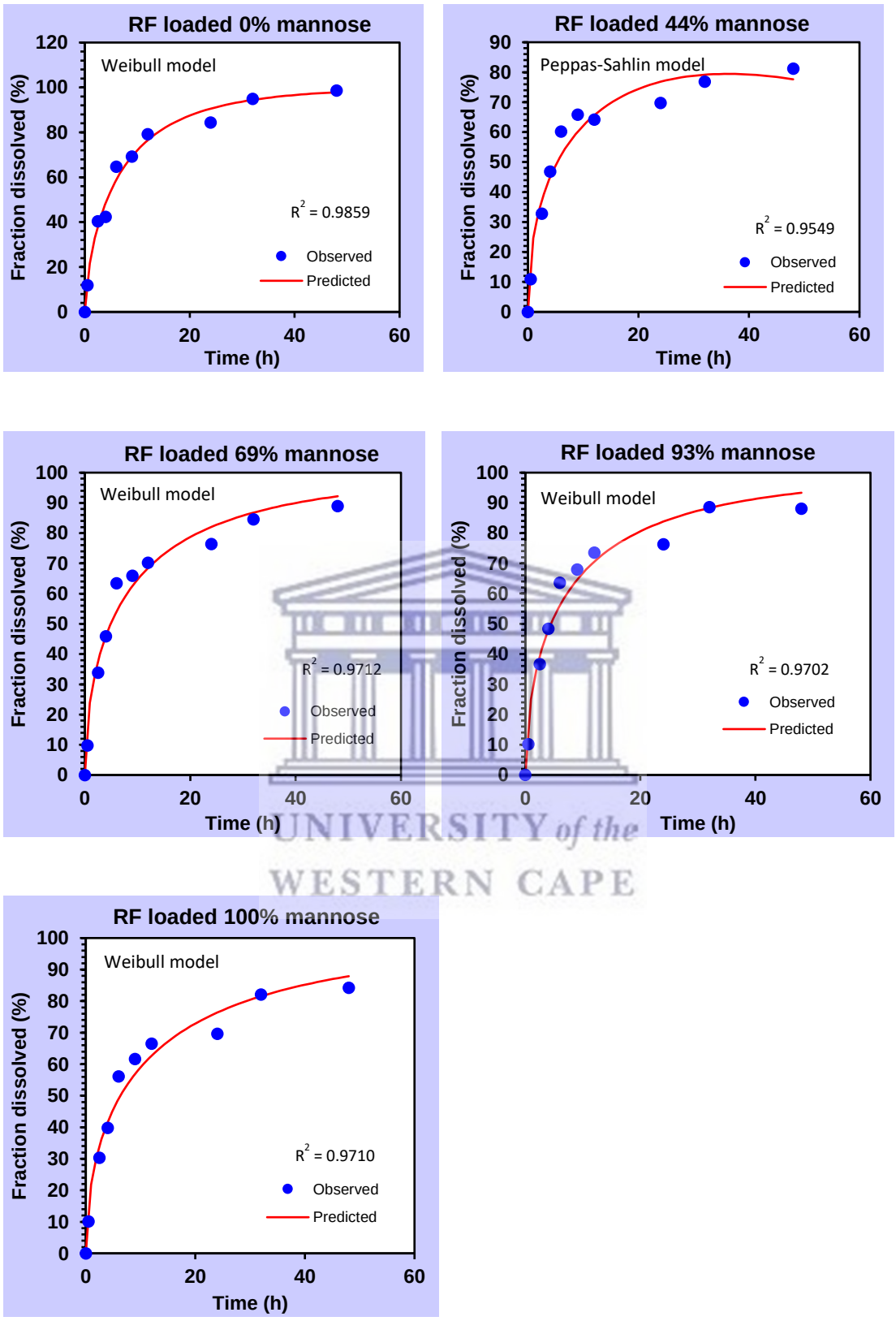

Figure 5.19 Kinetic models of best fit for *in vitro* release of rifampicin from mannosylated dendrimer nano-formulations at pH 4.5.

5.8 Conclusion

The release behaviour of the rifampicin from nanoformulations was assessed at pH 4.5 and pH 7.4 using the dialysis bag technique. Results indicated that the two types of surface-modifications, PEG conjugated PAMAM dendrimer as well as mannose conjugated PAMAM dendrimer, showed prolonged drug release in both media. Furthermore, results have verified that for each group the rate of drug release was inversely proportional to the content of conjugated molecules (PEG or mannose). In addition, the rate of drug release was higher in the acetate medium pH 4.5 compared to the PBS medium pH 7.4 in both groups. This characteristic could facilitate site-specific burst drug release at the phagolysosomal of the alveolar macrophages. Thus, surface-modified G4 PAMAM dendrimer (with PEG or mannose) is suggested as one of the promising pulmonary drug delivery systems with prolonged-release behaviour.

5.9 References

Abouelmagd, S.A., Hyun, H. and Yeo, Y., (2014). Extracellularly activatable nanocarriers for drug delivery to tumors. *Expert opinion on drug delivery*, *11*(10), pp.1601-1618.

Agata, Y., Iwao, Y., Miyagishima, A. and Itai, S., (2010). Novel mathematical model for predicting the dissolution profile of spherical particles under non-sink conditions. *Chemical and Pharmaceutical Bulletin*, *58*(4), pp.511-515.

Agrawal, S. and Panchagnula, R., (2004). In vitro analysis of rifampicin and its effect on quality control tests of rifampicin containing dosage forms. *Die Pharmazie-An International Journal of Pharmaceutical Sciences*, *59*(10), pp.775-781.

Asthana, A., Chauhan, A.S., Diwan, P.V. and Jain, N.K., (2005). Poly (amidoamine)(PAMAM) dendritic nanostructures for controlled sitespecific delivery of acidic anti-inflammatory active ingredient. *AAPS PharmSciTech*, *6*(3), pp.E536-E542.

Barraza, L.F., Jiménez, V.A. and Alderete, J.B., (2015). Effect of PEGylation on the structure and drug loading capacity of PAMAM-G4 dendrimers: a molecular modeling approach on the complexation of 5-fluorouracil with native and PEGylated PAMAM-G4. *Macromolecular Chemistry and Physics*, *216*(16), pp.1689-1701.

Bellini, R.G., Guimarães, A.P., Pacheco, M.A., Dias, D.M., Furtado, V.R., de Alencastro, R.B. and Horta, B.A., (2015). Association of the anti-tuberculosis drug rifampicin with a PAMAM dendrimer. *Journal of Molecular Graphics and Modelling*, *60*, pp.34-42.

Boas, U. and Heegaard, P.M., (2004). Dendrimers in drug research. *Chemical Society Reviews*, *33*(1), pp.43-63.

Burkersroda, F., Schedl, L. and Göpferich, A., (2002). Why degradable polymers undergo surface erosion or bulk erosion. *Biomaterials*, *23*(21), pp.4221-4231.

Calvo, P., Vila-Jato, J.L. and Alonso, M.J., (1996). Comparative in vitro evaluation of several colloidal systems, nanoparticles, nanocapsules, and nanoemulsions, as ocular drug carriers. *Journal of pharmaceutical sciences*, *85*(5), pp.530-536.

Cauchetier, E., Deniau, M., Fessi, H., Astier, A. and Paul, M., (2003). Atovaquone-loaded nanocapsules: influence of the nature of the polymer on their in vitro characteristics. *International journal of pharmaceutics*, *250*(1), pp.273-281.

Chidambaram, N. and Burgess, D.J., (1999). A novel in vitro release method for submicron-sized dispersed systems. *AAPS PharmSci*, *1*(3), pp.32-40.

Chilin, C. and Metters, A.T., 2006. Hydrogels in controlled release formulations: Network design and mathematical modelling. *Advanced Drug Delivery Reviews*, *58*, pp.1379-1408.

Costa, P. and Lobo, J.M.S., (2001). Modeling and comparison of dissolution profiles. *European journal of pharmaceutical sciences*, *13*(2), pp.123-133.

D'Souza, S., (2014). A review of in vitro drug release test methods for nano-sized dosage forms. *Advances in Pharmaceutics*, *2014*, *pp. 1-12*.

D'Souza, S.S. and DeLuca, P.P., (2005). Development of a dialysis in vitro release method for biodegradable microspheres. *AAPS PharmSciTech*, *6*(2), pp.E323-E328.

D'Souza, S.S. and DeLuca, P.P., (2006). Methods to assess in vitro drug release from injectable polymeric particulate systems. *Pharmaceutical Research*, *23*(3), pp.460-474.

Dash, S., Murthy, P.N., Nath, L. and Chowdhury, P., (2010). Kinetic modeling on drug release from controlled drug delivery systems. *Acta Pol Pharm*, *67*(3), pp.217-23.

Diaz, C., Guzmán, J., Jiménez, V.A. and Alderete, J.B., (2018). Partially PEGylated PAMAM dendrimers as solubility enhancers of Silybin. *Pharmaceutical development and*

technology, *23*(7), pp.689-696.

Dineshkumar, P., Panneerselvam, T., Deepti Brundavani, K., Selvaraj, K. and Vijayaraj Kumar, P., (2017). Formulation of Rifampicin Loaded PEGylated 5.0 G EDA-PAMAM Dendrimers as Effective Long-Duration Release Drug Carriers. *Current Drug Therapy*, *12*(2), pp.115-126.

Dutta, T., Agashe, H.B., Garg, M., Balasubramanium, P., Kabra, M. and Jain, N.K., 2007. Poly (propyleneimine) dendrimer based nanocontainers for targeting of efavirenz to human monocytes/macrophages in vitro. *Journal of drug targeting*, *15*(1), pp.89-98.

Dutta, T. and Jain, N.K., 2007. Targeting potential and anti-HIV activity of lamivudine loaded mannosylated poly (propyleneimine) dendrimer. *Biochimica et Biophysica Acta (BBA)-General Subjects*, *1770*(4), pp.681-686.

Freire, M.C.L.C., Alexandrino Jr, F., Marcelino, H.R., de Souza Picciani, P.H., de Holanda e Silva, K.G., Genre, J., de Oliveira, A.G. and Tabosa do Egito, E.S., (2017). Understanding Drug Release Data through Thermodynamic Analysis. *MATERIALS*, *10*(6), pp. 651.

Gao, Y., Zuo, J., Bou-Chacra, N., Pinto, T.D.J.A., Clas, S.D., Walker, R.B. and Löbenberg, R., (2013). In vitro release kinetics of antituberculosis drugs from nanoparticles assessed using a modified dissolution apparatus. *BioMed research international*, *2013, pp. 1-9.*

Gharbo, S.A., Cognion, M.M. and Williamson, M.J., (1989). Modified dissolution method for rifampin. *Drug Development and Industrial Pharmacy*, *15*(2), pp.331-335.

Gupta, U., Agashe, H.B. and Jain, N.K., (2007). Polypropylene imine dendrimer mediated solubility enhancement: effect of pH and functional groups of hydrophobes. *J Pharm Pharm Sci*, *10*(3), pp.358-67.

Heng, D., Cutler, D.J., Chan, H.K., Yun, J. and Raper, J.A., (2008). What is a suitable dissolution method for drug nanoparticles?. *Pharmaceutical Research*, *25*(7), pp.1696-1701.

Ho, M.N., Bach, L.G., Nguyen, T.H., Ho, M.H., Nguyen, D.H., Nguyen, C.K., Nguyen, C.H., Nguyen, N.V. and Thi, T.T.H., (2019). PEGylated poly (amidoamine) dendrimers-based drug loading vehicles for delivering carboplatin in treatment of various cancerous cells. *Journal of Nanoparticle Research*, *21*(2), p.43.

Holden, C.A., Tyagi, P., Thakur, A., Kadam, R., Jadhav, G., Kompella, U.B. and Yang, H., (2012). Polyamidoamine dendrimer hydrogel for enhanced delivery of antiglaucoma drugs. *Nanomedicine: Nanotechnology, Biology and Medicine*, 8(5), pp. 776–783.

ICH (2005) 'ICH harmonised tripartite guideline validation of analytical procedures: text and methodology Q2(R1)', *Geneva, Switzerland* (Vol. 11).

Jin, Y., Ren, X., Wang, W., Ke, L., Ning, E., Du, L. and Bradshaw, J., (2011). A 5-fluorouracil-loaded pH-responsive dendrimer nanocarrier for tumor targeting. *International journal of pharmaceutics*, *420*(2), pp.378-384.

Jindal, K.C., Chaudhary, R.S., Singla, A.K., Gangwal, S.S. and Khanna, S., (1994). Dissolution test method for rifampicin—isoniazid fixed dose formulations. *Journal of pharmaceutical and biomedical analysis*, *12*(4), pp.493-497.

Jain, K., Verma, A.K., Mishra, P.R. and Jain, N.K., 2015. Surface-engineered dendrimeric nanoconjugates for macrophage-targeted delivery of amphotericin B: formulation development and in vitro and in vivo evaluation. *Antimicrobial agents and chemotherapy*, *59*(5), pp.2479-2487.

Khan, M.F., Rita, S.A., Kayser, M., Islam, M., Asad, S., Bin Rashid, R., Bari, M., Rahman, M.M., Aman, A., Anwar, D.A. and Setu, N.I., (2017). Theoretically guided analytical method development and validation for the estimation of rifampicin in a mixture of isoniazid and pyrazinamide by UV spectrophotometer. *Frontiers in chemistry*, *5*, p.27.

Kojima, C., Kono, K., Maruyama, K. and Takagishi, T., (2000). Synthesis of polyamidoamine

dendrimers having poly (ethylene glycol) grafts and their ability to encapsulate anticancer drugs. *Bioconjugate chemistry*, *11*(6), pp.910-917.

Kostanski, J.W. and DeLuca, P.P., (2000). A novel in vitro release technique for peptide-containing biodegradable microspheres. *AAPS PharmSciTech*, *1*(1), pp.30-40.

Kumar, P.D., Kumar, P.V., Selvam, T.P. and Rao, K.S., (2013). PEG Conjugated PAMAM Dendrimers with a Anti-HIV Drug Stavudine for prolong release. *Research in Biotechnology*, *4*(2), pp. 10-18.

Kumar, P.V., Asthana, A., Dutta, T. and Jain, N.K., (2006). Intracellular macrophage uptake of rifampicin loaded mannosylated dendrimers. *Journal of drug targeting*, *14*(8), pp.546-556.

Lamprecht, A., Saulnier, P., Boury, F., Passirani, C., Proust, J.E. and Benoit, J.P., (2002). A quantitative method for the determination of amphiphilic drug release kinetics from nanoparticles using a Langmuir balance. *Analytical chemistry*, *74*(14), pp.3416-3420.

Langer, R. and Peppas, N., (1983). Chemical and physical structure of polymers as carriers for controlled release of bioactive agents: a review. *Journal of Macromolecular Science-Reviews in Macromolecular Chemistry and Physics*, *23*(1), pp.61-126.

Lee, I., Athey, B.D., Wetzel, A.W., Meixner, W. and Baker, J.R., (2002). Structural molecular dynamic studies on therapeutically-applied polyamidoamine dendrimers: the effects of pH and surface derivatization group. *Macromolecules*, *35(11)*, pp.4510-4520.

Lee, J.H. and Yeo, Y., (2015). Controlled drug release from pharmaceutical nanocarriers. *Chemical engineering science*, *125*, pp.75-84.

Lee, S.H., Mok, H., Lee, Y. and Park, T.G., (2011). Self-assembled siRNA–PLGA conjugate micelles for gene silencing. *Journal of controlled release*, *152*(1), pp.152-158.

Ly, T.U., Tran, N.Q., Hoang, T.K.D., Phan, K.N., Truong, H.N. and Nguyen, C.K., (2013). Pegylated dendrimer and its effect in fluorouracil loading and release for enhancing antitumor activity. *Journal of biomedical nanotechnology*, *9*(2), pp.213-220.

Bruschi, M.L., (2015). *Strategies to modify the drug release from pharmaceutical systems*. Woodhead Publishing.

Pan, G., Lemmouchi, Y., Akala, E.O. and Bakare, O., (2005). Studies on PEGylated and drug-loaded PAMAM dendrimers. *Journal of bioactive and compatible polymers*, *20*(1), pp.113-128.

Papadopoulou, V., Kosmidis, K., Vlachou, M. and Macheras, P., (2006). On the use of the Weibull function for the discernment of drug release mechanism. *Int. J. Pharm*, *309*(1-2), pp.44-50.

Patri, A.K., Myc, A., Beals, J., Thomas, T.P., Bander, N.H. and Baker, J.R., (2004). Synthesis and in vitro testing of J591 antibody− dendrimer conjugates for targeted prostate cancer therapy. *Bioconjugate chemistry*, *15*(6), pp.1174-1181.

Peppas, N.A., Bures, P., Leobandung, W.S. and Ichikawa, H., (2000). Hydrogels in pharmaceutical formulations. *European journal of pharmaceutics and biopharmaceutics*, *50*(1), pp.27-46.

Prabaharan, M., Grailer, J.J., Pilla, S., Steeber, D.A. and Gong, S., (2009). Amphiphilic multi-arm-block copolymer conjugated with doxorubicin via pH-sensitive hydrazone bond for tumor-targeted drug delivery. *Biomaterials*, *30*(29), pp.5757-5766.

Rajaram, S., Vemuri, V.D. and Natham, R., (2014). Ascorbic acid improves stability and pharmacokinetics of rifampicin in the presence of isoniazid. *Journal of pharmaceutical and biomedical analysis*, *100*, pp.103-108.

Samkange, T., D'Souza, S., Obikeze, K. and Dube, A., (2019). Influence of PEGylation on PLGA nanoparticle properties, hydrophobic drug release and interactions with human serum

albumin. *Journal of Pharmacy and Pharmacology*, *71*(10), pp.1497-1507.

Shabir, G. A. (2006). Step-by-Step Analytical Protocol in the Quality System Methods Validation and Compliance Industry. *Analytical Methods Validation*, 40(6), pp. 951–961.

Shetab Boushehri, M.A. and Lamprecht, A., (2015). Nanoparticles as drug carriers: current issues with in vitro testing. *Nanomedicine*, *10*(21), pp.3213-3230.

Shishoo, C.J., Shah, S.A., Rathod, I.S., Savale, S.S., Kotecha, J.S. and Shah, P.B., (1999). Stability of rifampicin in dissolution medium in presence of isoniazid. *International journal of pharmaceutics*, *190*(1), pp.109-123.

Sideratou, Z., Tsiourvas, D. and Paleos, C.M., (2001). Solubilization and release properties of PEGylated diaminobutane poly (propylene imine) dendrimers. *Journal of colloid and interface science*, *242*(1), pp.272-276.

Siegel, R.A. and Rathbone, M.J., (2012). Overview of controlled release mechanisms. In *Fundamentals and applications of controlled release drug delivery*. pp. 19-43. Springer, Boston, MA.

Siepmann, J. and Göpferich, A., (2001). Mathematical modeling of bioerodible, polymeric drug delivery systems. *Advanced drug delivery reviews*, *48*(2-3), pp.229-247.

Siepmann, J. and Siepmann, F., (2008). Mathematical modeling of drug delivery. *International journal of pharmaceutics*, *364*(2), pp.328-343.

Sievens-Figueroa, L., Pandya, N., Bhakay, A., Keyvan, G., Michniak-Kohn, B., Bilgili, E. and Davé, R.N., (2012). Using USP I and USP IV for discriminating dissolution rates of nano-and microparticle-loaded pharmaceutical strip-films. *AAPS PharmSciTech*, *13*(4), pp.1473-1482.

Reddy, N.S., Sowmya, S., Bumgardner, J.D., Chennazhi, K.P., Biswas, R. and Jayakumar, R., (2014). Tetracycline nanoparticles loaded calcium sulfate composite beads for periodontal management. *Biochimica et Biophysica Acta (BBA)-General Subjects*, *1840*(6), pp.2080-2090.

Singh, P., Gupta, U., Asthana, A. and Jain, N.K., (2008). Folate and folate− PEG− PAMAM Dendrimers: synthesis, characterization, and targeted anticancer drug delivery potential in tumor bearing mice. *Bioconjugate chemistry*, *19*(11), pp.2239-2252.

Singh, S., Mariappan, T.T., Sharda, N., Kumar, S. and ChakrabortI, A.K., (2000). The reason for an increase in decomposition of rifampicin in the presence of isoniazid under acid conditions. *Pharmacy and Pharmacology Communications*, *6*(9), pp.405-410.

Son, G.H., Lee, B.J. and Cho, C.W., (2017). Mechanisms of drug release from advanced drug formulations such as polymeric-based drug-delivery systems and lipid nanoparticles. *Journal of Pharmaceutical Investigation*, *47*(4), pp.287-296.

Sorokoumova, G.M., Vostrikov, V.V., Selishcheva, A.A., Rogozhkina, E.A., Kalashnikova, T.Y., Shvets, V.I., Golyshevskaya, V.I., Martynova, L.P. and Erokhin, V.V., (2008). Bacteriostatic activity and decomposition products of rifampicin in aqueous solution and liposomal composition. *Pharmaceutical chemistry journal*, *42*(8), pp.475-478.

Tawfik, M.A., Tadros, M.I. and Mohamed, M.I., (2019). Polyamidoamine (PAMAM) dendrimers as potential release modulators and oral bioavailability enhancers of vardenafil hydrochloride. *Pharmaceutical development and technology*, *24*(3), pp.293-302.

Thakur, S., Kesharwani, P., Tekade, R.K. and Jain, N.K., (2015). Impact of pegylation on biopharmaceutical properties of dendrimers. *Polymer*, *59*, pp.67-92.

Vijayaraj Kumar, P., Agashe, H., Dutta, T. and Jain, N.K., (2007). PEGylated dendritic architecture for development of a prolonged drug delivery system for an antitubercular drug. *Current drug delivery*, *4*(1), pp.11-19.

Wang, D. and Imae, T., (2004). Fluorescence emission from dendrimers and its pH dependence. *Journal of the American Chemical Society*, *126*(41), pp.13204-13205.

Williams, K.J. and Piddock, L.J., (1998). Accumulation of rifampicin by Escherichia coli and Staphylococcus aureus. *The Journal of antimicrobial chemotherapy*, *42*(5), pp.597-603.

Xie, L., Beyer, S., Vogel, V., Wacker, M.G. and Mäntele, W., (2015). Assessing the drug release from nanoparticles: Overcoming the shortcomings of dialysis by using novel optical techniques and a mathematical model. *International journal of pharmaceutics*, *488*(1-2), pp.108-119.

Yan, G.P., Zong, R.F., Li, L., Fu, T., Liu, F. and Yu, X.H., (2010). Anticancer drug-loaded nanospheres based on biodegradable amphiphilic ε-caprolactone and carbonate copolymers. *Pharmaceutical Research*, *27*(12), pp.2743-2752.

Yang, H., Morris, J.J. and Lopina, S.T., (2004). Polyethylene glycol–polyamidoamine dendritic micelle as solubility enhancer and the effect of the length of polyethylene glycol arms on the solubility of pyrene in water. *Journal of colloid and interface science*, *273*(1), pp.148-154.

Yang, L. and Da Rocha, S.R., (2014). PEGylated, NH2-terminated PAMAM dendrimers: a microscopic view from atomistic computer simulations. *Molecular Pharmaceutics*, *11*(5), pp.1459-1470.

Yoo, H.S. and Park, T.G., (2001). Biodegradable polymeric micelles composed of doxorubicin conjugated PLGA–PEG block copolymer. *Journal of controlled Release*, *70*(1-2), pp.63-70.

Zhang, Y., Huo, M., Zhou, J., Zou, A., Li, W., Yao, C. and Xie, S., (2010). DDSolver: an add-in program for modeling and comparison of drug dissolution profiles. *The AAPS Journal*, *12*(3), pp.263-271.

Chapter 6

In vitro cytotoxicity and permeability studies

6.1 Introduction

This chapter gives a detailed account of the materials, methods, and a clear description of the techniques applied to evaluate the cytotoxicity and the permeability potential of the nanoparticles that were developed in Chapters Three and Four. This chapter also shows the results, with discussion and conclusion.

6.2 Review of the literature

6.2.1 Toxicity and biocompatibility

The term toxicity is usually used by pharmaceutical companies to describe undesired side effect(s) and/or non-specific activity of drug molecules towards patient's cells, tissues, and organs (Figure 6.1) (Duncan and Izzo, 2005). Whilst the term biocompatibility is applied when a material is capable to mediate an effect with a suitable host reaction in a particular application (Figure 6.1) (Williams, 1989). For biocompatibility, it is necessiary to consider the potential effect of the material in the body, besides the impact of the biological environment on the performance of the material (Duncan and Izzo, 2005).

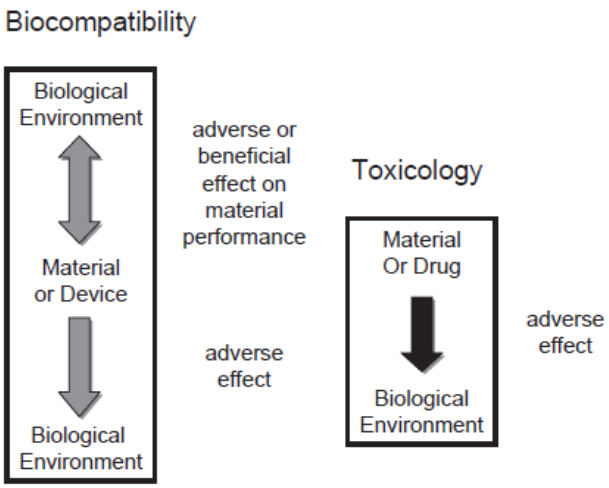

Figure 6.1 Difference between biocompatibility and toxicity [adapted from (Duncan and Izzo, 2005)].

6.2.2 Toxicity of drug delivery systems: Dendrimer toxicity

Generally, polymeric drug carriers such as dendrimers that are proposed for therapeutic applications are essentially meant to be non-immunogenic, non-toxic, and biodegradable. In addition, it should be characterized by appropriate body distribution that facilitates diffusion to the desired site of action. Assessing the toxicity of nanoparticles *via* simple *in vitro* tests such as cytotoxicity against various cell lines (Sgouras and Duncan, 1990) and red blood cells (RBCs) (Duncan *et al.*, 1991) have been recommended by many scientists before performing the *in vivo* analysis (Duncan and Izzo, 2005).

Although dendrimers have numerous characteristics, which were discussed in Chapter Two, that suggest they are one of the superior drug delivery systems, they experience significant toxicity that hamper their use (Duncan and Izzo, 2005). Dendrimers with cationic surface groups disrupt the biological membranes by interacting with negatively charged components of the lipid membrane to generate nano-holes that destabilize the cell membrane. This facilitates the diffusion of intracellular materials such as lactate dehydrogenase (LDH) enzyme and hemoglobin out of cells and causes cell lysis and hemolysis, respectively (Malik *et al.*, 2000; Chen *et al.*, 2004; Mecke *et al.*, 2005; Kolhatkar *et al.*, 2007), at experimental concentration > 200 nM (Fischer *et al.*, 2003; Hong *et al.*, 2004, 2006; Leroueil *et al.*, 2007, 2008). Dendrimers such as PPI, PAMAM, and poly-L-lysine (PLL) are examples of cationic dendrimers that exhibit significant toxicity due to their surface positively charged groups (Kolhatkar *et al.*, 2007). Chen and co-worker (2004) have confirmed that cationic melamine dendrimers with various peripheral groups were more toxic than anionic or surface-modified melamine dendrimers (Chen *et al.*, 2004). The manner through which dendrimers are expected to mediate the cytotoxicity is comparable to what has been previously reported by other cationic macromolecules, such as micelles and liposomes (Thakur *et al.*, 2015).

Many literature reports indicated that dendrimer toxicity was observed to be concentration and generation dependent, a superior level of cytotoxicity was associated with higher dendrimer generations (Fischer *et al.*, 2003; R Jevprasesphant *et al.*, 2003; Kolhatkar *et al.*, 2007). A similar observation was noticed for the hemolytic effect of dendrimers (Jain *et al.*, 2010). Compared to flexible linear polymers having amine groups, recent reports identified that cationic amine-terminated PAMAM dendrimers

showed lower toxicity possibly due to lower interactions of the globular-shaped dendrimers to the biological membranes (Thakur *et al.*, 2015).

Agashe and co-workers (2006) evaluated the cytotoxicity of 5.0 G PPI and surface-modified 5.0G PPI in HepG2 and COS-7 cell lines. The results indicated that for the unmodified 5.0 G PPI toxicity was observed to be a function of incubation time and dendrimer concentration, which perhaps due to the peripheral positive groups. Surface manipulation with mannose and lactose was significantly decreased by the cytotoxicity profile of 5.0 G PPI dendrimer. Agashe and co-authors concluded that surface optimization of PPI dendrimer was suggested as one of the techniques to develop biocompatible drug delivery systems (Agashe *et al.*, 2006).

Kolhatkar and co-workers (2007) studied the cytotoxicity of 2.0 G, 4.0 G PAMAM dendrimers, and functionalized 2.0 G, 4.0 G PAMAM dendrimers against Caco-2 cell lines (Kolhatkar *et al.*, 2007). Surface manipulation was done with various concentrations of the acetamide group. The results showed that surface acetylation decreased the cytotoxicity of PAMAM dendrimers by more than 10-folds, while the permeability of these nanoparticles across Caco-2 cell lines did not significantly differ from the unmodified PAMAM dendrimer. Accordingly, surface modification of PAMAM dendrimers with acetamide was suggested by Kolhatkar *et al.* to minimize the dendrimer toxicity without affecting their permeability across Caco-2 cells.

The toxicity of the dendrimers is not exclusively linked with the peripheral groups, some reports revealed that aromatic polyether core and anionic carboxylated peripheral groups showed hemolytic activity for RBCs of rats after 24 hrs of incubation (Liu, Kono and Fréchet, 1999). The authors suggested that the aromatic core of the dendrimer may perhaps interact with the RBCs membrane *via* hydrophobic interactions and induce hemolysis (Liu, Kono and Fréchet, 1999). Two factors may influence the interaction of the dendrimer core and the RBCs membrane, the number of generations as well as the rigidity of the dendrimer branches (Thakur *et al.*, 2015). A lower degree of interactions is expected with higher dendrimer generation and rigid dendritic shells.

Another explanation for the mechanism of dendrimer-mediated cytotoxicity is expected to occur through subcellular apoptotic events that are independent of the escape of cellular components. Earlier studies have revealed that cationic polymers are able to increase the endolysosomal pH, which was known as the proton sponge effect (Behr,

1993), as a result of lysosomal swelling and rupture (Kichler *et al.*, 2001; Sonawane, Szoka and Verkman, 2003; Akinc *et al.*, 2005). Thomas and co-worker (2009) studied the mechanism of toxicity of 5.0 G PAMAM dendrimer and acetylated surface-modified 5.0 G PAMAM dendrimer against human epidermoid carcinoma (KB) cells at concentrations up to 3 μM (Thomas *et al.*, 2009). The findings revealed that cytotoxicity is principally associated with the free surface amines of the dendrimer and that functionalization of > 80% of the surface amines did not exhibit any cytotoxic effects. Encapsulation of the cationic dendrimers into the lysosomal part of the KB cell confirmed the increase of lysosomal pH. The results also observed that the nano-hole formation and the escape of LDH enzyme, due to cationic surface groups, does not account for the early cytotoxicity of KB cells. Thomas and co-workers have suggested though that PAMAM dendrimer cytotoxicity is mainly mediated following the lysosomal apoptosis pathway, as a result of the proton sponge effect and the changes in the mitochondrial membrane potential. Many techniques have been developed to overcome the dendrimer toxicity and render them biocompatible molecules, the most common are summarized in Figure 6.2 (Boas and Heegaard, 2004; Satija, Gupta and Jain, 2007; Jain *et al.*, 2010, 2012; Schlick *et al.*, 2011).

6.2.3 Functionalization strategies

6.2.3.1 Surface-functionalized dendrimers

Drug molecules are usually conjugated to dendrimer scaffold either at their surface *via* chemical interactions or may be encapsulated within the dendrimer core *via* physical entrapment, H-bonding, and hydrophobic interactions. If the dendrimer periphery is manipulated with various molecules, the loading capability particularly that takes place at the surface is expected to increase (Mishra, Gupta and Jain, 2009).

Dendrimers have multiple surface sites that easily be modulated with a variety of functionalities *via* covalent or non-covalent bonds to develop multifunctional dendrimer molecules. Figure 6.2 summarizes some of the surface modification techniques, in this chapter we will focus on surface functionalization with PEG chains and mannose residues.

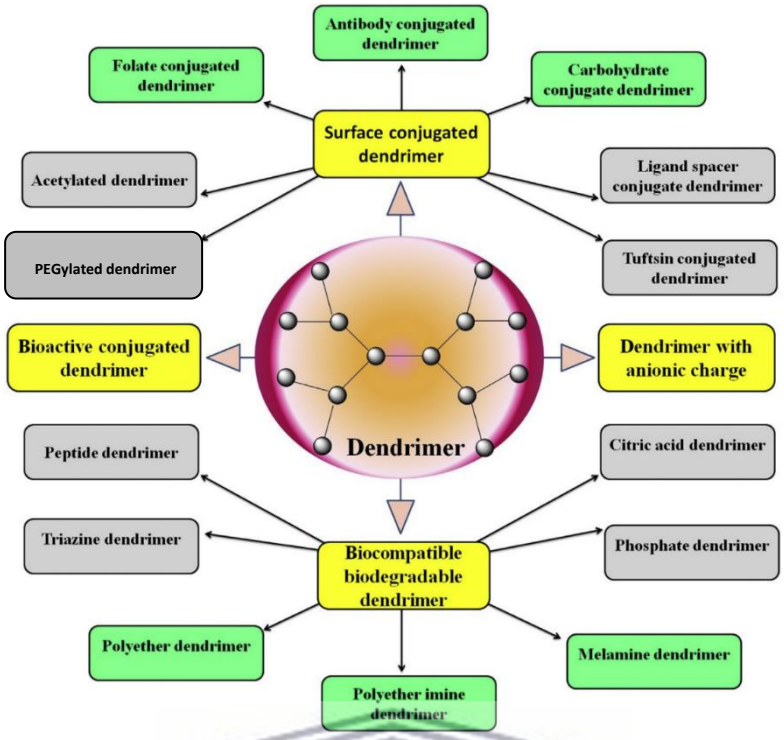

Figure 6.2 Commonly reported techniques to overcome dendrimer toxicity (Thakur *et al.*, 2015).

(a) Surface functionalization with PEG chains

PEG is extensively employed in the field of drug delivery due to its superior solubility in both organic and aqueous solutions, besides its biocompatibility properties (Mishra, Gupta and Jain, 2009). Functionalization of the surface of dendrimers with PEG chains

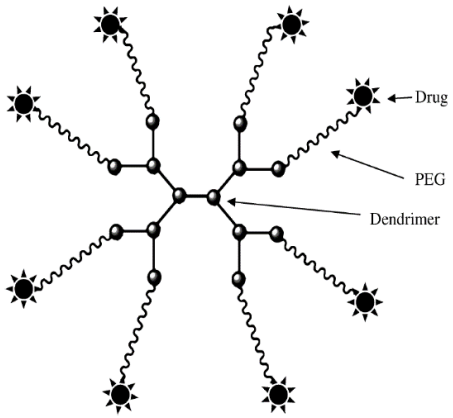

Figure 6.3 The structure of PEGylated dendrimer [adapted from (Mishra, Gupta and Jain, 2009)].

can alleviate some of the drawbacks associated with the use of dendrimers such as toxicity as well as immunogenicity. The PEGylated dendrimer can be considered as a single micelle molecule (Figure 6.3) (Newkome *et al.*, 1985; Heise *et al.*, 1999; Liu *et al.*, 1999).

Since dendrimer toxicity is a function of periphery chemistry, surface modification of cationic dendrimers with PEG chains (PEGylation) has been evidenced to minimize their toxicity as a result of shielding the positive functional groups (Mishra, Gupta and Jain, 2009). Furthermore, PEGylation can improve the drug loading potential of the dendrimer besides offering a prolonged-release manner, as discussed previously in Chapters Three and Five, respectively.

Wang and co-workers (2009) evaluated the cytotoxicity of 5.0 G PAMAM dendrimer and surface-modified 5.0 G PAMAM dendrimers using two molecular weights PEG chains. They evaluated the effect of PEGylation on the dendrimer mediated cytotoxicity, the change in the mitochondrial membrane potential (MMP), and reactive oxygen species (ROS). The results confirmed that PEGylation could successfully minimize the PAMAM dendrimer mediated cell apoptosis through attenuating the formation of ROS besides inhibiting MMP collapse. The IC_{50} concentrations of PEGylated dendrimers were approximately 12 – 105 times higher than the non-PEGylated dendrimers. Wang and co-workers observed that surface modification with a small quantity of lower molecular weight PEG chains does not significantly change the endocytic properties, whereas for added percentage of higher molecular weight PEG the toxicity was significantly decreased (Wang *et al.*, 2009).

Stasko and co-workers (2007) assessed the cytotoxicity and time-dependent membrane disruption induced by 5.0 G PPI dendrimer and surface-modified 5.0 G PPI dendrimers on human umbilical vein endothelial cells (HUVEC). The surface amines of the dendrimer were modified using high molecular weight PEG chains and acetamides. The analysis was performed using confocal fluorescent microscopy after labeling the dendrimers with a fluorescent dye. Dendrimers with a concentration of 3 µM were used. The LDH assay results revealed that surface-modified 5.0 G PPI dendrimers (PEG and acetamides) diminished the cytotoxicity of the dendrimers by inhibiting the interaction of the cationic amines with the cell membrane (Figure 6.4). While for the native 5.0 G

PPI with free amines, the analysis observed a time-dependent variation in the cell membrane's permeability and noticeable cytotoxicity (Stasko *et al.*, 2007).

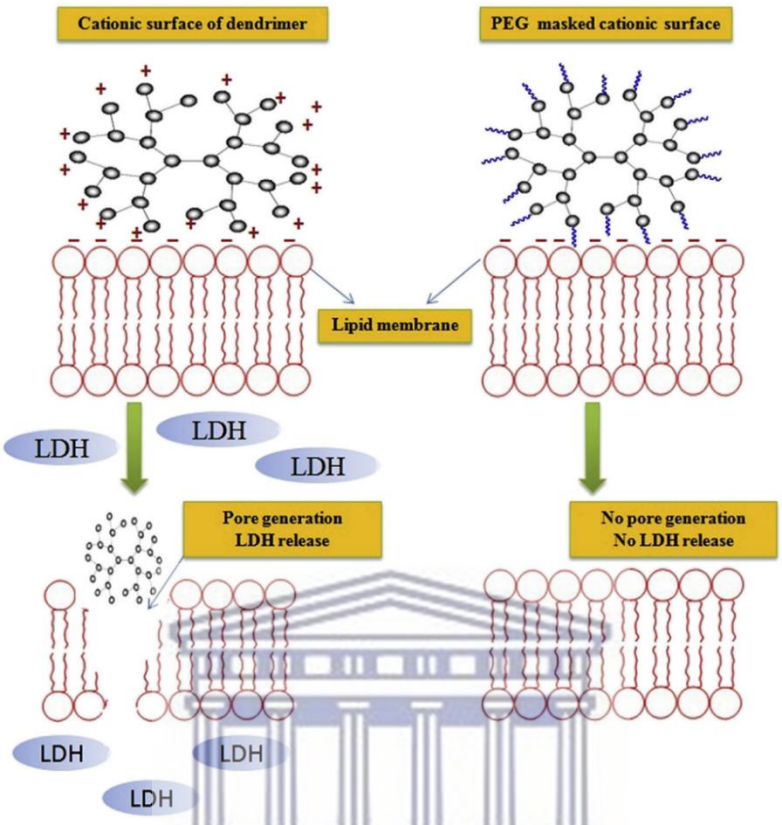

Figure 6.4 Illustration for the expected interaction between dendrimer and cell membrane [adapted from (Jain *et al.*, 2010; Thakur *et al.*, 2015)].

Zhu and co-workers (2010) encapsulated the anticancer drug doxorubicin (DOX) in surface-modified PAMAM dendrimer having different concentrations of PEG chains. The conjugation of DOX and dendrimer was achieved through acid-sensitive *cis*-aconityl linkage or acid-insensitive succinic linkage to generate PEG-PAMAM-*cis*-aconityl-DOX (PPCD) conjugated and PEG-PAMAM-succinic-DOX (PPSD) conjugates, respectively. PPCD nanoconjugates showed enhanced antitumor activity compared to the PPSD nanoconjugates. PPCD conjugates that had higher PEG content mediated an enhanced drug localization and tumor targeting as a result of decreased liver and spleen uptake. *In vitro* cytotoxicity of nanoconjugates against B16 melanoma cells was also examined, the results indicated that partial PEGylation reduced the cytotoxicity of the dendrimer nanoparticles. Although PPSD conjugates were accumulated into the tumors in higher quantities compared to PPCD conjugates at the same PEGylation degree, PPCD conjugates showed greater cytotoxicity compared to

PPSD conjugates. DOX release from PPCD was superior to that from PPSD due to acid-sensitive linkage. The advanced DOX release in the case of PPCD conjugate explains the enhanced antitumor efficacy as well as its related toxicity (Zhu *et al.*, 2010).

Kono and co-workers (2008) developed PEGylated PAMAM dendrimer using glutamic acid as a linker between the dendrimer scaffold and the PEG chains. The PEGylated dendrimer nanoparticles were employed as a carrier for the anticancer drug Adriamycin (ADR). ADR molecules were conjugated to the PEGylated dendrimer either *via* the amide bond [PEG–Glu(ADR)-G4] or *via* the hydrazone bond [PEG–Glu(NHN–ADR)-G4]. *In vitro* cytotoxicity studies on Hela cells indicated that the free Adriamycin drug exhibits higher toxicity comparative to the ADR conjugated dendrimers (Kono *et al.*, 2008).

Another study performed by Diaz and co-worker (2018) to assess the cytotoxicity of 4.0 G PAMAM dendrimer and PEGylated 4.0 G PAMAM dendrimer using two molecular weights PEG i.e., 550 and 2000 Da with analysis achieved using dendrimer concentration of 1 – 500 µM against HEK cell culture. The results revealed that for native 4.0 G PAMAM dendrimer the toxicity is a function of its concentration and the IC50 was 500 µM after three hours of study. For the PEGylated dendrimer formulation with 550 and 2000 Da PEG chains, no cytotoxic effect was observed for the 1 – 500 µM dendrimer concentration range. Furthermore, among the two molecular weight PEG chains, no significant difference was observed (Diaz *et al.*, 2018). Similar observations for the effect of PEGylation on decreasing the dendrimer toxicity were also reported by Ho and co-workers (Ho *et al.*, 2019) and Ly and co-workers (Ly *et al.*, 2013).

(b) Surface functionalization with carbohydrate moieties

The incorporation of carbohydrate molecules into the dendrimer structure generates what is known as glycodendrimers (Bhadra *et al.*, 2005). The most frequently used carbohydrates to synthesize glycodendrimers are lactose, mannose, and D-galactose (Figure 6.5). The carbohydrates molecules can either be applied to functionalize the outer surface of the dendrimer (Figure 6.5) or may represent the core and the branching units of the dendrimer structure (Jayaraman, Nepogodiev and Stoddart, 1997). As discussed in Chapter Four, the conjugation of mannose residues on the surface of a

dendrimer can decrease the toxicity by shielding the positively charged groups, besides the targeting capability of the lectin receptors located at the surface of alveolar macrophages.

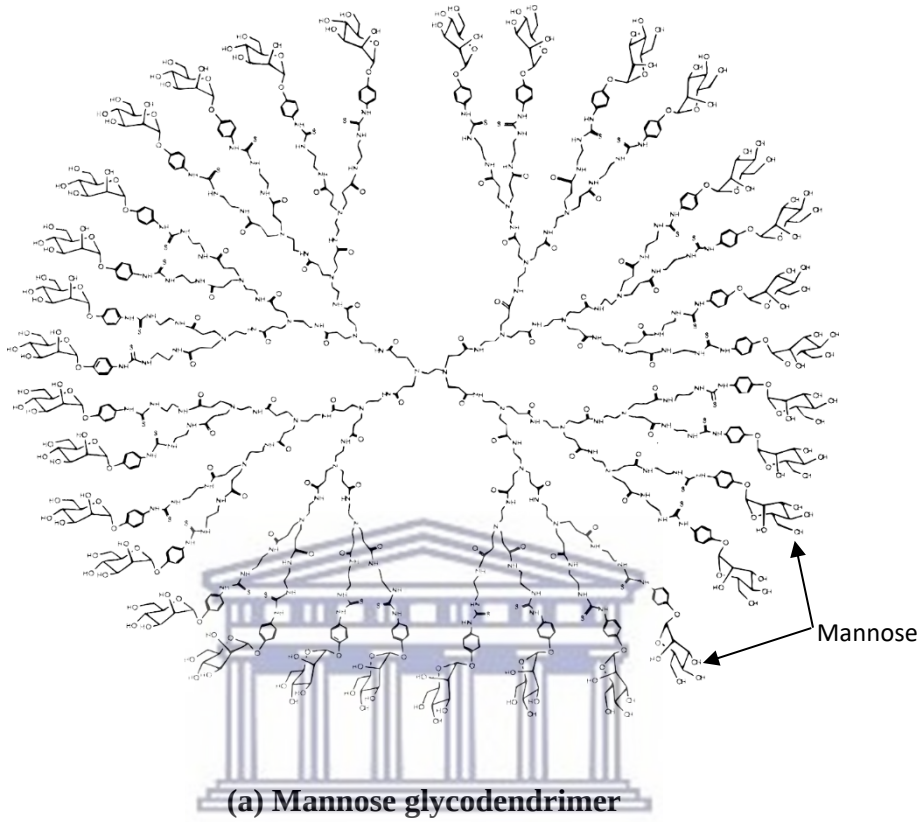

(a) Mannose glycodendrimer

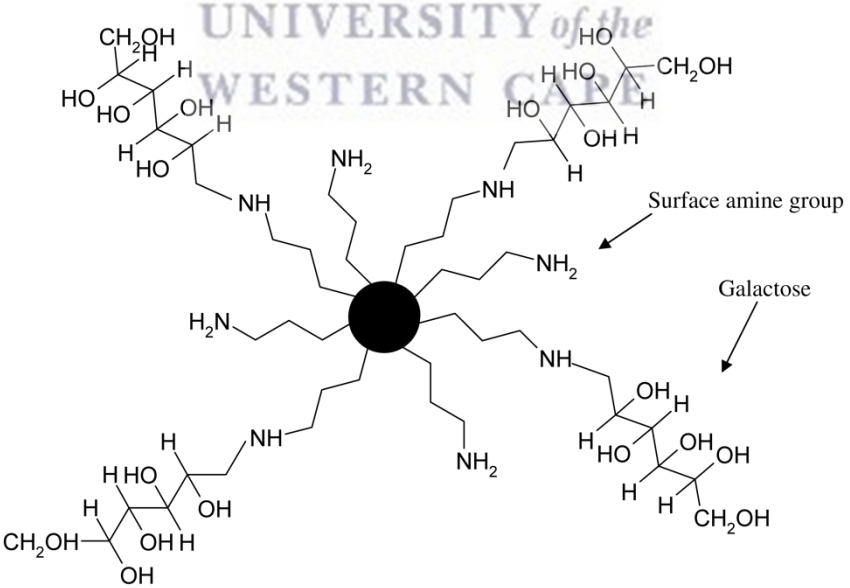

(b) Galactose glycodendrimer

Figure 6.5 Glycodendrimers structure of (a) surface-modified with mannose (Pagé and Roy, 1997), and (b) surface-modified with galactose (Mishra, Gupta and Jain, 2009).

A MTT assay performed by Kumar and co-workers (2006) to assess the cytotoxicity of rifampicin loaded into mannosylated 5.0 G PPI dendrimer in Vero cells revealed up to 100 µg/ml concentration of mannosylated dendrimer with negligible cytotoxicity observed. The pure rifampicin exhibited significantly higher toxicity towards Vero cells compared to the rifampicin loaded mannosylated dendrimer. When mannosylated dendrimer is loaded with rifampicin the toxicity was significantly increased, Kumar and co-workers explained that some of the physically bound drug molecules may leach to the surface of the dendrimer and account for the higher toxicity observed (Kumar *et al.*, 2006).

Another study was done by Dutta and co-workers (2007) to develop a 5.0 G PPI dendrimer nanocarrier to target the antiretroviral drug efavirenz (EFV) to human macrophages. The cytotoxicity of mannosylated PPI dendrimer with a range concentration of 0.001 – 1 mg/ml was significantly lower than the native PPI dendrimer which perhaps due to the shielding of the cationic peripheral groups of the dendrimer. Similarly, EFV-loaded mannosylated PPI was characterized by negligible cytotoxicity while the % of cell viability of native PPI was less than 20% for the analysis concentration of 0.3 mM EFV (Dutta *et al.*, 2007). Dutta and co-authors concluded that mannosylated PPI dendrimer is considered as one of the strategies that can be applied to decrease the dendrimer toxicity besides enhancing the targeting of EFV to macrophages.

Jain and co-workers (2015) synthesized 5.0 G PPI dendrimers having mannose residues attached to the periphery, for macrophage target delivery of amphotericin B. The MTT assay results confirmed that both loaded and unloaded mannosylated PPI dendrimers exhibited negligible cytotoxicity against J774A.1 macrophage cells after an incubation time of 18 hrs. IC_{50} of the pure drug was found 8.71 ± 0.37 µg/ml, whereas the mannosylated dendrimer did not display any cytotoxic activity up to a concentration of 50 µg/ml. The authors concluded that mannosylated PPI dendrimer is one of the suggested novel drug delivery systems of amphotericin B to the macrophages (Jain *et al.*, 2015).

6.2.3.2 Dendritic boxes

The dendritic box is synthesized by forming a densely-packed shell of protected amino acids around the PPI dendrimer surface (Figure 6.6) (Mishra, Gupta and Jain, 2009).

Usually, drug molecules are encapsulated within the PPI, then a shell will be formed around the surface of the dendrimer as a result of the interaction of peripheral amines with the amino acids to produce a box that stabilizes the encapsulated molecules.

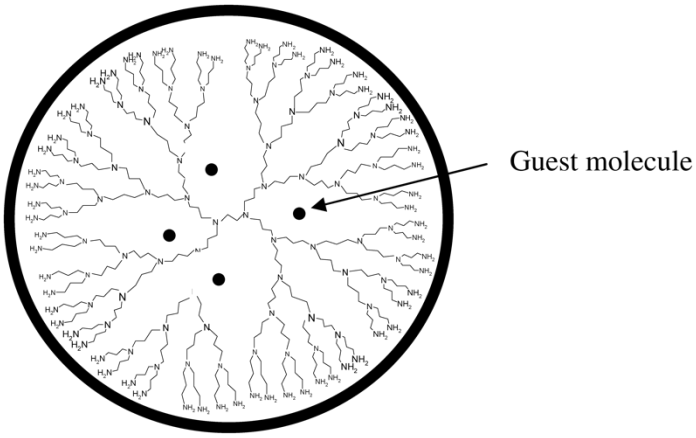

Figure 6.6 The structure of a dendritic box [adapted from (Mishra, Gupta and Jain, 2009)].

The dendritic box controls the release of entrapped molecules by the outer shell, and the release only occurs under particular conditions when partial or complete hydrolysis of the shell happens. Partial hydrolysis will liberate small-sized encapsulated molecules, whereas the release of all molecular sizes is facilitated once total hydrolysis takes place (Jansen, De Brabander-van den Berg and Meijer, 1994; Jansen, Meijer and de Brabander-van den Berg, 1995; Boas *et al.*, 2001).

6.2.4 Dendrimer cellular uptake

Cellular pharmacokinetics of dendritic polymers is one of the measures that play a major role in determining biological properties, such as efficacy and toxicity. The mechanism of cellular uptake of dendrimers is not clearly understood, however it has been significantly varied with dendrimer concentration, generation, periphery charge, and functionalization (Fox, Richardson and Briscoe, 2018). Cell type could also account to influence the internalization mechanism of dendrimers. The intracellular fate of dendrimer was observed to be affected by the mechanism of cellular uptake (Fox, Richardson and Briscoe, 2018).

According to many literature articles, dendrimer internalization can be achieved by various endocytic approaches, where caveolae-mediated endocytosis, clathrin-

mediated endocytosis, micropinocytosis, and other approaches independent of clathrin and caveolae are the most reported types (Conner and Schmid, 2003; Doherty and McMahon, 2009; Kumari, Swetha and Mayor, 2010; Vidal and Guzman, 2015). Clathrin-mediated endocytosis signifies the classic and the major pathway of endocytosis. The main difference between the clathrin-mediated endocytosis and caveolae-mediated endocytosis is that for the clathrin pathway the vesicles fuse with early endosomes followed by an acidification process that ends in lysosomes (McMahon and Boucrot, 2011), while for the caveolae pathway the vesicles fuse with Golgi or endoplasmic reticulum compartments in a non-acidification pathway (Kiss and Botos, 2009).

The cellular uptake of various molecules through receptor-mediated endocytosis is taking place by a particular endocytic route. For example, it is determined that cellular uptake by folate receptor is mediated *via* the caveolae endocytic pathway (Pelkmans and Helenius, 2002), while uptake by the transferrin receptor is mediated *via* the clathrin endocytic pathway (Tortorella and Karagiannis, 2014).

The internalization mechanism of PAMAM dendrimer is influenced by the nature of the surface charges as well as cell type. Previous reports indicated that dendrimer with negatively charged surface groups are usually internalized following the caveolae endocytic pathway, whereas those with positively charged groups and neutral groups appear to be internalized through caveolae- and clathrin-independent pathway in A549 lung epithelial cells (Perumal *et al.*, 2008). Another study in Hela cells indicated that positively charged dendrimers are confirmed to be internalized through clathrin endocytic pathway and micropinocytosis (Albertazzi *et al.*, 2010).

While the endocytic pathway (active process) represents the main route of PAMAM dendrimer internalization (Fox, Richardson and Briscoe, 2018), some of the cellular uptakes were reported to be mediated through passive diffusion mechanism (Fox, Richardson and Briscoe, 2018).

6.2.5 Dendrimer uptake by alveolar macrophages

The main role of alveolar macrophages is to mediate immunological and inflammatory responses to protect the lung against foreign substances and infectious pathogens (Patel, Gupta and Ahsan, 2015). The removal of pathogens and foreign substances by alveolar

macrophages is achieved by the phagocytosis mechanism. As discussed in Chapter Four, sometimes alveolar macrophages can be targeted using various drug delivery systems to treat some pathological conditions where their pathogens utilize the macrophages as a safe harbor for replication and further infection, as in the case of TB and HIV pathogens (Patel, Gupta and Ahsan, 2015). Sometimes avoiding the macrophage uptake could be important to enhance system absorption and circulation period, so drug delivery systems can be manipulated to escape recognition and engulfment by alveolar macrophages. Thus optimizing drug delivery systems may perhaps be implemented to enhance or minimize uptake by the alveolar macrophages based on the intended therapeutic effect.

6.2.5.1 Mechanisms of phagocytosis

Phagocytosis is defined as the active process that engulfs particulates and pathogens detected in monocytes, macrophages, neutrophils, and to some extent in dendritic cells (Kiama *et al.*, 2001). The first step of the phagocytosis is the opsonization process, which is the recognition of the foreign particulates after coating with soluble proteins, such as opsonin. The opsonized particulates conjugate to corresponding receptors on the phagocyte membrane such as complement or immunoglobulin receptors (Greenberg and Grinstein, 2002). The interaction of opsonized particulates with the phagocyte receptors activates them, then they induce structural rearrangement to generate pseudopods on the surface of the phagocyte which enable engulfing of the particulates. The successful engulfing and internalization of particulates will generate phagosome, afterwards, phagolysosome is developed upon fusion with the lysosome compartment to destroy the engulfed materials through acidification and enzymatic action (Figure 6.7).

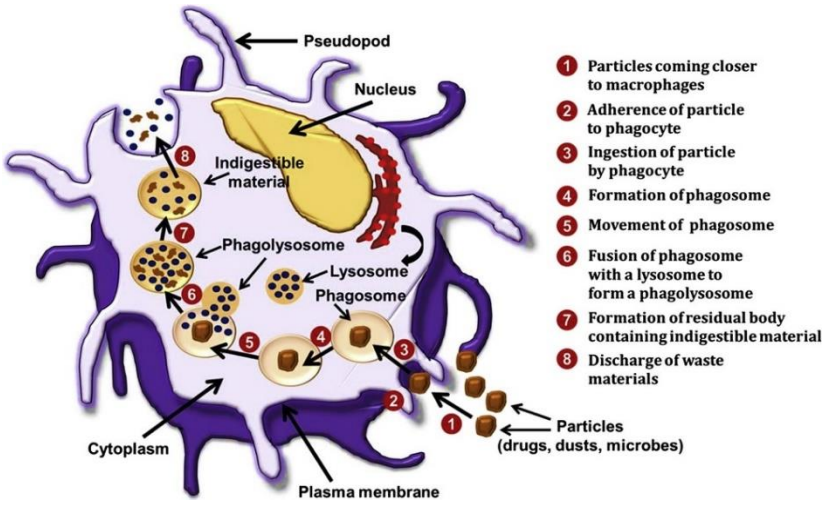

Figure 6.7 Illustration of the phagocytosis process by the alveolar macrophages [adapted from pathogens (Patel, Gupta and Ahsan, 2015)].

The process of recognition and engulfment of inhaled particulates is mediated by many receptors, the most common type occurs *via* a series of pattern recognition receptors (PRR) known as scavenger receptors (SRs). The main role of SRs is to remove altered endogenous molecules and apoptotic cells after being conjugated to modified low-density lipoprotein (LDL) (Palecanda *et al.*, 1999). Among the SRs class A family there is a macrophage receptor with collagen structure (MARCO) type, which is determined to participate in the elimination process of non-opsonized particulates and protect the lung tissues against inhaled foreign materials (Arredouani *et al.*, 2005). Other members of SRs that contribute to the process of recognition and phagocytosis include mannose receptors (CD206), toll-like receptors, and integrins (Palecanda and Kobzik, 2001; Stuart and Ezekowitz, 2005; Tricker and Cheng, 2008).

The process of opsonin-mediated phagocytosis is normally observed in the systemic circulation where the opsonin proteins are highly available in the blood, whereas due to the minimal existence of opsonin in the pulmonary region the phagocytosis of alveolar macrophages is predominantly mediated through opsonin-independent pathways (Donnelly and Barnes, 2012).

6.2.5.2 Manipulating drug carrier to influence alveolar macrophage engulfment process

The phagocytic potential of the alveolar macrophages can be modulated to enhance or decrease the uptake of inhaled drug carriers by optimizing some factors that influence the ability of macrophages to identify the foreign particulates. The two main approaches of macrophages targeting are passive and active. Passive targeting requires optimization of physicochemical features of the drug carrier including, size, shape, surface charge, and the nature of carrier constituents. While active targeting involves surface manipulation of the drug carrier with ligands to target particular receptors at the surface of the macrophage, such as lectin receptors (Patel, Gupta and Ahsan, 2015). Table 6.1 summarizes the common techniques that have been used to enhance or lessen the particulate internalization by the alveolar macrophages through active and passive approaches (Patel, Gupta and Ahsan, 2015).

Table 6.1 Approaches to increase or decrease the phagocytic potential of drug carriers by alveolar macrophages (Patel, Gupta and Ahsan, 2015).

Feature	Carrier feature to enhance uptake	Carrier feature to avoid uptake
Size	Particles between 100 to 200 nm and 1 - 6 µm	Particle size less than 1 µm and more than 6 µm
Shape	Spherical	Elongated, rod, and fibre-like
Composition	Particles having PS, PG, and hyaluronan	Particles having cholesterol and sphingomyelin
Surface charge	High positive or negative surface charge	Particles with relatively neutral surface charge
Density and rigidity	Hard/ stiff and non-porous particles	Soft and porous particles
Hydrophilic/ lipophilic	Insoluble and hydrophobic particles	Soluble and hydrophilic particles
Ligands	Particle's surface optimized with mannose, MBSA, tuftsin	Particle's surface optimized with PEG, poloxamers and poloxamines

* PS: phosphatidylserine; PG: phosphatidylglycerol; MBSA: mayelated bovine serum albumin; PEG: polyethylene glycol.

6.3 Aim and the Objectives of the Chapter

6.3.1 Aim

The study aimed to study the effect of surface modification (PEG or mannose) of 4.0 G PAMAM dendrimer on the cytotoxicity and cellular internalization of the nanoparticles against raw macrophages.

6.3.2 Objectives

i. To compare the cytotoxicity of the native G4 PAMAM dendrimer to the unloaded surface-modified G4 PAMAM dendrimers (PEG or mannose), at four concentrations (1.25 µM – 10 µM).

ii. To compare the cytotoxicity of rifampicin-loaded G4 PAMAM dendrimer to the rifampicin-loaded surface-modified G4 PAMAM dendrimer (PEG or mannose), at five concentrations (0.125 µM – 2 µM).

iii. To evaluate the cellular internalization of FITC-labelled PEGylated dendrimers into raw cells.

iv. To evaluate the cellular internalization of FITC-labelled mannosylated dendrimers into raw cells.

6.4 Materials

6.4.1 Consumables

96 well cell culture plate (flat well bottom, Cellstar® Greiner BIO-ONE, Germany), 12 well cell culture plate (flat well bottom, Cellstar® Greiner BIO-ONE, Germany), 6 well cell culture plate (flat well bottom, Cellstar® Greiner BIO-ONE, Germany), thiazolyl blue tetrazolium bromide (MTT) (Sigma, USA), Dulbecco's Modified Eagle's Medium (DMEM) (BioWhittaker®, Lonza, USA), Fetal Bovine Serum (FBS) (Gibco®, UK), Penicillin-Streptomycin (PENSTREP) mixture (Lonza, USA), trypsin ethylenediamine tetraacetic acid (EDTA) (Lonza, Belgium), Fluorescein isothiocyanates isomer I (Sigma Life Science, USA), T75-flask (SPL life sciences, Korea), 15 ml and 50 ml centrifuge tubes (SPL life sciences, Korea), mouse leukemic monocyte-macrophage cell line Raw 264.7 (ATCC, USA), phosphate buffer saline pH 7.2 (1X PBS) (Gibco®, UK), DMSO (Sigma Aldrich, Poland), Trypan blue solution (0.4%) (Sigma, UK), cell counting chamber slides (Countess™, Invitrogen™, USA), Pur-A-Lyzer MWCO 6 - 8 kDa dialysis tubes (Sigma, Israel), 31 mm sterile coverslips, and Fluoroshield Histology mounting media with diamino-2-phenylindole (DAPI) (Sigma, UK)

6.4.2 Equipment

Cell imaging system (Invitrogen EVOS™ XL core, Thermo Fisher Scientific, USA), CO_2 incubator (Thermo Electron Corporation, USA), automated cell counter (Invitrogen Countess™, Korea), microplate reader (POLARstar® Omega controlled with Omega software version 5.11 R3, BMG LABTECH, Germany), centrifuge (Sorvall® TC 6, USA), Flow Cytometer (BD Accuri™ C6 Plus, Singapore), and Fluorescence microscope (Leica microsystems DM2500 LED, Germany).

6.5 Methods

6.5.1 Cell culture

Raw 264.7 cell lines were grown in T75-flask using DMEM (supplemented with 10% FBS and 1% PENSTREP mixture) and maintained at 37˚C and 5% CO_2 atmosphere in a CO_2 incubator. The culture medium was changed every 2-3 days. Cells were passaged when attained 70% – 90% confluency using trypsin EDTA to dissociate adherent cells from the culture flask.

6.5.2 Cytotoxicity assay

The MTT assay technique was used to evaluate the toxicity of the dendrimer formulations against Raw 264.7 cell lines, following the previous protocol (Wen *et al.*, 2013; Hakkimane *et al.*, 2018). Cells were seeded at a density of 1 x 10^5 cells/ml (100 µl/well) in 96 flat-bottom well plates and incubated for 24 h for cell adherence. Then, plates were treated with the unloaded dendrimer formulations (1.25 µM – 10 µM) and rifampicin-loaded dendrimer formulations (0.125 µM – 2 µM) and kept in a CO_2 incubator. The MTT solution was prepared by adding MTT stock (5 mg/ml) to the DMEM medium to achieve a final concentration of 0.5 mg/ml. After 24 h, 48 h, and 72 h of incubation the supernatant was removed and 100 µl of MTT solution was added to each well and maintained in a CO_2 incubator for 3 hours. After this, MTT was removed and 100 µl of DMSO was added and the plates were kept for a further 30 mins to solubilize the formazan crystal. Lastly, the plates were analyzed under the POLARstar Omega microplate reader at 570 nm (with a reference wavelength at 700 nm) at 25˚C to determine the absorbance of formazan. Three replicates were done for each group in addition to an interference well. The untreated cells were considered as negative control and doxorubicin drug (5 µM and 10 µM) was regarded as a positive control. Cell viability was determined using **Equation 6.1**.

$$\%\ \text{cell viability} = \frac{\text{absorbance (sample)} - \text{absorbance (blank)}}{\text{absorbance (}-\text{ve control)} - \text{absorbance (blank)}} \times 100 \qquad \textbf{Equation 6.1}$$

6.5.3 Labeling of the dendrimer nanoparticles

Dendrimer nanoparticles were labeled with fluorescein isothiocyanates isomer I (FITC) to study their permeation across raw cell-lines, following previous protocols (Yu and Russo, 1996; Rachaneekorn Jevprasesphant *et al.*, 2003) with slight modification. The

isothiocyanates part of the FITC molecule can form a thiourea linkage with the primary amines of the dendrimer (Rachaneekorn Jevprasesphant *et al.*, 2003). Methanolic solutions of FITC (2.5 µmol) were prepared and added slowly to dendrimer solutions in PBS pH 7.4 (1 µmol). The mixtures were kept at slow stirring (50 rpm) at room temperature (25˚C) for 24h in dark. This was then dialyzed against dH_2O for another 24hrs to remove the unconjugated FITC molecules using 6 - 8 kDa MWCO dialysis tubes. The FITC-conjugated dendrimers were retrieved from solutions by lyophilization. ^1H NMR technique was employed to verify the conjugation of FITC as well as to estimate the number of attached molecules.

6.5.4 Cellular uptake studies

Raw cells were seeded in 12-well plates at a density of 1 x 10^5 cells/ml (500 µl/well) and incubated for 24h to adhere. Then, treated with 5µM of FITC-labeled native G4 PAMAM dendrimer and FITC-labeled surface-modified dendrimer formulations (PEG and mannose) and maintained for 24h. At the end of the incubation period, cells were collected and the excess of nanoparticles was removed by centrifugation at 2000 rpm for 5 mins. Cellular uptake was evaluated in a flow cytometer by counting 10,000 events. The percentage of +ve FITC-staining cells and the FITC mean fluorescence intensity (MFI) for each dendrimer formulation relative to the untreated cells were determined and recorded.

6.5.5 Fluorescence microscope analysis

Raw cells were seeded onto sterile 31 mm sterile coverslips in a 6-well. The cells were then treated with 5µM of FITC-labeled native G4 PAMAM dendrimer and FITC-labeled surface-modified dendrimer formulations (PEG and mannose) and incubated for 24h. After that, the media was removed and the cells were washed several times with PBS. The cells were then fixed by adding 1 ml of 4% paraformaldehyde (PFA) to each well and incubated for 15 mins at room temperature (25˚C). The fixative solution was removed and cells were washed with PBS three times and left in PBS. A few drops of Fluoroshield with DAPI were added to a sterile glass slide, the coverslips were removed from the plate, placed on the mounted slides, and maintained for 10 mins at room temperature. The internalized nanoparticles were qualitatively assessed under a fluorescence microscope.

6.6 Data analysis

The data were interpreted using GraphPad® Prism 7.04 and expressed as the mean ± standard deviation. One-way ANOVA and t-test were applied to set up the significance of any differences between means. Values were considered significant if the *p*-value was ≤ 0.05.

6.7 Results and discussion

6.7.1 Cytotoxicity studies

MTT assay technique was used to assess the cytotoxicity of G4 PAMAM dendrimer as well as surface-modified dendrimers (PEG or mannose). The toxicity study was performed in raw cell lines, by calculating the cell viability (%) after 24 hrs, 48 hrs, and 72 hrs of dendrimer incubation. For the unloaded dendrimer formulations, the toxicity was evaluated for increasing concentration from 1.25 µM – 10 µM, while for rifampicin-loaded dendrimer formulations the concentration range was from 0.125 µM – 2 µM.

6.7.1.1 PEGylated dendrimers

The toxicity of the dendrimer nanoformulations were studied by comparing the cell viability/survival (%) of the unmodified G4 PAMAM dendrimer to that of PEGylated dendrimers, which were synthesized earlier in Chapter three (38%, 49%, 70%, 85%, and 100% PEG).

For the unloaded dendrimers, the toxicity of the nanoparticles was assessed by treating the raw cells with G4 dendrimer or PEGylated dendrimers in an increasing concentration from 1.25 µM – 10 µM. After 24 hrs, 48 hrs, and 72 hrs of incubation, the cell survival (%) of unmodified G4 dendrimer was compared to that of PEGylated dendrimers at each concentration (Figure 6.8).

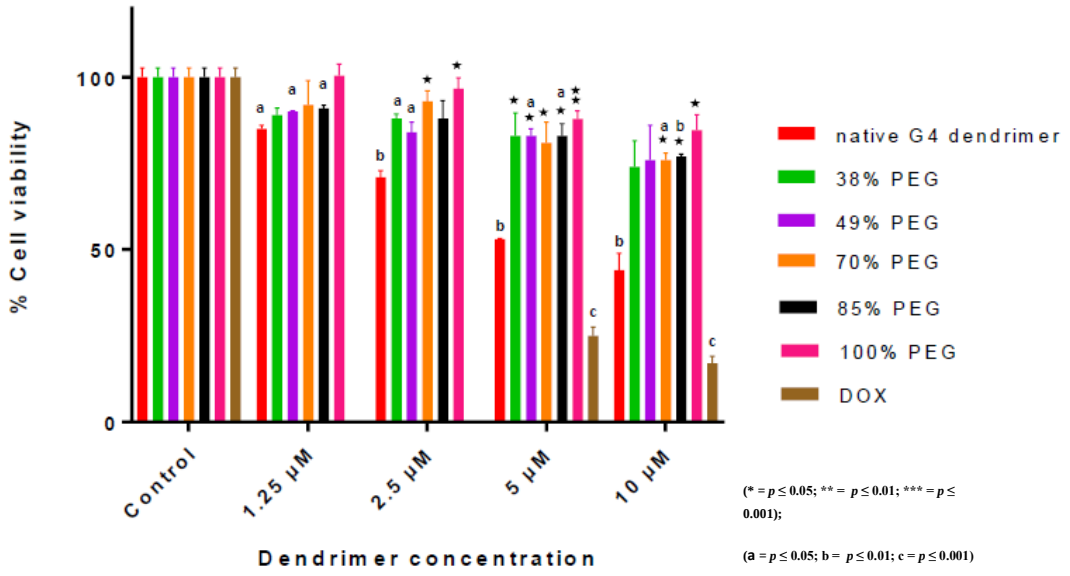

(* = $p \leq 0.05$; ** = $p \leq 0.01$; *** = $p \leq 0.001$);

(a = $p \leq 0.05$; b = $p \leq 0.01$; c = $p \leq 0.001$)

(a)

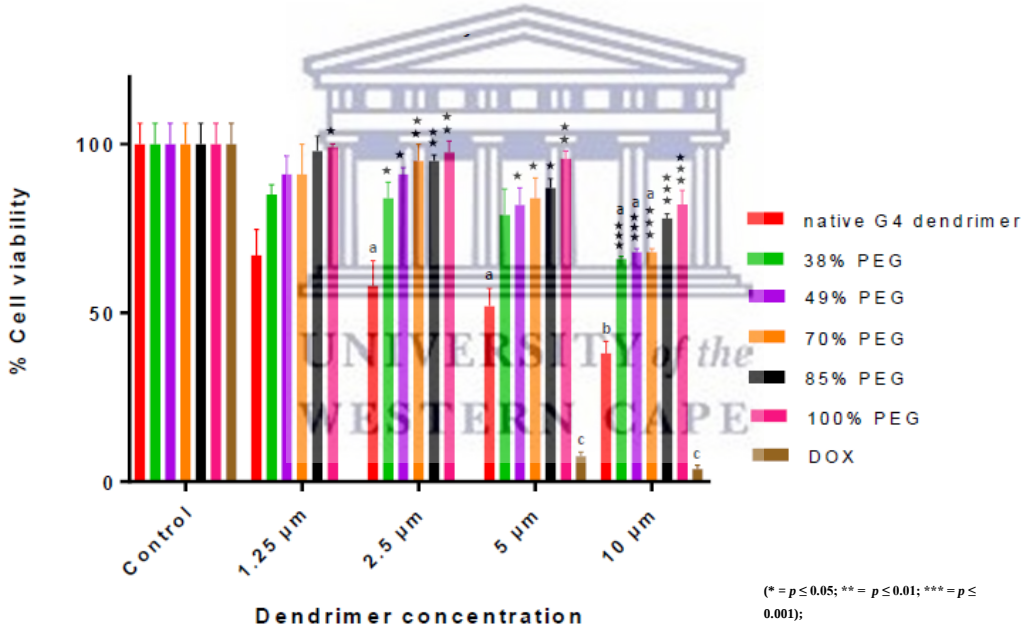

(* = $p \leq 0.05$; ** = $p \leq 0.01$; *** = $p \leq 0.001$);

(a = $p \leq 0.05$; b = $p \leq 0.01$; c = $p \leq 0.001$)

(b)

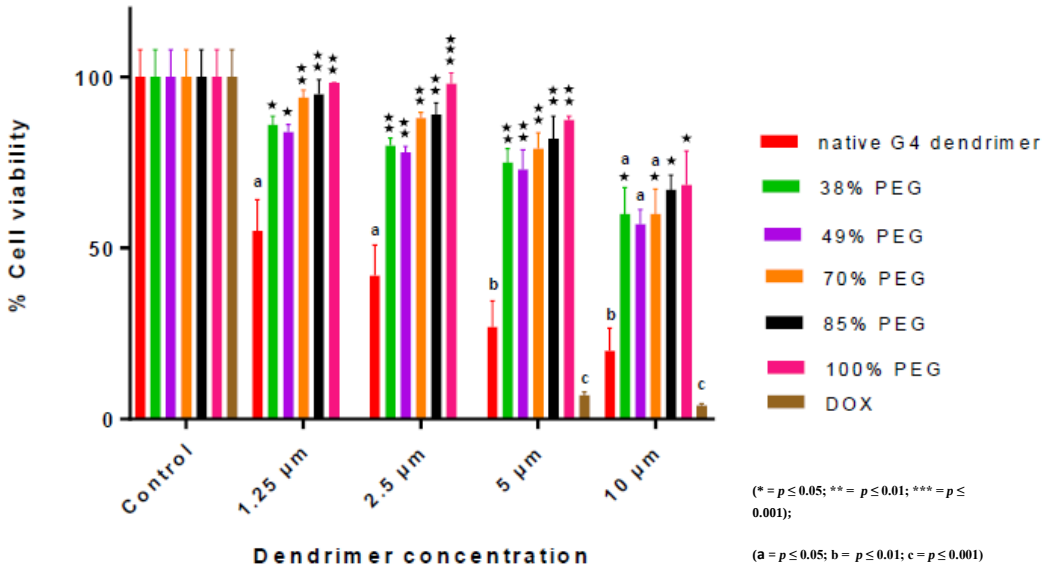

(c)

Figure 6.8 Cell survival (%) on raw cells for increasing PEGylated dendrimer concentrations (1.25 µM – 10 µM), after (a) 24 hrs, (b) 48 hrs, and (c) 72 hrs of incubation. The untreated cells were employed as a negative control and doxorubicin drug was used as a positive control. (n = 3). (*) denotes statistical significance difference compared to the unmodified dendrimer at each concentration, while letter (a,b, and c) symbols denote statistical significance difference compared to the control.

After 24 hrs of incubation (Figure 6.8 (a)), toxicity data indicated that PEGylation has improved the biocompatibility of dendrimer nanoparticles against raw cells compared to the unmodified dendrimer. PEGylated dendrimers have superior cell survival (%) comparative to the unmodified dendrimer and cell survival was directly proportional to the degree of dendrimer PEGylation. There was no statistical difference observed between the dendrimer formulations at the lowest concentration (i.e., 1.25 µM) ($p > 0.05$), while significant differences were detected between unmodified and PEGylated dendrimers by increasing dendrimer concentration. This observation could suggest that dendrimer toxicity is concentration dependant. Up to 5 µM, PEGylated dendrimers were non-toxic to the cell lines with cell survival (%) above 80%, whereas the unmodified dendrimer decreased cell population to 54%. For the entire study concentrations, the 100% PEGylated dendrimer does not exhibit toxicity to the cells compared to the viability control ($p > 0.05$).

After 48 hrs of incubation (Figure 6.8 (b)), the trend of cell viability of mannosylated dendrimers was comparable to what was observed for 24 hrs of incubation at all concentrations (statistically insignificant difference, $p > 0.05$). The cell viability of the unmodified dendrimer toxicity was decreased by increasing dendrimer concentration and a statistically lower cell population was noticed for the concentrations 2.5 µM, 5 µM, and µM 10 compared to the control viability ($p < 0.05$). For the entire concentration range, PEGylated dendrimers enhanced the cell viability and an extreme statistical difference between PEGylated and unmodified dendrimers was noticed at 10 µM. Up to 5 µM PEGylated dendrimer nanoparticles were non-toxic to raw cells with a viability above 80%. Both 85% and 100% PEGylated dendrimers did not show significant differences in their cell viability compared to the control viability throughout the concentration range.

After 72 hrs of incubation (Figure 6.8 (c)), the cell viability data of the mannosylated dendrimers showed comparable results to that at 24 hrs and 48 hrs (statistical insignificant difference, $p > 0.05$) at all concentrations. The unmodified dendrimer exhibited lower cellular population values compared to that at 24 hrs and 48 hrs. The reduction in cell population was a function of dendrimer concentration. Up to 2.5 µM, PEGylated dendrimers did not show toxicity to the raw cells and the cell survival was above 80%, while the unmodified dendrimer decreased cell viability to 42% at a similar concentration. Among PEGylated dendrimers, cell viability was also positively related to the extent of dendrimer PEGylation for the entire study concentrations.

The abovementioned finding in Figure 6.8, besides the data in Figure 6.9 indicated that the toxicity of G4 PAMAM dendrimer towards raw cells was concentration-dependent and time-dependent toxicity.

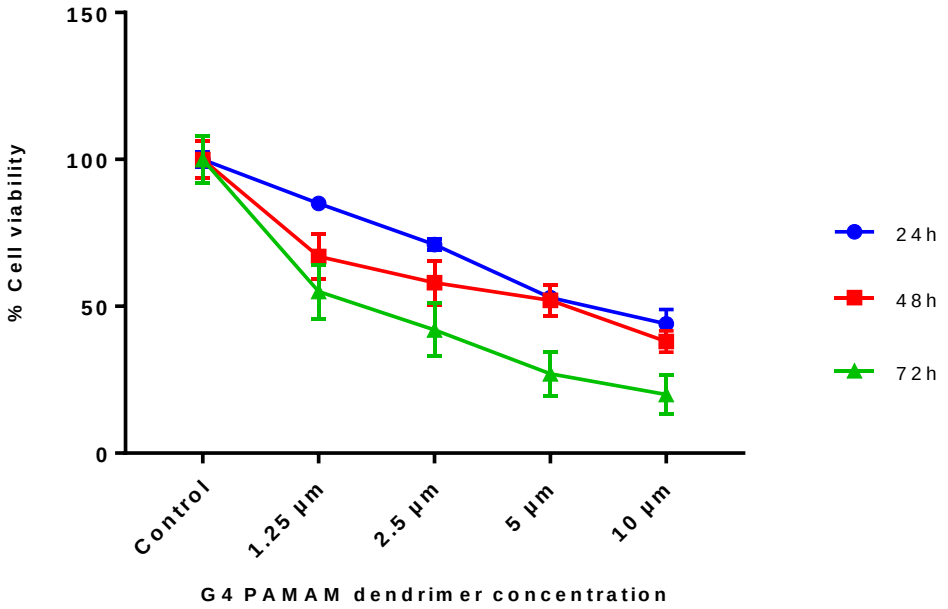

Figure 6.9 Cell survival (%) on raw cells for increasing unmodified G4 PAMAM dendrimer concentrations (1.25 µM – 10 µM), after 24 hrs, 48 hrs, and 72 hrs of incubation (n = 3).

The biocompatibility of any newly developed material is an essential element that controls its application for human use. There are various steps in drug development, starting from the preclinical phase that involves *in vitro* experiments (such as cytotoxicity test) and *in vivo* experiments (animal studies), followed by the clinical phase that involves testing the candidate material into humans (FDA, 2018). Hence, cytotoxicity is the frontline of biocompatibility testing. The novel dendrimer formulations were assessed firstly *in vitro* in cell lines before *in vivo* studies could even be considered to verify their safety.

The ISO standard (10993-5) illustrates the endpoint when evaluating the cytotoxicity of a candidate material by either: (i) assessing the cellular damage by morphological techniques, (ii) determining the cell damage, (iii) measuring the cell proliferation, (iv) measuring particular features of cellular metabolism (Kirkpatrick *et al.*, 1998). The MTT assay is a quantifiable test that measures the cell metabolic function (Kirkpatrick *et al.*, 1998). This assay can provide information regarding the effect of rifampicin, native dendrimer, loaded and unloaded surface-modified dendrimers on raw cells.

The raw 264.7 cells were selected as a testing cell line in this study. Raw 264.7 are monocyte/macrophage-like cells originating from Abelson leukemia virus-transformed cell line derived from BALB/c mice. They are widely used in literature and have been suggested as an appropriate model of macrophages (Taciak *et al.*, 2018). They are capable of doing pinocytosis and phagocytosis (Taciak *et al.*, 2018).

It has been well recognized that PAMAM dendrimers suffer from significant toxicity that hampers their use due to the presence of cationic charges at the dendrimer periphery at the physiological pH (Duncan and Izzo, 2005). The main two mechanisms of dendrimer toxicity that have been mentioned in the literature are either by the interaction of cationic surface groups of the dendrimer with the negatively charged components to generate nanoholes that destabilize cell membranes and causes cell lysis (mostly recommended mechanism) (Malik *et al.*, 2000; Chen *et al.*, 2004; Mecke *et al.*, 2005; Kolhatkar *et al.*, 2007) or cationic dendrimers could mediate cellular toxicity by increasing the endolysosomal pH (the proton sponge effect) (Behr, 1993). Various techniques have been applied to alleviate the dendrimer toxicity by manipulating the surface cationic groups to decrease the density of positive charges. Surface functionalization of dendrimers with PEG chains has been suggested as one of the strategies that could decrease dendrimer toxicity due to the shielding of the positively charged groups (Mishra, Gupta and Jain, 2009).

This study assessed the effect of PEG density on the toxicity of the dendrimer. Our results suggests that the toxicity of the unmodified dendrimer was concentration-dependent and time-dependent. Increasing the concentration of the unmodified dendrimer to 10 µM has decreased cell viability to 20% after 72 hrs of treatment. After PEGylation, the biocompatibility of the dendrimer nanoparticles was significantly enhanced due to the shielding effect of positive charges by PEG chains. The increasing trend in cell survival among PEGylated dendrimers for the entire study concentrations can be justified by the fact that lower PEG density shielded fewer surface groups and hence, some of the free positive charges may still interact with the cell membrane and cause cell lysis. While for the higher PEG density most of the dendrimer surface groups were covered and therefore PEG chains possibly interfere with dendrimer-cell membrane interactions. After 72 hrs of incubation, the IC_{50} of unmodified dendrimer was 1.601 µM, while the IC_{50} values of PEGylated dendrimers were not calculated since more than 50% of the cell populations were still alive at the highest dendrimer

concentration. These findings suggest that PEGylation has improved the biocompatibility of dendrimer towards raw cell lines.

For rifampicin-loaded dendrimer formulation, the MTT assay technique was applied to evaluate the toxicity of nanoparticles on raw cells. The analysis was done in an increasing concentration from 0.125 µM – 2 µM. After 24 hrs, 48 hrs, and 72 hrs of incubation, the cell survival (%) of unmodified G4 dendrimer was compared to that of PEGylated dendrimers at each concentration (Figure 6.10).

After 24 hrs of incubation (6.10 (a)), the cell viability of PEGylated dendrimers was higher compared to the unmodified dendrimer nanoparticles. For PEGylated dendrimers, the cell viability is positively associated with the degree of PEGylation. Dendrimer formulations that have the highest PEG density (i.e., 85% and 100%) showed significantly higher cell populations compared to the unmodified dendrimer especially at 0.5 µM, 1 µM, and 2 µM. The 49% and 70% PEGylated dendrimers were not toxic to cells up to 1 µM with viability above 80%. While the 85% and 100% PEGylated formulations were non-toxic to the cells for the entire study concentrations.

After 48 hrs of incubation (Figure 6.10 (b)), a similar trend in the cell viability was observed at 2 µM concentration. Whereas higher cell viability for 38%, 49%, and 70% PEGylated dendrimers was noticed in 0.125 µM, 0.25 µM, and 0.5 µM compared to 85% and 100% PEGylated dendrimers. Data analysis showed that up to 1 µM PEGylated dendrimers were non-toxic to the raw cells (cell viability ≥ 80%), except for 38% PEG dendrimer.

Similarly, after 72 hrs of incubation (Figure 6.10 (c)), PEGylated dendrimers exhibited higher cell viability compared to the unmodified dendrimer. Dendrimer formulations with higher PEG densities showed superior cell viability compared to those with lower PEG densities. Up to 0.5 µM concentration, 38%, 49%, and 70% PEG formulation were not toxic to the cells (cell viability ≥ 80%), whereas 85% and 100% PEG formulations did not exhibit toxicity to the cells up to 1 µM cell (viability ≥ 80%). This could suggest that increasing the density of PEGylation could enhance the biocompatibility of the dendrimer nanoparticles.

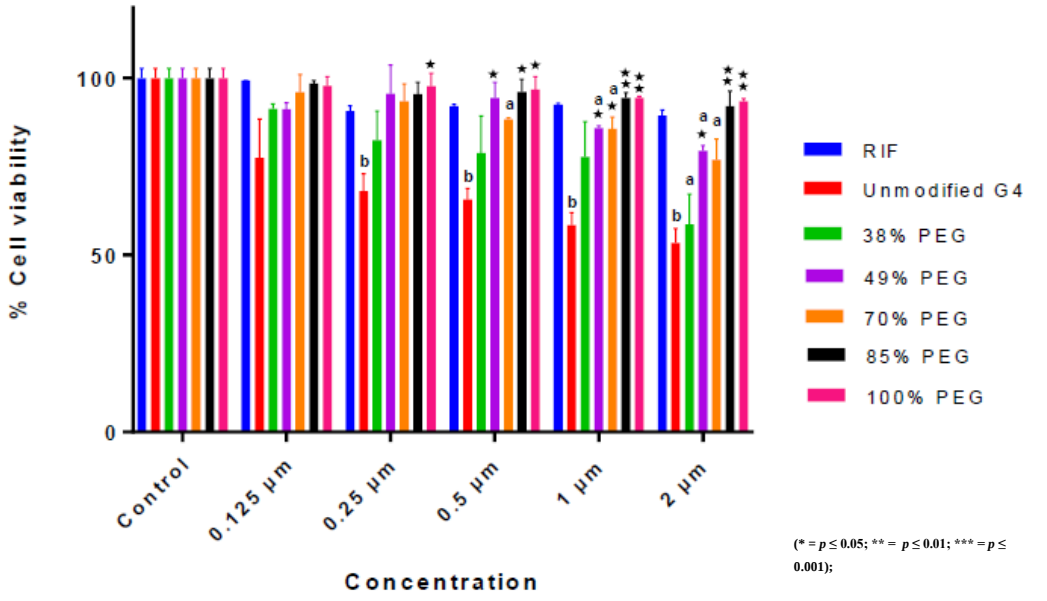

(* = $p \leq 0.05$; ** = $p \leq 0.01$; *** = $p \leq 0.001$);

(a = $p \leq 0.05$; b = $p \leq 0.01$; c = $p \leq 0.001$)

(a)

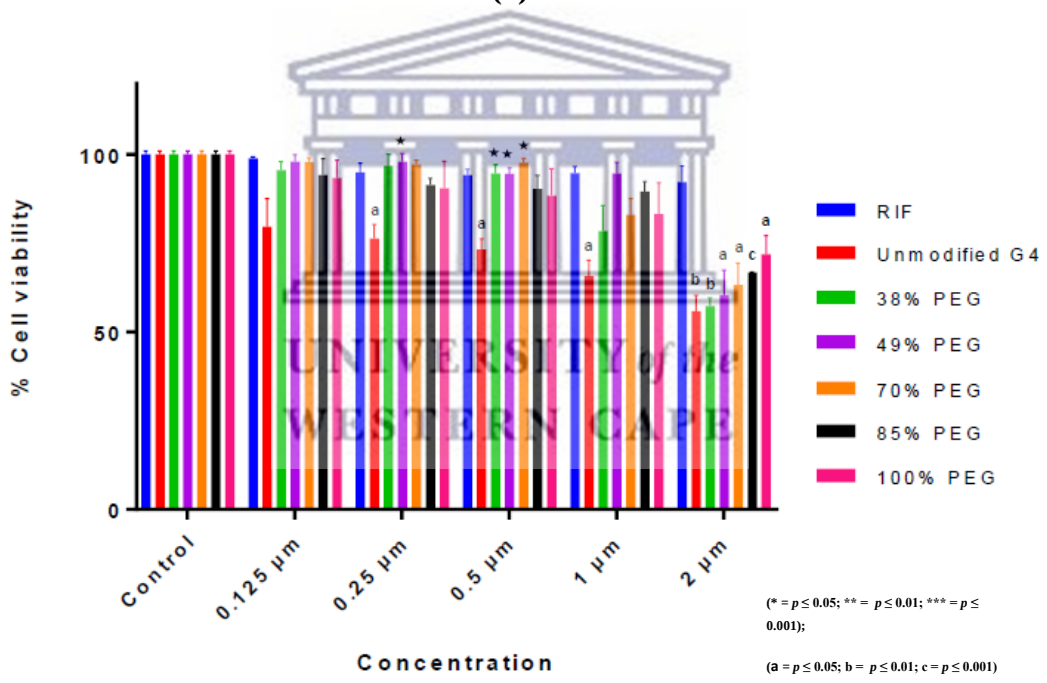

(* = $p \leq 0.05$; ** = $p \leq 0.01$; *** = $p \leq 0.001$);

(a = $p \leq 0.05$; b = $p \leq 0.01$; c = $p \leq 0.001$)

(b)

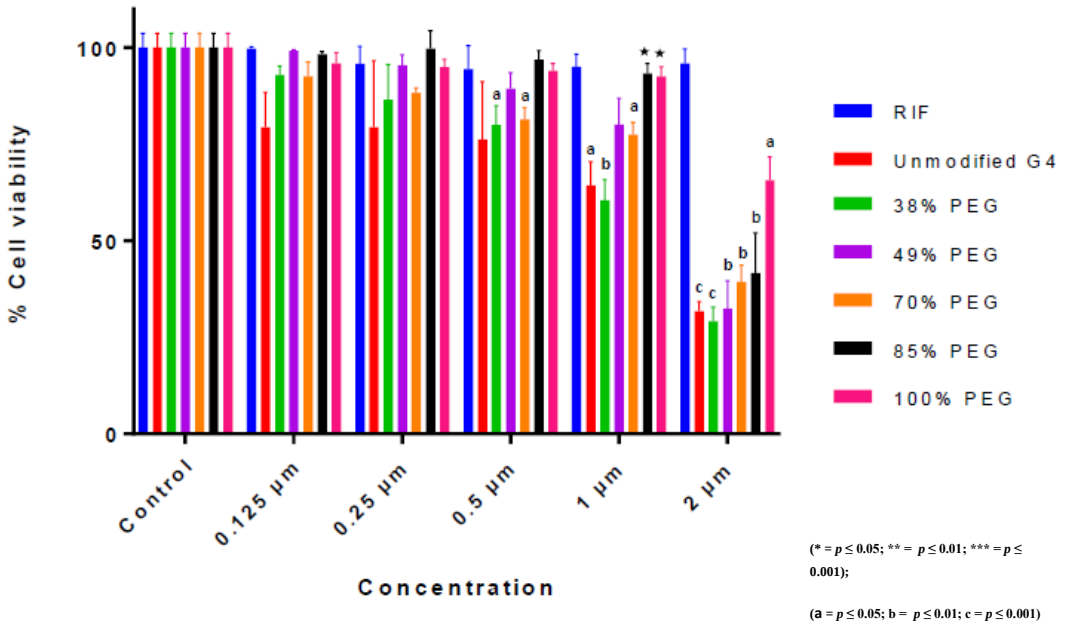

(c)

Figure 6.10 Cell survival (%) on raw cells for increasing rifampicin-loaded PEGylated dendrimer concentrations (0.125 µM – 2 µM), after (a) 24 hrs, (b) 48 hrs, and (c) 72 hrs of incubation. The untreated cells were employed as a negative control (n = 3). (*) denotes statistical significance difference compared to the unmodified dendrimer at each concentration, while letter (a,b, and c) symbols denote statistical significance difference compared to the control.

For rifampicin-loaded dendrimers, the toxicity of the nanoparticles was assessed for the concentration range from 0.125 µM – 2 µM. The higher cell viability for dendrimers with high PEG density can also be explained as a result of superior protection of surface cationic groups.

After 24 hrs of incubation, 49% PEG and 70% PEG formulations were non-toxic up to 1 µM. These results showed that with the developed dendrimers it is possible to use them as a drug delivery system up to this concentration, which corresponds to 60.2 µg/ml and 53.4 µg/ml of rifampicin, respectively. Therefore, a higher drug concentration than the reported bactericidal concentration of rifampicin against *MTB* (3.2 µg/ml) (Yamori *et al.*, 1992), can be used. Whilst for 85% and 100%, which were non-toxic to the cells for the entire study concentrations, it could be possible to use the PEGylated dendrimers with a concentration of 2 µM which correspond to 101.60 µg/ml and 127.20 µg/ml of rifampicin, respectively. Similar observations were also noticed after 48 hrs and 72 hrs of incubation. Overall data indicated that PEGylated dendrimers can be suggested as an appropriate carrier for the safe delivery of rifampicin.

6.7.1.2 Mannosylated dendrimers

For the unloaded mannosylated dendrimers, the toxicity of the nanoparticles was assessed by treating the cells with G4 dendrimer and mannosylated dendrimers in an increasing concentration from 1.25 µM – 10 µM. After 24 hrs, 48 hrs, and 72 hrs of incubation. The cell survival (%) of unmodified G4 dendrimer was compared to that of mannosylated dendrimers at each concentration (Figure 6.11).

After 24 hrs of incubation (Figure 6.11 (a)), mannosylated dendrimers showed better cell viability compared to the unmodified dendrimer for the entire concentrations, however, no statistical difference was detected. The mannosylated dendrimers, nanoparticles that possess higher mannose residues, exhibited an enhanced cell viability compared to those with a lower mannose percentage. Up to 5 µM concentration, all mannosylated dendrimers were non-toxic to the raw cells with viabilities ≥ 80%. Therefore, mannosylated dendrimers with a concentration of 5 µM can safely be used on raw cells.

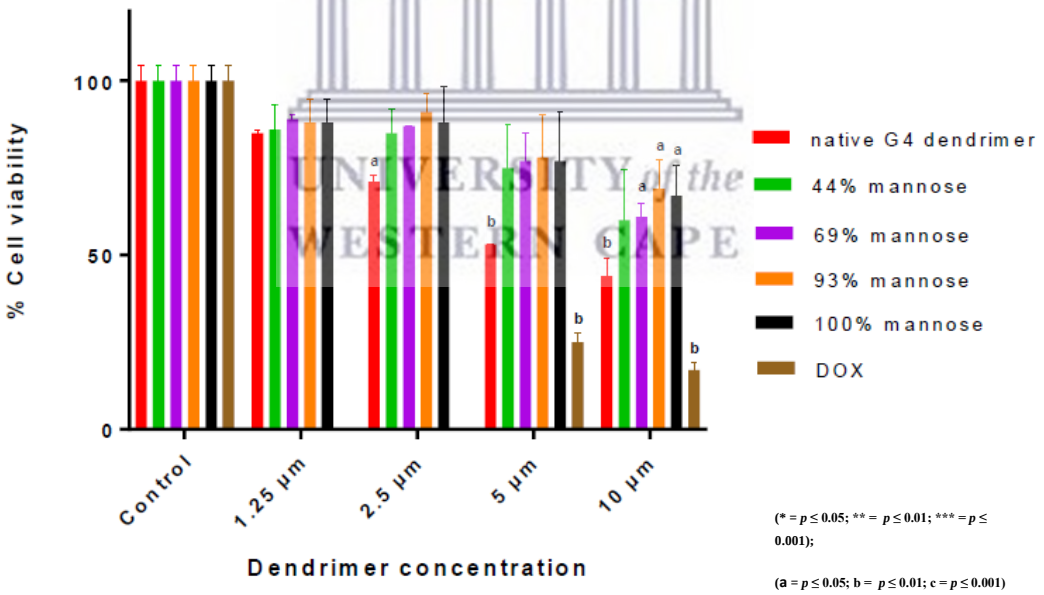

(a)

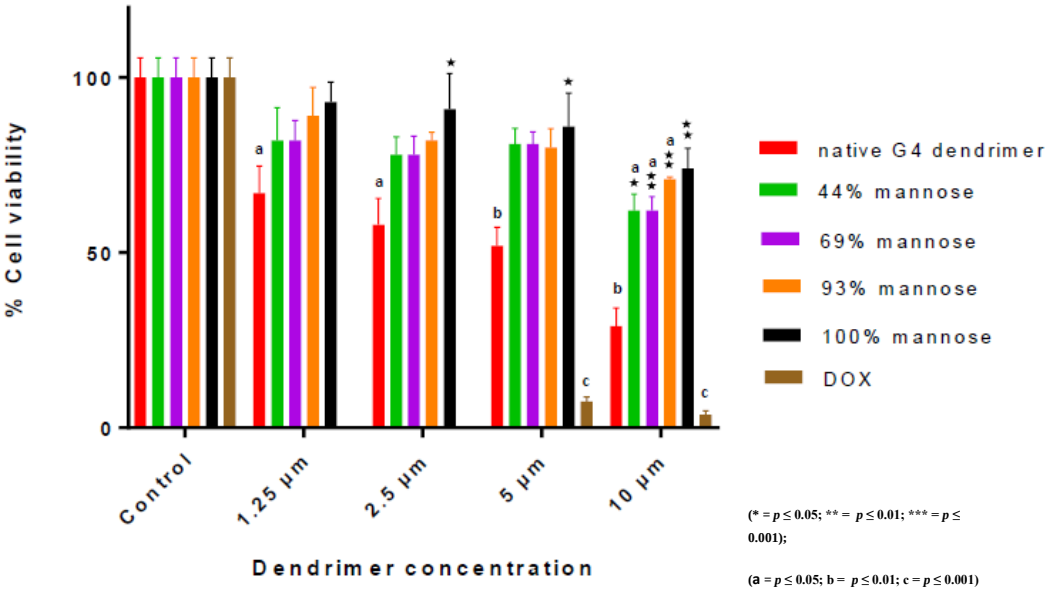

(b)

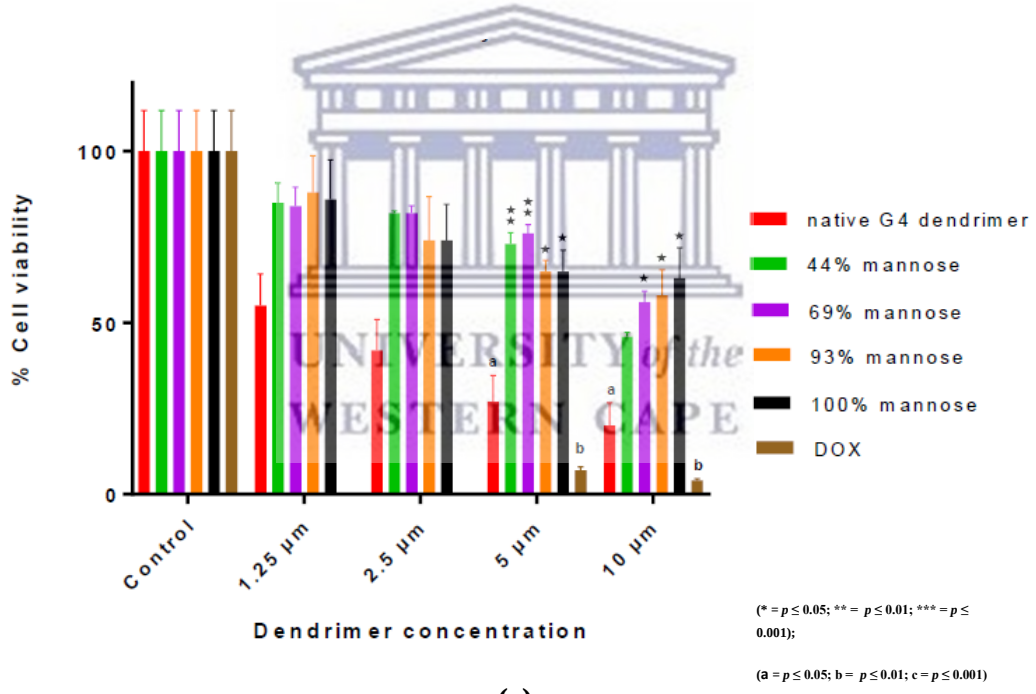

(c)

Figure 6.11 Cell survival (%) on raw cells for increasing mannosylated dendrimer concentrations (1.25 µM – 10 µM), after (a) 24 hrs, (b) 48 hrs, and (c) 72 hrs of incubation. The untreated cells were employed as a negative control and doxorubicin drug was used as a positive control (n = 3). (*) denotes statistical significance difference compared to the unmodified dendrimer at each concentration, while letter (a,b, and c) symbols denote statistical significance difference compared to the control.

After 48 hrs of incubations (Figure 6.11 (b)), mannosylated dendrimers displayed comparable observations to what was seen after 24 hrs of incubation (statistical insignificant difference, $p > 0.05$) at all concentrations. Mannosylated dendrimers exhibited a higher cell survival compared to the unmodified dendrimer for the entire study concentrations. Statistically significant differences between the unmodified and mannosylated dendrimers were observed at the higher concentration, i.e., 10 µM. Whereas, 100% mannosylated dendrimer showed significantly higher cell viability compared to unmodified dendrimer at 2.5 µM, 5 µM, and 10 µM concentrations. Considering mannosylated dendrimers, higher cell survival was linked to nanoparticles that have greater mannose content. Data analysis indicated that up to 5 µM mannosylated dendrimers were not toxic to the raw cells with viabilities ≥ 80%, which can safely be used to deliver drug molecules.

After 72 hrs of incubation (Figure 6.11 (c)), mannosylated dendrimers did not exhibit significant differences in toxicity compared to that at 24 hrs and 48 hrs ($p > 0.05$) at all the concentrations. Mannosylated dendrimers showed a higher cell viability compared to the unmodified dendrimer and significant differences between them were noticed at the higher concentrations i.e., 5 and 10 µM. At 2.5 µM and 5 µM mannosylated dendrimers with lower mannose content (i.e., 44% and 69%) exhibited higher cell survival than mannosylated dendrimers with higher mannose content (i.e., 93% and 100%), however no significant differences were detected. At the highest treatment concentration, the cell viability was positively related to the extent of dendrimer mannosylation with higher cell viability observed to dendrimers with higher mannose percentage. All mannosylated dendrimers were not toxic to raw cells at 1.25 µM concentration with viabilities ≥ 80, while 44% and 69% formulations were safe up to the concentration of 2.5 µM.

As mentioned earlier, cationic PAMAM dendrimers showed significant cytotoxicity towards biological membranes which hampers their use, due to the presence of positive charges at the dendrimer periphery at the physiological pH (Duncan and Izzo, 2005). Another technique that has been suggested in the literature to decrease the dendrimers toxicity is the surface functionalization with carbohydrate molecules (such as mannose residues) (Thakur *et al.*, 2015). Additionally, carbohydrate functionalization can enhance nanoparticle internalization into the macrophages by targeting the lectin receptors (Patel, Gupta and Ahsan, 2015). These two features of carbohydrates could

suggest mannosylated dendrimers as a potential site-specific targeting drug delivery system for anti TB drugs.

Most strategies used to decrease the dendrimer toxicity are focused to reduce the density of surface positive charges to inhibit the interaction with the negatively charged components of the biological membranes (Thakur *et al.*, 2015). Surface conjugation of carbohydrate molecules (such as mannose) could decrease the number of free primary amines and the total positive charges. In Chapter four, we verified the conjugation of mannose residues to the surface amines *via* thiourea linkages, so the density of surface positively charged groups, as well as their related toxicity, are expected to decrease. The decrease in the charge density is directly related to the number of conjugated mannose, so superior biocompatibility is expected to the dendrimer with higher mannose percentage (lower free primary amines).

The MTT results of the unloaded mannosylated dendrimers agreed with what was expected and with previous observations (Kumar *et al.*, 2006; Dutta and Jain, 2007). After 24 hrs, 48 hrs, and 72 hrs of incubation cell survival (%) was in a positive relationship with the extent of dendrimer mannosylation for the entire study concentrations. After 72 hrs of incubation, the IC_{50} of the unmodified dendrimer was 1.601 µM, while the IC_{50} values of 44% mannosylated were 9.795 µM, which indicated that the concentration of 44% mannosylation dendrimer that showed 50% of the cell population was 5.5-fold higher than that of the unmodified dendrimer. The IC_{50} values of other mannosylated dendrimers were not calculated since more than 50% of the cell populations were still alive at the highest dendrimer concentration of the study. These findings suggested that surface mannosylation of PAMAM dendrimer has improved their biocompatibility.

Our results concur with Dutta and co-workers (Dutta *et al.*, 2007), who observed that the unmodified 5.0 G PPI dendrimer experienced time and concentration-dependent toxicity in human hepatoma cell lines. After surface modification with mannose residue, negligible toxicity to the cells was noticed. The authors justified the significant decrease in the dendrimer toxicity after mannosylation could result from the shielding of the surface positive charges by the mannose residues. Comparable observations were also noticed earlier in the literature (Kumar *et al.*, 2006; Dutta and Jain, 2007; Jain *et al.*, 2015; He *et al.*, 2018).

For rifampicin-loaded mannosylated dendrimers (Figure 6.12), the cytotoxicity was assessed for the increasing concentration of dendrimer formulation from 0.125 µM – 2 µM. The MTT results represent a similar trend where the unmodified dendrimer formulation showed time-dependent and concentration-dependent toxicity, while for the mannosylated formulations higher cell viability was observed and the toxicity was inversely proportional to the degree of dendrimer mannosylation.

After 24 hrs of incubation (Figure 6.12 (a)), it was observed that mannosylated dendrimers showed a higher cell population compared to the unmodified formulation for the entire study concentrations, with significant differences between unmodified and 100% mannosylated dendrimer at all time points (except 0.125 µM). Mannosylated dendrimers with high mannose content (93% and 100%), a superior cell viability was exhibited compared to those with lower mannose content. Up to 1 µM, the nanoparticles were not toxic to the raw cells (viability ≥ 80%).

After 48 hrs of incubation (Figure 6.12 (b)), a similar trend to that after 24 hrs of incubation was observed. Up to 1 µM, the nanoparticles were not toxic to the raw cells (viability ≥ 80%).

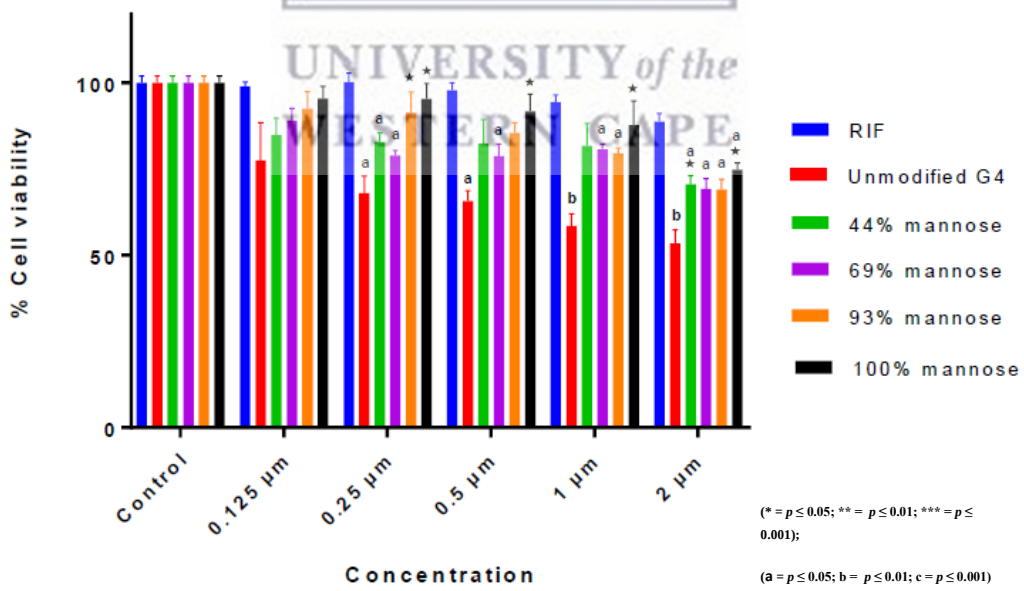

(a)

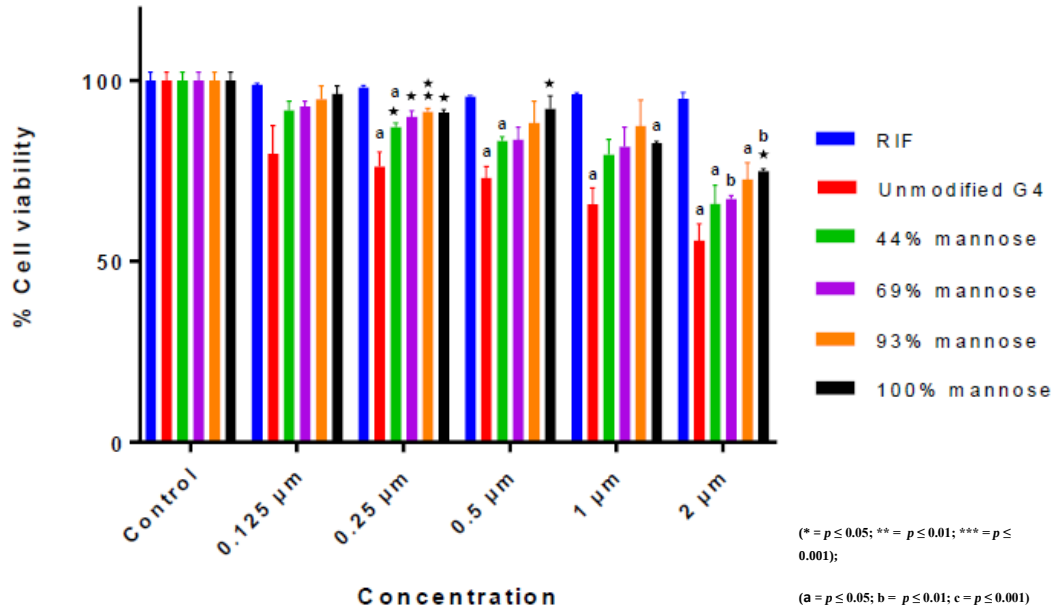

(b)

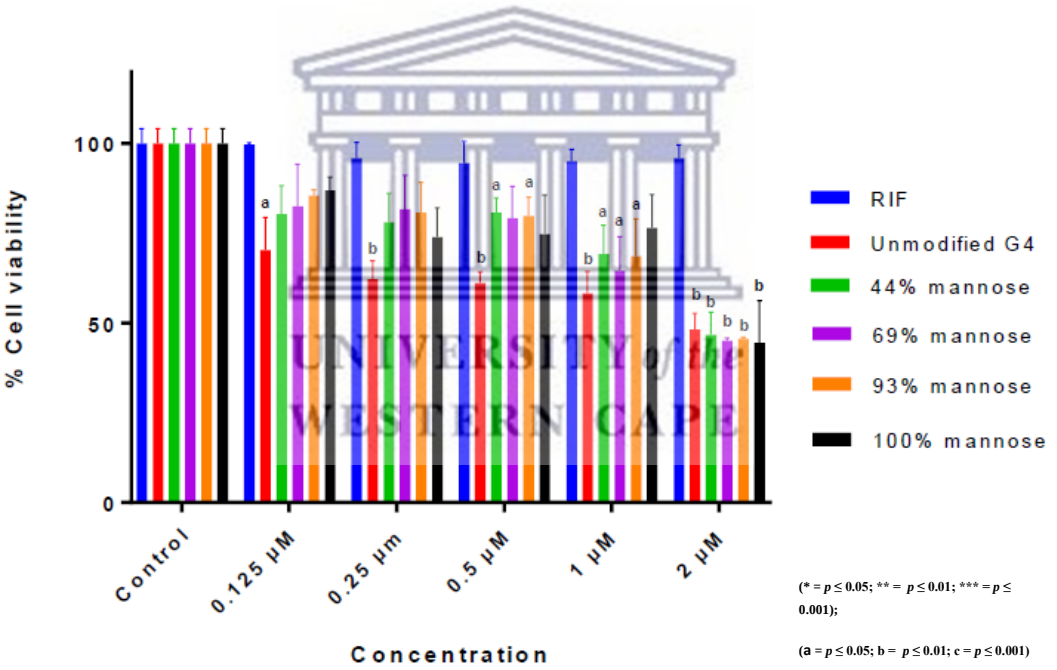

(c)

Figure 6.12 Cell survival (%) on raw cells for increasing rifampicin-loaded mannosylated dendrimer concentrations (0.125 µM – 2 µM), after (a) 24 hrs, (b) 48 hrs, and (c) 72 hrs of incubation. The untreated cells were employed as a negative control (n = 3). (*) denotes statistical significance difference compared to the unmodified dendrimer (0% mannose) at each concentration, while letter (a,b, and c) symbols denote statistical significance difference compared to the control.

After 72 hrs of incubation (Figure 6.12 (c)), mannosylated dendrimer formulations showed higher cell viability compared to the unmodified dendrimer at 0.125 µM, 0.25 µM, 0.5 µM, and 1 µM concentrations. Whereas at concentration 2 µM, comparable cell viability values were noticed between dendrimer formulations. The dendrimer formulations were non-toxic to raw cells at 0.125 µM with viability values ≥ 80%. The positive relationship between the degree of dendrimer mannosylation and their cell viability values were noticed at 0.125 µM and 1 µM concentrations, while the viability values for the other concentration were approximately similar.

For rifampicin-loaded dendrimers, the higher cell viability for dendrimers with high mannose density can also be elucidated as a result of higher shielding to the peripheral positive charges. After 24 hrs and 48 hrs of incubation, dendrimer formulations were non-toxic up to the concentration of 1 µM. This indicates that with the developed 44%, 69%, 93%, and 100% mannosylated dendrimers, it can be safely used as a drug delivery system up to this concentration, which corresponds to 35.50 µg/ml, 37.0 µg/ml, 45.80 µg/ml, and 57.90 µg/ml, respectively. Therefore, a higher drug concentration than the reported bactericidal concentration of rifampicin against *MTB* (3.2 µg/ml) (Yamori *et al.*, 1992), can be used. Likewise, after 72 hrs of incubation, the developed mannosylated dendrimers can be safely used up to 0.125 µM which corresponds to rifampicin concentrations that are higher than the reported bactericidal concentration of rifampicin against *MTB* (3.2 µg/ml) (Yamori *et al.*, 1992).

The overall MTT findings suggests that mannosylated dendrimers, especially those with higher mannose content (93% and 100%), is a promising drug delivery system for the anti TB drug rifampicin with negligible cytotoxicity against raw macrophages.

6.7.2 Microscopic analysis

Figure 6.13 displayed microscopic images of untreated cells, in addition to raw cells after 24 hrs of treatment with 5 µM of DOX and dendrimers. In the positive control, most of the cells were dead. Compared to the negative control, it was observed that the unmodified/native G4 exhibited cytotoxicity towards the raw cells, which was verified by the lower number of cells. For the surface-modified dendrimers, PEGylated and mannosylated dendrimers, the cell viability was significantly enhanced. It was observed that the survival rate was positively related to the density of PEG/mannose on the

dendrimer, negligible toxicity was noticed for dendrimers with high surface functionalization especially for the 100% dendrimer formulations.

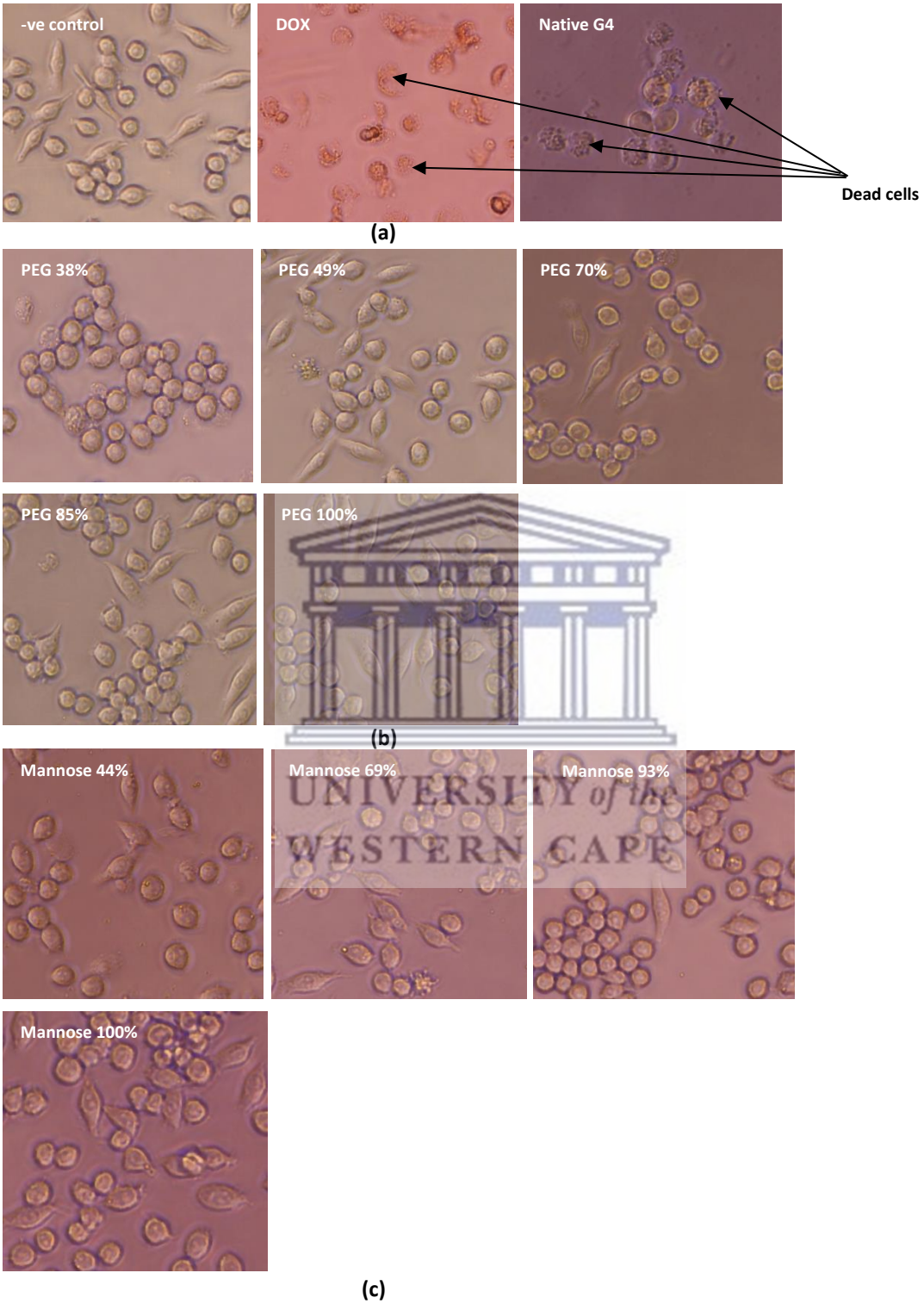

Figure 6.13 Microscopic images of raw cells treated with 5 µM of DOX and dendrimers for 24 hrs. The images were obtained by the Invitrogen EVOS cell imaging system. (a)

include the –ve control, +ve control and the native G4, (b) PEGylated dendrimers, and (c) mannosylated dendrimers.

6.7.3 Labeling of the dendrimer nanoparticles

Dendrimer nanoformulations were labeled with FITC molecules to assess nanoparticles' internalization into raw cells. FITC conjugation was verified by the ^{1}H NMR technique. Furthermore, the ^{1}H NMR technique was employed to determine the approximate number of FITC attached to the dendrimer. Calculating the integral ratio of the peak area which corresponds to the methylene protons next to the carbonyl groups of PAMAM dendrimer (δ = 2.19 ppm), to the peak area corresponds to the aromatic protons at chemical shifts (δ) 6.55 ppm, 6.61 ppm, and 6.68 ppm. An average molar ratio of 1:2.2 dendrimer:FITC was successfully achieved for all nanoformulations.

Figure 6.14 illustrates the ^{1}H NMR spectra of 38% PEGylated dendrimer and FITC-labeled PEGylated dendrimer (38%), the aromatic peaks that were highlighted with square shape were used to quantify the attached FITC molecules. Similar results were also obtained for mannosylated dendrimers.

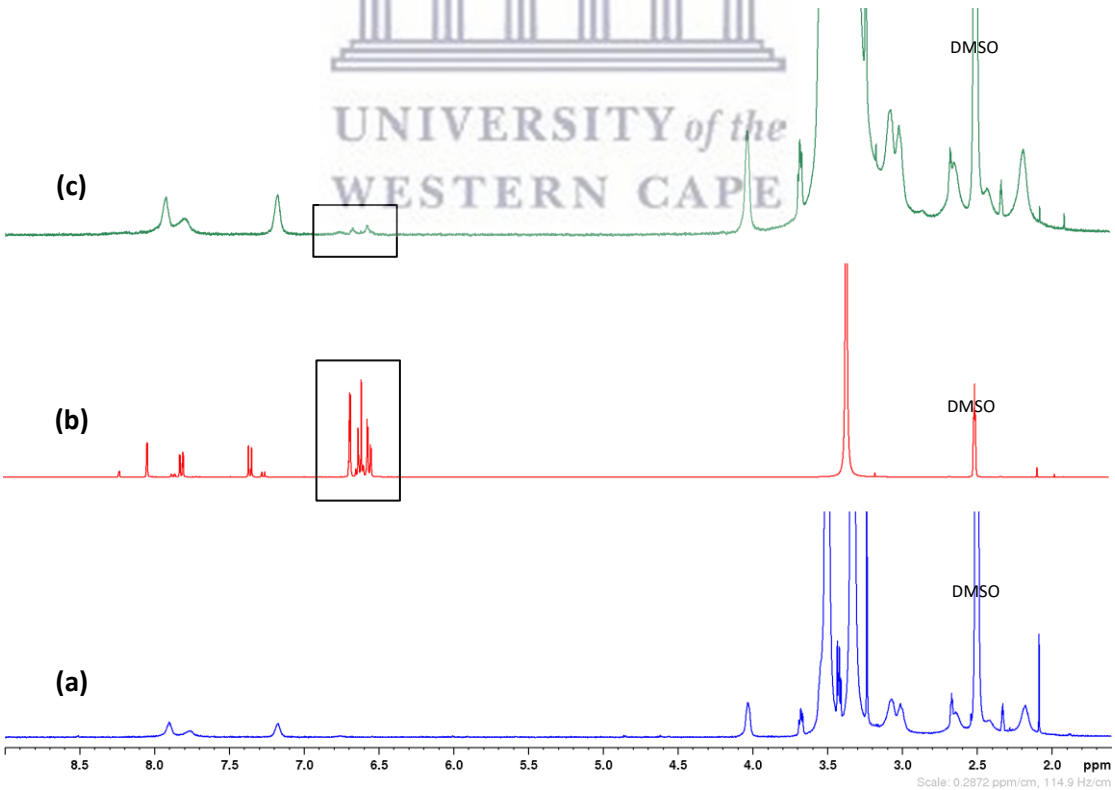

Figure 6.14 ^{1}H NMR spectra of (a) 38% PEGylated dendrimer, (b) FITC, and (c) FITC-labeled PEGylated dendrimer (38%).

6.7.4 Cellular uptake studies

The permeability of the unmodified G4 PAMAM dendrimer and surface-modified dendrimer formulations was assessed across raw macrophage cell lines. The study was performed by treating the raw cells with a predetermined non-toxic concentration of FITC labelled-dendrimers i.e., 5 µM. Cellular uptake of the FITC-labeled dendrimer nanoparticles was evaluated after 24 hrs of incubation by measuring the mean fluorescence intensity (MFI) of each dendrimer formulation using a flow cytometer.

6.7.4.1 PEGylated dendrimers

Cellular internalization of PEGylated dendrimers was studied under a flow cytometer. Figure 6.15, showed the internalized FITC labeled dendrimers as a function of their FITC-height (FITC-H) after 24 hrs of incubation. From Figure 6.15 (a), it was observed that dendrimers were successfully internalized into the raw cells due to the shift in the FITC-H peaks of the labeled dendrimers relative to the untreated cells (control). The percentage of positive FITC-staining cells (Figure 6.15 (b)) was directly related to the degree of dendrimer PEGylation. The highest percentage of +ve cells was noticed with the unmodified dendrimer. Among PEGylated dendrimers, the percentage of +ve cells was inversely associated with the PEG content of the dendrimer, and significantly lower +ve cells were observed for 85% and 100% PEGylated dendrimers compared to the unmodified dendrimer ($p < 0.05$).

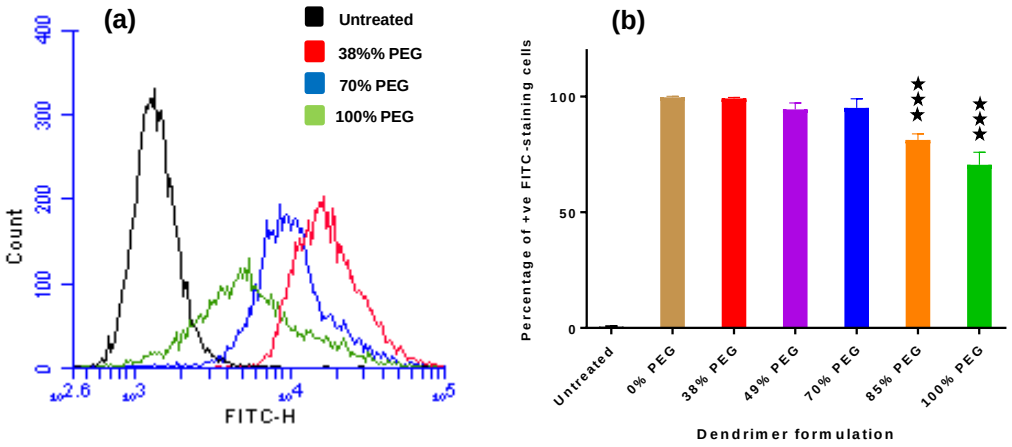

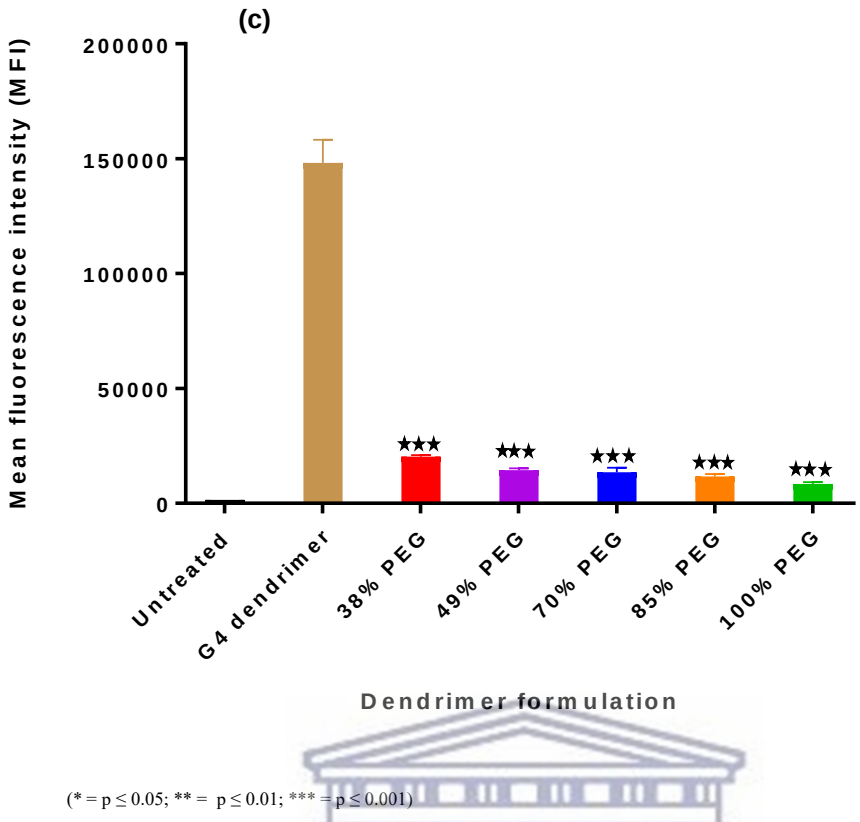

Figure 6.15 Endocytic uptake of FITC-labeled PEGylated dendrimers (5 µM) in raw cells after 24 hrs of incubation. (a) Flow cytometric analysis, (b) percentage of +ve-FITC-staining cells, and (c) mean fluorescence intensity of dendrimer nanoformulations (n = 3). (*) denotes statistical significance difference compared to the unmodified dendrimer.

The internalized nanoparticles were quantitatively assessed by determining the mean fluorescence intensity (MFI) of FITC-labeled dendrimers as illustrated in Figure 6.15 (c). Data analysis showed that surface PEGylation of dendrimers significantly decreased its permeability across the raw cells compared to the native G4 PAMAM dendrimer ($p < 0.05$). The order of internalization after 24 hrs of incubation was the unmodified G4 > 38% PEG > 49% PEG > 70% PEG > 85% PEG > 100% PEG. The MFI of 38% PEG, 49% PEG, 70% PEG, 85% PEG, and 100% PEG dendrimers were 7.3, 10.3, 11.0, 12.6, and 17.6-fold lower than the unmodified dendrimer ($p < 0.05$), respectively. Among PEGylated dendrimers, the MFI was inversely proportional to the extent of dendrimer PEGylation. No statistically significant differences were detected between PEGylated dendrimers ($p > 0.05$), the only exception was observed between 38% and 100% PEGylated dendrimers ($p < 0.05$).

6.7.4.2 Mannosylated dendrimer

Cellular internalization of mannosylated dendrimers was evaluated under a flow cytometer. In Figure 6.16 (a), it is observed that dendrimers were successfully internalized into the raw cells due to the shift in the FITC-H peaks of the labeled dendrimers relative to the untreated cells (control), and the extreme shift is observed for dendrimer with higher mannose content.

The percentage of positive FITC-staining cells (Figure 6.16 (b)) is almost similar for the dendrimer formulations which ranged from 99.97% – 96.57% ($p > 0.05$). These results indicate that approximately all the cells have engulfed the dendrimer nanoparticles.

Data analysis of the MFI of the internalized FITC-labelled dendrimers (Figure 6.16 (c)), showed that surface mannosylation has significantly increased cellular internalization of dendrimer nanoparticles across the raw cells after 24 hrs of incubation ($p < 0.05$). The extreme statistically significant differences were observed for 69%, 93%, and 100% mannosylated dendrimers compared to the unmodified dendrimer ($p < 0.05$).

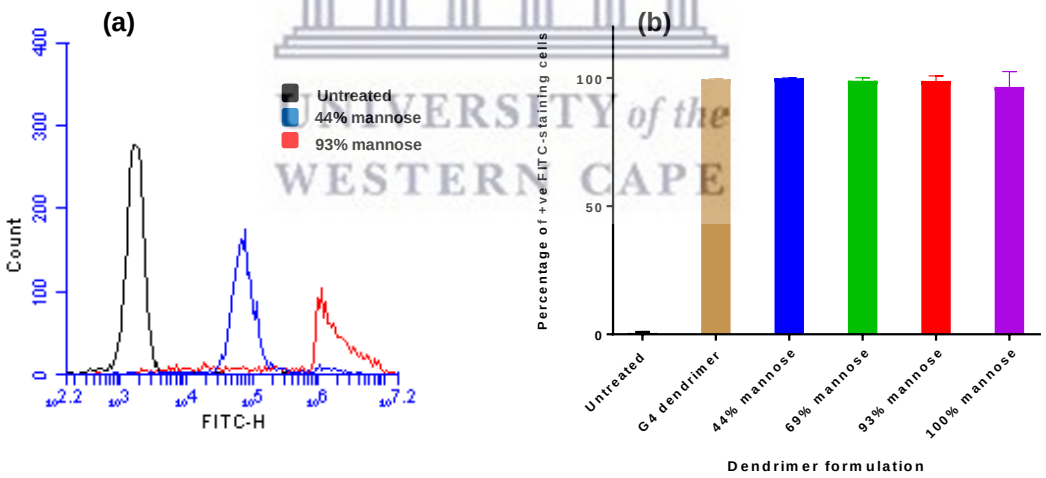

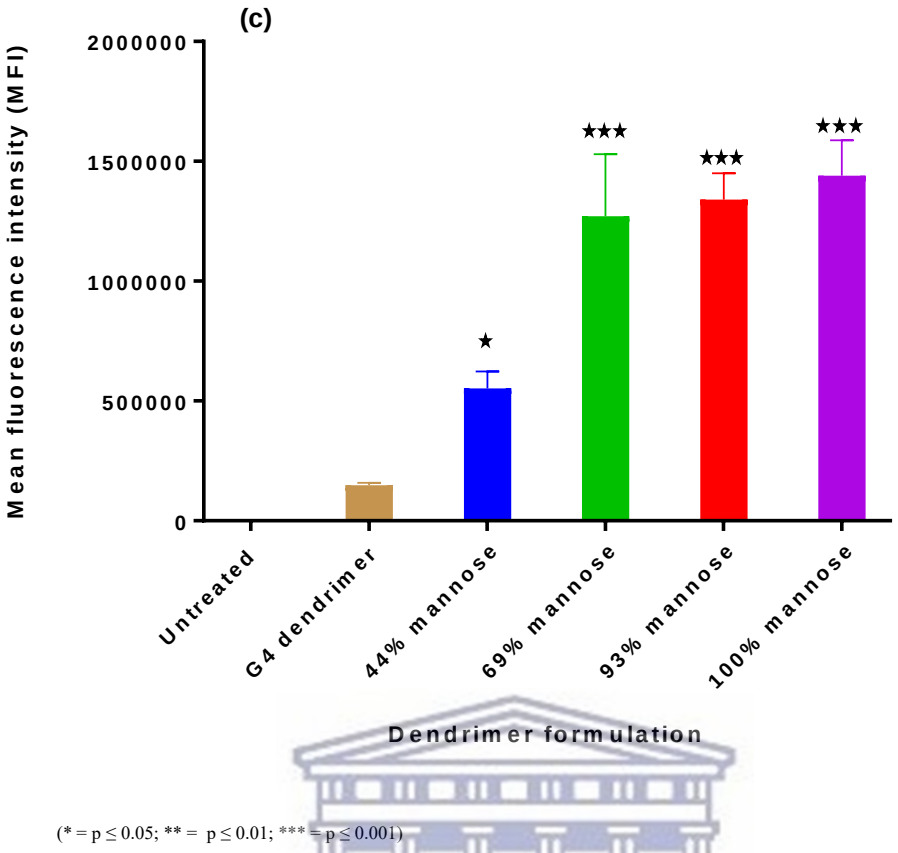

Figure 6.16 Endocytic uptake of FITC-labeled mannosylated dendrimers (5 µM) in raw cells after 24 hrs of incubation. (a) Flow cytometric analysis, (b) percentage of +ve-FITC-staining cells, and (c) mean fluorescence intensity of dendrimer nanoformulations (n = 3). (*) denotes statistical significance difference compared to the unmodified dendrimer.

The order of internalization after 24 hrs of incubation was the unmodified G4 < 44% mannose < 69% mannose < 93% mannose < 100% mannose. The MFI of 44%, 69%, 93%, and 100% mannosylated dendrimers were 3.7, 8.6, 9.1, and 9.7-fold higher than the unmodified dendrimer ($p < 0.05$), respectively. Among mannosylated dendrimers, the MFI was positively associated with the extent of dendrimer mannosylation. The MFI value of the 44% mannosylated dendrimer formulation was significantly lower than those with higher mannose content (69%, 93%, and 100%) ($p < 0.05$). No statically significant differences were noticed between 69%, 93%, and 100% mannosylated dendrimer formulations ($p > 0.05$).

Cellular permeability investigations showed that mannosylated dendrimers were intensively internalized by raw cells compared to the unmodified dendrimer as well as PEGylated dendrimers.

Endocytosis is an active cellular trafficking mechanism to uptake small molecules, macromolecules, and particles. Endocytosis is commonly classified into phagocytosis and pinocytosis (Mukherjee, Ghosh and Maxfield, 1997). Phagocytosis involves the transport of large particles (such as foreign particles and bacteria), whereas pinocytosis involves the transport of small particles (such as nanoparticles). The endocytotic trafficking and proper intracellular permeability is a privilege for the effective performance of drug delivery systems (Rejman, Bragonzi and Conese, 2005). Most of the literature reports indicated that cellular internalization of dendrimers is typically influenced by the surface nature of the dendrimer besides the cell model used (Perumal *et al.*, 2008; Wang *et al.*, 2009; Albertazzi *et al.*, 2010; Zhu *et al.*, 2010).

In Figure 6.15, it is observed that the cellular uptake is decreased as the PEG density on the dendrimer surface increases. The highest cellular uptake was observed for the unmodified dendrimer, as shown by the leveling off of the MFI values. While for the PEGylated dendrimers, the trend in cellular internalization was inversely associated with the PEG density. This can be attributed to the typical uptake mechanism of cationic dendrimers, which are assumed to take place by charge-mediation, facilitated by the presence of negatively charged components of the cell membrane i.e., proteoglycans (electrostatic interactions) (Perumal *et al.*, 2008). However, the MFI values of PEGylated dendrimers were gradually reduced with the increase in PEG density, which can be elucidated by the shielding of positive charges with PEG chains. Accordingly, a decrease in the interaction of dendrimer nanoparticles with the cell surface may result in lower surface adsorption that would subsequently lead to endocytosis (Perumal *et al.*, 2008; Sweet *et al.*, 2009). Minimum MFI was obtained by 100% PEG dendrimer because most of the surface charges were shielded by the PEG chain. Among the PEGylated dendrimers, the highest MFI was achieved by the 38% PEG formulation, since it has the superior unmodified surface amines.

A previous study was performed by Zhu and co-workers involving partial PEGylation of amino-terminated PAMAM dendrimer where increasing the density of PEG (i.e., 5000 Da) on the surface of the dendrimer, caused a significant decrease in the cellular uptake in murine B16 melanoma cells (Zhu *et al.*, 2010). The authors noticed that the decrease in the uptake had a strong association with the zeta potential of dendrimers. Increasing the density of PEG chains could negatively affect the cellular internalization of dendrimers by lowering the zeta potential of the nanoparticles and their surface

charges (Zhu *et al.*, 2010). Another study done by Sweet and co-workers involved using PEG 750 Da to manipulate the surface of G3.5 and 4.5 PAMAM dendrimers (anionic dendrimer) (Sweet *et al.*, 2009). Similarly, they observed that PEGylation reduced nanoparticle transport across Caco-2 cells due to the decrease in the dendrimer surface charges. Conversely, the addition of similar PEG chains had enhanced cellular internalization of G4.5 dendrimer on the same cell lines, signifying that appropriate charge density may be necessary for improving or decreasing the dendrimer transport into cells (Sweet *et al.*, 2009).

An earlier study carried out by Bharatwaj and co-workers using amino-terminated G3 PAMAM dendrimer had various PEG 1000 Da content (Bharatwaj *et al.*, 2015). A decrease in the cellular uptake (Human bronchial epithelial cell lines, Calu-3) was observed upon increasing the PEG density on the dendrimer. They suggested that the decrease in the cellular internalization could reveal that PEGylation had modulated the uptake of the nanoparticles, as determined by flow cytometry and cell lysis studies. Interestingly, the authors noticed a rapid increase in the transport rate across epithelial monolayers for dendrimer with higher PEG content compared to those with lower and 0% PEG content. Furthermore, *in vivo* data from both pulmonary and intravenous routes showed a significant increase in the plasma concentration of dendrimer with the highest PEG content compared to those with lower PEG and 0% PEG. This observation can be justified by the rapid transport of the PEGylated dendrimer across the Calcu-3 cells, which suggest higher absorption (evidenced by higher K_a), besides the characteristic of stealth dendrimer that enhances the circulation time by the lowest clearance (evidenced by lower K_{e1}) (Bharatwaj *et al.*, 2015). The overall results suggest that functionalizing the dendrimer with appropriate surface content of PEG chains can be used to modulate the uptake and the transport of the nanoparticles into and across the pulmonary epithelium which may be employed to develop such drug delivery systems for treating either local pulmonary diseases or targeting peripheral organs by using the pulmonary route of administration (Bharatwaj *et al.*, 2015).

On the other hand, one of the typical approaches that have been widely employed to promote the internalization of nanoparticles into macrophages (such as alveolar macrophages), is the active targeting technique (Patel, Gupta and Ahsan, 2015). Active targeting involves surface functionalization of the drug carrier with ligands to target particular receptors at the surface of the macrophage, such as lectin receptors (Patel,

Gupta and Ahsan, 2015). Targeting the mannose/lectin receptors using carbohydrate ligands (such as mannose residues) is mostly used to enhance drug delivery to the alveolar macrophages (Kumar *et al.*, 2006; Nimje *et al.*, 2009; Song *et al.*, 2015).

From Figure 6.16, the trend in cellular internalization, expressed as MFI, was positively associated with the density of mannose residues on the surface of dendrimers. The highest MFI value was obtained by dendrimer with 100% mannose density, while the minimal MFI value was obtained by unmodified dendrimer (0% mannose) followed by 44% mannose formulation. For active targeting, firstly the ligand epitope(s) should interact specifically with the binding spot(s) on the receptor before mediating endocytosis. Since C-type lectin receptors (mannose receptors) are highly expressed on the surface of the alveolar macrophages (Ishii and Akira, 2008), the concentration-dependent uptake can be attributed to the high possibility of interactions between the mannose epitopes and the receptor binding spot(s) on the cellular surface. By increasing the ligand density (mannose), both multivalent interactions and glycoside cluster effect are expected to be involved in the interaction mechanisms with lectin receptors of the raw macrophages. This observation can explain the higher cellular internalization of the dendrimer with high mannose content (100% mannose) compared to those with low or 0% mannose content.

As receptor-mediated endocytosis is more effective than the charge-mediated interactions (Dutta and Jain, 2007), this could elucidate the extremely significant increase in the cellular uptake of mannosylated dendrimers compared to the unmodified dendrimer ($p < 0.05$), especially for those with higher mannose density.

Many literature reports have verified the enhanced internalization of mannosylated dendrimer into cells which are highly expressed with lectin receptors (Kumar *et al.*, 2006; Dutta and Jain, 2007; Dutta *et al.*, 2007; Jain *et al.*, 2015; He *et al.*, 2018).

6.7.5 Fluorescence microscope analysis

Qualitative analysis of FITC-labeled dendrimers was performed for unmodified, PEGylated, and mannosylated formulations using fluorescence microscopy (Figure 6.17). The merged fluorescence image of the unmodified dendrimer (Figure 6.17 (a)) showed that the green colour of FITC-labeled dendrimer could be seen in most of the cells, which was accumulated in the cytoplasm. It was observed that the number of cells

decreased, which could result from the cytotoxic behaviour of the unmodified cationic dendrimer.

For PEGylated nanoformulations (Figure 6.17 (b & c)), dendrimers that have the highest and the lowest PEG density were selected for the analysis i.e., 38% and 100% formulations. Fluorescence images for both formulations showed that few cells picked up the green dye. Relatively a higher green fluorescein was noticed in cells treated with 38% PEG dendrimer compared to those treated with 100% PEG dendrimer. The internalized nanoparticles were accumulated in the cytoplasm, as the green colour surrounds the blue nuclei in all cells.

For mannosylated dendrimers (Figure 6.17 (d&e)), 44% and 69% mannosylated dendrimers were analyzed under fluorescence microscopy. A significant increase in the intensity of fluorescein was observed for both formulations compared to the unmodified and PEGylated dendrimers. It was observed that the increase in the fluorescein was positively related to the density of mannose, a higher intensity was noticed for 69% formulation. In addition to the cytoplasmic accumulation of the FITC-mannosylated dendrimers, some of the green dye overlapped the blue nuclei, which suggested that nanoparticles could enter the cell nucleus.

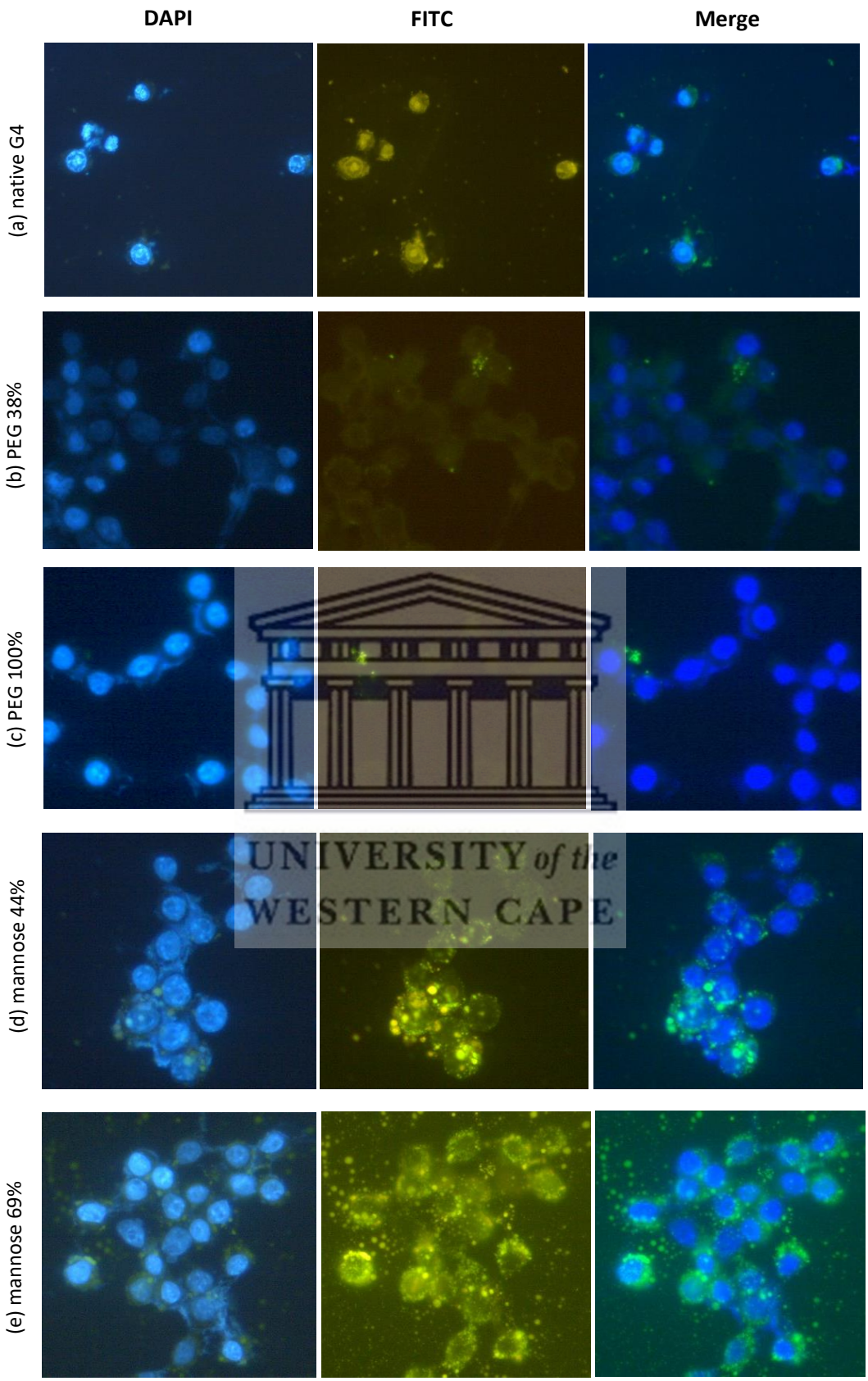

Figure 6.17 Fluorescence images of raw264.7 cells incubated with 5 µM of FITC-labeled dendrimers (green dye) (a) unmodified dendrimer, (b) 38% PEG-dendrimer, (c)

100% PEG-dendrimer, (d) 44% mannose-dendrimer, and (e) 69% mannose-dendrimer, showing uptake after 24 hrs. The nuclei were stained with DAPI (blue dye).

The fluorescence analysis agreed and further confirmed our flow cytometer results (Figures 6.15 and 6.16). The negative relationship between the nanoparticle's internalization and their PEG density was also observed here. As well as, the mannose concentration-dependent dendrimer uptake appeared in the fluorescence images of mannosylated dendrimers. Lower uptake in PEGylated dendrimers was previously illustrated in section 6.7.4, which was associated with the density of surface charges. For mannosylated dendrimers, the lectin receptor-mediated endocytosis probably facilitated the nanoparticle's uptake, which could elucidate the enhanced transport into raw cells.

The majority of the dendrimers were found in the cytoplasm, while the mannosylated dendrimers were also detected in the nucleus of some cells. This can be justified by the molecular weight of the mannosylated dendrimers which are less than 50 kDa. Since small molecules that are less than 6 nm in size or molecular weight less than 60 kDa are identified to be able to diffuse across the nucleus pores (Allen *et al.*, 2000), mannosylated dendrimers were expected to simply enter the nucleus. This observation was not seen in the case of PEGylated dendrimers, as their molecular weights are greater than 60 kDa.

6.8 Conclusion

In the present study, the toxicity and the permeability characteristics of the native G4, as well as the surface-modified dendrimer (PEG or mannose), were evaluated on raw 264.7 cells. MTT results verified that the toxicity of the native G4 was concentration-dependent and time-dependent. Whereas for the surface-modified dendrimers (PEG or mannose) the cytotoxicity was significantly reduced, and negligible toxicity was observed for dendrimers with 100% of PEG or mannose. Thus, they can establish the suitability of such dendrimer formulations as a delivery system for the anti TB drug, rifampicin. Flow cytometer findings besides the fluorescence microscopy analysis of the FITC-dendrimers on raw cells confirmed that the nanoparticles were successfully internalized and were imaged with cell's nuclei. Besides the cytoplasmic accumulation, mannosylated dendrimers were also seen in the nucleus of some cells due to their molecular weights (< 60 kDa). The uptake of mannosylated dendrimers was

significantly higher than the unmodified dendrimer as well as PEGylated dendrimer, due to lectin receptors-mediated endocytosis. The lower internalization of PEGylated dendrimers resulted from the decrease of surface charges by PEG conjugation, thus mannosylated dendrimers can be suggested as potential targeting drug delivery to the macrophages. PEGylated dendrimers can be used to modulate the uptake and the transport of nanoparticles into and across the pulmonary epithelium which may be employed to develop a drug delivery system for treating either local pulmonary diseases or targeting peripheral organs by using the pulmonary route of administration.

6.9 References

Agashe, H.B., Dutta, T., Garg, M. and Jain, N.K., (2006). Investigations on the toxicological profile of functionalized fifth-generation poly (propylene imine) dendrimer. *Journal of pharmacy and pharmacology*, *58*(11), pp.1491-1498.

Akinc, A., Thomas, M., Klibanov, A.M. and Langer, R., (2005). Exploring polyethylenimine-mediated DNA transfection and the proton sponge hypothesis. *The Journal of Gene Medicine: A cross-disciplinary journal for research on the science of gene transfer and its clinical applications*, *7*(5), pp.657-663.

Albertazzi, L., Serresi, M., Albanese, A. and Beltram, F., (2010). Dendrimer internalization and intracellular trafficking in living cells. *Molecular pharmaceutics*, *7*(3), pp.680-688.

Allen, T.D., Cronshaw, J.M., Bagley, S., Kiseleva, E. and Goldberg, M.W., (2000). The nuclear pore complex: mediator of translocation between nucleus and cytoplasm. *Journal of cell science*, *113*(10), pp.1651-1659.

Arredouani, M.S., Palecanda, A., Koziel, H., Huang, Y.C., Imrich, A., Sulahian, T.H., Ning, Y.Y., Yang, Z., Pikkarainen, T., Sankala, M. and Vargas, S.O., (2005). MARCO is the major binding receptor for unopsonized particles and bacteria on human alveolar macrophages. *The Journal of Immunology*, *175*(9), pp.6058-6064.

Behr, J.P., (1993). Synthetic gene-transfer vectors. *Accounts of Chemical Research*, *26*(5), pp.274-278.

Bhadra, D., Yadav, A.K., Bhadra, S. and Jain, N.K., (2005). Glycodendrimeric nanoparticulate carriers of primaquine phosphate for liver targeting. *International journal of pharmaceutics*, *295*(1-2), pp.221-233.

Bharatwaj, B., Mohammad, A.K., Dimovski, R., Cassio, F.L., Bazito, R.C., Conti, D., Fu, Q., Reineke, J. and da Rocha, S.R., (2015). Dendrimer nanocarriers for transport modulation across models of the pulmonary epithelium. *Molecular pharmaceutics*, *12*(3), pp.826-838.

Boas, U., Karlsson, A.J., De Waal, B.F.M. and Meijer, E.W., (2001). Synthesis and properties of new thiourea-functionalized poly (propylene imine) dendrimers and their role as hosts for urea functionalized guests. *The Journal of organic chemistry*, *66*(6), pp.2136-2145.

Boas, U. and Heegaard, P.M., (2004). Dendrimers in drug research. *Chemical Society Reviews*, *33*(1), pp.43-63.

Chen, H.T., Neerman, M.F., Parrish, A.R. and Simanek, E.E., (2004). Cytotoxicity, hemolysis, and acute in vivo toxicity of dendrimers based on melamine, candidate vehicles for drug delivery. *Journal of the American Chemical Society*, *126*(32), pp.10044-10048.

Conner, S.D. and Schmid, S.L., (2003). Regulated portals of entry into the cell. *Nature*, *422*(6927), pp.37-44.

Diaz, C., Guzmán, J., Jiménez, V.A. and Alderete, J.B., (2018). Partially PEGylated PAMAM dendrimers as solubility enhancers of Silybin. *Pharmaceutical development and technology*, *23*(7), pp.689-696.

Doherty, G.J. and McMahon, H.T., (2009). Mechanisms of endocytosis. *Annual review of biochemistry*, *78(1)*, pp.857-902.

Donnelly, L.E. and Barnes, P.J., (2012). Defective phagocytosis in airways disease. *Chest*, *141*(4), pp.1055-1062.

Duncan, R. *et al.* (1991) 'Soluble Polymeric Drug Carriers: Haematocompatibility', in *Progress in Membrane Biotechnology*. Birkhäuser Basel, pp. 253–265. doi: 10.1007/978-3-0348-7454-0_18.

Duncan, R., Bhakoo, M., Riley, M.L. and Tuboku-Metzger, A., (1991). Soluble polymeric drug carriers: haematocompatibility. In *Progress in membrane biotechnology*, pp. 253-265. Birkhäuser Basel.

Duncan, R. and Izzo, L.,(2005). Dendrimer biocompatibility and toxicity. *Advanced drug delivery reviews*, *57*(15), pp.2215-2237.

Dutta, T., Agashe, H.B., Garg, M., Balasubramanium, P., Kabra, M. and Jain, N.K., (2007). Poly (propyleneimine) dendrimer based nanocontainers for targeting of efavirenz to human monocytes/macrophages in vitro. *Journal of drug targeting*, *15*(1), pp.89-98.

Dutta, T. and Jain, N.K., (2007). Targeting potential and anti-HIV activity of lamivudine loaded mannosylated poly (propyleneimine) dendrimer. *Biochimica et Biophysica Acta (BBA)-General Subjects*, *1770*(4), pp.681-686.

FDA (2018) *The Drug Development Process | FDA*, *FDA*. Available at: https://www.fda.gov/patients/learn-about-drug-and-device-approvals/drug-development-process (Accessed: 18 November 2020).

Fischer, D., Li, Y., Ahlemeyer, B., Krieglstein, J. and Kissel, T., (2003). In vitro cytotoxicity testing of polycations: influence of polymer structure on cell viability and hemolysis. *Biomaterials*, *24*(7), pp.1121-1131.

Fox, L.J., Richardson, R.M. and Briscoe, W.H., (2018). PAMAM dendrimer-cell membrane interactions. *Advances in Colloid and Interface Science*, *257*, pp.1-18.

Greenberg, S. and Grinstein, S., (2002). Phagocytosis and innate immunity. *Current opinion in immunology*, *14*(1), pp.136-145.

Hakkimane, S.S., Shenoy, V.P., Gaonkar, S.L., Bairy, I. and Guru, B.R., (2018). Antimycobacterial susceptibility evaluation of rifampicin and isoniazid benz-hydrazone in biodegradable polymeric nanoparticles against Mycobacterium tuberculosis H37Rv strain. *International journal of nanomedicine*, *13*, pp.4303-4318.

He, H., Yuan, Q., Bie, J., Wallace, R.L., Yannie, P.J., Wang, J., Lancina III, M.G., Zolotarskaya, O.Y., Korzun, W., Yang, H. and Ghosh, S., (2018). Development of mannose functionalized dendrimeric nanoparticles for targeted delivery to macrophages: use of this platform to modulate atherosclerosis. *Translational Research*, *193*, pp.13-30.

Heise, A., Hedrick, J.L., Frank, C.W. and Miller, R.D., (1999). Starlike block copolymers with amphiphilic arms as models for unimolecular micelles. *Journal of the American Chemical Society*, *121*(37), pp.8647-8648.

Ho, M.N., Bach, L.G., Nguyen, T.H., Ho, M.H., Nguyen, D.H., Nguyen, C.K., Nguyen, C.H., Nguyen, N.V. and Thi, T.T.H., (2019). PEGylated poly (amidoamine) dendrimers-based drug loading vehicles for delivering carboplatin in treatment of various cancerous cells. *Journal of Nanoparticle Research*, *21*(2), p.43.

Hong, S., Bielinska, A.U., Mecke, A., Keszler, B., Beals, J.L., Shi, X., Balogh, L., Orr, B.G., Baker Jr, J.R. and Banaszak Holl, M.M., (2004). Interaction of poly (amidoamine) dendrimers with supported lipid bilayers and cells: hole formation and the relation to transport. *Bioconjugate chemistry*, *15*(4), pp.774-782.

Hong, S., Leroueil, P.R., Janus, E.K., Peters, J.L., Kober, M.M., Islam, M.T., Orr, B.G., Baker

Jr, J.R. and Banaszak Holl, M.M., (2006). Interaction of polycationic polymers with supported lipid bilayers and cells: nanoscale hole formation and enhanced membrane permeability. *Bioconjugate chemistry*, *17*(3), pp.728-734.

Ishii, K. J. and Akira, S. (2008). Innate immunity, in *Clinical Immunology*. Elsevier Ltd, pp. 39–51.

Jain, K., Kesharwani, P., Gupta, U. and Jain, N.K., (2010). Dendrimer toxicity: Let's meet the challenge. *International journal of pharmaceutics*, *394*(1-2), pp.122-142.

Jain, K., Verma, A.K., Mishra, P.R. and Jain, N.K., (2015). Surface-engineered dendrimeric nanoconjugates for macrophage-targeted delivery of amphotericin B: formulation development and in vitro and in vivo evaluation. *Antimicrobial agents and chemotherapy*, *59*(5), pp.2479-2487.

Jain, V., Swarnakar, N.K., Mishra, P.R., Verma, A., Kaul, A., Mishra, A.K. and Jain, N.K., (2012). Paclitaxel loaded PEGylated gleceryl monooleate based nanoparticulate carriers in chemotherapy. *Biomaterials*, *33*(29), pp.7206-7220.

Jansen, J.F., De Brabander-van den Berg, E. M. M, and Meijer, E.W., (1994). Encapsulation of guest molecules into a dendritic box. *Science*, *266*(5188), pp.1226-1229.

Jansen, J.F., Meijer, E.W. and de Brabander-van den Berg, E.M., (1995). The dendritic box: shape-selective liberation of encapsulated guests. *Journal of the American Chemical Society*, *117*(15), pp.4417-4418.

Jayaraman, N., Nepogodiev, S.A. and Stoddart, J.F., (1997). Synthetic Carbohydrate-Containing Dendrimers. *Chemistry–A European Journal*, *3*(8), pp.1193-1199.

Jevprasesphant, R., Penny, J., Attwood, D., McKeown, N.B. and D'emanuele, A., (2003). Engineering of dendrimer surfaces to enhance transepithelial transport and reduce cytotoxicity. *Pharmaceutical Research*, *20*(10), pp.1543-1550.

Jevprasesphant, R., Penny, J., Jalal, R., Attwood, D., McKeown, N.B. and D'emanuele, A., (2003). The influence of surface modification on the cytotoxicity of PAMAM dendrimers. *International journal of pharmaceutics*, *252*(1-2), pp.263-266.

Kiama, S.G., Cochand, L., Karlsson, L., Nicod, L.P. and Gehr, P., (2001). Evaluation of phagocytic activity in human monocyte-derived dendritic cells. *Journal of aerosol medicine*, *14*(3), pp.289-299.

Kichler, A., Leborgne, C., Coeytaux, E. and Danos, O., (2001). Polyethylenimine-mediated gene delivery: a mechanistic study. *The journal of gene medicine*, *3*(2), pp.135-144.

Kirkpatrick, C.J., Bittinger, F., Wagner, M., Köhler, H., Van Kooten, T.G., Klein, C.L. and Otto, M., (1998). Current trends in biocompatibility testing. *Proceedings of the Institution of Mechanical Engineers, Part H: Journal of Engineering in Medicine*, *212*(2), pp.75-84.

Kiss, A.L. and Botos, E., (2009). Endocytosis via caveolae: alternative pathway with distinct cellular compartments to avoid lysosomal degradation?. *Journal of cellular and molecular medicine*, *13*(7), pp.1228-1237.

Kolhatkar, R.B., Kitchens, K.M., Swaan, P.W. and Ghandehari, H., (2007). Surface acetylation of polyamidoamine (PAMAM) dendrimers decreases cytotoxicity while maintaining membrane permeability. *Bioconjugate chemistry*, *18*(6), pp.2054-2060.

Kono, K., Kojima, C., Hayashi, N., Nishisaka, E., Kiura, K., Watarai, S. and Harada, A., (2008). Preparation and cytotoxic activity of poly (ethylene glycol)-modified poly (amidoamine)

dendrimers bearing adriamycin. *Biomaterials*, *29*(11), pp.1664-1675.

Kumar, P.V., Asthana, A., Dutta, T. and Jain, N.K., (2006). Intracellular macrophage uptake of rifampicin loaded mannosylated dendrimers. *Journal of drug targeting*, *14*(8), pp.546-556.

Kumari, S., Swetha, M.G. and Mayor, S.,(2010). Endocytosis unplugged: multiple ways to enter the cell. *Cell research*, *20*(3), pp.256-275.

Leroueil, P.R., Hong, S., Mecke, A., Baker Jr, J.R., Orr, B.G. and Banaszak Holl, M.M.,(2007). Nanoparticle interaction with biological membranes: does nanotechnology present a Janus face?. *Accounts of chemical research*, *40*(5), pp.335-342.

Leroueil, P.R., Berry, S.A., Duthie, K., Han, G., Rotello, V.M., McNerny, D.Q., Baker Jr, J.R., Orr, B.G. and Banaszak Holl, M.M., (2008). Wide varieties of cationic nanoparticles induce defects in supported lipid bilayers. *Nano letters*, *8*(2), pp.420-424.

Liu, H., Jiang, A., Guo, J. and Uhrich, K.E., (1999). Unimolecular micelles: synthesis and characterization of amphiphilic polymer systems. *Journal of Polymer Science Part A: Polymer Chemistry*, *37*(6), pp.703-711.

Liu, M., Kono, K. and Fréchet, J.M., (1999). Water-soluble dendrimer–poly (ethylene glycol) starlike conjugates as potential drug carriers. *Journal of Polymer Science Part A: Polymer Chemistry*, *37*(17), pp.3492-3503.

Ly, T.U., Tran, N.Q., Hoang, T.K.D., Phan, K.N., Truong, H.N. and Nguyen, C.K., (2013). Pegylated dendrimer and its effect in fluorouracil loading and release for enhancing antitumor activity. *Journal of biomedical nanotechnology*, *9*(2), pp.213-220.

Malik, N., Wiwattanapatapee, R., Klopsch, R., Lorenz, K., Frey, H., Weener, J.W., Meijer, E.W., Paulus, W. and Duncan, R., (2000). Dendrimers:: Relationship between structure and biocompatibility in vitro, and preliminary studies on the biodistribution of 125I-labelled polyamidoamine dendrimers in vivo. *Journal of Controlled Release*, *65*(1-2), pp.133-148.

McMahon, H.T. and Boucrot, E., (2011). Molecular mechanism and physiological functions of clathrin-mediated endocytosis. *Nature reviews Molecular cell biology*, *12*(8), pp.517-533.

Mecke, A., Lee, D.K., Ramamoorthy, A., Orr, B.G. and Banaszak Holl, M.M., (2005). Synthetic and natural polycationic polymer nanoparticles interact selectively with fluid-phase domains of DMPC lipid bilayers. *Langmuir*, *21*(19), pp.8588-8590.

Mishra, V., Gupta, U. and Jain, N.K., (2009). Surface-engineered dendrimers: a solution for toxicity issues. *Journal of Biomaterials Science, Polymer Edition*, *20*(2), pp.141-166.

Mukherjee, S., Ghosh, R. N. and Maxfield, F. R. (1997). Endocytosis, *Physiological Reviews*. American Physiological Society, pp. 759–803.

Newkome, G.R., Yao, Z., Baker, G.R. and Gupta, V.K., (1985). Micelles. Part 1. Cascade molecules: a new approach to micelles. A [27]-arborol. *The Journal of Organic Chemistry*, *50*(11), pp.2003-2004.

Nimje, N., Agarwal, A., Saraogi, G.K., Lariya, N., Rai, G., Agrawal, H. and Agrawal, G.P., (2009). Mannosylated nanoparticulate carriers of rifabutin for alveolar targeting. *Journal of drug targeting*, *17*(10), pp.777-787.

Pagé, D. and Roy, R., (1997). Synthesis and biological properties of mannosylated starburst poly (amidoamine) dendrimers. *Bioconjugate chemistry*, *8*(5), pp.714-723.

Palecanda, A., Paulauskis, J., Al-Mutairi, E., Imrich, A., Qin, G., Suzuki, H., Kodama, T.,

Tryggvason, K., Koziel, H. and Kobzik, L., (1999). Role of the scavenger receptor MARCO in alveolar macrophage binding of unopsonized environmental particles. *The Journal of experimental medicine*, *189*(9), pp.1497-1506.

Palecanda, A. and Kobzik, L., (2001). Receptors for unopsonized particles: the role of alveolar macrophage scavenger receptors. *Current molecular medicine*, *1*(5), pp.589-595.

Patel, B., Gupta, N. and Ahsan, F., (2015). Particle engineering to enhance or lessen particle uptake by alveolar macrophages and to influence the therapeutic outcome. *European Journal of Pharmaceutics and Biopharmaceutics*, *89*, pp.163-174.

Pelkmans, L. and Helenius, A., (2002). Endocytosis via caveolae. *Traffic*, *3*(5), pp.311-320.

Perumal, O.P., Inapagolla, R., Kannan, S. and Kannan, R.M., (2008). The effect of surface functionality on cellular trafficking of dendrimers. *Biomaterials*, *29*(24-25), pp.3469-3476.

Rejman, J., Bragonzi, A. and Conese, M., (2005). Role of clathrin-and caveolae-mediated endocytosis in gene transfer mediated by lipo-and polyplexes. *Molecular Therapy*, *12*(3), pp.468-474.

Satija, J., Gupta, U. and Jain, N.K., (2007). Pharmaceutical and biomedical potential of surface engineered dendrimers. *Critical Reviews™ in Therapeutic Drug Carrier Systems*, *24*(3), pp. 257-306.

Schlick, K.H., Morgan, J.R., Weiel, J.J., Kelsey, M.S. and Cloninger, M.J., (2011). Clusters of ligands on dendrimer surfaces. *Bioorganic & medicinal chemistry letters*, *21*(17), pp.5078-5083..

Sgouras, D. and Duncan, R., (1990). Methods for the evaluation of biocompatibility of soluble synthetic polymers which have potential for biomedical use: 1—use of the tetrazolium-based colorimetric assay (MTT) as a preliminary screen for evaluation ofin vitro cytotoxicity. *Journal of Materials Science: Materials in Medicine*, *1*(2), pp.61-68.

Sonawane, N.D., Szoka, F.C. and Verkman, A.S., (2003). Chloride accumulation and swelling in endosomes enhances DNA transfer by polyamine-DNA polyplexes. *Journal of Biological Chemistry*, *278*(45), pp.44826-44831.

Song, X., Lin, Q., Guo, L., Fu, Y., Han, J., Ke, H., Sun, X., Gong, T. and Zhang, Z., (2015). Rifampicin loaded mannosylated cationic nanostructured lipid carriers for alveolar macrophage-specific delivery. *Pharmaceutical research*, *32*(5), pp.1741-1751.

Stasko, N.A., Johnson, C.B., Schoenfisch, M.H., Johnson, T.A. and Holmuhamedov, E.L., (2007). Cytotoxicity of polypropylenimine dendrimer conjugates on cultured endothelial cells. *Biomacromolecules*, *8*(12), pp.3853-3859.

Stuart, L.M. and Ezekowitz, R.A.B., (2005). Phagocytosis: elegant complexity. *Immunity*, *22*(5), pp.539-550.

Sweet, D.M., Kolhatkar, R.B., Ray, A., Swaan, P. and Ghandehari, H., (2009). Transepithelial transport of PEGylated anionic poly (amidoamine) dendrimers: implications for oral drug delivery. *Journal of controlled release*, *138*(1), pp.78-85.

Taciak, B., Białasek, M., Braniewska, A., Sas, Z., Sawicka, P., Kiraga, Ł., Rygiel, T. and Król, M., (2018). Evaluation of phenotypic and functional stability of RAW 264.7 cell line through serial passages. *PLoS One*, *13*(6), p.e0198943.

Thakur, S., Kesharwani, P., Tekade, R.K. and Jain, N.K., (2015). Impact of pegylation on biopharmaceutical properties of dendrimers. *Polymer*, *59*, pp.67-92.

Thomas, T.P., Majoros, I., Kotlyar, A., Mullen, D., Banaszak Holl, M.M. and Baker Jr, J.R., (2009). Cationic poly (amidoamine) dendrimer induces lysosomal apoptotic pathway at therapeutically relevant concentrations. *Biomacromolecules*, *10*(12), pp.3207-3214.

Tortorella, S. and Karagiannis, T.C., (2014). Transferrin receptor-mediated endocytosis: a useful target for cancer therapy. *The Journal of membrane biology*, *247*(4), pp.291-307.

Tricker, E. and Cheng, G., (2008). With a little help from my friends: modulation of phagocytosis through TLR activation. *Cell research*, *18*(7), pp.711-712.

Vidal, F. and Guzman, L., (2015). Dendrimer nanocarriers drug action: perspective for neuronal pharmacology. *Neural regeneration research*, *10*(7), pp. 1029-1031.

Wang, W., Xiong, W., Wan, J., Sun, X., Xu, H. and Yang, X., (2009). The decrease of PAMAM dendrimer-induced cytotoxicity by PEGylation via attenuation of oxidative stress. *Nanotechnology*, *20*(10), p.105103.

Wen, Z.S., Liu, L.J., Qu, Y.L., OuYang, X.K., Yang, L.Y. and Xu, Z.R., (2013). Chitosan nanoparticles attenuate hydrogen peroxide-induced stress injury in mouse macrophage RAW264. 7 cells. *Marine drugs*, *11*(10), pp.3582-3600.

Williams, D.F., (1989). A model for biocompatibility and its evaluation. *Journal of biomedical engineering*, *11*(3), pp.185-191.

Yamori, S., Ichiyama, S., Shimokata, K. and Tsukamura, M., (1992). Bacteriostatic and bactericidal activity of antituberculosis drugs against Mycobacterium tuberculosis, Mycobacterium avium-Mycobacterium intracellulare complex and Mycobacterium kansasii in different growth phases. *Microbiology and immunology*, *36*(4), pp.361-368.

Yu, K. and Russo, P.S., (1996). Light scattering and fluorescence photobleaching recovery study of poly (amidoamine) cascade polymers in aqueous solution. *Journal of Polymer Science Part B: Polymer Physics*, *34*(8), pp.1467-1475.

Zhu, S., Hong, M., Tang, G., Qian, L., Lin, J., Jiang, Y. and Pei, Y., (2010). Partly PEGylated polyamidoamine dendrimer for tumor-selective targeting of doxorubicin: the effects of PEGylation degree and drug conjugation style. *Biomaterials*, *31*(6), pp.1360-1371.

Chapter 7

Summary, conclusion, and recommendations

7.1 Summary and conclusion of the thesis

Tuberculosis is one of the serious bacterial infections caused by MTB that mainly affects the lungs. Sometimes, the MTB bacilli may diffuse out the pulmonary region and infect peripheral organs causing extra-pulmonary tuberculosis. Many therapeutic agents were developed over the past years to compact TB, however, the rapid emergence of resistant strains hampered their use. Accordingly, the WHO has suggested numerous guidelines for TB treatment to assist all national TB directors in settling policies to achieve cure without relapse or recurrence, minimize transmission, decrease drug resistance, and reduce global prevalence. Long term regimens with multi-drugs are typically advised. Moreover, most of the current anti TB drugs experience many challenges, which can be summarized in treatment regimen factors, co-infection, drug-drug interactions, route of administration, and physicochemical characteristics of drugs (such as permeability into alveolar macrophages). These challenges have a significant role in treatment failure and the emergence of resistant TB. Due to the lack of newly discovered anti-TB drugs, besides the absence of effective vaccines, many scientists have suggested the use of novel modalities for the current anti TB drugs to enhance their efficacy and overcome some of their drawbacks, one of these modalities is nanotechnology-based drug delivery systems.

The introduction of nanotechnology, which is using material at a nano-scale level, has expanded the application of different materials in many areas of science. Nanotechnology is paving the road for pharmaceutical industries from two perspectives, either through participation in the synthesis of new molecular entities that did not exist before or by improving the pharmacokinetic profiles of the existing molecules. Many advantages can be attained from the use of nanotechnology in drug delivery, including enhancing the delivery of poorly water-soluble drugs, precise site targeting of the drugs by using different routes of administration or targeting ligands, enhance drug permeability across various biological membranes, decrease the therapeutic toxicity, improve drug stability, and controlled or prolonged drug release.

This study aimed to develop a novel nanotechnology-based pulmonary delivery system for the treatment of TB. To attain that rifampicin was conjugated to the fourth-generation (G4) PAMAM dendrimer nanoparticles having a range of poly(ethylene glycol) densities or mannose residues, in order to overcome some of the shortcomings of the rifampicin and improve its efficacy.

Dendrimers are synthetic, globular-shaped, three-dimensional, hyperbranched, well-ordered polymeric nanoparticles. Dendrimers have precise constitutional and compositional properties such as size (less than 100 nm), shape, and molecular weight. Amongst the dendrimers family, polyamidoamine (PAMAM) and polypropylene imine (PPI) were extensively employed as drug carriers. The surface groups of PAMAM dendrimer can further be manipulated to improve dendrimer properties and enhance the drug/guest molecule's conjugation. G4 PAMAM dendrimer was employed in this study due to the affordable loading potential for various drugs, besides the lower toxicity compared to higher dendrimer generations.

Poly(ethylene glycol) (PEG) has been extensively applied in the field of drug delivery as characterizes by good solubility in both organic and aqueous solutions, besides its biocompatibility properties. The PEG 2 kDa was selected to manipulate the surface of the dendrimer to enhance the nanoconjugate characteristics, due to superior results that have been achieved in the literature by using this molecular weight. In addition, mannose residues were the second molecule used for surface functionalization of the dendrimer to enhance the targeting capability to the alveolar macrophages.

Rifampicin is one of the most essential therapeutic drugs of the first-line TB regimen. Due to its lipophilic nature and superior retention in the lungs, rifampicin was selected as a model drug to be loaded in native and surface-modified G4 PAMAM dendrimers.

At the beginning, the surface of the G4 dendrimer was functionalized with increasing concentrations of PEG or mannose *via* amide and thiourea linkages, respectively. Then rifampicin molecules were loaded in surface-modified dendrimer formulations by simple dissolution solvent evaporation technique. The loaded and unloaded dendrimer nanoparticles were verified and characterized using various analytical techniques such as NMR, FTIR, SEM, DSC, HPLC, and Zetasizer.

Drug release from unmodified and surface-modified (PEG or mannose) dendrimer formulations was assessed at pH 7.4 and pH 4.5 to predict the release behaviour at

physiological and phagolysosomal environments, respectively. Compared to pure rifampicin, all dendrimer formulations showed prolonged drug release at the physiological pH. Among the surface-modified dendrimers, the rate of drug release was inversely proportional to the density of the conjugated molecule (PEG or mannose). Relatively a higher release rate was observed in pH 4.5 compared to pH 7.4, which suggested the suitability of such carriers for the burst release of the loaded drugs inside the macrophage.

Considering that the novel drug delivery system will be used in human tissues *via* the pulmonary route, it is therefore should be biocompatible. Therefore, the cytotoxicity of the loaded and the unloaded dendrimer formulations was studied against raw cells, one of the widely used in literature and has been suggested as an appropriate model of macrophages. The toxicity results confirmed that the unmodified dendrimer experienced time-dependent and concentration-dependent cytotoxicity against the raw cells. These properties were significantly deceased after surface functionalization of a dendrimer with either PEG chains or mannose residues. The survival rate was positively associated with the density of the surface conjugated molecules (PEG or mannose). Dendrimer formulations with 100% PEG or mannose seemed to be biocompatible to the raw cells, with negligible toxicity. Similarly, the toxicity results of the drug-loaded dendrimers showed that the nanoconjugates are non-toxic up to concentrations that correspond to rifampicin concentration that are significantly higher than the reported bactericidal concentration against *MTB* (3.2 µg/ml). The toxicity results can therefore propose the safety of using the developed dendrimer nanoparticles as a novel pulmonary delivery for treating tuberculosis.

The developed dendrimer nanoparticles were successfully internalized into the raw cells. The order of nanoparticles permeability was PEG 100% < PEG 85% < PEG 70% < PEG 49% < PEG 38% < unmodified dendrimer < mannose 44% < mannose 69% < mannose 93% < mannose 100%. It was known that cellular internalization of the cationic dendrimers could occur *via* charge-mediated endocytosis, through which the internalization of the unmodified dendrimer was expected to take place. So, the decrease in uptake of the nanoparticles by increasing the PEG density can be elucidated by the shielding of positive charges with PEG chains. Minimum MFI was obtained by 100% PEG dendrimer because most of the surface charges were shielded by the PEG chain, while the highest MFI was achieved by the 38% PEG formulation. On the other

hand, mannose ligands significantly enhanced the macrophage uptake of the dendrimer nanoparticles due to their interactions with the lectin receptors that facilitated the endocytosis. Since receptor-mediated endocytosis is more effective than charge-mediated endocytosis, this could support the higher MFI values of mannosylated dendrimers compared to other dendrimer formulations.

Mannosylated dendrimers can be suggested as potential targeting drug delivery to the macrophages, while PEGylated dendrimers can be used to modulate the uptake and the transport of the nanoparticles into and across the pulmonary epithelium which may be employed to develop drug delivery systems for local pulmonary diseases or targeting peripheral organs by using the pulmonary route of administration.

7.2 Recommendations for this study

i. The antimicrobial efficiency of the novel rifampicin-loaded dendrimer formulations needs to be tested against the MTB bacilli.

ii. *In vivo* aspects related to the novel dendrimer formulations is an area that requires further investigation.

iii. The toxicity and permeability studies of the novel dendrimers were assessed only in raw macrophage cells. More cell lines, especially other pulmonary cells, are suggested be evaluated.

iv. The permeability study was only evaluated for one time period i.e., 24 hr. More time interval points are suggested to compare the rate of internalization of dendrimer formulations.

v. The study of the mechanism(s) of cellular internalization and intracellular trafficking of the nanoformulations needs further analysis.

vi. Functionalization of the surface of PAMAM dendrimers with both PEG and mannose ligands at the same time is an area that needs more exploring.

vii. Developing and optimization of dry powder inhalation of the novel dendrimer nanoformulations is an interesting field that needs further studies.